G R
HONI SOIT QUI MAL Y PENSE
DIEU ET MON DROIT

IMPERIAL INSTITUTE
OF
AGRICULTURAL RESEARCH, PUSA.

PROCEEDINGS

OF THE

ROYAL SOCIETY OF LONDON

SERIES A—MATHEMATICAL AND PHYSICAL SCIENCES

VOL CXLVII

LONDON
Printed and published for the Royal Society
By Harrison & Sons, Ltd., 44–47, St. Martin's Lane
Printers in Ordinary to His Majesty

December, 1934

LONDON:
HARRISON AND SONS, LTD., PRINTERS IN ORDINARY TO HIS MAJESTY
ST. MARTIN'S LANE

CONTENTS

SERIES A VOL CXLVII

No. A 860—November 1, 1934

PAGE

On the Cataphoresis of Gliadin. Part I—The Adsorption of Gliadin on Quartz. By I. Kemp and E. K. Rideal, F.R.S. 1

On the Cataphoresis of Gliadin. Part II—The Effect of Strong Electrolytes upon the Mobility. By I. Kemp and E. K. Rideal, F.R.S. 11

The Spectrum of H$_2$ (the Ordinary Hydrogen Molecule). Part I—The 3, $4d\,^3\Sigma$, Π, $\Delta \rightarrow 2p\,^3\Pi$ and $3s\,^3\Sigma \rightarrow 2p\,^3\Pi$ Systems. By O. W. Richardson, F.R.S., and T. B. Rymer 24

The Reaction between Oxygen and the Heavier Isotope of Hydrogen. By C. N. Hinshelwood, F.R.S., A. T. Williamson, and J. H. Wolfenden 48

Researches on the Chemistry of Coal. Part VII—An Investigation of German Brown Coals and Irish Peat. By W. A. Bone, F.R.S., and L. J. Tei 58

The Catalysis by Palladium of the Union of Hydrogen and Oxygen. A New Phenomenon of Contact Catalysis. By D. L. Chapman, F.R.S., and G. Gregory 68

On the Explicit Solution of Certain Difference Equations. By L. M. Milne-Thomson. Communicated by Harold Jeffreys, F.R.S. 76

The Diamagnetic Susceptibilities of Salts forming Ions with Inert Gas Configurations. Part I—The Halides of Sodium and Potassium. By F. E. Hoare. Communicated by Lord Rayleigh, For. Sec. R.S. 88

Measurement of Shot Voltage used to Deduce the Magnitude of Secondary Thermionic Emission. By E. B. Moullin. Communicated by E. V. Appleton, F.R.S. 100

The Thermal Decomposition of Methyl Alcohol. By C. J. M. Fletcher. Communicated by C. N. Hinshelwood, F.R.S. 119

The Sorption of Vapours by Ferric Oxide Gel. I—Aliphatic Alcohols. By A. G. Foster. Communicated by A. J. Allmand, F.R.S. 128

The Induction Period of the Photochemical Reaction between Hydrogen and Chlorine. By J. G. A. Griffiths and R. G. W. Norrish. Communicated by T. M. Lowry, F.R.S. 140

The Swelling of Charcoal. Part III—Experiments with the Lower Alcohols. By D. H. Bangham, N. Fakhoury, and A. F. Mohamed. Communicated by D. L. Chapman, F.R.S. 152

The Swelling of Charcoal. Part IV—Stoichiometric Relations for the Films of the Alcohols. By D. H. Bangham. Communicated by D. L. Chapman, F.R.S. 175

The Liquefaction of Helium by an Adiabatic Method. By P. Kapitza, F.R.S. 189

No. A 861—November 15, 1934

PAGE

On the Acoustic Radiation Pressure on Spheres. By L. V. King, F.R.S. 212

The Energies of Alpha, Beta, and Gamma Rays. By H. A. Wilson, F.R.S. .. 240

The Spectrum of H_2. Part II—The Band Systems due to Transitions from Four New Triplet States to $2p\,^3\Pi$. By O. W. Richardson, F.R.S., and T. B. Rymer 251

The Spectrum of H_2. Part III—New Bands and Band Systems ending on $2s\,^3\Sigma$ and an Extension of the Singlet System $^1Q \rightarrow 2p\,^1\Sigma$. By O. W. Richardson, F.R.S., and T. B. Rymer 272

The Determination of the Specific Heat of Gases at High Temperatures by the Sound Velocity Method. I—Carbon Monoxide. By G. G. Sherratt and Ezer Griffiths, F.R.S. 292

On Active Chlorine. By E. J. B. Willey and S. G. Foord. Communicated by F. G. Donnan, F.R.S. 309

The Catalytic Decomposition of Hydrogen Peroxide by Iron Salts. By F. Haber and J. Weiss. Communicated by Sir William Pope, F.R.S. 332

Some General Properties of the Formulæ of the Magneto-Ionic Theory. By H. G. Booker. Communicated by E. V. Appleton, F.R.S. 352

Pressure and the Water Relations of Proteins. I—Isoelectric Gelatin Gels. By D. J. Lloyd and T. Moran. Communicated by Dr. R. H. Pickard, F.R.S. 382

Applications of the Bloch Theory to the Study of Alloys and of the Properties of Bismuth. By H. Jones. Communicated by A. M. Tyndall, F.R.S. 396

No. A 862—December 1, 1934

The Behaviour of Electrolytes in Mixed Solvents. VI—The Electrical Conductivities of some salts in Water-Ethyl Alcohol Solutions. By L. E. Connell, R. T. Hamilton and J. A. V. Butler. Communicated by J. Kendall, F.R.S. 418

Absorption Bands of HCN in the Photographic Infra-red. By G. Herzberg and J. W. T. Spinks. Communicated by A. J. Allmand, F.R.S. (Plate 1) 434

The Low Energy β-Rays of Radium E. By H. O. W. Richardson. Communicated by C. D. Ellis, F.R.S. (Plate 2) 442

The Oxygen Afterglow. By E. M. Stoddart. Communicated by F. G. Donnan, F.R.S. 454

The Reflection of X-Rays from Powdered Anthracene. By B. W. Robinson. Communicated by Sir William Bragg, O.M., F.R.S. 467

The Principle of Least Action in Milne's Kinematical Relativity. By A. G. Walker. Communicated by E. A. Milne, F.R.S. 478

PAGE

The Structure of Surface Films. XXI—Surface Potentials of Dibasic Esters, Alcohols, Aldoximes, and Ketones. By N. K. Adam, F. J. Danielli and J. B. Harding. Communicated by F. G. Donnan, F.R.S. 491

The Magnetic Moment of the Nucleus of Cæsium. By D. A. Jackson. Communicated by F. A. Lindemann, F.R.S. 500

Spectrum of the Flame of Ethylene. By W. M. Vaidya. Communicated by A. Fowler, F.R.S. (Plate 3) 513

On the Quantization of the New Field Equations. I. By M. Born and L. Infeld. Communicated by P. A. M. Dirac, F.R.S. 522

The Mean Lives of Excited Hydrogen Atoms. By J. H. E. Griffiths. Communicated by F. A. Lindemann, F.R.S. 547

Slow Oxidations at High Pressures. I—Methane and Ethane; II—Methyl Alcohol, Ethyl Alcohol, Acetaldehyde, and Acetic Acid. By D. M. Newitt and P. Szego. Communicated by W. A. Bone, F.R.S. 555

The Upper Limits of the Continuous β-Ray Spectra of Thorium C and C″. By W. J. Henderson. Communicated by C. D. Ellis, F.R.S. 572

The Excitation Potential of the Nitrogen Second Positive Bands. By N. Thompson and S. E. Williams. Communicated by A. M. Tyndall, F.R.S. 583

A Note on the Spectrum of the Frequencies of a Polar Crystal Lattice. By M. Born and J. H. E. Thompson. Communicated by E. A. Milne, F.R.S. .. 594

Index 601

ERRATA

Paper by I. KEMP and E. K. RIDEAL, "On the Cataphoresis of Gliadin."
'Proceedings' A, vol. 147, p. 1 (November) 1934.

p. 9, line 17, *for* $\xi_1 \frac{e_1 + \xi_2 e_2}{kT}$ *read* $\frac{\xi_1 e_1 + \xi_2 e_2}{kT}$

p. 14, lines 7, 8 *for* "full" *substitute* "half."

„ line 14, *for* "$ka = 1 \cdot 6 \times 10^{-7}$" *read* "$Pka = 5 \cdot 5$"
"$kb = 1 \cdot 0 \times 10^{-11}$" *read* "$Pkb = 9 \cdot 7$"

„ line 18, *for* "$ka = 1 \cdot 0 \times 10^{-7}$" *read* "$Pka = 5 \cdot 9$"
"$kb = 0 \cdot 4 \times 10^{-11}$" *read* "$Pkb = 9 \cdot 8$"

p. 15, FIG. 2, *for* "gram mols of reagent" *read* "$\times 10^{-5}$ gram mols of reagent."

p. 17, lines 13, 15 *for* "k" *read* "K."

p. 19, equation (2.12), *for* "(HKa)" *read* "(1 + Ka)."

On the Cataphoresis of Gliadin

Part I—The Adsorption of Gliadin on Quartz

By IAN KEMP and ERIC K. RIDEAL, F.R.S., Colloid Science Laboratory, Cambridge

(*Received May* 26, 1934)

INTRODUCTION

There have been few systematic investigations of the physico-chemical properties of the more important plant proteins ; such investigations as have been carried out in the past have concerned themselves almost entirely with the better known animal proteins. It was, therefore, thought desirable to make a study of the physico-chemical properties of the protein gliadin, which, together with glutenin, forms the chief constituent of the gluten of flour.

Of all the methods employed for determining the mobility of colloid ions in an electric field, the micro-cataphoretic method is the most exact.* In studying the micro-cataphoresis of protein sols in which the particles are not visible in the ultramicroscope, it has been usual to make measurements using inert particles coated with protein. Although it was found possible to obtain gliadin sols containing visible submicrons, it was decided to make observations also on quartz particles covered with gliadin.

The investigations of Loeb,† Freundlich, and Abramson,‡ and especially those of Abramson,§ of Abramson and Michaelis,|| Daniel,¶ and

---

* *Cf.* Tuorila, 'Kolloid. Zsch.,' vol. 11, p. 44 (1928) ; Henry, 'Ann. Rep. Chem. Soc.' (193 ;

† 'J. gen. Physiol.,' vol. 5, pp. 395, 479, 505 (1922–3).

‡ 'Z. phys. Chem.,' vol. 128, p. 25 (1927) ; vol. 133, p. 51 (1928).

§ 'J. Amer. Chem. Soc.,' vol. 50, p. 390 (1928) ; 'J. gen. Physiol.,' vol. 13, p. 169 (1929–30) ; vol. 15, p. 575 (1931–2) ; vol. 16, p. 573 (1932–3) ; 'J. Phys. Chem.,' vol. 35, p. 291 (1931).

|| 'J. gen. Physiol.,' vol. 12, p. 587 (1929).

¶ 'J. gen. Physiol.,' vol. 16, p. 457 (1932–3).

of Prideaux and Howett,[*] have shown that particles coated with protein behave, as regards their cataphoretic behaviour, like natural proteins. Previous experiments had indicated that on the progressive addition of a protein to a quartz suspension, the mean velocity of the particles gradually changes to a value corresponding to the velocity of the protein itself, indicating that adsorption is taking place, and that the adsorption concentration relation approximates to that of a simple isotherm. No detailed examination of the process has, however, been attempted, and since the reaction between quartz particles and protein may be regarded as a macro-manifestation of a unimolecular reaction, it seemed desirable to study this process.

EXPERIMENTAL

The measurements of the cataphoretic velocity were carried out using a micro-cataphoresis cell of the Mattson type,[†] observations being made with a Leitz slit ultramicroscope. For determining the hydrion activities of the solutions, both hydrogen and quinhydrone electrodes were employed. Quartz suspensions were prepared by grinding up with water pieces of fused quartz which had been subjected to exhaustive cleaning treatment. Uniform suspensions could be obtained by using the upper portion of the liquid after sedimentation equilibrium had been attained.

Three samples of gliadin were used, no appreciable difference between the three being observed. The first was prepared by Dr. P. Halton in the laboratories of the Research Association of British Flour Millers, the method of preparation being described in the paper of Hughes and Rideal[‡]; the second was also prepared by Dr. Halton by the following method: washed-out gluten was dispersed in N/40 lactic acid, and alcohol was added until the concentration was 50%. The acid was then neutralized, and the precipitated glutenin removed. The remaining alcoholic solution of gliadin was concentrated *in vacuo* at low temperature, and the gliadin precipitated by pouring into water; it was subsequently purified in the usual manner. The third sample was obtained indirectly from Dr. R. Gortner, of Minnesota, the details of preparation being given in the paper of Hoffmann and Gortner.[§]

---

[*] 'Proc. Roy. Soc.,' A, vol. 126, p. 126 (1929).

[†] 'J. phys. Chem.,' vol. 32, p. 1532 (1928); vol. 37, p. 223 (1933).

[‡] 'Proc. Roy. Soc.,' A, vol. 137, p. 62 (1932).

[§] 'Colloid Symposium Monogr.,' vol. 2, p. 209 (1924).

ADSORPTION EQUILIBRIUM OF GLIADIN AT THE QUARTZ-LIQUID INTERFACE

It was found that the velocities of the particles of a quartz suspension show considerable variation in an electric field. These variations are due partly to errors in observation and partly to the Brownian agitation of the particles, which causes movements both in the direction of, and opposed to the migration due to, cataphoresis. Variations are also due to an alteration in depth and, in very dilute solutions, to the fact that the particles are not all identical in size. Similar observations have been made by Tuorila* for particles of a paraffin sol. It was found possible to construct velocity distribution curves by observing 200–300 particles, and such curves were found to be of the Gaussian type, fig. 2 (curve 1). The mobility of the quartz particles was found to be substantially independent of the hydrogen ion activity of the medium, as is shown in Table I.

TABLE I

Medium	N/15 phosphate				N/15 acetate					
Pa H	5·46	5·73	6·51	7·50	3·63	3·93	4·20	4·43	4·70	5·45
U in μ/sec/volt/cm	−2·30	−2·43	−2·32	−2·40	−1·90	−2·10	−1·95	−1·92	−2·00	−2·19

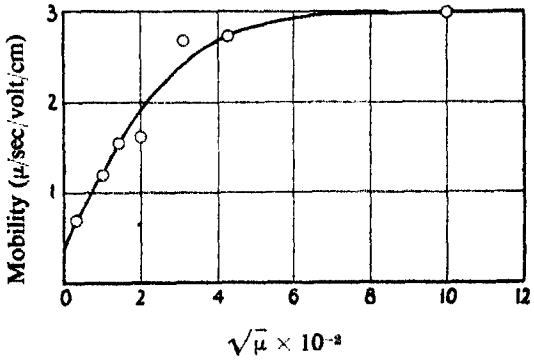

FIG. 1.

The mobility is determined, however, by the nature and ionic strength of the electrolyte present ; thus the mobility is greater in phosphate than in acetate solutions of the same ionic strength. Measurements in solutions of sodium acetate-acetic acid and of potassium chloride indicate that the mobility decreases as the ionic strength is decreased in uni-univalent electrolytes. In fig. 1 is shown the relationship between the mobility of quartz particles and the ionic strength of potassium chloride.

---

* 'Kolloid. Zsch.,' vol. 44, p. 11 (1928).

Thus the charge on the quartz is due in the main to ionic adsorption, and not to surface dissociation of a complex silicic acid.

On adding small amounts of gliadin to a quartz suspension the character of the velocity distribution curve becomes modified.

As the concentration is increased, the symmetrical monomodal Gaussian curve passes first into an asymmetrical monomodal curve, then into a bimodal curve, and finally into a symmetrical monomodal curve when surface saturation is reached (curves 1–6, fig. 2).

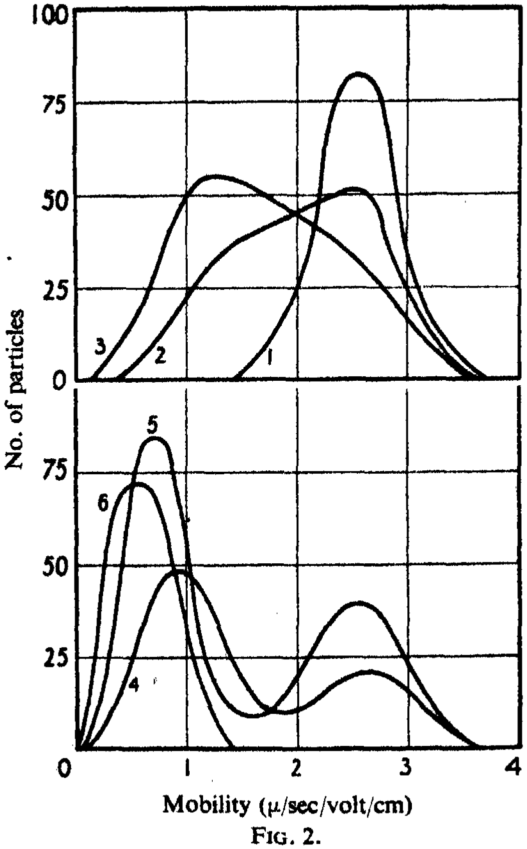

FIG. 2.

These curves reveal the existence of two adsorbing surfaces on the partly covered quartz, *i.e.*, that the protein is adsorbed not only on the

TABLE II

Curve	1	2	3	4	5	6
Concentration in gm/cc × 10^{-7}	0	7·5	12·4	15·1	22·4	81·4 (saturation)

quartz, but also, and preferentially, at those parts of the surface already covered with protein. Such increased probability of adsorption may be assigned to the modification of surface forces in the presence of adsorbed protein. Thus, in the immediate proximity of adsorbed protein molecules, the surface forces are modified and the work function is lowered. If we assume with Freundlich ("Kapillarchemie") that an energy of activation is necessary for such adsorption processes in solution, owing to the preliminary displacement from the quartz surface of a layer of adsorbed solvent, then we may write the probability of a molecule being adsorbed at a quartz-liquid interface as $e^{-\frac{\phi_1}{kT}}$ and for the protein-liquid interface as $e^{-\frac{\phi_2}{kT}}$ where ϕ_1 is greater than ϕ_2.

If the number of protein molecules striking unit area of surface per second be N_0, and θ be the fraction of the quartz surface covered with gliadin, the rate of adsorption, including that at the quartz and at the covered surface will be

$$\frac{\partial N}{\partial t} = k_1 N_0 \, e^{-\frac{\phi_1}{kT}} (1 - \theta) + k_2 N_0 \theta \, e^{-\frac{\phi_2}{kT}},$$

where k_1 and k_2 are constants characteristic of the surface. If the number of molecules on the surface be N and A the molecular area, then

$$\frac{\partial N}{\partial t} = N_0 \left(AN \left(k_2\alpha_2 - k_1\alpha_1\right) + k_1\alpha_1\right), \tag{1.1}$$

where

$$\left.\begin{aligned} \alpha_1 &= e^{-\frac{\phi_1}{kT}} \\ \alpha_2 &= e^{-\frac{\phi_2}{kT}} \end{aligned}\right\} \tag{1.2}$$

By equating the rate of adsorption to the rate of desorption

$$N_1 + N_2 = N$$

then we obtain as conditions of equilibrium a modified Langmuir adsorption isotherm of the type

$$x = \frac{kk_1k_2c}{1 + k\left(k_2 - k_3\right)c}$$

where

$$N_0 = kc \tag{1.3}$$

where x = amount adsorbed, c = concentration and k, k_1, k_2, k_3 are constants.

From measurements of the mobilities of quartz particles in the presence of varying concentrations of gliadin, the adsorption isotherm could be constructed. Thus, by plotting the mean mobility against the concentration of gliadin, we can follow the rate of change of the number of molecules of protein on the quartz surface with the concentration of protein. This is shown in fig. 3.

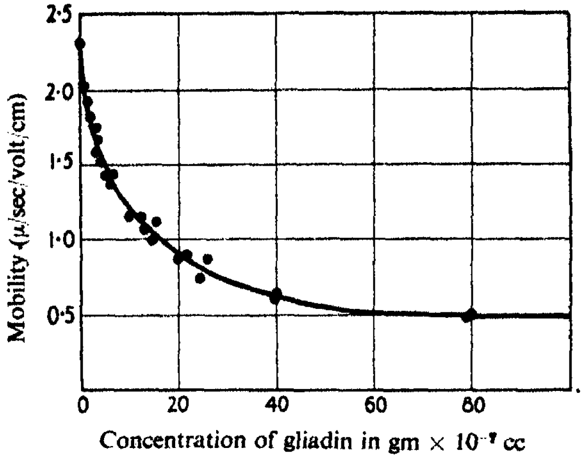

FIG. 3.

It is found that the form of the curve is that demanded by the theory

$$\Delta U = \frac{kC}{1 + k^1C} \tag{1.4}$$

where $k = 2{\cdot}90 \times 10^2$ and $k^1 = 1{\cdot}53 \times 10^6$, U being measured in cm/sec/volt/cm, and C in gm/cc.

The adsorption process is reversible ; thus, if to a mixture of quartz particles and gliadin an equal quantity of quartz be added, re-distribution is seen to have taken place, and the final mean mobility corresponds, on the adsorption isotherm, to a concentration of gliadin one-half of that originally present. Thus, in one experiment the measured mobility of quartz in a bulk concentration of gliadin of $24{\cdot}8 \times 10^{-7}$ gm/cc was $-\ 0{\cdot}94\ 10^{-4}$ cm/sec/volt/cm. On adding an equal amount of quartz, the equilibrium mobility was found to be $-\ 1{\cdot}08\,.\,10^{-4}$ cm/sec/volt/cm. This corresponds on the adsorption isotherm to a bulk concentration of $13{\cdot}0\,.\,10^{-7}$ cm/cc.

ON THE RATE OF ADSORPTION OF GLIADIN AT THE QUARTZ LIQUID INTERFACE

It was found possible to measure the velocity of adsorption of gliadin at the quartz surface for small concentrations of protein. The gliadin solution was added to a quartz suspension in a suitable electrolyte solution, and the apparatus filled with the freshly prepared solution. After suitable intervals of time, forty measurements of particle velocities were made, such a series taking about ten minutes.

The calculated maximum error in the mean velocity at each time is not greater than ± 10%.

In fig. 4 are shown the velocity curves for the adsorption of gliadin ions of opposite sign, the first in N/15 phosphate buffer at p_H 5·66, when the gliadin ion is negatively charged, and the second for an equal concentration of gliadin in N/15 acetate buffer of p_H 3·7 when the charge is positive. It will be noted that whereas the quartz particles in both buffer solutions possess a negative charge, the rate of adhesion of the gliadin to the quartz is much greater when the gliadin is positively charged than when the latter is negative, as would be expected.

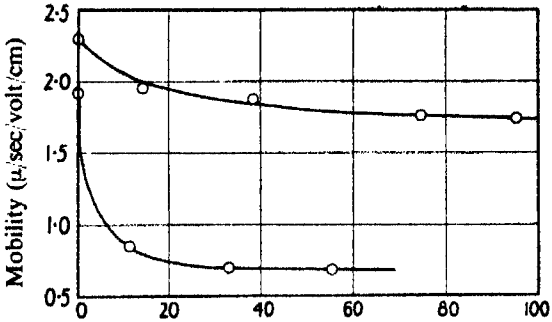

FIG. 4.

We note from (1·1) that the rate of adsorption should follow a unimolecular course, where

$$t = \frac{1}{N_0A\,(k_2\alpha_2 - k_1\alpha_1)} \log_e \left\{ AN \left(\frac{k_2\alpha_2}{k_1\alpha_1} - 1 \right) + 1 \right\} \qquad (1.5)$$

The values given in Table III for the unimolecular velocity constants were obtained at 20° C in N/15 phosphate buffer of p_H 5·66.

TABLE III

Concentration of gliadin × 10^{-7} gm/cc	1·14	1·71	2·28	2·85	3·42	3·84	3·99	4·56
$k \times 10^{-4}$ sec^{-1}	5·8	9·6	9·6	14·4	9·6	7·5	6·4	9·0
Concentration	5·13	5·36	6·03	6·75	9·35	11·2	15·1	21·3
$k \times 10^{-4}$ sec^{-1}	7·2	9·6	14·4	10·5	14·4	11·5	12·8	7·7

Mean value $k = 10{\cdot}2 \times 10^{-4}$ at 20° C.

For gliadin of concentration $3{\cdot}84 \times 10^{-7}$ gm/cc in N/15 acetate at p_{H} 3·7

$$k = 80{\cdot}0 \times 10^{-4}\ \mathrm{sec}^{-1}.$$

Within the limits of the experimental error the reaction velocity constant conforms to a unimolecular order, and the reaction velocity with the gliadin at p_{H} 3·7 (positively charged) is 10·7 times as great as for the gliadin at p_{H} 5·7 (negatively charged). Martin* has recently investigated the rates of adsorption of gliadin at the glass liquid interface by the method of streaming potentials ; his experimental values for the velocity constant are in substantial agreement with ours.

For a gliadin concentration of 20 × 10^{-7} gm/cc—

p_{H}	5·7	3·2
K × 10^{-4} sec^{-1}	9	70

For these dilute solutions of gliadin the reaction velocity can be written in the form, considering only adsorption at the quartz-liquid interface,

$$\frac{\partial \mathrm{N}}{\partial t} = k_1 \mathrm{N}_0 (1 - \theta) e^{-\frac{\phi_1}{k\mathrm{T}}}, \quad \text{or} \quad \frac{\partial \mathrm{N}}{\partial t'} = k\, e^{-\frac{\phi_2}{k\mathrm{T}}}.$$

The energy of activation ϕ for adhesion may be regarded as made up of two terms, the one involving the chemical energy of activation ω, which may be identified with the heat of hydration of the quartz surface, and the other determined by the electrical forces operative between the quartz and the protein. If the latter are taken as proportional to the ξ potential on the quartz, we have

$$\phi_1 = \omega - \xi_1 \varepsilon_1$$

$$\phi_2 = \omega + \xi_2 \varepsilon_2$$

---

* 'J. Phy. Chem.,' vol. 38, p. 213 (1934).

for the positively charged and negatively charged protein ions respectively, where ξ_1, ξ_2 are the electrokinetic potentials at the quartz liquid interface and ε_1 and ε_2 are the charges on the protein molecule.

Thus, for positively charged protein the rate of adsorption is

$$\left(\frac{dN}{dt}\right)_+ = kN_0\, e^{-\frac{(\omega-\xi_1 e_1)}{kT}}, \tag{1.6}$$

while for negatively charged protein the rate is

$$\left(\frac{dN}{dt}\right)_- = kN_0\, e^{-\frac{(\omega+\xi_2 e_2)}{kT}}. \tag{1.7}$$

The ratio

$$\frac{k_+}{k_-} = e^{\frac{(\xi_1 e_1+\xi_2 e_2)}{kT}}. \tag{1.8}$$

If we consider adsorption of protein at both quartz-liquid and quartz-protein interfaces, we have

$$\frac{\left(\frac{dN}{dt}\right)_+}{\left(\frac{dN}{dt}\right)_-} = \frac{N_0(AN(k_2\alpha_2 - k_1\alpha'_1) + k_1\alpha'_1)}{N_0(AN(k_2\alpha_2 - k_1\alpha_1) + k_1\alpha_1)} \quad \begin{matrix} \text{where} & \alpha'_1 = e^{-\frac{(\omega-\xi_1 e_1)}{kT}} \\ ,, & \alpha_1 = e^{-\frac{(\omega+\xi_2 e_2)}{kT}}. \end{matrix}$$

Thus

$$\frac{k^+}{k^-} = e^{\frac{\xi_1 e_1+\xi_2 e_2}{kT}} \cdot \frac{AN(e^{-\frac{\xi_1 e_1+\xi_2 e_2}{kT}}.k_2\alpha_2 - k_1\alpha_1) + k_1\alpha_1}{AN(k_2\alpha_2 - k_1\alpha_1) + k_1\alpha_1}, \tag{1.8A}$$

and this is strictly more valid than equation (1·8).

The ratio of velocity constants for protein adsorption at p_H 3·7 and at p_H 5·7, and a concentration of 3·84 × 10^{-7} gm per cc was found to be

$$\frac{k_\pm}{k_-} = 10{\cdot}7.$$

Thus $\log_e 10{\cdot}7 = \xi_1 \frac{e_1 + \xi_2 e_2}{kT}$ (from equation 1·8).

Hence $\xi_1 e_1 + \xi_2 e_2 = 61{\cdot}7 \times 10^{-3}$ electron volts.

The values of ξ_1 and ξ_2 calculated from the Henry expression (Part II, equation (2·8)), and using the measured mobilities are

$\xi_1 = 34{\cdot}5 \times 10^{-3}$ volts (in N/15 phosphate solution),

and

$\xi_2 = 28{\cdot}8 \times 10^{-3}$ volts (in N/15 acetate solution).

The thickness of the double layer is at this ionic strength less than the dimensions of the protein molecule, and we can, therefore, assume that the charged gliadin molecule may become attached by only one electronic charge.

Thus the value of $\xi_1 + \xi_2 = (34\cdot5 + 28\cdot8)\ 10^{-3} = 63\cdot3 \times 10^{-3}$ volts, which is in agreement with the value of the sum of the electrical work functions derived from velocity measurements :

$$61\cdot7 \times 10^{-3} \text{ electron volts.}$$

SUMMARY

(1) From the distribution curves of gliadin molecules over the surface of suspended quartz particles, it appears that preferential adsorption of gliadin occurs at the gliadin-liquid interface.

(2) The velocity of adsorption of gliadin molecules at the surface of suspended quartz particles is shown to be unimolecular.

(3) The velocity depends upon magnitude and sign of the charge on the gliadin molecule. From this relationship the electrical work function at the quartz liquid interface is shown to be of the order of the measured electrokinetic potential.

On the Cataphoresis of Gliadin

Part II—The Effect of Strong Electrolytes upon the Mobility

By Ian Kemp and E. K. Rideal, F.R.S.

(*Received* May 26, 1934)

Careful analyses of the cataphoretic velocity of a colloid particle suspended in an electrolyte solution have been made by Smoluchowski,[*] by Debye and Hückel,[†] by Hückel,[‡] and by Henry.[§]

No actual test of their theoretical conclusions over a sufficiently wide range of ionic strength appears yet to have been made, with the exception of some experimental work recorded by Audubert,[||] whose results indicate good agreement for particles of radius 60 — 130 A, but not for particles of radius 2–8 μ. Unfortunately, no details are given of the measurement of the sizes of such small particles. In adopting the hypothesis of Pauli that a colloidal particle behaves like a large polyvalent ion, it is assumed that on altering the electrolyte concentration there is no change in valency of the ion when the theory of Debye-Hückel and of Henry is applied. In practice those colloids whose charge is derived mainly from adsorption of ions do not exhibit constant valency on variation of the ionic strength of the electrolyte. According to Abramson,[¶] quartz particles covered with protein behave as ions of constant valency in solutions of the same ionic strength and hydrion activity. This assumption can be valid only over a restricted range of concentrations. Thus, at high ionic strengths, the valency may be altered appreciably by the adsorption of electrolyte ions, whilst it may reasonably be anticipated that at small ionic strengths the effect of the restriction of ions inside the double layer will lead to an alteration in the effective valency of the particle. In general a Donnan equilibrium is set up wherever one ionic species is constrained in any manner from free diffusion ; modification of the effective valency of the colloid ion may be expected in very dilute electrolyte solutions on this account.

---

[*] Grätz "Handbuch der Elektricität und Magnetismus" (1914); 'Bull. Acad. Sci. Cracovie,' vol. 182 (1903).

[†] 'Phys. Z.,' vol. 25, p. 49 (1924).

[‡] 'Phys. Z.,' vol. 25, p. 205 (1924).

[§] 'Proc. Roy. Soc.,' A, vol. 133, p. 106 (1931).

[||] 'J. Chim. Phys.,' vol. 30, p. 89 (1932).

[¶] 'J. Gen. Physiol.,' vol. 15, p. 575 (1931–2).

EXPERIMENTAL

Microcataphoretic experiments were carried out both with sols of gliadin (prepared by diluting alcoholic solutions with the suitable buffer mixtures) and with suspended particles of quartz covered with a complete layer of adsorbed gliadin. In both preparations the particles, judging from their ultramicroscopic appearance, were substantially spherical. In order to determine the size of the particles two methods were employed. In the quartz suspensions about 100 cc of suspension was evaporated, together with a control of an equal volume of distilled water. The weight of quartz in 100 cc could thus be determined, and the number of particles per cc was evaluated by ultramicroscopic counting in suitable dilutions. The mean radius by this method was found to be $a = 1{\cdot}27\ 10^{-5}$ cm.

The radius of the suspended particles was also derived by measurement of Brownian displacements using the equation of Einstein

$$\frac{\overline{\Delta x^2}}{t} = \frac{\mathrm{RT}}{3\pi\eta \mathrm{N}a}, \tag{2.1}$$

where $\overline{\Delta x^2}$ = the mean square displacement along a given axis in time t,

η = the viscosity of the solution,
R = gas constant,
T = °K,
N = Avogadro number,
a = radius of particle.

The suspended particles were observed in the cataphoresis tube, with a No. 4 Leitz objective, the graticule spacing being with this magnification 26 μ. Using this eyepiece graticule, the co-ordinates in the focal plane of each particle were noted before and after the elapse of a suitable interval of time, in this case 30 seconds, which was observed with an error of ± 0·5 sec. The co-ordinates of the particle were estimated to one-twentieth of a graticule spacing. The highest available magnification was employed in order to ensure maximum displacements, and, therefore, a minimum relative error.

The tube was lagged with cotton-wool to minimize temperature fluctuation and drifts in the tube resulting therefrom ; the temperature variation was not greater than 1° K in 300° K, but a correction for the variation of η with the temperature was necessary, the final error due to temperature variations being about 1%.

About two hundred particles of quartz and of gliadin were observed. The displacements Δx and Δy were deduced for each, and the mean displacements calculated. These revealed displacements of the distribution maxima due to drifts in the cell.

The values of $\overline{\Delta x^2}$ and of $\overline{\Delta y^2}$ were calculated from the corrected displacements. The values for the radii thus obtained were—

for quartz .. $a = (1 \cdot 1 \pm 0 \cdot 4) \times 10^{-5}$ cm,
„ gliadin .. $a = (1 \cdot 3 \pm 0 \cdot 4) \times 10^{-5}$ cm.

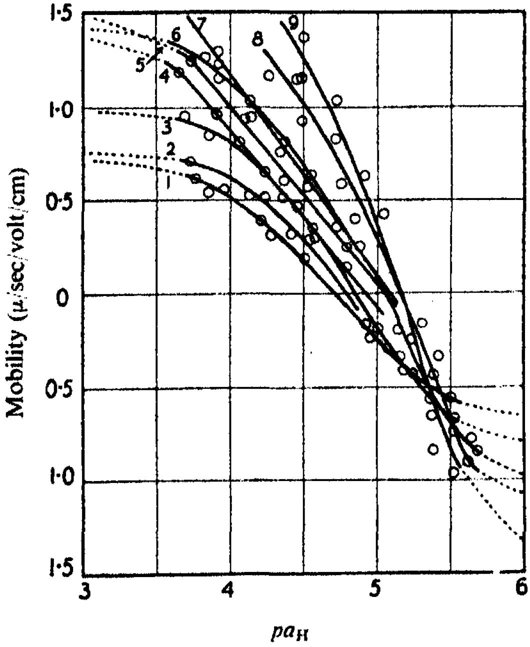

Fig. 1.

Curve	1	2	3	4	5	6	7	8	9
Normality of the solution ……	N/15	N/10	N/30	N/50	N/100	N/150	N/250	N/1500	N/2500

Solutions of gliadin-coated quartz particles and of gliadin particles were prepared in acetate buffer solutions of different p_H and of varying ionic strength. In fig. 1 are plotted the cataphoretic mobilities as a function of the hydrogen ion activity for these different solutions.

THE ISOELECTRIC POINT OF GLIADIN

It will be noticed from fig. 1 that the observed isoelectric point is markedly dependent upon the electrolyte concentration. The experimental figures are given in Table I.

TABLE I

Ionic strength	0·1000	0·0667	0·0333	0·0200	0·0133	0·0100	0·0067	0·0040	0·0007
Isoelectric point pa_H	4·78	4·70	4·83	4·90	5·00	5·02	5·05	5·08	5·10

All the curves are smooth, an indication that the protein may be considered in respect to its acid and basic dissociation constants as a monovalent ampholyte.

The full basic dissociation is given by the equation

$$\frac{kb}{kw}(\overset{+}{\mathrm{H}}) - \frac{ka}{(\mathrm{H})} = 1, \qquad (2.2)$$

whilst for full acid dissociation we have

$$\frac{ka}{(\mathrm{H})^+} - \frac{kb}{kw}(\overset{+}{\mathrm{H}}) = 1, \qquad (2.3)$$

where ka and kb are the acidic and basic dissociation constants respectively. By extrapolating the mobility-p_H curves, the values of a_{H^+} for limiting basic dissociation and for limiting acid dissociation can be determined approximately, and on substitution of these values in equations (2·2) and (2·3) the values of ka and kb can be calculated. The values calculated were

$$ka = 1\cdot6 \times 10^{-7}$$
$$kb = 1\cdot0 \times 10^{-11}.$$

In view of the extended extrapolation necessary (since the limiting ionizations are outside the p_H range of the buffer), these values are in reasonable agreement with those determined directly by titration, viz. :—

$$ka = 1\cdot0 \times 10^{-7}$$
$$kb = 0\cdot4 \times 10^{-11}.$$

For the electrometric titration of gliadin, the quinhydrone electrode was employed. The reagents were N/100 hydrochloric acid and N/200 caustic soda (freed from CO_2). Since the concentration of gliadin was never larger than $\frac{1}{2}$%, the protein error of the electrode could be neglected, but a correction was made for the secondary salt effect, the formula of Linderstrom-Lang and Lund* being used in this connection—

$$\bar{h} = \frac{pa_{\bar{H}} - pa_{H}}{\left(\frac{0{\cdot}308 \times 10^{-7}}{a\,(1 + ka)} + \frac{0{\cdot}8686}{q}\right)},$$

where

$\bar{h}$ = number of H^+ bound per gm mol,

a = ionic radius,

$2q$ = total number of ionizable groups,

$pa_{\bar{H}}$ = isoelectric point.

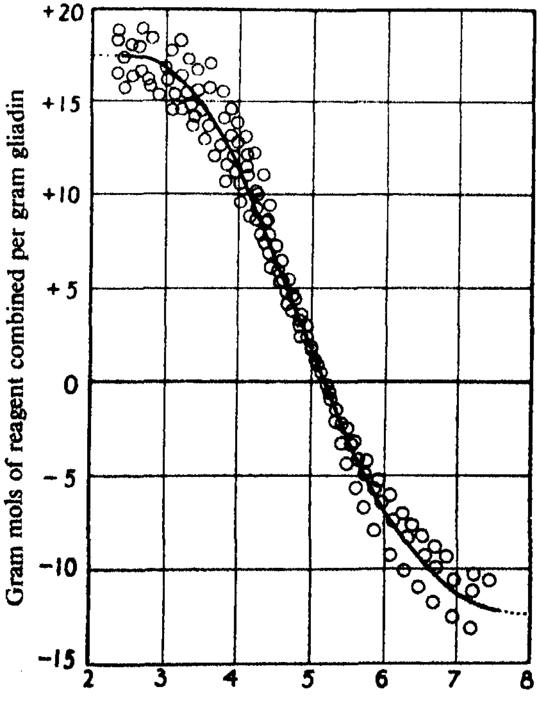

Fig. 2.

The titration curves are shown in fig. 2. The acid combination curve is derived from eleven titrations and the basic combination curve from five titrations.

---

* 'C.R. Trav. Lab. Carlsberg,' vol. 16, p. 5 (1926).

The accepted value for the isoelectric point of gliadin appears to be pa_{H} 6·5. Numerous[*] determinations have been made, all based upon the hypothesis that the protein possesses a minimum of solubility at the isoelectric point. In order to corroborate these results the variation in the solubility of gliadin with the p_{H} was investigated by two methods. In the first an ultramicroscopic estimation was made of the amount of gliadin precipitated from dilute alcoholic solutions in the presence of electrolytes. In the second, the turbidity maximum was determined by means of a turbidimeter designed by Dr. P. S. H. Henry, of this laboratory. The results of both methods were in substantial agreement, indicating that for acetate buffer solutions of ionic strength $\mu = 0{\cdot}006$ at 20° C, the point of minimum solubility lies between the values p_{H} 6 and 7. It seems certain that the isoelectric point of gliadin does not coincide with the point of minimum solubility—indeed, if we accept the hypothesis that the protein is present mainly in the form of zwitterions, there is no reason for the assumption that the solubility of a protein is a minimum at the isoelectric point.

APPLICATION OF THE THEORY OF STRONG ELECTROLYTES

The cataphoresis of an insulating particle suspended in a liquid has been considered by Smoluchowski (*loc. cit.*). Assuming the ionic envelope to be a diffuse layer of the type postulated by Gouy[†] he deduced the following relation for the velocity

$$U = \frac{DX\xi}{4\pi\eta}, \tag{2.4}$$

where U is the velocity, D the specific inductive capacity of the medium, η the viscosity, ξ the electrokinetic potential or potential difference across the double layer, and X the intensity of the electric field.

Debye and Hückel (*loc. cit.*) have made an analysis for a colloid particle of conductivity equal to that of the medium and surrounded by a diffuse ionic atmosphere ; the resultant expression obtained was

$$U = C\frac{DX\xi}{\eta}, \tag{2.5}$$

---

[*] Lüers, 'Kolloid. Zsch.,' vol. 25, p. 177 (1919–20) ; Pearsall and Ewing, 'Biochem. J.,' vol. 18, p. 329 (1924) ; Hoffmann and Gortner, 'Colloid. Symposium Monogr.,' vol. 2, p. 209 (1924) ; Tague, 'J. Amer. Chem. Soc.,' vol. 47, p. 418 (1925) ; Csonka Murphy and Jones, 'J. Amer. Chem. Soc.,' vol. 48, p. 767 (1926) ; Chibnall and Grover, 'Biochem. J.,' vol. 70, p. 108 (1926) ; Kondo and Hayashi, 'Mem. Coll. Agri. Kyoto Imp. Univ.,' vol. 2, p. 5 (1931) ; Martin, 'J. Phys. Col.,' vol. 35, p. 2065 (1931) ; de Jong, 'Trans. Faraday Soc.,' vol. 28, p. 798 (1932).

[†] 'J. Physique,' vol. 9, p. 457 (1910); 'Ann. Phys. Lpz.,' vol. 53, p. 239 (1917).

where C is a constant dependent on the shape of the particle, being $1/6\pi$ for a sphere and $1/4\pi$ for a cylinder moving axially to the field. The electrokinetic potential for a sphere was likewise found to be

$$\xi = \frac{e}{Da\,(1 + Ka)}, \tag{2.6}$$

where e is the charge on the sphere, a its radius and

$$K = \sqrt{\frac{4\pi\varepsilon^2}{DkT}\Sigma n_i \nu_i^2}, \tag{2.7}$$

where ε is the electronic charge, k Boltzmann's constant, T the absolute temperature, and n_i the number of ions of valency ν_i per cc of solution.

Since the ionic strength of a solution is defined as

$$\mu = \tfrac{1}{2}\Sigma c_i \nu_i^2,$$

where c_i = concentration (in gm ions/litre) of ions of valence ν_i, we may write

$$k = \sqrt{\frac{8\pi\varepsilon^2 N}{1000 \,.\, D \,.\, k \,.\, T} \cdot \mu}.$$

Thus for water at room temperature

$$k = 3\,.\,3 \times 10^7 \sqrt{\mu}\ \mathrm{cm}^{-1}.$$

For an insulating spherical particle in an ionic atmosphere of the Debye-Hückel type Henry (*loc. cit.*) has deduced the expression

$$U = \frac{DX\xi}{4\pi\eta} f(Ka), \tag{2.8}$$

where $f(Ka)$ can be computed approximately as the sum of a series ; thus the value of $f(Ka)$ is unity for $Ka > 300$ and Smoluchowski's expression is obtained, whilst for $Ka < 0, 5$ the limiting value of $f(Ka)$ is 2/3 and the Debye-Hückel equation is applicable.

For a sphere of charge e we obtain

$$e = 4\pi a^2 \sigma,$$

where σ is the surface charge density. Hence from (2.6) and (2.8) we obtain

$$U = \frac{X\sigma}{\eta}\,\frac{a}{1 + Ka} f(Ka). \tag{2.9}$$

Since the values of the constants X, a, η and σ can all be measured the theoretical relationship between U and Ka can be computed.

The determination of the radius a has already been described. To evaluate σ it is necessary to know the charge per gm of gliadin σ' and the weight of gliadin per sq cm of quartz surface, γ.

If γ be the weight of gliadin per sq cm then

$$\sigma = \gamma\sigma'.$$

The values of γ have been given by Hughes and Rideal (*loc. cit.*).

$\gamma_1 = 0{\cdot}4\ 10^{-7}$ gm/cm^2 for an expanded film

$\gamma_2 = 0{\cdot}7\ 10^{-7}$ gm/cm^2 for a condensed film

$\gamma_3 = 1{\cdot}5\ 10^{-7}$ gm/cm^2 for a gel film.

The value of σ' is known from the titration data.

The theoretical curve for the relationship between mobility u/X and Ka was constructed from equation (2.9) using the values $\sigma' = 7{\cdot}99 \times 10^{-1}$ E.M.U./gram, $\gamma = 0{\cdot}4 \times 10^{-7}$ gm/cm^2, $\eta_{20^\circ C} = 1{\cdot}006 \times 10^{-2}$ c.g.s., and $a = 1{\cdot}2 \times 10^{-5}$ cm. This could be compared with the experimental curve obtained from measurements of the cataphoretic mobility of gliadin in solutions of the same hydrogen ion activity but of varying ionic strength. In practice it was difficult to prepare very dilute buffer solutions of the same hydrogen ion activity and it was, therefore, necessary to extrapolate to the standard hydrogen ion activity, the isoelectric points being known for all concentrations of electrolyte (p. 14). The observed mobilities were reduced to U 20° C by a correction of 2% per degree in the viscosity.

Both the theoretical curve (1.1) and the experimental points, ○ are shown in fig. 3.

It will be seen that there is good agreement over the range of ionic strength $\mu = 0{\cdot}008$ to $\mu = 0{\cdot}013$ corresponding to a range of (Ka) from 35 to 45. Outside this range there is, however, a considerable discrepancy between the observed and calculated mobilities, the latter being considerably the greater.

ADSORPTION OF IONS BY GLIADIN IN SOLUTIONS OF HIGH IONIC STRENGTH

The discrepancy between the observed and calculated velocities for high ionic strengths (K$a > 45$) may quite reasonably be ascribed to the occurrence of adsorption of acetate ions in strong solutions. In fig. 1 it will be observed that the isoelectric point is dependent on the ionic strength of the medium for solutions of ionic strength greater than $\mu = 5 \cdot 10^{-3}$. The number of acetate ions adsorbed per molecule of gliadin can be computed from the shifts of the isoelectric point.

Thus if

P_{HO} be the isoelectric point at infinite dilution

P_{HC} be the isoelectric point at a concentration C

$\left(\frac{dU}{dP_H}\right)_C$ be the slope of the curve at concentration C

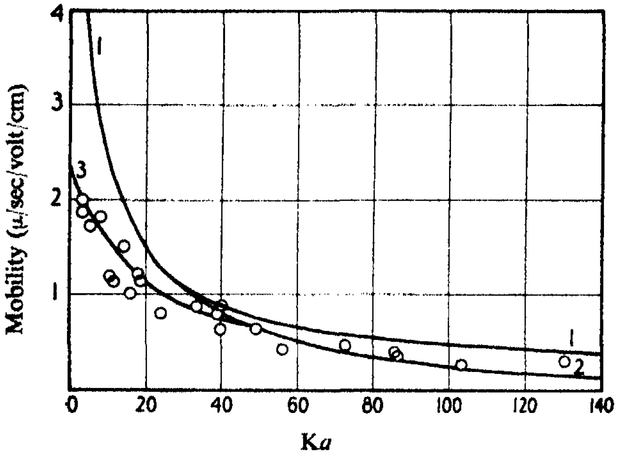

FIG. 3.

then the change in mobility due to anionic adsorption will be

$$\Delta U = -\left(\frac{dU}{dP_H}\right)_C (P_{HO} - P_{HC}). \tag{2.10}$$

From equation (2.9) we have

$$\Delta U = \left\{\frac{X}{\eta}\frac{a}{1 + Ka} f(Ka)\right\} \Delta\sigma,$$

and hence

$$\Delta\sigma = -\left(\frac{dU}{dpH}\right)_C (P_{HO} - P_{HC}) \frac{\eta}{X} \frac{1 + Ka}{af(Ka)}. \tag{2.11}$$

This is equivalent to the change in the surface charge density due to the adsorption of anions. The number of acetate ions adsorbed per molecule of gliadin is then given by

$$n_A = \frac{M\left(\frac{dU}{dpH}\right)_C (P_{HO} - P_{HC})\, \eta\, (HKa)}{\varepsilon\gamma\bar{N}Xaf(Ka)}, \tag{2.12}$$

where

M = molecular weight

ε = electronic charge.

$\bar{N}$ = Avogadro number

γ = No. of gm of gliadin per cm^2.

If the molecular weight of gliadin be taken as $M = 20{,}700$ the relationship between the number of acetate ions adsorbed per molecule of gliadin and the total ionic strength can be calculated from (2.12) the results of which are shown in fig. 4.

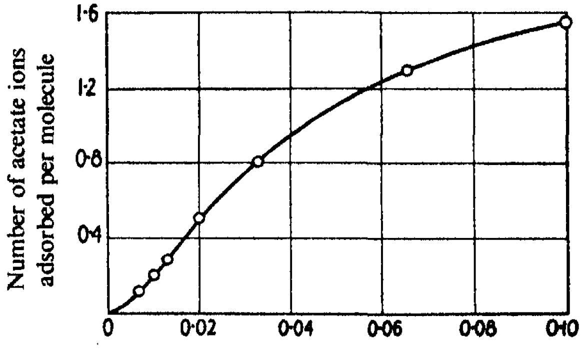

Fig. 4.

The adsorption of acetate ions commences to be appreciable at concentrations of $\mu = 0 \cdot 02$ and consequently the mobility of the colloid particle in electroytes of concentrations greater than this will be smaller than that calculated by the equation (2.9). The correction for adsorption was determined from the shift in the isoelectric points, fig. 1, and the theoretical mobility curve (1) shown in fig. 3 can be corrected for the effect of this adsorption ; the corrected curve (2) is shown in fig. 3 and it will be seen that the experimental and corrected theoretical curves are now in agreement over the region $\mu = 0 \cdot 005$ to the most concentrated solutions examined.

The agreement between theoretical mobilities (corrected for adsorption) and the observed values is given in Table II.

THE EFFECTS OF MEMBRANE EQUILIBRIUM ON THE CATAPHORETIC MOBILITY

It will be noted, fig. 3, that in solutions of very low ionic strength the mobilities observed for the protein-covered quartz particles fall far below the theoretical values anticipated from equation (2.9). It might be suggested (*vide* Abramson, *loc. cit.*) that the large particles of protein or of protein-covered quartz behave electrokinetically as single protein ions and hence that the velocity is independent of the sizes of the particles. This view is at variance with the theory of Debye-Hückel and Henry, which requires that the velocity should be independent of the radius only at high values of K*a*. Experimental verification of this point has not been forthcoming with the exception of the experiments of Mooney[*] whose results are only in rough agreement with the predictions of equation (2.9).

TABLE II

Estimated error in $a = \pm 20\%$. Estimated error in $\sigma = \pm 5\%$.

Reproducibility at any K*a* value of the mobility is $\pm 0{\cdot}08 \times 10^{-4}$ cm²/volt sec.

K*a*	U observed	U theoretical with max error	U theoretical − U observed	Max. possible deviation
33·5	0·93 ± 0·05	1·06 ± 0·27	+ 0·13	± 0·32
40·0	0·83	0·85 ± 0·21	+ 0·02	± 0·26
47·5	0·75	0·70 ± 0·18	− 0·05	± 0·23
73·0	0·50	0·38 ± 0·10	− 0·12	± 0·15
86·5	0·41	0·30 + 0·08	− 0·11	± 0·13
102·0	0·25	0·25 ± 0·06	0	± 0·11
133·3	0·35	0·22 ± 0·06	− 0·13	± 0·11

Preliminary experiments with gliadin have shown that in solutions of low ionic strength the velocity of cataphoresis is dependent upon the particle radius, although the agreement with the theory is for the results available at present only rough.

Thus for particles of radii about $1 \cdot 10^{-5}$ cm and $1 \cdot 10^{-4}$ cm respectively, suspended in solutions of ionic strength $\mu = 10^{-4}$ the ratio of the velocities should according to the theory of Henry be 0.6. The observed velocities were :—

U_1	U_2	U_1/U_2
	× 10^{-4} cm/sec/volt/cm	
0·72	0·93	0·77
0·71	0·91	0·78
0·90	1·14	0·79

It is clear that the velocity is not independent of the radius in solutions of low ionic strength, and hence we cannot explain the discrepancy in dilute solutions by the theory of Abramson.

Since there is agreement between the predictions of the Debye-Henry theory and the results of experimental observations over the range

---

[*] 'Phys. Rev.,' vol. 23, p. 396 (1924) ; 'J. Phys. Chem.,' vol. 35 p. 331 (1931).

K*a* 35—130, it is unlikely that the discrepancy can be due to a breakdown of the theory. We suggest that it is due to a diminution in the effective charge on the gliadin ion in dilute solutions of electrolyte. In considering the mechanism of such a variation in the charge on the ion it is unlikely that the mechanism of valency reduction is due to the linking up of ionizable groups in the absence of peptizing electrolytes; *e.g.*

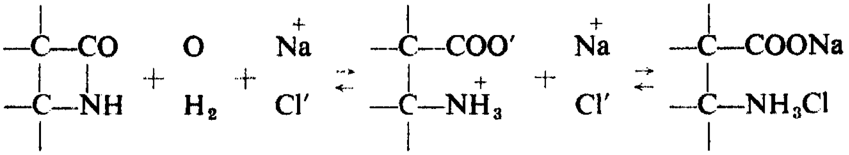

$$\begin{array}{l} -C-CO \\ \;\;|\;\;\;\;\;| \\ -C-NH \end{array} + \begin{array}{c} O \\ H_2 \end{array} + \begin{array}{c} \overset{+}{Na} \\ Cl' \end{array} \rightleftarrows \begin{array}{l} -C-COO' \\ -C-\overset{+}{N}H_3 \end{array} + \begin{array}{c} \overset{+}{Na} \\ Cl' \end{array} \rightleftarrows \begin{array}{l} -C-COONa \\ -C-NH_3Cl \end{array}$$

although this may prove to be an important factor in the coagulation of the less hydrated proteins such as the globulins. It is much more likely that the ionic equilibrium inside the double layer is governed by the conditions imposed by a Donnan ionic equilibrium. Inside the double layer the following ionic species are present, $\overset{+}{H}$, $\overset{+}{Na}$, CH_3COO' and $\overset{+}{G}$ the gliadin ions; the latter are restricted inside the double layer by adsorption at the interface and this must accordingly lead to a Donnan distribution. If one denotes the activities of the ions within and outside the double layer respectively by the suffixes 2 and 1, the following relationships must hold:

$$\frac{(CH_3CO\overset{-}{O})_1}{(CH_3CO\overset{-}{O})_2} = \frac{\overset{+}{Na}_2}{\overset{+}{Na}_1} = \frac{\overset{+}{H}_2}{\overset{+}{H}_1}. \tag{2.13}$$

Furthermore, the solutions are electrically neutral, thus

$$\overset{+}{Na}_1 + \overset{+}{H}_1 - (CH_3CO\overset{-}{O})_1 = 0 \tag{2.14}$$

$$\overset{+}{Gn}_2 + \overset{+}{Na}_2 + \overset{+}{H}_2 - (CH_3CO\overset{-}{O})_2 = 0, \tag{2.15}$$

where n_2 is the charge on the gliadin ion in solution of $\overset{+}{H}_2$. Thus

$$\overset{+}{Gn}_2 = (CH_3CO\overset{-}{O})_2 - (\overset{+}{Na}_2 + \overset{+}{H}_2) = \frac{\overset{+}{H}_1\,(CH_3CO\overset{-}{O})_1}{\overset{+}{H}_2} - \left(\frac{\overset{+}{H}_2}{\overset{+}{H}_1}\overset{+}{Na}_1 + \overset{+}{H}_2\right).$$

Now

$$\frac{\overset{+}{H}_1}{\overset{+}{H}_2} = \frac{\overset{+}{n}_1}{\overset{+}{n}_2},$$

where n_1 is the charge on the gliadin ion in solution of $\overset{+}{H}_1$. Thence

$$\overset{+}{Gn}_2 = \frac{n_1}{n_2}\,(CH_3CO\overset{-}{O})_1 - \left(\frac{n_2}{n_1}\overset{+}{Na}_1 + \frac{n_2}{n_1}\overset{+}{H}_1\right) = (CH_3CO\overset{-}{O})_1\left(\frac{n_1}{n_2} - \frac{n_2}{n_1}\right)$$

or

$$n_2 = \frac{(\mathrm{CH_3CO\bar{O}})_1}{\overset{+}{\mathrm{G}}} \left(\frac{n_1^2 - n_2^2}{n_1 n_2}\right),$$

therefore

$$\overset{+}{\mathrm{G}}\, n_1 n_2^2 = (\mathrm{CH_3CO\bar{O}})_1 (n_1^2 - n_2^2)$$

or

$$n_2 = n_1 \sqrt{\frac{(\mathrm{CH_3CO\bar{O}})_1}{\overset{+}{\mathrm{G}} n_1 + (\mathrm{CH_3CO\bar{O}})_1}}\,. \tag{2.16}$$

Thus in strong solutions the effective valency of the gliadin ion is the same as that associated with a hydrogen ion concentration of the external fluid, viz., $\overset{+}{\mathrm{H}}_1$, but as the concentration decreases the effective valency decreases since in dilute solutions the surface charge is that associated with $\overset{+}{\mathrm{H}}_2$, the hydrogen ion activity inside the double layer, and not with the hydrogen ion activity of the external fluid $\overset{+}{\mathrm{H}}_1$.

Assuming that the ratio n_1/n_2 is that given by (U theoretical)/(U observed) at low dilutions, it is possible to calculate the effective surface activity of the gliadin ions $\overset{+}{\mathrm{G}}$ and from this and equation (2.16) the variation of n_2 with the ionic strength. In this way the theoretical mobility curve corrected for the effects of the Donnan membrane equilibrium was obtained, fig. 3 (3), and, as will be seen, is in good agreement with the experimental one. From the curve it is seen that n_2 becomes equal to n_1 at a concentration of electrolyte corresponding to $Ka =$ *ca.* 45.

It is clear that the magnitude of the effects of the Donnan distribution on the cataphoretic mobility renders any calculation of the particle radius (such as was attempted by Audubert (*loc. cit.*)) directly from the mobility of doubtful value, but as we have seen the ionic distribution can readily be determined.

We are indebted to Drs. E. A. Fisher and P. Halton of the Research Association of British Flour-Millers for samples of gliadin, and to the Department of Scientific and Industrial Research for a maintenance grant (I. K.).

SUMMARY

The acid and basic dissociation constants of gliadin are calculated from mobility-p_{H} curves and from titration data.

The isoelectric point of gliadin depends upon the concentration of electrolyte. From this variation the numbers of acetate ions adsorbed per molecule of gliadin are calculated.

The Debye-Hückel-Henry expression for cataphoretic velocity is applicable to the systems investigated only over a limited range of concentrations ($\mu = 0 \cdot 008 - 0 \cdot 013$). For more concentrated solutions a correction for adsorption of ions becomes necessary. Application of this correction leads to a satisfactory agreement with theory for strong solutions. For more dilute solutions, it becomes necessary to take into account the fact that the effective surface charge on the protein is decreasing owing to the existence of a Donnan ionic equilibrium between ions inside and outside the double layer.

The Spectrum of H_2 (the Ordinary Hydrogen Molecule)

Part I—The 3, $4d\,{}^3\Sigma$, Π, $\Delta \rightarrow 2p\,{}^3\Pi$ and $3s\,{}^3\Sigma \rightarrow 2p\,{}^3\Pi$ Systems

By O. W. Richardson, F.R.S., Yarrow Research Professor of the Royal Society, and T. B. Rymer, B.A., King's College, London

(*Received June* 23, 1934)

§ 1 INTRODUCTION

As a result of a further examination of this spectrum we have found a number of new bands and band systems ending on the lowest triplet state $2p\,{}^3\Pi_{ab}$ which, collected together, form a considerable aggregate. They include :—

(*a*) Extensions of the $4d\,{}^3\Sigma\Pi\,\Delta$ complex → $2p\,{}^3\Pi$ systems :—

(1) The discovery of the $4d\,{}^3\Delta_a$ level which Richardson and Davidson* were unable to find.

(2) The substitution of new v' † = 2 and 3 levels in $4d\,{}^3\Pi_b$ for the levels given by Richardson and Davidson* which were regarded by them as dubious.

(3) The non-diagonal lines of $4d\,{}^3\Sigma$, Π_b, Π_a and $\Delta_b \rightarrow 2p\,{}^3\Pi$.

---

* Richardson, Davidson, Marsden and Evans, 'Proc. Roy. Soc.,' A, vol. 142, p. 40 (1933), referred to in this series of papers as R and D, Part III.

† The Italic *v* (*vee*) of this fount should not be confused with the Greek ν.

(*b*) Extension of the $3s\,^3\Sigma \rightarrow 2p\,^3\Pi$ system to the $v' = 0$, 2, 3 and 4 levels. Richardson and Davidson* were only able to find the $v' = 1$ level of this system.

(*c*) Extension of the $3d\,^3\Sigma\Pi\Delta$ complex $\rightarrow 2p\,^3\Pi$ to the v', $v'' = 4'$, $4''$ levels.

(*d*) Discovery of a system which is probably either $5d\,^3\Sigma \rightarrow 2p\,^3\Pi$ or $5g\,^3\Pi_a \rightarrow 2p\,^3\Pi$.

(*e*) Discovery of two systems of new types called provisionally $^3A \rightarrow 2p\,^3\Pi$, and $^3B \rightarrow 2p\,^3\Pi$. The upper levels, ^3A and ^3B, do not seem to fit in any obvious way into the orthodox scheme of singly excited electronic levels as set out, for example, by Richardson.† They may be the counterpart (or some of it) in the triplet system of the "abnormal" ^1K, ^1L, ^1M, ^1N, etc., singlet states which it has been suggested‡§ arise as a result of the simultaneous excitation of both the electrons in H_2. There is also a new system called $^3C \rightarrow 2p\,^3\Pi$, which is probably either $5d\,^3\Pi_b \rightarrow 2p\,^3\Pi$ or $5d\,^3\Delta_b \rightarrow 2p\,^3\Pi$.

The material under the heading (*a*) above may be regarded as an amplification and continuation of R and D, Part III, and that under (*b*) and (*c*) as in a similar relation to R and D, Part II.

In addition, we have found a number of new bands and band systems, going down either to the lowest odd singlet level, $2p\,^1\Sigma_u$, or the lowest even triplet level, $2s\,^3\Sigma_g$. These, and the new systems ending on $2p\,^3\Pi$, will be described in a separate paper or papers.

§ 2 THE $4d\,^3\Delta_a \rightarrow 2p\,^3\Pi$ SYSTEM

The lines of this system, which is weak, are set out in Table I. This, and similar tables of lines in this sequence of papers, is arranged so that the three theoretically possible lines R (K), Q (K + 1), P (K + 2), which come from the same (K + 1) initial rotational level, follow each other, at any rate in the diagonal bands which are the most strongly developed. The differences such as R (K) − Q (K + 1) or Q (K + 1) − P (K + 2) are final level differences. These are known very accurately in most cases, from the study of stronger band systems ending on the same final level, and most of them are tabulated in R and D, Part II, pp. 40–43. The

---

[*] 'Proc. Roy. Soc.,' A, vol. 140, p. 25 (1933), referred to in this series of papers as R and D, Part II.

[†] "Molecular Hydrogen and its Spectrum," p. 60, Yale University Press, New Haven (1934).

[‡] Richardson, *op. cit.*, p. 312.

[§] Weizel, 'Z. Physik,' vol. 65, p. 456 (1930).

defects of these rotational combinations compared with the standard values are shown on the left of the Table. The wave numbers of the lines are followed first by the intensity in Gale, Monk and Lee's* tables (G), then by Finkelnburg's† estimate (F), and then by Kapuscinski and Eymers'‡ measures (K), where these occur.

TABLE I—The Lines of $4d\,^3\Delta_a \rightarrow 2p\,^3\Pi$

The 0 → 0 *band*		
↑	R′ 1	23012·98 *ab* G 00F
+0·07	Q′ 2	(22892·12) *ab* G *ab* F
↓	P′ 3	22712·21 0*a* G 1F 2·6K He+ +
	R2	(23181·33) *ab* G *ab* F
∧	Q3	23001·29 *ab* G 0F
−0·05		
∨	P4	22763·67 1G 3F 7·3K ? He+ +
	R′ 3	(23368·39) *ab* G *ab* F
∧	Q′ 4	23130·32 *ab* G 0F
−0·14		
∨	P′ 5	22836·74 *ab* G 1F M.B. [−] line only observed by Merton and Barratt in presence of helium.
↑	R4	23560·92 1G 1F 6·6K, also 3 → 2, $4p\,^3\Pi_a \rightarrow 2s\,^3\Sigma$, Q3
−0·09	Q5	(23266·77) *ab* G *ab* F
↓	P6	22919·17 0*a* G 2F He+, also 0 → 0, $4d\,^3\Pi_a \rightarrow 2p\,^3\Pi$, R4
The 0 → 1 *band*		
	Q5	20967·59 0G 3F, also 2 → 4, $3d\,^1\Pi_b \rightarrow 2p\,^1\Sigma$, Q5, defect 0·03
The 1 → 0 *band*		
	R2	? 25377·36 *ab* G 00F, defect 0·13
	R4	25731·42 *ab* G *ab* F (*r*) Tanaka,§ defect 0·20
The 1 → 1 *band*		
	R′ 1	(22882·97) *ab* G *ab* F
∧	Q′ 2	22768·00 4G 4F 22·5K, also 0 → 0, $4d\,^3\Delta_b \rightarrow 2p\,^3\Pi$, Q2
+0·13		
∨	P′ 3	22596·22 0G 0F diffuse
The 1 → 1 *band*—(continued)		
	R2	(23044·23) *ab* G *ab* F
∧	Q3	22872·87 2G 3F 5·5K, also 0 → 0, $4d\,^3\Delta_b \rightarrow 2p\,^3\Pi$, Q4
−0·04		
∨	P4	22646·00 1G 1F 5·2K
↑	R′ 3	23227·87 1G 2F, also 0 → 0, $^1M \rightarrow 2p\,^1\Sigma$, R3
−0·05	Q′ 4	(23001·56) *ab* G *ab* F
↓	P′ 5	22721·18 0G 0F 2·2K, also λ4142 progression, $v'' = 1$, $K = 5$
∧	R4	23417·91 *ab* G 0F
+0·01		
×	Q5	23138·13 00G *ab* F 2·2K, also 2 → 2, $3\,^1K \rightarrow 2p\,^1\Sigma$, R3
−0·09		
∨	P6	22806·47 2G *ab* F 12·0 K, also 5 → 4, $4p\,^3\Pi \rightarrow 2s\,^3\Sigma$, Q1
	R′ 5	(23613·71) *ab* G *ab* F
∧	Q′ 6	23282·51 *ab* G 00F
−0·06		
∨	P′ 7	22901·72 *ab* G 00F
The 1 → 2 *band*		
	R2	? 20833·01 *ab* G 00F, defect 0·18
	R4	? 21225·29 *ab* G *ab* F (2) M.B., given also by McLennan, Grayson-Smith and Collins,‖ defect 0·27
	Q5	20959·69 *ab* G 0F, defect 0·08
	P6	20643·51 *ab* G 0F, defect 0·08

---

* 'Astrophys. J.,' vol. 67, p. 89 (1928).

† 'Z. Physik,' vol. 52, p. 27 (1928).

‡ 'Proc. Roy. Soc.,' A, vol. 122, p. 58 (1929).

§ 'Proc. Roy. Soc.,' A, vol. 108, p. 592 (1925).

‖ 'Proc. Roy. Soc.,' A, vol. 116, p. 277 (1927).

TABLE I—(continued)

The 2 → 1 band
P4 24644·18 *ab* G 00F, defect 0·16

The 2 → 2 band
R′ 1 (22678·69) *ab* G *ab* F
∧ Q′ 2 22569·29 *ab* G 1F
−0·04
∨ P′ 3 22405·64 1G ? F 2·9K

R2 (22830·81) *ab* G *ab* F
∧ Q3 22668·01 *ab* G 00F
+0·04
∨ P4 22451·67 3G 2F 13·9K, also 1 → 1, $4d\,^3\Pi_b \rightarrow 2p\,^3\Pi$, R′ 4

R′ 3 (23000·33) *ab* G *ab* F
∧ Q′ 4 22785·26 *ab* G 00F
+0·02
∨ P′ 5 22517·72 *ab* G 00F

∧ R4 23169·26 *ab* G 00F
0·00
× Q5 22903·49 0G 1F
+0·05
∨ P6 22586·89 0G 1F, also 0 → 0, $4d\,^3\Delta_b \rightarrow 2p\,^3\Pi$, P′ 4
or
↑ R4 23153·71 *ab* G 0F
−0·08 Q5 (22888·03) *ab* G *ab* F
↓ P6 22571·47 00G 0/1F

The 2 → 3 band
∧ Q3 ? 20583·28 *ab* G 00F, defect 0·12
−0·20
∨ P4 20377·44 1G 6·5K, defect 0·09

Alternative v′ = 2 level

The 2 → 1 band (alternative)
P4 24701·35 *ab* G 1F, defect 0·05
P6 ? 24791·42 *ab* G 00F, defect 0·03

The 2 → 2 band (alternative)
R′ 1 (22733·06) *ab* G *ab* F
∧ Q′ 2 22623·66 *ab* G 00F
−0·01
∨ P′ 3 22459·98 *ab* G 00F

R2 (22888·15) *ab* G *ab* F
∧ Q3 22725·35 *ab* G 00F
−0·04
∨ P4 22509·09 2G, also 1 → 1,
0·01 2F
$3d\,^1\Sigma \rightarrow 2p\,^1\Sigma$, R0

The 2 → 2 band (alternative)—(continued)

R′ 3 (23059·49) *ab* G *ab* F
∧ Q′ 4 22844·42 *ab* G 00F
+0·05
∨ P′ 5 22576·85 00G 0/1F 2·5K

R4 (23210·67) *ab* G *ab* F
∧ Q5 22944·90 00*a*G 0/1F
−0·06
∨ P6 22628·41 *ab* G 00F

The 2 → 3 band (alternative)
Q3 20640·76 0G ? 00F 7·3K, defect 0·02
Q5 20884·35 *ab* G 00F, defect 0·08

The 3 → 2 band
∧ Q3 24580·27 1G 2F 33·7K, also
−0·05 1 → 0, $3d\,^1\Delta_b \rightarrow 2p\,^1\Sigma$, Q4, defect zero
∨ P4 24363·92 *ab* G 0F, defect 0·03

The 3 → 3 band
R′ 1 (22500·77) *ab* G *ab* F
∧ Q′ 2 22396·83 *ab* G 0F
−0·06
∨ P′ 3 22241·07 1G 00F

R2 (22650·36) *ab* G *ab* F
∧ Q3 22495·66 *ab* G 00F
−0·01
∨ P4 22289·63 1G 2F, also 2 → 2, $4d\,^3\Pi_b \rightarrow 2p\,^3\Pi$, R3

∧ R′ 3 22808·88 0G *ab* F 1·7K
+0·08
× Q′ 4? 22604·57 1G, 3F, also 1 → 1, $4d\,^3\Pi_a \rightarrow 2p\,^3\Pi$, R′ 1, 0 → 0, $4d\,^3\Pi_b \rightarrow 2p\,^3\Pi$, R5, and 1 → 1, $3d\,^1\Sigma \rightarrow 2p\,^1\Sigma$, R8
+0·04
∨ P′ 5 22350·47 *ab* G 0/1F

The 3 → 4 band
Q3 20526·94 1G 4·5K, also 1 → 5, $^1N \rightarrow 2p\,^1\Sigma$, P3, defect 0·02
P4 20330·20 *ab* G *rd*^{a} Deodhar,[*] defect 0·21

---

[*] ' Proc. Roy. Soc.,' A, vol. 113, p. 420 (1926).

This is followed by any other information available, such as response to helium admixture, as recorded by Merton and Barratt,* and interference with other lines of known systems.

As the lines are so weak, the information we have about their properties is meagre ; so that the evidence for the reality of the bands must rest mainly on the combinations, together with a reasonable structure for the levels of the upper state and a reasonable distribution of intensity among the lines. We believe that these conditions are all satisfied. In addition to the rotational combinations referred to above, the lines of the axial bands which, as with all the other systems which come from the 3, $4d\,{}^3\Sigma\Pi\Delta$ complexes and go down to $2p\,{}^3\Pi$, are the best developed, are connected with lines of non-diagonal bands having the same electronic states. These final vibrational differences are also accurately known, and most of them are given in R and D, Part III, p. 50. Except for about the usual proportion of clashes with established lines of other systems, or with lines which are thought to be blends on observational grounds and one or two doubtful lines, the combinations, apart from a few lines found only in the tables of Merton and Barratt, Tanaka, or Deodhar, in which the errors of measurement are greater than in the tables of Gale, Monk and Lee or Finkelnburg, are very accurate, and the defects never exceed 0·08 wave number. The doubtful lines could be taken out without much detriment. They are, for the most part, merely suggestions for possible further examination. This double check in the combinations enhances the security of the arrangement very much. As we shall see later, there are other very strong reasons for believing in the essential correctness of the 0 → 0 band.

Considering the system as a whole, the P P′ branches of the bands are the best developed. In fact, any strength there is in the whole system seems to reside in these branches. It will be seen that there is a definite, though perhaps not very marked, tendency for the lines of Finkelnburg to be enhanced relatively to those of Gale, Monk and Lee at higher rotational numbers. This is in support of the reality of the bands, as Finkelnburg used a light-source with a much higher temperature. It will be noted that the 0 → 0 band includes at least two lines, and possibly four, enhanced by helium. In the other systems of the 3 and $4d\,{}^3\Sigma\Pi\Delta \rightarrow 2p\,{}^3\Pi$ complexes, this enhancement by helium is a feature which distinguishes the 0 → 0 bands from the other $v' \rightarrow v''$ bands, and thus its occurrence in the present case tends to confirm the allocation of the remaining lines of this band. There are no helium lines in the other bands of $4d\,{}^3\Delta_a \rightarrow 2p\,{}^3\Pi$, except possibly where the properties refer to blends with $0 \rightarrow 0$ lines of other bands. It is probable that the bad combination given by the P′ 5 line in the $0 \rightarrow 0$ band is due to Finkelnburg's line being a blend. Merton and Barratt's value removes the bad combination, and it seems likely that they were observing the band line since the P branch is clearly enhanced by helium. The rotational structure of the final state at $v'' = 0, 1, 2$ and 3 is described in R and D, Part II. The structure of this state at $v'' = 4$ will be given later in this paper (p. 43). The $1 \rightarrow 1$ band contains a larger number than usual of clashes with lines of other established systems. However, the only two of these which can be subjected to the test (the intervals for the dashed *s* lines are unknown) are backed up by combinations, in the case of one of them double, with lines off the axis. We do not ourselves think there is any reasonable doubt about the essential correctness of the $v' = 1$ level. At the $v' = 2$ level we meet with a difficulty of a different kind. There appear to be two $v' = 2$ progressions with the expected properties, and neither of them in quite the right position. In the first set of lines, as given in Table I, there is a further alternative for the R4, Q5, P6 lines of the $2 \rightarrow 2$ band. In the second set, which we shall refer to as belonging to the alternative $v' = 2$ level, Q5 looks too strong, but as it is marked *a* by Gale, Monk and Lee, it is probably a blend. P4 of the alternative $2 \rightarrow 2$ band is also claimed elsewhere, but the discrepancy between Gale, Monk and Lee's and Finkelnburg's measure of its wave-length suggests that it also is a blend. We shall return to the consideration of these alternatives at the $v' = 2$ level later. At the $v' = 3$, $K' = 5$ level, the final interval which would lead down to P6, the only line out of R4, Q5 and P6 which might have any strength, is unknown.

---

* 'Phil. Trans.,' A, vol. 222, p. 369 (1922).

The rotational structure of the initial level $4d\,{}^3\Delta_a$ is given in Table II. For comparison that of $3d\,{}^3\Delta_a$ is also included. There are two alternative possibilities for the $v' = 2$ level of $4d\,{}^3\Delta_a$. The first (shown at the top of Table II) uses the first set of lines in Table I, and the second (shown at the bottom of Table II) uses the alternative set. The general structure of the levels of $4d\,{}^3\Delta_a$, apart from a somewhat wider spacing, is quite similar to that of the levels of $3d\,{}^3\Delta_a$. It is also quite similar to what is known of the structures of $4d\,{}^1\Delta_a$ and $3d\,{}^1\Delta_a$, whichever of the two possible alternatives is chosen. This tends to confirm the reality and identification of the upper state. A further confirmation is obtained if we consider the detailed quantitative structure of the $v' = 0$ level and the intensities of the lines of the $0 \rightarrow 0$ band. The structure of the $v = 0$ level at $K = 2$, 3 and 4, and the relative intensities of the three lines going down from each of these levels have been calculated on the wave mechanics by Marsden and Evans (R and D, Part III). If we turn to their fig. 2 on p. 59 of that paper, we find that the calculated K = 2 level of $v' = 0$, $4d\,{}^3\Delta_a$, lies about 535 wave numbers above that of the K = 2 level of $v = 0$, $4d\,{}^3\Sigma_g$. This should be the same as the difference between the

TABLE II—Rotational Structure of $4d\,{}^3\Delta_a$ and $3d\,{}^3\Delta_a$

$4d\,{}^3\Delta_a$ with first alternative at $v = 2$

K ↓	$v = 0$	K ↓	$v = 1$	K ↓	$v = 2$	K ↓	$v = 3$
		6s					
			475·83				
5a		5a	→ 59·15	5a			
	430·42		416·68		(?) 384·72*		
4s	→ 63·59	4s	→ 61·45	4s	→ 51·86 (?)	4s	
	366·83		355·23		332·86		(?) 313·75
3a	→ 77·67	3a	→ 78·85	3a	→ 70·99	3a	→ (?) 59·71
	289·16		276·38		261·87		254·04
2s		2s		2s		2s	

$3d\,{}^3\Delta_a$

K ↓	$v = 0$	K ↓	$v = 1$	K ↓	$v = 2$	K ↓	$v = 3$
5a		5a		5a		5a	
	373·37		332·35		281·22 (?)		243·71 (?)
4s	→ 59·90	4s	→ 55·94	4s	→ 39·48 (?)	4s	→ 31·58 (?)
	313·47		276·41		241·74		212·13
3a	→ 63·65	3a	→ 63·88	3a	→ 57·51	3a	→ 50·05
	249·82		212·53		184·23		162·08
2s		2s		2s		2s	

$4d\,{}^3\Delta_a$ with second alternative at $v = 2$

K ↓	$v = 0$	K ↓	$v = 1$	K ↓	$v = 2$	K ↓	$v = 3$
		6s					
			475·83				
5a		5a	→ 59·15	5a			•
	430·42		416·68		(?) 366·99		
4s	→ 63·59	4s	→ 61·45	4s	→ 32·33 (?)	4s	
	366·83		355·23		334·66		(?) 313·75
3a	→ 77·67	3a	→ 78·85	3a	→ 69·81	3a	→ (?) 59·71 (?)
	289·16		276·38		264·85		254·04
2s		2s		2s		2s	

R′ 1 lines of $4d\,{}^3\Delta_a$ and $4d\,{}^3\Sigma$, which come respectively from these levels and go down to the same final level. Now R′1 of $4d\,{}^3\Delta_a$ at $0 \rightarrow 0$ is 23012·98, and R′1 of $4d\,{}^3\Sigma$, $0 \rightarrow 0 = 22477{\cdot}97$; so that the difference is 535·01, or exactly the calculated amount. From the same figure the calculated level spacing at $v = 0$ is $\mathrm{K}(3) - \mathrm{K}(2) \simeq 285$ and $\mathrm{K}(4) - \mathrm{K}(3) \simeq 350$. The experimental values are $\mathrm{K}(3) - \mathrm{K}(2) =$

---

* Based on R4 = 23169·26, etc. The alternative level gives 369·22.

289·16 and K (4) — K (3) = 366·83. This shows that the structure of the observed $4d\,{}^3\Delta_a$ level agrees with the predicted structure so far as that has been calculated.

Turning now to the intensity distribution, Marsden and Evans (*loc. cit.*, Table XI, p. 62) have calculated the relative intensities, within each group, of the three groups of lines coming from the K = 2, 3 and 4 levels of $v = 0$, $4d\,{}^3\Delta_a$ respectively. These are set out along with the observed eye estimates of Gale, Monk and Lee (G) and Finkelnburg (F) in Table III. Only two of the stronger lines belonging to different groups have been measured by Kapuscinski and Eymers, so that their data are not of use in this connection.

TABLE III—Comparison of Marsden and Evans' calculated with observed intensities

	Calc.	G.	F.		Calc.	G.	F.		Calc.	G.	F.
R′1	0·059	*ab*	00	R2	0·09	*ab*	*ab*	R′3	0·015	*ab*	*ab*
Q′2	0·16	*ab*	*ab*	Q3	0·115	*ab*	0	Q′4	0·08	*ab*	0
P′3	2·8	0*a*	1	P4	2·8	1	3	P′5	2·9	*ab*	1

It is clear from Table III that the eye estimates of the intensities are in good agreement with the calculated ratios. It is to be remembered that the calculation only applies to each one of the groups R′1, Q′2, P′3 or R2, Q3, P4 or R′3, Q′4, P′5 separately. Thus the intensity distribution, as well as the structure, is in agreement with theoretical prediction so far as that is known.

The vibrational intervals of $4d\,{}^3\Delta_a$ are set out, together with those of $4d\,{}^3\Delta_b$ and $4d\,{}^3\Pi_{ab}$ in Table VI, below. Only the values for the strong (*a*) levels can be determined, as the final vibrational intervals for the alternate weak (*s*) levels are unknown. Three alternative sets of values of the $2' - 1'$ and $3' - 2'$ intervals of $4d\,{}^3\Delta_a$ are given. The top set is based on the first set of lines coming from $4d\,{}^3\Delta_a$ at $v' = 2$ in Table I, whilst the middle set uses the alternative lines. If the resulting intervals are compared with those for $4d\,{}^3\Delta_b$ (K even) and for $4d\,{}^3\Pi_{ab}$, they both look rather irregular, and there is little or nothing to choose between them. The alternative $v' = 2$ progressions on which they are based are both very much alike, and of similar intensity and generally have the properties we expect for the $v' = 2$ progression of $4d\,{}^3\Delta_a$, judging by those of the other v' progressions. It is possible that the whole vibrational level at $v' = 2$ is split by a perturbation. Then, since the intensities of the lines are about the same for each progression, the unperturbed level should be the mean of both. If the separate intervals are averaged at $2' - 1'$

and $3' - 2'$ we get the values shown in the two lowest rows of Table VI. It is a fact that these average values remove the irregularity otherwise present in the intervals. It is even possible that the $v' = 2$ level is split into three. We find that the following pair of weak lines—R2, 22864·00 *ab* G (0) F ; Q3, absent ; P4, 22484·98 *ab* G (00) F, defect $-$ 0·08 occur at the positions interpolated from the $v' = 0$, 1 and 3 lines. There is a suspicion of a splitting of the higher rotational levels of the $v' = 0$ level of $3d\ {}^3\Pi_a$.*

§ 3 THE $4d\ {}^3\Sigma \rightarrow 2p\ {}^3\Pi$ AND $4d\ {}^3\Pi_b \rightarrow 2p\ {}^3\Pi$ SYSTEMS

We have nothing appreciable to add to the account of $4d\ {}^3\Sigma \rightarrow 2p\ {}^3\Pi$ given by R and D, Part III. The following doubtful additions may be made to the list of lines of the non-diagonal bands (*loc. cit.*, p. 43) : $1 \rightarrow 2$, P6 = (?) 19322·85 1G 9·0 K L +, also $1 \rightarrow 2$, ${}^1\mathrm{Q} \rightarrow 2p\ {}^1\Sigma$, R0, defect 0·02, $2 \rightarrow 3$ Q5 = (?) 19570·32 0*a* G 3·8 K, also $1 \rightarrow 6$, ${}^1\mathrm{N} \rightarrow 2p\ {}^1\Sigma$ R3, defect 0·21 and $3 \rightarrow 4$ Q1 = (?) 19861·92 *ab* G (*rd*) Deodhar, defect 0·29.

In dealing with $4d\ {}^3\Pi_b$, we shall mention at the outset a point in connection with the K = 1 level at $v' = 0$. In R and D, Part III, in the body of the paper, this level is fixed by the lines Q′ 1 = 22622·48 and P′ 2 = 22501·71, which determine the interval K (2) − K (1) given as (?) 35·19 in Table VII, p. 53. This level was determined before the structure of the $4d\ {}^3\Pi_b$ state had been computed, and was found not to agree very well with the results of the computations. In the Appendix to the paper, by Marsden and Evans, under fig. 2, p. 59, it is stated that the " K = 1 observed level corresponds to lines which are alternatives to those in the text." These alternative lines agree very well with the computed level, but what they are is nowhere stated. They are: Q′ 1 = 22651·41 (2) G (3) F 12·8 K He + + also R′ 2 of $2 \rightarrow 2$, $4d\ {}^3\Delta_b \rightarrow 2p\ {}^3\Pi$ and P2 of $0 \rightarrow 0$ $4d\ {}^3\Pi_a \rightarrow 2p\ {}^3\Pi$: and P′ 2 = 22530·62 (00) G *ab* F and they make the interval between K = 2 and K = 1 equal to $6 \cdot 43 - x_0$, instead of (?) $35 \cdot 19 - x_0$, in agreement with the theory. They have the further support that they give a perfect combination (defect 0·00), and that Q′ 1 is a He + + line. In this and allied systems only the lines of the $0 \rightarrow 0$ bands respond markedly to helium. The objections to the triple allocation of 22651·41 (2) are removed by considerations put forward in § 4 below.

In R and D, Part III, on p. 50, it is stated that " We are inclined to consider the $2 \rightarrow 2$ and $3 \rightarrow 3$ bands of $4d\ {}^3\Pi_{ab} \rightarrow 2p\ {}^3\Pi_{ab}$ as less secure than the others." The bands attributed to $4d\,^3\Pi_b$ at these vibrational levels seem particularly improbable as they lead to vibrational intervals for $4d\,^3\Pi_b$ (given in *loc. cit.*, Table VI, p. 51) which are very different from those for $4d\,^3\Pi_a$, although these are about right when compared with those for $4d\,^3\Sigma$, $4d\,^3\Delta_b$ and $4d\,^3\Delta_a$. It seemed difficult to justify such a situation, so we decided to make a new examination of this system. As a result we have found bands at these vibrational levels of $4d\,^3\Pi_b$ which remove the anomalies. It is true that they are weak, but this we expected. There are also alternative possibilities for some of the rotational levels, which make the interpretation of some of the details a little difficult and rather uncertain. This difficulty is augmented by the irregular rotational structure of the upper state due to uncoupling. In spite of this and of the fact that most of the strength arises from coincidences with stronger lines of other systems, we believe that there is sufficient coherence among the results to warrant the belief that the proposed bands are in the main correct.

---

* Richardson and Davidson, ' Proc. Roy. Soc.,' A, vol. 123, p. 466 (1929).

The lines, so far as they are different from those given by R and D, Part III, are set out in Table IV in the same way as those for $4d\,^3\Delta_a \rightarrow 2p\,^3\Pi$ in Table I. In the 2 → 2 band there are alternative possibilities at the $K' = 2$, 5 and 6 levels and in the 3 → 3 band at the $K' = 1$ level. The rotational structure of $4d\,^3\Pi_b$ is set out in Table V. At $v = 0$ the lowest interval, 6·43, is based on the alternative lines, already referred to, which agree with the results of the calculations of Marsden and Evans, otherwise the rest of the $v = 0$ levels and all the $v = 1$ levels are as given by R and D, Part III. The values on the left under $v = 2$ are those which correspond to the first set of alternative 2 → 2 lines, and also to the 2 → 1 lines in Table IV. These seem to agree with the trend of the intervals at the other vibrational levels better than the others which also have no confirmation at the 2 → 1 band.

TABLE IV—$4d\,^3\Pi_b \rightarrow 2p\,^3\Pi$

The 0 → 0 *band*

∧ Q′ 1 22651·41 2G 3F He+ + 12·8K,
also 2 → 2, $4d\,^3\Delta_b \rightarrow 2p\,^3\Pi$, R′2
0·00 and 0 → 0, $4d\,^3\Pi_a \rightarrow 2p\,^3\Pi$, P2
∨ P′ 2 22530·62 00G *ab* F

The rest of this band is as given by R and D, Part III, p. 44.

The 1 → 0 *band*

∧ Q2 24707·83 *ab* G 0F, defect 0·07
+0·13
∨ P3 24527·66 0*a* G 0/1F 1·6K, defect 0·06

The 1 → 0 *band*—(continued)

∧ R3 24790·49 0G 0/1F 3·1K, defect 0·11, also 2 → 1,
−0·28 $3d\,^1\Pi_a \rightarrow 2p\,^1\Sigma$, R1
∨ Q4 mixed with 24553·10 1G *ab* F 11·8K = 0 → 2,
$4d\,^1\Sigma \rightarrow 2p\,^1\Sigma$, R1

The 1 → 1 *band*

This band is as given by R and D, Part III, p. 44.

TABLE IV—(continued)

The 2 → 1 *band*

R5 24429·82 0G *ab* F, defect + 0·04,
also 2 → 2, $3\,{}^1O \rightarrow 2p\,{}^1\Sigma$, P2
P7 ? 23717·43 *ab* G 0F (*r*) D, defect
− 0·2 (interval uncertain)

The 2 → 2 *band*

∧ Q′ 1 22279·65 0G 0F
+0·06
∨ P′ 2 22170·19 *ab* G 0F

∧ R1 22320·25 3G 2F 11·0K, also
−0·17 3 → 3, $4d\,{}^3\Delta_b \rightarrow 2p\,{}^3\Pi$, Q4
∨ Q2 22210·65 *ab* G 0F
P3 (22047·85) *ab* G *ab* F

or

↑ R1 22316·72 2G *ab* F 4·1K
−0·06
| Q2 (22206·95) *ab* G *ab* F
↓ P3 22044·21 *ab* G 0/1F

∧ R′ 2 22304·85 1G *ab* F 7·0K, also
1 → 1, $3d\,{}^1\Sigma \rightarrow 2p\,{}^1\Sigma$, ? P3
and 3 → 3, $4d\,{}^3\Delta_b \rightarrow 2p\,{}^3\Pi$,
−0·19 Q′ 3
∨ Q′ 3 22141·35 2G 2F 7·6K, also
0 → 4, $4d\,{}^1\Sigma \rightarrow 2p\,{}^1\Sigma$, P1
and 2 → 3, $3d\,{}^1\Pi_a \rightarrow 2p\,{}^1\Sigma$, P6
P′ 4 (21926·28) *ab* G *ab* F

∧ R3 22289·63 1G 2F, also 3 → 3,
−0·04 $4d\,{}^3\Delta_a \rightarrow 2p\,{}^3\Pi$, P4
× Q4 22073·37 5G 2F, also 2 → 2,
$4d\,{}^3\Sigma \rightarrow 2p\,{}^3\Pi$, Q1 and 3 → 3,
−0·10 $4d\,{}^3\Pi_a \rightarrow 2p\,{}^3\Pi$, Q1
∨ P5 21807·51 *ab* G 0F

∧ R′ 4 22272·56 1G 3F 3·9K, also
+0·10 2 → 2, $4d\,{}^3\Delta_b \rightarrow 2p\,{}^3\Pi$, P′ 4
∨ Q′ 5 22004·94 *ab* G 00F
P′ 6 (21690·6) *ab* G *ab* F

↑ R5 22251·42 1G 00F
−0·09 Q6 (21934·87)
↓ P7 21573·46 10G 10F 485K, also
0 → 0, $3d\,{}^1\Sigma \rightarrow 2p\,{}^1\Sigma$, R2

or

∧ R′ 4 22267·82 0G *ab* F, also 1 → 1,
+0·06 $4d\,{}^3\Pi_a \rightarrow 2p\,{}^3\Pi$, P4
∨ Q′ 5 22000·24 *ab* G 2F
P′ 6 (21686·0) *ab* G *ab* F

The 2 → 2 *band*—(continued)

∧ R5 22239·18 1G 2F, also 1 → 1,
−0·11 $4d\,{}^3\Pi_b \rightarrow 2p\,{}^3\Pi$, Q4
∨
∧ Q6 21922·74 2G 1F 13·4K, also
−0·09 1 → 0, ${}^1Q \rightarrow 2p\,{}^1\Sigma$, R0
∨ P7 21561·33 *ab* G 0F

The 3 → 2 *band*

R1 ? 24252·11 *ab* G 0F, defect −0·17
R3 24208·91 ? G 1F, defect + 0·05
line measured as 24209·03 (2)
by G. M. L., defect + 0·17

The 3 → 3 *band*

∧ Q′ 1 22124·25 1G 2F, also the R3 line
−0·08
∨ P′ 2 22020·39 *ab* G 00F

or

∧ Q′ 1 22117·89 3G 4F 6·8K He + + Z
+0·05
∨ P′ 2 22013·90 *ab* G 0F

or

∧ Q′ 1 22112·51 *ab* G 1F
−0·02
∨ P′ 2 22008·59 *ab* G 0F

∧ R1 22154·24 0G 1F 4·4K
+0·05
× Q2 22049·71 *ab* G 00F
−0·14
∨ P3 21895·15 *ab* G 0F

↑ R′ 2 22139·41 3G 5F, also 1 → 1,
| $4p\,{}^3\Pi_b \rightarrow 2s\,{}^3\Sigma$, R′ 3
−0·07 Q′ 3 (21983·59) *ab* G *ab* F
↓ P′ 4 21779·44 *ab* G 1F

∧ R3 22124·25 1G 2F, also Q′ 1 ?
−0·02
∨ Q4 21918·23 1G 3F 20·9K, also
0 → 1, ${}^1M \rightarrow 2p\,{}^1\Sigma$, R2
P5 (21666·24) *ab* G *ab* F

∧ R′ 4? 22103·87 1G 0F 13·7K, also Q6
−0·04 of the 1 → 1 band
∨ Q′ 5 ? 21849·85 *ab* G 0F

At $v = 3$ the lowest interval, 36·35, inserted in Table V is the one which corresponds to the middle alternative set of Q′ 1, P′ 2 lines in Table IV. The first set would make this interval 29·92 and the third set 41·70. Owing to the abnormal spacing of the two lowest levels at $v = 0$ it is difficult to know what the trend of this interval should be.

TABLE V—Rotational Structure of $4d\,{}^3\Pi_b$

K ↓	$v = 0$	$v = 1$	$v = 2$	or $v = 2$	$v = 3$
7s		········			
		317 (?)			
6a	———	———→ 53 (?)	———	———	
	279·40	264·03	245·44	237·90	
5s	·····→ 54·12	·······→ 51·69	→ 46·96	→ 44·15	········
	225·28	212·34	198·48	193·75	184·39 (?)
4a	———→ 57·47	———→ 52·81	———→ 50·72	———→ 45·99	———→ 44·34(?)
	167·81	159·53	147·76	147·76	140·05
3s	→ 60·96	→ 56·18	→ 53·93	→ 50·10	→ 50·89
	106·85	103·35	93·83	97·66	89·16
2a	———→ 100·42	———→ 62·97	———→ 53·23	———→ 60·59	———→ 52·81
	6·43	41·38	40·60	37·07	36·35
1s		·······			

The first three rows of figures in Table VI give the *a* (strong, K even) vibrational intervals given by the lines in Table IV, together with the strong *a* (K, odd) intervals of $4d\,{}^3\Pi_a$. These are followed by the 2 − 1 and 3 − 2 intervals of $4d\,{}^3\Pi_b$, as they were given by R and D, Part III. Where there are alternatives, the upper set correspond to the lines which give the rotational structure shown on the left at $v = 2$ in Table V. From the point of view of vibrational structure, there seems to be little or nothing to choose between these alternatives. Lower down in the table are set out the intervals for $4d\,{}^3\Delta_b$ and $4d\,{}^3\Delta_a$.

The intervals for $4d\,{}^3\Sigma$ and $4d\,{}^3\Delta_b$ are as set out by R and D, Part III, p. 51. Whichever set of alternatives is chosen it will be seen that the new intervals remove the abnormal vibrational spacing which the old $4d\,{}^3\Pi_b$ state possessed when compared with all the other states of the $4d\,{}^3\Sigma\Pi\Delta$ complex.

What the old 2 → 2 and 3 → 3 bands of $4d\,{}^3\Pi_b$ are we do not at present know. It seems certain at least that the $K' = 4$ level of the 3 → 3 band represents something which goes down to $2p\,{}^3\Pi$ at $v'' = 3$ and $K'' = 3$, 4 and 5, because, in addition to giving the combinations R3 − Q4 = 206·14 (206·04) and Q4 − P5 = 251·95 (251·99)—the Q4 line is almost certainly a close blend—it gives combinations to the following lines, coming from the same upper level and going down to $2p\,{}^3\Pi$ at $v'' = 2$: R3 = 23898·10 *ab* G 00 F defect 0·01, Q4 = 23681·61 *ab* G 0 F defect 0·05, and P5 = 23415·94 *ab* G 00 F defect 0·08. There are no similar combinations from the K′ = 2 level of the old 3 → 3 band. The old 2 → 2 lines of the $4d\,{}^3\Pi_b$ also give the following, less convincing, combinations to $2p\,{}^3\Pi$ at $v'' = 1$: – Q2 = 24326·86 0 G 0 F 6·3 K, also 1 → 2, ^{1}N → $2p\,{}^1\Sigma$ R3 and 1 → 1, $5p\,{}^3\Pi_b \rightarrow 2s\,{}^3\Sigma$, P3 defect 0·05 and R3 = 24421·04 *ab* G *ab* F 0 Tanaka defect 0·07.

TABLE VI—Vibrational Intervals of $4d\,{}^3\Pi_{ab}$ and $4d\,{}^3\Delta_{ab}$

Vibrational Intervals of $4d\,{}^3\Pi_{ab}$

Δ*v*	K = 1 (Π_a)		K = 2 (Π_b)	K = 3 (Π_a)	K = 4 (Π_b)	K = 5 (Π_a)		K = 6 (Π_b)
1′–0′	2048·50*		2170·66	2171·54	2158·85	2173·03		2130·15
2′–1′	2028·61	or	2047·55 2043·90	†2034·95	2026·55†	2030·37	or	1994·04 1981·91 †
3′–2′	1877·80	or	1931·81 1935·54	†1890·9$_0$	1919·21†	1898·1$_0$		
2′–1′			1952·47‡		1955·07‡			1950·90$_5$‡
3′–2′			1693·3$_0$ ‡		1679·8$_8$ ‡			

Vibrational Intervals of $4d\,{}^3\Delta_{ab}$

	K = 2 (Δ_b)	K = 3 (Δ_a)	K = 4 (Δ_b)	K = 5 (Δ_a)
1′–0′	2166·75$_5$	2196·11	2140·32	2170·63
2′–1′	2042·06	1998·03	2012·06	1943·70
3′–2′	1917·4	1912·27	1875·47	
2′–1′		2055·39		1985·10
3′–2′		1854·92		
2′–1′		2026·71		1964·40
3′–2′		1883·60		

* Perturbed Interval.
† New Values.
‡ Old Values.

§ 4 THE $4d\,{}^3\Pi_a \rightarrow 2p\,{}^3\Pi$ AND $4d\,{}^3\Delta_b \rightarrow 2p\,{}^3\Pi$ SYSTEMS

In the account of the $4d\,{}^3\Pi_a$ state in R and D, Part III, there is a similar anomaly at the lowest rotational and vibrational level to that noted at the K = 1, $v = 0$ level of $4d\,{}^3\Pi_b$. In the body of the text the Q1, P2 lines which determine this level were chosen as that pair of lines giving the correct combination which made the lowest interval (see Table VII, *loc. cit.*, p. 53) continue the trend of the higher intervals at $v = 0$. However, the computations of Marsden and Evans (fig. 2, Appendix, p. 59) show that such regularity is contrary to the theoretical predictions, and that the K = 1 level should almost coincide with the K = 2 level. The experimental level in the text is shown with a question mark in their figure. We now find that there are alternative Q1, P2 lines in the positions to correspond with Marsden and Evans' predicted level. They are set out, together with some other additions we have found to the list of lines of $4d\,^3\Pi_a \rightarrow 2p\,^3\Pi$ given by R and D, Part III, in Table VII. The P2 line is also allocated as R′ 2 of 2 → 2, $4d\,^3\Delta_b \rightarrow 2p\,^3\Pi$, and as Q′ 1 of 0 → 0, $4d\,^3\Pi_b \rightarrow 2p\,^3\Pi$. The combinations are all good, and the line has the correct intensity for all three positions. In the 2 → 2 band of $4d\,^3\Delta_b \rightarrow 2p\,^3\Pi$ the intensity of R1 is 2G, 2F, 8·7 K and R3 is absent. This would make the expected intensity for R′ 2 about (0/1) G (1) F 3·0 K.* The ratio of the intensities of Q′ 1 and P′ 2 of $4d\,^3\Pi_b \rightarrow 2p\,^3\Pi$ is computed on the wave mechanics by Marsden and Evans* to be 1·5 : 1·5. If the P′ 2 line is correct, this would make the intensity of the Q′ 1 line of 0 → 0, $4d\,^3\Pi_b \rightarrow 2p\,^3\Pi$ (00) G *ab* F and < 1·0 K. If we add the expected intensity of this Q′ 1 to that of the R′ 2 line we get

TABLE VII—Lines of $4d\,^3\Pi_a \rightarrow 2p\,^3\Pi$

The 0 → 0 *band*

∧	Q1	22772·07 *ab* G 00F
−0·07		
∨	P2	22651·40 2G 3F 12·8K He++, also 2 → 2, $4d\,^3\Delta_b \rightarrow 2p\,^3\Pi$, R′ 2 and 0 → 0 $4d\,^3\Pi_b \rightarrow 2p\,^3\Pi$ Q′ 1

The rest of the band is as given in R and D, Part III.

The 0 → 1 *band*

P2	20318·18 1G 6·3K, also 3 → 6, $3d\,^1\Pi_b \rightarrow 2p\,^1\Sigma$, Q3, defect 0·04
Q3	20323·15 5G 11·4K, also 0 → 1, $3d\,^1\Sigma \rightarrow 2p\,^1\Sigma$ R5 and 3 → 1, $3p\,^3\Pi_a \rightarrow 2s\,^3\Sigma$, Q4, defect 0·04
R4	20605·50 *ab* G 0F, defect 0·04

The 1 → 0 *band*

Q1	24820·61 *ab* G 0/1F, defect 0·04
R2	? 24999·50 *ab* G 0F, defect 0·19
R4	25092·13 *ab* G 0F, defect 0·05

The 1 → 1 *band*

This band is as given in R and D, Part III.

The 1 → 2 *band*

P2	? 20155·48 *ab* G (*r*) Deodhar, defect 0·31

The 2 → 1 *band*

	P4	? 24302·60 *ab* G 0F, defect 0·18
∧	R4	24808·93 *ab* G 00F, defect 0·03
−0·08		
∨	P6	24197·49 2G 2F 27·1K, also 1 → 2, $^1N \rightarrow 2p\,^1\Sigma$, P2, defect 0·08

The 2 → 2 *band*

This band is as given in R and D, Part III.

The 2 → 3 *band*

R2	20396·79 0G, also 1 → 3, $3d\,^1\Pi_b \rightarrow 2p^1\Sigma$, Q7, defect 0·12

The 3 → 3 *band*

This band is as given by R and D, Part III.

The 3 → 4 *band*

∧	Q1	? 20091·21 0G, defect 0·25
−0·16		
∨	P2	? 19992·03 *ab* G [−] M.B. He++, defect 0·25
	R2	20311·06 00G, defect 0·07

---

* R and D, Part III.

(1) G (1) F 4·0 K. Subtracting this from the measured intensity of 22651·41 leaves (1) G (2) F, 8·8 K for the intensity of P2 of 0 → 0, $4d\ {}^3\Pi_a \rightarrow 2p\ {}^3\Pi$. The intensity of the Q1 line of this band is *ab* G 00 F *ab* K. These figures are just about what is required to agree with Marsden and Evans'* computation of the ratio of the intensities of these two lines, which they give as 0·1 : 2·5. The new K = 1 level now lies 5·31 wave numbers below the K = 2 level, instead of (?) 111·36 as given in the body of the paper. This agrees with its theoretical position to the probable accuracy of the computations. The new lines also have the additional confirmation that P2 is a He line, and therefore likely to belong to at least one 0 → 0 band.

In the $4d\ {}^3\Delta_b \rightarrow 2p\ {}^3\Pi$ system we have found a number of combinations with non-diagonal band lines. These are set out in Table VIII. As these lines do not introduce any new initial states, they merely tend to confirm without modification the conclusions reached in R and D, Part III.

TABLE VIII—Lines of $4d\,{}^3\Delta_b \rightarrow 2p\ {}^3\Pi$

The 0 → 0 *band*

The lines of this band are as given in R and D, Part III.

The 1 → 0 *band*

R1 25055·40 8G 7F 142K, also 3 → 2, $3d\,{}^1\Pi_b \rightarrow 2p\,{}^1\Sigma$, Q2, defect 0·07 which requires the strength

R3 ? 25250·86 rd^2 Deodhar, defect 0·01

The 1 → 1 *band*

The lines of this band are as given in R and D, Part III.

The 1 → 2 *band*

R3 20723·48 0G 00F, also 0 → 1, $3d\ {}^1\Pi_a \rightarrow 2p\,{}^1\Sigma$, R1, defect 0·05

The 2 → 1 *band*

R3 24938·46 2G 1F 10·1K, also 3 → 2, $3d\ {}^1\Sigma \rightarrow 2p\,{}^1\Sigma$, P2, defect 0·15

The 2 → 2 *band*

The lines of this band are as given in R and D, Part III.

The 2 → 3 *band*

Q4 20444·54 *ab* G *rd* Deodhar, defect 0·25

The 3 → 2 *band*

R3 24610·93 *ab* G 0/1F, defect 0·03

The 3 → 3 *band*

The lines of this band are as given in R and D, Part III.

The 3 → 4 *band*

Q4 20361·2 [ ] Tanaka, defect 0·2

§ 5 THE $3s\ {}^3\Sigma \rightarrow 2p\,{}^3\Pi$ SYSTEM

The $v' = 1$ progression of this system is described and analysed in R and D, Part II. What there is of the rest of this system is set out in Table IX. In the 0 → 0 band the P branch is probably the strongest, as it is in the 1 → 1 band. In the 2 → 2 band the P branch has disappeared. In the 0 → 0 branch there are two alternative possibilities at the $K' = 4$ and $K' = 5$ levels. The relative merits of these will be considered later. The presence of two He + lines in the 0 → 0 band is a satisfactory feature. In the 1 → 1 band the Q branch consists of five lines, all within a range of seven wave numbers. In the 2 → 2 band this compression of the Q branch has gone on still further, so that Q1, Q′ 2, Q3 and Q′ 4 are represented by a single line. It is true that the combinations of 16841·63 are practically all with lines claimed elsewhere, but it happens that in every case there are other grounds for believing the lines to be blends. The line 16841·63 has enough strength for all four positions. If this interpretation of it is correct, it means that the spacing of the $K = 1, 2, 3$ and 4 levels of $3s\,{}^3\Sigma$ at $v = 2$ is the same as that of the $K = 1, 2, 3$ and 4 levels of $2p\,{}^3\Pi$ at $v = 2$.

---

* R and D, Part III.

The rotational structure of what there is of $3s\,{}^3\Sigma$ is shown in Table X. If this is compared with Table VI, p. 45, of R and D, Part II, it will be seen that the intervals of $2p\,{}^3\Pi_a$ at $v = 2$ are identical with those of $3s\,{}^3\Sigma$ at $v = 2$. If the possible P′ 1 line of the 0 → 0 band is disregarded and the second alternative for the $K' = 5$, $v' = 0$ level is accepted, the value of $2B_0$ comes very near to 58·6. Putting $F_0\,(K) = B_0\,(K + \frac{1}{2})^2 + \beta_0\,(K + \frac{1}{2})^4$, values very close to 58·6 are got (1) by using the data for the $K = 1, 3$ and 5 strong *a* levels at $v = 0$, and eliminating β_0, and (2) by assuming the small quantity β_0 is $= -0{\cdot}02$, and using either the K (2) − K (1) or the K (3) − K (2) interval. The value $\beta_0 = -0{\cdot}02$ is a normal value, and is consistent with the values of β_v at $v = 1$ and $v = 2$; anyhow, any reasonable change in this small quantity cannot alter the value of B_0 much. If we accept the P′ 1 line and the first alternatives for the $K' = 4, 5$, $v' = 0$ levels, the rotational structure of the $v' = 0$ level shown in Table X is evidently somewhat perturbed. However, such perturbations seem not uncommon in $s\sigma$ states of H_2. This choice of rotational levels at $v' = 0$ points to a value of $2B_0$ close to 60. This agrees with the value of $2B_0$ (60·0) which is obtained by extrapolation from the values of $2B_1$, $2B_2$ and $2B_3$ (see Table XI, below).

There are the following additional grounds for believing that the choice of levels which leads to the higher value of $2B_0$ is the correct one : (1) This value of $2B_0$, combined with the value 2331·3 of ω_0 (see Table XII below), gives for Mecke's constant* (B_0/ω_0) the value 0·01287. This compares with 0·01287 for $2s\,{}^3\Sigma$ and 0·01302 for $1s\,\sigma^2\Sigma$ (the ion

---

[*] Nat. Res. Council Rep. on " Molecular Spectra in Gases," p. 233 (1926).

TABLE IX—The Lines of $3s\,^3\Sigma \rightarrow 2p\,^3\Pi$

The 0 → 0 *band*

P′ 1 16930·14 0G C++ or absent

Q1 absent
P2 16870·70 2G 10·5K C++, also
3 → 3, $3d\,^3\Delta_b \rightarrow 2p\,^3\Pi$, P3 and
? 3 → 3, $3d\,^3\Delta_a \rightarrow 2p\,^3\Pi$ P′ 3

↑ R′ 1 17108·41 0G
−0·03 Q′ 2 absent
↓ P′ 3 16807·74 1G 10·0K

∧ R2 17160·95 1G C++
+0·02
∨ Q3 16980·89 1G 11·0K H+ He+,
∧ also 4 → 4, $3d\,^3\Delta_b \rightarrow 2p\,^3\Pi$,
+0·05 R1
∨ P4 16743·17 3G 15·3K C+ He+,
also 6 → 2 $3p\,^3\Sigma \rightarrow 2s\,^3\Sigma$ P2,
where it is too strong

R′ 3 absent
∧ Q′ 4 16977·18 0G, also ? 1 → 1,
−0·42 $3d\,^3\Pi_b \rightarrow 2p\,^3\Pi$, R5
∨ P′ 5 ? 16683·88 0*h* G

R4 absent
∧ Q5 16976·03 5G 17·5K also 0 → 5,
−0·04 $3\,^1M \rightarrow 2p\,^1\Sigma$, R0 and 2 → 2,
∨ $3d\,^3\Delta_a \rightarrow 2p\,^3\Pi$, P4
P6 16628·47 00G

Alternative (less likely) for K′ = 4 and 5 levels.

R′ 3 Q′ 4 P′ 5 absent
∧ R4 ? 17244·91 0G, also 3 → 3,
−0·31 $3d\,^3\Delta_a \rightarrow 2p\,^3\Pi$ R′ 3
∨ Q5 ? 16950·98 0*a* G C+, also R′ 1 of
∧ the 2 → 2 band and 2 → 2,
+0·18 $3d\,^3\Delta_a \rightarrow 2p\,^3\Pi$ P′ 5
∨ P6 ? 16603·20 9G 27·0K, also 1 → 1,
$3d\,^3\Sigma \rightarrow 2p\,^3\Pi$, Q1

The 0 → 1 *band*

P2 14537·31 1G, defect 0·13

The 1 → 0, 1 → 1 *and* 1 → 2 *bands*

The lines of these bands are as given in R and D, Part II, p. 54.

The 2 → 1 *band*

Q1 19058·30 1G, also 1 → 4,
$3d\,^1\Pi_a \rightarrow 2p\,^1\Sigma$, R1, defect
−0·10 with Q1, 2 → 2

The 2 → 2 *band*

P′ 1 absent

Q1 16841·63 4G 10·3K He0
P2 (16731·86) *ab*

∧ R′ 1 16950·98 0*a* G, also ?Q5 of the
−0·05 0 → 0 band and 2 → 2,
∨ $3d\,^3\Delta_a \rightarrow 2p\,^3\Pi$, P′ 5
Q′ 2 16841·63 4G 10·3K
P′ 3 (16677·94) *ab*

∧ R2 17004·40 3*a*G 14·9K, also
−0·03 0 → 0, $3d\,^3\Pi_b \rightarrow 2p\,^3\Pi$, P′ 2
∨ Q3 16841·63 4G 10·3K
P4 (16625·33) *ab*

∧ R′ 3 17056·70 1G 9·3K, also 1 → 1,
0·00 $3d\,^3\Pi_a \rightarrow 2p\,^3\Pi$, Q′ 4
∨ Q′ 4 16841·63 4G 10·3K
P′ 5 (16574·11) may be concealed by
16573·94 (10)

The 2 → 3 *band*

Q1 14743·50 0*ah* G, defect +0·09
with Q1, 2 → 2

The 3 → 2 *band*

Q1 18870·92 0G, also 4 → 0,
$3p\,^3\Sigma \rightarrow 2s\,^3\Sigma$, P2, defect from
3 → 3 Q1, +0·14

The 3 → 3 *band*

P′ 1? 16720·26 2G

∧ Q1 16772·74 1G
+0·09
∨ P2 16668·17 0G

The 3 → 4 *band*

Q1 14790·72 00G, also 0 → 6,
$3d\,^1\Pi_a \rightarrow 2p\,^1\Sigma$, R2, defect 0·13

The 4 → 4 *band*

∧ Q1 ? 16715·37 0G
+0·05
∨ P2 ? 16615·98 0G
P4 ? 16472·46 00*a* G

H_2^+). This value for the constant is better than the value 0·01267 derived from the alternative value 58·6 of $2B_0$, for we should expect the value of the constant to approach that of $1s\,\sigma^2\Sigma$, the end of the series $ns\sigma^3\Sigma$, as n increases, and not to move away from it. Thus the values of the constant for the series $np\,{}^3\Pi_a$ are : $2p\,{}^3\Pi_a$, 0·01263 ; $3p\,{}^3\Pi_a$, 0·01280 ; $4p\,{}^3\Pi_a$, 0·01291 ; $1s\,\sigma^2\Sigma$, 0·01302. The value of B_0/ω_0 for $3p\,{}^3\Sigma$ is also 0·01287. (2) The value $2B_0 = 60·0$ also gives a slightly better agreement with Birge's empirical formula $2xB_e/\alpha_e = 1·4$, the value of $2xB_e/\alpha_e$ being 1·3. (3) It appears that the intensity of the Q branch increases relatively to the P and R branches with increasing rotational quantum number. This is a satisfactory feature, since the Hönl London formula* requires for a $\Sigma \rightarrow \Pi$ band that the Q branch should have about double the intensity of the P and R branches for high rotational quantum numbers, but that the P branch should tend to predominate at the lower rotational levels. A similar variation of intensity is observable in the lines of the $1 \rightarrow 1$ band. (4) The lines Q5 = 16976·03, P6 = 16628·47 give a much more probable value for the $\Delta v' = 1 - 0$ interval at $K' = 5$ than do the alternative lines which are queried in Table IX (see Table XII below).

TABLE X—Rotational Structure of $3s\,{}^3\Sigma$

K ↓	$v = 0$		$v = 1$		$v = 2$	$v = 3$	$v = 4$
5a	———————	———————	———————				
	↑ 292·91	↑	↑ 277·44				
4s	527·08 ……→58·74 or	501·74	502·16 ……→52·72		……		
	↓ 234·17	↓	↓ 224·72	>1·87	215·59		
3a	———→60·93	———	———→54·59		———→52·45		
	173·24		170·13	>1·37	163·14		
2s	……→56·27		……→55·96		……→53·79		
	116·97		114·17	>0·85	109·35		
1a	———→55·67 ?		———→56·81		———	———	? ———
	? 61·30		57·36	>0·55		? 52·4	
0s	……		……		……		

Objections to this alternative are the irregularity of the rotational structure and the bad combination between Q′4 and P′5. However, such a large defect is just possible where both lines are blends ; another possibility is that either Q′4 or P′5, or both, are absent.

The combinations are insufficient to fix the value of B_3. This depends on the assumption that the P′1 line of the $3 \rightarrow 3$ band is 16720·26. When this is combined with the P2 line and the known final interval we get $52·39 - x_3 = F'(1) - F'(0) = 2B_3 + 5\beta_3$. Putting $5\beta_3 = -0·1$

---

* *Cf.* Weizel, " Bandenspektren," p. 187.

and disregarding x_3, this gives $2B_3 = 52\cdot 5$. This value is in harmony with the values of $2B_v$ for the other levels, as can be seen from Table XI, where the values of $2B_v$ and β_v for the different vibrational levels are collected together.

TABLE XI—Values of $2B_v$ and β_v for $2s\,^3\Sigma$ and $3s\,^3\Sigma$

	$v \longrightarrow$	0	1	2	3	4
$2s\,^3\Sigma$	$2B_v \longrightarrow$	66·77	63·51	60·33	57·26	54·25
	$-\beta_v \longrightarrow$	0·022	0·020	0·0195	0·0190	0·0189
$3s\,^3\Sigma$	$2B_v \longrightarrow$	60·0*	57·44	54·99	(?) 52·5	
	$-\beta_v \longrightarrow$	*ca.* 0·02	0·020	0·017	(0·02)	

* Possible, but less likely alternative value, 58·6 (see text).

As was pointed out by Richardson and Davidson (Part II, p. 56), the value of B_1 for $3s\,^3\Sigma$ is lower than one would at first expect in comparison with that for $2s\,^3\Sigma$. This disparity persists at B_0, but an examination of Table XI shows that the discrepancy between the B_vs of $2s\,^3\Sigma$ and $3s\,^3\Sigma$ diminishes regularly as v increases. There can be little doubt that the value of B_0 found for $3s\,^3\Sigma$ is substantially correct, because it is confirmed by the vibrational data for this state. The vibrational intervals of $3s\,^3\Sigma$, which the known lines and known final $2p\,^3\Pi$ intervals enable us to determine, are set out in Table XII, together with those at the $K = 1$ level of $2s\,^3\Sigma$, $2p\,^3\Pi_a$ and $3p\,^3\Pi_a$ for comparison. From the $K = 1$ data for $3s\,^3\Sigma$ we deduce $\omega_0 = 2331\cdot_0$ and $x\omega_0 = 64\cdot_2$. Just as B_0 for $3s\,^3\Sigma$ is a long way from B_0 for $2s\,^3\Sigma$, so also is ω_0, when compared, for example, with the values for $2p\,^3\Pi_a$ and $3p\,^3\Pi_a$. However, the values are mutually consistent because, as we have seen, they satisfy the rule given by Mecke, which states that B_0/ω_0 is approximately constant during a transition.

TABLE XII—Vibrational Intervals of $2s\,^3\Sigma$, $3s\,^3\Sigma$, $2p\,^3\Pi$ and $3p\,^3\Pi$

	$\Delta v \longrightarrow$	1–0	2–1	3–2	4–3
$3s\,^3\Sigma$	$K = 5$ or	2233·92 2259·17 †			
$3s\,^3\Sigma$	$K = 3$	2258·98	2129·16		
$3s\,^3\Sigma$	$K = 1$	2264·96	2140·90	2029·15	1924·52
$2s\,^3\Sigma$	$K = 1$	2521·07	2385·12	2253·05	2123·85
$3p\,^3\Pi_a$	$K = 1$	2240·21	2114·84	1993·47	1875·49
$2p\,^3\Pi_a$	$K = 1$	2338·84	2216·77	2098·04	1981·89
For $3s\,^3\Sigma$ ..	$\omega_0 = 2331\cdot_0$, $x\omega_0 = 64\cdot_2$.				

† Less probable value which uses the R4, etc., lines queried in Table IX.

The extrapolated wave number of the P′ 1 line of the 0 → 0 band is about 16932. There is an unclassified line 16930·14 (0) G, C++. This is a line of the right type, being enhanced in the condensed discharge, according to Merton and Barratt ; but, as we have seen already, if it is the band line it makes the lowest rotational interval slightly irregular, $f'(1) - f'(0)$ being $61 \cdot 30 - x_0$. In any event, the interval $f''(1) - f'(0)$ is very close to 60, and from $P'(1) = \nu_0 + f'(0) - f''(1)$ we get $\nu_0 = 16990$. If we take 29635* as the ν_e of $2p\,^3\Pi$, measured from the ground state $1s\,\sigma^2\Sigma$ of the molecular ion, this makes $3s\,^3\Sigma$ lie 12645 wave numbers below $1s\,\sigma^2\Sigma$, and this corresponds to a Rydberg denominator of 2·94. That of $2s\,^3\Sigma$ got by a method entirely independent of this is 1·9333.*

§ 6 $3d\,^3\Sigma$, Π, Δ COMPLEX → $2p\,^3\Pi$

We have found the bands of these systems which involve the $v' = 4$ and $v'' = 4$ vibrational levels. The band lines are weak and not very numerous, as is to be expected, but the combinations are very accurate, and the distribution of intensity among the lines is quite reasonable, apart from obvious blends. From the development of the bands at the v', v'' levels in the range 0 → 3, we expected that we might find the 4 → 4, 3 → 4 and 4 → 3 bands coming down to $2p\,^3\Pi$ from each of the five states—$3d\,^3\Sigma$, $3d\,^3\Pi_b$, $3d\,^3\Pi_a$, $3d\,^3\Delta_b$ and $3d\,^3\Delta_a$. Out of this total of fifteen bands we find that only one is entirely missing, the 4 → 3 band of $3d\,^3\Delta_b \rightarrow 2p\,^3\Pi$. However, the 3 → 2 band of $3d\,^3\Delta_b \rightarrow 2p\,^3\Pi$ is weaker than 3 → 2 bands which come down from $3d\,^3\Sigma$, $3d\,^3\Pi_b$ and $3d\,^3\Pi_a$, so this result is not unreasonable.

The lines are set out in the usual way in Table XIII. So far we have only found the lines which correspond to transitions between the alternative strong (*a*) levels. If there are lines in the tables corresponding to transitions between the intervening weak (*s*) levels, they do not seem to be numerous enough to base any definite conclusions on. Nevertheless, this new material enables us to make some valuable additions to the information about these important states which was given by Richardson and Davidson in Parts II and III. The new rotational differences for $v'' = 4$ are set out, together with the corresponding data for the lower vibrational levels in Table XIV. The first and second horizontal differences are also inserted. These make very clear how extremely regular the change of these intervals is when the vibration quantum number varies. The value 237·40 for K (5) − K (4) is queried because the data on which it rests are sparse. The same pair of lines do duty as Q1 and

---

* “Molecular Hydrogen and its Spectrum,” final table.

TABLE XIII—Lines of New Bands of $3d\,{}^3\Sigma$, Π, Δ Complexes → $2p\,{}^3\Pi$

$3d\,{}^3\Sigma \rightarrow 2p\,{}^3\Pi$

The 3 → 4 *band*

Q1 13950·0 00G, defect 0·05
Q3 13826·2 4G, also 2 → 1,
$^1X \rightarrow 2p\,{}^1\Sigma$ P1, defect 0·15
R4 (13903·64) *ab* Q5 (13666·2) *ab*

The 4 → 3 *band*

∧ Q1 17501·97 1G, also 2 → 7,
−0·12 $3d\,{}^1\Pi_b \rightarrow 2p\,{}^1\Sigma$, Q4, defect
0·03
∨ P2 17397·61 1G, also 2 → 7,
$3d\,{}^1\Sigma \rightarrow 2p\,{}^1\Sigma$, R0, defect 0·18

∧ R2 17498·87 U G, defect 0·05
0·00
∨ Q3 17344·17 1G, defect 0·02
P4 (17138·13) *ab*

The 4 → 4 *band*

Q1 15520·05 3G 18·0K C ÷ also
4 → 4, $3p\,{}^3\Pi_a \rightarrow 2s\,{}^3\Sigma$, Q3
P2 (15420·71) *ab*

∧ R2 15522·10 0G
−0·02
∨ Q3 15375·49 1G
P4 (15178·91) *ab*

$3d\,{}^3\Pi_b \rightarrow 2p\,{}^3\Pi$

The 3 → 4 *band*

↑ R1 14463·86 00G
−0·11 Q2 (14364·57) *ab*
↓ P3 14218·0 00G

R3 (14507·40) ? 14507·89 (2)
Allibone
Q4 (14310·80) *ab*
P5 (14073·44) ? ? 14072·2 (1) G.
Interval not very certain.

The 4 → 3 *band*

R1 18063·55 0*a* G 2·0K, also 4 → 3,
$3d\,{}^3\Pi_a \rightarrow 2p\,{}^3\Pi$, Q1, defect
0·06

The 4 → 3 *band*—(continued)

Q2 (17959·07) *ab*
P3 (17804·37) *ab* G *ab* M.B.
? ? 17806·01 (rd^2) Deodhar

↑ R3 18074·26 0G, defect 0·03
−0·09 Q4 (17868·22) ? 17867·99 0G
↓ P5 17616·32 2G, also 1 → 6,
3′O → $2p\,{}^1\Sigma$, P2, where it is
probably too strong, defect
0·04

The 4 → 4 *band*

∧ R1 16081·72 0G, also 4 → 4,
−0·04 $3d\,{}^3\Pi_a \rightarrow 2p\,{}^3\Pi$, Q1
∨ Q2 15982·42 0G, also 4 → 4,
$3d\,{}^3\Pi_a \rightarrow 2p\,{}^3\Pi$, P2
P3 (15835·79) *ab*

↑ R3 16105·59 1G, also 3 → 3,
+0·02 $3d\,{}^3\Pi_b \rightarrow 2p\,{}^3\Pi$, P′ 4
Q4 (15909·01) *ab*
↓ P5 15671·59 2G 13·3K

$3d\,{}^3\Pi_a \rightarrow 2p\,{}^3\Pi$

The 3 → 4 *band*

Q1 (14406·43) *ab*
P2 14307·13 00G, also (doubtfully)
6 → 3, $3p\,{}^3\Sigma \rightarrow 2s\,{}^3\Sigma$, P4,
defect 0·02

R2 (14602·31) *ab*
Q3 14455·57 00G, defect 0·03
P4 (14259·07) *ab* R4 (14719·35) *ab*
Q5 (14482·10) *ab*

The 4 → 3 *band*

Q1 18063·55 0*a* G, also 4 → 3,
$3d\,{}^3\Pi_b \rightarrow 2p\,{}^3\Pi$, R1, defect
0·06
P2 (17959·14) *ab*

R2 (18191·53) *ab* Q3 (18036·91) *ab*
P4 (17830·89) *ab*

TABLE XIII—(continued)

The 4 → 4 band

∧ Q1 16081·72 0G, also 4 → 4,
−0·04 $3d\,^3\Pi_b \rightarrow 2p\,^3\Pi$, R1
∨ P2 15982·42 0G, also 4 → 4,
$3d\,^3\Pi_b \rightarrow 2p\,^3\Pi$, Q2

∧ R2 16214·81 0*a* G
+0·03
∨ Q3 16068·21 2G, also 2 → 2,
$3d\,^3\Pi_b \rightarrow 2p\,^3\Pi$, P7 ,where it is probably too strong
P4 (15871·63) *ab* G, might be in M and B

$3d\,^3\Delta_b \rightarrow 2p\,^3\Pi$

The 3 → 4 band

∧ R1 15148·00 0G, defect zero
−0·05
∨ Q2 15048·71 00G, defect 0·02
P3 (14902·08) *ab*
R3 (15271·00) *ab* Q4 (15074·42) *ab*
P5 ? 14837·04 *ab* G (1) Allibone, defect 0·02

The 4 → 3 band

R1 (18962·78) *ab* Q2 (18858·24) *ab*
P3 (18703·59) *ab*
R3 (19029·38) *ab* Q4 (18823·34) *ab*
P5 (18571·35) *ab*

The 4 → 4 band

∧ R1 16980·89 1G 11·0K H+ He+,
+0·03 also 0 → 0, $3s\,^3\Sigma \rightarrow 2p\,^3\Pi$, Q3
∨ Q2 16881·52 1G
P3 (16734·89) *ab*

∧ R3 17060·68 5G 20·5K L++
0·00
∨ Q4 16864·10 1G, also 0 → 4,
$3d\,^1\Pi_b \rightarrow 2p\,^1\Sigma$, Q4
P5 (16626·70) *ab*

$3d\,^3\Delta_a \rightarrow 2p\,^3\Pi$

The 3 → 4 band

R2 (15211·20) *ab*
Q3 15064·45 0G, also 0 → 5,
$3\,^1K \rightarrow 2p\,^1\Sigma$, P3, defect 0·06
P4 (14867·91) *ab*

The 4 → 3 band

R2 19008·37 1G, also 1 → 5,
$30 \rightarrow 2p\,^1\Sigma$, R2, defect 0·02
Q3 (18853·67) *ab* P4 (18647·63) *ab*

The 4 → 4 band

∧ R2 17031·67 1*a* G, also 1 → 1,
+0·10 $3s\,^3\Sigma \rightarrow 2p\,^3\Pi$, R′ 1
× Q3 16884·94 4G, also 0 → 0,
−0·04 $3d\,^3\Sigma \rightarrow 2p\,^3\Pi$, R′ 1
∨ P4 16688·40 4G,,also 1 → 1,
$3s\,^3\Sigma \rightarrow 2p\,^3\Pi$, P4

P2 of 4 → 4, $3d\,^3\Pi_a \rightarrow 2p\,^3\Pi$, and as R1 and Q2 of 4 → 4, $3d\,^3\Pi_b \rightarrow 2p\,^3\Pi$. They may not belong to both bands, but there appears to be no reason for preferring one position rather than the other.

The new rotational intervals at $v = 4$ for the initial levels are shown in the last column of Table XV. The values of the corresponding interval at the lower vibrational levels are included for comparison. At $3d\,^3\Delta_a$ $v = 4$ we have only one rotational level, K = 3, but the ν of this is about right with respect to the others. The value of F (3) − F (1) for $3d\,^3\Sigma$ looks to be too low at $v = 4$, but there is no evidence of any alternative for it. The reality of the K = 3 level is supported by good combinations between R2 and Q3 of the 4 → 4 band, and with Q3 of the 4 → 3 band. The combinations with Q3 of the 3 → 4 band and R2 of the 4 → 3 band may be illusory, owing to interference by blends. However, the rising trend of the separation F (3) — F (1) seen between $v = 1$ and $v = 3$ cannot go on indefinitely, as v increases, and the value found at $v = 4$ is still higher than those at $v = 0$ and $v = 1$. In the case of $3d\,{}^3\Pi_a$ also, the value at $v = 4$ looks rather low in comparison with the others. It is possible in both these states that the $v = 3$ level requires re-investigation. The values of F (4) — F (2) for the $3d\,{}^3\Pi_b$ and $3d\,{}^3\Delta_b$ states at $v = 4$ look to be about normal in comparison with those for the lower values of v.

TABLE XIV—Rotational Differences of $2p\,{}^3\Pi_{ab}$ (*a* States only)

v'' →	0		1		2		3		4
Q1 — P2 = R1 — Q2	120·74		115·14		109·77		104·48		99·34
		5·60		5·37		5·29		5·14	
			0·23		0·08		0·15		
Q2 — P3 = R2 — Q3	$180{\cdot}03_6$		$171{\cdot}33_9$		$162{\cdot}8_0$		154·70		146·63
		8·70		8·54		8·10		8·07	
			0·16		0·44		0·03		
Q3 — P4 = R3 — Q4	$237{\cdot}67_4$		226·91		$216{\cdot}3_0$		206·04		196·58
		10·764		10·61		10·26		9·46	
			$0{\cdot}15_4$		0·35		0·8		
Q4 — P5 = R4 — Q5	294·24		279·77		$265{\cdot}76_5$		251·99		237·40 ?
		14·47		$14{\cdot}00_5$		$13{\cdot}77_5$		14·59 ?	
			$0{\cdot}46_5$		0·23		−0·81 ?		

TABLE XV—Comparison of Rotational Structure of Initial Levels

v' →		0	1	2	3	4
$3d\,{}^3\Sigma$	F′(3) — F′(1) ..	100·15	96·65	107·46	122·24	101·39
$3d\,{}^3\Pi_b$	F′(4) — F′(2) ..	300·79	298·63	295·42	289·47	269·80
$3d\,{}^3\Pi_a$	F′(3) — F′(1) ..	350·10	345·04	321·89	295·19	232·42
$3d\,{}^3\Delta_b$	F′(4) — F′(2) ..	493·57	451·44	410·06	369·00	325·79

For the final level the following vibrational intervals can be added to Table V of R and D, Part III, p. 50 : $2p\,{}^3\Pi_b$, vibrational interval $\Delta v = 4 - 3$, at K = 2, 1976·72, at K = 4, 1959·22; $2p\,{}^3\Pi_a$, $\Delta v = 4 - 3$, at K = 1, 1981·89, at K = 3, 1968·70, at K = 5, 1944·69. For the initial levels the following vibrational intervals can be added to Table VIII of R and D, Part II, p. 47 : $3d\ ^3\Sigma$, $\Delta v = 4 - 3$, at $K = 1$, 1570·05, at $K = 3$, 1549·10; $3d\ ^3\Pi_b$, $\Delta v = 3 - 2$, at $K = 4$, 1807·18, $\Delta v = 4 - 3$, at $K = 2$, 1617·83, at $K = 4$, 1598·17 ; $3d\,^3\Pi_a$, $\Delta v = 4 - 3$, at $K = 1$, 1675·28, at $K = 3$, 1612·56 ; $3d\ ^3\Delta_b$, $\Delta v = 4 - 3$, at $K = 2$, 1832·86, at $K = 4$, 1789·66 ; $3d\ ^3\Delta_a$, $\Delta v = 4 - 3$, at $K = 3$, 1820·47.

All these vibrational intervals continue in a satisfactory manner the trend of the corresponding intervals for lower vibration quantum numbers given in the tables referred to.

SUMMARY

This paper describes a number of new bands and a new band system ending on the lowest triplet level $2p\,^3\Pi$ of H_2. They are: (1) the $4d\ ^3\Delta_a \rightarrow 2p\,^3\Pi$ system ; (2) the substitution of new $v' = 2$ and $v' = 3$ levels in $4d\ ^3\Pi_b$ for the levels given by Richardson and Davidson; (3) the non-diagonal bands and some minor alterations of and additions to $4d\ ^3\Sigma$, Π_{ba}, $\Delta_b \rightarrow 2p\,^3\Pi$; (4) the extension of the $3s\,^3\Sigma \rightarrow 2p\,^3\Pi$ system to the $v' = 0$, 2, 3 and (?) 4 levels ; (5) the extension of the $3d\,^3\Sigma\Pi\Delta$ complex $\rightarrow 2p\,^3\Pi$ to the v', $v'' = 4'$, $4''$ levels. The band constants and more important properties of the new levels are worked out.

The Reaction between Oxygen and the Heavier Isotope of Hydrogen

By C. N. HINSHELWOOD, F.R.S., Messel Research Fellow,
A. T. WILLIAMSON, International Research Fellow, and J. H. WOLFENDEN

(*Received June* 29, 1934)

INTRODUCTION

The reaction between hydrogen and oxygen is complex, and includes a variety of mechanisms, some depending upon quantities such as activation energies, and others upon purely physical properties such as diffusion coefficients.* A comparison between the two isotopes of hydrogen promises therefore not merely to add to our knowledge of the properties of deuterium, but to assist the theoretical interpretation of the hydrogen-oxygen reaction itself.

This paper deals with the rate of the surface reaction, the rate of the chain reaction in the gas, and the upper limit of the low pressure explosion. While the experiments were in progress, a communication† on the explosion limit appeared which seems to be in substantial agreement with this part of our work.

PREPARATION OF DEUTERIUM

Two grammes of heavy water, obtained commercially, were distilled *in vacuo*. The specific gravity of the distillate was measured in a pyknometer of 0·3 cc capacity and found to be 1·1033 at 14° C, relative to water at the same temperature. Accepting Taylor and Selwood's‡ recent estimate of the ratio of the specific gravities of light and heavy waters at 25° as 1·1079, and the data of Lewis and Macdonald§ for the thermal expansion of heavy water, the deuterium content of the distillate was 96·2%.

The heavy water was decomposed in portions of about 0·5 gramme by passing it over iron at about 600° C. The iron was obtained by the reduction of pure iron oxide. The deuterium was transferred to a storage vessel as it was formed with the aid of a Töpler pump device. Two passages of the heavy water over the hot iron were enough for 97% decomposition. In order to exclude the possibility that differences between the hydrogen and deuterium might be caused by some unexpected impurity introduced in the preparation of the latter, the earlier control experiments were made with hydrogen prepared from distilled water in exactly the same way as the deuterium. This hydrogen behaved in a manner indistinguishable from that of cylinder hydrogen, which was therefore used in the later control experiments.

---

* *Cf.* Hinshelwood and Williamson, "The Reaction between Hydrogen and Oxygen," Oxford, 1934.

† Frost and Alyea, 'J. Amer. Chem. Soc.,' vol. 56, p. 1251 (1934).

‡ *Ibid.*, vol. 56, p. 998 (1934).

§ *Ibid.*, vol. 55, p. 3059 (1933).

METHOD OF EXPERIMENT

The procedure was similar to that described in previous papers from this laboratory.* Every experiment with deuterium was immediately preceded and followed by an exactly similar experiment with hydrogen. The mean of the two control experiments with hydrogen served as a standard of comparison with deuterium. This systematic control is essential to obtain significant results with a reaction as sensitive to apparently trivial changes in experimental conditions as the combination of hydrogen and oxygen.

The reaction vessel was usually a cylindrical silica bulb, 7 cc in diameter and of 250 cc capacity. It was heated in an electric furnace, the temperature of which could be kept constant and measured to within half a degree. For the experiments on the surface reaction a bulb packed with small silica spheres was used. Its surface/volume ratio was sixteen times as great as that of the unpacked bulb. In measuring the upper limit of the " low pressure explosion," deuterium (or hydrogen) and oxygen were admitted to the bulb in equivalent proportions at a pressure well above the explosion limit. The gases were then slowly pumped out, and the pressure at which explosion occurred noted. The steady rates of reaction were measured by admitting deuterium or hydrogen at the appropriate pressure followed by oxygen, starting a stop-watch at the moment of mixing, and recording the times for uniform small intervals of fall of pressure.

THE SURFACE REACTION

The packed bulb was used at 525° C. Previous experience with this bulb had shown that the reaction was almost entirely heterogeneous, even at temperatures considerably higher than that chosen.

---

* Hinshelwood and Thompson, 'Proc. Roy. Soc.,' A, vol. 118, p. 170 (1928) ; Gibson and Hinshelwood, vol. 119, p. 591 (1928) ; Thompson and Hinshelwood, vol. 122, p. 610 (1929) ; Grant and Hinshelwood, vol. 141, p. 29 (1933).

The reaction was slow, and only initial rates were measured. The times, Δt, required for successive equal increments of steam formation are recorded in Table I for three typical experiments. In each the pressure of oxygen was 100 mm and that of hydrogen or deuterium 200 mm. The order of the measurements is indicated by numbers.

TABLE I

Steam formation mm	Δt (seconds)				Ratio rate D_2/rate H_2
	(1) H_2	(3) H_2	H_2 (mean)	(2) D_2	
0–4	87	80	83	125	0·66
4–8	95	93	94	145	0·65
8–12	151	129	140	245	0·57
12–16	225	198	211	275	0·77
16–20	300	250	275	435	0·63
				Mean :	0·66

A similar series of experiments made with 150 mm oxygen and 300 mm hydrogen or deuterium gave a mean ratio of 0·70.

THE UPPER EXPLOSION LIMIT

The " low pressure " explosion depends upon the branching of reaction chains, and the upper limit is reached when effective branching is balanced by de-activation in ternary collisions in the gas phase. The influence of various gases on its position is principally determined by the speeds and sizes of their molecules.

When hydrogen is replaced by deuterium the limit is raised—that is, the mixture becomes more explosive, in the sense that a larger pressure is required to keep the branching chains in check.

The results of experiments made by the " withdrawal " method, previously described, are given in Table II and plotted in fig. 1.

All measurements were made with equivalent proportions. P'_e and P''_e are the total pressures at the limit for hydrogen and deuterium mixtures respectively.

From the figure it may be seen that the lines obtained by plotting log P'_e and log P''_e against $1/T$ are parallel within the limits of experimental error. Thus P''_e/P'_e is constant, the mean value of the ratio being 1·31.

The difference between hydrogen and deuterium can be entirely accounted for by the difference in the molecular speeds. According to the simple theory of the upper limit given by Grant and Hinshelwood,* there is a probability ν that branching occurs at the encounter of two particles, X and Y, which meet in the course of the chain. If a third

TABLE II

Temperature °C	P'_e	P''_e
550	120	169
542	—	134
541	106	—
539	99	—
536	—	125
532	89	—
525	76	96
510	—	75
500	48	60
480	29	—
476	—	36
474	24	—

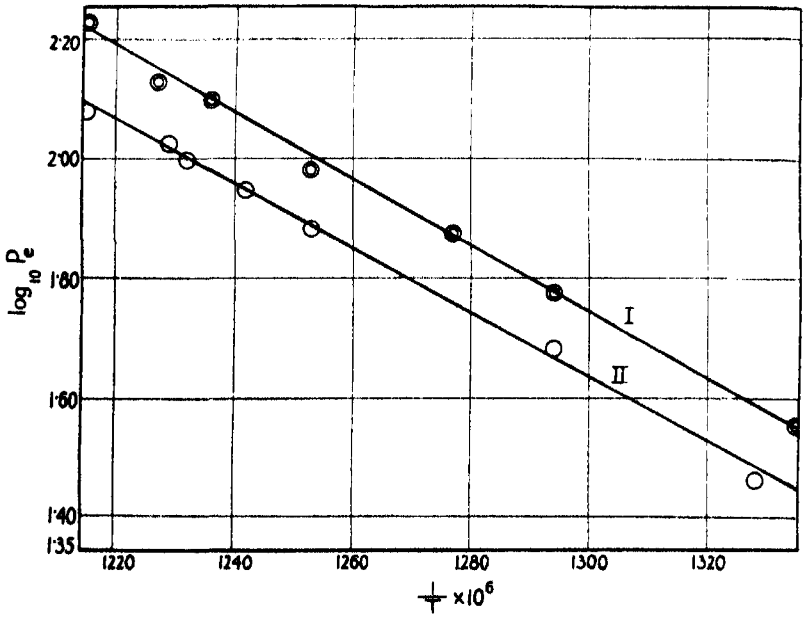

FIG. 1—I, deuterium ; II, hydrogen

molecule arrives while X and Y are in association, the branching is prevented. This leads to the following condition for the upper limit :—

$$\nu k [X] [Y] = Z_{H_2} [X] [Y] [H_2] + Z_{O_2} [X] [Y] [O_2],$$

---

* 'Proc. Roy. Soc.,' A, vol. 141, p. 29 (1933).

the Z factors being proportional to the collision frequencies of the "complex" XY with hydrogen or oxygen. This gives

$$Z_{H_2} . P_{H_2} + Z_{O_2} . P_{O_2} = C,$$

where C is a constant.

Since for equivalent proportions $P_{H_2} = 2\,P_{O_2} = 2/3\ P_e$,

$$P'_e \left[0{\cdot}667 + 0{\cdot}333\,\frac{Z_{O_2}}{Z_{H_2}}\right] = \frac{C}{Z_{H_2}},$$

Z_{O_2}/Z_{H_2} was found experimentally by Grant and Hinshelwood to be 0·33, whence we find $C/Z_{H_2} = 0{\cdot}777\ P'_e$.

Assuming ν and therefore C to be the same for the reaction with deuterium,

$$Z_{D_2} . P_{D_2} + Z_{O_2} . P_{O_2} = C,$$

and

$$P''_e \left[0{\cdot}667 + 0{\cdot}333\,\frac{Z_{O_2}}{Z_{D_2}}\right] = \frac{C}{Z_{D_2}},$$

$$P''_e \left[0{\cdot}667 + 0{\cdot}333\,\frac{Z_{O_2}}{Z_{H_2}}\,\frac{Z_{H_2}}{Z_{D_2}}\right] = \frac{C}{Z_{H_2}}\,\frac{Z_{H_2}}{Z_{D_2}},$$

whence

$$\frac{Z_{D_2}}{Z_{H_2}} = \frac{\left(0{\cdot}777\,\frac{P'_e}{P''_e} - 0{\cdot}110\right)}{0{\cdot}667}$$
$$= 0{\cdot}725.$$

The value of Z_M is proportional to $\sigma^2_{XYM}/\mu^{\frac{1}{2}}_{XYM}$ where σ is the sum of the molecular diameters of the complex XY and the third molecule M, and $\mu = m_{XY} . m_M/(m_{XY} + m_M)$, m_M, etc., being the molecular weights. The value of σ for the two isotopes will be the same. The calculation is not sensitive to the value taken for m_{XY} provided it is great compared with m_M, a condition which is certainly fulfilled here. m_M will be taken as approximately equal to $(m_{O_2} + m_{H_2})$ or to $(m_{O_2} + m_{D_2})$.

Thus

$$Z_{D_2}/Z_{H_2} = \sqrt{\frac{18 \times 2}{20}\Big/\frac{20 \times 4}{24}} = 0{\cdot}735.$$

The close agreement with the experimental value justifies the conclusion that ν is the same in both systems.

Thus the difference found with deuterium can be entirely accounted for by its smaller molecular velocity. The concordance is, indeed, good enough to serve as a confirmation of the general hypothesis that the upper limit is controlled by ternary collisions in the gas phase.

The value for the energy of activation of the branching process is 25,000 calories for deuterium, and does not differ significantly from the values 25,500 and 26,000 previously found for hydrogen.

THE GASEOUS REACTION

A typical comparison of deuterium and hydrogen is shown in fig. 2. The experiments were made with 150 mm oxygen and 300 mm deuterium or hydrogen at 557° C. Curve *d* represents an experiment made with deuterium between the two experiments with hydrogen represented in curves *a* and *b*. Curve *c* is the mean of *a* and *b*.

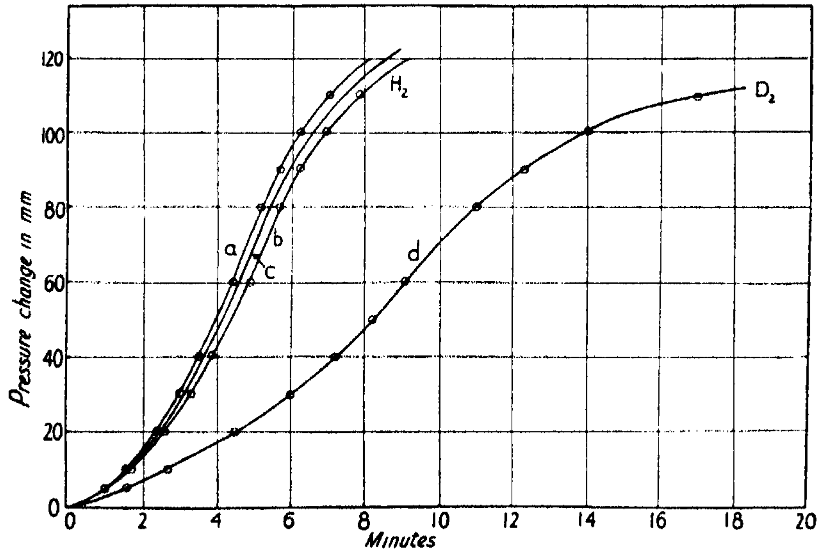

Fig. 2.

The ratios of the times required for a given percentage change with hydrogen and deuterium are given in Table III.

TABLE III

% change	Time H_2/time D_2
10	0·55
25	0·53
50	0·50
75	0·44

From this it appears that the initial rate with deuterium is about 60% of that with hydrogen. The divergence of the rates becomes greater as the combination proceeds. This is better shown by taking tangents to *the curves at various points.*

TABLE IV

% change	*Ratio of tangent slopes* D_2/H_2
0	0·60
20	0·47
40	0·47
60	0·41

The change being autocatalytic in form, the increasing divergence of the curves means that the accumulation of the product in the system assists the reaction of the heavier isotope less than that of the lighter. The steam increases the rate of reaction by delaying the diffusion of the chain propagating particles to the vessel wall, where most of them are ultimately destroyed. The difference in this respect between light and heavy steam must be inconsiderable, the molecular weights being so close. But the reacting gases themselves delay the diffusion, and in this respect deuterium will be markedly more effective than hydrogen, its molecular weight being double. In the early stages of the reaction, therefore, the " inert gas effect " of the deuterium will partly compensate for its lower reactivity. The " inert gas effect " of steam is great compared with that of either hydrogen or deuterium ; in the later stages of the reaction, therefore, most of the resistance to diffusion is due to the steam, and the difference of hydrogen and deuterium in this respect becomes far less important. Thus the inherent difference in reactivity reveals itself more clearly as the reaction proceeds.

Table V summarizes the results of several series of experiments made under various conditions. The absolute rates of reaction are not given, but it may be mentioned that in this region of temperature the reaction is rapid, and the rate approximately proportional to the cube of the initial pressure, for both isotopes.

The mean values, together with the ratios of the initial rates for the different pressures, are given in Table VI.

It is rather difficult to measure the tangents after about 60% reaction, but from the results as a whole it seems probable that the limiting value to which the ratio falls as reaction proceeds is, on the average, not far from 0·4.

Thus we may say that hydrogen can react about 2·5 times as rapidly as deuterium, but that the greater inert gas effect of deuterium reduces this ratio to 1·5 in the earlier stages of the reaction. The difference between the inert gas effects which must be attributed to hydrogen and deuterium is quite consistent with the known magnitude of the effect of helium on the combination of hydrogen and oxygen.

Since the addition of nitrogen causes a very great increase in the length of the path traversed by the chains on their way to the wall, and a consequent increase in reaction velocity, it seemed possible that experiments made in the presence of a considerable partial pressure of nitrogen might cause the difference between hydrogen and deuterium to stand out more clearly. Measurements were made at 550° with 200 mm hydrogen or deuterium, and 100 mm oxygen, with the addition of 380 mm nitrogen, the effect of which was to increase the total rate by a factor of some four times.

TABLE V

Temperature °C	Initial pressure H_2 or D_2	O_2	Ratio of tangent slopes D_2/H_2 At 25%	At 50%
549	400	200	0·61	0·52
550	400	200	0·40	0·45
550	400	200	0·66	0·50
550	300	150	0·44	0·35
553	300	150	0·61	0·44
553	300	150	0·49	0·47
557	300	150	0·46	0·41
560	300	150	0·55	0·47
550	200	100	0·40	0·28
550	200	100	0·44	0·31
553	200	100	0·36	0·31
557	200	100	0·41	0·32
560	200	100	0·35	0·28

TABLE VI

Initial pressures	Ratio of initial rates	Ratio of tangent slopes at 25%	50%
400/200	0·60	0·56	0·49
300/150	0·60	0·51	0·43
200/100	0·70	0·39	0·30

Ratio of tangent Slopes D_2/H_2

25%	0·51	0·47	0·57	0·53
50%	0·44	0·39	0·49	0·38

These ratios are not appreciably less variable with the progress of the reaction than before, which shows that the initial addition of nitrogen has less effect on the ratio than the steam formed in the reaction. The inert gas effect of steam is known to be greater than that of nitrogen, but the fact that the formation of 100 mm steam changes the ratio more than the addition of 380 mm nitrogen suggests a greater specificity in the action of steam in impeding the chain carriers than has hitherto been recognized.

The different inert gas effects of hydrogen and deuterium still make themselves felt in presence of nitrogen, the inert gas effect of which might have been expected to outweigh that of either. This is curious, but may have a special explanation. When the reaction rate is as high as in the experiments with nitrogen (time of half change, 5 minutes), the phenomenon of secondary activation*† can give rise to a more than linear increase of rate with inert gas concentration. Thus the addition of nitrogen may create conditions where the rate becomes much more sensitive to any small absolute differences in the total inert gas effect.

DISCUSSION

In the neighbourhood of the upper explosion limit deuterium is not less but more explosive than hydrogen. The shift of the limit can be entirely accounted for by the different molecular velocities of the two isotopes. The probability of chain branching must therefore be the same for both isotopes. It is just possible that the branching in deuterium is due to the small residual amount of hydrogen, but there is a simpler alternative. According to one theory,† chain branching depends upon whether or not an activated molecule of H_2O_2 breaks down into 2 OH. In this no link involving H or D is broken, and therefore the different zero point energies of the two isotopes will have only a second order effect or none.

In the surface reaction and the steady chain reaction, on the other hand, the rates depend not upon simple branching but upon initiation and propagation mechanisms, one or other of which must include the activation or dissociation of H_2 or D_2. The different zero point energies will then give rise to different activation energies, and hence to different rates. When corrected for the different chain lengths due to the changed diffusion coefficient, the ratio of the rates in hydrogen and deuterium seems to be about 2·5. If this all arose from an exponential factor $e^{-\Delta E/RT}$, then the value of Δ E would be 1500 calories. According to Eyring and Sherman,* the difference in the zero point energies of H_2 and D_2 is about 1800 calories, and of OH and OD about 1400 calories.

---

* Semenov, ' Z. phys. Chem.,' B, vol. 2, p. 169 (1929).

† Hinshelwood and Williamson, *op. cit.*

We are indebted to Imperial Chemical Industries, Ltd., for a grant with which materials have been purchased.

SUMMARY

Deuterium reacts more slowly than hydrogen with oxygen. For the surface reaction on silica the ratio of the rates is from 0·6 to 0·7 at 525° C. For the chain reaction in the gas at 550° to 560° C, the ratio is 0·6 in the early stages of the reaction, but falls to about 0·4 as steam accumulates in the system. In the early stages the smaller diffusion coefficient of the chain carriers in deuterium partly compensates for the lower reactivity, but, as the reaction goes on, the steam minimizes the compensation and allows the inherent difference in reactivity to appear more completely.

The upper limit of the " low pressure " explosion region is higher with deuterium than with hydrogen. The shift can be quantitatively accounted for in terms of the smaller number of deactivating ternary collisions made by the deuterium. No difference in the probability of chain branching need be assumed. This lends support to the hypothesis that the branching depends upon a process in which no hydrogen or deuterium linkages are broken.

---

* 'J. Chem. Phys.,' vol. 1, p. 345 (1933).

Researches on the Chemistry of Coal

Part VII—An Investigation of German Brown Coals and Irish Peat

By WILLIAM A. BONE, D.Sc., F.R.S., and LOUIS J. TEI, B.Sc.

(*Received July* 7, 1934)

In continuance of investigations in the Fuel Research Laboratories of the Imperial College, London, on the chemical constitution and maturing of coals, it was thought advisable to examine some representative German brown coals in the hope of obtaining further light upon the origin of those constituents of bituminous coals which are mainly responsible for their coking propensities. The present paper summarizes the results thereof which are supplemented by some observations on a typical Irish peat.

It may be recalled how in previous papers of the series* it has been shown in regard to the dry organic substance of brown coals (*e.g.*, Morwell brown coal, Italian and Canadian brown lignites) :—(i) that on being raised to a certain temperature, varying between 300 and 400° in different cases, it underwent an " internal condensation " characterized by the simultaneous elimination of oxides of carbon (but chiefly the dioxide) and steam without any appearance of oil, hydrogen, or more than a negligible amount of gaseous hydrocarbon ; (ii) that on further raising the temperature there followed another range (up to *circa* 500°) in which methane and heavy hydrocarbons also appeared, as though alkyl side-chains were being eliminated ; but (iii) that hydrogen was not evolved until the temperature exceeded 500°. Moreover, it was shown that on being extracted with benzene under pressure it yielded neutral oils, phenols (*plus* acidic bodies) and phenolic esters *plus* a " residue " (constituting upwards of 80% of the whole coal substance) which was largely benzenoid in character.

The present investigation was undertaken to ascertain (i) whether typical German brown coals—which in some other respects differ from those previously examined—would behave similarly when subjected to the said treatments, and (ii) how far previous conclusions, that the main " coking constituent " of bituminous coals probably originated in the phenols and phenolic esters of brown coals, would be borne out or need modifying.

---

* ' Proc. Roy. Soc.,' A, vol. 99, p. 236 (1921), and vol. 120, p. 523 (1928).

A—GENERAL DESCRIPTION AND PROXIMATE ANALYSIS OF THE COALS

The four brown coals selected for the investigation, procured for us from Germany by the Fuel Research Board, were as follows :—

Nos. 1 *and* 2—From the Rheinische Braunkohlen Syndikat of Cologne, being of tertiary origin from an open-working in which the seam had a total thickness of 50 metres with an " overburden " of 12 to 15 metres. No. 1 was an average sample of the coal between 20 and 25 metres, while No. 2 was an average of that between 30 and 50 metres, down the seam.

No. 3—From the open " Siegfried " mine near the village of Deuben (" Weissenfels-Zeitrer Bezirk "), about 30 kilometres S.S.E. of Halle, where the seam is 12 metres thick with an " overburden " of 20 metres.

No. 4—From the " Walters-Hoffnung " mine near the village of Stetden (" Oberoblingen Bezirk "), 15 kilometres W. of Halle, where the seam is 18 metres thick under an " overburden " of 50 metres. Deposits of potash occur in this district and the coal-ash contains it.

A *Proximate Analyses*—As received the two Rhenish coals were nearly in their natural state and contained 57·6 and 59·1%, respectively, of moisture. The two Saxon coals, however, had been partly dried (down to about 15% moisture-content) before being despatched to us. The ash contents of the dry coals were as follows :—

Rhenish		Saxon	
No. 1	No. 2	No. 3	No. 4
7·6%	5·2%	11·2%	11·0%

The " volatiles " yielded by the dry-ashless coal substance at 900° were as follows :—

	Rhenish		Saxon	
	No. 1	No. 2	No. 3	No. 4
Volatiles	55·9	54·6	60·3	60·1

B *Montan-Wax Content*—These German coals contained notably larger proportions of " montax wax " than did either the Australian or Canadian brown coals previously examined in our laboratories. Such wax—which in our specimens was readily extracted from the dry coal by boiling benzene at atmospheric pressure, and melted between 80 and 85°

—has usually been considered a mixture of higher fatty acids and their esters together with (may be) higher hydrocarbons. Thus, after hydrolysing it, Tropsch and Dilthey isolated myricyl alcohol $C_{30}H_{62}O_2$ (m.p. 88°), " bituminol " $C_{32}H_{66}O$, carbocerinic and montanic acids ($C_{27}H_{54}O_2$, m.p. 81·5 to 82°, and $C_{29}H_{58}O_2$, m.p. 86·5°) ; while Pschorr and Pfaff similarly isolated tetracosanol ($C_{24}H_{50}O$, m.p. 83°), as well as the foregoing substances from it. Recently Holde and Bleiberg have isolated *n* octocosanic acid ($C_{28}H_{56}O_2$, m.p. 89°).

The four coals in question yielded (when " dry ") the following percentages .of the wax :—

No. 1	No. 2	No. 3	No. 4
2·5	2·8	7·5	6·0,

as compared with the 1·3% yielded by the Morwell and the 0·4% by the Canadian brown coals previously examined. And if a small percentage of sulphur be disregarded, the ultimate compositions of the wax-contents (*vide* Table V) all closely approximated to the empirical formula $C_nH_{2n}O_2$ (with $n = 27$ to 32) requiring $C = 79{\cdot}0$ to $80{\cdot}0$, $H = 13{\cdot}15$ to $13{\cdot}35$, and $O = 7{\cdot}85$ to $6{\cdot}65$.

C *Ultimate Compositions of the Coal Substances*—The ultimate compositions of the dry-ashless coal substances, both (*a*) before and (*b*) after being " dewaxed " in each case, were as follows :—

TABLE I

Coal No.	1		2		3		4	
	(*a*)	(*b*)	(*a*)	(*b*)	(*a*)	(*b*)	(*a*)	(*b*)
C	64·30	65·85	66·50	66·35	68·45	68·95	69·50	70·05
H	5·85	4·70	5·65	4·85	6·40	5·30	5·95	5·45
N	0·50	0·55	0·85	0·70	0·55	0·55	0·55	0·55
S	0·40	0·30	0·30	0·30	3·80	4·20	3·90	4·70
O	28·95	28·60	26·70	27·80	20·80	21·00	20·10	19·25
C/H ratio..	11·0	14·0	11·75	13·7	10·7	13·0	11·7	12·85

If, as seems reasonable, the montan-wax in the original coal be regarded as an incidental rather than a basal constituent, the figures under (*b*) rather than those under (*a*) would represent the composition of the true coal substance. And although the two Rhenish have higher C/H ratios, their lower carbon and higher oxygen contents show them to be less mature than the two Saxon coals. Also, the much higher sulphur contents of the last named should be noted.

D *The Action of Heat upon the Dry and Dewaxed Coal Substance*—A quantitative study was made of the gases evolved during the fractional carbonization of the dry de-waxed coal-substance in successive temperature-ranges up to 800° when thermal decomposition had been almost completed. The results, while agreeing generally with those previously obtained with other brown coals, are of sufficient interest in themselves to warrant detailed consideration. Seeing, however, that there was a close similarity between the results from the two Rhenish coals as well as between those from the two Saxon coals, it will suffice for us to detail those of one from each area, and therefore we have selected the maturer of the two coals in each case, namely, Rhenish No. 2 and Saxon No. 4. The temperature at which oils first appeared was 300° with the former and 275° with the latter ; accordingly the results are tabulated (Tables III and IV) so as to show, in each case, the amounts and compositions of the gas evolved (i) up to such " oil point," and (ii) over selected temperature-ranges thereafter until thermal decomposition had been completed within each range.

Attention may be directed to the fact that with each of the four coals, practically all that happened up to its " oil point " was an expulsion of carbon dioxide and steam* in molecular ratios between 1 : 1·7 and 1 : 2·6, the mean being remarkably near the corresponding 1 : 2·25 ratio previously found with Morwell brown coal on undergoing much the same " internal condensation " up to its " oil point " of 375°. Thus for the present coals we obtained the results shown in Table II.

TABLE II

Coal	" Oil point "	Weight evolved per 100 gm of dry dewaxed coal substance		$\%CO_2$ in gas	$\frac{H_2O}{CO_2}$
		Gas	Steam		
No. 1	260°	4·9	5·0	93·2	2·6
No. 2	300°	6·1	4·0	91·4	1·7
No. 3	288°	4·6	3·5	90·9	2·0
No. 4	275°	3·9	3·8	92·9	2·5

A detailed investigation of the stage-wise carbonization of No. 2 up to 480° showed that its " oil point " synchronized with the first appearance of paraffin hydrocarbons (principally methane, ethane, and propane) among the gaseous products ; hydrogen first appeared between 400°

---

* There was also relatively little carbon monoxide expelled (*vide* Tables III and IV), but no other oxygenated product.

and 420°. The C/A ratios obtained in explosion analyses of the residual gases after removal of H_2S, CO_2, C_nH_{2n}, and CO were 1·6 at 315°, 1·75 at 420° (when propane, ethane, methane, and hydrogen were all present) and 2·2 at 450°, by which temperature the paraffin-constituent had become practically all methane. At 480° the C/A ratio had risen to 2·4, the residual gas consisting of methane and hydrogen only.

TABLE III—Gases evolved from Rhenish Coal No. 2; cc at N.T.P. per 100 gm of dry dewaxed coal substance

Temperature range °C	Total gas	H_2S	CO_2	CO	C_nH_{2n}	CH_4 and C_nH_{2n+2}	H_2	N_2
Up to 300	3196	Nil	2920	247	10	Nil	Nil	19
300 to 420	6190	18	4272	860	235	767	Nil	38
420 to 500	5114	10	1978	583	133	1890	496	24
500 to 600	4500	3	1104	850	41	1395	1000	107
600 to 700	7367	Nil	567	1739	44	1606	3160	251
700 to 800	5272	Nil	179	1108	5	691	3000	289
Totals	31639	31	11020	5387	468	6349	7656	728

TABLE IV—Gases evolved from Saxon Coal No. 4; cc at N.T.P. from 100 gm of dry dewaxed coal substance

Temperature range °C	Total gas	H_2S	CO_2	CO	C_nH_{2n}	CH_4* and C_nH_{2n+2}	H_2	N_2
Up to 275	2024	28	1874	85	4	6	Nil	27
275 to 400	6305	960	4388	543	98	299	Nil	17
400 to 500	6322	481	2584	668	357	2121	Nil	111
500 to 600	5750	93	1386	934	78	1933	1109	217
600 to 700	7807	14	995	2071	24	1461	3068	174
700 to 800	5281	Nil	221	1368	9	787	2730	166
Totals	33489	1576	11448	5669	570	6607	6909	712

* Mainly CH_4.

The results obtained with coals Nos. 2 and 4 over their complete carbonization ranges (Tables III and IV) showed that whereas 90% of the total H_2S, and 80% of the total yields of CO_2 and unsaturated C_nH_{2n} hydrocarbons, had been evolved below 500°, and about 80% of the total yield of paraffins (almost all methane) between 400 and 700°, 80% of the hydrogen and 60% of the total yield of carbonic oxide were not evolved until the temperature exceeded 600°.

Of the total sulphur in the coal the proportion eliminated as sulphuretted hydrogen up to 800° was only 15% in the case of No. 2 Rhenish, but as much as 48% in the case of the No. 4 Saxon coal. The question of the sulphur-distribution among the various carbonization products in the case of the last-named coal is, however, reserved for a future communication.

THE BENZENE PRESSURE-EXTRACTION OF THE DRY DEWAXED COAL

The Extraction Process—Each coal, having been thoroughly dried *in vacuo* at 105°, ground so as to pass through a 20- but not a 40-mesh screen, and suitably " dewaxed," was extracted Soxhlet-wise by boiling benzene in successive stages, namely, at 250, 500, and 700–750 lbs per sq inch (*i.e.*, at *circa* 210°, 260°, and 285°) according to our usual procedure. There was always some elimination of water and gas evolution (mainly CO_2), more particularly at the 250 lbs stage, indicative of some " internal condensation " of the coal substance having set in, but presumably such would not involve any breakdown of its essential chemical structure.

Fractionation of the Primary Benzene Pressure-Extract—A preliminary examination of the benzene solution of the combined pressure-extract in each case having shown it to be a complex mixture of phenolic substances and the like with hydrolysable esters, neutral oils and minute quantities of basic bodies, it was successively extracted with (*a*) 10% HCl aq, and (*b*) a series of three 10% aqueous alkaline ($NaHCO_3$, Na_2CO_3, and NaOH) solutions which effectively removed all basic, phenolic, and acidic constituents. Afterwards the neutral esters and non-hydrolysable oils were recovered from it for subsequent examination. During each of the extractions of the benzene solution referred to, some emulsified " tarry " matter was precipitated and could be removed by filtration only with great difficulty. The precipitate from (*a*) was entirely insoluble in ether ; that from (*b*) was soluble in water, and after reprecipitation with hydrochloric acid it was resolved into ether-soluble and ether-insoluble portions.

The quantitative results of the benzene pressure extraction and subsequent fractionation of the resulting primary extracts are summarized in Tables V and VI ; and the general properties of the various fractions were briefly as follows :—

(*a*) *The* HCl-*soluble Constituents*, which were present in very small amounts, were organic bases.

(*b*) *The Alkali-soluble Constituents*—These contained, besides p. cresol and catechol, certain other complex acidic bodies which "coupled" with diazotized bases and were presumably also mainly phenolic, although it is possible that some were not. This fraction will, therefore, be referred to as the "phenolic" constituents. And since they now (as it were) appeared in place of the characteristic fraction IV (*i.e.*, the main coking constituents) of the benzene pressure-extract obtained from bituminous coals, they may also be conveniently designated as the IV′ fraction.

(*c*) *The Tarry Constituents*—There was some evidence (though not conclusive) of these having been formed by polymerization or resinification from the alkaline solution of (*b*). They were further divided into ether-soluble and -insoluble portions, of which the former could be further resolved by our standard treatment (*q.v.*) into four fractions simulating the familiar fractions I to IV of the benzene pressure-extracts from bituminous coals. Albeit those now obtained were all acidic, instead of being mainly neutral, in reaction; and (like fractions III and IV from bituminous coals) they exhibited binding power when strongly heated in admixture with excess of finely divided coke. The ether-insoluble portion had no such binding power.

TABLE V—Percentage Yields from Benzene Pressure-Extractions referred to the Dry-ashless Coals

Coal	Montan wax	Fractions from benzene pressure-extraction								Dry† residue recovered
								Tarry constituents*		
		Basic	IA	IB	II	III′	IV′	Soluble in ether	Insoluble in ether	
Rhenish No. 1	2·5	Trace	0·7	2·5	0·6	0·4	1·4	2·3	2·2	71·5
„ No. 2	2·8	0·15	1·0	2·5	0·8	2·0	3·2	5·3	3·9	63·4
Saxon No. 3 ..	7·5	0·10	1·1	4·4	1·8	1·8	2·6	5·5	3·4	60·8
„ No. 4 ..	6·0	Trace	0·4	3·3	2·3	Trace	1·5	1·8	3·5	70·4

IA and B and II = neutral, non-hydrolysable oils; III′ = phenolic esters; IV′ = phenolic bodies.

* Polymerized bodies precipitated during fractionation.

† CO_2 and H_2O were also eliminated and there was some mechanical loss during each extraction.

(*d*) *The Neutral Constituents*—After removal of fraction IA by steam distillation, these were first of all resolved into hydrolysable phenolic-esters and non-hydrolysable viscous oils. Since the former appeared in place of fraction III of the extract from bituminous coals it may

TABLE VI—Ultimate Compositions of Montan Waxes; Benzene Pressure-Extracts IA and B and II; and Residues.

	Montan wax				IA				IB				II				Residue			
Coal No. :	1	2	3	4	1	2	3	4	1	2	3	4	1	2	3	4	1	2	3	4
C	78·6	80·0	79·1	79·0	83·2	79·7	80·0	78·6	83·0	82·0	82·1	81·1	80·7	78·6	79·8	78·4	71·8	73·0	72·5	72·9
H	11·6	12·8	12·3	12·8	9·6	9·3	10·1	10·8	10·1	10·7	10·6	10·5	8·0	10·2	10·0	10·2	4·3	4·0	4·3	4·7
N	Nil	Nil	Tr.	Nil	Nil	Nil	Nil	Nil	Nil	Nil	Nil	Nil	Nil	Tr.	Nil	Nil	0·6	1·3	1·0	0·9
S	0·2	0·1	0·7	1·6	Tr.	Tr.	Tr.	Tr.	0·3	0·3	1·3	1·4	0·7	0·6	1·7	2·6	0·4	0·6	0·9	3·7
O (diff.)	9·6	7·1	7·9	6·6	7·2	11·0	9·9	10·6	6·6	7·0	6·1	7·0	10·6	10·6	8·5	8·8	22·9	21·1	21·3	17·8
C/H ratio	6·8	6·2	6·4	6·2	8·6	8·6	7·9	7·3	8·2	7·6	7·8	7·8	10·1	7·7	8·0	7·7	16·7	18·2	17·0	15·7

conveniently be designated III′. The latter were further resolved into fractions soluble and insoluble in light petroleum (b.p. 40 to 60°) corresponding closely with the fractions I and II of the extract from bituminous coals, except that (as might be expected) their oxygen contents were higher than those of the last named. Moreover, although fractions IA and B and II were always non-nitrogenous (or practically so), IB and II always contained sulphur. Their ultimate compositions (*vide* Table VI) closely approximated to those of the corresponding fractions from the Morwell and Canadian brown coals previously examined*; and their low C/H ratios (with one exception all between 7·3 and 8·6) indicated a non-benzenoid constitution.

(*e*) *The Residues*—The C/H ratios (15·7 to 18·2) for the "residues" were all notably higher than those for the original dry dewaxed coals (*q.v.*), though below the 19·0 to 19·6 previously obtained for the corresponding "residues" from the Morwell and Canadian brown coals; and, as will be shown in a subsequent paper, like the latter, they were largely benzenoid in character.

THE BENZENE PRESSURE-EXTRACTION OF A TURRAUN IRISH PEAT

In view of the results obtained with brown coals, it was thought advisable to carry out a similar benzene pressure-extraction of a typical peat, and for this purpose a well-rotted sample of Irish peat, supplied to us through the Fuel Research Board by the Turraun Peat Company, was selected.

The sample reached us in an air-dried condition ($H_2O = 13\%$), but after the completion of its drying *in vacuo* at 105°, and deduction of its ash content (about 3%), the anhydrous and ashless peat substance contained :—

$$C = 57 \cdot 4, H = 5 \cdot 3, N = 1 \cdot 1, S = 0 \cdot 9, \text{and } O\,(\text{diff.}) = 35 \cdot 3\%.$$

It contained also 3·1% of wax ($C = 74 \cdot 3$, $H = 10 \cdot 2$, $O = 15 \cdot 5\%$) extractable by boiling benzene at atmospheric pressure. On further benzene pressure-extraction up to 750 lbs per sq in, during which some water and carbon dioxide were eliminated, the "dewaxed" peat substance yielded nearly 19% of total extract of much the same character as the extracts similarly obtained from brown coals; and like them it could be resolved, by the procedure already described, into fractions closely resembling the corresponding ones for brown coals. There was, in fact, little difference between the peat and brown coal fractions. The percentage yields on the dry peat substance are shown in Table VII.

---

* 'Proc. Roy. Soc.,' A, vol. 120, p. 537 (1928).

TABLE VII

Fractions of the benzene pressure-extract

Montan wax	Bases	IA	IB	II	III′ and IV′	Tarry substances: Soluble in ether	Tarry substances: Insoluble in ether
3·1	0·5	3·6	2·5	1·7	4·4	1·0	4·5

Fractions III′ and IV′ (like the corresponding fractions from brown coal) were composed of complex phenolic bodies, and the "tarry substances" formed during their extractions from benzene solution by means of aqueous alkaline solution also closely resembled the corresponding substances obtained from the brown coals.

The ashless residue after the benzene pressure-extraction contained :—

$$C = 69{\cdot}6,\ H = 4{\cdot}0,\ N = 1{\cdot}8,\ S = 1{\cdot}4, \text{ and } O = 23{\cdot}2\%.$$
$$\text{Ratio } C/H = 17{\cdot}4,$$

and it was also largely benzenoid in character.

The investigation as a whole thus supports the view that fractions III and IV of the benzene pressure extracts of bituminous coals have probably originated in the phenolic bodies comprising fractions III′ and IV′ of the benzene pressure-extract for peats and brown coals. The development of the benzenoid structure of the main organic substance throughout the lignin-peat-coal series will be discussed in a subsequent paper.

In conclusion, we desire to thank the Fuel Research Board of the Department of Scientific and Industrial Research for grants which have enabled the investigations to be carried out.

The Catalysis by Palladium of the Union of Hydrogen and Oxygen

A New Phenomenon of Contact Catalysis

By D. L. CHAPMAN, M.A., F.R.S., Fellow of Jesus College, Oxford, and G. GREGORY, B.A., Jesus College, Oxford

(*Received July* 10, 1934)

Researches conducted by Hughes and Bevan,* by Chapman, Ramsbottom, and Trotman,† and by Chapman and Hall‡ on the catalysis of the union of hydrogen and oxygen by nickel and silver lend support to the view that the reaction in both cases proceeds by the alternate oxidation and reduction of the metal surface. This theory was proposed more than a century ago by de la Rive and Harcet§ to account for the catalysis of hydrogen and oxygen by platinum.

It is by no means certain that the mechanism of the reaction in question is the same when catalysed by all metals. Thus, in the absence of evidence to the contrary it might be thought probable that a metal such as palladium, which has a strong affinity for hydrogen, would promote the formation of steam by the reverse process, namely, by the oxidation of hydrogen adsorbed on its surface. However, the experiments which we have performed with this metal support the hypothesis of de la Rive and Harcet, and show that the portion of the surface covered with adsorbed hydrogen is catalytically inoperative. Furthermore, when the metal has been subjected to suitable pre-treatment it does not immediately catalyse the union of hydrogen and oxygen when brought into contact with electrolytic gas, but only does so after it has been left in contact with electrolytic gas for considerable periods of time. There is a long inert period or "period of induction" during which we believe the metal to be completely covered with a protective layer of adsorbed hydrogen.

EXPERIMENTAL

The essential parts of the apparatus are depicted in fig. 1. A similar apparatus had been previously used by Corkhill and Morgan in an unpublished research on the catalysis of the same reaction by platinum.

---

* 'Proc. Roy. Soc.,' A, vol. 117, p. 100 (1927).

† 'Proc. Roy. Soc.,' A, vol. 107, p. 92 (1925).

‡ 'Proc. Roy. Soc.,' A, vol. 124, p. 478 (1929).

§ 'Ann. Chim. Phys.,' vol. 39, p. 328 (1828).

The reaction vessel A, of thick walled quartz glass of 3·4 cm diameter and 18 cm long, communicated by means of the wide quartz tube B with the quartz U-tube C. Connexion with the glass apparatus was made with the ground joint D, which was luted on with a mixture of three parts of metaphosphoric acid and one part of orthophosphoric acid, the mixture being solid at the temperature of the laboratory, but softening at about 80° C. D was surrounded with mercury to prevent the lute absorbing moisture from the air. Beyond D was a U-tube, E, and a mercury seal, F. The rest of the apparatus communicating with the left-hand limb of the seal F was essentially the same as that used by Hughes and Bevan, and Chapman and Hall, and comprised a pumping system, McLeod pressure gauge, gas reservoirs and apparatus for the preparation and purification of hydrogen and oxygen. The quartz tube A, which contained the palladium, could be heated in an electric furnace M. The furnace was supported on a carriage, on rails permitting easy removal. When in use the furnace was always kept at the temperature of 700° C.

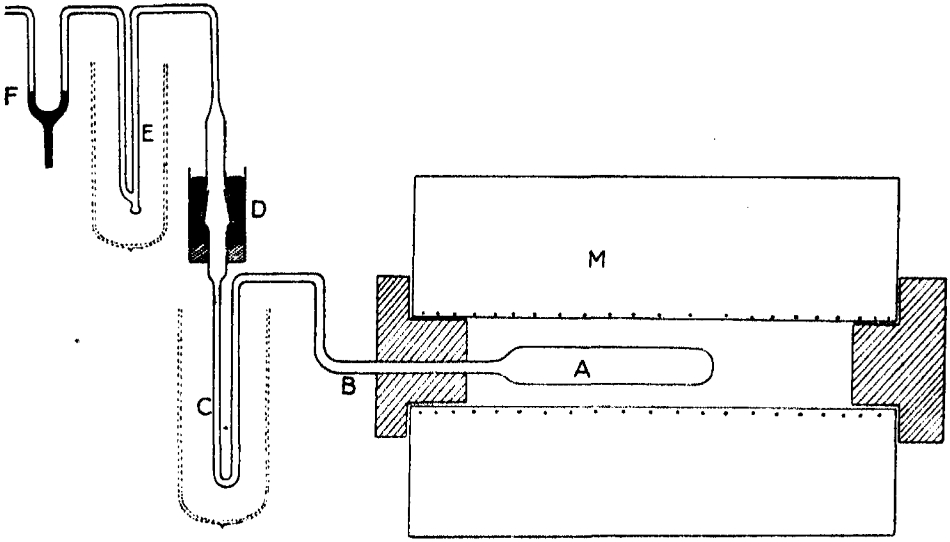

FIG. 1

The oxygen, prepared by heating re-crystallized potassium permanganate, was purified by leaving it in contact with sticks of potash enclosed in the container, and by its being passed through a U-tube surrounded with liquid air.

The hydrogen, prepared from arsenic-free zinc and sulphuric acid, was washed with caustic soda solution and purified by allowing it to diffuse through the walls of a palladium tube into the apparatus.

The U-tubes, E and C, were always kept at the temperature of liquid air to condense the water formed during an experiment, and to prevent mercury vapour from entering A and poisoning the palladium surface. The total volume of the reaction vessel, the U-tubes, the connecting tubing and the McLeod gauge was 682 ccs.

THE CATALYTIC ACTIVITY OF THE PALLADIUM

The palladium in the form of foil was the purest procurable. Its total surface was 40 square millimetres. With this surface the catalysis proceeded at a convenient rate at temperatures between 16° and 19° C. In the experiments the initial pressure of the mixture of hydrogen and oxygen was generally about 0·1 mm of mercury. At and below this pressure the water vapour diffused rapidly to the liquid air traps, and the McLeod gauge therefore measured with a sufficient degree of accuracy the pressure of the dry gas.

Preliminary experiments demonstrated that the activity of the catalyst depends in a surprising degree on its pre-treatment, although the same pre-treatment results in the surface having approximately the same activity. Palladium which has been heated in oxygen is much more active than that which has been heated in hydrogen.

THE PERIOD OF INERTNESS

On one occasion after the palladium had been kept at a temperature of 700° C in a high vacuum for several hours we were surprised to find that the metal had completely lost the property of catalysing the union of hydrogen and oxygen at the temperature of the laboratory. The pressure of the electrolytic gas remained quite steady for over two hours. It was left in this condition late in the evening ; but on taking a reading on the morning of the next day it was found that the electrolytic gas had entirely disappeared. Combination had started during the night after a long initial mestastable period.

Subsequent investigation showed that the same specimen of metal could by suitable pre-treatment always be brought into a condition with which this phenomenon of " induction " could be demonstrated. The best method of showing the phenomenon is to heat the metal for about one hour in hydrogen, and then for six or seven hours in a high vacuum at a temperature of 700° C. With the metal thus treated, induction periods of the order of 90 minutes have been observed. If the metal is heated for a longer time in vacuum; subsequent induction periods were still longer. Thus an induction period measured after the palladium had been heated in a vacuum for 14 hours was of 36 hours' duration.

All long induction periods are of similar character. There is no fall of pressure for a long time, but as soon as the pressure begins to fall its acceleration is very rapid, and the maximum rate of formation of steam is reached in a few minutes. Two typical induction periods are graphed as dotted curves IV and V in fig. 2. If, after the period of inertness has ended, the gas is pumped out of the apparatus and a fresh supply of electrolytic gas introduced, combination starts almost immediately at the former final rate.

For brevity we shall describe a surface which will not catalyse the combination of hydrogen and oxygen until it has been in contact with the mixed gases for some time as temporarily inert.

A surface which has been made temporarily inert by heating it in hydrogen and then in a vacuum, and has regained its activity by being exposed to electrolytic gas, can be again rendered temporarily inert by exposing it to an atmosphere of cold hydrogen. Examples of three induction periods observed after such treatment are recorded below.

In experiment 157 the palladium had been exposed to hydrogen for 1½ hours ; in experiment 166 the palladium had been exposed to hydrogen for 3 hours ; in experiment 185 the palladium had been exposed to hydrogen for 4½ hours.

Δ is the average fall in pressure in the five minutes preceding the reading.

TABLE I

No.	Time mins	Pressure in cm × 10^3	Δ	No.	Time mins	Pressure in cm × 10^3	Δ
157	1	8·410	—	166	1	10·180	—
	26	8·371	—		331	10·220	0·000
	56	8·390	0·002		386	8·058	0·197
	61	8·351	0·039		391	7·586	0·472
	66	8·233	0·118		396	7·153	0·433
	71	7·939	0·294		411	6·052	0·367
	76	7·643	0·296		421	5·404	0·324
	81	7·290	0·353				
	86	6·956	0·334	185	1	9·550	—
	96	6·269	0·344		6	9·530	0·020
	106	5·581	0·344		11	9·471	0·059
	116	4·933	0·325		16	7·506	1·965
	126	4·284	0·325		21	5·837	1·669
	136	3·694	0·295		26	4·067	1·778

An active surface which has been made temporarily inert by long exposure to cold hydrogen can again be rendered active by exposing it to oxygen for a short time. This fact was demonstrated by a large number of experiments performed in the following way : after the surface had been exposed to cold hydrogen for several hours the hydrogen was pumped out of the apparatus, and the surface shown to be inactive by testing it with electrolytic gas. Before reversion to activity had occurred, the reaction vessel was exhausted and oxygen at 0·1 mm pressure introduced, the oxygen being left in contact with the metal for different periods of time. After the removal of the oxygen the surface was always found to be active on testing it with electrolytic gas.

Four experiments are recorded in Table II.

TABLE II

No.	Pre-treatment	Rate—Pressure in cm × 10^3 at times, mins.			
		1	6	11	21
170	Cold H_2 for 12 hours ……	Induction period followed for 66 minutes.			
171	Cold O_2 for 3 hours ………	8·45	7·90	7·52	6·84
172	Cold H_2 for 18 hours ……	Induction period of 6 hours.			
206	Cold H_2 for 12 hours ……	Induction period followed for 5 hours.			
207	Cold O_2 for 1 hour…………	7·70	7·23	6·80	—
208	Cold H_2 for 12 hours ……	Induction period followed for 5½ hours.			
209	Cold O_2 for 15 minutes ….	5·34	4·74	4·24	
219	Cold H_2 for 12 hours ……	Induction period followed for 36 minutes.			
220	Cold O_2 for 15 minutes ……	10·38	9·98	9·73	9·04

A surface which has been rendered temporarily inert by heating the metal in hydrogen and then in a vacuum for a long time does not always revert to the active condition on exposing it to oxygen, as the following experiment, Table III, shows :—

TABLE III

No.	Pre-treatment	Rate
239	Heated in H_2 for 3 hours ; *in vacuo* 14 hours	No reaction for 46 minutes.
240	Exposed to cold O_2 for 12 hours ……….	Induction period of 36 hours.

We suggest as the cause of the observed temporary inertness a compact layer of adsorbed hydrogen covering the whole surface, which acts as a protective covering or " poison," and must be removed, at least partially, before catalysis by the process of alternate oxidation and reduction can occur. However, to account for some of the effects observed, other postulates must be made, though this cannot be done at present without ambiguity. The following suggestions are therefore put forward as working hypotheses which need to be further tested.

It seems necessary to assume that palladium which has been reduced with hydrogen, and subsequently heated for a long time in a high vacuum, has an abnormally great tendency to condense hydrogen on its surface. As, however, the surface ultimately reverts to an active condition in the presence of electrolytic gas, we must suppose that there are weak spots in the protective sheath of hydrogen through which oxygen molecules can penetrate under favourable conditions and form, with the palladium, an oxide of the metal. When this oxide is reduced by the surrounding hydrogen atoms the energy evolved might be sufficient to throw the atoms of palladium in the vicinity into a more normal configuration, in which the tendency to adsorb hydrogen did not considerably exceed the tendency to form oxide. In this way the area capable of attack by oxygen would grow, and its rate of growth would increase as the reaction proceeded.

It is not difficult to imagine how a surface of palladium left in contact with pure hydrogen would ultimately become covered with a compact layer of hydrogen.

Pease and Taylor[*] observed an " induction period " in the reduction of copper oxide by hydrogen, the rate of reduction being comparatively small until copper made its appearance, and they have suggested for the phenomenon an explanation similar to that given above.

We have obtained corroborative evidence of the assumption that catalysis does not proceed on that portion of the surface which is covered by adsorbed hydrogen from determinations of the rates of reaction, using mixtures of hydrogen and oxygen of varying composition. Using electrolytic gas, the rate of reaction is of an order between zero and the first, pointing to inhibition by one or other of the gases. That the gas which acts inhibitively is hydrogen was proved conclusively by the fact that the addition of hydrogen to electrolytic gas results in a pronounced reduction in the rate of reaction. The addition of oxygen has the opposite effect.

To illustrate the inhibitive effect of hydrogen, we have tabulated in Table IV the rates observed with mixtures in which the concentration of the oxygen was approximately the same, but that of the hydrogen different.

The readings are in centimetres of the McLeod gauge manometer, 1 cm fall of the McLeod gauge manometer corresponding to the removal of $1\cdot575 \times 10^{-7}$ mols of gas from the apparatus and to a fall of pressure of $3\cdot93 \times 10^{-4}$ cm of mercury, the volume of the apparatus being 682 cc. Δ is the fall of pressure in the 5 minutes preceding the reading.

---

[*] 'J. Amer. Chem. Soc.,' vol. 43, p. 3173 (1921); vol. 44, p. 1637 (1922).

TABLE IV

	Pressure of oxygen	Pressure of hydrogen	Δ
A	2·13	13·67	0·50
	2·16	4·32	1·25
B	1·31	12·02	0·38
	1·35	2·70	1·20
C	3·57	17·03	1·00
	3·63	7·25	1·55
D	2·98	15·85	0·75
	2·98	5·95	1·53
E	4·04	17·79	1·25
	4·04	8·09	1·68
F	7·63	15·27	0·40
	7·62	1·34	1·50

To ensure constancy of activity while the above determinations of rates were being made, the procedure adopted was as follows : starting at a pressure of 0·1 mm, several series of rates were taken until the measurements showed that the surface had arrived at a state of constant activity. Then two series of measurements were made with mixtures of hydrogen and oxygen of the same composition, but differing from that of electrolytic gas. Finally, it was shown with electrolytic gas that the activity of the surface had not altered.

The curves I, II, and III, fig. 2, show the consecutive readings made with mixtures of the respective compositions $2H_2 : O_2$; $H_2 : 2O_2$; $4H_2 : O_2$. It will be observed that with the mixture which contains more hydrogen than electrolytic gas the rates fall off gradually as the electrolytic gas disappears, whereas with the mixture which contains an excess of oxygen the rates remain constant until the electrolytic gas has been almost completely consumed. With the latter mixture a distinct increase of rate has been recorded on several occasions just before all the hydrogen had disappeared.

SUMMARY AND CONCLUSIONS

The mechanism of the catalysis of the union of hydrogen and oxygen by palladium is mainly one of alternate oxidation of metal and reduction of the oxide.

Adsorbed hydrogen does not react appreciably with oxygen at the temperature of the laboratory, and therefore adsorbed hydrogen can render the surface inoperative as a catalyst of the reaction in question.

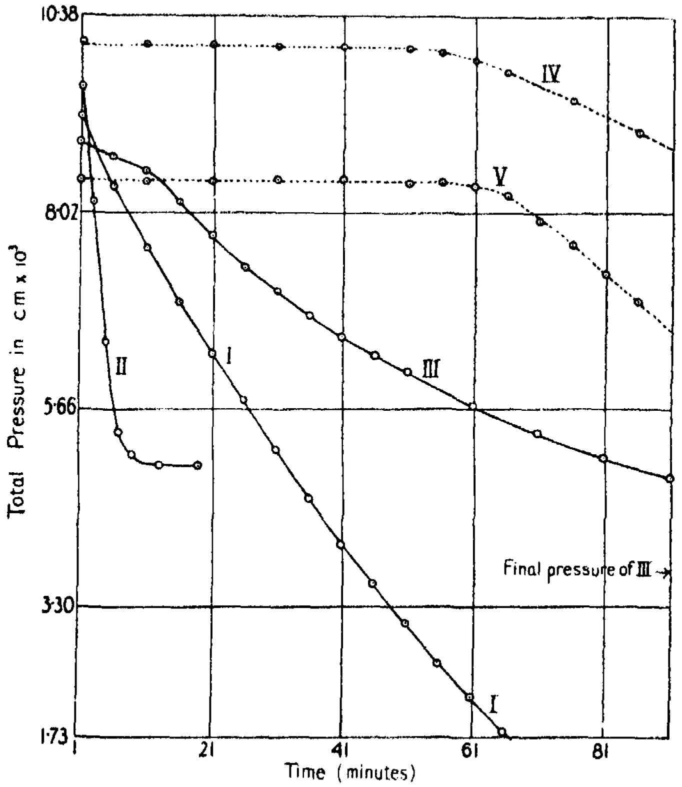

FIG. 2

By suitable treatment, the palladium can be rendered temporarily inert as a catalyst of the hydrogen and oxygen reaction. We believe that the temporary inertness is due to a compact layer of adsorbed hydrogen which prevents the oxygen molecules from reaching the surface.

In agreement with the above conclusions kinetic measurements show that hydrogen is an inhibitor and oxygen an accelerator of the reaction.

On the Explicit Solution of Certain Difference Equations

By L. M. MILNE-THOMSON

(*Communicated by Harold Jeffreys, F.R.S.—Received March* 28, 1934)

NOTATIONS

The operators used in this paper have the following definitions :—

$$\underset{\omega}{\Delta}\, u_x = \frac{u_{x+\omega} - u_x}{\omega},$$

$$\underset{\omega}{\nabla}\, u_x = \frac{u_{x+\omega} + u_x}{2}.$$

The summation* operator has the property that, if

$$u_x = \overset{x}{\mathcal{S}} f(t) \underset{\omega}{\Delta} t,$$

then

$$\underset{\omega}{\Delta}\, u_x = f(x),$$

and

$$\lim_{\omega \to 0} \overset{x}{\mathcal{S}} f(t) \underset{\omega}{\Delta} t = \int^x f(t)\, dt.$$

We also note that

$$\lim_{\omega \to 0} \underset{\omega}{\Delta}\, u_x = \frac{du_x}{dx}, \quad \lim_{\omega \to 0} \underset{\omega}{\nabla}\, u_x = u_x.$$

These notations are all due to N. E. Nörlund, their use allows us to consider general difference equations and to infer the corresponding results for differential equations.

THEOREM I

The difference equation

$$\overset{2}{\underset{\omega}{\Delta}}\, y_x + p(x) \underset{\omega}{\Delta}\, y_x + q(x)\, y_x = 0 \tag{1}$$

is transformed by the substitution

$$y_x = u_x \exp\left[\frac{1}{\omega} \overset{x-\omega}{\mathcal{S}} \log\left(1 - \tfrac{1}{2}\omega p(t)\right) \underset{\omega}{\Delta} t\right] \tag{2}$$

---

* For a brief account of the complete definition and properties of this operator, see Milne-Thomson, " Calculus of Finite Differences," London (1933), Chapter VIII.

into the form

$$\overset{2}{\underset{\omega}{\Delta}}\, u_x = \mathrm{I}\,(x)\, u_x, \tag{3}$$

where

$$\mathrm{I}\,(x) = \frac{\tfrac{1}{2}\underset{\omega}{\Delta}\, p\,(x-\omega) + \tfrac{1}{4}p\,(x)\,p\,(x-\omega) - q\,(x)}{(1-\tfrac{1}{2}\omega p\,(x-\omega))\,(1-\tfrac{1}{2}\omega p\,(x))}\,. \tag{4}$$

Proof—In the given equation (1) substitute

$$y_x = u_x v_x,$$

Then by the analogue of Leibniz' theorem

$$\underset{\omega}{\Delta}\, y_x = u_x \underset{\omega}{\Delta}\, v_x + v_{x+\omega} \underset{\omega}{\Delta}\, u_x,$$

$$\overset{2}{\underset{\omega}{\Delta}}\, y_x = u_x \overset{2}{\underset{\omega}{\Delta}}\, v_x + 2 \underset{\omega}{\Delta}\, u_x \underset{\omega}{\Delta}\, v_{x+\omega} + v_{x+2\omega} \overset{2}{\underset{\omega}{\Delta}}\, u_x.$$

The coefficient of $\underset{\omega}{\Delta}\, u_x$ in the transformed equation will therefore vanish if

$$\underset{\omega}{\Delta} \log v_{x+\omega} = \frac{1}{\omega} \log\,[1-\tfrac{1}{2}\omega p\,(x)],$$

and therefore by summation

$$v_{x+\omega} = \exp\left[\frac{1}{\omega} \overset{x}{\mathop{\mathcal{S}}} \log\,(1-\tfrac{1}{2}\omega p\,(t))\, \underset{\omega}{\Delta} t\right]. \tag{5}$$

Changing $x+\omega$ to x we have the required transformation (2), and the given equation then assumes the form (3), where

$$\mathrm{I}\,(x) = \frac{\overset{2}{\underset{\omega}{\Delta}}\, v_x + p\,(x) \underset{\omega}{\Delta}\, v_x + q\,(x)\, v_x}{-\,v_{x+2\omega}}\,.$$

Now

$$\underset{\omega}{\Delta}\, v_x = -\tfrac{1}{2} v_x\, p\,(x-\omega),$$

and therefore

$$\overset{2}{\underset{\omega}{\Delta}}\, v_x = -\tfrac{1}{2} v_x \underset{\omega}{\Delta}\, p\,(x-\omega) + \tfrac{1}{4} v_x\, p\,(x)\, p\,(x-\omega).$$

It follows that

$$\mathrm{I}\,(x) = [\tfrac{1}{2} \underset{\omega}{\Delta}\, p\,(x-\omega) + \tfrac{1}{4} p\,(x)\, p\,(x-\omega) - q\,(x)]\; v_x / v_{x+2\omega}. \tag{6}$$

Now from (5)

$$\log \frac{v_{x+2\omega}}{v_x} = \frac{1}{\omega} \mathop{\mathcal{S}}^{x+\omega} \log (1 - \tfrac{1}{2}\omega p(t)) \underset{\omega}{\Delta} t$$
$$- \frac{1}{\omega} \mathop{\mathcal{S}}^{x-\omega} \log (1 - \tfrac{1}{2}\omega p(t)) \underset{\omega}{\Delta} t$$
$$= 2 \underset{\omega}{\Delta} \underset{\omega}{\nabla} \mathop{\mathcal{S}}^{x-\omega} \log (1 - \tfrac{1}{2}\omega p(t)) \underset{\omega}{\Delta} t$$
$$= \log (1 - \tfrac{1}{2}\omega p(x - \omega)) + \log (1 - \tfrac{1}{2}\omega p(x)), \tag{7}$$

and (4) therefore follows from (6) and (7). This completes the proof.

When $\omega \to 0$ we get the corresponding result for the differential equation of the second order, namely, that the equation

$$\frac{d^2y}{dx^2} + p(x)\frac{dy}{dx} + q(x)\,y = 0 \tag{8}$$

is transformed by the substitution

$$y = u \exp\left[- \int^x \tfrac{1}{2} p(t)\, dt \right] \tag{9}$$

into the form

$$\frac{d^2u}{dx^2} = \mathrm{I}_0(x) \,.\, u, \tag{10}$$

where

$$\mathrm{I}_0(x) = \tfrac{1}{2}\frac{dp(x)}{dx} + \tfrac{1}{4}(p(x))^2 - q(x). \tag{11}$$

The function I (x) defined by (4) will be called the *discriminant* of the difference equation (1). All second order linear difference equations with the same discriminant are equivalent in the sense that their solution may be made to depend upon that of the canonical form (3).

It should be observed that the discriminant is a function of the two variables x and ω when the equation is presented in the form (1). If we start with the canonical form (3) we can suppose I (x) to be independent of ω.

When the discriminant vanishes the solution of (3) is immediate. We have, in fact,

$$u_x = \varpi_1 x + \varpi_2,$$

where ϖ_1 and ϖ_2 are arbitrary periodic functions; that is to say, arbitrary periodic functions of x with period ω. We have therefore for the complete solution of (1)

$$y_x = (\varpi_1 x + \varpi_2) \exp\left[\frac{1}{\omega} \mathop{\mathcal{S}}^{x-\omega} \log (1 - \tfrac{1}{2}\omega p(t)) \underset{\omega}{\Delta} t \right].$$

When the discriminant is constant we can also complete the solution of (1) for if

$$\mathrm{I}(x) = a^2$$

we have

$$u_x = (1 + a\omega)^{x/\omega}\,\varpi_1 + (1 - a\omega)^{x/\omega}\,\varpi_2, \tag{12}$$

and (2) then gives the solution. The form (12) will also hold if a is a periodic function.

When $\omega \to 0$ the form (12) gives

$$u_x = e^{ax}\,c_1 + e^{-ax}\,c_2,$$

where c_1 and c_2 are now arbitrary constants, for a periodic function with zero period is a constant, and this is the general solution of (10).

THEOREM II

The difference equation

$$\overset{2}{\underset{\omega}{\Delta}}\, u_x = \mathrm{I}(x)\, u_x \tag{3}$$

is transformed by the substitution

$$w_x = \frac{\underset{\omega}{\Delta}\, u_x}{u_x} \tag{13}$$

into the first order equation

$$\underset{\omega}{\Delta}\, w_x + w_x w_{x+\omega} = \mathrm{I}(x). \tag{14}$$

Proof—

$$\underset{\omega}{\Delta}\, w_x = \frac{u_{x+\omega}\,\overset{2}{\underset{\omega}{\Delta}}\, u_x - \underset{\omega}{\Delta}\, u_x\,\underset{\omega}{\Delta}\, u_{x+\omega}}{u_x u_{x+\omega}}.$$

Therefore

$$\frac{\overset{2}{\underset{\omega}{\Delta}}\, u_x}{u_x} = \underset{\omega}{\Delta}\, w_x + w_x w_{x+\omega},$$

which gives the required result.

When $\omega \to 0$ equation (14) becomes

$$\frac{d^2w}{dx^2} + w^2 = \mathrm{I}(x), \tag{15}$$

which is a particular case of Riccati's differential equation. We shall therefore refer to (14) as the canonical form of Riccati's (difference) equation. It will be proved later (Theorem VII) that the general form of difference equation corresponding to Riccati's differential equation can be reduced to the canonical form (14).

THEOREM III

The canonical form of Riccati's (difference) equation

$$\underset{\omega}{\Delta} w_x + w_x w_{x+\omega} = \mathrm{I}(x) \tag{14}$$

has a uniquely defined formal solution $\phi(x, \omega)$ *which is defined by the continued fraction*

$$1 + \omega\phi(x, \omega) = \frac{1 - \omega^2 \mathrm{I}(x)}{2 -}\,\frac{1 - \omega^2 \mathrm{I}(x + \omega)}{2 -}\,\frac{1 - \omega^2 \mathrm{I}(x + 2\omega)}{2 -}\dots \tag{16}$$

Proof—We have from (14)

$$w_{x+\omega} - w_x + \omega w_x w_{x+\omega} = \omega \mathrm{I}(x)$$

and therefore

$$\omega w_x = -1 + \frac{1 - \omega^2 \mathrm{I}(x)}{1 - \omega w_{x+\omega}}.$$

By repeated application of this recurrence relation we obtain

$$\omega w_x = -1 + \frac{1 - \omega^2 \mathrm{I}(x)}{2 -}\,\frac{1 - \omega^2 \mathrm{I}(x + \omega)}{2 -}\,\frac{1 - \omega^2 \mathrm{I}(x + 2\omega)}{2 -}\dots$$

$$= -1 + 1 + \omega\phi(x, \omega) \qquad \text{from (16)}$$

and therefore $\phi(x, \omega)$ is a formal solution. To justify the notation we observe that, when $\omega = 0$, the continued fraction reduces to unity.

Corollary—The differential equation

$$\frac{dw}{dx} + w^2 = \mathrm{I}(x)$$

has the particular solution

$$w = \lim_{\omega \to 0} \phi(x, \omega) = \phi(x), \text{ say.}$$

To state sufficient conditions for convergence of the continued fraction is simple for it has been shown by Pringsheim* that the continued fraction

$$\frac{b_1}{a_1 +}\,\frac{b_2}{a_2 +}\,\frac{b_3}{a_3 +}\dots$$

---

* Perron, "Die Lehre von den Kettenbrüchen," 2nd ed., Leipzig, 1929, § 53.

is convergent if

$$|a_\nu| \geqslant |b_\nu| + 1, \quad \nu = 1, 2, 3, \ldots$$

a condition which is satisfied in the case of (16) provided that

$$|1 - \omega^2 \mathrm{I}(x + \nu\omega)| \leqslant 1, \quad \nu = 0, 1, 2, 3, \ldots \tag{17}$$

Moreover, the convergence is uniform provided that the series

$$\sum_{\nu=1}^{\infty} (|a_1| - 1)(|a_2| - 1)\ldots(|a_\nu| - 1)$$

is uniformly divergent which is certainly true in the present case since $a_\nu = 2$.

Thus, if x and ω lie in regions in which condition (17) is satisfied, $\phi(x, \omega)$ then gives a particular solution of (14) which is a continuous function of x and ω. It is evident that the portion of the x plane in which x varies must contain all the points $x + \nu\omega$, $\nu = 0, 1, 2, \ldots$. These conditions would be realized in particular when $\mathrm{I}(x)$ is representable by a series of inverse factorials and the real part of x is taken sufficiently great in the half plane of convergence. Condition (17) is merely a sufficient condition and it may be possible to extend the scope of Theorem III to cases where the continued fraction diverges by employing a suitable summation method for the fraction. This is another branch of enquiry which we shall exclude from the present paper by supposing that our remarks apply only to those forms of $\mathrm{I}(x)$ for which Theorem III yields a solution.*

THEOREM IV

The general solution of the canonical form of Riccati's equation can be expressed in terms of the solution defined in Theorem III.

Proof—In (14) put

$$w_x = \phi(x, \omega) + \frac{1}{z_x},$$

The equation then becomes

$$\mathop{\Delta}_{\omega} z_x - z_x \frac{\phi(x, \omega) + \phi(x + \omega, \omega)}{1 - \omega\phi(x + \omega, \omega)} = \frac{1}{1 - \omega\phi(x + \omega, \omega)},$$

---

* A continued fraction into which ours can easily be transformed has been considered, in connection with the second order linear difference equation, by Watson ('Proc. Lond. Math. Soc.,' vol. 8, p. 125 (1910) ; vol. 10, p. 211 (1912)). Reference should be made to these papers for a development in considerable detail of asymptotic properties of this type of continued fraction.

which is a linear equation of the first order whose general solution is*

$$z_x = \left\{ \exp\left[\frac{1}{\omega} \mathop{\mathcal{S}}^{x} \log \frac{1+\omega\phi(t,\omega)}{1-\omega\phi(t+\omega,\omega)} \underset{\omega}{\Delta} t \right] \right\}$$

$$\times \left\{ \varpi + \mathop{\mathcal{S}}^{x} \left(\frac{1}{1-\omega\phi(t+\omega,\omega)} \exp\left[-\frac{1}{\omega} \mathop{\mathcal{S}}^{t+\omega} \log \frac{1+\omega\phi(p,\omega)}{1-\omega\phi(p+\omega,\omega)} \underset{\omega}{\Delta} p \right] \underset{\omega}{\Delta} t \right) \right\}, \tag{18}$$

where ϖ is an arbitrary periodic function.

If we now put

$$h(x) = \exp\left[\frac{1}{\omega} \mathop{\mathcal{S}}^{x} \log \frac{1-\omega\phi(t+\omega,\omega)}{1+\omega\phi(t,\omega)} \underset{\omega}{\Delta} t \right], \tag{19}$$

we obtain

$$w_x = \phi(x,\omega) + \frac{h(x)}{\varpi + \mathop{\mathcal{S}}^{x} \dfrac{h(t+\omega)}{1-\omega\phi(t+\omega,\omega)} \underset{\omega}{\Delta} t}, \tag{20}$$

which is the required general solution.

Theorem V

The general solution of the canonical form of Riccati's equation can be expressed by means of the single function

$$k(x) = \mathop{\mathcal{S}}^{x} \frac{h(t)}{1-\omega\phi(t,\omega)} \underset{\omega}{\Delta} t, \tag{21}$$

where $h(t)$ is given by (19), *in the form*

$$w_x = -\frac{1}{2} \frac{\overset{2}{\underset{\omega}{\Delta}} k(x)}{\underset{\omega}{\nabla}\underset{\omega}{\Delta} k(x)} + \frac{\underset{\omega}{\Delta} k(x) \underset{\omega}{\Delta} k(x+\omega)}{[\varpi + k(x+\omega)] \underset{\omega}{\nabla}\underset{\omega}{\Delta} k(x)}. \tag{22}$$

Proof—We have

$$\underset{\omega}{\Delta} k(x) = \frac{h(x)}{1-\omega\phi(x,\omega)}. \tag{23}$$

Taking logarithms and using (19) we obtain

$$\frac{1}{\omega} \mathop{\mathcal{S}}^{x} \log \frac{1-\omega\phi(t+\omega,\omega)}{1+\omega\phi(t,\omega)} \underset{\omega}{\Delta} t$$

$$= \log(1-\omega\phi(x,\omega)) + \log \underset{\omega}{\Delta} k(x).$$

---

* Milne-Thomson, 'Proc. Camb. Phil. Soc.,' vol. 29, p. 373 (1933).

Operating with $\underset{\omega}{\Delta}$ we get

$$\frac{1-\omega\phi(x,\,\omega)}{1+\omega\phi(x,\,\omega)}=\frac{\underset{\omega}{\Delta}\,k\,(x+\omega).}{\underset{\omega}{\Delta}\,k\,(x)}$$

Thus

$$\phi(x,\,\omega)=-\tfrac{1}{2}\,\frac{\underset{\omega}{\overset{2}{\Delta}}\,k\,(x),}{\underset{\omega}{\nabla}\,\underset{\omega}{\Delta}\,k\,(x)}, \tag{24}$$

and therefore

$$\begin{aligned}1-\omega\phi(x,\,\omega)&=\frac{2\underset{\omega}{\nabla}\,\underset{\omega}{\Delta}\,k\,(x)+\omega\underset{\omega}{\overset{2}{\Delta}}\,k\,(x)}{2\underset{\omega}{\nabla}\,\underset{\omega}{\Delta}\,k\,(x)}\\&=\frac{\underset{\omega}{\Delta}\,k\,(x+\omega).}{\underset{\omega}{\nabla}\,\underset{\omega}{\Delta}\,k\,(x)}\end{aligned} \tag{25}$$

Now from (20) and (23)

$$w_x=\phi(x,\,\omega)+\frac{[1-\omega\phi(x,\,\omega)]\;\underset{\omega}{\Delta}\,k\,(x).}{\varpi+k\,(x+\omega)}$$

Using (24) and (25) the required result (22) follows at once.

THEOREM VI

The solution of the general homogeneous linear difference equation of the second order can be expressed in terms of the function k (x) of Theorem V which depends solely on the discriminant of the given equation.

Taking equation (1) we have from Theorem II (13)

$$\underset{\omega}{\Delta}\log u_x=\frac{1}{\omega}\log(1+\omega w_x),$$

and therefore

$$u_x=\varpi'\exp\Big[\mathop{\mathrm{S}}^{x}\frac{1}{\omega}\log(1+\omega w_t)\,\underset{\omega}{\Delta t}\Big],$$

where ϖ' is an arbitrary periodic function, and therefore from Theorem I (2)

$$\begin{aligned}y_x=\varpi'\exp\Big[\frac{1}{\omega}&\mathop{\mathrm{S}}^{x-\omega}\log\big(1-\tfrac{1}{2}\,\omega p(t)\big)\,\underset{\omega}{\Delta t}\\&+\frac{1}{\omega}\mathop{\mathrm{S}}^{x}\log(1+\omega w_t)\,\underset{\omega}{\Delta t}\Big].\end{aligned} \tag{26}$$

If in this result we substitute the value of w_x from Theorem V (22) we have y_x expressed in terms of $k(x)$ and of course certain summations. Since w_x contains an arbitrary periodic function ϖ the value of y_x contains two arbitrary periodic functions.

It will be seen that the case of the difference equation is somewhat complex. The case of the differential equation is comparatively simple.

Taking the equation (8) we have from (26) when $\omega \to 0$

$$y = a \exp \left[\int^x \left(-\tfrac{1}{2} p(t) + w_t \right) dt \right],$$

where from (22)

$$w_x = -\tfrac{1}{2} \frac{k''(x)}{k'(x)} + \frac{k'(x)}{b + k(x)},$$

where the primes denote differentiation with respect to x. Here $k(x)$ is obtained from (19) and (21), namely,

$$k(x) = \int^x \exp \left[\int^t -2\phi(t)\, dt \right] dt,$$

where

$$\phi(t) = \lim_{\omega \to 0} \phi(t, \omega).$$

Now

$$w_x = -\tfrac{1}{2} \frac{d}{dx} \log k'(x) + \frac{d}{dx} \log (b + k(x)).$$

Hence

$$\exp \int^x w_t\, dt = \frac{b + k(x)}{\sqrt{k'(x)}},$$

so that

$$y = a \left[\exp \int^x -\tfrac{1}{2} p(t)\, dt \right] [b + k(x)] \Big/ \sqrt{k'(x)},$$

which is the general solution of the general homogeneous linear difference equation of the second order.

THEOREM VII

The solution of the general form of Riccati's difference equation can be effected by the method of Theorem III.

Proof—The general form in question may be written

$$\underset{\omega}{\Delta} y_x = p(x)\, y_x\, y_{x+\omega} + q(x)\, y_x + r(x). \tag{27}$$

The form (14) with which we have hitherto been occupied corresponds to $p(x) = -1, q(x) = 0$. We shall now show that the solution of (27) may be made to depend upon the form (14).

Let

$$y_x = -\frac{\underset{\omega}{\Delta} u_x}{u_x\, p(x)}, \tag{28}$$

Then

$$\underset{\omega}{\Delta} y_x - p(x)\, y_x\, y_{x+\omega} = -\frac{1}{u_x} \underset{\omega}{\Delta} \left(\frac{\underset{\omega}{\Delta} u_x}{p(x)}\right).$$

and therefore the equation becomes

$$\overset{2}{\underset{\omega}{\Delta}} u_x - \left[\frac{p(x+\omega)\, q(x)}{p(x)} + \frac{\underset{\omega}{\Delta} p(x)}{p(x)}\right] \underset{\omega}{\Delta} u_x + p(x+\omega)\, r(x)\, u_x = 0, \tag{29}$$

which is a linear equation of the second order. To this equation we can apply the method of Theorem VI which depends essentially on the application of Theorem III; that is to say, on the canonical type of Riccati's difference equation. The solution of (29) will therefore be given by an expression of the form (26). It will be seen that the periodic function ϖ' of (26) will disappear when we apply the transformation (28) to the solution of (29) so that there is, in fact, only one arbitrary periodic function in the solution.

The same method furnishes a solution of the general Riccati differential equation, namely,

$$\frac{dy}{dx} = p(x)\, y^2 + q(x)\, y + r(x).$$

Explicit forms could easily be given, but they do not essentially differ from those already obtained.

Theorem VIII

The non-linear difference equation of the third order

$$-\frac{1}{2} \frac{\overset{3}{\underset{\omega}{\Delta}} u_x}{\underset{\omega}{\nabla} \underset{\omega}{\Delta} u_{x+\omega}} + \frac{\overset{2}{\underset{\omega}{\Delta}} u_x (\overset{2}{\underset{\omega}{\Delta}} u_x + 2\, \overset{2}{\underset{\omega}{\Delta}} u_{x+\omega})}{4\, \underset{\omega}{\nabla} \underset{\omega}{\Delta} u_x\, \underset{\omega}{\nabla} \underset{\omega}{\Delta} u_{x+\omega}} = \mathrm{I}(x)\,, \tag{30}$$

has the general solution

$$u_x = \frac{\varpi_1\, k(x) + \varpi_2}{\varpi_3\, k(x) + \varpi_4}, \tag{31}$$

where $k(x)$ is given by Theorem V (21) and ϖ_1, ϖ_2, ϖ_3, ϖ_4 are arbitrary periodic functions.

Proof—From (24) we have

$$\phi(x,\,\omega) = -\tfrac{1}{2}\,\frac{\underset{\omega}{\overset{2}{\Delta}}\,k(x)}{\underset{\omega}{\nabla}\,\underset{\omega}{\Delta}\,k(x)},$$

and by Theorem III

$$\underset{\omega}{\Delta}\,\phi(x,\,\omega) + \phi(x,\,\omega)\,\phi(x+\omega,\,\omega) = \mathrm{I}(x). \tag{32}$$

It follows at once by direct substitution in (32) that $k(x)$ is a solution of (30).

If for brevity we write

$$k_s = k(x+s\omega), \quad s = 0, 1, 2, 3,$$

we have, since k_0 satisfies 30,

$$\begin{aligned}\omega^2\mathrm{I}(x)\,(k_2-k_0)\,(k_3-k_1) \\ = -\,(k_3-3k_2+3k_1-k_0)\,(k_2-k_0) \\ +\,(k_2-2k_1+k_0)\,(2k_3-3k_2+k_0),\end{aligned}$$

whence we easily obtain

$$\mathrm{I}(x) = \frac{(k_3-k_0)\,(k_2-k_1)}{\omega^2\,(k_2-k_0)\,(k_3-k_1)} + \frac{3\,(k_3-k_2)\,(k_0-k_1)}{\omega^2\,(k_2-k_0)\,(k_3-k_1)}.$$

The right-hand member is invariant under the substitution

$$\frac{\varpi_1 k(x)+\varpi_2}{\varpi_3 k(x)+\varpi_4},$$

for $k(x)$. It follows that (31) is the general solution of (30), and the theorem is therefore proved.

The interest of this result lies in the fact that the left-hand member of (30) may be regarded as a generalization of the Schwarzian differential invariant, for when $\omega \to 0$ we get

$$-\tfrac{1}{2}\,\frac{u'''}{u'} + \tfrac{3}{4}\,\frac{(u'')^2}{u'^2},$$

which is invariant under the substitution

$$\frac{a_1u+a_2}{a_3u+a_4}.$$

CONCLUSION

If a particular solution of the canonical Riccati's equation could be obtained by inspection, the foregoing results could then be applied to the general solution of the types enumerated. The particular interest of our results is that the algorism of Theorem III renders the matter independent of guesswork and forms a basis for attacking what at first appear to be three independent problems.

SUMMARY

The object of this paper is to reduce to the solution of a single canonical type of Riccati's equation the general solution of the following three classes of difference equations—

(i) Riccati's difference equation.
(ii) The general homogeneous linear difference equation of the second order.
(iii) A certain non-linear difference equation of the third order.

An algorism is given for the solution of the canonical equation and explicit solutions are then obtained for the general solution of the above three classes of equations. The general solutions of the corresponding types of differential equation emerge as particular cases.

The Diamagnetic Susceptibilities of Salts forming Ions with Inert Gas Configurations

Part I—The Halides of Sodium and Potassium

By F. E. HOARE, Ph.D., A.R.C.S., D.I.C.

(*Communicated by Lord Rayleigh—Received May* 9, 1934)

1—INTRODUCTION

Although the subject of diamagnetic susceptibility has attracted the attention of many experimental and theoretical investigators during the past decade, it is remarkable that no complete systematic investigation of the susceptibilities of salts forming ions with inert gas configurations has been made. As a result, in comparing experimental and theoretical work, results for various salts obtained by quite different methods are used in conjunction with one another, and it is hardly surprising that the agreement should be of an approximate quantitative nature only in view of the wide discordance of the experimental results. The work of Ikenmeyer* is the most complete investigation, but here the susceptibilities of certain salts, notably the fluorides, have not been measured. This is a serious omission for the data upon fluorides should prove to be amongst the most interesting.

The present investigation is part of an attempt to obtain a series of results under the same experimental conditions and with the same apparatus, in order that the comparative values so obtained may be as accurate as possible.

2—METHOD OF EXPERIMENT

Before finally deciding upon the method of experiment to be employed various methods were considered in detail. At first it was thought that the Curie-Chéneveau magnetic balance would give the greatest accuracy because of its large and easily adjusted sensitivity. A balance incorporating the improvements suggested by Gray and Farquharson† was constructed and tried for some months. As has been stated elsewhere,‡ the results obtained with this apparatus were most inconsistent. The inconsistency apparently arose from the fact that it is almost impossible to ensure that the specimen is always located in exactly the same position with respect to the magnet, with a consequent variation in the force experienced by the specimen under test. Although many investigations have been made using the Curie-Chéneveau balance, this difficulty has not been mentioned previously in the literature dealing with such measurements, but the variation in the deflections for water found by Gray and Dakers* are probably to be attributed to this cause.

---

* 'Ann. Physik,' vol. 1, p. 169 (1929).

† 'J. Sci. Insts.,' vol. 9, p. 1 (1932).

‡ Hoare, 'Nature,' vol. 132, p. 514 (1933).

The method finally adopted was that of Gouy, in which the force on the specimen in an inhomogeneous magnetic field is directly measured with an ordinary sensitive balance.

A large electromagnet, capable of producing fields up to 50,000 gauss, was used to obtain the magnetic field. This magnet was fitted with conical pole pieces, one centimetre in diameter at their smallest cross-section, separated by a distance of a little more than one centimetre. The specimens were contained in either of two glass tubes, hereinafter called tubes B and C, of approximately 0·7 cm diameter and 16 cm length. These were suspended by a fine wire from one arm of a Sartorius balance, the top of the specimen contained in the tube being almost exactly central between the pole pieces. Since water was to be used as the calibrating liquid, *i.e.*, the results were to be obtained in terms of the diamagnetic susceptibility of water, taken as $0{\cdot}72 \times 10^{-6}$ c.g.s. units at the temperature of the experiment, it was necessary that the specimen tube should always be located the same with respect to the magnetic field in order that the calibration measurements could be repeated as desired. This was ensured in the following manner: the top of each tube was ground perfectly square to its length, and a fine scratch made with a diamond lengthways along the tube. Brass stoppers, over part of which were slipped small pieces of rubber tubing, and which carried small hooks for attachment to the suspension from the balance, were used to close the open ends of the tubes. These stoppers had a small rim which fitted down tightly on the ground tops of the tubes, and a small scratch on the lower part of the stopper was made to coincide with the scratch on the glass in each case. In this way it was possible to arrange that the tube and specimen were in the same position with regard to the field each time, as was shown by a series of tests in which the increase in weight of a specimen with the field on was found a number of times, the tube being removed from the suspension, the stopper withdrawn and replaced between each measurement. The consistency of these results indicated that no error was likely to be caused by variations in the location of the tube. This conclusion was further strengthened during the course of the experiments by the consistency of the apparent increase in mass per unit mass with water in the tubes (Table I), and also the increase in weight of the empty tubes with the field on. Another advantage of the stoppers made to this design was the close sealing of the tubes which they effected. This was shown very clearly with the extremely hygroscopic salt potassium fluoride in the tube, when, during a period of twenty-four hours, an increase in weight of only two parts in five thousand occurred.

---

* 'Phil. Mag.,' vol. 11, p. 81 (1931).

Unfortunately the magnet possessed no cooling devices, and if run at full load of twelve amperes, the windings then dissipating approximately one kilowatt, there was some likelihood that the small rise of temperature might change the permeability of the iron. Consequently the magnet was run at only six amperes, which considerably reduced the sensitivity of the apparatus, as the magnetic repulsion is proportional to the difference of squares of field strengths. With this current, however, the magnet did not become heated in the time required for an experiment. Furthermore, the drain on the laboratory accumulators being small, the current remained steady and easily regulated to six amperes. Maintenance of the current at this fixed value was the only method employed to keep the field steady, but here again the consistency of the results for water and the empty tubes, taken over a period of four months, shows that variations in the field strength, if any, were very slight. Actually, at six amperes it was found that a variation of a twentieth of an ampere in the current had a just measurable effect with water in the specimen tubes. Since the current could be adjusted to one hundredth of an ampere, it is not at all likely that such slight variations in current as are inevitable in experimental work had any effect upon the results. Measurements with a fluxmeter and search coil showed that the approximate value of the maximum field strength was $1{\cdot}40 \times 10^4$ gauss, and at distances of 2, 4 and 6 cm from the centre of the pole pieces along the line in which the specimen lies $0{\cdot}53 \times 10^4$, $0{\cdot}29 \times 10^4$ and $0{\cdot}13 \times 10^4$ gauss respectively.

The masses of the specimens and apparent increases in mass with the field on were all found in terms of the same set of weights, which had been calibrated in terms of the fifty-gramme weight by the usual substitution method.

All the experiments were conducted in a small room, originally built as a photographic dark-room, in the corner of a larger laboratory. The temperature was thermostatically controlled, and the air kept in continuous circulation by means of an electric fan. For all the measurements the temperature was between 20° C and 22° C. Sufficient time was always allowed for a fresh specimen to attain the temperature of the surroundings.

The salts used in the present investigation were all supplied by the British Drug Houses, Ltd. The chlorides of sodium and potassium were of A.R. standard, whilst the other salts were specially purified by the same firm.

For the purpose of the magnetic measurements the salts were finely powdered and dried in a quartz crucible, with the exception of the two fluorides and sodium chloride, which were dried in a platinum dish. The salts were introduced into the specimen tubes a little at a time and tightly packed by ramming down each instalment with a glass rod of nearly the same diameter as that of the interior of the tubes. The packing was continued until the tightly packed salt reached a filling mark scratched on the tube. The end of the rod being ground off square to its length, the top level of the specimen after packing was flat and definitely located.

In general, four different samples of each salt were used, *i.e.*, two different samples in each of two tubes, and two measurements made on each sample. This gives four independent results for each salt, or eight results in all. Owing to the extremely finely divided character of the sodium fluoride supplied, some difficulty was experienced in packing it uniformly in the specimen tubes. Consequently, the results with this salt were more variant than with the others. Altogether, eleven different specimens of sodium fluoride were used, the mean of all the results being given in section 4*c*.

The tubes were carefully washed between each filling, first with tap water and then with distilled water, afterwards being thoroughly dried with a current of hot air. The weight of the empty tube, and its increase in weight in the magnetic field, were taken before each experiment. Calibration measurements with distilled water were taken from time to time throughout the course of the investigation.

3—REDUCTION OF RESULTS

The force F exerted in the direction x by a non-uniform magnetic field on a small particle of magnetic susceptibility K_S can be written

$$F = \frac{V}{2}(K_S - K_A)\frac{dH^2}{dx},$$

where V is the volume of the specimen, K_A the susceptibility of the surrounding medium, and H the field strength.

For a specimen of finite length, the total force can be obtained by a simple integration. If the cross-section of the specimen is A, and H^2

and H_0^2 are the values of the square of the field strength at the top and bottom of the specimen, its apparent increase in mass m in the magnetic field is given by

$$m = \mathrm{C.A.}\,(\mathrm{K_S} - \mathrm{K_A})\,(\mathrm{H}^2 - \mathrm{H}_0^2),$$

where C is a constant. If it is always arranged that the top of the specimen is between the pole pieces of the magnet, H^2 will be the same, and as the bottom of the specimen is at the bottom of the tube, which is accurately located in the same position by means of the device adopted for suspension, H_0^2 will also be the same. In this case the apparent increase in mass is proportional to the cross-sectional area of the specimen and the difference in the volume susceptibilities.

It is frequently assumed that calibration with water is sufficiently accurate to find the constants of the apparatus. This is so, provided allowance is made for the volume of liquid in the meniscus. Thus, if in the calibration experiments it is arranged that the bottom of the meniscus is on the fixed filling mark of the tube, a mass of water, W, being in the tube, and the distance of the filling mark from the bottom of the tube is l, the mean cross-section is not $\mathrm{W}/(d \times l)$, where d is the density of water, but $(\mathrm{W} - c)/(d \times l)$, where c is a small correction term for the mass of liquid in the meniscus whose value can be ascertained from tables* if the radius r of the tube is known.

(Alternatively, the correction c can be regarded as the allowance for the mass of liquid occupying a space which is not afterwards occupied by the specimen upon which magnetic measurements are to be made. It should be noticed that this correction does not become smaller as the radius of the tube increases, as has been pointed out by Porter.†)

Hence, if $\delta\mathrm{W}$ is the apparent increase in mass W of water in the tube, when placed in the magnetic field

$$\delta\mathrm{W} = \mathrm{C} \times \frac{\mathrm{W} - c}{d \times l}\,(\mathrm{K_W} - \mathrm{K_A})\,(\mathrm{H}^2 - \mathrm{H}_0^2),$$

which can be written

$$\delta\mathrm{W} = \mathrm{M} \times \frac{\mathrm{W} - c}{d}\,(\mathrm{K_W} - \mathrm{K_A}),$$

by combining the constant terms.

With a powdered salt in the tube, the top of the specimen coincides with the filling mark. If S is the mass of the specimen, $\delta\mathrm{S}$ its apparent increase in mass in the magnetic field, σ its density and K_s its susceptibility, we have

---

* 'Int. Crit. Tables.,' vol. 1, p. 72.

† 'Phil. Mag.,' vol. 17, p. 511 (1934).

$$\delta S = M \times \frac{S}{\sigma}(K_S - K_A).$$

Hence

$$\frac{\delta S}{\delta W} = \frac{S}{\sigma} \cdot \frac{d}{W - c} \cdot \frac{K_S - K_A}{K_W - K_A},$$

or

$$K_S = \frac{W - c}{S} \cdot \frac{\sigma}{d} \cdot \frac{\delta S}{\delta W} \cdot K_W + K_A\left(1 - \frac{W - c}{S} \cdot \frac{\sigma}{d} \cdot \frac{\delta S}{\delta W}\right).$$

If the mass susceptibilities of the specimen and water be represented by χ_S and χ_W respectively, we have

$$\chi_S = \frac{K_S}{\sigma}, \quad \chi_W = \frac{K_W}{d},$$

and hence

$$\chi_S = \frac{W - c}{S} \cdot \frac{\delta S}{\delta W} \cdot \chi_W + K_A\left(\frac{1}{\sigma} - \frac{W - c}{S} \cdot \frac{1}{d} \cdot \frac{\delta S}{\delta W}\right).$$

In reducing the results the following numerical values were assumed :—

Mass susceptibility of water between 20° C and 22° C

$$= \chi_W = -0{\cdot}72 \times 10^{-6} \text{ c.g.s.} ;$$

Volume susceptibility of air between 20° C and 22° C

$$= K_A = +0{\cdot}29 \times 10^{-9} \text{ c.g.s.}$$

Density of water between 20° C and 22° C

$$= d = 1{\cdot}000 \text{ gm}^{*}/\text{cc.}$$

Density[†] sodium fluoride = 2·79 ; density potassium fluoride = 2·48 ; density sodium chloride = 2·163 ; density potassium chloride = 1·988 ; density sodium bromide = 3·205 ; density potassium bromide = 2·75 ; density sodium iodide = 3·667 ; density potassium iodide = 3·123.

Determination of the correction " *c* "—The radii of the tubes were found by filling to two different levels with water and measuring the difference in level and in weight in the two cases. In this way it was found that the radius was 0·3462 cm for each tube. Using tables[‡] it was found that the

---

[*] This value for the density of water is sufficiently accurate, as it only enters into a small term in the nature of a correction term.

[†] Densities from 'Int. Crit. Tables,' vol. 1, p. 106.

[‡] 'Int. Crit. Tables,' vol. 1, p. 72.

volume of water in the meniscus was 0·0343 cc, the surface tension of water being taken as 72·75 c.g.s. at 20° C.[*]

This value appeared so large, amounting to 3% of the water (in one of the tubes) when filled to the filling mark, that the shape of the meniscus was found by microscopic measurement, and the volume found by graphical integration. The result obtained by this method agreed with that found from tables to closer than one-half of one per cent and was therefore regarded as sufficient confirmation of the accuracy of this correction.

4—RESULTS

(*a*) *Water*—Table I shows the results obtained with water in one tube (B).

The mean value $(\mathrm{W} - c)/\delta\mathrm{W} = 42{\cdot}40 \pm 0{\cdot}16$. The last column, headed Δ, gives the deviation from the mean value of $(\mathrm{W} - c)/\delta\mathrm{W}$, and $\pm 0{\cdot}16$ is the average deviation from the mean. This table is given in full to show the approximate accuracy obtainable by the method of experiment adopted. It will be seen that this is better than 0·5%.

TABLE I—Apparent Increase in Mass per Unit Mass with Water in Specimen Tube

W gm	$\mathrm{W} - c$ gm	$\delta\mathrm{W}$ gm	$\mathrm{W} - c/\delta\mathrm{W}$	Δ
1·3060	1·2717	0·0300	42·39	−0·01
1·3062	1·2719	0·0302	42·12	−0·28
1·3109	1·2766	0·0301	42·41	+0·01
1·3101	1·2758	0·0303	42·11	−0·29
1·3100	1·2757	0·0302	42·24	−0·16
1·3002	1·2659	0·0300	42·20	−0·20
1·2999	1·2656	0·0299	42·33	−0·07
1·3047	1·2704	0·0300	42·35	−0·05
1·3044	1·2701	0·0298	42·62	+0·22
1·3064	1·2721	0·0301	42·26	−0·14
1·3064	1·2721	0·0300	42·40	0·00
1·3038	1·2695	0·0299	42·46	+0·06
1·3036	1·2693	0·0299	42·45	+0·05
1·3123	1·2780	0·0299	42·74	+0·34
1·3121	1·2778	0·0298	42·88	+0·48

With another tube (C) the value of $(\mathrm{W} - c)/\delta\mathrm{W}$ was $35{\cdot}83 \pm 0{\cdot}14$.

(*b*) *Iodides of Sodium and Potassium*[†]—Tables II and III, for the iodides of sodium and potassium, show the order of agreement obtainable for the mass susceptibility using two specimen tubes (B and C). It will be noticed that the amounts of salt contained in the tubes are widely different, but the very close agreement in the final results is adequate proof of the suitability of the method for the accurate measurement of magnetic susceptibility.

---

[*] 'Int. Crit. Tables,' vol. 4, p. 447.

[†] It is to be understood that all the following results are diamagnetic—that is, negative—susceptibilities.

TABLE II—Sodium Iodide

Tube	S gm	δS gm	$\chi_s \times 10^6$
B	2·0923	0·0256	0·381
	2·0923	0·0255	0·379
	2·2438	0·0275	0·381
	2·2441	0·0271	0·381
C	1·7049	0·0244	0·376
	1·7047	0·0245	0·378
	1·7528	0·0254	0·381
	1·7532	0·0253	0·379

Mass susceptibility sodium iodide = 0·380 ± 0·001 (5) × 10^{-6} c.g.s.

TABLE III—Potassium Iodide

Tube	S gm	δS gm	$\chi_s \times 10^6$
B	2·4030	0·0306	0·395
	2·4033	0·0306	0·395
	2·4317	0·0311	0·397
	2·4313	0·0311	0·397
C	1·9642	0·0298	0·398
	1·9643	0·0298	0·398
	1·9906	0·0300	0·395
	1·9903	0·0300	0·395

Mass susceptibility potassium iodide = 0·396 ± 0·001 (3) × 10^{-6} c.g.s.

The figures in Tables II and III correspond to molecular susceptibilities, *i.e.*, susceptibilities per gramme molecule, of 57·0 × 10^{-6} and 65·7 × 10^{-6} for sodium and potassium iodide respectively.

(*c*) ***Bromides, Chlorides, and Fluorides of Sodium and Potassium***—The complete tables of results for the remaining salts are not given, since the order of agreement is approximately the same as for the iodides.

In Table IV the molecular susceptibilities, as calculated from the following results as well as the results obtained recently by other workers, are collected for the purposes of comparison.

The following mean values for the mass susceptibilities were obtained :

sodium bromide	$0\cdot399 \pm 0\cdot002\ (2) \times 10^{-3}$ c.g.s. ;
sodium chloride..........	$0\cdot517 \pm 0\cdot002\ (4) \times 10^{-6}$ c.g.s. ;
sodium fluoride	$0\cdot371 \pm 0\cdot004\ (5) \times 10^{-6}$ c.g.s. ;
potassium bromide	$0\cdot413 \pm 0\cdot001\ (4) \times 10^{-3}$ c.g.s. ;
potassium chloride	$0\cdot521 \pm 0\cdot001\ (2) \times 10^{-3}$ c.g.s. ;
potassium fluoride........	$0\cdot407 \pm 0.001\ (1) \times 10^{-6}$ c.g.s.

TABLE IV—Experimental Values of Molecular Susceptibility

Salt	Molecular Susceptibility × 10^6					
	Hoare	Ikenmeyer†	Hocart‡	Kido§	Ishiwara‖	Gray and Farquharson¶
NaF ..	$15\cdot6\pm0\cdot19$	—	—	19·6	—	—
KF ..	$23\cdot6\pm0\cdot06$	—	—	25·7	—	—
NaCl..	$30\cdot2\pm0\cdot14$	30·0*	30·1	29·6	29·2	—
KCl ..	$38\cdot8\pm0\cdot09$	36·2*	39·1	35·8	—	36·15
NaBr	$41\cdot1\pm0\cdot23$	43·2*	—	42·9*	—	—
KBr ..	$49\cdot2\pm0\cdot17$	52·6*	49·15	48·2	—	48·12
NaI ..	$57\cdot0\pm0\cdot23$	60·4*	—	60·6*	—	—
KI ..	$65\cdot7\pm0\cdot22$	67·8*	63·8	67·2	—	63·9

* These results were obtained from measurements upon aqueous solutions.

† 'Ann. Physik,' vol. 1, p. 169 (1929).

‡ 'C.R. Acad. Sci. Paris,' vol. 188, p. 1151 (1929).

§ 'Sci. Rep. Tôhoku Imperial University,' vol. 21, pp. 149, 288 (1932). (Kindly communicated to me by Dr. G. W. Brindley.)

‖ 'Sci. Rep. Tôhoku Imperial University,' vol. 3, p. 303 (1914).

¶ 'Phil. Mag.,' vol. 10, p. 191 (1930).

5—DISCUSSION OF RESULTS

For the results obtained in this investigation, it is only for sodium fluoride and sodium bromide that the average deviation from the mean is greater than 0·5%, as will be seen from Table IV. With sodium bromide the average deviation only just exceeds 0·5%, and for sodium fluoride 1%. The reason for the greater scatter of the results for the latter salt has already been indicated.

As compared with the results found by Ikenmeyer, the values for the bromides and iodides are low. Hocart measured the susceptibilities of the chlorides in the crystalline form and in aqueous solution, finding the results in the former state to be less than in the latter. It would appear, therefore, from the results for the bromides and iodides, that the result found by Hocart for two salts might very well be in agreement with a general principle. This conclusion is strengthened by Kido's results.

For sodium chloride and the chloride and bromide of potassium, the results of the present investigation are in excellent agreement with those found by Hocart.

Kido's result for sodium fluoride appears to be too high and for potassium chloride too low.

6—THE ADDITIVITY OF IONIC SUSCEPTIBILITIES

It is frequently assumed that the molecular susceptibility of a given salt is merely the sum of the susceptibilities of the ions of which it is composed. Clearly, if this is so, there should be a constant difference between the molecular susceptibilities of the halides of the same metallic radicle. To test this, it is necessary to compare results obtained under the same conditions, and it is unfortunate that only the results of Ikenmeyer, *loc. cit.*, and those of the present investigation satisfy this condition for any number of salts. Table V, however, illustrates how far the additivity principle is fulfilled in these two investigations.

TABLE V—Application of Additivity Principle

Salt	Ikenmeyer		Hoare	
	Mol. sus. $\times 10^6$	Difference	Mol. sus. $\times 10^6$	Difference
NaF	—	—	15·6	8·0
KF	—	—	23·6	
NaCl........	30·0	6·2	30·2	8·6
KCl	36·2		38·8	
NaBr........	43·2	9·4	41·1	8·1
KBr	52·6		49·2	
NaI	60·4	7·4	57·0	8·7
KI	67·8		65·7	

It will be seen that no conclusive evidence as to the validity of the additivity principle can be derived from this table, especially from Ikenmeyer's results; the results of the present investigation do indicate, however, that it may be true to a first approximation.

7—COMPARISON OF OBSERVED SUSCEPTIBILITIES WITH THEORETICAL VALUES

If it is assumed that the additivity method is valid for obtaining molecular susceptibilities from ionic susceptibilities, the experimental results can be compared with those obtained from theoretical considerations.

The diamagnetic susceptibility of a symmetrical atom can be written*

$$\chi = -\frac{e^2}{6mc^2}\Sigma\,\overline{r^2}$$

e being the electronic charge, m the mass of an electron, c the velocity of light, and $\overline{r^2}$ the mean square distance of an electron from the nucleus, the summation extending over all the electrons.

Stoner† has calculated $\Sigma\overline{r^2}$ in certain cases from the charge distributions obtained by Hartree's‡ method. Brindley§ has obtained corresponding values of $\Sigma\overline{r^2}$ by making use of an approximate method of obtaining wave functions developed by Slater.|| In this way the theoretical values of the susceptibilities of ions having an inert gas configuration have been calculated. The experimental and theoretical values of the susceptibilities are compared in Table VI, the theoretical values in the last two columns being the sum of the ionic susceptibilities as given by Brindley.§

TABLE VI—Comparison of Experimental and Theoretical Molecular Susceptibilities

Salt	Molecular Susceptibility × 10^6		
	Expt. (Hoare)	Hartree	Slater
NaF	15·6	23·0	12·5
KF	23·6	34·9	22·7
NaCl	30·2	46·1	30·0
KCl........	38·8	58·0	40·2
NaBr	41·1	—	44·3
KBr	49·2	—	54·5
NaI	57·0	—	64·0
KI	65·7	—	74·2

---

[*] Van Vleck, "Electric and Magnetic Susceptibilities," p. 206.

[†] 'Proc. Leeds Lit. Phil. Soc.,' vol. 1, p. 484 (1929).

[‡] 'Proc. Camb. Phil. Soc.,' vol. 24, pp. 89, 111 (1928).

[§] 'Phil. Mag.,' vol. 9, p. 786 (1931).

[||] 'Phys. Rev.,' vol. 36, p. 57 (1930).

8—CONCLUSIONS

The work here described has demonstrated that, by using intense fields and a sensitive balance in conjunction with a carefully calibrated set of weights, the method adopted is capable of an accuracy at least equal to that of any investigation yet made. Although the measurements are not absolute but depend upon the assumed susceptibility of water, in view of the good agreement between the most recent determinations of this quantity, there can be but little uncertainty in the results from this cause. In many ways it is an advantage to have results expressed in terms of water, since the determination of dH^2/dx presents considerable difficulty, and there is generally more uncertainty in this determination than in a calibration with water. Thus, if results are obtained by different investigators by methods involving calibration with water, there is less chance of large variations between the various measurements, provided the same value for the susceptibility of water is used in reducing the results, than would occur if absolute methods were used. The present method, depending directly upon weighings, is less likely to introduce serious errors than those involving the torsion of wires, the accurate centering of rotating systems, or complicated subsidiary apparatus. The difficulty of packing the specimen uniformly is the most serious disadvantage of the present method, but the agreement of the results with different samples in the specimen tubes is sufficient proof that if care is taken this difficulty can be overcome.

Lastly, I wish to record my gratitude to Professor F. H. Newman, who throughout the course of this work provided every facility for its prosecution, besides being ready at all times to discuss difficulties and contribute to their solution. My thanks are also due to Dr. G. W. Brindley, who made many helpful suggestions.

SUMMARY

The diamagnetic susceptibilities of the sodium and potassium halides have been measured by Gouy's method between the temperatures of 20° C and 22° C. The salts were used in the crystalline state, and their susceptibilities evaluated by comparison with the behaviour of water whose susceptibility was taken as $0 \cdot 72 \times 10^{-6}$ c.g.s.

A correction has been applied for the volume of the liquid meniscus. Neglect of this correction introduces an error of as much as 3%.

Two specimen tubes, and at least four different specimens of each salt were used. Special precautions were taken to ensure the same location of the specimen tubes throughout the experiments.

The average deviation of the results from the mean values is approximately 0·5%, and this figure probably represents the limit of accuracy of the method.

Measurement of Shot Voltage used to Deduce the Magnitude of Secondary Thermionic Emission

By E. B. MOULLIN

(*Communicated by E. V. Appleton, F.R.S.—Received May* 23, 1934)

I—INTRODUCTION

The electric current passing from filament to anode of a thermionic valve is a stream of individual electrons; the passage and arrival of each of these will cause a disturbance among the electrons already on the anode. Hence the current which passes through the circuit connecting the anode to the kathode will contain ripples which are due to the arrival on the anode of individual electrons. The electrons arrive with random phase distribution, and hence the circuit receives a succession of shock impulses. There will be a fluctuating potential difference across the circuit, and the mean square value of this can be measured after adequate amplification. The root mean square value of this potential difference is commonly termed the shot voltage, because the pattering of the electrons on the anode has been likened to the pattering of small shot on a target. The shot voltage will depend on the rate of arrival of the electrons and on the characteristics of the circuit which they shock into excitation.

The shot voltage was predicted by Schottky* in 1918, and measured roughly by Hartmann† in 1921. Schottky developed an expression for the magnitude of the shot voltage and, according to him, it should be proportional to the charge on an electron. Schottky's formula was tested experimentally by Hull and Williams.‡ They used a lightly damped

* ' Ann. Physik,' vol. 57, p. 541 (1918).

† ' Ann. Physik,' vol. 65, p. 51 (1921).

‡ ' Phys. Rev.,' vol. 27, p. 147 (1925).

circuit having a natural frequency of about 10^6 c/s, and their measurements yielded a value for *e* which agreed with Millikan's value to within $\frac{1}{3}$%. A further set of measurements were made by Williams and Vincent* where the receiving circuit was a graphite line drawn on a glass tube, and thus formed a system aperiodic to its fundamental mode. They observed the shot voltage by a selective amplifier, which gave appreciable response only to frequencies near 120 k.c./s. With this apparatus they obtained a value for *e* which agreed with Millikan's value to closer than one part in a thousand. Williams and Huxford† made a further series of measurements with improved apparatus, and again obtained the correct value for *e*; they used an amplifier which had appreciable response only between 112 and 121 k.c./s.

A similar series of measurements was made by J. B. Johnson,‡ but whereas the experimenters named previously had used a receiving circuit whose natural frequency was greater than 100 k.c./s., Johnson used a network whose natural frequency ranged from 6 k.c./s. down to 8 c/s. He found that the apparent value of *e* depended very much on the natural frequency of the network and on the material of the kathode, and obtained values ranging from 0·7 to 100 times the accepted value.

The writer, together with H. D. Ellis,§ has made lately some measurements of shot voltage in small receiving triodes, and has extended Schottky's formula to apply to valves in which there is space charge limitation. In the appendix to their paper§ will be found an experimental test of their expression, which is found to be substantially correct over a very wide range of valve parameters. It is true they yield a value of *e* which is too small, but there the authors were concerned in checking a formula which could be used in technical applications where an error of some 30% would not be important.

2—The Theory of the Shot Effect

The theory of the shot effect has been developed by Schottky (*loc. cit.*), Fry,|| Ballantine,¶ Thatcher and Williams,** Ellis and Moullin§ and others.

---

* 'Phys. Rev.,' vol. 28, p. 1250 (1926).

† 'Phys. Rev.,' vol. 33, p. 773 (1929).

‡ 'Phys. Rev.,' vol. 26, p. 71 (1925).

§ Moullin and Ellis, 'J. Inst. Elect. Eng. Lond.,' vol. 72, p. 323 (1934).

|| 'J. Franklin Inst.,' vol. 199, p. 203 (1925).

¶ "Contrib. Radio Frequency Laboratories," No. 7, p. 159 (1928).

** 'Phys. Rev.,' vol. 39, p. 474 (1932).

For the sake of completeness we will derive one form of the expression by means of a simple theorem due to Campbell,* and brought lately to the writer's notice. The theorem is as follows : Suppose an instrument is affected by events which are distributed at random in time, but are subject to the condition that on the average these events happen at a rate N. Let the happening of one event cause the instrument to perform an excursion such that its reading θ at time t subsequent to the happening is given by $\theta = f(t)$; let $\theta = 0$ when $t = \infty$, so that $f(\infty) = 0$. Let the effects be additive. Let $\overline{\theta^2}$ be the mean square deviation in reading of the instrument, which is to be determined by observing the value of θ at random moments and taking the mean of their squares. Then the theorem can be stated in the form

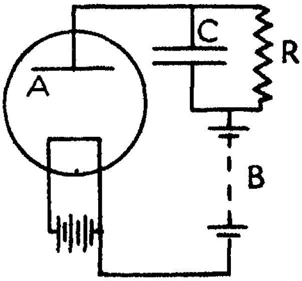

Fig. 1

$$\overline{\theta^2} = \mathrm{N}\int_0^\infty f^2(t)\,dt. \tag{1}$$

Consider fig. 1, which represents a thermionic valve in which the anode A is connected to the battery B by means of R and C in parallel. In this system C may be a concentrated capacitance or it may represent only the electrode capacitance of the valve, together with the distributed capacitance of the sensibly non-inductive resistance R. The valve is supposed to be operating in a condition of voltage saturation, so that the current flowing to the anode is independent of fluctuations of anode potential.

If an electron of charge e is suddenly communicated to the capacitance C, it will produce a voltage v† at subsequent time t, such that

$$v = \frac{e\,\varepsilon^{-\frac{1}{\mathrm{RC}}t}}{\mathrm{C}}$$

therefore

$$\begin{aligned}\overline{v^2} &= \frac{\mathrm{N}e^2}{\mathrm{C}^2}\int_0^\infty \varepsilon^{-\frac{2}{\mathrm{RC}}t}\,dt \\ &= \frac{\mathrm{N}e^2\mathrm{R}}{2\mathrm{C}} \\ &= \frac{\mathrm{I}e\mathrm{R}}{2\mathrm{C}},\end{aligned} \tag{2}$$

where I is the average value of the anode current.

---

* 'Proc. Camb. Phil. Soc.,' vol. 15, p. 117 (1909).

† The italic v of this fount should not be confused with the Greek ν.

This expression agrees with the limiting form of that developed by Schottky, when the inductance L of the circuit becomes vanishingly small.

In practice the voltage must be amplified before it is indicated by a pointer instrument. No amplifier is capable of amplifying a voltage having an indefinitely great rate of change, and in practice an upper limit may be intentionally imposed, by suitable design. Thus in practice the amplifier will record a voltage which is less than that given by the previous expression. If the amplifier has a uniform response k to sinusoidal voltages of all frequencies from zero up to $f = q/2\pi$, and thereafter zero response, then the writer has shown*, by the use of a Fourier integral, that it will record a voltage given by the expression

$$
\begin{aligned}
V_s^2 &= \frac{IeRk}{\pi C} \tan^{-1} RCq \\
&\doteqdot 2IeR^2fk\left(1 - \frac{R^2C^2q^2}{3}\right), \qquad \text{if} \qquad RCq \ll 1. \qquad (3)
\end{aligned}
$$

If RCq is very small, then it is not necessary that k should be constant within the frequency range $0 - f$, and the appropriate value of k in the foregoing formula is the average value within the range $0 - f$.

In practice a valve is always used in the condition of temperature saturation, and then the shot voltage causes sympathetic fluctuations of anode current. Ellis and Moullin (*loc. cit.*) have developed an argument showing that then

$$
V_s^2 = 2Iefk\left(\frac{R\rho}{R + \rho}\right)^2, \qquad (4)
$$

where ρ is the slope of the anode current—anode voltage characteristic.

The writer wished to repeat J. B. Johnson's experiments, in which he found the apparent value of e was much larger than the true value, when the natural frequency of the receiving circuit was within the acoustic range. For this purpose it would be undesirable to use the expression containing ρ, since this expression may not be exact. But when the modern type of screen grid valve is operated in its normal conditions, the value of ρ is about one or two megohms, and hence for small values of R must necessarily approach closely to the ideal conditions appropriate to Shottky's analysis, in which ρ is considered to be infinite. The original expression of Shottky may be applied to such a valve, and used to determine the apparent value of e obtaining in the small receiving valves in commercial production. Starting with this purpose, the writer realized

* Moullin and Ellis, 'J. Inst. Elect. Eng. Lond.,' vol. 74, p. 323 (1934).

that measurement of the shot voltage gives a method of examining the secondary emission which occurs when the potential of the anode is less than that of the screen, and which manifests itself by a negative slope in the characteristic. For the mean square shot voltage is proportional to the total number of events happening at the anode, and cannot depend on whether an electron is arriving or departing. When there is secondary emission, the space between anode and cathode will contain electrons moving in opposite directions, and consist of P electrons per unit time arriving at the anode and S electrons per unit time leaving the anode. The recorded shot voltage will thus be proportional to a current of value $P + S$, whereas the current entering the external circuit is equal to $P - S$. The secondary stream is thus equal to half the difference between the apparent current recorded from the shot voltage and the mean anode current. This paper describes how the apparent magnitude of the secondary stream was determined in this manner for two types of small receiving valve ; the accuracy of the process of measurement is checked by some evaluations of e. The measurements have also revealed some other effects which may be due to the production of ionization, and may be akin to the "flicker effect" recorded by J. B. Johnson.*

3—THE EXPERIMENTAL PROCEDURE

Both the amplifier and its characteristics have been described elsewhere.† The final indicator was a pointer galvanometer actuated by a thermocouple ; the average sensitivity of the amplifier was such that it had a "transfer resistance" of about $1 \cdot 3 \times 10^{-3}$ ohms. The thermojunction was fed through a carefully designed low-pass filter, whose characteristics were such that there was no appreciable response if the voltage applied to the amplifier had a frequency greater than 10 k.c./s. A curve was obtained relating the deflection of the galvanometer with the frequency of applied harmonic P.D. of constant value, for a large number of frequencies between 50 c/s and 11,000 c/s, and from such a curve it was found that the average response in the range 0–10 k.c./s. was 0·56 of the maximum response, which occurred at a frequency of 1·5 k.c./s. Such curves were obtained at intervals over a period of three months, and such tests suggest that the figure 0·56 is probably correct to an accuracy of about ± 2%.

The process of measuring the shot voltage is as follows : the input terminals of the amplifier were connected across a resistance, corresponding to R in fig. 1, through which was passing the current from the anode of a valve. A curve was obtained relating the deflection of the galvanometer with the value of the anode current. The galvanometer deflections were then calibrated by applying a known harmonic voltage, of frequency 1·5 k.c./s. to the input terminals of the amplifier. It was the practice to plot the reading of the galvanometer against the reading of a thermo-ammeter used to measure the current which produced the calibrating voltage. This curve should be, and always was, a straight line through the origin. The method of producing the known calibrating voltage, of value up to 21 μV, has been described in great detail elsewhere.* The process of reducing the results will be made more clear in the subsequent sections of the paper.

---

* 'Phys. Rev.,' vol. 26, p. 7 (1925).

† Moullin and Ellis, *loc. cit.*

4—MEASUREMENT OF *e*, USED TO CHECK THE MEASUREMENT

A Mazda screen-grid valve,† type AC/S2, was used with a potential of some 200 V on the anode, and a screen potential which could be varied between 12 and 70 V. Within most of this range of screen-grid potential, the anode current is almost independent of anode potential, and the slope resistance is of the order of 1MΩ. The resistance, typified by R in fig. 1, was 4.0$k\Omega$, and hence the condition of infinite anode impedance, implicit in Schottky's analysis, is simulated closely, and a factor of the form $R\rho/(R + \rho)$ differs insensibly from unity. But the magnitude of the anode current can be varied widely by changing the potential of the screen grid and yet not invalidate the condition of very large anode impedance.

Fig. 2 shows galvanometer deflection plotted against the value of the anode current. The dotted line on the same figure relates the galvanometer deflection with the square of the calibrating voltage, of frequency 1·5 k.c./s., and which is plotted along the axis of anode current. The value is such that an abscissa corresponding to 12 on the scale of anode current is equivalent to a calibrating voltage of 21 μV R.M.S. That the four observation points, marked with a cross, lie on the dotted line which passes through the origin, shows that the amplifier is responding proportionately to the square of the applied voltage, and is not subject to any excitation other than that applied through the known calibrating channel. The deflections due to shot voltage lie in groups having an abscissa near to 1·2, 2·5, 4, 6, 7·5 and 9 *m*A. The meaning of the groups is as follows: each group corresponds to a definite potential of the screen-grid. If the condition of very large anode resistance is fulfilled, then a wide change of anode potential should cause an insensible change of anode current. The three points corresponding to a current of approximately 5·75 *m*A were obtained with three different anode potentials between 100 and 200 V. Thus increasing the anode potential from 100 to 200 V increased the anode current from 5·7 to 6 *m*A ; it follows from this that the mean anode resistance within this range was 300 *k*Ω, compared with which an external resistance of 4 *k*Ω is negligible. With a screen potential giving 4 *m*A, the points are just distinguishable; below this they were indistinguishable. It may be seen that when the screen potential sufficed to produce an anode current of 8 *m*A and 9·5 *m*A, then the anode current is appreciably dependent on anode potential. In these regions the condition of a relatively large anode resistance is not fulfilled, but the points are included because the observations are important to part of the ensuing argument. It may be seen that for currents below 6 *m*A, the curve connecting galvanometer, deflection and anode current is a straight line through the origin. In this region the square of

---

* 'Proc. Camb. Phil. Soc.,' vol. 28, p. 386 (1932).

† *Some details respecting valves used in the measurements*—Type AC/S2 and AC2/HL, manufactured by the Cosmos Lamp Works, Ltd., have electrodes of flattened tubular type constructed of pure nickel. The cathodes are of rectangular cross-section, and are coated with a mixture of barium and strontium oxide. A magnesium "getter" is used in the AC/S2, and a barium "getter" in the AC2/HL. The PM4 valve, manufactured by the Mullard Co., has a molybdenum grid and nickel anode, and a filamentary cathode prepared by the barium-azide process.

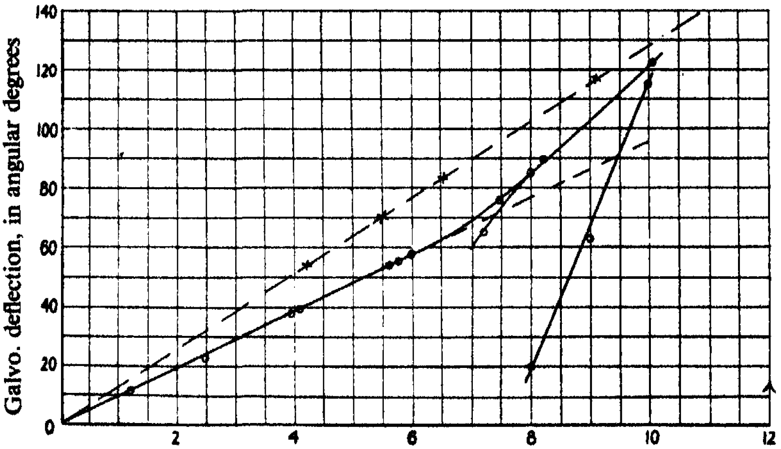

Anode current in *m*A,
also square of calibrating voltage

FIG. 2—Mazda valve, type AC/S2

the shot voltage is proportional to the current, and this is in accordance with Schottky's formula, equation (3).

To find the value of e it is now necessary to put numerical values in equation (3). It has been stated previously that the amplifier response was arranged to fall to a very small value at a frequency of 10 k.c./s. Hence f in equation (3) is to be taken as 10^4. The resistance R was 4 $k\Omega$, and C was due only to residual capacitance, whose value is unlikely to be as much as 100 $\mu\mu$F. Taking this value of C it follows that $R^2C^2q^2 = 6 \cdot 3 \times 10^{-4}$, and is negligible compared with unity. As a further check on the permissibility of ignoring this factor, a capacitance of 1000 $\mu\mu$F was connected across C. It was impossible to detect any change of deflection, whether this capacitance was in circuit or not.

Giving e the value $1 \cdot 59 \times 10^{-20}$ em units, it follows that the relation between V_s in μV and I in mA should be

$$V_s^2 = 51 \text{ I.}$$

Now consider the line in fig. 2, on which lie the points corresponding to currents less than 6 mA. The calibration line shows that 21 μV at 1·5 k.c./s. produced a deflection of 153. Hence the frequency characteristic of the amplifier implies that the average deflection due to 21 μV for any frequency up to 10 k.c./s. would be $153 \times 0 \cdot 56 = 85 \cdot 6$. Reference to the straight line produced, shows that a deflection of 85·6 would have corresponded to a current of 9.0 mA. But from the foregoing relation between V_s^2 and I, the current should be $\frac{441}{51} = 8 \cdot 7$ mA, whereas in fact it is 9·0. Thus from these observations we deduce a value for e which is 3·4% less than the accepted value. Separate determinations on other occasions yielded values which were respectively 10% and 11% greater than the accepted value. The values deduced for e were thus found to be above and below the true value, and presumably the discrepancies may be attributed to errors of measurement, the overall accuracy of which would appear to be of the order of ± 5%. It may be seen from fig. 2, that for currents above 6 mA the points lie above the straight line. The two groups of points show that in this region the anode current is appreciably dependent on anode potential, and that hence the anode resistance is not indefinitely great. But reference to equation (4) will show that if the factor $\rho/(R + \rho)$ is less than unity, there should result a reduction in the value of V_s^2. That this is so is apparent from the deflection resulting from a current of 8 and of 9 mA. But since increasing the anode potential brings this factor more nearly to unity, the observation points should approach the line and never lie above it. Reference to the figure shows that they do lie above it, and hence, with such currents, the shot voltage is greater than would be expected. Thus for a current of 10 *m*A, the apparent value of *e* is at least 30% in excess of the accepted value. Fig. 2 shows definitely that when the screen potential is such as to produce an anode current greater than 6 *m*A ($V_s > 43$ V), then there is some new factor in the process of conduction. Presumably, this factor is ionization, and is perhaps caused by liberation of gas from the screen or anode, due possibly to the increase of power absorbed in them. In this region of anode current the experience agrees with that of J. B. Johnson (*loc. cit.*) in finding the apparent value of *e* is too large. It is interesting to note that in this valve the appearance of "flicker effect" is a function of screen potential, and is absent when this potential is less than about 45 V.

4—DEDUCING THE VALUE OF THE SECONDARY EMISSION CURRENT

When the potential of the anode is less than that of the screen, there is a region of the characteristic in which an increment of anode potential is accompanied by a decrease of anode current. In this region there is either reflection or true secondary emission from the anode. In this particular valve the anode current could become negative, proving that then true secondary emission is occurring.

If the magnitude of the shot voltage is recorded as a function of anode potential, it is possible to deduce the value of the apparent anode current by means of the equation

$$V_s^2 = 2\mathrm{I}ef\left(\frac{\rho \mathrm{R}}{\mathrm{R}+\rho}\right)^2, \tag{4}$$

provided that the value of ρ can be found from the slope of the static characteristic.

Though the principle of the method is sound, it must be admitted that the validity of equation (4) rests on reasoning much less simple and rigorous than that used to develop equation (3). The anomalous values of *e* found by J. B. Johnson (*loc. cit.*) were deduced from an equation equivalent to (4). Hence if this equation is used to deduce the apparent value of the current, it presumes that the apparent value of *e* is $1 \cdot 59 \times 10^{-19}$ coulombs. It is known that fictitious values are sometimes found for *e*, and it is difficult to devise a means by which equation (4) can be subjected to rigorous experimental verification. The valve used to obtain the results shown in fig. 2 was used as a triode, by connecting together the anode and screen-grid, and the shot voltage was plotted as a function of anode current when the resistance R had the value 10 *k*Ω. This curve is shown in fig. 3, and also the curve calculated from equation (4) ; in this range of anode current, ρ ranged from 8·3 to 5 *k*Ω. For currents up to 3 *m*A, the observed and calculated values are in agreement. When the current is 9 *m*A, the observed value of V_s^2 is 10% less than the calculated, but it is thought that this discrepancy can probably be accounted for in the determination of ρ. But equation (4) does not always represent the facts with as much success as fig. 3 suggests.

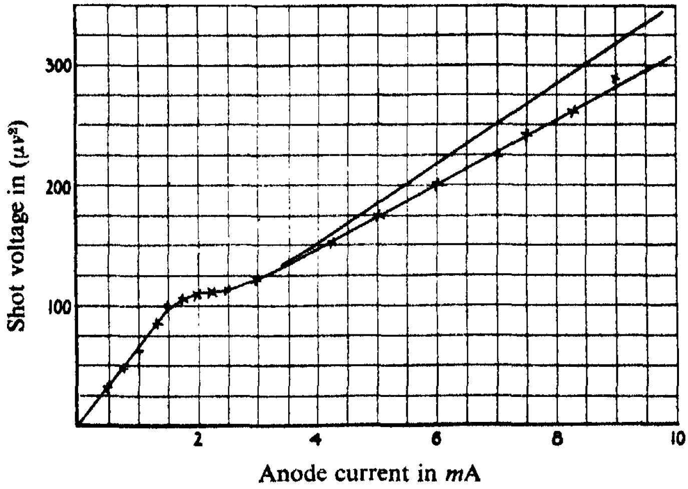

Fig. 3—Mazda valve AC/S2 used as a triode ; — calculated ; ×–×–× observed.

Thus measurements were made on a Mazda AC 2HL valve, in which the value of R/ρ was changed from 1/13 to 7, while the anode current was maintained at a constant value ; it was found that the curve relating V_s with Rρ/(R + ρ) was accurately a straight line through the origin, and it seems there can be no doubt that the effect of the valve resistance is accounted for correctly by equation (4). But when R was kept constant and the current was changed, which also involved some change of ρ, it was found that the observed and calculated values of V_s^2 were not in agreement and not in a constant ratio. For values of I between 3 and 12 *m*A, the observed value of V_s^2 was half the calculated, and for currents less than 1 *m*A it was about 20% greater than the calculated value. Hence in this valve the values deduced for *e* would be between 1·2 and 0·5 of the correct value. That the apparent value should be less than the true one is particularly difficult to understand. (Note : J. B. Johnson (*loc. cit.*) records values for *e* which are 70% of the true value.) It would seem that our present knowledge of the mechanism of the shot effect is incomplete. Hence with reservations respecting the absolute values of the final results, the method of deducting the magnitude of the primary and secondary stream will now be described. This paper is more concerned with describing a new technique than with discussing the interpretation of the measurements.

Turning now to the measurement of shot voltage in a valve where secondary emission is present. Fig. 4 shows both anode current and also deflection of the output galvanometer plotted as a function of anode potential, and it will be noticed that the galvanometer deflection changes enormously with the anode potential, and passes through two sharp maxima. It is instructive to consider the curve of deflection in its relation to the curve of anode current. In the region OA, ρ is positive, and has a mean value of about 1 $k\Omega$; hence the factor $\left(\frac{\rho}{R+\rho}\right)^2$ is of the order of 1/25, since $R = 4\ k\Omega$. Thus in general the deflection in the region O to A is likely to be much less than it is at the point A. In the region between A and B, ρ is negative and has a mean value of about 7 $k\Omega$. Hence, in this region $\left(\frac{\rho}{R+\rho}\right)^2$ is greater than unity, and is of the order of 4 ; in consequence, the shot voltage should be effectively augmented by the characteristic of the valve. If the curve of galvanometer deflection is now examined, it will be seen that the deflection

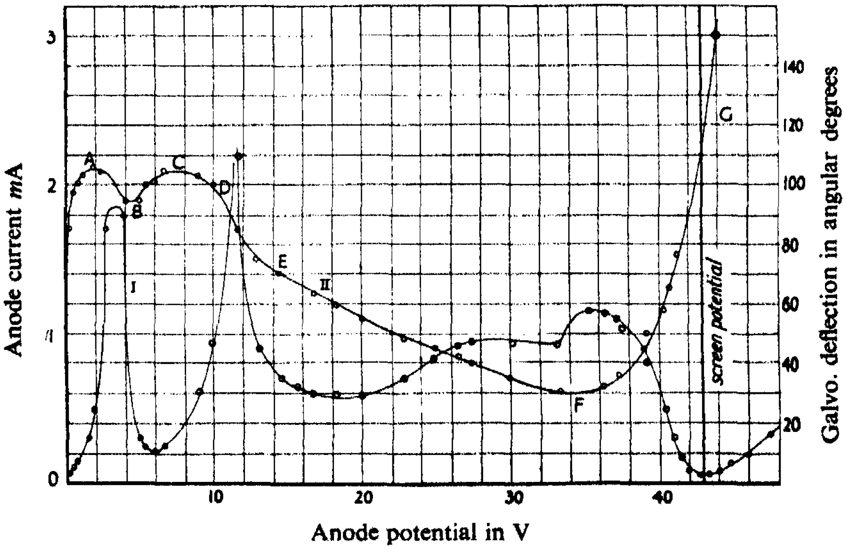

FIG. 4—Mazda valve AC/S2 ; I characteristic ; II deflection due to shot voltage.

is small in the region OA, rises to a maximum near the middle of the region AB, and falls to a minimum somewhere in the region BC, corresponding to the point of maximum positive slope. In the region CD, the deflection is increasing since ρ is there negative. In the region DE the deflection is large, since ρ is small and negative. Near the point E the negative slope diminishes rapidly, and remains substantially constant until the potential approaches the value corresponding to the point F. In the region EF the deflection is less than that in the region DE, which is to be expected. In the region FG, ρ is positive and decreasing, which should correspond with, and does correspond with, a decreasing deflection. Thus throughout the wide changes of ρ met with in the characteristic, the galvanometer deflection always follows the trend of the factor $\left(\frac{\rho}{R+\rho}\right)^2$.

The curves were plotted for values of anode potential up to 200 V, but the region between 48 and 200 is not shown in fig. 4. As described in the previous section the anode current tends to a constant value, and likewise the galvanometer deflection, as indeed is implied by fig. 2.

If the value of the factor $\left(\frac{\rho}{R+\rho}\right)^2$ can be deduced from the static characteristic, it will be possible to deduce the apparent value of the anode current, and hence to deduce the values of P and S, as described in section 2.

The characteristic showed definite signs of changing a measurable amount in a short time, hence it was desirable to plot the characteristic simultaneously with the galvanometer deflection. Since the potential has to be measured by a moving coil voltmeter of finite resistance, it is impracticable to measure the anode potential directly ; but it can be deduced by subtracting IR from the measured value of the battery voltage. The characteristic shown in fig. 4 was deduced in this manner, and the procedure was to record both anode current and galvanometer deflection as a function of the voltage of the anode battery. The process of reduction can be illustrated by using a point in fig. 4 to work back to the observed result. Thus a current of 1 *m*A is seen to occur when the anode potential is 22·5 V; since 1 *m*A reached the anode through a resistance of 4 *k*Ω, the voltage of the battery would be $22{\cdot}5 + 4 = 26{\cdot}5$ V. The characteristic was deduced by the converse of the process just illustrated. At A, B, C and F the factor $\left(\frac{\rho}{R+\rho}\right)^2$ is unity ; over much of the region EF it is constant, and there the value of ρ can be deduced from fig. 4 with considerable accuracy. By the help of such points it is possible to plot a curve relating the factor to the anode potential, and obtain this function with considerable accuracy over much of the range of V_a. Thus in the range $V_a = 14$ to $V_a = 35$ the factor ranges slowly from 1·6 to 1, and the probable value corresponding to a given V_a can be found with considerable accuracy. In the regions V_a 0–14 and 35–50, the factor changes rapidly and wanders over a wide range, and there can be determined only very roughly. Hence it is mostly in the region E to F that the values of P and S can be separated with much certainty. An example will make clear the method of reducing the results. Reference to a curve relating the factor with V_a would show that when $V_a = 25$, $\left(\frac{\rho}{\rho + R}\right)^2 = 1 \cdot 4$. Reference to fig. 4 will show that when $V_a = 25$, $\theta = 42$ and $I_a = 0 \cdot 9$ *m*A. The calibration at a frequency of 1·5 k.c./s. showed that 21 μV gave a deflection of 148; hence the average deflection for 21 μV in the frequency range 0–10 k.c./s. was $0 \cdot 56 \times 148 = 83$. Since the deflection is proportional to the square of the applied P.D., it follows that a deflection of 42 corresponds to a mean square voltage of 225 $(\mu V)^2$. With the relevant value of R

$$V_s^2 = 51 \left(\frac{\rho}{R + \rho}\right)^2 I,$$

hence it follows that $I = 3 \cdot 1$ *m*A.

$$\text{Hence} \quad S + P = 3 \cdot 1,$$

$$\text{and} \quad I_a = P - S = 0 \cdot 9,$$

therefore

$$P = 2\, mA \quad \text{and} \quad S = 1 \cdot 1.$$

Fig. 5 shows the apparent anode current, deduced from shot voltage, and the actual anode current plotted as a function of anode potential. It will be noticed that the curve of apparent current is shown dotted in the range 0–12 V, but that there are three isolated observation points in this range. Intermediate observation points are not shown because they are considered to be unreliable, since they are in a region where ρ ranges between very wide limits. Reference to fig. 4 will show that at the points A, B and C, ρ is infinite; hence at these points the joint resistance of R and ρ in parallel is R. Reference to fig. 4 will show that, as far as can be judged, the shot voltage corresponding to the points A, B and C is the same, and gives a galvanometer deflection of 25. Such a deflection indicates an apparent current of 2·6 *m*A. The three observation points on the dotted branch correspond to the points A, B and C. Intermediate points have been deduced, and appear to indicate currents between 1 and 5 *m*A, but these values depend so much on the supposed value of ρ that they have been considered unreliable.

Before using fig. 5 to deduce the two components of anode current, it is necessary to consider various interpretations of an elementary event. Since the anode current never falls to zero in the characteristic of fig. 4, only some primary electrons are reflected or cause the emission of secondary electrons ; consequently, there is more than one type of elementary event which occurs at the anode. If, when an electron is reflected or causes the emission of a single secondary, all departures occur at the same interval of time after the arrival, such an event would be negligible compared with the permanent acceptance of an electron.

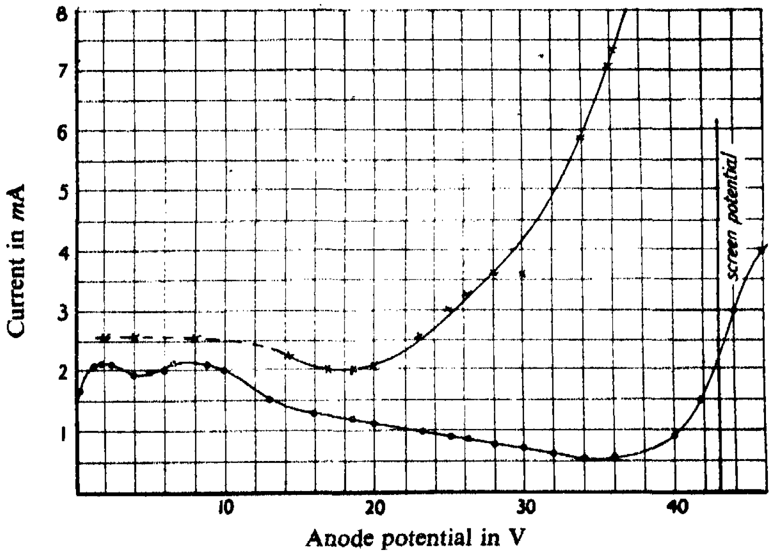

FIG. 5—Mazda valve AC/S2 ; O actual characteristic ; × apparent characteristic.

In such circumstances the effective events at the anode would number P − S, and then the apparent anode current would be equal to the true anode current; the curve of fig. 5 does not accord with this supposition. If the phase of the secondary emission with respect to the primary impact has a random distribution, then all events at the anode will be similar in magnitude, and their number will be P + S. This will be true if some primary electrons cause the emission of several secondary electrons, provided that there is random phase between all the secondaries emitted by one primary. But if one primary electron always causes the emission of *m* secondaries in the same phase, then the events will be of two classes, *m* being any integer including zero. Primary events P in number, bringing a charge e and N secondary events removing a charge me, where $m = 1, 2, 3,$ etc. In such circumstances

$$V_s^2 = ke^2(P + n_1 + 4n_2 + 9n_3 \ldots),$$

in which

$$n_1 + n_2 + n_3 + \ldots = N,$$

and

$$S = e\,(n_1 + 2n_2 + 3n_3 + \ldots).$$

Measurement of shot voltage can give no information about n_1, n_2, etc. Hence it seems possible to separate the apparent current into components P and S only if it is assumed that n_2, n_3, etc., are zero. According to this assumption

$$I = P + S$$

and

$$I_a = P - S.$$

It is according to this assumption that fig. 6 has been deduced. It will be noticed that when $V_a > 50$ V, the apparent current is in substantial agreement with the measured anode current. In this region secondary emission will have ceased to be apparent since the anode is then appreciably positive to the grid. The sharp maxima in the curve of P and S is a feature of interest, especially since the maximum value of P is 6·5 *m*A, whereas the limiting value of P is but 5·2 *m*A. The total current emitted by the filament (sum of grid current and anode current) was found to be independent of V_a and equal to 7·3 *m*A. Since the maximum value of the apparent primary current exceeds the limiting value of 5·2 *m*A, it must be supposed either that some primary impacts cause charges $2e$, $3e$, etc., to be emitted, or else that some electrons perform several journeys between screen and anode when these two electrodes are at nearly the same potential. It is necessary to enquire whether the accuracy of observation suffices to justify drawing the peak in fig. 6. Reference to fig. 6 will show that the peak of P and S occurs in the range of V_a, say, from 34 to 40 V. Reference to fig. 4 will show that this region corresponds to a large range in the value of the factor $\left(\frac{\rho}{R + \rho}\right)^2$, but that in this range the galvanometer deflections are sufficient to permit considerable fractional accuracy of reading. The factor $\left(\frac{\rho}{R + \rho}\right)^2$ has been determined with great care, and when plotted as a function of V_a it is found to be linear over the range 30 to 44 V. Owing to this fortuitous occurrence the factor is presumably known with considerable accuracy over the range in which the peak occurs. The writer thinks that in the peak range the values deduced for P are certainly reliable to an accuracy of ± 10%.

A test such as that represented by fig. 4 was made with the screen at 64 V ; the total current emitted from the filament was then 12·4 *m*A. In these conditions the limiting current is 9·6 *m*A, and reference to fig. 2 will show that this is in the region where the value deduced for *e* is too large, or, in other words, there is appreciable flicker effect. When the voltage on the screen is 64 V, the anode current reverses, being zero at $V_a = 46$ and $V_a = 62$ V.

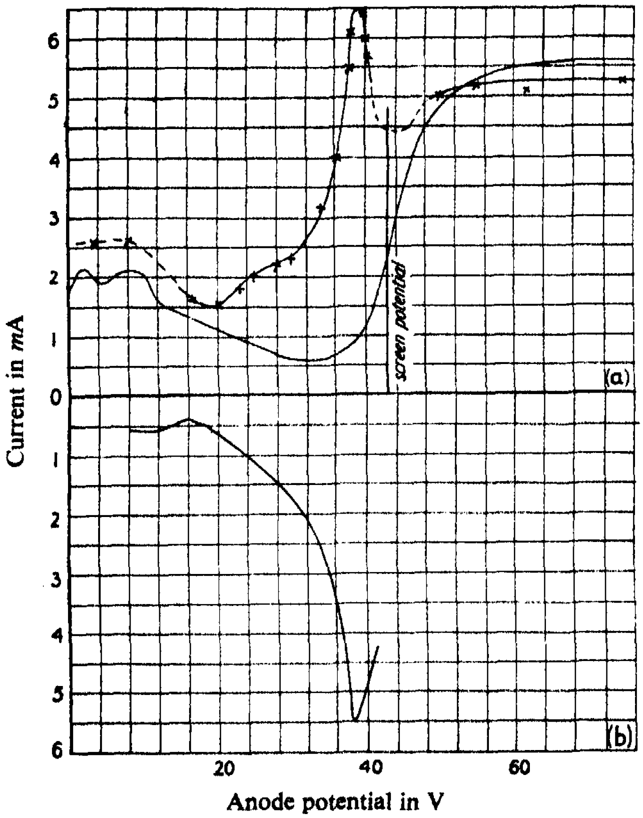

FIG. 6—Mazda valve AC/S2 ; (*a*) ×–×– apparent primary current, —— characteristic; (*b*) apparent secondary emission current

Fig. 7 shows the characteristic plotted over the range of anode potential from 40 to 140 V, and also shows the curve of primary emission, deduced from measurement of shot voltage. It will be observed that the shot voltage reveals the presence of impacts on the anode when the anode current is zero and shows that these impacts are equivalent to the effect of a uni-directional current of 9 *m*A or 22 *m*A. Deduction from the shot voltage shows that the apparent anode current tends to a limiting value of 15·5 *m*A, whereas in fact the limiting value is 9·6 *m*A. With the valve working in this condition the flicker effect is such that the apparent value of *e* is about 60% in excess of the true value. Fig. 7 shows that when the anode and the screen are nearly at the same potential, the primary current rises to a peak which is greater than 20 *m*A. In order to determine the rising portion of the curve of P with as much certainty as possible, the shot voltage was measured in the range 40–65 V, with the sensitivity of the amplifier adjusted to be as great as the deflection would permit, a sensitivity which would have been unsuited to study the whole range of V_a. Consequently the rising branch in fig. 7 is more to be depended on than the corresponding branch in fig. 5, and confirms that the total apparent number of impacts may exceed the total rate of emission from the filament when the two electrodes are at nearly the same potential.

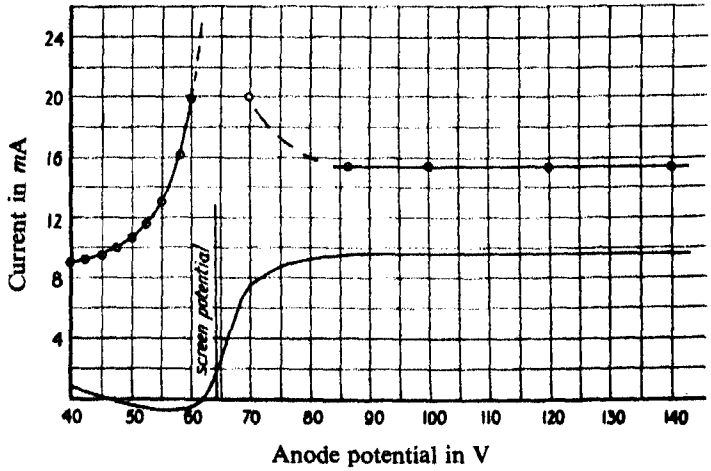

FIG. 7—Mazda valve AC/S2 ; O apparent primary current ; — characteristic.

Since the limiting apparent current in fig. 7 is 15·5 *m*A, when the true value was 9·6 *m*A, it might have been preferable to assume that, from ionization or some other cause, the apparent value of the electron charge should have been taken as $\frac{15\cdot 5e}{9\cdot 6} = 1\cdot 6e$. If this had been done, then the ascending branch of the curve deduced for P would have been sensibly that shown, but with ordinates reduced in the ratio 9·6/15·5.

The characteristic of the AC/S2 valve is unsuitable for studying the secondary emission in the neighbourhood of the first maximum of anode current. To study the behaviour in this neighbourhood an LS5 valve was used with its grid at a potential of 196 V and a total emission of 22 *m*A. The characteristic, in the range V_a 0–100, is shown in fig. 8. The same figure shows the curves deduced for P and S on the supposition that the apparent value of *e* was $1\cdot59 \times 10^{-}$ coulombs. The curve deduced for P seems very improbable, for though its maximum value is a little less than the total current emitted by the filament, yet it seems most unlikely that P should pass through a maximum. On the other hand, the same apparent effect is exhibited in fig. 6. When the total apparent current (to be obtained from fig. 8 by adding corresponding ordinates of P and S) is plotted against I_a, the two are found to be proportional to one another in the range of V_a 12–40 V, and in the ratio 2·2. It may be suspected from this that the apparent value of the electron charge for this valve was 2·2 *e*.

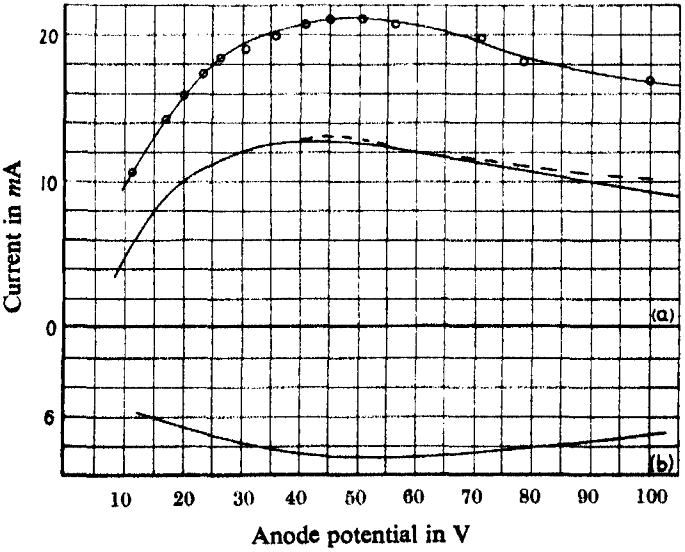

FIG. 8—Screen potential 194 V, valve type LS5 ; (*a*) — apparent primary current : — and — — characteristic ; (*b*) apparent secondary current.

On this supposition a fresh curve of P has been deduced, and is represented by the dotted curve in fig. 8. There is evidently no value of *e* which will make the curve of P increase continuously with V_a. Similar tests were made on a certain PM4 valve, in which it was found that the anode current was constant at 14 *m*A for values of V_a between 25 and 72 V, when the grid potential was 103 V. In this range of the characteristic the shot voltage was constant, and such as to indicate an apparent current of 250 *m*A. Since the apparent current was fourteen times the actual current, presumably there must have been severe ionization.

5—SUMMARY

This paper describes a technique for deducing the magnitude of secondary thermionic emission by measuring the "shot" voltage developed in a thermionic valve. The theory of shot effect is reviewed briefly, and the experimental method and its accuracy are discussed and illustrated by measurements of the electron charge, in conditions where secondary emission is absent, both in the presence and absence of space charge.

The shot voltage is presumed to be proportional to the total rate of events occurring at the anode ; hence if secondary emission is present it will give a measure of the sum of primary and secondary electrons agitating the anode circuit. The difference between the number of primary and secondary electrons is measured by the anode current. The sum is deduced from the shot voltage, and the difference from the anode current, and hence the magnitude of each component can be deduced. Some deduced curves of primary and secondary current are shown for two types of valve working in the dynatron condition. These curves appear to show that a complicated system of emission occurs when the grid and anode are nearly at the same potential. The paper is concerned mainly with discussing the application of shot voltage to measurement of secondary emission and does not make a serious attempt to discuss the unexpected features of the deduced curves. The measurements were made in the Engineering Laboratory of Oxford University.

The Thermal Decomposition of Methyl Alcohol

By C. J. M. FLETCHER

(*Communicated by C. N. Hinshelwood, F.R.S.—Received May* 30, 1934)

A comparison of the thermal decomposition of methyl alcohol with those of formaldehyde, the ethers, and other compounds of similar structure seems of interest in relation to kinetic problems.

Methyl alcohol is known to decompose catalytically in the presence of zinc oxide to formaldehyde and hydrogen at 300° C.* The same reaction occurs thermally at a measurable speed between 650° and 750° C. The presence of formaldehyde can be detected by Schryver's test. Formaldehyde at these temperatures rapidly decomposes into carbon monoxide and hydrogen,† so that the resultant equation is

$$CH_3OH = CO + 2H_2.$$

Analyses of the end-products of the reaction, made for initial pressures of approximately 200 mm, show that the gas consists entirely of hydrogen and carbon monoxide. The ratios in three analyses were 1·92, 1·83, and 1·85.

TABLE I—Temperature 669° C Unpacked bulb

a/(mms)	$t_{\frac{1}{2}}$/(secs)	$t_{\frac{1}{2}}/t_{\frac{1}{4}}$	$t_{\frac{3}{4}}/t_{\frac{1}{4}}$	End-point %
370	237	1·59	—	—
313	234	1·59	—	—
284	241	1·60	1·75	—
254	265	1·58	—	183
221	264	1·59	1·78	185
189	274	1·66	1·84	186
157	277	1·58	1·79	—
132	296	1·65	1·83	188
116	299	1·60	—	190
91	308	1·64	—	191
69	310	1·62	1·80	—
57	294	1·62	1·79	190
42	301	1·60	—	188
28	291	1·63	—	188
16·3	291	1·62	—	187
10·8	282	1·57	1·88	182
6·7	285	1·65	1·86	180
2·6	330	1·57	1·94	150

---

* Dohse, 'Z. phys. Chem.,' B, vol. 8, p. 159 (1930).

† Fletcher, 'Proc. Roy. Soc.,' A, vol. 146, p. 357 (1934).

The apparatus and method used were that described in a number of previous papers.* Methyl alcohol purified for use in conductivity work was used. A silica vessel of 300 cc volume was used. The manometer and tubing connected to the reaction vessel were heated with nichrome wire to above 80° C to prevent condensation of methyl alcohol, or polymerization of formaldehyde. For initial pressures below 10 mm a McLeod gauge was used.

THE PRESSURE INCREASE DURING THE REACTION

As formaldehyde undergoes certain condensation reactions which are more prominent at high pressures and in a packed vessel, it is not surprising that the pressure increase during the decomposition of methyl alcohol decreases as the initial pressure increases, and depends upon the vessel surface. A number of determinations of the final end-points were made at different initial pressures (*a*), and a curve constructed showing the variation of the percentage increase with *a*. The results are given in Table I. The curve has a maximum value of 191% between 30 and 100 mm and falls off slightly at higher pressures, and more rapidly at lower pressures. The variations of the final end-point with pressure for two packed bulbs (A and B), having respectively a surface-volume ratio 7 and 18 times greater than the unpacked bulb, were similar, but at any one initial pressure the end-point becomes smaller as the proportion of surface increases (Table IV). The marked decrease in the end-points at lower pressures in the unpacked bulb may be due to the increasing predominance of surface condensation reactions as the pressure falls. On this account the reaction could not be studied satisfactorily below 6 mm.

THE COURSE OF THE REACTION

As formaldehyde at 669° C decomposes approximately ten times as fast as methyl alcohol, the rate of the reaction is principally determined by the speed at which the first of the two stages

$$CH_3OH = H_2 + H\,.\,CHO$$
$$H\,.\,CHO = H_2 + CO$$

takes place. The pressure change with time is characteristic of consecutive reactions, *i.e.*, the rate at which the pressure increases, becomes greater as the reaction proceeds, owing to the contribution which is made by the ensuing decomposition of the formaldehyde (Table II).

---

* Hinshelwood and Hutchison, 'Proc. Roy. Soc.,' A. vol. 111, p. 245 (1926); Fletcher and Hinshelwood, *ibid.*, vol. 141, p. 41 (1933).

In order to determine the rate of the first stage, it is necessary to know the kinetics of the second stage. Previous work has shown that the rate of decomposition of pure formaldehyde is proportional to the square of its initial pressure ; but in the presence of excess of hydrogen and carbon monoxide, such as occurs in the present reaction, the rate is nearly proportional to the first power of the formaldehyde pressure, as the molecules can be activated by collisions with the products of decomposition as well as by collisions with their own kind. If, in addition, the decomposition of methyl alcohol into formaldehyde and hydrogen is assumed to be unimolecular, the course of the pressure-time curve can be satisfactorily explained. The velocity of the reaction for a given initial pressure may therefore be expressed by the equations:—

$$-\frac{d\,[\mathrm{CH_3OH}]}{dt} = k_1\,[\mathrm{CH_3OH}] \tag{1}$$

$$\frac{d\,[\mathrm{H\,.\,CHO}]}{dt} = k_1\,[\mathrm{CH_3OH}] - k_2\,[\mathrm{H\,.\,CHO}]. \tag{2}$$

The constant k_1 may be determined as follows. If a is the initial concentration in millimetres of methyl alcohol, and $(a - x)$ the concentration after time t, when the amounts of formaldehyde and carbon monoxide present are respectively y and z then

$$-\frac{d\,(a-x)}{dt} = k_1\,(a-x),$$

so that $(a - x) = ae^{-k_1t}$. Also

$$\frac{dy}{dt} = k_1\,(a-x) - k_2y = k_1ae^{-k_1t} - k_2y. \tag{3}$$

The solution of this equation gives

$$y = \frac{k_1}{k_2 - k_1}\,.\,a\,.\,(e^{-k_1t} - e^{-k_2t}). \tag{4}$$

Further

$$\frac{dz}{dt} = k_2y = \frac{k_1k_2}{k_2 - k_1}\,.\,a\,.\,(e^{-k_1t} - e^{-k_2t}),$$

so that

$$z = a\left\{1 - \frac{1}{k_2 - k_1}\,(k_2e^{-k_1t} - k_1e^{-k_2t})\right\}. \tag{5}$$

The pressure increase (p) for the simple decomposition of methyl alcohol into hydrogen and carbon monoxide is $y + 2z$. From equations (4) and (5) it follows that

$$e^{-k_1 t} = 1 - \left(\frac{p + y}{2a}\right),$$

so that

$$k_1 = \frac{1}{t} \log_e \left\{1 - \left(\frac{p + y}{2a}\right)\right\}^{-1}.$$

The constant k_1 may therefore be determined from a knowledge of the pressure increase and of the amount of formaldehyde present at different times. The latter were measured, for an initial pressure of approximately 150 mm by removing the gas mixture and titrating against iodine. A curve was constructed from which the proportion of formaldehyde (y/a) at any time could be read off. Table II shows that the expression $\frac{1}{t} \log_e \left\{1 - \left(\frac{p + y}{2a}\right)\right\}^{-1}$ is constant. Its mean value may be taken as k_1. Its constancy indicates that the course of the reaction

$$CH_3OH = H_2 + H\,.\,CHO$$

at this pressure is unimolecular.

TABLE II—Initial pressure (a)—154 mm of methyl alcohol.
Temperature 669° C

Time (secs) t	Pressure increase (p)	$\frac{y}{a}$	$10^3 \times \frac{1}{t} \log_e \left\{1 - \frac{p+y}{2a}\right\}^{-1}$
18	9	0·040	2·82
28	14	0·052	2·73
43	24	0·061	2·72
57	34	0·063	2·68
70	44	0·064	2·75
86	54	0·065	2·71
124	79	0·061	2·72
150	94	0·058	2·72
167	104	0·055	2·72
187	114	0·053	2·70
216	129	0·049	2·72
248	144	0·046	2·72
273	154	0·043	2·70
		Mean	2·72

From the maximum proportion of formaldehyde (y_{max}/a) formed and from the time (t_{max}) at which the maximum formaldehyde concentration is obtained it is possible, assuming knowledge of k_1, to derive

k_2. For at the time $t_{\max}$, $dy/dt = 0$, and so from equation (3) it follows that

$$k_2 = k_1 \cdot \frac{a}{y_{\max}} \cdot e^{-k_1 t_{\max}}.$$

The values of $t_{\max}$ and $y_{\max}/a$ are 81 seconds and 0·065 respectively. The value of k_2 is therefore $33 \cdot 6 \times 10^{-3}$, *i.e.*, the formaldehyde decomposes 12·3 times faster than the methyl alcohol. Knowing the value of k_2, the proportion of formaldehyde at different times may now be calculated from equation (4) and compared with those experimentally observed. The two sets of values are in close agreement.

TABLE III

Time (secs)	y/a (calculated)	y/a (observed)
10	0·022	0·024
20	0·038	0·040
30	0·049	0·053
40	0·056	0·060
50	0·061	0·063
60	0·063	0·064
80	0·065	0·065
100	0·064	0·064
150	0·058	0·058
200	0·051	0·052
300	0·039	0·040
400	0·029	0·028
500	0·023	0·018

The rate of decomposition of formaldehyde thus calculated may be compared with that obtained from direct measurements at lower temperatures and the known temperature coefficient. Making the calculation for 669° C, we find a value $6 \cdot 6 \times 10^{-4}$ for the constant k of the equation

$$-\frac{d\,[\text{HCHO}]}{dt} = k\,[\text{H . CHO}]^2;$$

i.e., $k = \dfrac{k_2}{[\text{H . CHO}]}$. From the value of k_2, and the maximum value of [H . CHO], the value of k found is $33 \cdot 6 \times 10^{-4}$, for an initial pressure of methyl alcohol of 150 mm. But if the formaldehyde is activated, not only by collisions with itself, but also by collisions with the other molecules present, then

$$-\frac{d\,[\text{HCHO}]}{dt} = k\,[\text{H . CHO}] \, . \, \text{P},$$

where P is the total pressure. Here $k = k_2/\mathrm{P}$, which gives k the value $2 \cdot 24 \times 10^{-4}$. The actual value of k, as found from the temperature coefficient, is intermediate between these two values, but nearer to the latter, thereby justifying the assumption that the other gases present can activate formaldehyde.

In practice it is convenient to derive the constant k_1 at different initial pressures from the time of half-change ($t_{\frac{1}{2}}$). This was taken as the time for the pressure to increase to half the observed end-point. At 154 mm the end-point is 188%. The time taken for the pressure to increase by 94% is 250 seconds. If the decomposition followed a simple unimolecular course, k_1 would be equal to $1/t_{\frac{1}{2}} \log_e 2$, *i.e.*, to $2 \cdot 78 \times 10^{-3}$. The more accurate value from the expression $1/t \log_e \left\{1 - \frac{p+y}{2a}\right\}^{-1}$ is $2 \cdot 72 \times 10^{-3}$, *i.e.*, 2% less. Similarly for an initial pressure of 284 mm the values of k_1 derived in the two ways are $2 \cdot 85 \times 10^{-3}$ and $2 \cdot 69 \times 10^{-3}$. In general, therefore, the velocity constant k_1 may be simply derived from the reciprocal of the half-time. Table I gives the results for some typical experiments. The times $t_{1/3}$ and $t_{3/4}$ are the times respectively for a pressure increase of a third and three-quarters of the final increase. The constancy of the ratios $t_{1/2}/t_{1/3}$ and $t_{3/4}/t_{1/2}$ indicates that the shape of the pressure: time curve is similar at different *initial* pressures. Apart from the initial inflexion the course of the curve is roughly characteristic of a unimolecular reaction. The theoretical values of $t_{1/2}/t_{1/3}$ and $t_{3/4}/t_{1/2}$ for such a reaction are $1 \cdot 71$ and $2 \cdot 00$ respectively.

THE INFLUENCE OF THE SURFACE

The extent to which any surface reaction occurs was found by measuring the rate of reaction in the two packed bulbs A and B. It is apparent from Table IV that some decomposition of methyl alcohol does occur on the surface. The contribution of the surface reaction, however, is approximately the same over the whole pressure range investigated. Thus the ratio of the value of $1/t_{1/2}$ in bulb B to that in the unpacked bulb is $1 \cdot 8$ at 250 mm and $1 \cdot 6$ at 40 mm. As the surface-volume ratio of bulb B is 18 times that of the unpacked, while $1/t_{1/2}$ at 250 mm is only increased by 80%, the decomposition on the surface is probably not more than 5% of the total decomposition occurring at this pressure.

THE INFLUENCE OF THE INITIAL PRESSURE

The dependence of the rate of reaction on the initial pressure may be judged from the values of $1/t_{1/2}$. For a unimolecular reaction $1/t_{1/2}$ does not vary with the initial pressure. For methyl alcohol $1/t_{1/2}$ increases very slightly above 100 mm (*e.g.*, by 20% between 100 and 370 mm), but is constant below 100 mm. In quasi-unimolecular reactions $1/t_{1/2}$ falls considerably for pressures below a certain value. No such behaviour is apparent in this case ; this constancy of $1/t_{1/2}$ is furthermore not fortuitous, and simply the result of a balance between an actual decrease in the rate of the homogeneous reaction and an increase in the proportion of the heterogeneous reaction as the pressure falls. For, if this were so, the ratio of $1/t_{1/2}$ in the packed and unpacked bulbs would not be so nearly equal at different pressures. In addition, if one makes the most unfavourable assumption possible, *i.e.*, that the reaction in the packed bulb B at the lowest pressures investigated (10 mm) is entirely heterogeneous, so that $1/t_{1/2}$ for the surface reaction equals $5 \cdot 0 \times 10^{-3}$, the contribution of the surface in the unpacked bulb is only an eighteenth of this, *i.e.*, $0 \cdot 28 \times 10^{-3}$. As the observed value of $1/t_{1/2}$ in the unpacked bulb at 10 mm is $3 \cdot 4 \times 10^{-3}$, the homogeneous reaction must predominate.

TABLE IV—Temperature 669° C

Pressure range	Unpacked bulb	Packed bulb A	Packed bulb B
	Mean value of $t_{\frac{1}{2}}$ (secs)		
300–400 mm	234	—	—
200–300 mm	254	237	145
150–200 mm	271	247	157
100–150 mm	295	256	166
50–100 mm	302	270	178
15–50 mm	297		195
Mean ratio $t_{\frac{1}{2}}/t_{\frac{1}{4}}$	1·62	1·65	1·63
„ $t_{\frac{3}{4}}/t_{\frac{1}{2}}$	1·82	1·90	1·88
End-point at 250 mm......	184%	170%	140%
„ 150 mm......	188%	180%	147%
„ 50 mm......	190%	183%	162%
„ 20 mm......	187%	180%	168%

The homogeneous decomposition of methyl alcohol appears therefore to be mainly unimolecular, and to show no marked decrease in the rate of reaction at pressures down to 10 mm, below which experimental difficulties limit investigation.

TEMPERATURE COEFFICIENT

The rate of reaction was measured for initial pressures of approximately 200 mm over the temperature range of 626°–730° C. The end-points and the ratios $t_{1/2}/t_{1/3}$ and $t_{3/4}/t_{1/2}$ were not found to vary for different temperatures. It is reasonable therefore to assume that the course of the reaction is the same at each temperature. $\text{Log}_{10}\, 1/t_{1/2}$ plotted against $1/T$ gives a straight line. The experimental values and those calculated from the equation

$$\log_e \frac{1}{t_{1/2}} = 30 \cdot 8 - \frac{68{,}000}{RT}$$

are given in Table V. The correction to be applied to $1/t_{1/2}$ in deriving k_1 will vary slightly with temperature, as the energy of activation of formaldehyde is much lower (44,000 cals.). As the correction, however, is in this case small, the energy of activation will only be raised slightly, and for practical purposes may be taken as 68,000 calories.

TABLE V

Temperature °C	$\text{Log}_{10}(10^4 \times 1/t_{1/2})$ Observed	Calculated
730	2·55	2·58
710	2·25	2·23
689·5	1·90	1·91
669	1·58	1·58
647·5	1·18	1·20
626	0·82	0·81

MOLECULAR STATISTICS

The number of molecules reacting at any temperature is greater than that given by the simple expression $k_1 = Z \,.\, e^{-\frac{E}{RT}}$. However, as it is not known at what pressure, if at all, the value of k_1 begins to fall, it is only possible to derive a minimum value for the number of square terms which must be introduced to explain the observed rate of reaction.

At 669° C and for an initial pressure of 200 mm the number of molecules reacting in 1 cc may be derived from the value of k_1. The value so given is $4 \cdot 98 \times 10^{15}$. Taking the diameter of the methyl alcohol as 5×10^{-8} cm the expression $Z \,.\, e^{-\frac{E}{RT}}$. has the value $6 \cdot 1 \times 10^{11}$. At this pressure, therefore, the number of molecules reacting is about 8000 greater than the simple expression predicts. If the value of k_1 were to fall in this region of pressure in the manner of a quasi-unimolecular reaction, the observed rate could be explained if the energy of activation was divided among 12 square terms. As, however, the rate does not fall off until some lower pressure, 12 is a minimum for the number of square terms which must be involved for the decomposition into formaldehyde and hydrogen.

DISCUSSION

The decomposition of methyl alcohol is of interest in that it shows clearly that the reaction takes place in two distinct stages. On account of the large difference in rate of the two steps, it has been possible to study the kinetics of the primary decomposition into formaldehyde and hydrogen. The methyl ethers are similar to methyl alcohol in that they possess the general formula $CH_3—O—R$; in some cases they also decompose primarily into an aldehyde which subsequently undergoes further decomposition. Dimethyl ether* decomposes into formaldehyde and methane ; methyl ethyl ether† decomposes mainly into acetaldehyde and methane, but partly into formaldehyde and ethane. It may be noted that in each case the main decomposition involves the migration of a hydrogen atom and the removal of the less complex group attached to the oxygen atom. With methyl alcohol this involves the breaking of the —O—H link and not the —O—C link present, even though the bond energy of the former is the greater.

The influence of the nature of the radicle R on the rate of decomposition may best be illustrated by comparing the temperatures at which the limiting high pressure rate (k') attains a given value. For $k' = 2 \cdot 75 \times 10^{-3}$, these temperatures and the values of the energies of activation are :—

for methyl alcohol 669° C, E = 68,000 ;
for dimethyl ether 527° C, E = 58,000 ;
for methyl ethyl ether 539° C, E = 63,000.

The higher energy of activation necessary to decompose methyl alcohol may be connected with the fact that in this case an O—H bond and not an O—C bond must be broken.

I wish to thank Mr. C. N. Hinshelwood for his much valued advice and interest in this work.

SUMMARY

The thermal decomposition of methyl alcohol takes place in the two stages $CH_3OH \rightarrow H_2 + H.CHO \rightarrow 2H_2 + CO$, and, under the experi-

---

* Hinshelwood and Askey, 'Proc. Roy. Soc.,' A, vol. 115, p. 215 (1927).

† Ure and Young, 'J. Phys. Chem.,' vol. 37, p. 1169 (1933).

mental conditions, is very largely homogeneous. The first stage, which determines the rate of reaction, is mainly unimolecular over the whole pressure range of 10–400 mm investigated, and requires an energy of activation of 68,000 calories. The minimum number of energy terms which must be involved to account for the measured rate of reaction is 12.

The Sorption of Vapours by Ferric Oxide Gel

I—Aliphatic Alcohols

By A. Graham Foster, King's College, London

(*Communicated by A. J. Allmand, F.R.S.—Received June* 1, 1934)

In this paper isothermals of a series of alcohols on ferric oxide gel at 25° C are described. The sorption of methyl, ethyl, n. and iso-propyl, and n. butyl alcohols has been investigated in order to determine how the nature of the isothermal alters with the size of the adsorbed molecule. Isothermals of benzene and ethyl alcohol on ferric oxide gel have been described previously,* and an examination of these data† leads to the conclusion that the hysteresis phenomena are associated with a capillary condensation process which follows a true adsorption process on the surface of the pores. The application of the Kelvin equation to the calculation of the capillary radii at corresponding volumes gives the values 16 and 18 A respectively, from the benzene and alcohol isothermals. The lack of complete agreement may, of course, be due to the fact that the limit of validity of the equation has been reached, but there remains a possibility that the difference actually arises from the variation in the thickness of the adsorbed layer with the size of the adsorbed molecules. A similar conclusion was arrived at from an examination of the isothermals of methyl and ethyl alcohol on a specimen of silica gel which exhibits hysteresis,‡ and the present series has therefore been determined in order to provide more extensive data for testing the validity of the Kelvin equation.

---

* Lambert and Clark, 'Proc. Roy. Soc.,' A, vol. 122, p. 497 (1929). Lambert and Foster, *ibid.*, vol. 136, p. 363 (1932).

† Foster, 'Trans. Faraday Soc.,' vol. 28, p. 645 (1932).

‡ Foster, 'Proc. Roy. Soc.,' A, vol. 146, p. 129 (1934).

EXPERIMENTAL

A large amount of ferric oxide gel was prepared in 1926 by Lambert and Clark (*loc. cit.*) for the determination of the benzene isothermals, and the sample used by Lambert and Foster (*loc. cit.*) for the ethyl alcohol isothermals in 1932 belonged to the same batch. The remainder of the preparation had been allowed to stand unactivated since 1926 and the gel used in the present work was taken from this batch, which shows a slight structural alteration, as the isothermals of ethyl alcohol which were re-determined, differ somewhat from those previously described. The present specimen holds 225 mg per gm at saturation whereas the original held 213 ; and the calculated mean radii of the capillaries are 20 and 18 A respectively.

The technique employed for the determination of the isothermals at 25° C was identical with that used for the investigation of methyl and ethyl alcohol on silica gel.* Owing to the lower vapour pressures of n.propyl and butyl alcohols it was necessary to use smaller amounts of gel, about 1 gm, so that the points obtained by the pressure change method should not fall too close together.

The gel after evacuation at 150° C was charged up with vapour until there were visible signs of condensation of liquid on the gel particles. The container was then weighed and transferred to the measuring system; after evacuation of this part of the apparatus, the saturation pressure of the sorbed liquid was checked at 25° C. A series of desorption points was then determined by the pressure change method, the system being maintained isothermally at 25° C until the end of the hysteresis area was reached. The container was then removed and weighed, in order to check the concentration values. At lower pressures the majority of points were obtained by direct weighing, when the amount of vapour removed from the system by evacuating the dead space was less than 2 mg per gm. At pressures below 0·3 to 0·2 mm the removal of vapour from the gel became difficult, even with a liquid air trap in addition to the mercury vapour pump; isothermals were therefore not investigated below this region.

After the determination of the initial desorption curve the gel was flushed out by heating to about 80°C for several hours before the remainder of the charge was removed by evacuation at 150° C. The second desorption curves usually followed the first closely until the lower end of the hysteresis area was reached, below which a slight shift towards the pressure axis was generally observed. After this flushing out treatment the isothermals were found to be reproducible, but on account of the tendency to shift towards the pressure axis, the actual readings are not recorded here, and the results are shown graphically in figs. 1, 2 and 3.

---

* Foster, 'Proc. Roy. Soc.,' A, vol. 146, p. 129 (1934).

The methyl and ethyl alcohols were those used in the experiments with silica gel. The other alcohols were prepared by fractionation of large amounts of the best commercial products obtainable. The saturation pressures of the lower alcohols at 25° C in the presence of the gel, were in good agreement with the values given by Landolt-Börnstein, but the vapour pressure of butyl alcohol was found to be definitely higher than that recorded by Kahlbaum.* The vapour pressure of the pure alcohol was checked by distilling about 1 cc *in vacuo* into an empty gel container, and then taking pressure readings in the manner normally employed for the determination of isothermals by the pressure change method. The pressures remained constant during the vaporization of the entire sample, showing definitely that the high value was not due to the presence of impurity. At 25° C the observed vapour pressure of n. butyl alcohol was 6·75 mm as compared with the value 6·45 mm derived by graphical interpolation from Kahlbaum's data between 18·7° C and 31° C.

Methyl Alcohol

A sample of gel weighing 5·050 gm was evacuated at 150° C and charged with methyl alcohol vapour. Unfortunately the amount added was insufficient to saturate the gel completely, so that the first desorption points fell inside the hysteresis area and not on the true "descending" branch of the loop. After flushing out, a second desorption curve was determined, which showed a considerable shift towards the pressure axis, curve ii, fig. 1. A sorption curve was then determined followed by a third desorption curve which was practically coincident with the second ; this is not shown in fig. 1. A further desorption was carried out, starting from a concentration corresponding to that at which the first run had been commenced, in order to determine where the true "descending" branch of the loop was reached. The dotted portion of curve i indicates the region where the points fall definitely inside the loop and the pressures do not represent true desorption equilibria.

The hysteresis loop begins at 90 mg per gm and the saturation value is 218 mg per gm. The point of inflexion in the final desorption curve is at $q = 155$ mg per gm and $p = 85·75$ mm. The original curve shows a displacement of about 10 mg/gm towards the right, so that it is reasonable to suppose that the initial saturation value was about 228 mg/gm, with the hysteresis beginning at about 100 mg/gm. Readings were taken at intervals of 3 mg/gm in some of the experiments, but the isothermals show no signs of being discontinuous.

---

* 'Z. phys. Chem.,' vol. 26, p. 603 (1898).

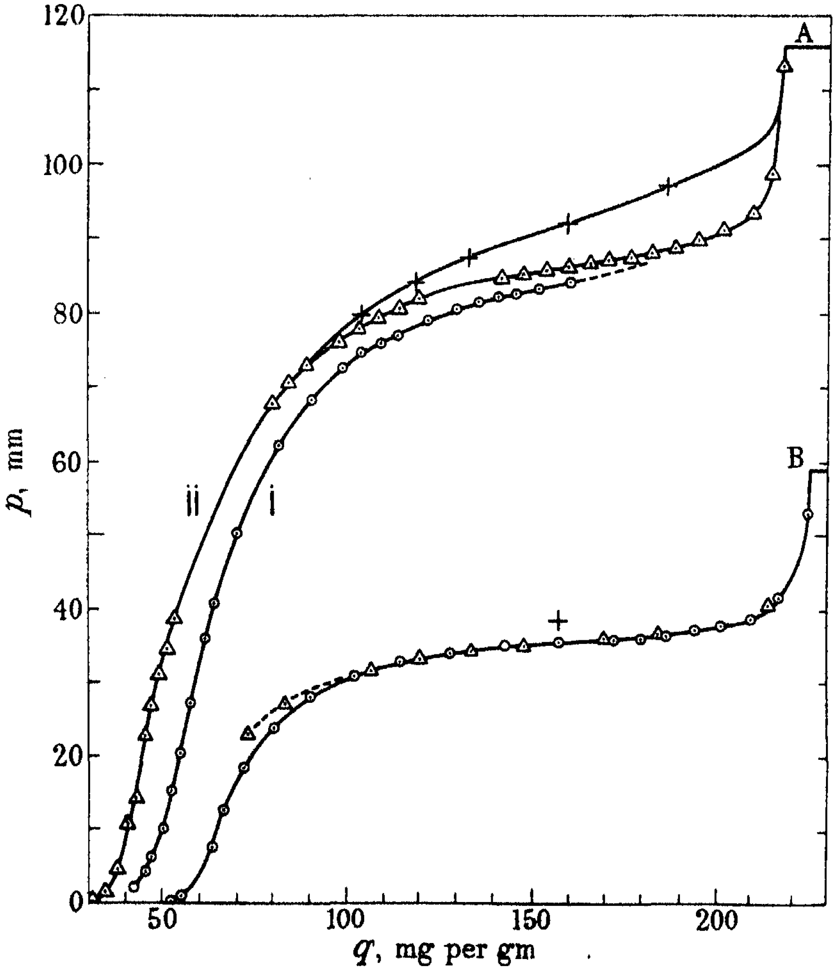

Fig. 1.—A, methyl alcohol ; B, ethyl alcohol; ⊙ first desorption points; △ second desorption points; + sorption points.

Ethyl Alcohol

A sample of gel weighing 1·144 gm was used. After the first desorption the gel was flushed out at 80° C for several hours, evacuated and recharged. The second series of desorption points fell, on the original curve, fig. 1, curve B, throughout the hysteresis area, but showed a shift towards the pressure axis at lower pressures. Only two ascending points were determined, since the previous investigation* had dealt fully with the hysteresis phenomena. The hysteresis area begins at about 100 mg/gm and the saturation value is 223 mg/gm, whilst the point of inflexion in the desorption curve is $q = 160$ mg/gm.

n.Propyl Alcohol

2·206 gm gel was used. The points obtained by the pressure change method fell rather close together, the average separation being about 3 mg per gm in the middle of the hysteresis area. Three quite definite "breaks" were observed during the first desorption before the gel had been subjected to any flushing out treatment. As the following figures show, the breaks are not quite horizontal like the steps reported by Burrage† in the sorption of carbon tetrachloride by silica gel—

(1) $q = 208$ to 191 mg/gm ; p falls from 12·05 to 11·90 mm.

(2) $q = 188$ to 166 mg/gm ; p remains constant at 11·70 mm.

(3) $q = 150$ to 135 mg/gm ; p falls from 11·10 to 11·00 mm.

The gel containing about 60 mg per gm of propyl alcohol was heated to 120° C for several hours and evacuated at 150° C before re-charging. The second series of desorption points followed the original curve closely, but the discontinuities were slightly less definite. At lower pressures the shift towards the pressure axis amounted to only about 3 mg/gm.

Iso-Propyl Alcohol

1·951 gm gel was used. The first desorption curve, curve B, fig. 2, showed no signs of any discontinuities, the average distance between consecutive points being 5 mg/gm in the hysteresis area. After flushing out the isothermal showed a considerable shift towards the pressure axis and a slight alteration in shape at higher pressures. This curve is not shown in fig. 2. The initial saturation value was about 228 mg/gm, as compared with 223 for the normal alcohol.

---

* Lambert and Foster, 'Proc. Roy. Soc.,' A, vol. 136, p. 363 (1932).

† 'J. Phys. Chem.,' vol. 37, p. 735 (1933).

n.Butyl Alcohol

The weight of the gel sample was 0·9990 gm. This was allowed to stand for 48 hours after saturation with vapour since it was thought that equilibrium might not be attained very rapidly, owing to the low vapour pressure of butyl alcohol. The first pressure reading, taken whilst there were still visible signs of liquid in contact with the gel, was 7·15 mm, which is considerably higher than the saturation pressure of 6·75 mm. This may be attributed to the presence of water, removed from the gel by the alcohol, since the effect disappeared after the gel had twice been flushed out at 100° C and re-charged. During the third desorption, the

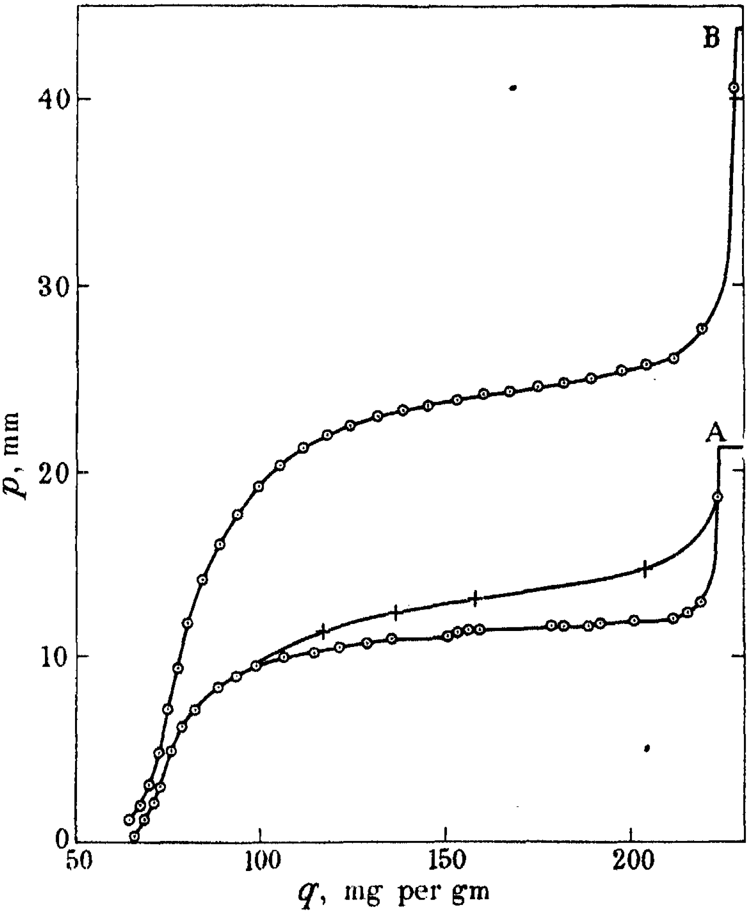

Fig. 2.—A, normal propyl alcohol ; B, iso-propyl alcohol ; ⊙, desorption ; +, sorption.

initial pressures remained constant at 6·75 mm whilst liquid was present. A few sorption points were then determined, followed by some desorption points to check the reproducibility of the previous curve, which is shown in fig. 3 together with the lower portion of the initial desorption curve. There is a slight discontinuity at 3·55 mm, $q = 210$ mg/gm, a further break between 3·35 and 3·30 mm, $q = 203$ to 182, and another between $q = 174$ and 147 mg/gm, where the pressure remains constant at 3·15 mm. The saturation value is 223 mg/gm, and did not alter during the series. The hysteresis begins at $q = 88$ mg/gm in the final run, and the same pressure would correspond to a concentration of about 103 mg/gm for the initial curve.

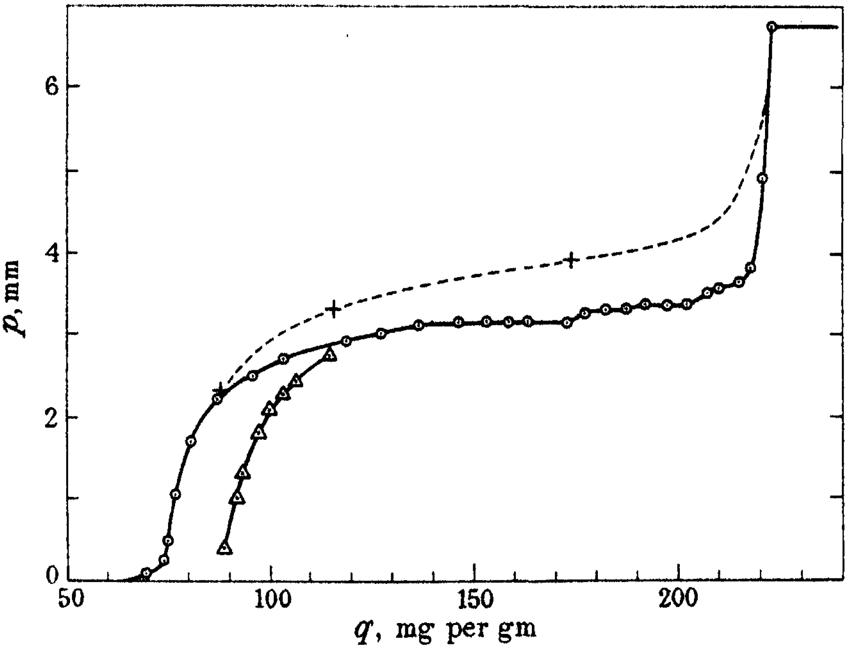

FIG. 3.—n.Butyl alcohol; △, first desorption points; +, final sorption points; ⊙, final desorption points.

DISCUSSION

The general similarity of the isothermals of all five alcohols is at once apparent from a comparison of figs. 1, 2, and 3. The amounts taken up at saturation vary between 223 and 229 mg/gm, corresponding to a volume of about 0·280 cc per gram of gel. The inflexion in the middle of the desorption curve occurs at about 160 mg/gm in each case, but the relative pressures at this point show a gradual decrease from methyl to butyl alcohol.

In Table I are given the actual and relative pressures at the point of inflexion, and also the capillary radii, calculated from the Kelvin equation, corresponding to these pressures. With the exception of ethyl alcohol the agreement is remarkable, three of the five liquids giving identical values. It is of interest to mention that in a similar series of isothermals on silica gel* three of the five alcohols give identical values of 14 A for the capillary radius, so that the agreement obtained with the present series can hardly be attributed to coincidence and would appear to establish the validity of the Kelvin equation for comparative purposes.

TABLE I

Alcohol	Pressure mm	Relative pressure	Capillary radius A
Methyl†	84·5	0·73	22·9
Ethyl................	35·5	0·60	19·9
n.propyl	11·6	0·55	22·9
iso-propyl	22·4	0·56	21·8
n.butyl	3·15	0·47	22·9

† The values for methyl alcohol are taken from the initial desorption curve and not from the final curve, where the radii at corresponding points are about 2 A higher, indicating that a slight change has occurred in the structure of the gel. A similar change has been observed with methyl alcohol on silica gel (Foster, *loc. cit.*), and also with water on ferric oxide gel (Lambert and Clark, *loc. cit.*), where the effect is, however, much more pronounced. With n. propyl and n. butyl alcohol, where the isothermals are discontinuous, the pressures given are those at which the long horizontal break occurs in the middle of the desorption curve.

An examination of the data at low pressures shows that the amounts of the various alcohols adsorbed at corresponding pressures below about one-hundredth of the saturation value are approximately proportional to their molecular weights. Fig. 4 shows the lower portions of the five curves plotted on a large scale and it is evident that the isothermals are falling so steeply that the exact value of the relative pressure at which the q values are compared makes very little difference to the ratios of these values in this region. The values obtained by extrapolation to zero pressure are given in Table II, column 1, whilst the corresponding values of q/M are shown in column 2. (The q values for the points at which the relative pressure is 0·01 show a similar variation, the q/M values being 1·31, 1·17, 1·10, 1·03 and 1·15 from methyl to butyl respectively.)

---

* Foster, unpublished work.

The third column gives the values of the expression $q/M.(M/d)^{2/3}$, which should be constant for the covering of a constant surface area with a film of adsorbed liquid.* These figures increase with increasing molecular weight in contrast with the q/M values which remain constant.

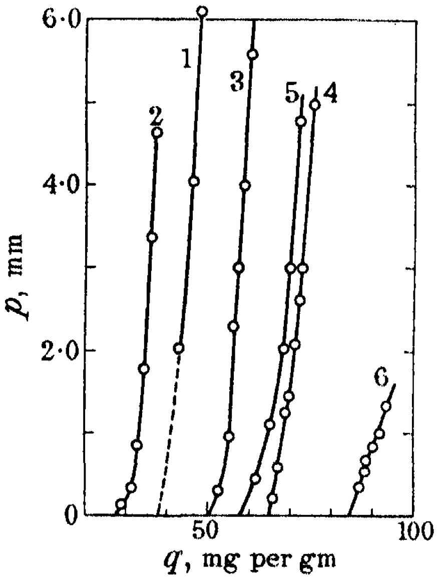

FIG. 4—1, Methyl (initial); 2, methyl (final); 3, ethyl; 4, n.propyl; 5, iso-propyl; 6, n.butyl.

TABLE II

Alcohol	q mg/gm	q/M	$q/M.(M/d)^{2/3}$
Methyl..............	36	1·13	13·4
Ethyl................	51	1·11	16·7
n.propyl	65	1·08	19·2
iso-propyl.	58	0·97	17·4
n.butyl..............	85	1·15	23·4

A comparison of the curves represented in figs. 1, 2 and 3 with the isothermals described by McBain† on highly purified sugar charcoals shows the remarkable difference in shape due to the different structure of the two adsorbents. It was suggested by McBain that the hysteresis phenomena observed with ferric oxide gel would disappear after complete removal of all impurities by flushing out, and that isothermals of rectangular type would then be obtained. This prediction is clearly not confirmed by the present series of experiments, but it is evident that the low pressure isothermals represented in fig. 4 are closely analogous to McBain's rectangular type and show the same abrupt transition from a horizontal to a vertical direction. In both cases therefore, it may be assumed that the *initial* stages of the sorption process are similar and consist in the formation of a unimolecular layer as originally suggested by Langmuir. On the ferric oxide gel, however, this layer occupies only a small fraction of the total volume of the pores, so that further sorption occurs almost entirely by capillary condensation, as may be seen from the shape of the butyl alcohol isothermal, where the 85 mg/gm which is firmly held, may definitely be attributed to a true surface adsorption. Since hysteresis begins at about 103 mg/gm (on the initial curve), there remains out of the total 223 mg only the small amount of 18 mg to be accounted for ; this is only one-fifth of the quantity necessary to complete a second adsorbed layer.

---

* Goldmann and Polanyi, 'Z. phys. Chem.,' vol. 132, p. 321 (1928).

† "The Sorption of Gases by Solids," Routledge, 1932.

With methyl alcohol there is a discrepancy of about 60 mg/gm between the amount assumed to be held in the first layer and that present when condensation begins. This must be held either on the less active points of the surface, if this is not already completely covered, or in a second layer. If the constant values of q/M indicate the existence of a constant number of active centres at which the strongly adsorbed molecules are attached to the surface, it is evident that although the butyl alcohol molecules appear to cover practically the entire surface, the smaller methyl alcohol molecules will be unable to do so. If the further sorption is still taking place in the first layer, it is difficult to understand why there should be such an abrupt change in the potential at which the molecules are held. On the other hand, it is known that the forces acting on a second layer of adsorbed molecules can only be about one-tenth of the magnitude of those operating at the surface, since the potential due to the adsorptive forces falls off as the cube of the distance according to London's theory.* It is also important to mention two factors which tend to assist the formation of an additional adsorbed layer on a non-planar surface : (1), the potential does not fall off so rapidly with the distance from the surface of a narrow cavity as from a plane surface† ; (2), the capillary forces are by no means negligible in comparison with the residual adsorption forces, and there is a potential due to the cylindrical meniscus effect which is approximately one-half that due to capillary condensation in pores of the same size.* The fact that the isothermals of methyl alcohol are convex to the pressure axis above $q = 55$ suggests that the capillary forces are operating, since it is difficult to see how this type of curve can arise from any simple layer adsorption process.

---

* 'Z. phys. Chem.,' B, vol. 11, p. 222 (1930).

† Polanyi, 'Trans. Faraday Soc.,' vol. 28, p. 325 (1932).

An alternative explanation of the results is to assume that in all cases the surface is completely covered by the adsorbed liquid. The constant q/M values would then indicate a definite orientation at the interface similar to that of the long chain fatty acids on water, where it is known that the carbon chains have a constant minimum cross-section of 20·5 A^2 which is independent of the length of the molecule. Using this value for the sectional area per molecule it follows that the minimum surface area required to accommodate 0·0011 gm mol (the amount held at low pressures) is of the order $1 \cdot 4 \times 10^5$ cm^2 per gram of gel.

Now an approximate estimate of the surface area can also be made from the capillary radius which has already been derived by means of the Kelvin equation from the sorption data at higher pressures. The ratio of the surface of a cylinder to its volume is $2/r$, so that a system of cylindrical pores of radius 23 A and volume 0·15 cc (the volume range of the hysteresis area during which the condensation process occurs), must have a surface of at least $1 \cdot 3 \times 10^5$ cm^2. This is also a minimum value since the surface of the adsorbed layer which is covered during the condensation process is less than that of the adsorbent itself, even if the irregular nature of the latter is ignored, but the agreement between two entirely independent methods of calculation suggests that the main assumptions are substantially correct.

In connection with the interpretation of the present results, the experiments of Garner, McKie and Knight,† on the sorption of alcohols from solution by charcoal are of interest. They found that the number of molecules of n.butyl and n.propyl alcohol adsorbed in the unimolecular layer was practically identical, but iso-amyl alcohol gave a lower value. In the present series the value of q/M for iso-propyl alcohol is considerably lower than that for the normal alcohol. This is, of course, easily explained by the larger cross-section of the branched chain, whereas the conception of isolated active centres would require the same amounts of each to be taken up. Another objection to the latter hypothesis is that the calculated surface area of the gel is approximately 3 × 10^6 cm^2 if the butyl alcohol molecules are assumed to lie flat on the surface. This value is of the same order as the highest estimates of the surface of active charcoals, which must have a much finer structure than ferric oxide gel. The value calculated by Garner, McKie and Knight was only 0·67 × 10^6 cm.[2]

---

* When a gram molecule of liquid of molar volume V condenses in a pore of radius r, the free surface of the liquid diminishes by an amount equal to $2V/r$, from which is derived the Kelvin equation. If, however, the same volume condenses in a layer of thickness d on the walls of the capillary, the decrease in free surface is only $2V/(2r - d)$, which reduces to half the former expression when d is small compared with r.

† 'J. Phys. Chem.,' vol. 31, p. 641 (1927).

The constant value obtained for the capillary radius suggests that the thickness of the adsorbed layer is the same for butyl as for methyl alcohol, whereas for a single layer with a definite orientation perpendicular to the surface there should be a difference of the order 4 A. Since it is essential according to the latter hypothesis to assume the partial formation of a second layer of the lower alcohols, in order to account for the amounts held before condensation begins, this second layer must compensate for the variations in the thickness of the first. In other words, there may be a tendency for the adsorbed layer to build up to a constant thickness (or volume) which results in the formation of a second layer when the first does not fill the volume available for layer adsorption.

Further experimental data are essential before it is possible to decide between the two alternative explanations of the present results. Some preliminary experiments with water vapour which are now being carried out, indicate that the amount held at a relative pressure of 0·01 is about 44 mg per gm or 0·0024 gm mol, as compared with 0·0011 gm mol for the alcohols. This result is in excellent agreement with the orientation hypothesis, since the number of molecules adsorbed in the saturation unimolecular layer should be inversely proportional to their sectional area. The value 21 A^2 has already been suggested for the alcohols, and the value for water is about 10 A^2. On the other hand, it is difficult to explain this result in terms of active centres unless it is assumed, either that the centres capable of holding a water molecule firmly are twice as numerous as those which can hold an alcohol molecule at the same potential, or that water is adsorbed as a double molecule. At present therefore, the evidence favours the alternative hypothesis that the entire surface is covered by the strongly adsorbed unimolecular layer.

The author wishes to acknowledge the receipt of a Senior Award from the Department of Scientific and Industrial Research, during the tenure of which the present work has been carried out.

SUMMARY

Isothermals of the following series of alcohols on ferric oxide gel have been determined at 25° C :—methyl, ethyl, normal and iso-propyl,

and normal butyl. All are reproducible and show a large hysteresis loop which extends over almost half the entire range.

The relative pressures at which hysteresis occurs diminish with increasing molecular weight, but the capillary radius (calculated by means of the Kelvin equation from the pressure at the point of inflexion in the desorption curves) remains constant, the average value being about 22 A.

The amounts of the various alcohols held at one hundredth of the saturation pressure are proportional to their molecular weights and correspond to approximately 0·0011 gm mol per gram of gel. This amount is assumed to represent the formation of a unimolecular layer on the surface of the pores. With butyl alcohol this process is followed almost immediately by capillary condensation, but with the smaller molecules there exists an intermediate stage in the sorption process which may represent the partial formation of a second layer.

The Induction Period of the Photochemical Reaction between Hydrogen and Chlorine

By John G. A. Griffiths, and Ronald G. W. Norrish

(*Communicated by T. M. Lowry, F.R.S.—Received June* 23 1934)

The induction period of the photochemical hydrogen-chlorine reaction was discovered by Draper in 1843* ; van't Hoff suggested that contrary to the earlier belief of Bunsen and Roscoe this phenomenon is not inherent in the mechanism of the reaction but due to the neglect of some precaution. This was confirmed by Burgess and Chapman in 1906,† who proved that the inhibition is due to the presence of impurities, mainly of an ammoniacal character, in the reacting gases and the water of the actinometer. When precautions were taken to remove these impurities, the induction period disappeared, but could be produced artificially by the addition of ammonia.

Although Chapman and McMahon,‡ using the water actinometer, found that nitrogen trichloride is one of the most powerful inhibitors and suggested that inhibition by ammoniacal substances is to be interpreted in terms of this compound, neither the actual mechanism by which it exerts its profound influence nor the process by which it is removed during the induction period have been established.

---

* 'Phil. Mag.,' vol. 23, p. 401 (1843).

† 'J. Chem. Soc.,' vol. 89, p. 1399 (1906).

‡ 'J. Chem. Soc.,' vol. 95, p. 1717 (1909) ; vol. 97, p. 847 (1910).

It has been shown by us* that in the absence of water, nitrogen trichloride is produced quantitatively in accordance with the equation :

$$4NH_3 + 3Cl_2 = NCl_3 + 3NH_4 Cl$$

when excess of chlorine is added to ammonia at pressures less than 25 mm. Under these circumstances, the addition of hydrogen produces a mixture in which the photochemical hydrogen-chlorine reaction is completely inhibited. If, however, the pressure of ammonia be greater than the above limit there is a slight explosion and the nitrogen trichloride first formed is decomposed :

$$2NCl_3 = N_2 + 3Cl_2.$$

There is then no observable induction period. These results show that (1) nitrogen trichloride is the inhibiting substance produced when chlorine and hydrogen are added to ammonia, and (2) the ammonium chloride produced at the same time has no effect provided water is excluded from the reaction system.

In the present paper we have attempted to elucidate the mechanism of this inhibition and offer an interpretation of hitherto unexplained phenomena germane to this problem ; this involves three questions, viz :

(1) The nature of the photochemical reaction between chlorine and nitrogen trichloride.

(2) The connection, if any, between this reaction and the process of inhibition.

(3) The degree of inhibition, as measured by the relative quantum yields of hydrogen chloride during and after the period of induction.

The first question has already been answered by our study of the decomposition of nitrogen trichloride photosensitized by chlorine.† This work was undertaken when preliminary experiments revealed that a gradual increase of pressure occurred during the induction period. Typical experimental curves are given in fig. 1 in which the onset of the rapid formation of hydrogen chloride is indicated by the sudden pressure change (Draper Effect) due to the exothermic character of the reaction. The slow irreversible rise of pressure which precedes this was attributed to the reaction :

---

* Griffiths and Norrish, 'Proc. Roy. Soc.,' A, vol. 130, p. 591 (1931).

† Griffiths and Norrish, 'Proc. Roy. Soc.,' A, vol. 135, p. 69 (1932).

$$2NCl_3 = N_2 + 3Cl_2.$$

It was then shown that this decomposition is quantitative, that it is homogeneous and effected only by light which is absorbed by the chlorine in the system, and that it occurs independently of the presence of hydrogen. The quantum yield of the decomposition, which has values as high as 15, and decreases towards a limiting value of *ca* 2 with increasing pressure of chlorine or added foreign gases, shows that we are here dealing with a chain reaction in which the length of chains is dependent upon the total pressure of the system. At the same time the effect of the various gases was found to be specific, and the quantum yield (γ) could be expressed by the following formula :

$$\gamma = \frac{1}{k_1[Cl_2] + k_x[X]} + 2 \cdot 5,$$

where [X] is the pressure of the foreign gas. The value of k_x was found for a series of gases, its magnitude increasing in the following order :

$$He,\ A,\ N_2,\ Cl_2,\ CO_2$$

and being roughly proportional to the diameter of the molecule concerned.

These facts are accounted for by the following chain mechanism :

$$\begin{array}{llll} Cl_2 + h\nu & = Cl + Cl & & (1) \\ Cl + NCl_3 & = NCl_2 + Cl_2 & & (2) \\ NCl_2 + NCl_3 & = N_2 + 2Cl_2 + Cl & & (3) \\ Cl + NCl_3 + X & = NCl_4 + X' & & (4) \end{array}$$

The chain is propagated by reactions (2) and (3) and ended by reaction (4), which is subject to stabilization by ternary collision and accounts for the foreign gas effect.

The experimental part of this paper is concerned with the second and third questions raised above. It has been found that during the induction period the nitrogen trichloride is decomposed by the photosensitized process already investigated, and that hydrogen acts only as an inert gas, taking its place beside helium in the series given above. Further, during the induction period the quantum efficiency of formation of hydrogen chloride is very small, and definitely less than unity, in contrast with values of between 10^3 and 10^5 in the absence of inhibitors, whilst over the first three-quarters of the induction period the amount of hydrogen chloride formed is not measurable by the most delicate method of detection. It would thus appear that inhibition by the nitrogen trichloride must be applied at the very inception of the hydrogen-chlorine chain. This may be interpreted in terms of the two alternative reactions for chlorine atoms:

$$Cl + NCl_3 = NCl_2 + Cl_2$$
$$Cl + H_2 \quad = HCl \ + H.$$

The latter is known to have a probability of 10^{-4} per collision* ; the former must therefore have a probability of the order of unity in order that the propagation of the hydrogen-chlorine chain should, on the average, be stopped at the first chlorine atom, in the presence of a relatively small quantity of nitrogen trichloride. These points will be further discussed after the experimental data have been considered.

EXPERIMENTAL

For the determination of the kinetics of the induction period, an apparatus similar to that employed in the study of the photosensitive decomposition of nitrogen trichloride was employed (*loc. cit.*). Briefly, it consisted of (1) a mixing chamber in which mixtures of chlorine and nitrogen trichloride were prepared by adding excess of chlorine to ammonia, (2) a reaction vessel with plane ends to which chlorine containing nitrogen trichloride and hydrogen were added, and (3) a sensitive Bourdon gauge, which served to measure both total pressures by the null method, and small pressure changes by observation of the deflection by a travelling microscope. Both the reaction vessel and Bourdon gauge were maintained at constant temperature by water pumped from an electrically regulated thermostat. The light beam, furnished by a mercury vapour lamp running at a constant voltage of 150, was focussed by a system of lenses and stops through the thermostat tank and reaction vessel, on to the sensitive surface of a Moll thermopile which was used in conjunction with a Broca galvanomenter. The beam had been calibrated in absolute measure by means of a carbon filament lamp standardized by the National Physical Laboratory. The reactants were prepared by various standard methods and carefully purified—the chlorine and ammonia as already described in our earlier work, and the electrolytic hydrogen by passage over hot palladized copper and drying with phosphoric oxide. The colour filters used were those described in the previous paper : copper sulphate solution to exclude the heat rays, a Wratten (18A) filter for the ultra-violet (365$m\mu$) light, and cuprammonium sulphate and quinine sulphate for the blue (436$m\mu$) light.

---

* Norrish and Ritchie, 'Proc. Roy. Soc.,' A, vol. 140, p. 713 (1933).

In carrying out an experiment, the intensity of the light was first measured with the reaction vessel evacuated. The mixture of gases was then prepared, and allowed to attain homogeneity. When it was certain that all was steady, the irradiation was commenced by raising a screen. After a slight Budde effect (which was equal to the same effect given by pure chlorine) the pressure immediately increased linearly with respect to time and was followed on the Bourdon gauge. This corresponded to the gradual destruction of the nitrogen trichloride. At the end of this period, the hydrogen-chlorine reaction suddenly became manifest by the relatively large Draper effects registered by the gauge ; typical curves are reproduced in fig. 1. An examination of these curves reveals the fact that they are in every way analogous to the curves obtained in the chlorine photosensitized decomposition of nitrogen trichloride, with the difference that the end of the decomposition of nitrogen trichloride is in this case marked by the Draper effect instead of by the semi-explosive change recorded in the previous work.

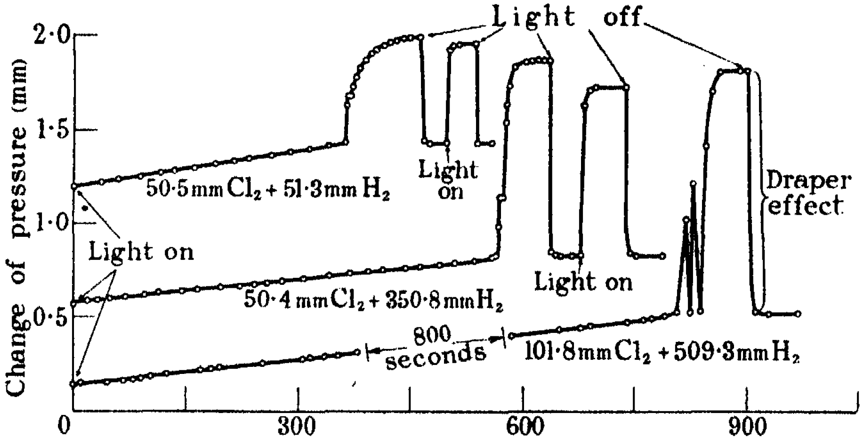

FIG. 1.

At the end of the induction period the apparatus was evacuated, and the light intensity again measured; the mean of the initial and final intensities (which never differed by more than 3%) was taken and from this the number of quanta absorbed by the chlorine calculated from the known extinction coefficient (von Halban and Siedentopf,* Griffiths and Norrish, *loc. cit.*) and the calibration figure for the thermopile.† The number of molecules of nitrogen trichloride decomposed per second was calculated from the dimensions of the vessel (75 cc) and the slope of the curves (*cp* fig. 1). The quantum efficiencies of removal of nitrogen trichloride during the induction period were evaluated by means of the relation: (molecules decomposed per second)/(quanta absorbed per second), and are tabulated in Table I.

TABLE I—" Inert gas effect " of hydrogen

P_{NCl_3}	P_{Cl_2}	P_{H_2}	Incident light galv. defln.	Absorbed light galv defln.	T	γ	γ
mm	mm	mm	cm	cm	sec	obs.	calc.
	50·5						7·7
0·234	50·4	20·3	7·65	3·4	360	7·2	7·3
0·233	50·5	51·3	8·25	3·65	370	6·5	6·7
0·233	50·9	150·1	8·1	3·65	480	5·0	5·5
0·240	50·1	249·8	7·7	3·4	600	4·4	4·9
0·242	50·4	350·8	8·0	3·55	568	4·5	4·4
0·281	50·5	558·5	7·65	3·4	780	4·0	3·9
	100·5						5·1
0·652	100·4	100·2	7·4	5·1	1080	4·5	4·6
0·430	100·2	308·4	7·2	4·95	900	3·6	4·0
0·691	101·8	509·3	7·5	5·25	1380	3·6	3·7

These quantum efficiencies are represented by the formula :

$$\gamma = \frac{1}{0\cdot0038\ P_{Cl_2} + 0\cdot0009\ P_{H_2}} + 2\cdot5,$$

and the figures calculated in the last column of Table I are for comparison.

It is thus clear that the removal of nitrogen trichloride during the induction period follows the same kinetic equation as found in our previous work, the quantum efficiency being depressed towards 2 as the total pressure of the gas mixture is increased. The hydrogen acts solely as an inert gas in this respect, the coefficient being equal to that found for helium (*loc. cit.*).

---

* 'Z. phys. Chem.,' vol. 103, p. 80 (1922).

† The calibration figure, calculation, and procedure were exactly as given in our paper on the photosensitized decomposition of nitrogen trichloride, Part I. 'Proc. Roy. Soc.,' A, vol. 130, p. 591 (1931).

From this result it follows that the period of inhibition, T, is increased by added gases to an extent depending upon their pressure, P_x, and specific "inert gas effect," k_x ; the complete relationship deduced is

$$T = \frac{P_{NCl_3}}{L_{abs.}} \left[\frac{k}{2 \cdot 5 + 1/\Sigma P_x k_x} \right]$$

where $L_{abs.}$ is the light absorbed and k depends upon the volume of the reaction vessel and the units employed. This formula accords with Norrish's conclusion* that the induction period is proportional to the weight of ammonia taken, since it was found that the yield of nitrogen trichloride bears a constant relation to the ammonia used (see p. 141).

Furthermore, the data may be employed in a complete interpretation of the results of earlier workers, and of these, the observation of Draper that pre-illumination of chlorine before the addition of hydrogen diminishes the induction period is to be explained in terms of the photosensitized decomposition of nitrogen trichloride produced from ammoniacal impurities in the actinometer liquid.

As we have observed, ammonium chloride did not cause inhibition in our experiments whereas in those of Burgess and Chapman there was an effect approximately proportional to the weight of ammonium chloride taken. This is to be explained by the fact that in the water of the actinometer, chlorine converts ammonium compounds into nitrogen trichloride† whereas in our research, water was excluded from the reaction system, and under these circumstances chlorine and ammonium chloride do not interact.

PHOTOSYNTHESIS OF HYDROGEN CHLORIDE DURING THE INDUCTION PERIOD

The work of Bunsen and Roscoe, and of Burgess and Chapman indicates that hydrogen chloride begins to be formed at a gradually increasing rate towards the end of the induction period.

The sharpness of the Draper effect, which, in the present investigation, marked the conclusion of the induction period, proved that the rate of formation, if any, of hydrogen chloride suddenly increased enormously, and it is of considerable importance to the accurate understanding of the mechanism to determine to what extent hydrogen chloride is formed during the various stages of the induction period.

---

* 'J. Chem. Soc.,' vol. 127, p. 2323 (1925).

† Chapin, 'J. Amer. Chem. Soc.,' vol. 51, p. 2112 (1929) ; vol. 53, p. 912 (1931).

Experiment showed that the light transmitted by the gaseous mixture during the induction period did not change appreciably and therefore very little chlorine could have reacted to form hydrogen chloride. It may be pointed out that during the few seconds previous to the development of the Draper effect the slope of the pressure-time curve sometimes increased very slightly, indicating either a perceptibly greater rate of decomposition of the nitrogen trichloride or, much more probably, a slight evolution of heat owing to the formation of small quantities of hydrogen chloride.

Analytical—Since it was desired to detect possible traces of hydrogen chloride in chlorine the following method was adopted. After the reactive mixture had been illuminated for the appropriate length of time in a special Pyrex reaction vessel of 220 cc capacity, fig. 2, the tap between the Bourdon gauge and the reaction vessel was closed, and about 20 cc of strong freshly prepared potassium iodide solution were rapidly admitted from the closed funnel, F, by opening tap T. The chlorine reacted with the potassium iodide, and any hydrogen chloride present dissolved. After a few minutes, dry carbon dioxide-free air was admitted to the reaction vessel which was then disconnected from the rest of the apparatus at the ground joint. The iodine liberated was exactly titrated with sodium thiosulphate, starch being the indicator. Potassium iodate was added to the colourless liquid and any acid present liberated an equivalent quantity of iodine in accordance with the equation

$$KIO_3 + 5KI + 6HCl = 3I_2 + 3H_2O + 6KCl.$$

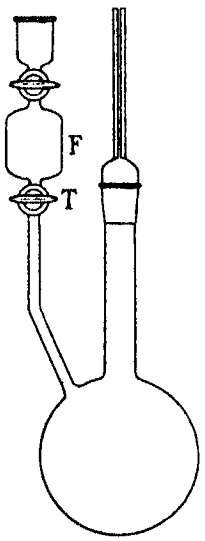

FIG. 2.

The iodine liberated in 2–5 minutes was titrated with 0·01 N sodium thiosulphate. The addition of one drop (0·025 cc) of 0·01 N-HCl produced a pronounced blue colour, this is equivalent to 0·021 mm of hydrogen chloride in the Pyrex reaction vessel.

In Table II are recorded the measurements of the quantum yield of hydrogen chloride for light of wave-length 365 $m\mu$, (*a*) in mixtures of pure hydrogen and chlorine alone, and (*b*) in the presence of nitrogen trichloride, over a period corresponding to 80 to 100% of the induction period. In the former case an immediate Draper effect on illumination showed that the gases were free from inhibitors. The figures for the light flux are subject to a correction factor of 1·49 to allow for absorption and reflexion of the light by the glass of the optical system (Griffiths and Norrish, *loc. cit.*), and the quantum efficiencies were calculated from the calibration data for the thermopile (1 cm galvanometer deflexion corresponded to 2·41 . 10^2 ergs per sec). In the last column are shown the values of the quantum efficiency calculated from the general formula of Ritchie and Norrish,* due allowance being made for the difference in size of the reaction vessels.

TABLE II

			Light flux galv. defln.					Quantum efficiency of HCl formation	
P_{NCl_3}	P_{Cl_2}	P_{H_2}	Incident	Mean absorbed	Time	NCl_3 decomposed	P_{HCl} formed	obs	calc
mm	mm	mm	cm	cm	sec	%	mm		
Nil	50·8	50·5	11·55	8·05	30	—	3·42	1520	1860
Nil	51·1	51·3	11·45	8·05	30	—	3·44	1530	1880
0·19	26·0	28·8	11·25	5·2	300	79	nil	<0·5	1360
0·46	50·0	54·0	9·3	6·7	660	78	nil	<0·2	2300
0·47	51·3	51·5	10·9	7·7	485	83	nil	<0·2	2070
0·88	104·1	113·0	12·1	11·1	1028	100	0·017	<0·2	3940

It will be seen (1) that values of the quantum yield in good agreement with the general formula are found for the pure hydrogen-chlorine mixture, and (2) that in the presence of nitrogen trichloride, during at least four-fifths of the induction period the quantum yield was definitely less than 0·2, our limit of measurement.

Thus the inhibition was virtually complete and quantities of nitrogen trichloride constituting less than 0·1% of the total gas mixture reduced the quantum efficiency by a factor of at least 10^4.

This very significant conclusion received independent support from the fact that the total increase of pressure due to the photosensitized decomposition of nitrogen trichloride is not affected by the presence of hydrogen (see pp. 142, 144) but would be less than indicated by the equation

$$2NCl_3 = 3Cl_2 + N_2$$

were hydrogen chloride present, because hydrogen chloride and nitrogen trichloride vapours interact rapidly, independently of illumination, producing a decrease of pressure.

---

* 'Proc. Roy. Soc.,' A, vol. 140, p. 112 (1933).

This is attributed to the occurrence in the gas phase of the reaction

$$NCl_3 + 4HCl = NH_4Cl + 3Cl_2$$

which is known to be quantitative in carbon tetrachloride solution.* Consistent with this view, a typical experiment, in which 47·5 mm of chlorine containing 0·85 mm of nitrogen trichloride were added to 4·56 mm of hydrogen chloride in a vessel from which light was excluded, showed that the observed total decrease of pressure, 1·74 mm, was almost exactly double the initial pressure of nitrogen trichloride.

Therefore, since in the induction period experiments there was no apparent deficiency of nitrogen trichloride as measured by the increase of pressure (see pp. 142, 144), it is inferred that no appreciable quantity of hydrogen chloride was formed during the induction period.

DISCUSSION OF RESULTS

The data recorded above establish the fact that during almost the whole of the induction period the photosensitized decomposition of the nitrogen trichloride occurs by the normal mechanism, practically to the exclusion of the formation of hydrogen chloride.

Since during the induction period the quantum yield of hydrogen chloride is less than 0·2 it is obvious that the first link of the Nernst chain

$$Cl + H_2 = HCl + H$$

can but rarely be completed. It follows that inhibition must be exercised by reaction of the nitrogen trichloride with the chlorine atoms rather than with the hydrogen atoms of the Nernst chain.

The only scheme of reaction which accounts satisfactorily for the photosensitized decomposition of nitrogen trichloride appears to be the chain mechanism given on p. 142.

This has now to be co-ordinated with the Nernst chain mechanism for the formation of hydrogen chloride, simplified by the fact that all chains must end by reaction of chlorine atoms with nitrogen trichloride, *i.e.*,

$$\begin{array}{llll} Cl_2 + h\nu & = Cl + Cl & \ldots\ldots\ldots & k_1 \\ Cl + H_2 & = HCl + H & \ldots\ldots\ldots & k_2 \\ H + Cl_2 & = HCl + Cl & \ldots\ldots\ldots & k_3 \\ H + HCl & = H_2 + Cl & \ldots\ldots\ldots & k_4 \\ Cl + NCl_3 & = \text{ends chain} & \ldots\ldots\ldots & k_0 \end{array}$$

---

* Noyes and Tuley, 'J. Amer. Chem. Soc.,' vol. 47, p. 1336 (1925).

Remembering that during the induction period [HCl] is zero, we obtain for the quantum efficiency of formation of hydrogen chloride,

$$\gamma = \frac{2k_1k_2[H_2]}{k_0[NCl_3]}.$$

Now $k_1 = 2$, representing two atoms of chlorine formed per quantum of light absorbed and the ratio k_2/k_0 represents approximately the relative collision efficiencies of the reactions

$$Cl + H_2 = HCl + H$$

and $$Cl + NCl_3 \quad \text{ends chain.}$$

Hence, taking the collision efficiency of the first reaction as 10^{-4} and using the data $\gamma < 0 \cdot 2$ when $[NCl_3] \sim 0 \cdot 1$ mm and $[H_2] \sim 50$ mm, we may calculate the collision efficiency of the chain ending process as of the order unity. Thus, every chlorine atom which collides with a nitrogen trichloride molecule is *permanently* put out of action for the formation of hydrogen chloride, and this in spite of the fact that it is regenerated by the nitrogen trichloride chain mechanism.

We are thus forced to the conclusion, suggested by Rollefson,* that the chlorine atoms starting the Nernst chains are in a special condition of activation. This is quite possible, since one of the atoms generated by the light is in the metastable $^2P_{\frac{1}{2}}$ state. Further this, or some other condition of activity must be preserved by the chlorine atoms in the hydrogen chloride reaction chain owing to the exothermic character of the process:

$$H + Cl_2 = HCl + Cl + 44 \cdot 8 \text{ k. cal.}$$

while it is not so preserved in the nitrogen trichloride reaction chain.

All this is in agreement with the view that the nearly thermoneutral reaction

$$Cl + H_2 = HCl + H - 1 \text{ k. cal.}$$

certainly requires some activation.† Thus the nitrogen trichloride is to be conceived as exerting its inhibiting effect by reacting preferentially with the activated chlorine atoms of the chain, and replacing them by an inactive species.

The authors wish to express their thanks to the Government Grant Committee of the Royal Society and the Research Grant Committee of

---

* 'J. Amer. Chem. Soc.,' vol. 51, p. 770 (1929).

† 'Richie and Norrish, 'Proc. Roy. Soc.,' A, vol. 140, p. 112 (1933).

the Chemical Society for grants towards the purchase of apparatus ; they are further greatly indebted to the Governing Body of Emmanuel College for a Research Grant and to the Department of Scientific and Industrial Research for a Research Assistantship granted at different stages of the investigation.

CONCLUSIONS AND SUMMARY

During the induction period of the photochemical hydrogen-chlorine reaction, due to nitrogen trichloride produced by interaction of dry ammonia and chlorine, nitrogen trichloride is decomposed photosensitively by the chlorine in a zero order reaction. In the absence of water, ammonioum chloride does not cause an induction period since it does not react with chlorine.

The quantum efficiency of the decomposition is given by

$$\gamma = 2 \cdot 5 + 1/(0 \cdot 0038 P_{Cl_2} + 0 \cdot 0009 P_{H_2})$$

Hence, hydrogen behaves like the " inert " gases already studied* in shortening the chain length of the photosensitized decomposition of nitrogen trichloride. It is therefore inferred that the induction period is increased by added gases.

During the period of inhibition, which persists until all the nitrogen trichloride is decomposed, the yield of hydrogen chloride is less than 0·2 molecules per quantum absorbed as compared with yields of the order of 1500 molecules obtained with mixtures of pure hydrogen and chlorine.

It is calculated that approximately every collision between a chlorine atom and a nitrogen trichloride molecule renders the chlorine incapable of taking part in the propagation of hydrogen-chlorine chains. Since the mechanism of the decomposition of the inhibitor involves chlorine atoms, it is concluded that only chlorine atoms in the $^2P_{\frac{1}{2}}$ or some other specially activated state, lead to the synthesis of hydrogen chloride, as suggested by Rollefson,† whereas atoms in this special state of activation are not preserved in the nitrogen trichloride reaction chain.

* Griffiths and Norrish, ' Proc. Roy. Soc.,' A, vol. 135, p. 69 (1932).

† ' J. Amer. Chem. Soc.,' vol. 51, p. 770 (1929).

The Swelling of Charcoal

Part III—Experiments with the Lower Alcohols

By D. H. BANGHAM, N. FAKHOURY, and A. F. MOHAMED, the Egyptian University, Cairo

(*Communicated by D. L. Chapman, F.R.S.—Received June* 25, 1934)

1—INTRODUCTION

When a rod of well-baked wood charcoal contained in an extensometer is plunged into methyl alcohol, a noise like the quenching of hot iron is produced, and the moving parts of the extensometer are violently disturbed, as by a sudden impact. Though such effects are to be classed as irreversible and even irreproducible (where the charcoal is visibly fractured), quantitative investigation shows the expansion phenomenon to be no more inherently so than are the effects which accompany the admission of gas to an evacuated vessel. There can be no doubt that the primary factor determining the violence of the effect is the ability of the adsorbed molecules to spread over the surface of the charcoal, not (as has been suggested by analogy with other systems) in a series of infrequent jumps, but with great rapidity. With increase of molecular weight of the alcohol, the effect becomes less violent, especially if only one end of the charcoal is immersed in the liquid ; but in none of the systems so far examined has a time-lag been found between adsorption and expansion.

Granted the free mobility of a fraction of the molecules forming the adsorbed phase on charcoal, mere economy of hypothesis demands that one should enquire, before making *ad hoc* assumptions as to the nature of the charcoal surface, whether or not the phenomena are quantitatively similar to the better understood effects which occur at the surfaces of liquids; the present communication records an attempt to provide an answer to this question by appeal to experiments carried out with a series of adsorbates of closely related constitution. On the basis of the results described in this and in earlier papers, it can be asserted without hesitation that the two sets of phenomena do in fact run parallel to a remarkable degree. No doubt remains that the expansion actually provides a measure of the lowering of the surface energy of the charcoal mass ; this is comprehensible, so far as when wood is carbonized the tendency of the carbon to reduce its surface energy to a minimum must be a primary cause of its shrinkage, and must determine, among other factors, the extent to which this shrinkage takes place. Further, a direct comparison of our expansion data with those for the lowering of the surface tension of mercury by the vapours of the same alcohols brings to light so many points of resemblance as to indicate a similarity of mechanism in the two cases. No evidence whatever was found in favour of the view (of which one of the present authors was an original advocate)[*] that the swelling is a lattice distortional effect caused by sessile adsorbed molecules; and though the investigation of other systems may reveal the existence of an expansion effect where the molecular motions are confined to isolated areas of low potential (and so make it necessary ultimately to reconcile the two conflicting viewpoints), such a development is not foreshadowed in the data here presented.

The principal results given in our earlier contributions[†] may be summarized as follows :—

1. Over certain ranges of concentration the relations between the percentage linear expansion x and the adsorption-value s approximate to those anticipated on the basis of the Schofield-Rideal equation of state,

$$\mathrm{F}\,(\mathrm{A} - \mathrm{B}) = i\mathrm{RT} \tag{1}$$

if the assumption is made that the surface pressure F is given by the equation

$$x = \lambda\,\mathrm{F} \tag{2}$$

where λ is a constant. In equation (1) A and B are respectively the actual and the " incompressible " areas occupied by 1 gram molecule ; i is a dimensionless constant determined by the inter-molecular forces.

2. In most of the cases examined, the relations between x, s, and the pressure p of gas or vapour have approximated to the form required by the Gibbs thermodynamic relationship if the lowering of surface energy is assumed to be proportional to x. Writing Σ for the specific surface of the charcoal, and noting that s is the weight adsorbed per gram, we should have, according to this equation,

$$d\mathrm{F}/s\,d\log_e p = \mathrm{RT}/\mathrm{M}\Sigma. \tag{3}$$

---

[*] Bangham, ' Phil. Mag.,' vol. 5, p. 737 (1928).

[†] Part I, ' Proc. Roy. Soc.,' A, vol. 130, p. 81 (1930) ; Part II, *ibid.*, vol. 138, p. 162 (1932) ; see also Bangham and Fakhoury, ' J. Chem. Soc.,' p. 1324 (1931).

Since $dF = dx/\lambda$, and at zero adsorption $F_0A_0 = RT$ (where $F_0 = x_0/\lambda$ and $A_0 = M\Sigma/s_0$), there follow the relations

$$Mx_0/s_0 = \lambda\, RT/\Sigma \tag{4}$$

$$M dx/s\, d\log_e p = \lambda\, RT/\Sigma = Mx_0/s_0 = \text{constant.} \tag{5}$$

Small deviations from constancy on the part of the expression on the left-hand side of (5) might reasonably be attributed to inequalities in the charcoal surface ; but in one case where the deviations were great (water and charcoal IIA), the x, s relations were, except in one particular,* precisely those which obtain between the pressure and concentration of a substance undergoing condensation by isothermal compression. The Gibbs equation is invalid when two surface phases are present at equilibrium.

2—THE MOLECULAR EXPANSION CURVES OF THE ALCOHOLS : THE CONSTANTS λ AND Σ FOR CHARCOAL II

The molecular expansion graphs resulting from experiments carried out with charcoal II† under isothermal conditions at room temperature are shown in fig. 1. The continuous curves refer to the four straight-chain alcohols, and the broken lines to the branched-chain isomers; the steeply falling initial sections which characterize certain of the curves are here omitted, and representative points only are included in the figure, the lowest curve of all refers to water adsorbed on the same charcoal, and has been inserted for purposes of comparison.

According to equation (2), these graphs should have the same significance as the FA–F curves for surface films on liquids. There is, however, this distinction, that whereas the latter give at once full information as to the equation of state of the adsorbed films, in the case of the former further evidence is required as to the values of the constants λ and Σ.

The ratio λ/Σ *for Charcoal II*—Attempts to evaluate λ/Σ by extrapolation of the molecular expansion graphs to zero conditions (see equation (4)) have not proved of value,‡ and as an alternative method equation (5)

---

* Reversal of sign of the heat of liquefaction ; see Part II.

† A pinewood charcoal, part of the original stock carbonized by Meehan, 'Proc. Roy. Soc.,' A, vol. 115, p. 199 (1927) ; evacuated at 560° C, and previously used for many of the experiments described in Part II.

‡ The use of an extensometer of low magnification ratio to investigate the properties of highly "imperfect" gaseous films may be partly responsible for the difficulty in obtaining consistent values of Mx_0/s_0 by extrapolation, but the imperfection of the charcoal surface is probably also a contributory cause. Suggestive

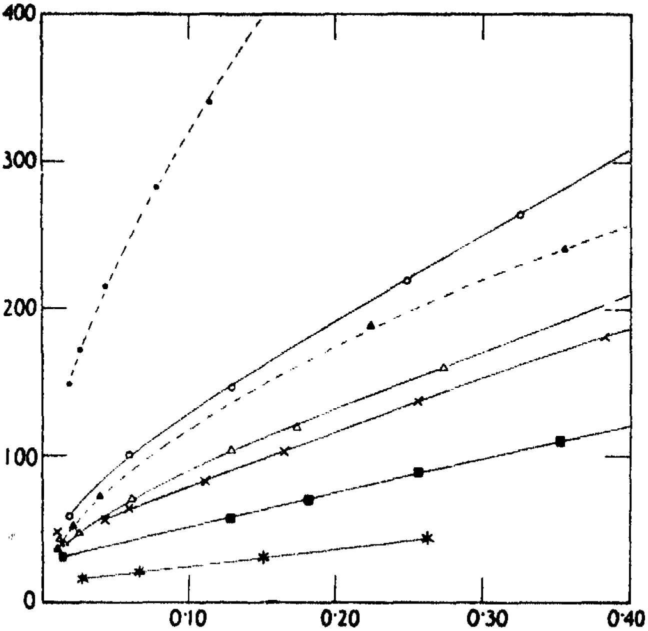

FIG. 1.—Molecular expansion curves of the alcohols and of water, adsorbed on charcoal II.

● Primary iso-butyl alcohol ; ○ n.butyl alcohol ; ▲ iso-propyl alcohol ; △ n.propyl alcohol, ; × ethyl alcohol ; ■ methyl alcohol ; * water.

evidence on this point is provided by the experiments at low temperatures, wherein abnormally high expansion values were invariably recorded in the region of low concentration. The following are examples :—

	s gm/gm	x%	Mx/s × 273/T
CH_3OH, t = −78° C	0·0040	0·016	180
	0·0075	0·021	126
	0·0110	0·027	108
	0·0220	0·044	90
n-C_3H_7OH (−30°)	0·0093	0·018	130
	0·0151	0·024	105
n-C_3H_7OH (−30°)	0·0059	0·011	130
	0·0121	0·019	108

Though the molecular expansion is here falling sharply with increase of concentration, the values are consistently higher than those found for Mx_0/s_0 by the alternative method described in the text. Such anomalous results were obtained only at lower temperatures, and were more conspicuous for some more strongly pre-heated charcoals. The change with temperature of the zero-point of the extensometers was frequently checked in the course of the investigation, and, as concordant results were invariably obtained, no error is assignable to this cause. The crowding together of molecules in areas of minimum potential is a possible explanation ; it is readily understandable has been used in connection with the pressure data. The investigation has yielded in two cases data of high accuracy whereby the validity of this equation may be tested. With methyl alcohol in contact with charcoal II the values of Mx_0/s_0 and λ/Σ so calculated were found to be independent of x over about four-fifths of the total range of expansions ; independent evidence points to the co-existence of two surface phases as the most probable cause of the deviation in the first-fifth of the range. With ethyl alcohol the agreement was almost equally good. The values obtained were* :—

Methyl alcohol :

$$Mx_0/s_0 \text{ at } 0^\circ \text{ C} = 66{\cdot}4\% \; ; \; \lambda/\Sigma = 2{\cdot}93 \times 10^{-9} \text{ ergs}^{-1}$$

Ethyl alcohol :

$$Mx_0/s_0 \text{ at } 0^\circ \text{ C} = 68{\cdot}3\% \; ; \; \lambda/\Sigma = 3{\cdot}01 \times 10^{-9} \text{ ergs}^{-1}$$

TABLE I

(The saturation adsorption values have been found by extrapolating the molecular expansion curves to the saturation values of the expansion ; the latter, which have been determined experimentally, were found to have small negative temperature coefficients.)

	CH_3OH 20°C	C_2H_5OH 30°C	n-C_3H_7OH 20°C	n-C_4H_9OH 30°C
Saturation adsorption gm/gm	0·149	0·137	0·157	0·133
Saturation expansion %	1·029	1·018	1·011	1·029

Though the necessarily less accurate data for the less volatile alcohols provide no independent proof of the accuracy of equation (5), they are, at all events, consistent with its validity. The most reliable values of λ/Σ found for n. and iso-propyl alcohols do not differ widely from those given by methyl and ethyl, though a slight progressive increase with molecular weight is also not precluded. A comparison of the saturation values of the adsorption and expansion in the case of the four straight-chain alcohols (see table above) reveals an absence of progressive change

---

that differences in the force field which may be insignificant at one temperature would become important at a lower one. With rise of concentration the influence of the intermolecular forces (attractive and repulsive) becomes more and more important, and it is these, rather than the deviations of the surface from the equipotential, which then appear to determine the distribution of molecules in the films.

* Values of the percentage linear expansion x are dimensionless ratios, as are also those of the molecular expansion; the constant λ has the dimensions of a length (centimetre) per unit force (dyne).

with molecular weight that is certainly best explained in terms of values of λ and of Σ that are common to all four of these alcohols.

Slopes of the Molecular Expansion Curves—The arbitrary assumption that the films are unimolecular, and that Σ takes the same value in all cases, leads at once into difficulties. For example, the slopes of the molecular expansion curves of primary iso-butyl alcohol and water, given in fig. 1, stand in the ratio of about 16 : 1. The cross-section of the water molecule being near 10 A, that of the alcohol would then be some 160 A, a figure about three times too great. At first sight it appears probable that Σ takes a smaller value for the alcohol on account of the much larger size of its molecules, and some support is lent here by the fact that the still less flexible and less slender molecules of the tertiary isomer $(CH_3)_3COH$ were not adsorbed by charcoal II. Experiments with the simpler alcohols at lower working temperatures, however, revealed the transient existence of unstable films for which the molecular expansion curves were quite as steep, in proportion to molecular size, as that of primary iso-butyl alcohol. In the sections which follow these are referred to as " primary " films. If, after each addition of vapour, the charcoal was first warmed and then allowed to cool slowly to the temperature of reading, the effect at all but the lowest concentrations was to produce films characterized by much flatter molecular expansion curves ; the slopes of these curves for the normal alcohols were as small, in comparison with molecular size, as that of water on the same charcoal. The term " annealed " is used to designate this second type of film, it being desirable to use a term carrying no implications as to structure. That the curves for the heat-treated films actually differ but little from those shown in fig. 1 may be expressed in the statement that the films undergo self-annealing at room temperature, this being particularly rapid with methyl and ethyl alcohols ; in other cases the curves for the annealed films are rather flatter, especially near the axis.

Estimates of Σ based on data for other charcoals—Water adsorbed on charcoal IIA (a charcoal of the same origin as charcoal II, but pre-heated for a longer period) gave a molecular expansion curve different from that shown in fig. 1, and resembling the PV–P graph of a vapour undergoing liquefaction by isothermal compression.* On the supposition (*cf.* Semenoff†) that the film was unimolecular at the point where a sudden expansion indicated the disappearance of the surface vapour phase (the molecules being now everywhere in contact), it was calculated that Σ for charcoal IIA lay between the limits of 160 and 190 m^2/gm. Attempts to obtain similar data for charcoal II have not proved successful, for, although sharp break-points were found in certain experiments, these appear to relate to an isothermal transition from the primary to the annealed type of film, and evidence of actual liquefaction is lacking.*

---

* Part II.

† 'Z. phys. Chem.,' B, vol. 7, p. 471 (1930).

Experiments with charcoal III, which was pre-heated to 1000° C, were more successful; when methyl alcohol was adsorbed on this charcoal at 20° C, there was no measurable expansion until 0·059 gm/gm had been adsorbed, but a marked expansion at 0·07 gm/gm, beyond which point the expansion increased steadily. The exact dimensions and orientation of the methyl alcohol molecules being unknown, this datum does not permit a very close estimate to be made of Σ; the assumption of spherical symmetry is unlikely, however, to lead to a large error in this case, and the upper and lower limits calculated on this basis are 220 and 185 m^2 respectively.

The four natural wood charcoals examined by us have shown remarkably little variation in the volumes (reckoned in terms of the normal liquids) of different substances adsorbed at or near saturation.† It is legitimate to conclude that the variation of Σ from one to another of these charcoals is not great. Although not referring, therefore, to the charcoal mainly concerned in this investigation, the estimates of 160–190 m^2 and 185–220 m^2 for charcoals IIA and III respectively are of importance as providing data for comparison with values found by other methods.

Calculation of Σ by comparison with the behaviour of films on mercury—The molecular expansion graphs for both the primary and the annealed films of the first four straight-chain alcohols find their counterpart in the FA–F curves derived from the data of Cassel and Salditt‡ for the lowering of the surface tension of mercury by their unsaturated vapours. Certain of the results arrived at in Part IV of this series, where a full comparison of the two sets of data is made, may here be anticipated :—

1. From the relative slopes of the molecular expansion and FA–F graphs for the primary films of n.propyl alcohol there is obtained, as a rough estimate, $\Sigma = 200$ m^2 ; values similarly calculated from the more fragmentary data for the other alcohols are of the same order.

---

* See, in particular, the section dealing with methyl alcohol.

† To give examples : charcoal III adsorbed 0·152 gm/gm of methyl alcohol at a pressure 95% of saturation, as against 0·153 gm/gm adsorbed by charcoal II at 98% of saturation, the temperature in both cases being 20° C ; charcoal IIA took 0·123 gm/gm of water at 94% of saturation, as against 0·130 gm/gm adsorbed by charcoal II at about the same relative humidity.

‡ 'Z. phys. Chem.,' vol. 155, p, 321 (1931).

2. From the respective positions of the two sets of curves for the annealed films relative to Mx_0/s_0 on the one hand and to F_0A_0 on the other there is obtained, as the mean value for the four alcohols, $\Sigma = 176$ m². This estimate assumes a common value of Mx_0/s_0 for all four alcohols ; also that at equal surface concentrations of each adsorbate the surface pressures are equal in the two cases. Both assumptions are supported by the data, since the values calculated for each alcohol separately do not differ greatly from this mean value.

The general agreement between all seven determinations of Σ affords a striking vindication of the interpretation placed on the expansion data, and shows the latter to be self-consistent when expressed in terms of known molecular and other magnitudes. Whilst values of the specific surface of charcoal of the same order have been given by a number of authors, the assumptions on which most of these rest are such as would invalidate comparison,* even if it were not for the divergence of properties shown by charcoals of different origin.

Taking $\lambda/\Sigma = 2 \cdot 97 \times 10^{-9}$ ergs^{-1} and $\Sigma = 176$ m² (these being in both cases the average values of the most reliable estimates), the value found for λ is 0·0052 cm/dyne ; thus each abscissa scale division of fig. 1 would correspond to a surface energy lowering of about 19 dynes. Whilst caution is desirable in assuming the validity of these constants in the case of adsorbates of widely different constitution, they will be taken as the basis of calculations of the film thicknesses and molecular areas of the alcohols.†

---

* This remark does not apply to the determinations of Bartell and Ying Fu (' Colloid Symposium Annual,' vol. 7, p. 138 (1930)). These authors found for the specific surface of an activated sugar charcoal values of some 630 m² ; judging from the heats of wetting recorded in their paper, this charcoal was characterized by an adsorptive capacity much greater than the inactive wood charcoals used by us.

† For these calculations, see Part IV. The values of Mx_0/s_0 found for benzene and pyridine adsorbed on charcoal II (see Part II) were somewhat higher than those given here for the alcohols. Although reference to unpublished data gives some grounds for suspecting that the former determinations, which depend much on the accuracy of one or two observations where the temperature control may not have been perfect, may be a little high, the assumption that the values of λ and Σ here given are common to all adsorbates would be quite unwarranted. The only reliable determinations of Mx_0/s_0 are those in which the coefficient $dx/d \log p$ is proved accurately proportional to s over a range of expansions. Fortunately, since an error in λ affects only the scale, and not the shape, of the molecular expansion graphs, an uncertainty in the value of this constant does not place a very serious obstacle in the way of their interpretation. A large difference in the Σ values for two adsorbates would probably be rendered conspicuous by a marked departure from the well-known rule of Gurvitsch.

The Effect of Temperature—It appears to be characteristic of the annealed films that the expansions corresponding to a given adsorption are proportional, or very nearly so, to the absolute temperature; the molecular expansion graphs for these films at different temperatures are thus brought into coincidence by multiplying both abscissa and ordinate variables by 273/T. This rule affords some justification for assuming a zero temperature coefficient for λ. It is not unlikely that λ is related to the elastic constants of the charcoal,* the temperature coefficients of which would be but very small.

3—DISCUSSION

The assumption upon which the above conclusions rest, namely, that the adsorbed films of the alcohols are characterized by the same equation of state whether adsorbed on mercury or on charcoal II, appears justified, in the case in point, by the experimental evidence alone.† Such an assumption does not lack justification in terms of accepted theories as to the nature of adsorptive forces, but it raises the question as to why such a variety of behaviour should be shown by different charcoals. According to the "potential" theory of Polanyi,‡ now based on a consideration of the additive nature of van der Waals or "dispersion" forces, the same equation of state should apply, in simple cases, when the molecules of a substance form an adsorbed film as when they form a phase in three dimensions. This simple result requires modification for long molecules with active head-groups, for here orientation effects will clearly play an important part.§ With the reservation that accidents of molecular geometry may in special cases give rise to the opposite effect, it is to be expected that molecules adsorbed at a surface will usually be so oriented as to render the forces between them less powerful than they are under conditions of random orientation. There will therefore be less tendency for the molecules to cohere as liquid, and the heat of liquefaction will be reduced; it may even become negative if the liquefaction requires that a sufficiently large amount of work should be done in re-orienting the molecules.* With increasing temperature the orientation effects will become less marked, and the departure from the equation of state of the bulk material correspondingly reduced. All these results are in accordance with the experimental facts relating to charcoals II and IIA, and we conclude that orientation effects play an important part in determining the behaviour of the films formed on them.

---

* The following calculation based on the numerical values of λ and Σ is of interest. A plane non-porous lamina 50 A in thickness would have about the same area per gram as that assigned to charcoal II, if both sides contribute to the area and the density of the material is that of graphite. If it be supposed that a surface "pressure" of F dynes/cm has the same stretching effect as a mechanically applied longitudinal tension of 2F, the elasticity modulus calculated from the value found for λ amounts to about $7 \cdot 7 \times 10^{10}$ dynes/cm.^{2} This result is of the same order as the longitudinal (Young's) modulus of such materials as wood, and about one-half that of lead. Strictly such comparison is not justified, since in the case of Young's modulus a contraction takes place in both directions normal to the applied tension. Nevertheless the calculation is of interest, and the fairly high value obtained casts some doubt on the suggestion made in Part I, that the occurrence of an expansion may be dependent on the presence of gross irregularities in the surface. The value of the modulus found is to be regarded as a minimum, for it has been assumed that the stress is shared equally by all the atoms forming the section of the lamina.

† See Part IV, which follows.

‡ London and Polanyi, 'Naturwiss,' vol. 18, p. 1099 (1930).

§ *Cf.* Fowler, 'Faraday Soc. General Discussion,' p. 442 (1932).

Such evidence as is available suggests that gaseous films of readily condensible substances are less persistent in charcoals more strongly pre-heated; the contrasting behaviour of water on charcoal II, heated to 560° C, and on charcoal IIA, heated for a longer period to the same temperature, and of methyl alcohol on charcoal II and on charcoal III, heated to 1000° C, are examples. Two causes may contribute to these differences of behaviour, though much more evidence is required before any conclusions can be drawn. First it is possible that, either by the re-arrangement of the carbon atoms in the surface, or by the removal of some of them in combination with hydrogen or oxygen, a distortion of the equipotential surface is brought about, with the production of localities where conditions favour the formation of liquid nuclei.† A further effect of heat may be the removal of adsorbed impurities, of which the molecules, if mobile, would hinder the growth of liquid nuclei in much the same way as a small admixture of permanent gas will hinder the condensation of vapour in the cooled end of a capillary tube.

Whilst the possible presence of unremoved impurities is an inherent difficulty in investigations with charcoal, it is not easy to see what impurities could hinder liquefaction of the films of the alcohols on the freshly formed mercury surfaces of Cassel and Salditt. It appears more probable that in the absence of surface irregularities the orientations assumed by the molecules are statistically unfavourable to the formation of liquid nuclei. As is shown elsewhere, the annealed films of the normal alcohols contain molecular aggregates between which only weak cohesive forces are acting. Whether or not such aggregates would be stable in the presence of liquid nuclei, it seems certain that their stability has much to do with the absence of liquefaction.

---

* The authors can find no justification for the assumption, often made, that spontaneously occurring processes taking place at surfaces are necessarily exothermic.

† *Cf.* Allmand and Burrage, 'Proc. Roy. Soc.,' A, vol. 130, p, 629 (1931).

To sum up, the validity of the calculation of Σ by the method of comparing the data for mercury and charcoal II does not necessarily require that the substrate should be without determining influence on the behaviour of the adsorbed films, but merely that there should be similarity of orientation in the two cases. The existence of well-defined regularities common to both sets of data makes it certain that this condition is at least approximately satisfied.

The "Retrograde" or "Relaxation" Effect—The transition of the "primary" to the "annealed" type of film was accompanied, where the pressure was sufficiently low, by a contraction of the charcoal. This phenomenon, termed by McBain* the "relaxation" effect, has already been recorded in earlier papers, where it was suggested that it might be due either to re-orientation of the molecules, or to a fraction of their number taking up fixed positions on the surface. These interpretations may now be replaced by a more general conception: given that the total adsorption remains constant, or nearly so, an effect of the kind described is to be anticipated whenever the surface film tends to a state of lower free energy, whether by the disappearance of an unstable phase or by a re-adjustment of molecular condition in homogeneous phase. The explanation of the effect recently given by Burrage,† who ascribes it to the "flushing out" of gases previously forming part of a spongy complex (the swelling of which is supposed by him to be the cause of the expansion), is directly contrary to the facts. Our data for charcoal II show the expansion measurements to be precisely reproducible, within the very small reading error, after a four-year interval, during which the charcoal was flushed out perhaps seventy times with gas-free saturated vapours, but came in contact with no other source of oxygen. It follows that such minimal quantities of gases as were flushed out (these quantities were unmeasurably small in the experiments here described) were entirely without influence on the expansion measurements.‡

---

* McBain, Porter and Sessions, 'J. Amer. Chem. Soc.,' vol. 55, p. 2294 (1933).

† 'Trans. Faraday Soc.,' vol. 29, p. 458 (1933).

‡ The authors would be reluctant to describe any wood-charcoal as gas-free. Judging by its failure, however, to evolve gases when exposed to saturated vapours, charcoal II was more carefully evacuated than many that have been so described. The statement of McBain, Porter and Sessions (*loc. cit.*) that air was not thoroughly excluded during the course of our earlier experiments of this series is contrary to fact, and clearly arises through a misunderstanding of our experimental conditions.

4—APPARATUS AND MATERIALS

The apparatus and technique employed in the measurements have already been described fully in Part II. The charcoal, designated charcoal II in Part II, was the identical piece used for the experiments with benzene, pyridine, etc., and had at no time been exposed to air since the apparatus was set up in its final form ; it was part of the stock originally prepared by Meehan.

The methyl alcohol was prepared by the hydrolysis of re-crystallized methyl oxalate. The product was dried over ignited potassium carbonate and fractionally distilled. The distillate, after being refluxed over metallic calcium, gave a product of normal boiling point. After introduction into the sealed apparatus, the alcohol was again fractionated several times to free it from dissolved air; it then gave the following vapour pressures at the temperatures indicated:—

$t =$	$-3°$	$0°$	$5°$	$10°$ C
$p =$	25·05	30·06	40·75	54·67 mm

These values are in fair agreement with data of Ramsay and Young quoted in the Landolt-Börnstein tables.

The ethyl alcohol was obtained by refluxing a good grade of absolute alcohol over metallic calcium and fractionating the product. The n.propyl iso-propyl and n. and iso-butyl alcohols were Kahlbaum's purest quality preparations, and were used after prolonged drying over ignited barium oxide, followed by repeated fractionation. The boiling points were in all cases normal after this treatment. Each alcohol, after introduction into the apparatus, was fractionated under low pressure to free it from dissolved air. In view of the anomalous results obtained with n.propyl alcohol, which are described in a later section, the stock was removed from the apparatus and more drastically purified, the same procedure being followed. The product gave the following values of the vapour pressure at the temperatures indicated :—

$t =$	$0°$	$3·8°$	$6·5°$	$10·6°$ C
$p =$	3·55	4·49	5·76	7·52 mm

These are again in fair agreement with the values based on Ramsay and Young's measurements recorded in the tables.

The tertiary butyl alcohol was prepared from the hydrated liquid, which, after a preliminary drying, was refluxed with metallic calcium. The supernatant liquid was fractionated, using a long column. The fraction passing over at 83° C solidified, giving fine dry needles, which gave a sharp melting point (temperature unrecorded). The alcohol was further purified by vacuum sublimation after introduction into the apparatus. The following are the sublimation pressures measured at the temperatures indicated :—

t = 0°	4·2°	10·1°	15·6°	19·2° C
p = 4·70	7·42	12·99	19·96	26·85 mm

Deadspace measurements—In calculating the quantities of vapour present in the different parts of the calibrated system the validity of the ordinary gas laws was assumed. Control experiments carried out along the lines described in Part II showed this to be justified. In Table II are given, in arbitrary units, the values of the product pv of quantities of four of the alcohols as measured at different pressures and room temperature.

TABLE II

CH_3OH		C_2H_5OH		n-C_3H_7OH		$(CH_3)_3COH$		$(CH_3)_2$ CHOH	
p mm	pv	p mm	pv	p mm	pv	p mm	pv	p mm	pv
15·8	1·000	12·6	1·000	2·6	1·000	12·1	1·000	7·1	1·000
21·6	1·005	17·3	1·002	3·5	0·982	16·75	1·001	9·8	0·991
34·1	0·989	27·2	0·989	5·5	0·974	27·9	1·001	15·7	0·957
77·7	0·977	61·8	0·971	13·1	?1·003				

Such deviations as appear are probably due to a wall effect,* and the errors introduced into the burette measurements are therefore not cumulative.

5—EXPERIMENTS WITH METHYL AND ETHYL ALCOHOLS

Eight experiments were carried out with methyl alcohol, covering the range of temperatures from −78° to 0° C. The usual tests for displaced gas gave negative results throughout. Except at −78° C steady values of p and x were rapidly attained, and were unaffected by annealing the films at 50° C.

Molecular expansion graphs of methyl alcohol—The molecular expansion graphs resulting from these measurements are shown in fig. 2 ; both abscissa and ordinate variables have here been multiplied by 273/T in order to render the results at different temperatures more readily comparable. As the diagram indicates, the curves for 50°, 20° and 0° C are thus brought into coincidence over a great part of their range. The curve common to the three temperatures is very nearly linear over much of its course, and in both shape and position is typical of what have been termed the "annealed" films of the normal alcohols. If the linear portion be produced back to cut the axis, it does so at $Mx/s = 28\%$, and not at the origin; the coincidence of the curves for different temperatures is not, therefore, due to liquefaction.

---

* See Part II.

At 0° C the characteristics of the annealed films do not appear until the adsorption exceeds some 0·06 to 0·07 gm/gm ; when s is smaller than this, the molecular expansion graph at this temperature follows the course of the broken line shown in the lower graph of fig. 2. These higher values of the molecular expansion persist even if the films are heated to 50° before each reading at 0°. As a further test of reversibility, a desorption experiment was carried out at 0° C. In this the molecular expansion values followed the normal curve until the adsorption fell below 0·08 gm/gm. Thereafter the readings, both of the pressure and of the expansion became somewhat irregular. Some of the results of this experiment are included in fig. 2.

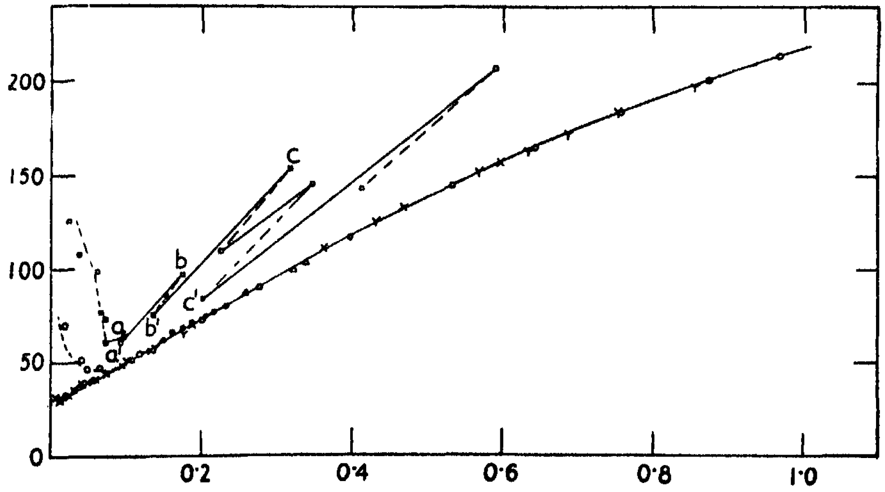

Fig. 2—Lower graph: molecular expansion graph, reduced to 0° C, for annealed films of methyl alcohol ; 50°, Δ ; 20°, ×, Y ; 0°, adsorption increasing, O; 0°, adsorption decreasing, ●. The broken line shows deviation from normal curve at 0° and low concentration.

Upper graph : molecular expansion graph, reduced to 0° C, for films of methyl alcohol at —78° □

Since, other things being equal, the influence of intermolecular forces is to reduce the expansion effect, it appears that at low concentration these forces are less effective at lower temperatures. This is more strikingly shown by the results at −78° C, also included in fig. 2. The large and immediate expansions produced by the addition of small quantities of vapour at this temperature were stable until the minimum point on the molecular expansion graph was reached ($s = 0\cdot039$ gm/gm), but at higher concentrations a marked relaxation effect was observed. In the graph points a, b, c, . . . refer to observations made as soon as possible after each addition of vapour, and points a', b', c', . . . to others made after standing for much longer periods. Since the retrograde movement set in rather sharply, but later became very slow, the former points do not necessarily represent the full extent of the forward movement, nor the latter that of the backward drift. The conditions rendered the prolongation of this experiment difficult, and it remains an open question whether, given sufficient time, the retrograde movement would

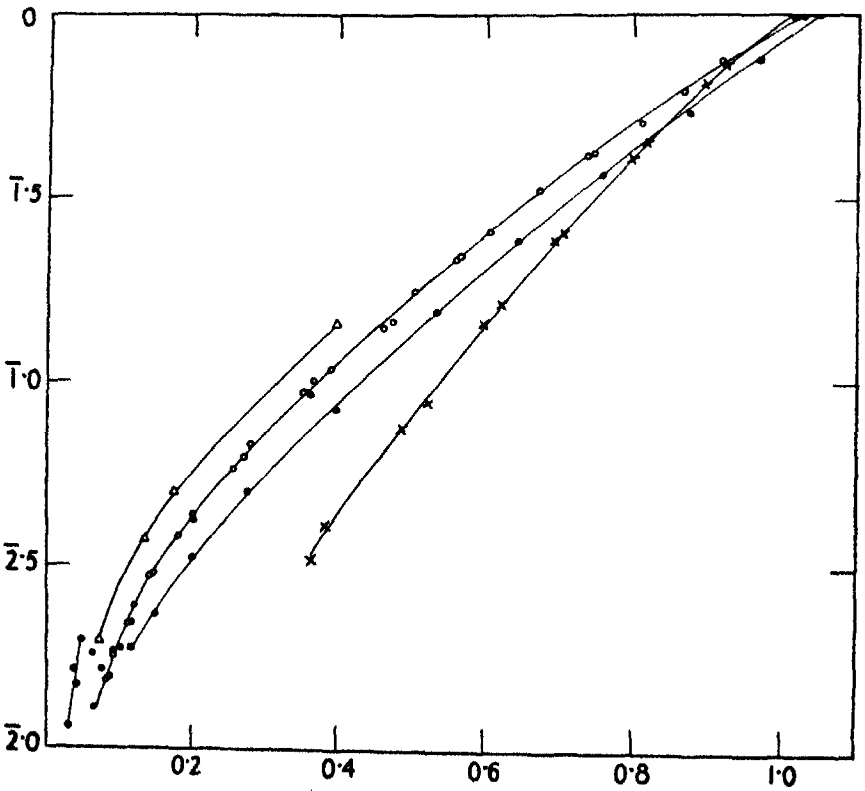

Fig. 3—Abscissæ, values of x ; ordinates, values of $\log_{10} p/p_0$. Methyl alcohol at 0° C, ● ; at 20°, ○ ; at 50°, △ ; ethyl alcohol at 30°, ×

have continued so far as to cause the reduced molecular expansion curve to coincide with that common to the other temperatures.

Pressure relations—Four concordant series of results at 20° C provide suitable data for testing the validity of equation (5), the criterion being the constancy of Mx_0/s_0 as calculated therefrom. The graphs of $\log p/p_0$ against x, where p_0 is the saturation pressure, are shown in fig. 3, which includes the corresponding curves for 50° and 0° C. Values of $dx/d\log_{10}p$ and of Mx_0/s_0 are given in Table III. As a check on the former, graphs of $\log p$ against $\log x$ have also been used, these showing slight curvature in the opposite sense. Where the results differ, a mean value has been recorded in the table; the difference never exceeds 0·02.

TABLE III

Temp. °C	p/p_0	$x\%$	s gm/gm interpolated	$dx/d\log_{10}p$	Mx_0/s_0	$273Mx_0/Ts_0$
20°	0·020	0·100	0·0635	0·21	46	—
	0·056	0·250	0·0930	0·47	70	65
	0·093	0·350	0·1020	0·53	72	67
	0·136	0·450	0·1100	0·57	72	67
	0·172	0·550	0·1175	0·59	70	65
	0·301	0·650	0·1240	0·635	71	66
	0·419	0·747	0·1305	0·67	71	66
	0·615	0·868	0·1375	0·74	74	69
50°	0·028	0·100	0·0580	0·225	54	—
	0·050	0·176	0·0760	0·41	75	63
0°	0·050	0·277	0·0970	0·46	(66)	—
	0·242	0·644	0·1250	0·60	67	67
	0·540	0·874	0·1390	0·69	69	69

Mean value of Mx_0/s_0 at 0° C = 66·4 ± 0·4

As Table III indicates, the values of Mx_0/s_0 are nearly constant from $p = 0{\cdot}05\ p_0$ to $p = p_0$, a range which includes four-fifths of the total variation of x and adsorption values greater than 0·07 gm/gm. In the last column the values falling within this range have been reduced to 0° C; the smallness of the deviations from the mean value of 66·4% affords strong evidence of the validity of equation (5).

At pressures lower than $0{\cdot}05\ p_0$ the values calculated for Mx_0/s_0 are abnormally low. Since at 20° C $0{\cdot}05\ p_0$ is only about 4·5 mm, the systematic error necessarily involved in applying the ordinary capillarity corrections to readings of meniscuses exposed to the alcohol vapour may become significant in this region. The fact that the run at 50° C shows a similar deviation, however, in spite of the much larger saturation pressure, lends support to the accuracy of the low pressure measurements, and suggests that the deviation may be real; the cause possibly lies in the occurrence of a phase-change, the evidence of which will now be discussed.

The data for 0° C are of unusual interest on account of the occurrence of two breakpoints in the low pressure range; these are illustrated by the broken form of the $\log p - x$ curve, see fig. 3, ●, and of the isotherm, fig. 4, ●; the abscissa variable in the latter graph is the logarithm of the relative pressure p/p_0, and the ordinate s. It is true that in the region of the breaks the pressures were too small, *ca.* 0·6 mm, for assured accuracy of measurement. Reasons have been given, however, for regarding the low pressure readings as substantially correct. Moreover, there appears no good reason why adventitious irregularities should appear at this stage—the first break occurs at the minimum point on the molecular expansion graph—whilst readings of still smaller pressures showed normal increase with each admission of vapour.

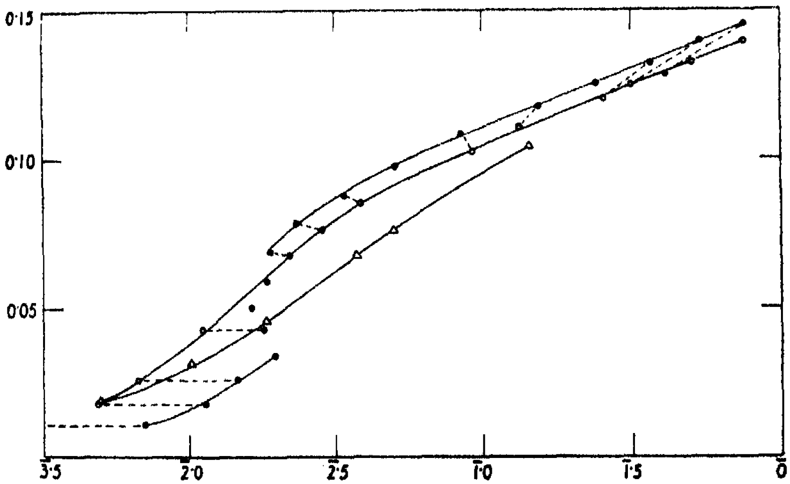

FIG. 4—Isotherms of methyl alcohol; abscissæ, values of $\log_{10} p/p_0$; ordinates values of s; 0° C, ●; 20° C, ○; 50° C, △

The experiments at 20° C having given no evidence of such breaks, the method was adopted of taking alternate readings at the two temperatures, all admissions of vapour being made at 0°, and each reading at 20° being sandwiched between a pair of readings at 0° C. Two such experiments were carried out, and in both cases the 0° curves showed breakpoints, whilst the 20° curves showed none. In fig. 4, where the semi-log isothermals are plotted, the black and the white circles joined by broken lines refer to paired observations made at these two temperatures in the manner indicated. Between the second breakpoint and saturation the two isotherms run nearly parallel, indicating that the differential heat of adsorption is here nearly constant ; it exceeds the latent heat of vapourization by rather less than 3000 cals/gm mol.* This constancy of the heat of adsorption indicates that heat of compression is here unimportant, in spite of the rapid rise of the surface pressure in this region.

The graphs of log p/p_0 against x are also nearly parallel, fig. 3, the saturation expansion being 1·029% at 20° as against 1·049% at 0° C.

Obscurity remains as to the precise relation between the effects observed at − 78° and at 0° C, and also as to the extent to which either or both of these sets of phenomena can be called upon to account for the deviations (supposing these to be real) from equation (5) at low pressure. All that can be stated with certainty is that the first break occurs at a concentration (*ca.* 0·035 gm/gm) roughly equal to that at which the film at −78° first showed instability ; and the second at $s =$ *ca.* 0·070 gm/gm, which is near the lower limit for the validity of the equation. Whilst it is probable that the change associated with the 0° breakpoints may occur in a more continuous manner at 20° and at 50°, it is remarkable that the molecular expansion graphs at these temperatures should give no indication of it.

Experiments with Ethyl Alcohol—These call for but little special comment. The results were very accurately reproducible, and no anomalous effects were observed ; experiments at lower temperatures were not, however, attempted. The graph of log p/p_0 against x at 30° C is shown in fig. 3 by ×. Both this and the double logarithmic graph show only very slight curvature, and the values of $dx/d \log p$ derived from these two graphs agree to within 0·01. The values of Mx_0/s_0 at 30° and at 0° C derived with the aid of equation (5) are given in Table IV; the mean value at the latter temperature is seen to differ very little from the value found for methyl alcohol.

The s, x relations for ethyl alcohol at 30° C are typical of the " annealed " films, and no relaxation effect was observed, the self-annealing process being rapid at this temperature. The molecular expansion curve is shown in fig. 1 by ×.

---

[*] The latent heat of vapourization being about 9000 cals, the heat of adsorption is about 12,000 cals/gm mol. ; it is of interest to note that, near saturation, values very little different have been obtained by other workers using *activated* charcoal. See Pearce and McKinley, 'J. Phys. Chem.,' vol. 32, p. 360 (1928) ; Kruyt and Modderman, 'Chem. Rev.,' vol. 7, p. 259 (1930).

TABLE IV

Temp. °C	p/p_0	x%	s gm/gm interpolated	$dx/d\ log_{10}p$	Mx_0/s_0	$273\ Mx_0/Ts_0$
30	0·159	0·615	0·1125	0·42	75	67
	0·251	0·703	0·1175	0·45	77	69
	0·398	0·795	0·1235	0·47 (5)	77	69
				Mean value of Mx_0/s_0 at 0° =		68·3

6—EXPERIMENTS WITH THE PROPYL ALCOHOLS

It was observed towards the end of each of the earlier experiments with n.propyl alcohol that the vapour in contact with the charcoal gave, on condensation, a liquid of which the vapour pressure did not quite correspond to that of the original stock. At first this was attributed to the displacement of gas from the charcoal, but the behaviour of the mixture at low temperatures suggested rather the presence of a lower boiling impurity in the original alcohol, the concentration of which may have become augmented by selective adsorption of the main constituent. The alcohol was therefore removed from the system, and the stock carefully refractionated after thorough drying. The vapour pressure data quoted in an earlier section refer to the product thus obtained. The molecular expansion curve found on re-charging the charcoal with the freshly purified alcohol was little different from that found previously, though the vapour pressure curve of the unadsorbed residue was now normal.

Molecular expansion curves of n.propyl alcohol—The relaxation effect with this alcohol was well marked both at 20° and at 0° C. The retrograde movement became so slow, however, some time after each admission of vapour, that the practice of annealing the films at 50° C[*] between readings was resorted to, this treatment being repeated until no further change took place. The results for the films so obtained are illustrated in fig. 5A, curve III, where ● denote readings taken at 0° and × readings at 20° C. Both abscissa and ordinate variables have here been multiplied by the factor $273/T$, a procedure which again brings the curves for the annealed films at the two temperatures into coincidence.

---

[*] A higher temperature could not be used on account of the risk of decomposing the alcohols under the catalytic action of the metal surfaces ; the fact that in the experiments described the unadsorbed residue gave a normal vapour pressure curve indicates that significant decomposition did not occur, and that the reaction between carbon and the alcohols, described by Zelinski and Gaverdovskaja ('Ber. deuts. chem. Ges.,' vol. 64, p. 435 (1931)) as taking place when activated charcoal is exposed to the vapours of these substances at 300° C, was also absent.

The results of a desorption experiment are also included in fig. 5A; in this experiment readings were taken both at 20° and at 0°. The fact that the points fall on the curve indicates that at all events within the limited range of this experiment the state of the film is here independent of its history. The desorption of the vapour was found to be a very slow process.

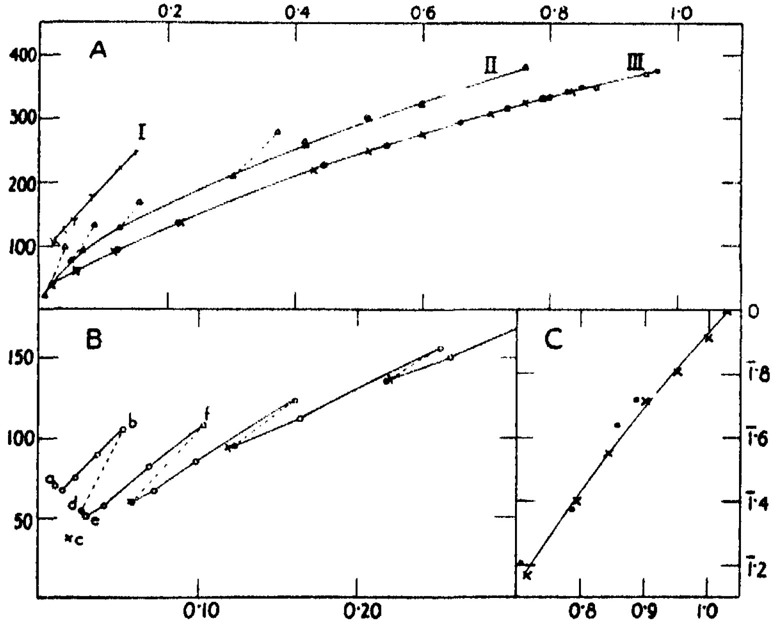

FIG. 5A—Molecular expansion graphs of the propyl alcohols, reduced to 0° C. I, primary film of normal alcohol at −30° Y ; II, iso-propyl alcohol at 20° C, readings before Δ and after ▲ annealing the films. III, annealed films of n.propyl alcohol ; readings at 0° C, ● ; at 20°, × ; desorption readings at 20°, ■ ; desorption at 0°, □. FIG. 5B—Molecular expansion graph of n.propyl alcohol, reduced to 0° C; readings before and after the annealing of the films ; 0° before annealing, ○; 0° after annealing, ●; 20° after annealing ×. FIG. 5C—Abscissæ, values of x ; ordinates, values of $\log_{10} p/p_0$. Desorption ■ and resorption ×, with n.propyl alcohol at 25° C.

Fig. 5B also illustrates the effect of making several rapid additions of vapour under isothermal conditions at 0°. When this was done at the beginning of an experiment, the points obtained lay along the curve *ab*. When the reading at the point *b* had been taken the film was twice annealed at 50° ; points *c* and *d* denote the values obtained at 20° and at 0° respectively after this treatment. The former point is seen to lie on and the latter rather above the curve for the annealed film, although the reading at 20° preceded that at 0°. Further rapid additions at the lower temperature then gave rise to the points lying about the curve *ef*. At this stage, however, both the 0° and 20° points obtained after annealing lie on the continuous curve characteristic of the annealed film, and thereafter even rapid additions made at 0° cause only very slight deviation from this curve.

The behaviour of the primary film was further examined by experiments carried out at − 30°, the vapour being added as quickly as the necessary readings could be taken. The results of two of these experiments appear in fig. 5A, curve I. As in other similar cases, the self-annealing or relaxation effect took place much more slowly at this lower temperature, and the readings were correspondingly easier to take. The film became highly unstable, however, when some 0·037 gm/gm had been taken up.

The saturation pressure of n.propyl alcohol being only some 15 mm at the highest working temperature, great accuracy cannot be claimed for the pressure measurements. From the results of a desorption and a resorption experiment at 16° the calculated value of Mx_0/s_0 at 0° C is found to lie between 63 and 73%, but a somewhat higher value is not precluded. These results are graphed in fig. 5C.

Iso-propyl alcohol—The adsorption of this compound being very much slower than that of its straight-chain isomer,* it was not found possible to obtain valid data for the primary film. The expansion gradually increased until most of the vapour generated had been adsorbed, and then gradually diminished. By annealing the films at 50° C the retrograde effect could be brought to completion, but, with the exception now to be noted, the expansion corresponding to a given adsorption remained substantially greater than had been the case with the annealed film of the normal alcohol. The exception refers to the state of affairs at very small *s*-values, it being found that quantities of the order of 0·004 gm/gm caused no measurable expansion. The molecular expansion graph therefore passes through the origin, as was suspected to occur with the annealed film of benzene (Part II).

The molecular expansion data are plotted in fig. 5A (curve II), where points Δ refer to the maximum forward movement and ▲ to the film in its permanent condition after annealing. Allowing for the difference of molecular size, the curve passing through the latter points is remarkably similar to that of benzene ; it differs in the characteristics already noted from that of the annealed film of the normal alcohol.

---

* *Cf.* Pearce and Taylor, 'J. Phys. Chem.,' vol. 35, p. 1091 (1931).

On account of the slowness with which equilibrium was established, the minimum quantity necessary to give a permanent expansion could not be measured accurately ; such quantity is, however, far smaller than would be necessary to cover the surface with a unimolecular layer of liquid, and is certainly no more than one-tenth of this.

The value of Mx_0/s_0 at 0° C calculated by equation (5) from the pressure data is a little over 70% ; this estimate is, however, given with considerable reserve, on account of the difficulty in attaining equilibrium. The saturation expansion was 0·97%, a rather smaller figure than that recorded for the straight-chain alcohols.

7—EXPERIMENTS WITH THE BUTYL ALCOHOLS

N.Butyl alcohol—The behaviour of this alcohol was so similar to that of n.propyl alcohol as to render a special description of the experiments unnecessary. The relaxation effect was slower, however, and as the primary adsorption was rapid it was possible to determine the x, s relations for the primary film by working at 0° C. The results of such an experiment are shown in fig. 6 by Δ ; the broken lines indicate the course of the retrograde movement taking place when the system was allowed to stand for a shorter or a longer period without addition of further vapour. The course of the molecular expansion curve at room temperature has been indicated in fig. 1.

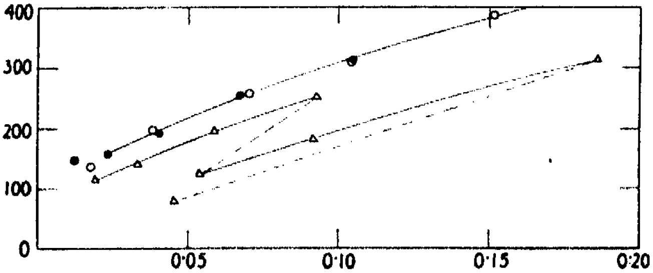

FIG. 6—Molecular expansion graph of primary iso-butyl alcohol ●, ○, reduced to 0° C ; and of n.butyl alcohol at 0° C Δ

The saturation pressure of this alcohol was too small to permit an accurate determination of Mx_0/s_0 by the use of equation (5). Vapour pressure measurements made with the desorbed vapour and unadsorbed residue showed these to be free from contamination.

Iso-butyl alcohol $(CH_3)_2CH\ CH_2\ OH$—This alcohol was adsorbed with extreme slowness. As the material had been freed from dissolved gases by repeated fractionation under vacuum conditions after introduction into the sealed apparatus, the extreme disparity between its rate of adsorption and that of the normal alcohol can only be regarded as an effect due to constitution. When exposed to the saturated vapour of the iso-alcohol, the charcoal expanded at a fairly uniform rate for 48 hours, and thereafter at a gradually diminishing rate. After 15 days the expansion had reached 0·66%, but, as there was no indication of its complete cessation, the saturation expansion is probably much greater than this.

The reduced molecular expansion graph resulting from experiments carried out isothermally at 25° C is shown in fig. 6 (circles). The course of the curve near the axis remains uncertain, but over the experimental range it is seen to be very little steeper than that of the primary film of the straight-chain isomer, which is shown in the same figure. No data are available for the annealed film of the iso-alcohol.

Tertiary butyl alcohol—Preliminary experiments having shown this alcohol to be exceptional in causing no measurable expansion in charcoal rods immersed in its melt, it was of interest to discover whether this was due to inactivity or to the formation of a solid film. Measurements of the deadspace vapour present in the adsorption vessel after the introduction of successive quantities of the alcohol gave values representing respectively 100·4%, 99·6% and 99·7% of the quantities generated. The system was unchanged after standing overnight at a pressure 60% of saturation, and on raising the pressure to saturation the extensometer still recorded zero expansion. It appears safe to conclude that even at this pressure there was no adsorption.

8—SUMMARY

Using the apparatus, technique, and pinewood charcoal rod described in Part II, adsorption-expansion measurements have been made with the series of lower alcohols. The view that the expansion is proportional to the surface pressure in the adsorbed phase is confirmed. The Gibbs equation is accurately valid for ethyl alcohol and methyl alcohol, except in the region of low pressures, where two breakpoints occur in the 0° isothermal of the latter substance. The four lowest straight-chain alcohols form two distinct types of film (the "primary" and the "annealed"); transition from the former to the latter proceeds more rapidly at high temperatures than at low. A comparison of the expansion data with those for the lowering of the surface tension of mercury by

the vapours of the same alcohols permits estimates to be made of the specific of surface the charcoal, and of the expansion per dyne increase of surface pressure. For a given adsorption value, the branched-chain alcohols give rise to larger expansions than their straight-chain isomers, and they are characterized also by a much slower rate of adsorption. Tertiary butyl alcohol was not adsorbed by the charcoal used.

The Swelling of Charcoal

Part IV—Stoichiometric Relations for the Films of the Alcohols

By D. H. BANGHAM

(*Communicated by D. L. Chapman, F.R.S.—Received June* 25, 1934)

1—THE RULE OF GURVITSCH

According to the well-known rule of Gurvitsch,[*] the quantities of different substances adsorbed by a porous substance at saturation represent equal volumes of the normal liquids. If this rule were strictly obeyed, molecular structure could not be considered a factor determining adsorption under saturation conditions. It has been shown by Coolidge,[†] however, that the rule is of no more than approximate validity ; deviations may be due either to differences in the " adsorption space " occupied by the films of different substances, or to the fact that the densities of the bulk liquids form no more than a rough criterion as to the densities of the saturated films.

The lower alcohols form a series particularly well suited for the study of the influence of structure, for not only are the densities of the normal liquids nearly equal at equal temperatures, but Bridgman[‡] has shown that this applies also to the liquids under high pressure. Without postulating for the adsorbed phases of these alcohols properties identical with those of the bulk liquids, one may justifiably anticipate that were it not for the

[*] 'J. Russ. Phys. Chem. Soc.,' vol. 47, p. 805 (1915) ; for discussion of this rule, see McBain, " The Sorption of Gases by Solids," p. 135 (1932).

[†] 'J. Amer. Chem. Soc.,' vol. 46, p. 596 (1924).

[‡] 'Proc. Acad. Arts Sci.,' vol. 49, p. 3 (1913) ; " The Physics of High Pressure," p. 128 (1931).

factors—such as molecular size, shape, and state of aggregation—which make for deviations from Gurvitsch's rule, the quantities of the different alcohols giving rise to equal *surface* pressures would themselves be equal. As a measure of the surface pressure, we have the expansion of the charcoal.

Fig. 1 shows how far this generalization applies. Using the data for the " annealed " films described in Part III, values of the expansion per unit adsorption* (x/s) have here been plotted against the expansion x, both variables being reduced to 0° C by multiplying by the factor 273/T†. The curves for the first four straight-chain alcohols are seen to lie close together, methyl, ethyl and n-butyl alcohols all giving curves intermediate between those of n-propyl alcohol and its isomer. The lowest curve of all refers to water, and on account of the different pressure-density relations of this substance is not comparable with the others in the figure. For any given value of x, the s-values for the straight-chain alcohols do not deviate by more than about 10% from the mean, and over most of

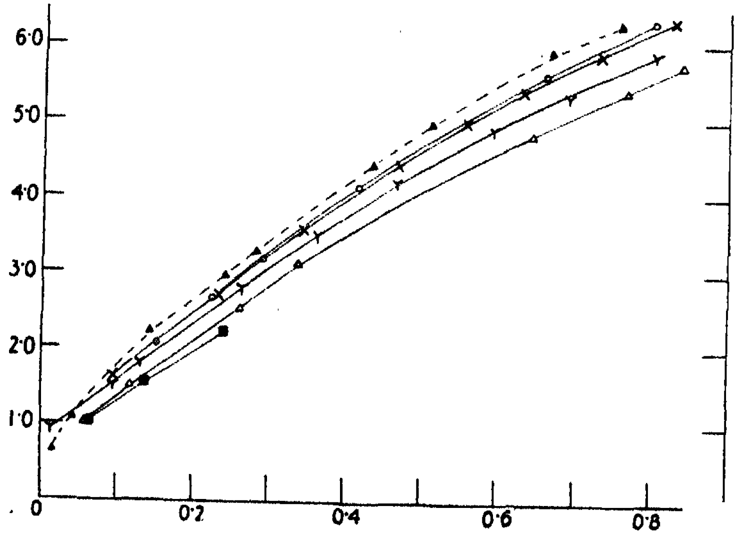

FIG. 1—Abscissæ, values of x ; ordinates, values of x/s, for the annealed films of water and the alcohols adsorbed on charcoal II. Iso-propyl alcohol, – – ▲ – –; n.butyl alcohol, ○; ethyl alcohol, ×; methyl alcohol, Y; n-propyl alcohol, Δ; water, ■

---

* x is the linear expansion per cent. ; s is expressed in gm/gm of charcoal.

† As stated in Part III, this procedure renders the curves for the annealed films of the *normal* alcohols independent of the temperature ; this may not apply to the other graphs in the figure.

the range the deviation is considerably smaller. Considering the small numbers of carbon atoms they contain, the similarities of behaviour of these alcohols are more striking than the differences. Neither in direction nor in magnitude are the deviations such as would be anticipated if the molecules formed unimolecular films of thickness proportional to the lengths of their chains. As the figure indicates, the ratio x/s is smallest not with n.butyl but with n.propyl alcohol, and greatest not for methyl but for n.butyl alcohol. Equally unsatisfactory is the view that the films are unimolecular ones in which the axes of the chains are parallel with the surface ; were this so, the quantities giving rise to equal expansions might well be nearly equal, but this would not account for the existence of the primary* films, in which the molecules occupy a much greater effective area.

2—COMPARISON WITH THE DATA OF CASSEL AND SALDITT FOR THE FILMS ON MERCURY

It is expedient, before attempting to draw further conclusions as to the structure of the films, to make a comparison of the expansion data with the data of Cassel and Salditt,† who measured the lowering of the surface tension of mercury caused (in the absence of air) by the unsaturated vapours of a number of organic liquids. The measurements were made by a drop pressure method at a temperature of 50° C. Assuming the validity of the Gibbs equation, Cassel and Salditt calculate the number of molecules adsorbed per cm^2 at different fractions of the saturation pressures. Fig. 2B illustrates the results obtained; the abscissæ are values of the surface tension lowering F (in dynes/cm), and the ordinates those of the product FA (A in Angstroms).

In the companion figure, 2A, are the molecular expansion graphs‡ for the same series of vapours adsorbed on charcoal II ; the three continuous lines near the ordinate axis refer to the primary films of n.butyl alcohol, benzene, and n.propyl alcohol at 0° C ; the two continuous lines near the x-axis refer to the highly unstable primary film of methyl alcohol at −78° C ; and the four broken lines to the annealed films of the four straight-chain alcohols. The two diagrams are seen to have much in common ; the irregular form of the graphs in the right-hand figure, their bend parallel to the axis after the initial steep rise, and the flatter rising sections of the curves of n.propyl and n.butyl alcohols are features highly suggestive of a gradual change-over from the primary to the annealed type of film. A closer scrutiny leaves no room for doubt that this is so: attention is drawn to the following points:—

---

* See Part III.

† 'Z. phys. Chem.,' vol. 155, p. 299 (1931).

‡ Corrected for temperature in the same manner as for the graphs of fig. 1.

1. If, instead of bending parallel to the x-axis, the FA—F curve for propyl alcohol continued its steep upward course, this would imply the existence of a limiting adsorption value of about $2 \cdot 5 \times 10^{14}$ molecules per cm^2, or $2 \cdot 5 \times 10^{-4}$ gm per m^2. The limiting adsorption value for this alcohol, similarly calculated from the curve for the primary film on charcoal, is about 0·055 gm/gm. If the molecular cross-sectional area is the same in the two cases, it follows that the specific surface of the charcoal is 220 m^2, as a rough estimate. A similar calculation, using the rather more accurate data of two concordant runs with n.propyl alcohol at − 30° C (see Part III), gives for Σ a value about 10% lower, viz. 200 m^2.

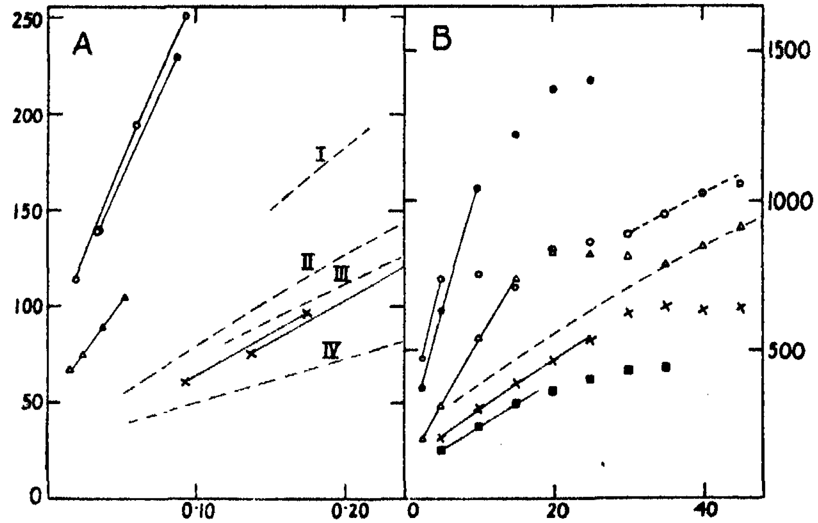

FIG. 2A—Molecular expansion curves for primary, ———, and annealed, — — —, films on charcoal II. In order of steepness, primary films : n.butyl alcohol, ○ ; benzene, ● ; n.propyl alcohol, Δ ; methyl alcohol, ×. Annealed films: curve I, n.butyl alcohol; II, n.propyl alcohol ; III, ethyl alcohol; IV, methyl alcohol.

B—Abscissæ, values of F; ordinates, values of FA (F in dynes, A in Angstroms) for films on mercury (Cassel and Salditt). n.butyl alcohol, ○ ; benzene, ● ; n.propyl alcohol, Δ ; ethyl alcohol, × ; methyl alcohol, ■

2. If the graphs in the two figures are plotted on scales so chosen that the curves for the primary films of n.propyl alcohol are parallel in the

two cases, the corresponding curves for methyl, alcohol, benzene and n.butyl alcohol are also nearly parallel, implying that values of Σ of the same order would result were the rather fragmentary data for these substances used as the basis for a similar calculation.

3. In the region of higher concentration the FA—F curves of fig. 2B are in all cases more curved than those in 2A, and the final upward bend is absent for methyl and ethyl alcohols. It does not necessarily follow, however, that the films on mercury are more compressible than those on charcoal, for even at the highest concentrations the change to the annealed type of film may have been incomplete under the dynamical conditions of the surface tension experiments. In this region, however, a further important relation is to be noticed: as with the films on charcoal the quantities of the normal alcohols giving rise to equal surface pressures are themselves nearly equal. Table I serves to establish this point.

TABLE I—Data of Cassel and Salditt for mercury surfaces

Surface tension lowering in dynes	Quantities adsorbed per cm^2 ; unit = 10^{-8} gm			
	CH_3OH	C_2H_5OH	$n-C_3H_7OH$	$n-C_4H_9OH$
25	3·28	3·54	3·03	3·57
30	3·64	3·64	3·67	4·12
35	4·14	4·09	4·42	4·49
40	—	4·76	4·67	4·74
45	—	5·35	4·90	5·21

The deviations are of the same order, though seldom in the same sense, as those which occur in the case of charcoal. The regularity does not extend to the region of low concentration.

4. From Table I it is seen that, on mercury, a surface concentration of about $4\cdot73 \times 10^{-8}$ gm/cm^2 of each of ethyl, propyl and butyl alcohols gives rise to a surface pressure equivalent to 40 dynes/cm at 50° C. Let it be supposed that at an equal concentration the films on charcoal II exert an equal pressure at the same temperature. If Σ be the specific surface of the charcoal and λ the percentage expansion per dyne,* we should have, corresponding to an adsorption of $4\cdot73 \times 10^{-8} \times \Sigma$ gm/gm, an expansion of $40\,\lambda$ at 50° C. Applying to the x-value the temperature correction which is known to be valid for the annealed films, it becomes $40\,\lambda \times 273/323$ or $33\cdot8\,\lambda$ at 0° C, at which temperature we should have

$$\frac{x}{s} = \frac{33\cdot8\lambda}{4\cdot73 \times 10^{-8} \times \Sigma}\ \%\ \text{per gm.}$$

---

* See equation (2), Part III.

Equation (5) of Part III permits the evaluation of λ/Σ in terms of RT and Mx_0/s_0, the expansion per gm mol (M gm) at zero concentration. Assigning to RT the usual value of $273 \times 8{\cdot}32 \times 10^7$ ergs, and to Mx_0/s_0 the value of 67% at 0° C, which is known to be accurate for methyl and ethyl alcohols and is not widely incorrect for the higher members, we have, on substituting,

$$\frac{x}{s} = \frac{33{\cdot}8 \times 67}{4{\cdot}73 \times 273 \times 10^{-8} \times 8{\cdot}32 \times 10^7} = 2{\cdot}12\% \text{ per gm.}$$

With the aid of the graphs of fig. 1, the values of x and s for which this equation is valid are readily determined ; to solve for λ and Σ it is now necessary only to put $F = 33{\cdot}8$ dynes/cm, and $s/\Sigma = 4{\cdot}73 \times 10^{-8}$ gm/cm². The values of x, s, λ^{-1} and Σ are set out in Table II.

TABLE II

	CH_3OH	C_2H_5OH	n–C_3H_7OH	n–C_4H_9OH	Mean
$x\%$	0·176	0·162	0·205	0·162	—
s gm/gm	0·0832	0·0766	0·0968	0·0766	—
$\lambda^{-1} = 33{\cdot}8/x$ dynes/cm ..	192	208	165	208	192
$\Sigma = s/4{\cdot}73 \times 10^{-4}$ m² ..	176	162	205	162	176

5. The values of Σ so calculated are in striking agreement not only with the rough estimate obtained from the curves for the primary films of propyl alcohol, but also with other estimates based on totally different evidence and data. The significance of this fact, translated into terms of the graphs of fig. 2, is that although the slopes of Cassel and Salditt's curves at high concentration do not accord well with those of the molecular expansion curves for the annealed films, their *positions*, relative to F_0A_0 in the one case and Mx_0/s_0 in the other, are in very fair agreement.* A similar result is obtained if the surface concentrations at F = 35 or F = 45 dynes are taken as the basis for comparison; the mean of all twelve values of Σ is identical with the mean value given in Table II, 176 m².

---

* As stated in Part III, the deadspace pressure data do not preclude the possibility that Mx_0/s_0, and therefore λ/Σ, may increase slightly on ascending the series, though the relative positions of the curves of fig. 1 render this unlikely. For the calculation of film thicknesses and molecular areas given in a later section it is desirable to use a value of Σ which is not subject to the errors of particular experiments, or dependent on the peculiarities of individual alcohols. It is readily understood that in a thin film of oriented molecules the ease of packing might well depend on the relative positions of the OH and of the terminal CH_3 groups—that is, on whether the molecule contains an odd or an even number of carbon atoms; it is possible that the larger adsorption values shown by methyl and n.propyl alcohols are due to an effect of this kind.

Comparison of experimental conditions—The close connection between the two sets of data is the more striking in view of the very different experimental conditions. It will bear emphasis that the "relaxation" effect, which alone renders the self-annealing process conspicuous, is always liable to be obscured by another consequence of the same process, namely, the adsorption of further vapour from the deadspace. Unless the pressure is so small that very little vapour remains for further adsorption, the effect observed on allowing the closed system to stand after an addition of vapour is not a contraction, but a gradual disappearance of vapour accompanied by little or no expansion. It is easy to show, on thermodynamic grounds, that in the extreme case where the pressure of the vapour is kept constant, as, for example, by the presence of liquid within the closed system, the transition of the surface film from an unstable state to a stable must always be accompanied by a lowering of the surface energy of the adsorbent.*

Cassel and Salditt's measurements were made under constant pressure conditions. The surface concentrations calculated by them with the aid of the Gibbs equation may be presumed valid both in the region of very low concentrations, where the primary film has probably a definite range of stability, and in that of high concentration, where it is probably so unstable that the transition is nearly complete within the lifetime of the drops; were the latter not so, it is difficult to see why so simple a relation should obtain between the data for the four alcohols. It is in the intermediate region that the calculation is open to suspicion. Cassel and Salditt were careful to vary the age of the drops, and rejected all observations which showed a drift of the surface energy when the drop age was increased from 20 seconds to 2 minutes ; this drift, when it appeared, they attributed to the presence of impurities. The life of the drops was, however, quite negligibly short in comparison with the age of the films examined by us, and in view of the mutually compensating nature of its effects, it is not surprising that the transition escaped notice. Supposing, for simplicity, that during the lifetime of the drops the increase of surface pressure due to increased adsorption just balanced the decrease due to molecular rearrangement, the Gibbs equation would clearly give values too small for the concentrations in the aged films, but approximating to those obtaining at the time of attainment of equilibrium between the vapour phase and the primary film. The calculated values of FA would thus be too high in this region. Reference to the graphs of fig. 2 will indicate that a correction having the effect of decreasing the FA values at intermediate concentrations would render them even more strikingly similar to those of the companion figure. The fact that their slopes at high concentration are uniformly less than those of the molecular expansion curves of the annealed films is thus accounted for.

---

* Let it be supposed that an adsorbed substance can exist in two states, the one stable at low and the other at high concentration. Let the equation of state of the former be $A = f_1(F)$ and that of the latter $A = f_2(F)$, where A is the area per molecule and $f_1 > f_2$ for all equal values of the surface pressure F. In the absence of any transition both f_1 and f_2 are single-valued continuous functions, and so must also be the functions $\log p = \phi_1(F)$ and $\log p = \phi_2(F)$ obtained with the aid of the general free energy equation or of the Gibbs equation. According to the latter, if k is the gas constant per molecule, $A = kT\, d\phi_1/dF$ for the phase stable at low concentration, and $A = kT\, d\phi_2/dF$ for that stable at high concentration, and it follows, since $A_1 > A_2$, that $d\phi_1/dF > d\phi_2/dF$ for all equal values of F. At the transition point the two phases have common values of F and $\log p$; it follows that for values of F that are smaller than this we have $\phi_1(F) < \phi_2(F)$, whilst for values that are greater $\phi_1(F) > \phi_2(F)$. Thus, given a common value of F, the stable phase is the one for which $\log p$ is smaller; conversely, given any common value of $\log p$, the stable phase has the greater value of F. It is possible that the absence of a relaxation effect in the experiments of McBain, Porter, and Sessions ('J. Amer. Chem. Soc.,' vol. 55, p. 2294 (1933)) was due to an approximation to constant pressure instead of to constant adsorption conditions.

3—Structure of the Films

Straight-chain Alcohols : Primary films—The calculation of molecular areas from FA—F or molecular expansion graphs is justified only when these are proved to be linear, or nearly so, over a fairly wide range of concentrations. The only data for the primary films at all reliable for this purpose are those for n.propyl alcohol. Assuming $\Sigma = 176$ m^2 for the films on charcoal, the following are the calculated values of the "incompressible" area per molecule of this substance :—

From the molecular expansion graph at 0° C ..	32 A
From the molecular expansion graph at $-30°$ C .	35 A
From the data of Cassel and Salditt	40 A

Bosworth,[*] who measured by an interferometric method the quantities of the lower fatty acids adsorbed at the surface of mercury drops, concluded that the films of propionic, butyric, and valeric acids were each capable of existence in two states, one stable at low and the other at high concentration.[†] In the former state the area per molecule of propionic acid was 36 A, which is in fair agreement with the values given above for the alcohol. Bosworth found that in the films stable at low concentration the molecular areas increased in arithmetical progression on ascending the homologous series, and concluded from this that in these the molecules lie flat on the surface. Whilst this conclusion is possibly not fully warranted,* there is a very strong probability that the primary films both of the acids and of the alcohols, are of no greater thickness than the width of the carbon chains. The molecular expansion graphs give evidence of considerable intermolecular attraction for methyl alcohol, but this becomes less marked, especially at lower temperatures, with increase of molecular weight.

---

[*] 'Trans. Faraday Soc.,' vol. 28, p. 903 (1932).

[†] In addition to measuring the adsorption directly, Bosworth determined the change of surface tension of mercury at different partial pressures of the vapours, using the method of Iredale. Here also evidence of transition was found.

Straight-chain alcohols: Annealed films—The structure of the annealed films is a matter of considerable interest. The molecular expansion graphs of all four straight-chain alcohols are nearly linear below $x = 0 \cdot 5\%$, representing a range of nearly 100 dynes in the surface tension lowering. The limiting adsorption values calculated from their slopes in the region of fairly low compression are but little less than the saturation adsorptions found by extrapolating the curves to the saturation expansions. By far the greater part of the adsorption must therefore occur without great increase of film thickness; moreover, so far from there being a progressive increase of film thickness on ascending the homologous series, there is a slight apparent decrease.† In Table III, B stands for the incompressible area per molecule calculated from the slopes of the graphs, and B^1 for the area per molecule at saturation; in both cases a film area of 176 m^2 per gramme of charcoal has been assumed. The values of the film thickness Δ given in the fourth column have been derived with the aid of Bridgman's PV data for the bulk liquids under moderate pressures, the incompressible *volumes* per molecule being calculated in precisely the same manner as the corresponding areas. In the last column under Δ^1 are given the film thicknesses calculated on the basis of the assumption that at saturation the density of each adsorbed film is equal to that of the corresponding bulk liquid at 20° C and 2200 atmospheres pressure.*

---

* On account of possible rotation about C–C links, it does not appear quite certain that such a simple additive rule would be closely followed in films of this description.

† The low value of Δ for n.butyl alcohol may be due to the fact that in the absence of data for the annealed film under very low compression, the slope of its molecular expansion curve has been read at rather higher x-values than in other cases. The behaviour of the alcohols is in complete contrast to that reported by Bosworth (*loc. cit.*) for fatty acid films of high concentration on mercury. According to Bosworth the area per molecule remained constant on ascending the series, the film thickness increasing with each addition of CH_2.

TABLE III

	Limiting adsorption values gm/gm calculated from molecular expansion graphs in region of low compression	B in A	Δ in A	Saturation adsorption values gm/gm	B^1 in A	Δ^1 in A
CH_3OH	0·137	6·8	9·2	0·149	6·2	9·4
C_2H_5OH	0·123	10·9	8·3	0·137	9·8	8·8
n-C_3H_7OH ..	0·125	13·9	8·3	0·157	11·1	9·9
n-C_4H_9OH ..	0·117	18·4	7·8	0·133	16·1	8·4

To account for the formation of these relatively thick films in the region of low compression, it is necessary to suppose that the intermolecular forces giving rise to association should be effective mainly in the direction normal to the surface ; any other distribution of these forces would clearly permit the crowding of molecules into the innermost layer, under the attractive force of the substrate, and the instability of the primary films shows that there is a sharp limit to the extent to which this can occur.

A measure of the degree of association is provided by producing the molecular expansion graphs to cut the axis, and comparing the ordinate value at the intersection with that of Mx_0/s_0. Taking 67% for the latter, the association factor† found for both methyl and n.propyl alcohols is about 2·4. It is important to note that this factor is, at all events as a first approximation, independent of the temperature. Considered in conjunction with the fact that the films are about two carbon chains width in thickness, an association factor of rather more than two points strongly to the formation of fairly stable doublets, so oriented that the line joining the centres of the oxygen atoms is nearly normal to the surface, whilst the axes of the carbon chains are parallel, or nearly so, to the plane of the surface. No other arrangement appears capable of explaining the remarkable constancy of Δ and of the degree of association. It remains an open question, however, whether the value of 2·4 for the latter is to be explained by a tendency of the film to thicken further by association of a similar type (as the rather large value of Δ for methyl alcohol suggests may here occur), or whether the excess over the whole number is due to the operation of forces parallel to the surface. The constancy of the heat of adsorption of methyl alcohol in the region of high concentration provides independent evidence that the latter are relatively unimportant.*

---

* The saturation values of x correspond to a surface force of about 200 dynes/cm. The thickness of the films being in all cases about 9 A, the surface pressure, if equally distributed throughout this thickness, would be about 2200 atmospheres. (*Cf.* Adam, "Physics and Chemistry of Surfaces," p. 52.) Whilst this calculation is open to objection, it appears to form the most reasonable basis for comparing the film thicknesses near saturation with those obtaining under low compression. That the values of Δ^1 are no more than approximate is shown by the fact that the films have neither the compressibility nor the dilatation coefficients characteristic of the bulk liquids at the pressure in question (see section 4).

† The association factor here referred to is the reciprocal of i in the Schofield-Rideal equation of state $F(A - B) = iRT$, A being the area per molecule. The data for ethyl and n.butyl alcohols do not extend sufficiently into the region of low concentration to permit the evaluation of i. Cassel and Salditt ('Z. Elektrochem.,' vol. 37, p. 642 (1931)) found for ethyl alcohol adsorbed on mercury an association factor of 2·5 at 50° as against 2·3 at 25° C. Their method of calculation makes it probable that these figures refer to the primary films; nevertheless, they are of interest as affording another example where the cohesive forces are, if anything, more effective at higher temperature (*cf.* Part III). The value found by them for methyl alcohol was 4.

There can be no doubt that one of the chief factors affecting the stability of a given orientation in the adsorbed state is the tendency of the hydroxyls to lie in juxtaposition; not only does this tendency largely determine the crystal form of many oxygen-containing compounds, but Stewart† has shown that it extends also to the liquids. Smyth,‡ whose conclusions are based on the molecular polarization curves of the alcohols in non-polar solvents, recognizes two types of molecular association in these substances: in the first the dipole axes of a pair of molecules are aligned and pointing in the same direction, and in the second they are parallel and pointing in opposite directions. Since in the straight-chain alcohols the dipole axes are roughly normal to the axes of the chains, these orientations are identical with those assigned above to the aggregates in the annealed and in the primary films respectively if the dipole axes are also normal to the surface.

Iso-alcohols—Although iso-propyl alcohol shows a marked relaxation effect, indicating re-orientation, the interpretation to be placed on its molecular expansion curve§ remains obscure. The curve for the annealed film shows marked curvature near the axis, and, like the corresponding curve for benzene, appears to dip sharply down towards the origin. So far from the intermolecular forces being directed mainly along the normal to the surface, they appear, at all events at low concentration, to act predominantly in a tangential direction. It is readily understood that, on account of their screening effect, the presence of CH_3 groups near the hydroxyl would diminish the tendency to assume the first of the orientations described above: Smyth attributes the abnormally low dielectric constants and polarizations of certain tertiary alcohols to this cause. In the absence of adsorption data for the corresponding hydrocarbons, it is difficult to judge how far the diminished rate of adsorption of the iso-alcohols and its complete absence in the case of tertiary butyl alcohol are to be explained along these lines.

---

* Cassel and Salditt (*loc. cit.*) found a similar constancy for ethyl alcohol at high concentrations.

† Stewart and Morrow, 'Phys. Rev.,' vol. 30, p. 232 (1927); Stewart and Skinner, *ibid.*, vol. 31, p. 1.

‡ Smyth and Stoops, 'J. Amer. Chem. Soc.,' vol. 51, p. 3330 (1929); Smyth, "Dielectric Constant and Molecular Structure," New York (1931).

§ Part III. The form of the curve may be gauged from the curve for this alcohol in fig. 1.

In the region of high concentration the $x/s - x$ curve for iso-propyl alcohol actually deviates less from those of ethyl and n.butyl alcohols than do methyl and n.propyl.

4—THERMAL DILATATION AND COMPRESSIBILITY OF ANNEALED FILMS OF THE NORMAL ALCOHOLS

With the aid of certain simplifying assumptions it is possible to calculate approximate values for the coefficients of thermal dilatation and compressibility of the matter composing the annealed films. Reasons have been given for regarding λ, the expansion per dyne increase of surface pressure, as invariable ;* in the special case of the annealed films of the *normal* alcohols it appears that, at all events as a first approximation, Δ, the film thickness, can also be considered as independent of temperature and of (surface) pressure. Granted these conditions, we have, writing V for the specific volume,

$$\alpha = (\partial \log_e \mathrm{V}/\partial \mathrm{T})_{\mathrm{F}} = -(\partial \log_e s/\partial \mathrm{T})_x$$

For the calculation of β it is necessary to make the more questionable assumption that the pressure is equally supported throughout the thickness of the films. We have then, writing P for the pressure in bars,

$$\begin{aligned}\beta = -(\partial \log_e \mathrm{V}/\partial \mathrm{P})_{\mathrm{T}} &= 10^6 \times \Delta\,(\partial \log_e s/\partial \mathrm{F})_{\mathrm{T}} \\ &= 10^6 \times \Delta\lambda\,(\partial \log_e s/\partial x)_{\mathrm{T}}.\end{aligned}$$

The intention of the calculation being merely to compare the values of α and β so obtained with those of the bulk liquids, it is sufficient to assign a round figure of, say, 9 A to Δ. By plotting log s against x, a series of curves[*] is obtained, which become parallel and show but slight curvature as saturation is approached. For the calculation of α, suitable data are provided by the experiments with methyl and with propyl alcohol, in which duplicate readings were taken at 0° C and at room temperature. The derived values of α and β, together with those for the bulk liquids both at low and at high pressure,[†] are given in Table IV.

---

* The coincidence of the molecular expansion curves when corrected for temperature ; the value of λ used in the calculation is 0·0052 cm/dyne (see Part III).

TABLE IV

	$\alpha \times 10^3$			$\beta \times 10^4$ (per bar)		
	Liquid 1 atm.	Liquid 2000 kg/cm² (1940 atm.)	Annealed film near saturation	Liquid 1–4 atm. 0° C	1000–2000 kg/cm² (970–1940 atm.) 20° C	Annealed film near saturation
CH_3OH	1·19	0·68	1·3	1·01	0·47	1·9
$n\text{–}C_3H_7OH$ ..	0·87	0·56	0·9	0·86	0·38	2·0

The values found for α are not widely different from those of the bulk liquids under normal conditions, but far exceed those of the liquids under pressure of 2000 atmospheres;[‡] those of β are greater under all conditions. The coefficient $(\partial p/\partial T)$, which is given by the ratio α/β, amounts to about 7 bars per degree for methyl alcohol near saturation, and about 4·5 for n.propyl. Both these values are much smaller than those of the bulk liquids, whether at low or at high pressure. Whilst the presence, near saturation, of even a small amount of loosely adhering liquid phase would lead to too high a result being given for β, it is noteworthy that all three coefficients for the nearly saturated films of methyl alcohol agree fairly well with those for air at 0° and 2000 atmospheres ($\alpha = 1{\cdot}16 \times 10^{-3}$, $\beta = 1{\cdot}6 \times 10^{-4}$, $\alpha/\beta = 7$ bars per degree ; data of Amagat). It is legitimate to conclude that these data near saturation are fully consistent with the view that the films are probably gaseous.

---

[*] These are not shown here.

[†] The compressibilities of the liquids at low pressure are taken from the Landolt-Börnstein tables ; the rest of the data from Bridgman's measurements.

[‡] Compare Coolidge, 'J. Amer. Chem. Soc.,' vol. 48, p. 1795 (1926) ; also Goldmann and Polanyi, 'Z. phys. Chem.,' vol. 132, p. 321 (1928). A distinction is to be made between the coefficient of dilatation as above defined, and that derived from *saturation* data at different temperatures. With both the above alcohols the difference is, however, negligible ; the value of α given above for methyl alcohol agrees well with the data of Coolidge for this alcohol.

5—SUMMARY

With the annealed films of the first four straight-chain alcohols, the quantities of each alcohol giving rise to equal expansions of the charcoal were found to be approximately equal. The same applies, according to the data of Cassel and Salditt, to the adsorbed quantities of these alcohols having equal effect on the surface tension of mercury, provided that the surface concentration is sufficiently great. A comparison of the FA—F curves for the films on mercury with the corresponding molecular expansion graphs derived from the charcoal data shows that on mercury also there occurs, with rise of concentration, a transition from the primary to the annealed type of film. The primary films are probably unimolecular, whilst the thickness of the annealed films is about equal to that of two carbon chains. The state of aggregation of the annealed films is discussed, and it is shown that, in those of the normal alcohols, the intermolecular forces are operative mainly in the direction of the normal to the surface. On the basis of certain simplifying assumptions, values are calculated for the coefficients of compressibility and of dilatation of the annealed films of the normal alcohols.

The Liquefaction of Helium by an Adiabatic Method

By P. Kapitza, F.R.S., Messel Professor of the Royal Society,
Royal Society Mond Laboratory, Cambridge

(*Received August* 22, 1934)

INTRODUCTION

The liquefaction of helium by Kammerlingh Onnes has led in the past thirty years to discoveries of the greatest importance to the study of the solid state. In spite of this, very few laboratories are now equipped with the apparatus necessary for the production of liquid helium. It is therefore very desirable that the complicated technique necessary for its production should be simplified to allow of its more extensive use. In this paper we shall describe a more efficient liquefier, based on an adiabatic principle, which we hope will considerably simplify the production of liquid helium for scientific work.

At present two principal methods are used for the cooling and liquefying of gases. The first method is based on cooling produced by adiabatic expansion where the expanding gas is cooled by doing external work. This phenomenon was observed by Clèment and Desormes in 1819* when they discovered the cooling of a gas in a container when its pressure was reduced by letting out some of the gas through a tap. It can be shown that on expanding, the gas remaining in the container has done work in communicating kinetic energy to the escaped gas, and therefore has been cooled adiabatically. Olszewski† in 1895 applied this method to the liquefaction of hydrogen; he compressed the gas to 190 atmospheres and pre-cooled it with liquid oxygen boiling at reduced pressure (−211° C); on releasing the pressure, he observed a fog of liquid hydrogen drops. From this experiment he was able to determine the critical data for hydrogen. This method has also been used recently by Simon‡ for liquefying helium. Simon took advantage of the fact that at very low temperatures the thermal capacity of the container is so small that it practically absorbs no cold from the liquefied helium. The limitations of this method are that it can only conveniently be applied for obtaining small amounts of liquid helium; it is not suited for a continuous output of helium, and also there is necessarily a loss of cold due to the gas which leaves the container. The method is also complicated by the fact that high pressures are required, and that pre-cooling with liquid hydrogen boiling at reduced pressure is necessary.

---

* 'J. Phys. Chim. Hist. nat.,' vol. 89, pp. 321, 428 (1819).

† 'Wiedemann's Ann. Physik,' vol. 56, p. 133 (1895) ; 'Phil. Mag.,' vol. 39, p. 188 (1895).

‡ 'Z. Physik,' vol. 81, p. 816 (1933).

The great advantage of liquefying gases by making them do direct work on a mechanical system has been long recognized, and this method is now commonly used for the liquefaction of most gases. Unfortunately, however, this method is not easily applied to helium and hydrogen, the reasons being mainly technical and due to the difficulty of constructing an expansion engine which will operate at very low temperatures; for this reason the adiabatic method of cooling has not yet been used to liquefy any gas with a lower liquefying point than air.

The alternative method of cooling consists in allowing the gas which is to be liquefied to expand and do internal work. The phenomenon is known as the Joule-Thomson effect and was originally employed by Kammerlingh Onnes* for the liquefaction of helium, and is still used for the production of liquid helium on a large scale. Since helium approaches very closely to the requirements for an ideal gas, the Joule-Thomson effect is very small, and it is only by pre-cooling the helium to the temperature of liquid hydrogen boiling at reduced pressure that the magnitude of the effect is sufficient to liquefy the gas. The efficiency of this method is very low—Meissner† estimates that it is only 1% of the efficiency which would be obtained by using an adiabatic method. Actually, to produce 1 litre of liquid helium, Meissner estimates that 6 litres of liquid air and 5 litres of liquid hydrogen are required. This figure gives some idea of the difficulties encountered in cryogenic work with helium.

POSSIBLE EXPANSION ENGINES

In view of the low efficiency and complication of the Joule-Thomson process for liquefaction and of the possibility of increasing the efficiency by a factor of approximately one hundred by the use of an adiabatic process, we have developed an expansion engine which will work continuously at low temperatures to enable this process to be realized.

A number of methods are possible *a priori* to extract heat adiabatically from compressed gases at low temperatures. The one which would seem to be the most natural would be to use a turbine, and at first sight this idea seems to be very attractive, since in the first place no lubricant would be required, and lubrication is one of the great difficulties encountered at low temperatures. From the theory of the efficiency of turbines it is known that the velocity of the moving blades must be near the critical velocity of the gas, and under normal conditions this tends to be rather high and makes construction difficult. At temperatures approaching its liquefaction point, however, the critical velocity of helium is very much reduced—for instance, at 15° K it is only 153 metres per second—and therefore undue high speed of the turbine blades would not be required. After detailed calculation, however, we found that the chief difficulty would arise from the size of the actual turbine. For instance, at 15° K and 30 atmospheres pressure, treating about 30 cubic metres of helium per hour (which would be necessary for the liquefaction of a few litres of helium per hour), the cross-section of the nozzle would have to have an area as small as 1/10 sq mm. The other dimensions of the turbine would have to be on a correspondingly small scale; and it would appear, therefore, that unless helium is to be liquefied on a really large scale, the turbine method is not practicable. Actually, as will be seen from the description of our present machine, which has a high efficiency, it will probably be difficult to improve on this efficiency even with a turbine used for large scale production.

---

* ' C. R. Acad. Sci. Paris,' vol. 147, p. 421 (1908).

† " Geiger u. Scheel," ' Handb. der Physik,' vol. 11, p. 320.

Another possible machine is an ordinary reciprocating piston type. The great technical difficulty in designing this kind of machine for very low temperatures is to devise a method whereby the piston can move in the cylinder without friction but at the same time without leakage. In an ordinary reciprocating engine this is achieved by the introduction of a lubricant between the piston and the cylinder wall—but at the temperatures of liquid hydrogen and helium it is impossible to find a lubricant. The first successful use of an expansion engine for low temperature work is due to Claude.* In the first instance Claude overcame the lubrication difficulty by using liquid air itself to lubricate the piston, but eventually he found that liquid aid is not an efficient lubricant,† and at present he only uses his expansion engine down to −140° C at which temperature ether and petrol still keep their lubricating properties. If liquid air is not found to be a very satisfactory lubricant, it is evident that liquid helium with its low surface tension would probably have no lubricating properties at all, and therefore Claude's solution of the difficulty would not be possible for a helium liquefier.

---

* 'C. R. Acad. Sci. Paris,' vol. 134, p. 1568 (June 30, 1902).

† *Ibid.*, vol. 141, p. 762 (November 13, 1905).

In order to overcome the difficulty of lubrication we have been working for some time in this laboratory on the development of a reciprocating expansion engine working on an entirely different principle in which the piston does not require any lubricant at all, and which will work at any temperature.* The main feature is that the piston is loosely fitted in the cylinder with a definite clearance, and when the gas is introduced into the cylinder at high pressure, it is allowed to escape freely through the gap between the cylinder and the piston. The expansion engine is arranged in such a way that the piston moves very rapidly on the expanding stroke, and the expansion takes place in such a small fraction of a second that the amount of gas escaping through the gap is very small and does not appreciably affect the efficiency of the machine. Actually the efficiency of this expansion machine has been found to be about 60% which is very high. With the machine which we describe in this article, helium was successfully liquefied without pre-cooling by liquid hydrogen.

THE GENERAL ARRANGEMENT OF THE LIQUEFACTION CIRCUITS

In designing the helium liquefier our general aim, besides high efficiency, has been to build a machine with the maximum output and a small starting time. To describe in detail all the calculations necessary for the design of a machine embodying these features is beyond the scope of this paper since most of them involve purely routine work of an engineering character. We shall therefore only discuss here the general principles of the machine.

The first question we had to settle was that of the choice of the liquefier circuit. Using our type of expansion machine it would be quite possible to liquefy helium without any pre-cooling, either by liquid hydrogen or liquid air; to do this, however, a very large expansion engine and compressors would be required and the whole liquefier would be very bulky. For example, to start from room temperature and then liquefy 1 kg of helium it would be necessary to extract 380 calories of cold. On the other hand, to liquefy the same amount of helium starting at the temperature of liquid nitrogen boiling at reduced pressure (65° K), it is only necessary to extract 84 calories of cold. Therefore a plant which did not make use of pre-cooling by liquid nitrogen would be about four times larger than one which used liquid nitrogen. With an ideal heat exchanger only $\frac{1}{2}$ litre of liquid nitrogen per litre of liquid helium would be required for pre-cooling, so that, taking into consideration the cheapness of liquid nitrogen, it pays in laboratory practice to use it for initial pre-cooling. Further pre-cooling to 20° K by means of liquid hydrogen would reduce the amount of cold to be extracted to 25 calories, but this advantage is discounted by the precautions and complications involved in running a hydrogen liquefier.

---

* Kapitza, 'Nature,' vol. 133, p. 208 (1934).

The scheme of heat exchangers we have adopted is shown on fig. 1. Compressed helium enters tube 1 and passes through a heat exchanger A, and is then cooled down to 65° K by passing round a ring shaped container N where liquid nitrogen is kept boiling at reduced pressure. The compressed helium then goes through the heat exchanger B to the expansion engine E. After leaving the expansion engine it passes through heat exchangers C, B, and A back to the compressor through tube 2. By means of these regenerating heat exchangers, the temperature of the outlet gas from the expansion engine could gradually be lowered until part of the helium would leave the expansion engine in the liquefied state. If we then separated the liquid from the gas we should have a liquefaction circuit similar to that originally used by Claude (*loc. cit.*) for the liquefaction of air. Such an arrangement, however, appears to be inefficient, and the reasons for this can easily be seen. Let us assume that the gas enters the expansion engine at a pressure p_1 where it fills a volume v_1 at a temperature T_1, and is then expanded to a volume v_2 at a pressure p_2 and temperature T_2. During this expansion the process follows the well-known formula:

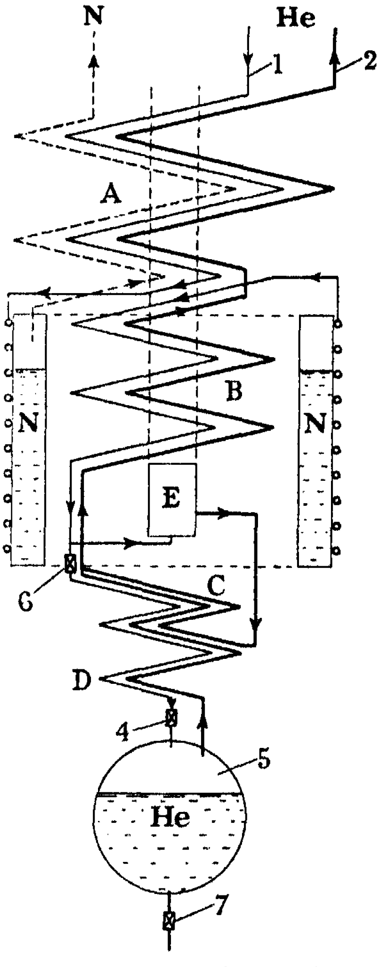

FIG. 1—The heat exchanger circuits of the liquefier.

$$pv^{\gamma} = \text{constant}, \tag{1}$$

where γ is the ratio of the specific heats. The amounts of cold obtained from a single expansion would be,

$$\Delta i = \eta j p_1 v_1 \frac{\gamma}{\gamma - 1}\left[1 - \left(\frac{p_2}{p_1}\right)^{\frac{\gamma-1}{\gamma}}\right], \tag{2}$$

where η denotes the efficiency of the expansion engine which in an ideal engine would be unity, and j the thermodynamical equivalent of heat. From (2) we see that the amount of cold we get from the expansion engine with a perfect gas is independent of the temperature at which the expansion engine works. The density of the helium which fills the expansion engine will be inversely proportional to the temperature T_1. Therefore, as T_1 is lowered the amount of gas which the compressor has to supply is increased, but the amount of cold produced by the expansion engine will be the same. We reach this conclusion by assuming that helium follows almost exactly the equation for a perfect gas. Actually it can be shown that deviation from the equation will not alter our conclusions but strengthen them, since the quantity of cold produced, Δi, diminishes as the temperature approaches nearer to the liquefaction temperature. From more detailed consideration it appears that it is preferable to keep T_1 as high as possible and to cool the helium by means of the expansion engine, to a temperature T_2 well above its boiling point, and endeavour to effect the final stages down to actual liquefaction by some other means.

Three possibilities are open to us: the first corresponds to Claude's method for the liquefaction of air, and means that we must have the temperature T_2 slightly below the critical temperature for helium liquefaction (5·2° K) and then carry out the liquefaction in a vessel cooled to this temperature at a pressure above the critical one (2·26 atmospheres). This method, however, proves to be impracticable for helium since the margin between the critical temperature and the liquefaction temperature is only 1° which is too small.

A second method would be to allow the exhaust gases to cool the helium in a container at considerable pressure, and then by reducing the pressure the helium could be liquefied by the Simon method. The vessel would then be emptied and the process repeated.

The third method, which is the one we have actually adopted, is similar to that used by Heylandt* for the liquefaction of air, where the last stage of the liquefaction is effected by means of the Joule-Thomson effect. The circuit used is shown on fig. 1. After passing through the heat exchanger B a fraction of the high pressure helium is passed through heat exchanger C, where it is cooled down to the temperature T_2 of the exhaust helium from the expansion engine. It then passes through heat exchanger D and the throttling valve 4 to the liquefaction vessel 5. After a part of it has liquefied, the remainder again passes through heat exchangers D and C and finally joins the outlet gas from the expansion engine.

---

* Meissner, *loc. cit.*, p. 314.

In order to calculate the output efficiency of our liquefier we have to know the equation of state for helium near its critical point. This, however, is not known analytically with any precision and it is much more convenient to make use of " Entropy diagrams " or " Mollier diagrams." Keesom and Houthoff* have actually prepared such diagrams for helium, and we found them most helpful in our work. From the diagrams we obtained the following data : (i) The total heat i_n and i'_n corresponding to pressures p_1 and p_2 at the temperature T_n at which the compressed helium leaves the liquid nitrogen container. (ii) The total heat, i_1, at the temperature T_1 of the inlet gas to the expansion engine. (iii) The total heat, i'_2, at temperature T'_2 after the gas has expanded adiabatically to pressure p_2. Actually, owing to different losses in the expansion mechanism the gas comes to a point p_2, T_2, and i_2, this point being related to the ideal point p_2, T'_2, i'_2 by the efficiency coefficient of the expansion engine

$$\eta = \frac{i_1 - i_2}{i_1 - i'_2} . \tag{3}$$

If we pass D kilograms of helium through the liquefier, a fraction of which, K, goes through the expansion engine, the amount of cold produced would be $DK\eta\,(i_1 - i'_2)$, but all this cold is not available for liquefaction—some of it being lost owing to imperfections in the heat exchanger B. If we take the efficiency of the heat exchanger B to be ϕ, the amount of cold carried away by the gas will be $D\,(i'_n - i_1)\,(1 - \phi)$. There will be some losses owing to the difference in total heats at the temperature T_n, this loss of cold being equal to $D\,(i'_n - i_n)$ is actually very small compared with the other terms.

A fraction of the gas $(1 - K)$ is used for the Joule-Thomson effect, being throttled from pressure p_3 to p_4. The corresponding total heats at temperature T_2 will be found on the entropy diagram to be i_3 and i_4, and in a liquid state and at a pressure p_4 it will be i'_4. To liquefy 1 kilogram of helium we require $i - i'_4$ calories, therefore the amount of gas liquefied will be

$$L = D\left[\frac{K\eta\,(i_1 - i'_2) - (1 - \phi)\,(i'_n - i_1) - (i'_n - i_n)}{i_n - i'_4}\right] . \tag{4}$$

---

* 'Commun. phys. Lab. Univ. Leiden,' vol. 17 (1924–1928), supplement 65e (1928).

The amount of helium liquefied by the Joule-Thomson effect wil then be*

$$L = D(1 - K)\frac{i_3 - i_4}{i_3 - i'_4}. \tag{5}$$

The value K is determined from equations (4) and (5), and it will be seen that there is a temperature T_2 at which L/D will be a maximum. The two equations (4) and (5) only begin to have a meaning for helium when T_2 is below 40° K and the Joule-Thomson effect has a positive sign. On reducing the value of T_2, $i_1 - i'_2$ will diminish and K will increase. Finally the product will reach a maximum at which the liquefier will have the maximum efficiency. From experiments this maximum would appear to be about 10° K, but we were unable to settle this from the diagram since, although the values obtained from it were accurate down to 15° K and 20 atmospheres pressure, at lower temperatures the accuracy was not so reliable. We shall discuss this point in a later section of this paper, and only mention it here because we found that the inversion pressure for the Joule-Thomson effect was lower than we expected from the diagram, and this made it necessary to introduce another throttling valve (6) which reduced the pressure of the helium entering the regenerating spirals C and D from 30 to about 17 atmospheres.

From equation (4) we see that the total output and efficiency of the liquefier does not depend entirely on the efficiency η of the expansion engine, but also on the efficiency ϕ of the heat exchanger B.

In practice we find that $(i_n - i_1) = 61$ calories while the cold produced by the expansion engine $K(i'_1 - i'_2) = 9 \cdot 7$ calories. The heat exchanger used has an efficiency ϕ of 92%, but even with this high figure, about half of the cold produced by the expansion engine is carried away. The necessity for a very efficient heat exchanger B has made it necessary to make it rather large and heavy as will be seen from fig. 3.

To avoid using such a bulky system of heat exchangers, it can be seen that a much more efficient liquefier could be made if a number of expansion engines were used in series, the outlet gas of one cooling the inlet gas for the next. In practice it will be found that if three machines are used, the exhaust gases of the last machine will have reached a sufficiently low temperature to be used for cooling the compressed helium to be liquefied by the Joule-Thomson effect. A liquefier working on this plan would practically dispense with heat exchanger B and would probably have at least three times the output of the present liquefier, using the same amount of compressed helium. The scheme has not yet been carried out merely because it involves building three expansion engines, and this technical complication was not justified in the initial stages of development.

---

* See Keesom, 'Commun. phys. Lab. Univ. Leiden,' vol. 17 (1924–1928), supplement 65f (1928).

THE EXPANSION MACHINE

In this section we shall describe the general principles on which the expansion engine is designed, and also the details of its construction. The first thing to be settled before designing an expansion engine is the choice of its working pressure p_1. From expression (2) we see that by increasing the working pressure the specific cold production $\Delta i/v_1 p_1$ is only increased slightly. On the other hand, increase of the inlet pressure greatly complicates the construction of the machine and also makes it more bulky. The most convenient pressure to use, however, depends on so many factors that it can only be found from experience; actually we have chosen this pressure to be between 25 and 30 atmospheres. The size of the expansion engine depends on the amount of gas to be treated and on the number of strokes the machine will make per minute. The inlet volume and expansion ratio are determined from the specific volumes of helium on the state diagram.

Our present expansion engine works at a rate of 100 to 120 strokes per minute and treats about 30 cubic metres of helium per hour at room temperature and normal pressure. The diameter of the piston is 31 mm (1¼ inches) and the stroke varies between 3·5 and 5 cm. In choosing the ratio between the diameter of the piston and the length of the stroke, we have to consider a number of factors : the thermal conductivity of the metal, the leakage through the space between the piston and the cylinder, the ease of operation of the cam mechanism, etc. Having settled the general size of the machine, the next point is to find a mechanism which will allow the piston to move quickly on the expanding stroke and do work, and then move slowly back again. It is evident that a crank shaft mechanism is not suitable for this purpose. It would probably be possible to find some cam mechanism which would fulfil the requirements, but technically it appeared to be simpler to use a hydraulic mechanism. The general principle of the mechanism is as shown in fig. 2. The expansion machine E is connected with the hydraulic mechanism H by a connecting rod 3. When the gas enters the expansion engine, it moves the piston 13 which in turn moves piston 8 in the hydraulic machine, and since the space above the piston 8 is filled with water this is forced out as a jet through the hole 9. In this way the work done by the expanding gas is transferred as kinetic energy to the jet of water. After the expansion stroke is finished and the outlet valve of the expansion engine is opened, the cylinder of the hydraulic machine is gradually filled with water, and the piston of the expansion machine returns slowly to its original position. The cooled expanded helium enters tube 10 from the cylinder, the gland 12 preventing it from escaping, and then passes through tube 11 into the heat exchangers. It should be noted that the diameter of the connecting rod 3 in gland 12 is chosen to be equal to the diameter of the piston in the expansion engine; therefore, on the expansion stroke, the volume of the gas in tube 10 is not altered, and no sudden increase of pressure occurs. On the down-stroke the gas in 10 is slowly compressed and made to circulate through the heat exchangers with a uniform velocity.

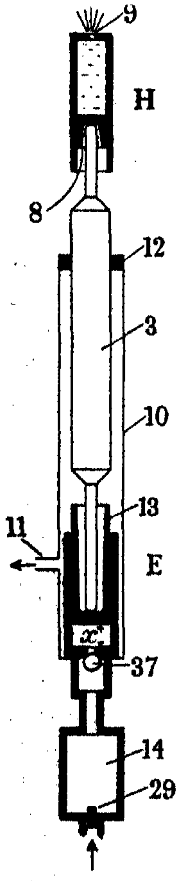

FIG. 2—Schematic outline of the expansion engine.

As will be seen from the diagram, the expansion engine is placed in a long thin-walled tube 10 (0·05 mm), and the connecting rod 3 is also in the form of a thin tube (0·5 mm); this provides thermal insulation from the cold produced in the expansion machine.

The motion of the system can be expressed by the following equation

$$M\ddot{x} + C\dot{x}^2 + F = P, \tag{6}$$

where x is the displacement of the piston in the expansion engine, M the mass of the two pistons and the connecting rod, F the frictional forces arising mainly from the gland, and P the resultant force which is equal to

$$P = (p - p_0)\,\pi R^2, \tag{7}$$

where R is the radius of the piston 13 of the expansion engine and p_0 the atmospheric pressure. The term $C\dot{x}^2$ represents the force due to the energy absorbed by the jet of water, while C is a constant which is determined as follows:—

$$C = \pi r^6 \sigma / 2\rho^2 a^4, \tag{8}$$

where r is the radius of the piston 8 of the hydraulic mechanism and a is the radius of the opening for the jet 9; σ is the density of water, and ρ the contraction of the jet which may be taken as equal to 0·6. During the time of filling of the expansion engine with gas at constant pressure, P is constant, and we get:

$$\dot{x}^2 = \dot{x}_0^2\left(1 - e^{-\frac{2Cx}{M}}\right) \tag{9}$$

where

$$\dot{x}_0^2 = \frac{P - F}{C}. \tag{10}$$

We see that if the factor 2Cx/M is large, the influence of the inertia on the motion will be small and the piston will assume practically at once the velocity given by (10). Therefore, if the mass of the moving part of the expansion engine is small and C large, we may assume that the motion is according to formula (10) all the time, even if P is a variable. The change in P after the inlet valve is closed is given by expression (1), and then the velocity of the piston can be estimated from (10) at any point in the stroke. For our present purposes this method of calculation is sufficiently accurate, although a more complete solution of (6) is obtainable by means of series.

It will be seen from (10) that the hydraulic arrangement has the advantage that it provides a faster motion of the piston at the beginning of the stroke when the pressure is high and the leakage losses between the piston and the cylinder are largest, and then the velocity of the stroke diminishes as the pressure drops. There is also the advantage that the length of the stroke is not fixed and can vary with the pressure or temperature of the inlet gas in such a way that the outlet pressure will always be the same, which results in a higher efficiency in the expansion.

Theoretically in choosing the actual speed of the motion, which is done by adjusting the diameter of the hole 9, we find the only factor which limits the speed of the piston is that it should be less than the critical velocity of helium, and at first sight it appears that the quicker we make the motion of the piston the shorter will be the time of the stroke, and therefore the leakage losses will be less through the gap between the cylinder and the piston. In practice we find that the speed of the piston is limited by the difficulty of filling the cylinder with gas in a short time, as this is limited by the size of the inlet valve. In fixing the size of the valve the following requirements have to be satisfied: to avoid a big pressure drop the area of the opening of the valve must be sufficiently large to make the velocity of the gas through the opening well below its critical velocity. On the other hand, the valve must not be made too large as it would require rather large forces for its operation, and also it must not have too great a mass because the inertia would interfere with quick operation. Taking all these conditions into consideration we have chosen a circular valve for our expansion engine with a diameter of 1 cm and an opening of 1 mm. This size of valve has proved satisfactory when the total time of the stroke from beginning to end is about 1/10 second, and this is achieved with the following dimensions of the hydraulic arrangement: diameter of cylinder 8, 25 mm; the diameter of hole 9, 2·7 mm.

If we know the velocity of the motion of the piston during its stroke, it is easy to estimate the width of the gap between the piston and the cylinder wall which will not cause too great a leakage of gas. The maximum value of the gas losses can be estimated from classical formulæ by assuming that the gas flows out as a viscous fluid. The value for the viscosity of helium at low temperatures was obtained from the measurements of Kammerlingh Onnes and Sophus Weber.* The leakage losses in this case will be found to be proportional to the cube of the width of the gap and have the maximum value when the piston is pushed to one side of the cylinder and the gap is not uniform. Actually, however, the flow is not a viscous but a turbulent one, and therefore the amount of gas lost will be less in practice than the amount estimated in this way. Accurate measurements of the gap are difficult, and for our practical purposes we estimated the losses by observations on the velocity with which the piston when loaded drops in the cylinder when all the valves are shut. Knowing the weight of the piston and of the load, we can by using a similarity formula extrapolate the magnitude of the leakage to the conditions at low temperatures and high pressures. In this way we find that with a gap of 0·04 to 0·05 mm, which is the gap used in our case, the losses do not exceed a few per cent. of the helium used.

The detailed arrangement of the expansion engine is shown on fig. 3. As in all engineering constructions, many of the devices which are used could be equally well replaced by other mechanisms, but there are also some details of the construction which are peculiar to the machine and essential for its efficient working which will now be referred to in detail.

Since there is no lubrication between the cylinder and piston, it is essential that there should be no sideway forces on the piston, and to ensure this there are two universal joints 26 and 28 so that in practice there are no side pressures on the cylinder other than those introduced by errors in the alignment of the axis of the cylinder and the axis of the connecting rod.

Another important detail is the necessity for cutting small grooves, ¼ mm deep and ¼ mm broad at a distance apart of about 5 mm, round the circumference of the piston. This is because we found it practically impossible, even with very great care, to make the surfaces of the cylinder and the piston perfectly even, and there are always small irregularities. As has been mentioned before, the resistance of the gap to the leaking gas

---

* 'Commun. phys. Lab. Univ. Leiden,' vol. 13, No. 134b (1913–14).

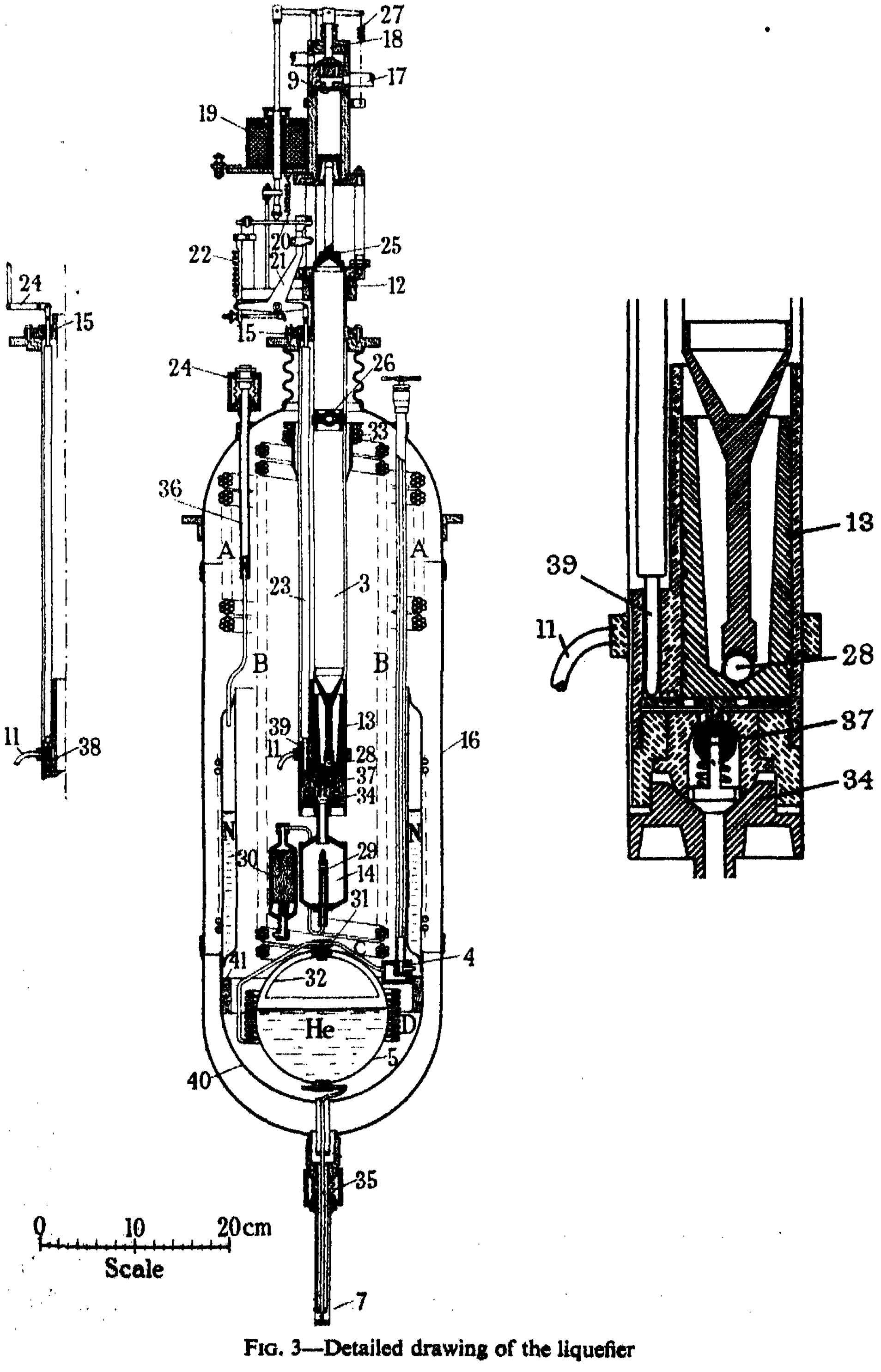

Fig. 3—Detailed drawing of the liquefier

depends on the cube of the width, and therefore even small variations will have a considerable influence on the pressure drop between the piston and the cylinder, and since this pressure drop may vary on different sides of the piston, considerable sideway forces may develop. The small grooves, however, equalize the pressure all round the piston. In practice we found that if we did not have these grooves the sideway forces are so high that the piston siezes almost immediately.

To ensure smooth working of the piston in the cylinder it is essential that there should be no foreign particles in the helium, and we therefore filter the gas before it enters the expansion machine. Also minute traces of impurity such as air, when cooled, form solid crystals on the side of the cylinder which cause scratching and wearing and even seizure of the piston, and the efficiency of the machine is considerably impaired. We found that the purity of the helium must be very high indeed, and to purify it to the required degree it was found necessary to pass it through a charcoal trap 30 before it enters the expansion engine.

Finally it is essential to have a high pressure container 14 which we have chosen to hold about ten times the volume of the gas used for a single expansion. This reservoir is necessary to avoid a pressure drop of the supplied gas during the inlet time, since this would obviously affect the efficiency of the engine.

The expansion engine is placed in the centre of the liquefier the whole being surrounded by casing 16. The necessary thermal insulation is produced by evacuating the casing to a very high vacuum with the help of charcoal 4.

It is essential that all internal parts of the expansion engine should be accessible for examination, and this is done by means of a special key with which the cylinder can be unscrewed from the seating 34. The inlet valve 37 can also be removed.

The inlet valve 37 consists of a steel ball of $\frac{1}{2}$ inch diameter pressed in a well-polished seating made of phosphor bronze. The construction of this valve is of primary importance. At low temperatures when the viscosity of the gas is small the problem of having a really tight valve is a difficult one. To make the valve shut tightly the same part of the ball is always used which is done by means of a pin inserted in a hole drilled in the ball which prevents it from rotating in the seating. The outlet valve 38 shown separately on the drawing is made in the side of the cylinder. The inlet valve is operated by push rod 39 which fits well into a cylindrical hole in the cylinder. The amount of gas leakage through the gap round the rod 39, as in the case of the piston and the cylinder, is small owing to the rapidity of the expansion. On the top of the expansion engine there are three glands, two for the valve push rods, 15, and one, 12, for the connecting rod. The dimensions of most of the operating parts in the expansion engine can be estimated from standard calculations of applied mechanics.

The operation of the expansion engine is as follows: The stroke is started by the electromagnet 19 which first of all opens water valve 18 which releases the water pressure above the piston, and then kicks down the trigger 20 which keeps the lever 21 in a fixed position. After release the lever is pulled down by the spring 22 and operates the inlet valve by means of the connecting rod 23. At the same time, by means of the lever 24, the outlet valve is closed. The pressure of the helium entering the cylinder sets the piston in motion and after it has moved about 0·7 cm and the filling of the expansion engine with gas is completed, the cam 25 presses the roller on the lever 21, the lever moves up, and this shuts the inlet valve. For the remainder of the stroke, the gas is allowed to expand adiabatically and a jet of water through hole 9 absorbs the work. The water is not wasted but is sent to the compressor where it is used for cooling purposes. When the stroke is ended, the current is broken in the electromagnet, its armature is pulled up by the spring 27 which opens the outlet valve and lets the trigger 20 fall back, and finally closes the water valve 18. The water then enters by tube 17 and fills the cylinder and the piston gradually moves back, pushing the cooled helium through the outlet tube 11 into the circulating system. The cycle is then finished.

The electromagnet 19 is automatically operated by means of a special contact which is operated by friction in such a way that it shuts off the current on the upward stroke of the piston and breaks it on the down stroke. This valve mechanism works quite well, but we think it could be considerably simplified and hope to do this in our next model.

Besides the question of design, a very important point in the construction of an expansion engine is the choice of proper materials. It is a well-known fact that a number of materials which are flexible at ordinary temperatures become as brittle as glass at low temperatures. This is especially true of common mild steel. Although the tensile strength of the material increases at low temperatures the absence of plasticity makes its use impossible. We had, therefore, to choose materials which keep their plasticity at low temperatures. Secondly, the tubes which connect the expansion engine with the hydraulic mechanism must have a small thermal conductivity and great strength. We found that a very suitable material was Firth's " Staybrite " steel. This non-corrodible steel has a very low thermal conductivity (0·033), keeps its plasticity at low temperatures, and can be drawn into very thin walled tubes. For our liquefier we used tubes having wall thicknesses of from 0·5 to 0·2 mm. There is one possible difficulty about using " Staybrite " steel, namely, that it belongs to the class of austenitic steels where the iron is in the non-magnetic γ-modification. On cold working the steel acquires magnetic properties which suggests that it may be in a state of unstable equilibrium between the α and the γ modification, and we might expect a gradual conversion to the α condition at low temperatures; should such a transition take place it would probably seriously affect the mechanical properties of the steel. To satisfy ourselves on this point, we kept a number of samples of different brands of " Staybrite " at the temperature of liquid hydrogen for 8 days. We are indebted to Dr. Hatfield, of the Research Laboratories of Messrs. Thomas Firth and John Brown, Ltd., who was kind enough to make a thorough examination of these samples after they were subjected to the low temperature treatment. Most of the samples showed no alteration in any of their physical properties, and we finally chose the " F.S.T." brand for our work. Another property of " Staybrite " steel is that it has a larger coefficient of thermal expansion than ordinary steel and actually approaches very near to the thermal expansion of copper. This makes the steel especially suitable for the construction of the piston of the expansion engine. At first sight it appeared that the best scheme would be to make both the piston and cylinder of the same material, but we found that when we made them both of phosphor bronze the piston seized, and on examination it appeared that this was due to foreign particles entering the gap, and since both surfaces were of equal hardness they did not get embedded in either of them. If, on the other hand, the piston is made of " Staybrite " and the cylinder of phosphor bronze, foreign particles will bury themselves in the latter. It is very important that all materials used for the construction of parts of the machine which are subjected to low temperatures should be well softened so that no internal stresses develop.

THE HEAT EXCHANGERS

The design of the heat exchangers is of obvious importance in obtaining the maximum efficiency from the liquefier. Generally speaking, the greater the size of the heat exchangers the greater their efficiency; on the other hand, in laboratory apparatus, efficiency is not the only consideration—greater size involves a much heavier and bulkier apparatus which is a disadvantage because it will have a larger cold consumption during the preliminary cooling and will therefore increase the starting up time.

In constructing our liquefier, therefore, we have been prepared to sacrifice a certain amount of efficiency for the sake of speed in starting and economy in preliminary cooling, and have tried to keep the heat exchangers as small as possible.

The general theory of the heat exchangers and the calculations for their construction have been obtained from the work of Nusselt.* In actual practice we only made the preliminary estimates of the dimensions of our heat exchangers from Nusselt's formulæ, and after making and examining them we then improved them by using similarity formulæ. From Nusselt's formulæ it will be seen that for a system of parallel tubes the heat transfer capacity of an exchanger treating a given amount of gas will be proportional to $n^{0 \cdot 21}$, $l^{0 \cdot 95}$ and $d^{-0 \cdot 79}$ where n is the number of tubes in parallel, d the diameter of the tubes, and l the length of the exchanger. Therefore to increase the heat transfer capacity of the exchanger we can make it longer and reduce the diameter of the tubes, but changing the number of tubes in parallel will not have much influence.

In choosing the dimensions of the tubes of the exchanger it is extremely important to ensure that the pressure drop is not too high, particularly in the return tubes. If we are treating a constant amount of gas, it can be shown that the pressure drop is proportional to $n^{-1 \cdot 75}$, l and $d^{-4 \cdot 75}$, which shows that even a slight variation of the diameter will greatly influence the pressure drop. It is evident that the best way of diminishing the pressure drop without affecting the heat exchanges is to increase the number n of tubes in parallel.

In our liquefier the heat exchangers consist of a high pressure tube with six low pressure tubes round it for the return gas. The tubes are made of cupro-nickel (composition 80/20) and are all soldered together and bound in a spiral. The heat exchanger A, figs. 1 and 3, is rather complicated and could be considerably improved. The top part of it is 4 metres long and consists of seven tubes of 4 mm inside diameter ; the lower part is 3 metres long and consists of seven tubes of 5 mm inside diameter. Three of these tubes in the lower part are used for the return of evaporated nitrogen.

The heat exchanger on the liquid nitrogen bottle N is 8 metres long and is made of 5 mm tubes.

The heat exchanger B is the longest and the most important. It is 16 m long and its length is divided into three sections, the inside diameters of the tubes being 4 mm, 3·5 mm, and 2·3 mm, respectively.

---

* Gröber, "Warmeübertragung," Springer (1926), p. 84.

Heat exchangers C and D are 2 m and 6 m long respectively and both consist of 2·3 mm tube.

If we do not take special precautions the expansion engine will send the gas in impulses to the heat exchangers which will considerably reduce the efficiency, especially for the exchanger B. We have already seen that gland 12, fig. 2, is made of the same dimensions as the piston, and this provides a uniform flow of the return gas. To obtain a more uniform flow of the inlet gas a nozzle 29, fig. 3, is placed at the bottom of the container 14 which introduces a resistance in the flow of gas. This nozzle has a diameter of 4 mm and a length of 1 cm and can be screwed out when the piston and cylinder are dismantled.

We found that particular care had to be taken in soldering all the tubes and parts of the liquefier in order to ensure vacuum tightness, satisfactory methods being developed by experience.

Of other details of the liquefier we should mention the centrifugal separator for removing the small drops of liquid helium from the cooled gas. After passing the throttling valve 4, fig. 3, the helium passes through three nozzles 31 which communicate the rotating motion required for separation to the gas in the gap between the wall of the container and the hemisphere 32.

The liquid nitrogen container N has a copper hemisphere 40 at the bottom which is kept at a low temperature by heat conductivity, and which surrounds the helium heat exchanger and expansion machine and protects it from loss of cold. The outside tube of the expansion engine is cooled down to the temperature of liquid nitrogen by the return flow of helium gas at the point 33, thus diminishing the thermal conductivity losses from the expansion engine to the exterior.

A number of pressure indicators are incorporated in the liquefier, and there are two simplified helium thermometers to measure the gas temperature before and after it passes through the expansion engine; there are also level indicators for the helium in the container and for the liquid nitrogen in the outer vessel. The liquid helium is drawn off at the bottom of the apparatus through a tap 7; this consists of two thin-walled " Staybrite " tubes, 0·2 mm thick, the inner one having a nozzle which is closed by pressing on an appendix fixed to the outer one, the whole being made tight by means of a flexible bellows 35. A similar tap 36 is used for letting liquid nitrogen into the outer container. The functioning of this type of tap was found to be very satisfactory.

For successful working of the liquefier it is absolutely essential to keep the helium free from contamination, and we have taken special care to work out a storage system in which there is no possibility of air or other impurities getting in. The helium is kept in a cylinder at 10 atmospheres pressure from which it is automatically discharged on demand into a ½ cu. m gasholder which is filled with rather heavy compressor oil (we found that only very heavy oil can be used for this purpose otherwise air diffuses into the helium). When the gasholder is filled with helium the surplus is automatically pumped back to the cylinder by means of a small totally enclosed pump. The system is made to hold about 7 to 8 cu. m of helium. A general view of the liquefier is shown on fig. 4, and a view of the layout of the installation on fig. 5.

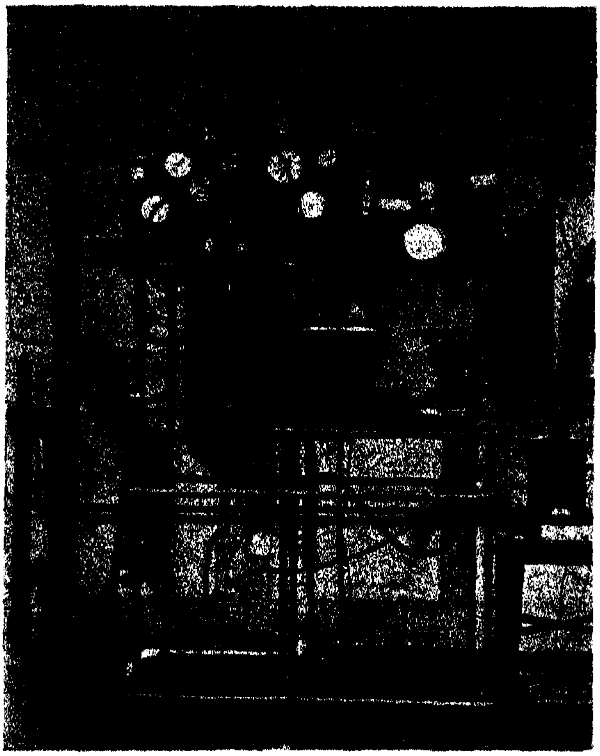

FIG. 4—General view of the liquefier.

PERFORMANCE OF THE LIQUEFIER

The expansion engine has proved to be a very efficient machine from a thermodynamical point of view. With inlet and outlet pressures of 30 and 2·2 atmospheres respectively, the inlet temperature of the gas is 19° K and the exhaust temperature 10° K, so that from the state diagram, 60% of the free energy of the gas is turned into mechanical work. This high efficiency for such a small machine is probably due to the very small friction losses between the piston and the cylinder. Apparently the small amount of gas which leaks through the gap acts as an "ideal" lubricant. This is borne out by the fact that we found that even after working for many hours there was no appreciable wearing of the surface of the cylinder or piston, and the small scratches and markings made in the construction remained untouched.

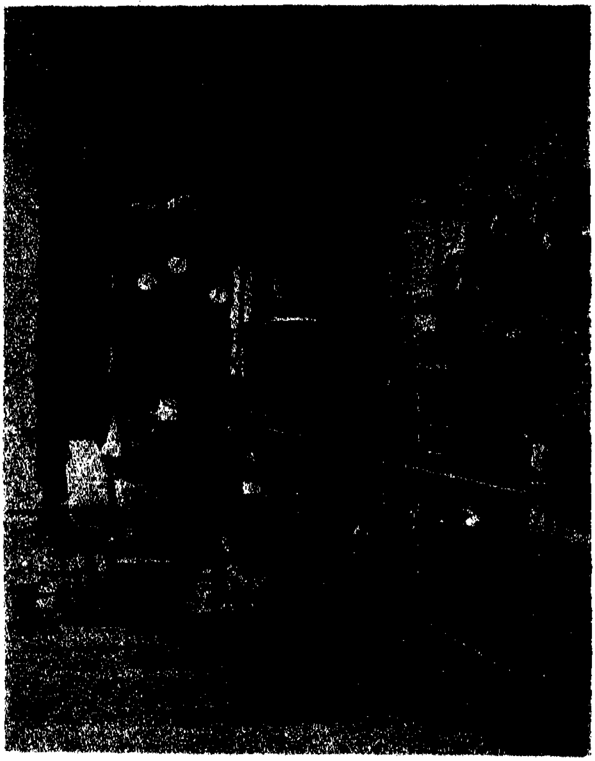

FIG. 5—General view of the installation.

From the data given above, assuming that 32 cu. m of gas are delivered by the compressor per hour, of which 28 cu. m passes through the expansion engine, 49 calories will be available per hour. This should be sufficient to liquefy 4·7 litres of helium, but actually our best output is only 1·9 to 2 litres per hour, the difference being mainly due to losses in heat exchanger B as discussed before.

The starting up of the liquefier is carried out as follows: Bottle N, fig. 1, is filled with liquid nitrogen, and at the same time the expansion engine is started. To get the heat exchangers cooled down quickly, a large amount of helium is kept circulating through tube 1, bottle 5 and tap 7, and back to the gasholder without passing through return tube 2. In 45 minutes the whole apparatus is at the temperature of liquid nitrogen and then the expansion engine brings it down in 25 to 30 minutes to 10° K. To cool the bottle 5 to this temperature as soon as possible, a weaker continuous stream of helium is still maintained through tap 7. Tap 7 is then shut and liquid helium starts to accumulate in the container practically at once. For starting the liquefier 7 kilograms of liquid nitrogen are required.

Experiments have shown that the speed of liquefaction depends very much on the throttling pressure. We noticed that when working at 30 atmospheres, helium is produced at first, but the rate gradually diminishes and the temperature of the expansion engine becomes lower, until finally liquefaction stops almost completely. This phenomenon puzzled us at first, and the only satisfactory solution seems to be that at these temperatures and pressures there is an inversion of the Joule-Thomson effect. When the amount of gas used for the Joule-Thomson effect does not remove enough cold for liquefaction the temperature of the expansion engine becomes lower, and with this diminishing temperature but the same pressure the magnitude of the Joule-Thomson effect becomes less owing to inversion. Finally when the temperature of the outlet gas from the expansion engine reaches a value of 6° K, the stroke becomes shorter and the output of cold is so small that it is only sufficient to balance the cold losses in the heat exchanger B, and liquefaction practically stops. At present there are no definite data on the existence of such an inversion pressure at low temperatures ; Meissner discusses this point without coming to any definite conclusion.* The entropy diagram of Keesom and Houthoff (*loc. cit.*) does not indicate an inversion point at about 14° K and 20 to 25 atmospheres pressure where we should expect it from our experiments. Kammerlingh Onnes found that the most efficient pressure for liquefying helium was 20 atmospheres, and he suggested that at higher pressures the speed of liquefaction diminishes because drops of helium are carried away by the return stream of helium. At first we thought this explanation could be applied in our case too, but on improving the separation of liquid gas by the centrifugal arrangement 31, fig. 3, as already described, we found that there was no improvement in the liquefaction. By decreasing the throttling pressure by means of valve 7, fig. 1, from 30 to 17 atmospheres, but at the same time keeping the stream of gas through the throttle constant so that the carrying away of drops was constant, we increased the rate of liquefaction from 0·6 to 2 litres. It seems probable from our experience that the maximum of liquefaction observed by Kammerlingh Onnes was also due to this inversion phenomenon. Our liquefier is not suited for accurate study of the equation of state for helium at low temperatures, but it is difficult to put forward any other convincing explanation for the phenomena described. We actually found that with a throttling pressure of 17 to 18 atmospheres we attained a maximum rate of liquefaction of about 2 litres per hour, while the consumption of liquid nitrogen is of the order of 2 kilograms per hour. Therefore to make approximately 1 litre liquid helium, we require just under 1·5 litres of liquid nitrogen.

---

* *Loc. cit.* ' Handb. Physik,' p. 326.

CONCLUDING REMARKS

The same type of expansion engine may have other applications besides the liquefaction of helium, where an apparatus has to be cooled down to a temperature of 7° to 8° K. We have also used it for the liquefaction of hydrogen, but apparently this is only of practical advantage when liquid hydrogen is to be produced on a large scale.

The present liquefier has been working for several months and most of the troubles which hindered us have been overcome, and it is now a reliable machine. We are contemplating various improvements such as simplification of the valve mechanism, and reduction of the weight of the cooling part of the apparatus. We are also planning several expansion engines working in series as described in a previous paragraph which should at least double the output, and probably halve the starting time.

For a considerable amount of our success in making this machine we are indebted to a number of firms who have co-operated in supplying us with materials, and my thanks are due to Messrs. Thomas Firth & John Brown for the " Staybrite " steel ; Messrs. Accles & Pollock for very special work in drawing thin walled " Staybrite " tubes ; The Yorkshire Copper Works for supplying and specially drawing cupro-nickel tubes for the heat exchangers ; and The Hoffmann Manufacturing Company for the specially accurate balls with holes drilled in them.

The liquefier was constructed in the Laboratory workshop by Mr. H. Pearson, and experiments and tests were carried out with the assistance of Mr. E. Laurmann.

I wish to express my grateful thanks to the Department of Scientific and Industrial Research and the Royal Society for the provision of

funds to develop the cryogenic apparatus now installed in the Royal Society Mond Laboratory.

SUMMARY

An expansion engine is described which works without lubrication at low temperatures, and an account is given of its use for the liquefaction of helium. The liquefier is pre-cooled by liquid nitrogen only, and further cooling of the helium is done in two stages: down to 10° K by means of the expansion engine, and finally down to liquefaction point by using the Joule-Thomson effect.

It has been found that it is probable that the Joule-Thomson effect has a pressure inversion point at these low temperatures and that this appears at a pressure of about 17 atmospheres.

The starting time of the liquefier is 1¼ hours, and the output is 2 litres per hour, using 1½ litres of liquid nitrogen to produce 1 litre of liquid helium.

On the Acoustic Radiation Pressure on Spheres

By LOUIS V. KING, F.R.S., Macdonald Professor of Physics, McGill University, Montreal

(*Received June* 14, 1934)

SECTION 1—INTRODUCTION

Although frequent reference is made to acoustic radiation pressure in treatises and memoirs on sound, there appears to be no systematic theoretical development of the subject enabling actual pressures on obstacles of simple geometrical form to be calculated. In the audible range of acoustic frequencies, it is possible to devise, in a number of ways, means of measuring pressure amplitudes in sound waves as first-order effects. At supersonic frequencies, however, these methods are no longer serviceable. When the dimensions of resonators of diaphragms become comparable with the wave-length, the physical effects which enable the pressure amplitude to be measured involve intractable diffraction problems, while the extremely high frequencies and small amplitudes involved make the employment of stroboscopic methods of observation extremely difficult.

It has been shown, however, that at supersonic frequencies the acoustic radiation pressures on spheres and discs become sufficiently large to be measured easily, at any rate, in liquids. The mean pressure is generally assumed to be proportional to the energy density in the neighbourhood of the obstacle, and on this basis relative measurements can be made, for instance, in the radiation field of a supersonic oscillator.* Such formulæ may be obtained without restriction as to wave-length, for spheres in plane progressive and stationary radiation fields, and the magnitude of the pressure is found to be of entirely different orders of magnitude in the two cases.

In stationary radiation fields, the magnitude of the radiation pressure is found to be sufficiently large to account, in part, for the formation of the well-known dust-figures observed in resonance tubes filled with gas and, in particular, to explain the main features of dust striations in supersonic radiation fields in water observed by Boyle and his co-workers.

In the present paper the effect of the compressibility of the spheres and the viscosity of the medium are not taken into account, although the analysis may be extended to include these factors. The formulæ for rigid spheres in a frictionless medium may, however, be expected to give correct orders of magnitude, and, in particular, to enable spherical torsion balances to be designed for optimum sensitivity in the measurement of radiation pressures. Should such instruments prove to be suitable for sound measurements, the procedure outlined in the present paper may be extended to obtain more refined formulæ including the compressibility of the spheres and viscosity of the medium.

---

* Boyle and Lehmann, 'Can. J. Res.,' vol. 3, p. 491 (1930).

SECTION 2—PRESSURE IN COMPRESSIBLE FLUID

If we denote by ρ the density of the medium, p the pressure intensity, (u, v, w) the velocity components, the equations of motion are

$$\rho\frac{\mathrm{D}u}{\mathrm{D}t} = -\frac{\partial p}{\partial x}, \qquad \rho\frac{\mathrm{D}v}{\mathrm{D}t} = -\frac{\partial p}{\partial y}, \qquad \rho\frac{\mathrm{D}w}{\mathrm{D}t} = -\frac{\partial p}{\partial z}, \tag{1}$$

where

$$\frac{\mathrm{D}}{\mathrm{D}t} = \frac{\partial}{\partial t} + u\frac{\partial}{\partial x} + v\frac{\partial}{\partial y} + w\frac{\partial}{\partial z}.$$

It is convenient to introduce ϖ defined by

$$\varpi = \int\frac{dp}{\rho}, \tag{2}$$

in terms of which the equations of motion may be rewritten,

$$\frac{\mathrm{D}u}{\mathrm{D}t} = -\frac{\partial\varpi}{\partial x}, \qquad \frac{\mathrm{D}v}{\mathrm{D}t} = -\frac{\partial\varpi}{\partial y}, \qquad \frac{\mathrm{D}w}{\mathrm{D}t} = -\frac{\partial\varpi}{\partial z}. \tag{3}$$

When the motion is irrotational, we have, in terms of the velocity potential ϕ,

$$u = -\frac{\partial\phi}{\partial x}, \qquad v = -\frac{\partial\phi}{\partial y}, \qquad w = -\frac{\partial\phi}{\partial z}. \tag{4}$$

The equations of motion (3) are, then, completely satisfied if

$$\varpi = \int\frac{dp}{\rho} = \dot{\phi} - \tfrac{1}{2}(u^2 + v^2 + w^2) = \dot{\phi} - \tfrac{1}{2}q^2, \tag{5}$$

where, as usual, we denote $q^2 = u^2 + v^2 + w^2$.

We have, in addition, the equation of continuity,

$$\frac{\partial\rho}{\partial t} + \frac{\partial}{\partial x}(\rho u) + \frac{\partial}{\partial y}(\rho v) + \frac{\partial}{\partial z}(\rho w) = 0, \tag{6}$$

which may be written

$$\frac{1}{\rho}\frac{\mathrm{D}\rho}{\mathrm{D}t}=\nabla^2\phi. \tag{7}$$

For a medium in which $dp/d\rho = c^2$, a constant, the exact differential equation for ϕ is easily found to be

$$\frac{1}{c^2}\frac{D^2\phi}{\mathrm{D}t^2}+\frac{1}{2c^2}\frac{\mathrm{D}}{\mathrm{D}t}\left\{\left(\frac{\partial\phi}{\partial x}\right)^2+\left(\frac{\partial\phi}{\partial y}\right)^2+\left(\frac{\partial\phi}{\partial z}\right)^2\right\}=\nabla^2\phi. \tag{8}$$

In acoustic problems, we may usually neglect the ratio q^2/c^2 in which circumstances ϕ may be obtained as an appropriate solution of the wave-equation

$$\nabla^2\phi=\frac{1}{c^2}\frac{\partial^2\phi}{\partial t^2}. \tag{9}$$

More generally, we consider a medium in which p is a function of ρ only (barotropic fluid), and write

$$p=f(\rho). \tag{10}$$

In terms of the condensation $s=(\rho-\rho_0)/\rho_0$, we have the expansion

$$p=f(\rho_0+s\rho_0)=f(\rho_0)+s\rho_0 f'(\rho_0)+\tfrac{1}{2}s^2\rho^2{}_0 f''(\rho_0)+\ldots, \tag{11}$$

so that

$$dp=\rho_0(f'+s\rho_0 f''+\ldots)\,ds,$$

while

$$\rho^{-1}=\rho_0{}^{-1}(1-s+s^2-\ldots).$$

Thus,

$$\varpi=\dot{\phi}-\tfrac{1}{2}q^2=\int\frac{dp}{\rho}=sf'+\tfrac{1}{2}s^2(\rho_0 f''-f')+\ldots, \tag{12}$$

no constant of integration being required since s and ϖ vanish together.

Solving (12) for s in terms of ϖ we find,

$$s\sim\frac{\varpi}{f'}-\tfrac{1}{2}\frac{(\rho_0 f''-f')}{f'}\frac{\varpi^2}{f'^2}+\ldots,$$

and substituting in (11),

$$p-p_0=\rho_0 f'\left\{\frac{\varpi}{f'}-\tfrac{1}{2}\frac{(\rho_0 f''-f')}{f'}\frac{\varpi^2}{f'^2}\right\}+\tfrac{1}{2}\rho_0{}^2\frac{f''}{f'^2}\varpi^2+\ldots,$$

or,

$$p-p_0=\rho_0\varpi+\tfrac{1}{2}\frac{\rho_0}{c^2}\varpi^2+\ldots, \tag{13}$$

where we have written $c^2=f'(\rho_0)$.

Finally, in terms of $\dot{\phi}$ and q^2, equation (13) gives the pressure variation in the medium

$$\delta p = p - p_0 = \rho_0 \dot{\phi} + \tfrac{1}{2} \frac{\rho_0}{c^2} \dot{\phi}^2 - \tfrac{1}{2}\rho_0 q^2. \tag{14}$$

The equation (14) is correct to terms of the order q^2/c^2 and in these circumstances it is sufficiently accurate to calculate ϕ from the approximate wave equation (9). When, however, we proceed to obtain the pressure variation over the surface of a rigid obstacle, the boundary conditions require us to refer ϕ to an origin suitably placed with reference to the boundary. The first order term in (14) integrated over the boundary will, unless the obstacle is fixed, lead to dynamical equations of motion, as a result of which the obstacle performs small linear and angular oscillations. If $(\dot{\xi}, \dot{\eta}, \dot{\zeta})$ are the velocities of translation thus determined, ϕ is referred to a moving origin and

$$\dot{\phi} = \frac{D\phi}{Dt} - \dot{\xi}\frac{\partial \phi}{\partial x} - \dot{\eta}\frac{\partial \phi}{\partial y} - \dot{\zeta}\frac{\partial \phi}{\partial z} = \frac{D\phi}{Dt} + u\dot{\xi} + v\dot{\eta} + w\dot{\zeta}. \tag{15}$$

The last three terms give rise to second-order contributions to the pressure variation over the boundary and are of the same order of magnitude as the last two terms of (14).*

In the following sections we use (14) and (15) to calculate the mean resultant pressure on a rigid sphere free to move under the influence of a prescribed radiation field. The final result is correct to the order q^2/c^2. Higher accuracy for acoustic radiation pressure in waves of finite amplitude would require a determination of ϕ from an exact equation of the type (5) adapted to the condition $p = f(\rho)$, using in addition an expression for the pressure variation δp of the form (14) carried to higher approximations.

---

* If we identify $(\dot{\xi}, \dot{\eta}, \dot{\zeta})$ with the motion (u, v, w) of a particle of the medium, $\dot{\phi} = D\phi/Dt + q^2$, so that (14) becomes $\delta p = \rho_0 D\phi/Dt + \frac{1}{2}(\rho_0/c^2)\dot{\phi}^2 + \frac{1}{2}\rho_0 q^2$, giving the pressure variation in the medium at a point which partakes of the motion of the medium. Taking time averages, the first term drops out while the last two give the average total density of energy in the medium. This is the theorem due to Langevin, quoted by P. Biquard ('Rev. d'Acoust.,' vol. 1, p. 93 (1932)). In a frictionless fluid, the velocity of a point on the boundary is not equal to the velocity of a particle immediately in contact with it, so that Langevin's theorem as it stands is not applicable to the calculation of the mean pressure components on an obstacle. The equation (14) is, however, employed by Kotani ('Proc. Phys. Math. Soc. Japan,' vol. 15, p. 32 (1933)), who calculated therefrom the mean pressure on a *rigidly fixed* circular disc. When the obstacle is free to move under the influence of the incident sound waves, the pressure contribution arising from a moving origin according to (15) cannot be omitted.

[*Note added in proof, October 13th*, 1934.—In a later paper ('Rev. d'Acoust.,' vol. 1, p. 315), Biquard continuing his edition of Langevin's lectures ('Collège de France,' 1923), arrives at the fundamental formula (14) suitable for the calculation of acoustic radiation pressures on rigid or freely suspended rigid obstacles.]

SECTION 3—BOUNDARY CONDITIONS

We confine ourselves for the present to dealing with a rigid spherical obstacle of mass M and mean density ρ_1, so that $M = \frac{4}{3}\pi a^3 \rho_1$. If the incident radiation field possesses radial symmetry with respect to the sphere, it will perform small oscillations along the z-axis, the dynamical equation of motion being

$$2\pi a^2 \int_0^\pi \delta p \cos\theta \sin\theta \, d\theta = -M\ddot{\zeta}, \tag{16}$$

where δp is given by

$$\delta p = \rho_0 \dot{\phi} - \tfrac{1}{2}\rho_0 q^2 + \tfrac{1}{2}\frac{\rho_0}{c^2}\dot{\phi}^2. \tag{17}$$

If $D\phi/Dt$ refers to an origin at the centre of the sphere moving with velocity $\dot{\zeta}$, we have, according to (15),

$$\dot{\phi} = \frac{D\phi}{Dt} - \dot{\zeta}\cos\theta\frac{\partial\phi}{\partial r} + \dot{\zeta}\frac{\sin\theta}{r}\frac{\partial\phi}{\partial\theta}. \tag{18}^*$$

To determine the motion of the sphere, it is sufficiently accurate to take into account first order terms in δp, so that on integration with respect to t, we have the dynamical equation

$$2\pi a^2 \rho_0 \int_{-1}^{1} \phi\mu \, d\mu = -M\dot{\zeta}, \tag{19}$$

where, as usual, we denote $\mu = \cos\theta$.

Since the fluid must remain in contact with the sphere, we also have,

$$-(\partial\phi/\partial r)_{r=a} = \dot{\zeta}\cos\theta. \tag{20}$$

---

[*] Lamb, 'Hydrodynamics,' §. 92, p. 124 (1932).

SECTION 4—SOLUTION OF THE WAVE EQUATION

It is well known that the solution of the wave equation, referred to the centre of the sphere as origin may be expressed in the form

$$\phi = \sum_{n=0}^{\infty} \{A_n \psi_n(\kappa r) + A'_n f_n(\kappa r)\}(\kappa r)^n S_n, \tag{21}$$*

where, as usual, the frequency f of the wave is given by $\omega = 2\pi f$ and $\kappa = \omega/c$. S_n is a surface-harmonic of order n, while $\psi_n(\kappa r)$ and $f_n(\kappa r)$ are spherical wave functions, the latter being appropriate to the expression for a divergent wave. The following well-known properties of these functions are used in the sequel :—

$$\psi_n(\zeta) = \zeta^{-n}\left(\frac{\pi}{2\zeta}\right)^{\frac{1}{2}} J_{n+\frac{1}{2}}(\zeta), \quad \phi_n(\zeta) = (-1)^n \zeta^{-n}\left(\frac{\pi}{2\zeta}\right)^{\frac{1}{2}} J_{-n-\frac{1}{2}}(\zeta) \tag{22}$$

$$\psi_n(\zeta) = \frac{1}{1.3....(2n+1)}\left\{1 - \frac{\zeta^2}{2(2n+3)} + \frac{\zeta^4}{2.4(2n+3)(2n+5)} - \dots\right\} \tag{23}$$

$$\phi_n(\zeta) = \frac{1.3....(2n-1)}{\zeta^{2n+1}}\left\{1 - \frac{\zeta^2}{2(1-2n)} + \frac{\zeta^4}{2.4.(1-2n)(3-2n)} - \dots\right\} \tag{24}$$

The spherical wave function appropriate to a diverging wave is,

$$f_n(\zeta) = \phi_n(\zeta) - i\psi_n(\zeta) = \left(-\frac{1}{\zeta}\frac{d}{d\zeta}\right)^n \frac{e^{-i\zeta}}{\zeta}, \tag{25}$$

* The principal properties of these functions are given in Lamb's 'Hydrodynamics,' 6th ed., 292, p. 503 (1932). See also Bateman, 'Partial Differential Equations,' 651, p. 384 (1932). Three types of notation are employed, as shown in the following table :—

Lamb	Bateman	Bessel-function notation
$\psi_n(x)$	$\frac{1}{x^{n+1}}\psi_n(x)$	$\frac{1}{x^{n+1}}(\frac{1}{2}\pi x)^{\frac{1}{2}} J_{n+\frac{1}{2}}(x)$
$\Psi_n(x) = \phi_n(x)$	$\frac{1}{x^{n+1}}\chi_n(x)$	$\frac{(-1)^n}{x^{n+1}}(\frac{1}{2}\pi x)^{\frac{1}{2}} J_{-n-\frac{1}{2}}(x) = -\frac{1}{x^{n+1}}(\frac{1}{2}\pi x)^{\frac{1}{2}} Y_{n+\frac{1}{2}}(x)$
$f_n(x)$	$-\frac{i}{x^{n+1}}\zeta_n(x)$	$-\frac{i}{x^{n+1}}(\frac{1}{2}\pi x)^{\frac{1}{2}} H^{(2)}_{n+\frac{1}{2}}(x)$

In this paper Lamb's notation is followed with the exception that $\phi_n(x)$ is written for $\Psi_n(x)$ as being more easily distinguished from $\psi_n(x)$ in writing and in print.

the expansion being

$$f_n(\zeta) = \frac{i^n e^{-i\zeta}}{\zeta^{n+1}} \left\{ 1 + \frac{n(n+1)}{2(i\zeta)} + \frac{(n-1)(n).(n+1)(n+2)}{2.4(i\zeta)^2} + \dots \right.$$
$$\left. + \frac{1.2.3.\dots(2n-1)}{2.4.6.\dots\ 2n} \frac{1}{(i\zeta)^n} \right\}. \quad (26)$$

Considerable use is made of the following recurrence formulæ satisfied by all the functions $\psi_n(\zeta)$, $\phi_n(\zeta)$, $f_n(\zeta)$:

$$\left.\begin{aligned} &\psi'_n(\zeta) = -\zeta\psi_{n+1}(\zeta) \\ &\phi_n(\zeta)\,\psi_{n-1}(\zeta) - \psi_n(\zeta)\,\phi_{n-1}(\zeta) = 1/\zeta^{2n+1} \\ &\phi_{n+1}(\zeta)\,\psi_{n-1}(\zeta) - \psi_{n+1}(\zeta)\,\phi_{n-1}(\zeta) = (2n+1)/\zeta^{2n+3} \end{aligned}\right\}. \quad (27)$$

From the foregoing we easily see that the appropriate form for the velocity potential ϕ is, writing $\alpha = \kappa a$,

$$\phi = \sum_{n=0}^{\infty} A_n \frac{\{F_n(\alpha)\,\psi_n(\kappa r) - G_n(\alpha)\,\phi_n(\kappa r)\}}{F_n(\alpha) - iG_n(\alpha)} (\kappa r)^n P_n(\mu), \quad (28)$$

while the incident velocity potential is

$$\phi_i = \sum_{n=0}^{\infty} A_n \psi_n(\kappa r) . (\kappa r)^n P_n(\mu). \quad (29)$$

In order to satisfy the boundary conditions (20), we easily find, on making use of (27),

$$F_n(\alpha) = \alpha^2\phi_{n+1} - n\phi_n, \quad G_n(\alpha) = \alpha^2\psi_{n+1} - n\psi_n, \quad (n \neq 1), \quad (30)$$

where, for brevity we have omitted the argument α on the right-hand side of the above equations.

For $n = 1$, the dynamical equation (19) requires that

$$F_1(\alpha) = \alpha^2\phi_2 - (1 - \rho_0/\rho_1)\phi_1, \quad G_1(\alpha) = \alpha^2\psi_2 - (1 - \rho_0/\rho_1)\psi_1. \quad (31)$$

On making use of the recurrence equations (27), we easily find that for all values of n, including $n = 1$

$$F_n(\alpha)\,\psi_n(\alpha) - G_n(\alpha)\,\phi_n(\alpha) = 1/\alpha^{2n+1}, \quad (32)$$

while

$$F_{n+1}(\alpha)\,G_n(\alpha) - F_n(\alpha)\,G_{n+1}(\alpha) = \{\alpha^2 - n(n+2)\}/\alpha^{2n+3}, \quad (n \neq 1). \quad (33)$$

In particular

$$\left.\begin{aligned} &F_1(\alpha)\,G_0(\alpha) - F_0(\alpha)\,G_1(\alpha) = 1/\alpha \\ &F_2(\alpha)\,G_1(\alpha) - F_1(\alpha)\,G_2(\alpha) = \{\alpha^2 - 3(1 - \rho_0/\rho_1)\}/\alpha^5 \end{aligned}\right\}. \quad (34)$$

We now have, on making use of (19), the velocity of the centre of the sphere,

$$\dot{\zeta} = -\frac{A_1}{\alpha^3}\kappa\frac{\rho_0}{\rho_1}\frac{1}{F_1 - iG_1}. \tag{35}$$

At the surface of the sphere, the expression for the velocity potential takes the particularly simple form

$$\phi = \sum_{n=0}^{\infty}\frac{A_n}{\alpha^{n+1}}\frac{P_n(\mu)}{F_n(\alpha) - iG_n(\alpha)}. \tag{36}$$

SECTION 5—CALCULATION OF ACOUSTIC RADIATION PRESSURE ON A SPHERE

In general the coefficients A_n of the incident radiation field (29) will be complex, so that we write

$$A_n = |A_n|\, e^{i(\omega t + \alpha_n)}. \tag{37}$$

It is also convenient to write

$$F_n(\alpha) + i\,G_n(\alpha) = H_n(\alpha)\, e^{i\epsilon_n},$$

where

$$H_n(\alpha) = \{F_n^2(\alpha) + G_n^2(\alpha)\}^{\frac{1}{2}},\ \cos\epsilon_n = \frac{F_n(\alpha)}{H_n(\alpha)},\ \sin\epsilon_n = \frac{G_n(\alpha)}{H_n(\alpha)}. \tag{38}$$

We are thus enabled to write (36) in the form

$$\phi = \cos\omega t\ \Sigma\, R_n P_n(\mu) + \sin\omega t\ \Sigma\, S_n P_n(\mu), \tag{39}$$

where

$$R_n = \frac{|A_n|}{H_n(\alpha)}\frac{\cos(\alpha_n + \epsilon_n)}{\alpha^{n+1}},\quad S_n = -\frac{|A_n|}{H_n(\alpha)}\frac{\sin(\alpha_n + \epsilon_n)}{\alpha^{n+1}}. \tag{40}$$

Since ϕ is the velocity potential referred to, the moving centre of the sphere as origin, it follows from (17), (18), and (39) that the first-order pressure variation δp_1 at the surface of the sphere, is given by

$$\delta p_1 = \rho_0 c\kappa\{\cos\omega t\ \Sigma\, S_n P_n(\mu) - \sin\omega t\ \Sigma\, R_n P_n(\mu)\}. \tag{41}$$

Evidently the time average of this expression vanishes, so that δp_1 contributes nothing to the mean acoustic pressure.

If we denote by P_ϕ the contribution of the term $\frac{1}{2}\rho_0\dot{\phi}^2/c^2$ in (17) to the integrated component over the sphere of the z-component of the pressure variation, we have

$$P_\phi = -\frac{\pi a^2\rho_0}{c^2}\int_0^\pi \dot{\phi}^2 \sin\theta\cos\theta\, d\theta = -\frac{\pi a^2\rho_0}{c^2}\int_{-1}^{+1}\dot{\phi}^2\mu\, d\mu. \tag{42}$$

Substituting from (39) we find on taking the time average,

$$\overline{P}_\phi = -\tfrac{1}{2}\pi\alpha^2\rho_0 \int_{-1}^{1} [\{\Sigma\, R_n P_n(\mu)\}^2 + \{\Sigma\, S_n P_n(\mu)\}^2]\, \mu d\mu. \qquad (43)$$

It is easily proved that if $m \geqslant n$,

$$\int_{-1}^{1} \mu P_n(\mu)\, P_m(\mu)\, d\mu = \frac{2(n+1)}{(2n+1)(2n+3)} \qquad \text{for } m = n+1$$

$$= 0 \qquad \text{for } m > n+1.$$

As a result of using this theorem, we obtain from (43),

$$\overline{P}_\phi = -2\pi\alpha^2\rho_0 \sum_{n=0}^{\infty} \frac{n+1}{(2n+1)(2n+3)} (R_n R_{n+1} + S_n S_{n+1}). \qquad (44)$$

Similarly, we denote by P_q the contribution of the term $-\tfrac{1}{2}\rho_0 q^2$ in (17) to the integrated component over the sphere of the z-component of the pressure variation.

Then we have

$$P_q = \pi a^2\rho_0 \int_0^\pi q^2 \cos\theta \sin\theta\, d\theta = \pi a^2\rho_0 \int_{-1}^{1} q^2 \mu\, d\mu. \qquad (45)$$

At the surface of the sphere we have, according to (20),

$$\partial\phi/\partial r = -\dot{\zeta}\cos\theta,$$

so that (44) becomes

$$P_q = \pi a^2\rho_0 \int_{-1}^{1} \left\{\dot{\zeta}^2\mu^2 + \frac{1}{a^2}\left(\frac{\partial\phi}{\partial\theta}\right)^2\right\} \mu\, d\mu.$$

The first term of the integral evidently vanishes, and we are left with

$$P_q = \pi\rho_0 \int_{-1}^{1} \left(\frac{\partial\phi}{\partial\mu}\right)^2 (1-\mu^2)\, \mu\, d\mu. \qquad (46)$$

On introducing the value of $\partial\phi/\partial\mu$ from (39), we find, after taking the time average, that

$$\overline{P}_q = \tfrac{1}{2}\pi\rho_0 \int_{-1}^{1} [\{\Sigma R_n\, P'_n(\mu)\}^2 + \{\Sigma S_n\, P'_n(\mu)\}^2]\, (1-\mu^2)\, \mu\, d\mu. \qquad (47)$$

It is easily proved that if $m \geqslant n$,

$$\int_{-1}^{1} P'_n(\mu)\, P'_m(\mu)\, (1-\mu^2)\, \mu\, d\mu = \frac{2n(n+1)(n+2)}{(2n+1)(2n+3)} \quad \text{if } m = n.$$

$$= 0 \qquad \text{if } m > n.$$

Applying this result to (47), we obtain

$$\bar{P}_q = 2\pi\rho_0 \sum_0^\infty \frac{n\,(n+1)\,(n+2)}{(2n+1)(2n+3)}(R_n R_{n+1} + S_n S_{n+1}). \tag{48}$$

Finally, we denote by P_ζ the contribution to the *z*-component of δp arising from the motion of the origin according to (17) and (18). Remembering that for $r = a$, $(\partial\phi/\partial r) = -\dot{\zeta}\cos\theta$, we have,

$$P_\zeta = -2\pi\rho_0 a^2\,\zeta \int_0^\pi \left(\dot{\zeta}\cos^2\theta + \frac{\sin\theta}{a}\frac{\partial\phi}{\partial\theta}\right)\sin\theta\cos\theta\, d\theta.$$

The first term vanishes, and on integrating the second by parts we find,

$$P_\zeta = 2\pi\rho_0 a\dot{\zeta} \int_{-1}^{1} 2P_2(\mu)\,\phi\, d\mu. \tag{49}$$

On substituting for ϕ from (39), it is evident that only those terms survive for which $n = 2$. There results,

$$P_\zeta = 2\pi\rho_0 a\dot{\zeta}\,\frac{4}{5}\{R_2\cos\omega t + S_2\sin\omega t\}. \tag{50}$$

From (35) and (40), we may write

$$\dot{\zeta} = -\kappa\,\frac{\rho_0}{\rho_1}\frac{1}{\alpha}\,\{R_1\cos\omega t + S_1\sin\omega t\}. \tag{51}$$

On substituting in (50), and taking the time average, we obtain

$$\bar{P}_\zeta = -2\pi\rho_0 \,.\, \frac{2}{5}\frac{\rho_0}{\rho_1}(R_1 R_2 + S_1 S_2). \tag{52}$$

The total mean pressure is given by

$$\bar{P} = \bar{P}_\phi + \bar{P}_q + \bar{P}_\zeta.$$

The sum of the three contributions given by (44), (48), and (52) combine to give the series

$$\bar{P} = -2\pi\rho_0\Big[\frac{1}{1\,.\,3}(R_0R_1+S_0S_1)\,\alpha^2 + \frac{2}{3\,.\,5}(R_1R_2+S_1S_2)\left\{\alpha^2 - 3\left(1-\frac{\rho_0}{\rho_1}\right)\right\}$$
$$+ \sum_{n=2}^{\infty}\frac{n+1}{(2n+1)(2n+3)}(R_nR_{n+1} + S_nS_{n+1})\,\{\alpha^2 - n\,(n+2)\}\Big]. \tag{53}$$

SECTION 6—ON THE NUMERICAL COMPUTATION OF COEFFICIENTS

According to (40), we easily deduce

$$R_nR_{n+1} + S_nS_{n+1}$$
$$= \frac{|A_n| \cdot |A_{n+1}|}{H_n\,H_{n+1}\,\alpha^{2n+3}}\{\cos(\alpha_{n+1} - \alpha_n)\,.\,\cos(\varepsilon_{n+1} - \varepsilon_n)$$
$$- \sin(\alpha_{n+1} - \alpha_n)\,.\,\sin(\varepsilon_{n+1} - \varepsilon_n)\}.$$

We find from (38),

$$\cos(\varepsilon_{n+1}-\varepsilon_n) = \frac{F_{n+1}\,F_n+G_{n+1}\,G_n}{H_{n+1}\,H_n},\ \sin(\varepsilon_{n+1}-\varepsilon_n) = \frac{G_{n+1}\,F_n-F_{n+1}\,G_n}{H_n\,H_{n+1}}.$$

We thus have, for purposes of computation,

$$R_n\,R_{n+1} + S_nS_{n+1} = \frac{|A_n| \cdot |A_{n+1}|}{H_n^2\,H_{n+1}^2\,\alpha^{2n+3}}$$
$$\times\{\cos(\alpha_{n+1}-\alpha_n)(F_{n+1}F_n+G_{n+1}\,G_n)+\sin(\alpha_{n+1}-\alpha_n)(F_{n+1}G_n-G_{n+1}F_n)\}. \qquad (54)$$

From (33) and (34),

$$F_{n+1}\,G_n - G_{n+1}\,F_n = \{\alpha^2 - n(n+2)\}/\alpha^{2n+3} \qquad (n \neq 1), \qquad (55)$$

from which we easily derive

$$(F_{n+1}\,F_n + G_{n+1}\,G_n)^2 + \frac{\{\alpha^2 - n(n+2)\}^2}{\alpha^{4n+6}} = H_{n+1}^2H_n^2 \quad (n \neq 1). \quad (56)$$

In particular, for $n = 1$, we have from (34)

$$F_2G_1 - F_1G_2 = \{\alpha^2 - 3(1 - \rho_0/\rho_1)\}/\alpha^5,$$

so that

$$(F_2F_1 + G_2G_1)^2 + \{\alpha^2 - 3(1 - \rho_0/\rho_1)\}^2/\alpha^{10} = H_2^2H_1^2. \qquad (57)$$

There now remains the problem of computing $H_n^2 = F_n^2 + G_n^2$. On making use of (30),

$$F_n^2 + G_n^2 = \alpha^4(\phi_{n+1}^2 + \psi_{n+1}^2)$$
$$- 2\alpha^2 n(\phi_{n+1}\phi_n + \psi_{n+1}\psi_n) + n^2(\phi_n^2 + \psi_n^2). \qquad (58)$$

Since $-\alpha\phi_{n+1} = \phi'_n$ and $-\alpha\psi_{n+1} = \psi'_n$, we have

$$-\alpha(\phi_{n+1}\phi_n + \psi_{n+1}\psi_n) = \phi_n\phi'_n + \psi_n\psi'_n = \frac{1}{2}\frac{d}{d\alpha}(\phi_n^2 + \psi_n^2),$$

Remembering that $f_n = \phi_n - i\psi_n$ we write $\phi_n^2 + \psi_n^2 = |f_n|^2$, and if we notice that

$$\frac{1}{\alpha^{n-1}} \frac{d}{d\alpha}\{\alpha^n \, |f_n|^2\} = \alpha \frac{d}{d\alpha} |f_n|^2 + n \, |f_n|^2,$$

we easily find from (58),

$$G_n^2 + F_n^2 = \alpha^4 \, |f_{n+1}|^2 + \frac{n}{\alpha^{n-1}} \frac{d}{d\alpha}\{\alpha^n |f_n|^2\}.$$

In terms of Bateman's function $\zeta_n(\alpha)$, we have*

$$f_n(\alpha) = -i\alpha^{-n-1} \zeta_n(\alpha),$$

so that

$$G_n^2 + F_n^2 = \frac{|\zeta_{n+1}|^2}{\alpha^{2n}} + \frac{n}{\alpha^{n-1}} \frac{d}{d\alpha} \left\{ \frac{|\zeta_n|^2}{\alpha^{n+2}} \right\}. \tag{59}$$

Bateman† gives for $|\zeta_n(\alpha)|^2$ the following finite series,

$$|\zeta_n(\alpha)|^2 = 1 + \tfrac{1}{2} n(n+1) \, . \frac{1}{\alpha^2} + \tfrac{1}{2} \, . \, \tfrac{3}{4} (n-1) \, n \, (n+1)(n+2) \frac{1}{\alpha^4} + \dots$$
$$+ \frac{1 \, . \, 3 \dots (2n-1)}{2 \, . \, 4 \dots 2n} \, . \, (2n)! \frac{1}{\alpha^{2n}}, \tag{60}$$

or

$$|\zeta_n(\alpha)|^2 = \sum_{s=0}^{n} \left(\frac{1}{2} \cdot \frac{3}{4} \cdots \frac{2s-1}{2s} \right) \frac{(n+s)!}{(n-s)!} \frac{1}{\alpha^{2s}}.$$

By means of (59) it is thus possible to express $H_n^2 = F_n^2 + G_n^2$ as polynomials in $1/\alpha^2$. Remembering that according to (31) the case $n = 1$ is exceptional, we easily find

$$|\zeta_1|^2 = 1 + \frac{1}{\alpha^2}, \quad |\zeta_2|^2 = 1 + \frac{3}{\alpha^2} + \frac{9}{\alpha^4}, \quad |\zeta_3|^2 = 1 + \frac{6}{\alpha^2} + \frac{45}{\alpha^4} + \frac{225}{\alpha^6}, \text{ etc.,}$$

and, in consequence, using (59),

$$\left.\begin{aligned}
H_0^2 &= \frac{1}{\alpha^2}(1 + \alpha^2) \\
H_1^2 &= \frac{4}{\alpha^6} \left\{ \left(1 + \frac{\rho_0}{2\rho_1}\right)^2 + \frac{1}{2}\alpha^2 \left(1 + \frac{\rho_0}{2\rho_1}\right) \frac{\rho_0}{\rho_1} + \tfrac{1}{4}\alpha^4 \right\} \\
H_2^2 &= \frac{81}{\alpha^{10}} \left\{ 1 + \frac{1}{9}\alpha^2 - \frac{2}{81}\alpha^4 + \frac{1}{81}\alpha^6 \right\} \\
H_3^2 &= \frac{16 \times 225}{\alpha^{14}} \left\{ 1 + \frac{1}{10}\alpha^2 + \dots \right\} \\
H_n^2 &= \frac{\{1 \, . \, 3 \, . \, 5 \dots (2n-1)\}^2}{\alpha^{4n+2}} \left\{ 1 + \frac{n-1}{(n+1)(2n-1)} \alpha^2 + \dots \right\}
\end{aligned}\right\} . \tag{61}$$

---

* Footnote to Section 4.

† "Partial Differential Equations," § 6.51, p. 387.

With these formulæ it is found that in plane waves two terms of the series (53) are accurate to better than 1/10% for $\alpha = \kappa a = 2\pi a/\lambda = 1$.

For large values of α exceeding 3 or 4, H_n^2 may be computed from Bessel function tables* according to the formulæ

$$\left.\begin{aligned} H_n^2 &= \tfrac{1}{2}\pi \frac{1}{\alpha^{2n+1}} \{n^2 (J_{n+\frac{1}{2}}^2 + J_{-n-\frac{1}{2}}^2) + 2n\alpha (J_{-n-\frac{1}{2}} J_{-n-\frac{3}{2}} - J_{n+\frac{1}{2}} J_{n+\frac{3}{2}}) \\ &\qquad + \alpha^2 (J_{n+\frac{3}{2}}^2 + J_{-n-\frac{3}{2}}^2)\}, \qquad (n \neq 1) \\ H_1^2 &= \tfrac{1}{2}\pi \frac{1}{\alpha^3} \left\{\left(1 - \frac{\rho_0}{\rho_1}\right)^2 (J_{\frac{3}{2}}^2 + J_{-\frac{3}{2}}^2) + 2\alpha \left(1 - \frac{\rho_0}{\rho_1}\right) (J_{-\frac{3}{2}} J_{-\frac{5}{2}} - J_{\frac{3}{2}} J_{\frac{5}{2}}) \right. \\ &\qquad \left. + \alpha^2 (J_{\frac{5}{2}}^2 + J_{-\frac{5}{2}}^2)\right\} \end{aligned}\right\} . \qquad (62)$$

SECTION 7—RADIATION PRESSURE ON A SPHERE IN A PLANE PROGRESSIVE WAVE

To express a plane wave in terms of spherical wave functions, we use an expansion due to Bauer,† and write for the velocity potential of the incident radiation field.

$$\phi_i = Ae^{-i\kappa z} = A \sum_{n=0}^{\infty} (2n + 1)(- i)^n \psi_n (\kappa r) \,.\, (\kappa r)^n P_n (\mu). \qquad (63)$$

From (37) it follows that

$$A_n = (2n + 1)\, |A|\, e^{i(\omega t - \frac{1}{2}n\pi)}, \qquad \text{so that} \qquad \alpha_n = - \tfrac{1}{2}n\pi,$$

and

$$|A_n| = (2n + 1)\, |A|.$$

Referring to (54), we have $\alpha_{n+1} - \alpha_n = - \frac{1}{2}\pi$, and in consequence,

$$R_n R_{n+1} + S_n S_{n+1} = - \frac{|A|^2 (2n + 1)(2n + 3)}{H_n^2\, H_{n+1}^2\, \alpha^{2n+3}} \{F_{n+1} G_n - G_{n+1} F_n\}. \qquad (64)$$

If we use (55), we find that the general formulæ (53) for the mean pressure gives,

$$\bar{p} = 2\pi\rho_0 \frac{|A|^2}{\alpha^2} \left[\frac{1}{H_0^2 H_1^2} + \frac{2}{H_1^2 H_2^2} \frac{\{\alpha^2 - 3(1 - \rho_0/\rho_1)\}^2}{\alpha^8} \right.$$
$$\left. + \sum_{n=2}^{\infty} \frac{(n + 1)}{H_n^2 H_{n+1}^2} \frac{\{\alpha^2 - n(n + 2)\}^2}{\alpha^{4n+4}}\right]. \qquad (65)$$

---

* "Report Brit. Assoc.," 1925, p. 221.

† Watson, 'Theory of Bessel Functions,' 4.82 (1922) ; also Lamb, 'Hydrodynamics,' Section 296.

It is evident from this expression that the radiation pressure on a sphere in a progressive wave is always positive, *i.e.*, in the direction of wave propagation.

Radiation Pressure on Small Spheres ($\alpha = \kappa a \ll 1$)

When the circumference of the sphere is very small compared to the wave-length, we find on using (61) that (63) yields

$$\bar{P} = 2\pi\rho_0 |A|^2 \alpha^6 \frac{\{1 + \frac{2}{9}(1 - \rho_0/\rho_1)^2\}}{(2 + \rho_0/\rho_1)^2} + \text{terms in } \alpha^8 \text{ and higher powers.} \quad (66)$$

It is interesting to note that the relative density factor

$$F(\rho_0/\rho_1) = \frac{1 + \frac{2}{9}(1 - \rho_0/\rho_1)^2}{(2 + \rho_0/\rho_1)^2}, \quad (67)$$

is always finite and positive in the interval $0 < \rho_0/\rho_1 < \infty$, and has a minimum at $\rho_0/\rho_1 = 3$. Its value is tabulated below :—

ρ_0/ρ_1	0	1	3	∞
$F(\rho_0/\rho_1)$	0·305	0·111	0·075	0·222

The last entry is the value appropriate to a rigid bubble.

The mean total energy-density in the wave is $\bar{E} = \frac{1}{2}\rho_0\kappa^2|A|^2$. We may write (66) in the form

$$\frac{\bar{P}}{\pi a^2} \sim 4(\kappa a)^4 F(\rho_0/\rho_1) \,.\, \bar{E} = 4\left(\frac{2\pi a}{\lambda}\right)^4 F(\rho_0/\rho_1) \,.\, \bar{E} \quad (68)$$

as the results of observation are usually expressed in this manner.

Radiation pressure on a sphere for which $\alpha = \kappa a = 1$

We easily find that the third term of (65) is of the order $\frac{49}{89 \times 1200}$. Neglecting this and higher terms, we find

$$\bar{P} \sim \pi\rho_0 |A|^2 \frac{1}{89} \frac{95 - 48(\rho_0/\rho_1) + 36(\rho_0/\rho_1)^2}{5 + 6(\rho_0/\rho_1) + 2(\rho_0/\rho_1)^2}. \quad 69)$$

In the case of sound waves in water, we take $\rho_0/\rho_1 = 1$. We then find that

$$\frac{\bar{P}}{\pi a^2} \sim \frac{166}{13 \times 89} \bar{E} = 0{\cdot}143\, \bar{E}. \quad (70)$$

The mean pressure in this case is very much greater than that given by (68). It is found, however, that when such a sphere is made up into a torsion balance of optimum sensitivity[*] of 10 seconds period, it requires waves transmitting 49 erg/cm^2 (107 decibels), on a 2 cm wave-length in water to give a deflection $\theta = 1/(2000)$, *i.e.*, 1 mm on a scale at 1 metre. We conclude that in a progressive plane wave in water the radiation pressure on a sphere is too small to be observed except when the intensity exceeds a level of 100 decibels.

SECTION 8—RADIATION PRESSURE ON A SPHERE IN A PLANE STATIONARY WAVE

If the centre of the sphere be at distance h from a fixed plane of reference, the incident velocity potential referred to the mean position of the centre as origin may be written

$$\phi_i = \tfrac{1}{2}\mathrm{A}\{e^{-i\kappa(z+h)} + e^{i\kappa(z+h)}\}, \quad \text{where} \quad \mathrm{A} = |\mathrm{A}|\, e^{i\omega t}. \tag{71}$$

According to (63) we may write

$$e^{i\kappa(z+h)} = \sum_0^\infty (2n+1)\, e^{i(\kappa h + \frac{1}{2}n\pi)}\, \psi_n(\kappa r).(\kappa r)^n\, \mathrm{P}_n(\mu),$$

and have, on changing the sign of i and adding,

$$\phi_i = \mathrm{A} \sum_0^\infty (2n+1) \cos(\kappa h + \tfrac{1}{2}n\pi) \quad \psi_n(\kappa r).(\kappa r)^n \quad \mathrm{P}_n(\mu). \tag{72}$$

From (29) and (37) it follows that $|\mathrm{A}_n| = |\mathrm{A}|\,(2n+1)\cos(\kappa h + \frac{1}{2}n\pi)$ and $\alpha_n = 0$.

Equations (40) give

$$\mathrm{R}_n = \frac{|\mathrm{A}|}{\mathrm{H}_n\, \alpha^{n+1}}(2n+1)\cos(\kappa h + \tfrac{1}{2}n\pi)\cos\epsilon_n,$$

$$\mathrm{S}_n = -\frac{|\mathrm{A}|}{\mathrm{H}_n\, \alpha^{n+1}}(2n+1)\cos(\kappa h + \tfrac{1}{2}n\pi)\sin\epsilon_n,$$

from which it follows that

$$\mathrm{R}_n\mathrm{R}_{n+1} + \mathrm{S}_n\mathrm{S}_{n+1} = \frac{(2n+1)(2n+3)}{2\,\alpha^{2n+3}}|\mathrm{A}|^2(-1)^{n+1}\sin 2\kappa h\,\frac{(\mathrm{F}_{n+1}\mathrm{F}_n + \mathrm{G}_{n+1}\mathrm{G}_n)}{\mathrm{H}_n^{\,2}\,\mathrm{H}_{n+1}^{\,2}}. \tag{73}$$

---

[*] Theoretical considerations on the design of torsion balances of optimum sensitivity using radiation pressures on spheres and circular discs is dealt with in another paper.

Finally, the general formula (53) gives for the mean pressure

$$\overline{\mathrm{P}} = \pi\rho_0\,|\mathrm{A}|^2 \sin 2\kappa h \left[\frac{1}{\alpha^3}\frac{(\mathrm{F}_0\mathrm{F}_1 + \mathrm{G}_0\mathrm{G}_1)}{\mathrm{H}_0^{\,2}\,\mathrm{H}_1^{\,2}}\,\alpha^2 - \frac{2}{\alpha^5}\frac{(\mathrm{F}_1\mathrm{F}_2 + \mathrm{G}_1\mathrm{G}_2)}{\mathrm{H}_1^{\,2}\,\mathrm{H}_2^{\,2}}\{\alpha^2 - 3\,(1 - \rho_0/\rho_1)\} \right.$$
$$\left. + \sum_{n=2}^{\infty} (-1)^n \frac{(n+1)}{\alpha^{2n+3}} \frac{(\mathrm{F}_{n+1}\mathrm{F}_n + \mathrm{G}_{n+1}\mathrm{G}_n)}{\mathrm{H}_n^{\,2}\,\mathrm{H}_{n+1}^{\,2}}\{\alpha^2 - n\,(n+2)\}\right]. \quad (74)$$

Radiation Pressure on Small Spheres ($\alpha = ka \ll 1$)

It is obvious from (23) and (24) that $\mathrm{G}_{n+1}\mathrm{G}_n \ll \mathrm{F}_{n+1}\mathrm{F}_n$. Using (30), we find when $\alpha \ll 1$ the approximate expansions,

$$\mathrm{F}_0 \sim \frac{1}{\alpha}, \quad \mathrm{F}_1 \sim \frac{1}{\alpha^3}(2 + \rho_0/\rho_1), \quad \mathrm{F}_2 \sim \frac{9}{\alpha^5}, \quad \mathrm{F}_3 \sim \frac{60}{\alpha^7}, \text{ etc.,}$$

and, in general, $\mathrm{F}_n \sim 1\,.\,3\,.\,\ldots\,(2n-1)\,(n+1)/\alpha^{2n+1}$.

In the present circumstances the first three terms of (74) give

$$\overline{\mathrm{P}} \sim \pi\rho_0|\mathrm{A}|^2 \sin 2\kappa h \left[\frac{1}{\alpha}\cdot\frac{1}{\mathrm{F}_0\mathrm{F}_1} - \frac{2}{\alpha^5}\frac{\{\alpha^2 - 3\,(1-\rho_0/\rho_1)\}}{\mathrm{F}_1\mathrm{F}_2} + \frac{3\,(\alpha^2-8)}{\alpha^7\,\mathrm{F}_2\mathrm{F}_3} - \ldots\right], \quad (75)$$

from which we derive the approximate expression

$$\overline{\mathrm{P}} = \pi\rho_0|\mathrm{A}|^2 \sin 2\kappa h\, \alpha^3 \frac{\{1 + \frac{2}{3}\,(1-\rho_0/\rho_1)\}}{2 + \rho_0/\rho_1} + \text{terms in } \alpha^4 \text{ and higher terms.} \quad (76)$$

It is important to notice that the leading term is of the order $(\kappa a)^3$, so that the mean radiation pressure on a small sphere due to stationary waves is of a much greater order of magnitude than that exerted by progressive waves, the maximum amplitude being the same in both cases.

According to (71), the velocity potential of the field is

$$\phi_i = |\mathrm{A}|\cos \kappa h \cos \omega t,$$

so that the particle velocity is $\dot{\xi} = \mathrm{A}\kappa \sin \kappa h \cos \omega t$.

The nodes ($\dot{\xi} = 0$) are at $h = 0, \pm \pi/\kappa, \pm 2\pi/\kappa, \ldots \pm s\pi/\kappa$, and the loops are situated at $h = \pm \frac{1}{2}\pi/\kappa, \pm \frac{3}{2}\pi/\kappa, \ldots \pm (s + \frac{1}{2})\,\pi/\kappa$.

It will readily be seen that for a relatively dense sphere ($\rho_0/\rho_1 < 2\cdot5$), the mean radiation pressure is such as to urge it away from the nodes towards the loops. On the other hand, a relatively light sphere ($\rho_0/\rho_1 > 2\cdot5$) is urged away from the loops towards the nodes. The question is examined in greater detail in the following section.

As in §7, the mean total energy-density in a stationary wave field is $\overline{\mathrm{E}} = \frac{1}{2}\rho_0\kappa^2|\mathrm{A}|^2$ at all points of the field. We may thus write (76) in the form,

$$\frac{\overline{\mathrm{P}}}{\pi a^2} \sim 2\,(\kappa a)\sin 2\kappa h\,\mathrm{F}\,(\rho_0/\rho_1)\,.\,\overline{\mathrm{E}}, \tag{77}$$

where, in this case, the relative density factor is

$$\mathrm{F}\,(\rho_0/\rho_1) = \frac{1 + \frac{2}{3}\,(1 - \rho_0/\rho_1)}{2 + \rho_0/\rho_1}. \tag{78}$$

It is interesting to notice that (77), as regards its linear dependence on κa follows the early trend of observations by Boyle and Lehmann* relating to pressures on circular discs of lead placed in the central beam of a supersonic piezo-electric oscillator, where the radiation field is of quasi-stationary character, and where the stationary component of the field is the dominant one.

It is possible to use (76) or (77) as the basis for the design of " spherical torsion balances " of optimum sensitivity for use in liquid or gaseous media, the detailed consideration of which must, however, be left to a future paper.

It is now evident on comparing (66) and (76) that the mean radiation pressure on a small sphere does not depend on the local specifications of the field, such as the total mean energy-density. The pressure depends, in fact, on the nature of the field as a whole as related to the mode of generation of the sound waves. In other than the simple types of field discussed in this paper, the computation of the components of radiation pressure is extremely difficult, especially if the sphere is free to oscillate as the effect of the first-order pressure. Its centre will, in general, move in a small three-dimensional orbit, with the result that the relative density factor will be different for the three components of the mean radiation pressure. The procedure of the present paper might, without difficulty, be generalized to give the mean radiation pressure in a complex progressive or stationary plane wave, or a complex wave made up of progressive and stationary components. The final result is, however, of no very great interest, as the main features of pressure effects are well illustrated by the simple problems considered in Sections 7 and 8.

---

* 'Can. J. Res.,' vol. 3, p. 505 (1930). The writer has, in fact, obtained for the radiation pressure on small thin circular discs in progressive and stationary plane waves formulæ similar to (66) and (76) except for the relative density factor which takes different forms. The investigation will be published in a later paper.

SECTION 9—ON THE MOTION OF SMALL SPHERES IN A PLANE STATIONARY RADIATION FIELD

If the sphere is free to move under the influence of the mean radiation pressure, we must add to the velocity potential ϕ the term

$$\phi_s = \dot{h}a^3 \cos \theta / r^2$$

appropriate to the mean velocity $\dot{h}$ and satisfying the boundary condition $-(\partial \phi_s / \partial r)_{\kappa=a} = \dot{h} \cos \theta$. The pressure arising from this mean velocity when integrated over the sphere is easily found to be

$$\overline{\mathrm{P}}_s = -\mathrm{M}'\ddot{h}, \quad \text{where} \quad \mathrm{M}' = \tfrac{2}{3} \pi a^3 \rho_0. \tag{79}$$

The equation of motion of the sphere under the influence of the mean radiation pressure is thus seen to be

$$\mathrm{M}\ddot{h} = \overline{\mathrm{P}} + \overline{\mathrm{P}}_s. \tag{80}$$

On using (76) for the value of $\overline{\mathrm{P}}$ in a plane stationary wave and (79) for the value of $\overline{\mathrm{P}}_s$ due to the mean motion, the equation (80) may be written

$$(\mathrm{M} + \mathrm{M}')\ddot{h} = \pi\rho_0 |\mathrm{A}|^2 \sin 2\kappa h \, (\kappa a)^3 \frac{\{1 + \frac{2}{3}(1 - \rho_0/\rho_1)\}}{2 + \rho_0/\rho_1}. \tag{81}$$

If we introduce the new variable θ given by $2\kappa h = \pi - \theta$, equation (81) takes the form

$$\ddot{\theta} + n^2 \sin \theta = 0, \tag{82}$$

where

$$n^2 = 3|\mathrm{A}|^2 \kappa^4 \frac{\rho_0}{\rho_1} \frac{\{1 + \frac{2}{3}(1 - \rho_0/\rho_1)\}}{(2 + \rho_0/\rho_1)^2}. \tag{83}$$

From the last two equations it is easily seen that the position of stable equilibrium depends on the sign of the relative density factor. We have the two cases :

(1) for relatively dense spheres ($\rho_0/\rho_1 < 2{\cdot}5$), the position of stable equilibrium is at $\theta = 0$, *i.e.*, at $h = \pm \frac{1}{2}\pi/\kappa$ and, in general, at $h = \pm (\mathrm{S} + \frac{1}{2}) \pi/\kappa$, *i.e.*, at the loops of the standing waves.

(2) for relatively light spheres ($\rho_0/\rho_1 > 2{\cdot}5$), the position of stable equilibrium is at $\theta = \pi$, *i.e.*, at $h = 0$, and in general, at $h = \pm s\pi/\kappa$, *i.e.*, at the nodes of the standing waves.

It is interesting to notice that the motion as governed by equations (82) and (83) is *independent of the radius of the sphere*, and is of the same nature as the oscillations of a simple pendulum. The time of a complete oscillation from a position of rest at $h = h_0$ is easily seen to be

$$T = \frac{2\pi}{n} \cdot \frac{2}{\pi} K(k), \tag{84}$$

where $K(k)$ is the complete elliptic integral to modulus $k = \cos \kappa h_0$.

In terms of the velocity amplitude of the sound waves, $|\dot{\xi}| = \kappa |A|$, the wave-length given by $\kappa = 2\pi/\lambda$, and the relative density factor $f(\rho_0/\rho_1)$ given by

$$f(\rho_0/\rho_1) = \left\{\frac{(2 + \rho_0/\rho_1)^2}{(\rho_0/\rho_1)(5 - 2\,\rho_0/\rho_1)}\right\}^{\frac{1}{2}}, \tag{85}$$

while we have for the time of oscillation of small spheres of all radii such that $\kappa a \ll 1$, the convenient formula,

$$T = \frac{\lambda}{|\dot{\xi}|} f(\rho_0/\rho_1) \cdot \frac{2}{\pi} K(k), \quad \text{where} \quad k = \cos(2\pi h_0/\lambda). \tag{86}$$

For relatively dense spheres ($\rho_0/\rho_1 > 2{\cdot}5$), it is evident from (85) that the factor $f(\rho_0/\rho_1)$ is infinite at $\rho_0/\rho_1 = 0$, and at $\rho_0/\rho_1 = 2{\cdot}5$. In the interval it has a minimum at $\rho_0/\rho_1 = 10/13$, for which value $f(\rho_0/\rho_1) = 1{\cdot}67$ and the time of oscillation is a minimum. In these circumstances we have,

$$T_{\min} = 1{\cdot}67\,(\lambda/|\dot{\xi}|)\,\frac{2}{\pi} K(k), \tag{87}$$

the oscillations in this case being across a loop of the standing wave system.

The amplitude factor $(2/\pi)$ $K(k)$ varies slowly with the distance of the initial position from the loop as shown in the following table :—

Distance from loop	0	$\frac{1}{4}\lambda$	$\frac{1}{3}\lambda$	$\frac{5}{12}\lambda$	$\frac{1}{2}\lambda$ (node)	
$\frac{2}{\pi} K(k)$	1	1·18	1·37	1·76	∞	(88)

The formula (87) has a bearing on the well-known phenomena exhibited when small particles are introduced in a high-frequency stationary wave field. For instance, in water, a velocity amplitude $|\dot{\zeta}| = 1{\cdot}53$ cm sec at wave-length $3{\cdot}77$ cm corresponds to a very moderate radiation density of $0{\cdot}0175$ watts/cm², emitted by a piezo-electric oscillator o

30 cm radius surrounded by an infinite rigid flange and radiating 50 watts.* Near the disc the radiation-field is very nearly of a stationary character. According to the results of the present section sharply defined "dust striations" are best observed with spherical particles of optimum density 1·3, since the time of oscillation across a loop is then a minimum.

With the above values we find

$$T_{\min} = 4 \cdot 1 \times \frac{2}{\pi} K(k) \text{ sec.} \tag{89}$$

A reference to (88) tells us that if the particles are initially equally distributed, almost all of them with the exception of those near the nodes will be swept towards the nearest loop in a time of the order $\frac{1}{4}T_{\min}$, *i.e.*, in a time interval of 1 or 2 seconds. It is thus probable that radiation pressure alone is the explanation of the remarkable striations observed by Boyle† and his co-workers in the radiation field of a supersonic piezoelectric oscillator. The sharpness of definition of the striations is no doubt due to the fact that the motion is independent of particle size.

When the particles are very small, the influence of viscosity on the mean motion cannot be ignored, we therefore discuss this aspect of the problem in greater detail in a later section.

SECTION 10—ON THE INFLUENCE OF RADIATION PRESSURE ON DUST STRIATIONS IN RESONANCE TUBES

It appears probable to the writer that radiation pressure plays an important part in the formation of the well-known striated patterns which light particles in a resonance tube assume when standing waves are excited therein.‡ The mean features of the phenomena are described in all text-books on sound and are familiar to all students of physics. Recently, the formation of these striations have been studied under carefully controlled conditions by Andrade.§

---

* The properties of this type of radiation field have been worked out in detail by the author in a recent paper, (Can. J. Res., Vol. 11, p.135, August, 1934).

† Boyle, Lehmann, and Reid, 'Trans. Roy. Soc. Canada,' vol. 19, Section 3, p. 167 (1925). Boyle and Lehmann, *Ibid.*, p. 159. It is stated, (p. 161) that particles of cinder dust settle in nodal planes in a stationary radiation field. According to a private communication from Dr. Boyle the density of the dust used in these experiments was: ashes, 0·72; lignite, 1.1; bituminous coal, 1·2–1·5. These densities are considerably less than 2·5, the particles are "relatively light," and a required by theory are driven by acoustic radiation pressure towards the nodes.

‡ Rayleigh, "Theory of Sound," vol. II pp. 46, 50 (1896).

§ 'Phil. Trans.,' A, vol. 230, p. 413 (1932).

Considering the problem in the light of a radiation pressure effect, we shall suppose that we have to deal with small spherical particles still sufficiently large that their inertia is the important term in the equation of motion (80) and that viscosity plays a minor role. In these circumstances, the efficacy of radiation pressure in forming striations may be judged by the time of oscillation given by (86). In air, it is obviously impossible to adjust the relative density factor to a minimum. The best that can be done is to choose a material for the particles for which ρ_0/ρ_1 is as close as possible to the optimum ratio 0·755 ; that is we have to use very light particles such as cork spherules, for which $\rho_1 = 0{\cdot}24$.

Taking $\rho_0 = 0{\cdot}0012$ as the density of air, $\rho_0/\rho_1 = 5 \times 10^{-3}$ and $f(\rho_0/\rho_1) = 12{\cdot}5$.

In his paper Andrade quotes observed displacement amplitudes of aerial vibrations of the order $|\zeta| = 10^{-2}$ cm at a frequency $f = 500$. This corresponds to a velocity amplitude $|\dot{\zeta}| = 31{\cdot}4$ cm/sec at a wavelength of $\lambda = 68{\cdot}8$ cm.

Since $\rho_0/\rho_1 < 2{\cdot}5$, the motion is that characteristic of relatively dense spheres which according to (86) oscillate across the loops or anti-nodes with a period

$$T = 27{\cdot}4 \times \frac{2}{\pi} K(k) \text{ seconds.}$$

In the light of (88) it is evident that, if the particles are initially equally distributed, they will with the exception of those near the nodes be swept towards the nearest loop or anti-node in a time of the order $\frac{1}{4}$T, *i.e.*, in 7–13 secs. At the higher frequencies and greater acoustic amplitudes at which the experiment is usually carried out this time of formation of the striations will be very much less.

Reference to the illustrations in Andrade's paper show that when precautions are taken to generate pure waves of moderate amplitudes, and to minimize the transmission of waves by the walls of the resonance tube, small particles tend to gather at the loops of the standing waves in the form of sharply defined *antinodal discs*. Circulation of air in the form of vortex patterns undoubtedly play an important part in the phenomenon, the particles forming the antinodal discs must be held against gravity by a radial vortex circulation, but their extreme sharpness of definition is apparently due to the effect of radiation pressure. The mutual effect of particles in close proximity is such as to further enhance this sharpness of definition as explained by Konig.*

---

* Rayleigh, "Theory of Sound," p. 46 (1896).

As usually performed, Kundt's experiment gives rise to prominent striations at the nodes of the stationary wave system. If the tube walls are thin, stationary fluxual waves in the tube are set up, and these again give rise to an associated wave-system in the air. A node in the original longitudinal sound waves will correspond to a node in the fluxual waves of the tube which consist of stationary swellings and contractions. The velocity potential corresponding to the aerial waves thus set up reveals the existence of longitudinal amplitudes of motion having maximum values or loops across the nodes close to the wall and diminishing rapidly with distance from it. In this radiation field, small spherical particles near the walls will be driven by radiation pressure to the loops of these secondary transverse waves, which for certain wall constants may attain high amplitudes of a resonance type. It is thus possible to account for the formation of the "nodal wall striations" which often make their appearance.

To explain the inter-nodal fine structure striations frequently observed at high intensities, it must be remembered that even if the source of the sound, such as an oscillating diaphragm, has a purely harmonic motion, the resulting waves of large amplitude have a complex character, the higher harmonics being present.* These react on the walls giving rise to fluxual oscillations, which in turn generate secondary stationary sound waves in which radiation pressure may collect light particles into inter-nodal striations in the manner already explained.

It is also probable that in a similar way radiation pressure in the acoustic radiation field associated with vibrating plates may play a part in driving relatively heavy particles towards the nodes, while extremely small particles in the motion of which viscosity plays the leading part are caused to drift towards the loops by the vortex circulation engendered. A detailed mathematical investigation of the part played by radiation pressure in the formation of Chladni and Savart's sand figures† is, however, beyond the scope of the present paper.

SECTION 11—ON THE INFLUENCE OF RADIATION PRESSURE ON THE FORMATION OF DUST STRIATIONS IN STATIONARY WAVES

We consider a system of plane stationary waves whose nodal planes N, fig. 1, are vertical. A small sphere of density ρ_1 is released at a distance x_0 from the nearest anti-nodal plane L which contains the axis of z measured vertically downwards, the origin being taken in the horizontal plane in which the particle is released. The effect of viscosity is to introduce a force $\mu\dot{x}$ opposing the motion which, introduced in equation (81) gives

---

* Lamb, "Dynamical theory of sound," Arnolds, p. 180 (1910); also King, 'Phil. Trans.,' A, vol. 218, p. 221 (1919).

† Rayleigh, "Theory of Sound," vol. 1, p. 367 (1894).

$$(\mathrm{M} + \mathrm{M}')\ddot{h} + \mu\dot{h} = 2\pi\rho_0(\kappa a)^3 f(\rho_0/\rho_1) \sin \kappa h \cos \kappa h, \tag{90}$$

where

$$f(\rho_0/\rho_1) = \{1 + \tfrac{2}{3}(1 - \rho_0/\rho_1)\}/(2 + \rho_0/\rho_1). \tag{91}$$

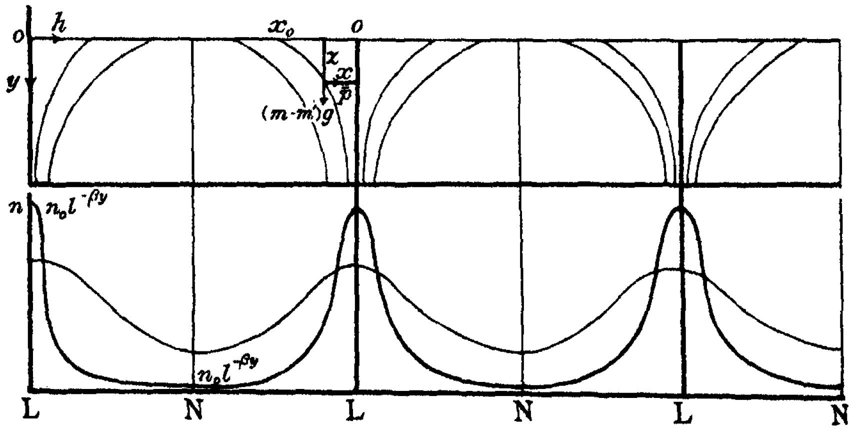

FIG. 1 (*a*)—Sketch of trajectories of small spheres moving under the effect of gravity, viscosity, and radiation pressure in a system of horizontal plane standing waves. FIG. 1 (*b*)—Sketch of relative densities of small particles after falling through a vertical distance z in the radiation field of fig. 1 (*a*). The initial density distribution over the plane $z = 0$ is constant.

The position of the sphere is defined by the distance h measured from left to right from an arbitrary plane of reference. If we are dealing with relatively dense spheres ($\rho_0/\rho_1 > 2{\cdot}5$), the motion will take place towards the nearest loop. In terms of the co-ordinate x of fig. 1 (*a*) measured from right to left from the axis of z situated in the plane of loops, we write

$h = \tfrac{1}{2}\pi/\kappa - x$, and (91) becomes

$$(\mathrm{M} + \mathrm{M}')\ddot{x} + \mu\dot{x} = -2\pi\rho_0 |\mathrm{A}|^2 (\kappa a)^3 f(\rho_0/\rho_1) \sin \kappa x \cos \kappa x, \tag{92}$$

while the equation of motion under the effect of gravity is

$$(\mathrm{M} + \mathrm{M}')\ddot{z} + \mu\dot{z} = \tfrac{4}{3}\pi a^3(\rho_1 - \rho_0) g. \tag{93}$$

When the particles are sufficiently small, the effect of viscosity predominates, and we may neglect the acceleration terms in (92) and (93). In these circumstances the integrals of the equations of motion are

$$\frac{\mu}{\kappa}\log\frac{\tan\kappa x_0}{\tan\kappa x} = 2\pi\rho_0\,|A|^2(\kappa a)^3 f(\rho_0/\rho_1)t, \text{ and } \mu z = \tfrac{4}{3}\pi a^3(\rho_1 - \rho_0)gt, \tag{94}$$

so that on eliminating t, the equation of the trajectory is, on using (90),

$$\tan\kappa x = \tan\kappa x_0\, e^{-\beta z}, \tag{95}$$

where

$$\beta = \frac{|A|^2\kappa^4}{2g}\,\frac{(5 - 2\,\rho_0/\rho_1)\,.\,\rho_0/\rho_1}{(2 + \rho_0/\rho_1)(1 - \rho_0/\rho_1)}. \tag{96}$$

It is interesting to note that the trajectory is independent of particle radius and viscosity so that all trajectories from the same initial position are identical.

We now suppose the particles to be initially equally distributed in the plane $z = 0$, so that the number between x_0 and $x_0 + dx_0$ is $n_0 dx$, n_0 being constant. Then if at depth z the number between x and $x + dx$ is ndx, we must obviously have

$$ndx = n_0\, dx_0. \tag{97}$$

We accordingly find from (95) that the density distribution at depth z is given by

$$n = \frac{n_0}{\cosh\beta z - \cos 2\kappa x \sinh\beta z}. \tag{98}$$

Two such distribution curves are sketched in fig. 1 (*b*). For relatively dense particles the density distribution n has minima $n_0 e^{-\beta z}$ at the nodes and maxima $n_0 e^{\beta z}$ at the loops.

Numerical Examples

(i) Take $\rho_0/\rho_1 = 0{\cdot}5$, $\lambda = 3{\cdot}77$ cm, $|\dot{\xi}| = \kappa|A| = 1{\cdot}53$ cm/sec. As in Section 9, $|\dot{\xi}|$ is the velocity amplitude of the approximately stationary field near the disc of a piezo-electric oscillator emitting 0·0175 watts/cm². Supposing the particles to fall through 30 cm, we easily find from (96) that $\beta z = 0{\cdot}159$, so that relative densities of the particles at this depth at the loops and nodes is $e^{\beta z} : e^{-\beta z} = 1{\cdot}17 : 0{\cdot}85$, which is just detectable.

(ii) Boyle's experiments were carried out at $f = 570{,}000$ for which $\lambda = 0{\cdot}258$ cm. For the same velocity amplitude $|\dot{\xi}| = 1{\cdot}53$ cm/sec corresponding to the same radiation density as in the previous example, we find for

$$z = 10 \text{ cm},\ \beta z = 11{\cdot}1, \text{ and } e^{\beta z} : e^{-\beta z} = 6\times 10^4 : 1{\cdot}7\times 10^{-4},$$

while for $z = 5$ cm, $\beta z = 5{\cdot}6$, and $e^{\beta z} : e^{-\beta z} = 257 : 0{\cdot}0039$.

At these extremely high frequencies it is evident that radiation pressure is able to produce very sharp striations in the pattern of small relatively dense particles allowed to fall through moderate distances. A large variety of these patterns have been observed by Boyle, Lehmann, and Reid, to whose paper the reader is referred for experimental details.

It is worthy of notice that if a count or microphotometric record of particle density be made in a plane stationary wave field resulting from an initially uniform distribution allowed to fall under gravity through a distance z, βz may be roughly evaluated from (98). If the wave-length and density of the particles are known, equation (96) allows the velocity amplitude $|\xi| = \kappa\,|A|$ to be evaluated. The same object may be achieved if it is possible to photograph the trajectory of a single particle.

We may notice that relatively light spherules ($\rho_0/\rho_1 > 2\cdot5$), such as air bubbles, tend to move towards the nodal planes. Observations on the motion of such particles do not appear to have been published, and their investigation would be of great interest.*

If we start with an initially uniform distribution of N_0 particles per unit volume, the final distribution N per unit area at depth z is easily found to be,

$$N = \int_0^z \frac{dx}{dx_0}\,dz = \frac{N_0}{\beta}\,\frac{\tan^{-1}(e^{\beta z}\tan\kappa x) - \kappa x}{\sin\kappa x\cos\kappa x}. \tag{99}$$

At the loops, ($\kappa x = 0$), $N_L = (N_0/\beta)\,(e^{\beta z} - 1)$, while at the nodes $N_N = (N_0/\beta)\,(1 - e^{-\beta z})$, and $N_L : N_N = 1 : e^{-\beta z}$. The "contrast" of particle density at the loops and nodes is thus less accentuated than when the particles are initially uniformly distributed in a plane. In the numerical example (i) above, $N_L : N_N = 1 : 0\cdot85$, while in example (ii) we have for $z = 10$ cm, $N_L : N_N = 1 : 1\cdot7 \times 10^{-4}$, and for $z = 5$ cm, $N_L : N_N = 1 : 3\cdot9 \times 10^{-3}$. In the latter case the striations are as sharply accentuated as could be desired.

SECTION 12—ON THE SUSPENSION OF SMALL SPHERICAL PARTICLES AGAINST GRAVITY

Of some interest from the experimental point of view is the possibility of suspending small spherical particles against gravity in a vertical column of fluid in which supersonic stationary waves are generated by a piezo-electric oscillator. If we equate $\bar{F}$ given by (76) to the buoyancy, we obtain for the velocity amplitude $|\dot{\xi}| = \kappa\,|A|$ the equation

---

* This conclusion is verified by Boyle's observations. (Boyle, Taylor and Froman, 'Trans. Roy. Soc. Canada', vol. 23, section III, p. 189 (1929)). It is distinctly stated that bubbles collect at the nodes of the stationary waves as required by theory.

$$|\dot{\xi}|^2 = \frac{2\lambda g}{\pi}\,\frac{1}{\sin 2\kappa h}\cdot\frac{(1-\rho_0/\rho_1)\,(2+\rho_0/\rho_1)}{(\rho_0/\rho_1)\,(5-2\,\rho_0/\rho_1)}. \tag{100}$$

Numerical Examples

(i) *Light particles in air*—If we consider small spherules of cork in a vertical column of air for which $\rho_1 = 0{\cdot}24$, $\rho_0 = 0{\cdot}0012$, the necessary velocity amplitude for equilibrium at a loop is given by $|\dot{\xi}|^2 = 51\ \lambda g$. Even at supersonic frequencies the velocity amplitude required is much beyond that experimentally realizable.

(ii) *Small particles in water*—It is evident that by taking $\rho_1/\rho_0 \sim 1$, equilibrium is always possible at the loops for nearly buoyant spherules.

If we take $\rho_0/\rho_1 = 0{\cdot}5$, $\lambda = 0{\cdot}258$ cm as in the example (ii) of Section 11, we find for the minimum velocity amplitude for which equilibrium is possible at a loop,

$$|\dot{\xi}|^2 = \tfrac{5}{4}\lambda g/\pi,\ \text{giving}\ |\dot{\xi}| = 10\ \text{cm/sec},$$

a value which should be easily attainable in practice.

If, in the same circumstances, we take ρ_0/ρ_1 very large, the corresponding minimum velocity amplitude for which small rigid bubbles can be held in equilibrium at a node is $|\dot{\xi}|^2 = \lambda g/\pi$, giving $|\dot{\xi}| = 9$ cm/sec, also realizable experimentally.

These results are of interest in connection with experiments of Biquard* in which the velocity amplitude of stationary waves shows a marked exponential decrease with distance from the piezo-electric oscillator not accounted for by the usual theory of viscosity. The actual measurement of radiation pressure on a small sphere by means of a sensitive balance might supplement Biquard's observations which were made by an optical method. Computations of the type made in the present section indicate that radiation pressures may be easily measurable in this manner. For high precision the exact formula (74) should be employed, corrected for the compressibility of the sphere and the effect of viscosity on the scattered wave. A consideration of these points must, however, be left to a future investigation.

---

* 'C. R. Acad. Sci. Paris,' vol. 197, pp. 309–311 (1933).

SECTION 13—SUMMARY AND CONCLUSIONS

1. The pressure variation in a compressible medium in which the pressure is any function of the density is given by

$$\delta p = \rho_0 \dot{\phi} + \tfrac{1}{2} \frac{\rho_0}{c^2} \dot{\phi}^2 - \tfrac{1}{2} \rho_0 q^2. \qquad \text{(i)}$$

The velocity potential ϕ is the solution of the wave equation with appropriate boundary conditions. The differentiation with respect to the time implied in $\dot{\phi}$ refers to an origin at rest. If $D\phi/Dt$ refers to an origin having components of velocity $(\dot{\xi}, \dot{\eta}, \dot{\zeta})$,

$$\dot{\phi} = D\phi/Dt + u\dot{\xi} + v\dot{\eta} + w\dot{\zeta}, \qquad \text{(ii)}$$

where, as usual $(u, v, w) = -\operatorname{grad} \phi$, are the velocity components referred to these axes.

2. To second-order terms, the time average of the acoustic radiation pressure on a sphere is given by

$$\bar{P} = \bar{P}_\phi + \bar{P}_q + \bar{P}_\xi, \qquad \text{(iii)}$$

where $\bar{P}_\phi$ and $\bar{P}_q$ are contributed by the second and third terms of (i), and $\bar{P}_\xi$ is contributed by the last three terms of (ii) arising from the motion of the origin at the centre of the spherical obstacle which performs small oscillations under the influence of the first-order radiation pressure.

3. In radially symmetrical radiation fields for which the velocity potential can be expanded as a series of spherical wave functions in the form,

$$\phi_i = \sum_{n=0}^{\infty} A_n \psi_n(\kappa r) \, . \, (\kappa r)^n \, P_n(\mu), \qquad \text{(iv)}$$

a general expression is obtained for the radiation pressure including the three terms of equation (iii).

4. In a plane progressive wave for which $\phi_i = Ae^{-i\kappa x}$ the radiation pressure $\bar{P}$ is always positive. For spheres whose circumference is small compared to the wave-length

$$\frac{\bar{P}}{\pi a^2} \sim 4 (\kappa a)^4 F(\rho_0/\rho_1) \bar{E} \qquad \text{(v)}$$

where $\bar{E}$ is the mean total energy-density in the medium and $F(\rho_0/\rho_1)$ is the relative density factor

$$F(\rho_0/\rho_1) = \frac{1 + \frac{2}{9}(1 - \rho_0/\rho_1)^2}{(2 + \rho_0/\rho_1)^2}. \qquad \text{(vi)}$$

5. In plane stationary waves for which $\phi_i = A \cos \kappa (z + h)$, the radiation pressure $\bar{P}$ is periodic, depending on the position of the centre of the sphere with respect to the planes of loops and nodes. For small spheres

$$\frac{\bar{P}}{\pi a^2} = 2\,(\kappa a) \sin 2\kappa h \; F\,(\rho_0/\rho_1)\,\bar{E} \tag{vii}$$

where $F\,(\rho_0/\rho_1)$ is the relative density factor

$$F\,(\rho_0/\rho_1) = \frac{1 + \frac{2}{3}\,(1 - \rho_0/\rho_1)}{2 + \rho_0/\rho_1}. \tag{viii}$$

It is important to note that in this case the radiation pressure in a stationary wave is of a much higher order of magnitude than in a progressive wave.

6. In general, the radiation pressure on a small sphere does not depend on the local specifications of the field, but on the nature of the field as a whole as related to the mode of generation of the sound waves.

7. The motion of a small sphere in a stationary plane radiation field is discussed in the light of equation (vii) above. When its mass is sufficiently great so that viscous resistance is negligible, the equations of motion are similar to that of a simple pendulum, oscillations taking place across the loops for relatively dense spheres ($\rho_0/\rho_1 < 2{\cdot}5$), and across loops for relatively light spheres ($\rho_0/\rho_1 > 2{\cdot}5$). The " time of formation " of striations is of the order $\frac{1}{4}T$, where T is the time of a complete oscillation, and is independent of the radius of the spherical particles.

For small particles in water, T is a minimum for the density ratio $\rho_1/\rho_0 = 1{\cdot}3$. In a supersonic radiation field of moderate intensity, $\frac{1}{4}T_{\min}$ is of the order of 1 second.

For particles of cork-dust in stationary air-waves having a velocity amplitude of 31·4 cm/sec at a frequency of 500, $\frac{1}{4}T$ is of the order of 7 seconds.

It appears probable that radiation pressure plays an important part in the formation of the familiar " dust striations " observed in resonance tubes.

8. When the particles are extremely small, so that the motion is principally controlled by viscosity, the trajectories of spherules falling vertically in a stationary radiation field having vertical nodal planes are obtained, and shown to be independent of the radius. If the particles are initially equally distributed over a horizontal plane, the density distribution after falling a depth z is determined. For relatively dense particles the density distribution has minima $n_0 e^{-\beta z}$ at the nodes and

maxima $n_0 e^{\beta z}$ at the loops, where β depends on the amplitude, wavelength, and the relative density, but is independent of the radius. In a supersonic stationary radiation field for which the velocity amplitude is 1·53 cm/sec at 570,000 cycles, the ratio of maximum to minimum density of the particle after falling through 5 cm is 257·2 : 0·0039, thus accounting for the very sharp striations observed by Boyle, Lehmann, and Reid.

9. The suspension of small particles and bubbles against gravity in a vertical stationary radiation field is discussed.

10. The results of the present investigation may be used in the design of torsion balances of optimum sensitivity for the measurement of amplitudes in stationary supersonic radiation fields.

The Energies of Alpha, Beta, and Gamma Rays

By H. A. Wilson, F.R.S., Rice Institute, Houston, Texas

(*Received June* 25, 1934)

This paper contains a continuation of the discussion of the energies of alpha, beta, and gamma rays on the theory previously suggested by the writer.* According to this theory the energies of beta and gamma rays are equal to $nq + \Sigma N_m E_m$ where $q = 3 \cdot 85$, $n = 0, 1, 2, 3 \ldots\ldots$, E_m denotes an electronic energy level and $N_m = 0, 1, 2, 3 \ldots\ldots$ The unit 10^5 electron volts will be used throughout.

We should expect elements with the same atomic number to give rays of equal energies. The chance of the emission of a ray with any given possible energy must depend on the nucleus as well as on the electronic system so that the relative intensities of the rays from different elements, having the same atomic number, may not be the same. The different elements may emit nuclear gamma rays with different values of the integer *n* and with different intervals between the emissions.

The three elements radium B, thorium B, and actinium B have the same atomic number 82 so we should expect to find beta and gamma rays of the same energies from these elements. The beta rays from actinium (B + C) and those from thorium B and its products have been observed, but there is some doubt as to which of the observed rays belong to actinium B and thorium B. The energy values used in this paper for radium B, radium C′, thorium B and its products are those of Ellis* For the other elements the values used are those given in " Radiations from Radioactive Substances" by Rutherford, Chadwick, and Ellis.

---

* 'Proc. Roy. Soc.,' A, vol. 144, p. 280 (1934), vol. 145, p. 447 (1934).

Table I gives the energies of the most intense beta ray from radium B the two rays associated with it and the rays of nearly equal energies from actinium (B + C) and thorium B and its products.

TABLE I

Radium B	Actinium (B + C)	Thorium B, etc.
$2\cdot600 + 0\cdot903\ (K) = 3\cdot503$	$2\cdot647 + 0\cdot903 = 3\cdot550$	$2\cdot609 + 0\cdot903 = 3\cdot512$
$3\cdot334 + 0\cdot163\ (L_1) = 3\cdot497$	$3\cdot396 + 0\cdot163 = 3\cdot559$	—
$3\cdot456 + 0\cdot040\ (M_1) = 3\cdot496$	$3\cdot519 + 0\cdot040 = 3\cdot559$	$3\cdot465 + 0\cdot040 = 3\cdot505$

The beta ray 2·609 from thorium products has been attributed to thorium C″ so that the nearly equal ray from thorium B if present may be very weak. The ray about 3·36 is not observed with thorium B. The thorium ray 3·465 is attributed to thorium C. Thus the thorium B rays equal to these radium B rays may be absent or very weak. The gamma ray energies got from the radium B beta rays by the addition of the K, L_1, and M_1, levels decrease from K to M_1, whereas the actinium B gamma ray energies increase. If we take the means of the radium B and actinium B beta ray energies we get the sums $2\cdot624 + 0\cdot903 = 3\cdot527$, $3\cdot365 + 0\cdot163 = 3\cdot528$, and $3\cdot488 + 0\cdot040 = 3\cdot528$, which are very nearly equal. It seems probable therefore that the radium B energies are rather too low and the actinium energies too high.

Table II gives another set of radium B and thorium B rays. The rays 1·504 and 1·477 are both of great intensity. Corresponding rays are not found with actinium B.

TABLE II

Radium B	Thorium B	Mean Values
$1\cdot504 + 0\cdot903 = 2\cdot407$	$1\cdot477 + 0\cdot903 = 2\cdot380$	$1\cdot491 + 0\cdot903 = 2\cdot394$
$2\cdot242 + 0\cdot163 = 2\cdot405$	$2\cdot217 + 0\cdot163 = 2\cdot380$	$2\cdot230 + 0\cdot163 = 2\cdot393$
$2\cdot367 + 0\cdot040 = 2\cdot407$	$2\cdot340 + 0\cdot040 = 2\cdot380$	$2\cdot354 + 0\cdot040 = 2\cdot394$

The energy 1·491 is equal to $K + L_1 + L_2 + 2L_3$.

Table III gives the energies of another radium B beta ray, the two rays associated with it and the nearly equal rays from thorium B. The rays 2·04 and 2·09 are both of great intensity.

---

* 'Proc. Roy. Soc.,' A, vol. 138, p. 318 (1932), vol. 143, p. 350 (1934).

TABLE III

Radium B	Thorium B	Mean Values
$2 \cdot 04 + 0 \cdot 90 = 2 \cdot 94$	$2 \cdot 09 + 0 \cdot 90 = 2 \cdot 99$	$2 \cdot 07 + 0 \cdot 90 = 2 \cdot 97$
$2 \cdot 77 + 0 \cdot 16 = 2 \cdot 93$	$2 \cdot 83 + 0 \cdot 16 = 2 \cdot 99$	$2 \cdot 80 + 0 \cdot 16 = 2 \cdot 96$
$2 \cdot 88 + 0 \cdot 04 = 2 \cdot 92$	$2 \cdot 96 + 0 \cdot 04 = 3 \cdot 00$	$2 \cdot 92 + 0 \cdot 04 = 2 \cdot 96$

The differences between the radium B and thorium B lines in Table III are greater than we should expect if these lines are really of equal energies. The mean value 2·07 agrees nearly with the value found by Ellis in 1924 for radium B.

Ellis* found that several low energy beta rays of radium B agree nearly with rays from thorium B. The radium B beta ray 1·141 agrees nearly with the thorium B ray 1·139. The mean value 1·140 is equal to $K + L_2 + 2M_1$.

Radiothorium and radioactinium have the same atomic number. Radiothorium gives only a few beta rays of low energy which are attributed to the electronic system. Table IV gives the beta rays of radiothorium and the rays of nearly equal energies from radioactinium.

TABLE IV

Radiothorium	Radioactinium
0·547	—
0·567	0·567
0·656	—
0·688	0·689
0·801	0·791
0·834	0·834

Radium and actinium X have the same atomic number. The strong beta ray 1·71 from actinium X agrees nearly with the line 1·72 from radium.

Thorium C″ and actinium C have the same atomic number. Table V gives the beta rays from thorium C″ which agree nearly with rays from actinium (B + C).

TABLE V

Actinium (B + C)	Thorium C″
2·65	2·61
3·52	3·47
3·91	3·86

This comparison of the beta ray energies from different elements having the same atomic number shows that there are approximate agreements in several cases. The number of such agreements, however, is not very large. It is probable that the number of beta rays found for any element depends greatly on the strength of the source used. With stronger sources many more beta rays would doubtless be obtained and so perhaps more cases of such agreements.

---

* 'Proc. Roy. Soc.,' A, vol. 139, p. 336 (1933).

A list of pairs of radium C′ beta and gamma ray energies having sums equal to multiples of 3·85 was given in the previous paper. Table VI gives a number of similar pairs of the ray energies of other elements.

TABLE VI

Thorium B and its products : 26·19 + 8·46 = 34·65
26·08 + 8·55 = 34·63
3·85 × 9 = 34·65
26·19 + 0·77 = 26·96
26·08 + 0·86 = 26·94
25·31 + 1·64 = 26·95
3·85 × 7 = 26·95
8·68 + 6·74 = 15·42
8·55 + 6·82 = 15·37
8·46 + 6·91 = 15·37
7·96 + 7·59 = 15·55
7·72 + 7·72 = 15·44
3·85 × 4 = 15·40

Mesothorium 2 : 16·46 + 2·74 = 19·20
16·06 + 3·19 = 19·25
14·97 + 4·27 = 19·24
16·06 + 3·18 = 19·24
10·06 + 9·13 = 19·19
10·58 + 8·61 = 19·19
3·85 × 5 = 19·25
9·70 + 5·67 = 15·37
14·97 + 0·42 = 15·39
3·85 × 4 = 15·40

Radium B : 3·89 + 3·79 = 7·68
4·24 + 3·46 = 7·70
4·36 + 3·33 = 7·69
4·39 + 3·31 = 7·70
4·78 + 2·94 = 7·72
3·85 × 2 = 7·70
2·41 + 1·43 = 3·84
2·57 + 1·28 = 3·85
2·73 + 1·14 = 3·87
3·31 + 0·53 = 3·84
3·33 + 0·52 = 3·85
3·46 + 0·40 = 3·86
3·49 + 0·37 = 3·86

Values of $\Sigma N_m E_m$ like $K + L_1 + 2L_2$ and similar combinations of K with three L levels occur among the values of C in the expression $nq + C$ for the energy of a beta or gamma ray. Table VII gives a number of such values.

TABLE VII

$\Sigma N_m E_m$	AcX		Mesoth. 2		RaC′	
	Cal.	Obs.	Cal.	Obs.	Cal.	Obs.
$K + L_2 + 2L_3$	1·445	1·435	—	—	1·368	1·362
$K + L_1 + 2L_3$	1·452	1·463	1·620	1·624	—	—
$K + 2L_2 + L_3$	1·472	1·471	1·646	1·644	—	—
$K + L_1 + L_2 + L_3$	1·479	1·481	1·654	1·658	—	—
$K + 2L_1 + L_3$..............	1·486	1·483	1·662	1·663	1·406	1·406
$K + L_1 + 2L_2$	1·506	1·509	1·688	1·685	—	—
$K + 2L_1 + L_2$	1·513	1·513	—	—	1·430	1·438

	RaB		Radioac.		RaD	
	Cal.	Obs.	Cal.	Obs.	Cal.	Obs.
$K + L_2 + 2L_3$	—	—	1·528	1·522	—	—
$K + L_1 + 2L_3$	—	—	—	—	1·334	1·336
$K + 2L_2 + L_3$	1·350	1·347	—	—	—	—
$K + L_1 + L_2 + L_3$	—	—	—	—	—	—
$K + 2L_1 + L_3$	1·364	1·372	1·573	1·579	1·364	1·364
$K + L_1 + 2L_2$	—	—	—	—	—	—
$K + 2L_1 + L_2$	1·387	1·392	1·604	1·602	—	—

The observed and calculated values agree very closely. This must be partly due to chance because the possible errors in the observed values are probably ± 0·01.

The relative frequency with which the different values of $C = \Sigma N_m E_m$ occur has been examined by calculating the C's for all measured beta rays of known origin. The values for the different elements were multiplied by the ratio of the combination of radium C′ energy levels to the same combination of energy levels of the element in question. These ratios are nearly the same for any combination of the energy levels. The values so obtained are equal to C's for radium C′ with the N's the same as in the C's for the different elements. Fig. 1 shows the number of values so obtained in ranges of 0·03 plotted against the value of C.

It appears that certain values occur with relatively great frequencies. Table VIII gives these values, the number of times they occur and an approximate representation of them as sums of multiples of the radium C′ energy levels, taking $K = 0{\cdot}93$, $L = 0{\cdot}17$, and $M = 0{\cdot}04$.

TABLE VIII

C	Number	$\Sigma N_m E_m$
0·03	8	M
0·08	6	2M
0·29	18	2L − M
0·38	16	2L + M
0·53	16	K − 2L − M
0·68	12	K − L − 2M
0·74	12	K − L
0·92	16	K
0·98	10	K + M
1·07	12	K + L
1·19	8	K + L + 2M
1·28	24	K + 2L
1·41	8	K + 3L − M
1·52	12	2K − 2L
1·67	12	2K − L
1·82	10	2K − M
1·88	12	2K, 2K + M

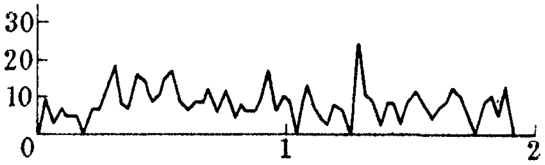

FIG. 1.

It appears that K + 2L is the most frequently occurring combination of the energy levels. We should expect the more commonly occurring combinations to appear with the beta rays of great intensity. Table IX gives the most intense beta rays from radium C′.

TABLE IX

$5{\cdot}90 = 2q - 1{\cdot}80$
$1{\cdot}79 = 1{\cdot}79$
$17{\cdot}46 = 5q - 1{\cdot}79$
$21{\cdot}04 = 5q + 1{\cdot}79$
$13{\cdot}23 = 3q + 1{\cdot}68$
$13{\cdot}96 = 4q - 1{\cdot}44$
$16{\cdot}81 = 4q + 1{\cdot}41$
$12{\cdot}86 = 3q + 1{\cdot}31$
$5{\cdot}14 = q + 1{\cdot}29$
$14{\cdot}11 = 4q - 1{\cdot}29$
$10{\cdot}28 = 3q - 1{\cdot}27$
$16{\cdot}67 = 4q + 1{\cdot}27$

$6{\cdot}73 = 2q - 0{\cdot}97$
$16{\cdot}36 = 4q + 0{\cdot}96$
$8{\cdot}40 = 2q + 0{\cdot}70$
$11{\cdot}45 = 3q - 0{\cdot}10$

The values 1·27 to 1·31 nearly equal to K + 2L occur most frequently in Table IX also. After K + 2L the values 2L − M, 2L + M, K − 2L − M and K are next in frequency of occurrence among the C's for all the beta rays. Values between 1·26 and 1·32 also occur most frequently among the C's for the alpha rays which have been measured accurately.*

Table X gives the radium C′ gamma rays and the internal K conversion coefficients found experimentally and calculated theoretically for quadripole emission by the nucleus.† For dipole emission the values are about one-third of those for quadripole emission.

TABLE X

Gamma ray energies	Conversion observed	Coefficients calculated	Half values
$6\cdot07 = 2q - 1\cdot63$	0·0060	0·016	0·008
$13\cdot79 = 4q - 1\cdot61$	0·0015	0·0035	0·0017
$17\cdot61 = 5q - 1\cdot64$	0·0018	0·0024	0·0012
$21\cdot93 = 6q - 1\cdot17$	0·0012	0·0017	0·0009
$9\cdot33 = 2q + 1\cdot63$	0·0060	0·0072	0·0036
$12\cdot38 = 3q + 0\cdot83$	0·0060	0·0045	0·0023
$11\cdot20 = 3q - 0\cdot35$	0·0060	0·0053	0·0027
$7\cdot66 = 2q - 0\cdot04$	0·0048	0·011	0·0055

The calculated coefficients are for an atom containing two K electrons. The first four lines in Table X have C's indicating that the electronic system received energy greater than K so that one K electron was removed before the emission of the gamma ray. The K conversion should therefore be for an atom containing only one K electron and so should be about half that calculated. The observed coefficients for these rays are all less than those calculated and on the whole agree better with the half values given in the last column.

The next three rays in Table X have C's either positive or small so that the atoms are left with two K electrons and the observed coefficients agree fairly well with those calculated for quadripole emission with an atom containing two K electrons.

The gamma ray 7·66 may be a dipole emission since the conversion coefficient for dipole emission is about 0·0038 which does not differ much from the observed value 0·0048. It appears that the observed coefficients are consistent with quadripole emission except for the last line 7·66. The possible errors in the observed values are quite large.

---

* 'Phys. Rev.,' vol. 44, p. 858, November 15 (1933).

† Taylor and Mott, 'Proc. Roy. Soc.,' A, vol. 138, p. 665 (1932).

A list of eleven pairs of alpha ray disintegration energies, having sums equal to multiples of 3·85 was given in a previous paper.* Six more pairs have since been found which are given in Table XI. Radium C′ rays are not included in Table XI or in the previous list.

TABLE XI

Th X, An_{a_2}	57·86 + 65·31 = 123·17	3·85 × 32 = 123·20
Ra A, Th C_{a_1}	61·12 + 62·04 = 123·16	3·85 × 32 = 123·20
Ac A	75·08 + 75·08 = 150·16	3·85 × 39 = 150·15
Ac C_a	67·39 + 67·39 = 134·78	3·85 × 35 = 134·75
Rn	55·80 + 55·80 = 111·60	3·85 × 29 = 111·65
Ac, Ac C_a	75·08 + 67·39 = 142·47	3·85 × 37 = 142·45

Thus there are 17 such pairs formed by the 20 disintegration energies. The mean deviation of the 17 pairs from multiples of 3·85 is 0·03. The most probable number of pairs deviating to this extent from multiples of 3·85 due to accidental coincidences is 200 × 0·06/3·85 which is about three. There are therefore about five times as many pairs as might be expected due to chance. There are four sums which occur more than once, viz. : 123·20, 111·65, 119·35, and 142·45. The number to be expected due to chance is about 3 × 3/40 = 0·22, so that the number found is about 18 times the number to be expected. The sum 123·20 occurs three times. The number of sums to be expected to occur three times is 0·22 × 3/40 = 0·016 so that the number found is about 60 times the number to be expected due to chance.

It is clear that the chance that the observed sums equal to multiples of 3·85 are due to accidental coincidences is very small.

Similar considerations may be applied to the pairs, with sums equal to multiples of 3·85, formed by the gamma and beta ray energies. For example, there are five pairs formed by the gamma and beta ray energies of radium C′ equal to 46·21 or 46·22, which are almost equal to 3·85 × 12 = 46·20. The number of beta and gamma rays which could help to form these pairs is 20, which give a total of 200 pairs with sums between about 40 and 52. The number to be expected due to chance between 46·21 and 46·22 is about 200 × 0·02/12 = 0·33. The number found is therefore 15 times the number to be expected due to chance.

Table XII gives the values of $nq \pm 1 \cdot 29$ and the nearly equal beta ray energies of radium C′.

The mean deviation of the observed energies from the calculated values is 0·02. There are about 60 beta rays in the range from 2 to 25,

---

* 'Proc. Roy. Soc.,' A, vol. 144, p. 280 (1934).

TABLE XII

	Observed		Observed
$3\cdot85 + 1\cdot29 = 5\cdot14$	5·14	$3\cdot85 - 1\cdot29 = 2\cdot56$	2·54
$2 \times 3\cdot85 + 1\cdot29 = 8\cdot99$	8·98	$2 \times 3\cdot85 - 1\cdot29 = 6\cdot41$	—
$3 \times 3\cdot85 + 1\cdot29 = 12\cdot84$	12·86	$3 \times 3\cdot85 - 1\cdot29 = 10\cdot26$	10·28
$4 \times 3\cdot85 + 1\cdot29 = 16\cdot69$	16·67	$4 \times 3\cdot85 - 1\cdot29 = 14\cdot11$	14·11
$5 \times 3\cdot85 + 1\cdot29 = 20\cdot54$	20·58	$5 \times 3\cdot85 - 1\cdot29 = 17\cdot96$	17·89
$6 \times 3\cdot85 + 1\cdot29 = 24\cdot39$	—	$6 \times 3\cdot85 - 1\cdot29 = 21\cdot81$	21·82

so that the chance of a number selected at random agreeing within 0·02 with a beta ray is about 1/10. We should therefore expect about one agreement in the above twelve cases whereas we actually get ten. The ten beta rays in Table XII give 25 pairs with sums nearly equal to multiples of 3·85.

Recent results with elements of low atomic weight appear to show that the nuclei of these elements have possible energies or resonance levels differing by about 3·85. Thus Chadwick and Constable[*] found four levels in aluminium equal to 52·5, 48·6, 44·9, and 40. The differences between these are 3·9, 3·7, and 4·9. Also Kirsch and Slonek[†] found levels in beryllium equal to 52·5, 48·5, 44, 40, and 37, with differfences 4, 4·5, 4, and 3. Bonner and Mott-Smith[‡] here have also recently found similar series of levels in boron, beryllium, and fluorine. These results are not exact enough to show that the differences are equal to 3·85, but they suggest that it is possible. It seems likely therefore that the nuclei of all the atoms have possible energies equal to nq like those of the radioactive atoms.

In the previous paper it was shown that the differences between disintegration energies are frequently equal to prominent gamma and beta ray energies. A more detailed examination of the differences yields interesting results. Table XIII gives all the differences between disintegration energies and the radium C′ rays between 10 and 14·20.

All the beta and gamma rays of radium C′ in Table XIII are equal within the limits of error to disintegration energy differences. Some of the agreements may be accidental coincidences, but it seems unlikely that the general agreement can be due to chance.

Table XIV gives the differences and radium C′ rays between 5 and 7.

The very intense gamma ray energy 6·07 and the beta rays 5·14 and 5·90 associated with it are clearly present among the disintegration energy differences.

---

[*] 'Proc. Roy. Soc.,' A, vol. 135, p. 48 (1932).

[†] 'Naturwiss.,' vol. 4, p. 62 (1933).

[‡] 'Phys. Rev.,' vol. 46, p. 258, Aug. 15 (1934).

TABLE XIII

Disintegration Energy Differences	Beta Rays	Radium C′ Intensity	Gamma Rays
10·21, 10·28, 10·33, 10·36	10·28	13	
10·48, 10·50, 10·50, 10·56, 10·58, 10·80, 10·85, 10·90	10·63	1	
11·01, 11·11	11·04	2·1	
11·13, 11·14, 11·18, 11·24, 11·25	11·16	1	11·20
11·50, 11·51, 11·57, 11·59, 11·64	11·45	3·6	
11·87, 11·87, 11·98	11·87	0·85	
12·16, 12·24	12·22	0·85	
12·30, 12·36, 12·48, 12·59	12·40	0·20	12·38
12·82, 12·83, 12·85, 12·98, 13·04	12·86	0·90	
13·17, 13·22, 13·22	13·23	25	
13·33, 13·44, 13·45	13·36	1	
13·66, 13·77, 13·85	13·59	0·4	13·79
13·95, 13·99	13·96	3·7	
14·07, 14·12, 14·14, 14·17	14·11	1·4	14·14

TABLE XIV

Disintegration Energy Differences	Beta Rays	Radium C′ Intensity	Gamma Rays
5·01, 5·03	—		
5·10, 5·14	5·14	40	
5·35, 5·43, 5·46, 5·49, 5·49	—		
5·54, 5·56, 5·57, 5·58	5·57	2·6	
5·71, 5·75	5·72	2·6	
5·89, 5·96, 5·97, 5·97	5·90	9·0	
6·03, 6·04	6·05	1·6	
6·07, 6·08, 6·08, 6·12, 6·12	—	—	6·07
6·24, 6·44, 6·52	—		
6·69, 6·75	6·73	3·2	
6·81, 6·82, 6·84, 6·93	—		

Table XV gives the disintegration energy differences and the radium C′ rays between 16 and 18.

TABLE XV

Disintegration Energy Differences	Beta Rays	Radium C′ Intensity	Gamma Rays
16·04	16·17	0·2	
16·29	16·36	0·7	
16·60, 16·60, 16·64, 16·65	16·67	4·2	
16·98	16·81	0·85	
17·20, 17·22	17·05	0·30	
17·33, 17·43	17·46	0·95	
17·62	—	—	17·61
17·79, 17·94, 17·95	17·89	0·2	

Here again the intense beta ray energy 16·67 is clearly present among the disintegration differences and also the beta ray 17·46 and the associated gamma ray 17·61.

It seems clear that the disintegration energies contain terms determined by the electronic energy levels. It was pointed out in " Radiations from Radioactive Substances," by Rutherford, Chadwick, and Ellis that the beta and gamma rays from radiothorium are probably purely electronic emissions and that the electronic system must be excited by an alpha ray because there are no nuclear gamma rays available. If in this case the alpha rays give energy to the electrons we should expect the same thing to happen in many other cases.

The nuclear energies *nq* seem to require a very simple nucleus. If the nucleus contained particles describing orbits we should expect the possible energies to depend on the number of the particles and so on the atomic weight just as the electronic energy levels depend on the number of electrons. It seems possible therefore that the nucleus does not contain particles describing orbits but acts like a single particle.

SUMMARY

This paper contains a continuation of the discussion of the energies of alpha, beta, and gamma rays on the theory previously proposed by the writer. The energies of beta rays from elements having the same atomic number are compared and it is found that they agree approximately in a number of cases in accordance with the theory. Pairs of beta and gamma ray energies having sums equal to multiples of 3·85 are found for several elements. The relative frequencies with which the different values of $\Sigma N_n E_m (N_m =$ integer, $E_m =$ electronic energy level) occur in the observed energies are determined. It is found that K + 2L occurs most frequently. The internal conversion coefficients for the radium C′ gamma rays are considered and found to be consistent with the theory. The chance that the agreements with the theory are due to accidental coincidences is considered and shown to be very small.

The Spectrum of H_2

Part II—The Band Systems due to Transitions from Four new Triplet States to $2p\,^3\Pi$

By O. W. RICHARDSON, F.R.S., Yarrow Research Professor of the Royal Society, and T. B. RYMER, B.A., King's College, London

(*Received July* 6, 1934)

§ 1 INTRODUCTION

In this paper we describe and discuss four new band systems which end on the lowest triplet state $2p\,^3\Pi$ of H_2. The upper states are all new and it is impossible at this stage to settle their electronic configurations with complete definiteness so we call them provisionally ^{3}A, ^{3}B, C and ^{3}G. ^{3}A has a Rydberg denominator just under 4 and a fairly regular rotational and vibrational structure as H_2 molecules go; it has, however, some peculiar features which make the interpretation of its electronic structure difficult. ^{3}G is a $^3\Sigma_g$ or a $^3\Pi_{ag}$ state with a denominator almost exactly 5 and it is practically certain that it is either $1s\sigma\,5d\sigma\,^3\Sigma_g$ or $1s\sigma\,5g\pi\,^3\Pi_{ag}$. The denominator of ^{3}C is about 4·93. It is an even Δ_b or possibly Π_b state with pronounced uncoupling and is most probably $1s\sigma\,5d\delta\,^3\Delta_b$ or $1s\sigma\,5d\pi\,^3\Pi_b$. ^{3}B has a denominator close to 4·63. It is unlikely that it is any orthodox state with a single excited electron. It is probably the analogue in the triplet systems of one of the numerous " abnormal " singlet states ^{1}K, ^{1}L, ^{1}M, ^{1}N, etc.

The form of the tables and the notations used are the same as in our previous paper, Part I.

§ 2 THE SYSTEM $^3G \rightarrow 2p\,^3\Pi$

These bands appear to belong to the d^3 or g^3 complexes at principal quantum number 5. They are, of course, weak and $0' \rightarrow 3''$ is the only certain band we have found off the diagonal axis; but they are quite definite. They have only been found at the $v' = 0$ and 1 levels, but as the upper state at $v = 2$ has about enough energy to go spontaneously into the ground state of H_2+, the end of the nd^3 and ng^3 series, this is not surprising. The lines are given in Table I. In both the $0 \rightarrow 0$ band and the $1 \rightarrow 1$ band the R branch is strongest and the P branch weakest.

TABLE I—LINES OF $^3G \rightarrow 2p\,^3\Pi$

The 0 → 0 *band*

P′1 ? 25264·42 0 G 0/1 F.

∧ Q1 25221·65 1*a* G 1 F.
−0·11
∨ P2 25101·02 *ab* G 0 F.

∧ R′1 25213·00 1*a* G 0 F.
+0·08
∨ Q′2 25092·13 *ab* G 0 F.
P′3 (24912·22) *ab* G *ab* F.

∧ R2 25126·71 1 G 3 F 9·6 K, also 0 → 0, $^3F \rightarrow 2s\,^3\Sigma$, R1.
+0·04
∨ Q3 24946·63 *ab* G 0/1 F.
P4 (24708·96) *ab* G *ab* F.

∧ R′3 25031·45 2 G 3 F 14·6 K, also 3 → 2, $3d\,^1\Pi_a \rightarrow 2p\,^1\Sigma$, P2.
−0·05
∨ Q′4 24793·57 *ab* G 0 F.
P′5 (24499·85) *ab* G *ab* F.

∧ R4 24935·04 0*a* G 1F 6·7 K, also 3 → 2, $3d\,^1\Pi_a \rightarrow 2p\,^1\Sigma$, P5.
−0·07
∨ Q5 24640·87 0*a* G 1 F 3·4 K, also 0 → 2, $4d\,^1\Sigma \rightarrow 2p\,^1\Sigma$, R5 and 1 → 1, $5p\,^3\Pi \rightarrow 2s\,^3\Sigma$ R1.
P6 (24293·27) *ab* G *ab* F.

The 0 → 1 *band*

P6 ? 22010·06 *ab* G 00 F defect −0·10.

The 0 → 2 *band*

Q1 20665·94 *ab* G 00 F, defect 0·10

The 0 → 3 *band*

P2 18463·55 0*a* G, also 1 → 4 $3\,^1K \rightarrow 2p\,^1\Sigma$, P3, defect +0·06.
∧ R2 18489·33 1 G, also 1 → 0 $3d\,^3\Sigma \rightarrow 2p\,^3\Pi$, Q5, defect −0·03.
−0·07
∨
P4 18128·66 2 G 7·9 K, defect −0·06.

The 0 → 3 *band*—continued

R4 18354·75 2 G 4·0 K, also 2 → 1, $3p\,^3\Pi \rightarrow 2s\,^3\Sigma$, Q4, defect −0·09.

The 1 → 1 *band*

P′1 ? 25101·94 1 G *ab* F.

∧ Q1 25055·40 8 G 7 F 142·0 K, also 3 → 2, $3d\,^1\Pi_b \rightarrow 2p\,^1\Sigma$, Q2 and 1 → 0, $4d\,^3\Delta_b \rightarrow 2p\,^3\Pi$, R1.
−0·01
∨ P2 24940·27 *ab* G 0 F.

∧ R′1 25046·08 0 G *ab* F.
+0·06
× Q′2 24930·99 0 G 0 F, also 5 → 3, $4p\,^3\Pi_a \rightarrow 2s\,^3\Sigma$, Q1.
+0·12
∨ P′3 ? 24759·22 *ab* G 0 F.

∧ R2 24962·64 0*a* G *ab* F, also 0 → 0, $^3B \rightarrow 2p\,^3\Pi$, R5.
−0·12
∨ Q3 24791·42 *ab* G 00 F.
P4 (24564·51) *ab* G *ab* F.

∧ R′3 24878·55 0 G 1 F.
−0·06
∨ Q′4 24652·27 2 G 4 F 20·6 K, also 0 → 0, $3\,^1N \rightarrow 2p\,^1\Sigma$, P6.
P′5 (24371·88) *ab* G *ab* F.

∧ R4 24798·47 2 G 2 F 11·4 K, also 0 → 0, $5p\,^3\Pi_a \rightarrow 2s\,^3\Sigma$, Q3.
0·00
∨ Q5 24518·70 *ab* G 0 F.
P6 (24186·95) *ab* G *ab* F.

The 1 → 2 *band*

P6 ? 22023·79 *ab* G 0 F, defect 0·12.

The 1 → 3 *band*

P2 20636·07 *ab* G 0/1 F, defect 0·05.

The 1 → 4 *band*

Q5 18335·03 2 G 2·7 K, also 2 → 1, $3d\,^3\Sigma \rightarrow 2p\,^3\Pi$, Q3, defect 0·04.

In this respect they resemble $3d\,^3\Sigma \rightarrow 2p\,^3\Pi$ and $4d\,^3\Sigma \rightarrow 2p\,^3\Pi$. In fact the resemblance is most remarkably close, because, in each of the three systems, the P branch fails entirely in each band except for the two lines P′ 1 and P2, apart from two very weak lines P6 and P′ 7 in the tail of $4d\,^3\Sigma \rightarrow 2p\,^3\Pi$, $0 \rightarrow 0$. The usual enhancement in Finkelnburg's higher temperature source compared with Gale, Monk and Lee's of the lines of higher rotational quantum number is scarcely noticeable, but this is not very surprising; owing to the pronounced inversion of the lower rotational levels all the lines of each band are confined within a range of less than 300 wave numbers, so that the Boltzmann factor exp. $-w/k\mathrm{T}$ can have little effect.

It seems fairly certain that the $0 \rightarrow 3$ band is real in spite of the coincidences. The combinations are good. Every R and P line for which the vibrational interval is known is present. Both the R2 and P2 lines look slightly too strong in their present allocations. The fact that the P2 line is marked *a* in Gale, Monk and Lee's tables is an additional reason for supposing the line to be a blend.

The rotational structure of the upper levels is shown in Table II together with that of the corresponding levels of $3d\,^3\Sigma$ and $4d\,^3\Sigma$ for comparison. The lowest interval at each vibrational level is shown queried because it depends on the P′ 1 line for which there is of necessity no combinational support. However, there are few suitable lines to choose from and in the $1 \rightarrow 1$ band, the P′ 1 line looks pretty secure. The peculiar lowest intervals of $3d\,^3\Sigma$ and $4d\,^3\Sigma$ also have no combinational support ; but these can now be regarded as certain, since they are confirmed by the wave mechanics calculations. The trend of the rotational intervals is clearly a continuation of that of 3 and $4d\,^3\Sigma$. In $3d\,^3\Sigma$ the $\mathrm{K} = 0$ level is slightly inverted being just above $\mathrm{K} = 1$. In $4d\,^3\Sigma$ the $\mathrm{K} = 0$ level is much inverted being just under $\mathrm{K} = 3$, the $\mathrm{K} = 1$ level is almost inverted being just under $\mathrm{K} = 2$. At the upper state of the present bands this process has gone a step further. Both $\mathrm{K} = 0$ and $\mathrm{K} = 1$ are inverted; $\mathrm{K} = 1$ lies above $\mathrm{K} = 2$ and $\mathrm{K} = 0$ well above $\mathrm{K} = 3$.

The 1′—0′ vibrational intervals of the upper state are compared with those of $3d\,^3\Sigma$ and $4d\,^3\Sigma$ in Table III. They evidently also continue the trend of $nd\,^3\Sigma$ at $n = 3$ and 4. It will be noticed* that they are increasing and approaching the values for the molecular ion H_2+, the end of the series *nd* or $g\,^3\Sigma$, as *n* increases. In this respect they resemble the series $np\,^3\Sigma$. The series $np\,^3\Pi$ and $ns\,^3\Sigma$, on the contrary, have

---

* *Cf.* Richardson, " Molecular Hydrogen and its Spectrum," p. 251.

TABLE II—ROTATIONAL STRUCTURE OF $nd\,^3\Sigma$, $n = 3, 4$ AND UPPER STATE OF PRESENT BANDS

The $v = 0$ levels

K	$3d\,^3\Sigma$	$4d\,^3\Sigma$	^3G
7a			
	278·30	308·64	
6s	→ 52·15	→ 62·91	
	226·15	245·73	
5a	→ 52·61	→ 65·90	
	173·54	179·83	141·29
4s	→ 53·03	→ 66·34	→ 56·55
	120·51	113·49	84·74
3a	→ 50·42	→ 60·31	→ 50·21
	70·09	53·18	34·53
2s	→ 40·03	→ 51·27	→ 43·33
	30·06	1·91	−8·80
1a	→ 32·13	→ 51·17	→ 33·97 (?)
	−2·05	−49·26	−42·77 (?)
0s			

The $v = 1$ levels

K	$3d\,^3\Sigma$	$4d\,^3\Sigma$	^3G
7a			
	263·87		
6s	→ 48·20		
	215·68		
5a	→ 49·26		
	166·42	161·90	146·54
4s	→ 49·39	→ 53·43	→ 59·18
	117·03	108·47	87·36
3a	→ 47·65	→ 54·16	→ 55·50
	69·38	54·31	31·86
2s	→ 42·11	→ 53·06	→ 41·10
	27·27	1·25	−9·24
1a	→ 29·96	→ 52·12	→ 37·30 (?)
	−2·69	−50·87	−46·54 (?)
0s			

TABLE III—1′ — 0′ VIBRATIONAL INTERVALS OF $3d\,^3\Sigma$, $4d\,^3\Sigma$ AND ^3G

	K = 1		K = 3		K = 5	
^3G	2172·55		2169·26		2177·09	
		>24·84		>21·07		>51·95
$4d\,^3\Sigma$	$2147{\cdot}71_5$		2148·19		2125·14	
		>60·52		>64·47		>52·20
$3d\,^3\Sigma$	2087·19		2083·72		2072·94	

values of these intervals which diminish as n increases, since the values at the lowest n are larger than those for H_2+.

Whilst all this makes the identification of the upper level with $5d\,^3\Sigma$ plausible, more is required to make it certain. Assuming that the P′ 1 lines belong to the bands the rotational structure shows that it is some kind of a Σ level with pronounced uncoupling. Four such orthodox levels are now known, viz., $3d\,^3\Sigma$, $4d\,^3\Sigma$, $3d\,^1\Sigma$ and $4d\,^1\Sigma$ so that we are becoming fairly familiar with their properties. The fact that the $K = 0$ level is an s level shows that it is a Σ_g (even) level and this is also required by the fact that it goes down to the odd level $2p\,^3\Pi$. As the position of the level with reference to $1s\sigma\,^2\Sigma$, the ground state of the H_2+ ion, gives it a " denominator " close to 5, if it is a level with only one electron excited we expect it to be an $n = 5$ level. There are two possible Σ_g levels at $n = 5$ which it might be, namely, $5d\,^3\Sigma_g$ and $5g\,^3\Sigma_g$. Until we know more about the other states at $n = 5$ it seems impossible to decide definitely between the claims of these two which should probably have very similar properties. We have attempted to decide the question by using a Rydberg formula to predict the $P'\,1$ line of the $0 \rightarrow 0$ band from the $P'\,1$ lines of the $0 \rightarrow 0$ bands at $3d\,^3\Sigma$ and $4d\,^3\Sigma$, the $P'\,1$ lines being chosen because the $v' = 0$, $K' = 0$ levels of these states are unperturbed. This placed the $P'\,1$ line about 200 wave numbers below where we find it. This favours $5g\,^3\Sigma_g$ which should lie a little higher than $5d\,^3\Sigma_g$ but the question is quite uncertain.* It is not unlikely that $5g\,^3\Sigma_g$ would follow the trend of the rotational and vibrational structure of $3d\,^3\Sigma_g$ and $4d\,^3\Sigma_g$ in a somewhat similar manner to that expected of $5d\,^3\Sigma$.

The status of ^3G is considered further in § 6.

§ 3 THE SYSTEM $^3A \rightarrow 2p\,^3\Pi$

This is another rather weak system, but it seems fairly extensive, there being some evidence of it at all the vibrational levels v' and v'' from 0 to 4. As with all the other known systems which end on $2p\,^3\Pi$ the diagonal bands are the strongest. In them the R branches are the most strongly developed; in the Q and P branches many of the lines are missing and the rest usually weak. The $0 \rightarrow 0$ band is a weak band, the $1 \rightarrow 1$ band is the strongest and the intensity falls off steadily as v', v'' increase from 1 to 4. The non-diagonal development seems more extensive than usual, but a good many of the non-diagonal lines listed may be coincidences. The lines are set out in the usual way in Table IV. There are several close alternative lines between the claims of which it is difficult

---

* Since this passage was written we have found (see Part III) the odd level $1s\sigma\,5f\sigma\,^3\Sigma_u$ which proves to have a denominator of about 5·3. This would make the value found for ^3G about right for $1s\sigma\,5d\sigma\,^3\Sigma_g$ and probably too low for that of $1s\sigma\,5g\sigma\,^3\Sigma_g$.

TABLE IV—LINES OF $^3A \rightarrow 2p\,^3\Pi$

The 0 → 0 *band*

	Q′1	[22486·68] *ab*.
	P′2	22365·89 *ab* G 0/1 F.
↑	R1	22545·27 1 G 1 F 5·3 K.
+0·04	Q2	(22424·50) *ab* G *ab* F.
↓	P3	22244·45 *ab* G 0 F.
or (less likely)		
↑	R1	22546·36 *ab* G 0/1 F 0 Tanaka.
+0·03	Q2	(22425·60) *ab* G *ab* F.
↓	P3	22245·55 *ab* G 00 F.
∧ +0·22	R′2	22541·66 2 G 2 F 8·7 K, also 2 → 2, $4d\,^3\Delta_b \rightarrow 2p\,^3\Pi$, R1.
∨	Q′3	22361·53 1 G 0 F 3·7 K, also 1 → 1, $3\,^1K \rightarrow 2p\,^1\Sigma$, R1, and 3 → 3, $4d\,^3\Delta_b \rightarrow 2p\,^3\Pi$, R1.
	P′4	(22123·71) *ab*.
∧ −0·14	R3	22532·01 *ab* G 00 breit F.
∨ ∧ 0·00	Q4	22294·48 1 G *ab* F 3·2 K, also 0 → 0, $3d\,^1\Delta_a \rightarrow 2p\,^1\Sigma$, P5.
∨	P5	22000·24 *ab* G 2 F, also Q6 of the 2 → 2 band.
↑	R′4	22517·72 *ab* G 00 F.
−0·07	Q′5	(22224·03) *ab* G *ab* F.
↓	P′6	21875·65 *ab* G 00 F.
or (less likely)		
↑	R′4	22515·62 *ab* G 0 F.
−0·02	Q′5	(22221·90) *ab* G *ab* F.
↓	P′6	21873·50 *ab* G 00 F.
↑	R5	22498·68 0*h* G 1·8 K, also 1 → 1 $4d\,^3\Pi_a \rightarrow 2p\,^3\Pi$, Q′4. 22498·80 0 F, also 1 → 1, $4d\,^3\Pi_a \rightarrow 2p\,^3\Pi$, Q5.
+0·07	Q6	(22151·14) *ab* G *ab* F.
↓	P7	21750·50 *ab* G 0 F.

The 0 → 1 *band*

	Q2	20091·21 0 G, defect 0·04.
	Q4	19980·86 9 G 40·0 K C+, also 1 → 3, $3d\,^1\Sigma \rightarrow 2p\,^1\Sigma$, R0 defect 0·09.

The 0 → 2 *band*

	P3	17717·06 3*a* G 5·9 K, also 0 → 0, $3d\,^3\Delta_a \rightarrow 2p\,^3\Pi$, R2, defect 0·05.

The 0 → 3 *band*

	Q2	? 15787·23 5 G 32·1 K, also 3 → 3, $3p\,^3\Pi_a \rightarrow 2s\,^3\Sigma$, Q2 defect 0·13.

The 1 → 0 band

	R3	24746·25 *ab* G 00 F, defect 0·08.
	Q6	? 24356·50 *r* Deodhar, defect 0·18. (Line measured as 24356·08 (00) by Finkelnburg.)

The 1 → 1 *band*

∧ +0·09	Q′1	22376·38 0*a* G 0/1 F 3·0 K 76·54 in F.
∨	P′2	22261·26 1*a* G 1 F, also 0 → 2, $3\,^1N \rightarrow 2p\,^1\Sigma$, P1.
∧ +0·16	R1	22432·02† 3 G 4 F 26·4 K 32·12 in F. Z = 0 RT 24 LA 21 He 0, also 2 → 2, $4d\,^3\Delta_b \rightarrow 2p\,^3\Pi$, Q2, and 0 → 0, $3d\,^1\Delta_b \rightarrow 2p\,^1\Sigma$, Q4.
× −0·19	Q2	22316·72 2 G *ab* F 4·1 K 0 MB
×	P3	22145·57 3 G 5 F 4·6 K H + Z = 0 RT 9½ LA 6 He++, also 0 → 0, $3d\,^1\Pi_b \rightarrow 2p\,^1\Sigma$, Q8.
∧ +0·16	R′2	22427·50 1 G 1 F 4·6 K 27·44 in G.
∨	Q′3	22255·69 1*h* G 0 F 55·89 in F.
	P′4	(22029·52) *ab* G *ab* F.

---

† Properties affected by blends other than the coincidences mentioned.

TABLE IV—(continued)

The 1 → 1 *band*—(continued)

↑ R3 22421·63† 3 G 4 U F 20·0 K,
Z RT 15½ LA 10 He+, also
0 → 0, $3d\,^1\Delta_a \rightarrow 2p\,^1\Sigma$, P6.
0·05 Q4 (22194·72) *ab* G *ab* F.
↓ P5 21914·90 *ab* G 0 F.

R′4 22414·29 0 G 1 F 2·0 K 14·33
in F.
Q′5 (22133·90) *ab* P′6 (21802·7) *ab*.

∧ R5 22405·26 ? G 1 F 2·9 K 05·64
+0·14 (1) in G, also 2 → 2, $4d\,^3\Delta_a \rightarrow$
$2p\,^3\Pi$, P′3.
∨ Q6 22073·37 5 G 2 F 7·6 K, also
2 → 2, $4d\,^3\Sigma \rightarrow 2p\,^3\Pi$, Q1,
3 → 3, $4d\,^3\Pi_a \rightarrow 2p\,^3\Pi$, Q1,
and 2 → 2, $4d\,^3\Pi_b \rightarrow 2p\,^3\Pi$,
Q4.
P7 (21693·14) *ab* G *ab* F.

The 1 → 2 *band*

R5 20226·86 3 G 10·7 K, also
1 → 3, $3d\,^1\Pi_b \rightarrow 2p\,^1\Sigma$, Q5,
defect 0·04.

The 1 → 3 *band*

R3 18134·00 1 G He++, also (?)
1 → 3, $^1Q \rightarrow 2p\,^1\Sigma$, P4, defect
0·12.

The 1 → 4 *band*

∧ Q2 ? 16035·56 *ab* G *r* Deodhar
−0·38 defect 0·29.
∨ P3 15889·31 *ab* G 0 MB, defect
0·05.

The 2 → 0 *band*

R3 ? 26847·58 *r* Deodhar, defect
0·10, 47·05 (0) in F.

The 2 → 1 *band*

∧ Q2 24427·71 *ab* G 0 F, defect 0·05.
−0·17
∨ P3 24256·54 *ab* G 0 F, defect 0·10.

The 2 → 2 *band*

∧ Q′1 22274·90 *ab* G 1*d* F.
−0·07
∨ P′2 22165·57 *ab* G 0 F.

↑ R1 22326·03 1 G 1 F 25·97 in F
3·0 K.
−0·08 Q2 (22216·26) *ab* G *ab* F.
↓ P3 22053·54 (?) G 4 breit F, in G
53·66 (4), = 2 → 3, $3d\,^1\Sigma \rightarrow$
$2p\,^1\Sigma$, R0, R3.

R′2 (22321·91) *ab* G *ab* F.
∧ Q′3 22158·22 (?) G (?) F, may be
0 mixed with 22158·45 (4) G =
∧ 58·37 (3) F = 0 → 2, $^1N \rightarrow$
0·15 $2p\,^1\Sigma$, P5 and 0 → 1,
∨ $^3B \rightarrow 2p\,^3\Pi$, P3.
∨ P′4 21943·15 *ab* G 0 F.

↑ R′2 22321·37 *ab* G 1 F ⎫ alternative
+0·05 ⎬
↓ Q′3 22157·63 0 G 2 F ⎪ R′2 Q′3
P′4 (21942·59) *ab* G *ab* F ⎭ P′4.

R3 22320·24 3 G 2 F 11·0 K, also
∧ 3 → 3, $4d\,^3\Delta_b \rightarrow 2p\,^3\Pi$, Q4.
+0·07
× Q4 22103·87 (?) G 0 F, 22103·67 (1)
G 13·7 K = 1 → 1, $4d\,^3\Pi_b \rightarrow$
$2p\,^3\Pi$, Q6.
+0·04
∨ P5 21838·29 *ab* G 0 F.

∧ R′4 22318·21 1 G (?) F, 22318·46 (0)
+0·04 F.
× Q′5 22050·65 *ab* G 0 F.
? ∧
There is only one other known value 314·29 of this interval. It involves a blend. The present lines make it 314·57.
∨
∨ P′6 ? 21736·08 *ab* G 0 F.

∧ R5 22316·72 2 G *ab* F, also Q2 of
+0·07 the 1 → 1 band.
× Q6 22000·24 *ab* G 2 F, also P5 of
the 0 → 0 band.
−0·03
∨ P7 21638·64 *ab* G 0 F

TABLE IV—(continued)

The 2 → 3 *band*

P3 ? 19969·2 *ab* G [*d*] Tanaka, defect 0·3.

P5 19777·54 2*a* G, also 1 → 3, $3\,^1K \rightarrow 2p\,^1\Sigma$, P1, defect 0·12.

The 2 → 4 *band*

R1 ? 18245·8 [ ] Tanaka, defect 0·27.

Q4 18070·20 0 G, defect 0·13.

R5 18311·28 8 G 43·0 K, also 1 → 1 $4d\,^1\Pi_b \rightarrow 2p\,^1\Pi$, R1*, defect 0·09.

The 3 → 3 *band*

∧ Q′1 22184·97 *ab* G 0 F.

+0·03

∨ P′2 22081·00 0 G 1 F 80·90 in F = 2 → 3, $3d\,^1\Sigma \rightarrow 2p\,^1\Sigma$, P1 and 0 → 0, $3d\,^1\Pi_a \rightarrow 2p\,^1\Sigma$, P7.

or

∧ Q′1 22183·74 00 G *ab* F, also 2 → 2, $4d\,^3\Pi_a \rightarrow 2p\,^3\Pi$, P2.

0·00

P′2 22079·80 1 F

→ 22079·72 2 G } = 2 → 2, $4d\,^3\Sigma \rightarrow 2p\,^3\Pi$, R′1 and 1 → 1, $4d\,^3\Pi_b \rightarrow 2p\,^3\Pi$, P′4.

∧ R1 22232·45 1 G 2 F 14·0 K, coincident with the R3 line.

+0·03

∨ Q2 22128·00 2 G 1 F 6·7 K 28·06 in F, also 0 → 2, $^1N \rightarrow 2p\,^1\Sigma$, P5.

∧

−0·02

∨ P3 21973·25 *ab* G 0 F.

↑ R′2 22230·34 3 G 3 F 9·0 K, also 0 → 0, $4d\,^3\Sigma \rightarrow 2p\,^3\Pi$, Q3, and 2 → 4, $3\,^1O \rightarrow 2p\,^1\Sigma$, R2.

−0·14 Q′3 (22074·38) *ab* G *ab* F.

↓ P′4 ?21870·15 0 G *ab* F.

↑ R3 22232·45 1 G 2 F 14·0 K 32·49 in F, coincident with the R1 line

+0·04 Q4 (22026·41) *ab* G *ab* F.

↓ P5 21774·38 *ab* F 00F.

The 3 → 4 *band*

R3 ? 20263·88 4 G 30·0 K, also 0 → 1, $3d\,^1\Sigma \rightarrow 2p\,^1\Sigma$, R3, defect 0·13.

The band lines coming from $v = 4$ are probably either

∧ R1 22154·57 0 G 1 F 4·4 K, also R1 of 3 → 3, $3d\,^3\Pi_b \rightarrow 2p\,^3\Pi$.

+0·13

∨ Q2 22055·10 *ab* G 0 F.

P3 (21908·54) *ab* G *ab* F.

↑ R3 22160·21 1 G *ab* F 4·3 K, also 2 → 4, $3\,^1O \rightarrow 2p\,^1\Sigma$, R1.

+0·04

↓ Q4 21963·59 3 G 3 F, also 2 → 2, $4d\,^3\Sigma \rightarrow 2p\,^3\Pi$, P2, R′3 and 2 → 3, $3\,^1K \rightarrow 2p\,^1\Sigma$, R1.

or

The 4 → 3 *band*

Q2 ? 24023·10 1 G 0 F 6·2 K, also 2 → 2, $^1L \rightarrow 2p\,^1\Sigma$, P2, defect 0·15.

The 4 → 4 *band*

R1 22145·57 3 G 5 F† H+ He++ Z = 0, RT 9½, LA 6, also 0 → 0, $3d\,^1\Pi_b \rightarrow 2p\,^1\Sigma$, Q8.

Q2 (22046·23) (?) G (?) F, may be mixed with 22046·37 (6) G = 6·39 (4) F = 2 → 3, $3d\,^1\Pi_b \rightarrow 2p\,^1\Sigma$, Q2.

P3 (21899·61) *ab* G *ab* F.

↑ R3 22152·66 1 G 6 F† He++

−0·09 Q4 (21956·08) *ab* G *ab* F.

↓ P5 21718·77 *ab* G 00 F.

* This is the only line in this singlet band. It is obviously much too strong for both positions combined.

† Properties may be affected by blends.

to decide, owing to a slight irregularity in the rotational structure. The details of the 3 → 3 band must be regarded as somewhat uncertain as there are a number of lines in the same region having suitable rotational combinations. The 4 → 4 band is uncertain owing to the impossibility of identifying the R′ 2, Q′ 3, P′ 4 level for which the combination differences are unknown.

The rotational structure of the initial (upper) state, which is set out in Table V, is peculiar. It is some kind of a Π or Σ state because the $K = 1$ level is present at each of the vibrational levels $v' = 0, 1, 2$ and 3. The only evidence that it may possibly be a Σ state rests on the occurrence of an unclassified line 22376·54 (0*a*) G (0/1) F with about the correct intensities in Gale, Monk and Lee and in Finkelnburg at the expected position for the P1 line of the 1 → 1 band. This line has no support from non-diagonal combinations. In the 0 → 0 band there does not seem to be a line suitable for P1. But in all except the 1 → 1 band the rotational structure is rather irregular, so that we cannot foretell the precise position of the P1 line should it exist; furthermore, all these bands are so weak that it may not occur on that account. There is a weak and uncertain level $4\,^1O$ which one of us* has provisionally assigned to $4s\,^1\Sigma_g$ which has a similar ν_e and a similar structure except that the *a* (strong) and *s* (weak) levels are interchanged. This shows that if ^3A is a Σ level it is an odd level so that it cannot be $4s\,^3\Sigma_g$. For the same reason it cannot go down to $2p\,^3\Pi$ which is also an odd level but it does. If there were nothing but the transitions and the structure of the levels to contend with we should conclude without doubt that ^3A was an even Π state.

The difficulty about this is that there is no unknown even Π state with a single excited electron which can have a " denominator " so near to 4 as that of ^3A unless it is a state with principal quantum number > 4 perturbed to a degree which seems impossible. We shall postpone the further consideration of the possible electronic structure of ^3A until two additional systems ending on $2p\,^3\Pi$ have been described.

The vibrational intervals of ^3A are set out in Table VI. These are very similar to the corresponding intervals of $4p\,^3\Pi$ the only known odd triplet Π level at $n = 4$. Where alternative values are given they correspond to the lines which come first in Table IV.

The ν_0 of the 0 → 0 band is very close to 22580. If we take the ν_0 of the final state to be 29635,† the value got by applying a Rydberg formula to the series $3d\,{}^3\Sigma$, Π, $\Delta \rightarrow 2p\,{}^3\Pi$, $4d\,{}^3\Sigma$, Π, $\Delta \rightarrow 2p\,{}^3\Pi$, this makes ν_e for ^{3}A to be 7055, and the Rydberg denominator 3·943. The values of ν_e for other well-known $n = 4$ triplet states of H_2 are : $4p\,{}^3\Pi$, $\nu_e = 7067$; $4d\,{}^3\Sigma$, $\nu_e = 7106$; $4d\,{}^3\Pi$, $\nu_c = 6980$; $4d\,{}^3\Delta$, $\nu_e = 6815$. The values given for the $4d^3$ complex are those for the theoretical unperturbed states.

---

* Richardson, " Molecular Hydrogen and its Spectrum," pp. 142, 311.

† An alternative extrapolation from the series $np\,^3\Pi$, $n = 3, 4, 5$ to $n = 2$ using a Rydberg-Ritz formula gave 29503. Richardson, 'Proc. Roy. Soc.,' A, vol. 113, p. 368 (1926).

TABLE V—ROTATIONAL STRUCTURE OF ^{3}A LEVEL

K ↓	$v = 0$		$v = 1$		$v = 2$		$v = 3$		$v = 4$
6a	—		—		—				
	275·08 − x_0		271·93 − x_1		265·03				
5s	…	→ 51·64	…	→ 52·39	…	→ 51·5_1			
	223·44 + x_0		219·24 + x_1		213·5_2				
4a	—	→ 52·86	—	→ 53·53	—	→ 52·0_5	—		—
	170·58 − x_0		165·71 − x_1		161·47		157·46		↑
3s	…	→ 53·48	…	→ 55·23	…	→ 56·25	…	→ 55·67	251·67
	117·10 + x_0		110·48 + x_1		105·22		101·79		↓
2a	—	→ 58·52	—	→ 54·81	—	→ 54·09	—	→ 54·28	—
	58·58 − x_0		55·67 − x_1		51·13 − x_2		47·51 − x_3		
1s	…		…	→ 55·83 ?	…		…		
			? −0·16 + x_1						
		? 0a	—						
	or less likely				or		or		or
					…				
					213·52				
4	—				—	51·48			—
	170·58				162·04				↑
3	…	→ 54·57			…	57·38	…		253·06
	116·01				104·66		101·79		↓
2	—	→ 56·34			—	53·53	—	→ 53·04	—
	59·67				51·13		48·75		
1	…				…		…		

TABLE VI—VIBRATIONAL INTERVALS OF ^{3}A

Δv at → ↓	K = 2	K = 4	K = 6
1′ − 0′	2225·48	2213·99	2205·51
	or 2224·38		
2′ − 1′	2110·88	2101·52	2089·91
3′ − 2′	2004·41	1996·79	
4′ − 3′	1903·95	1896·44	
	or 1895·01	or 1888·94	

Both the vibrational intervals of ^{3}A and the position ν_e of this electronic level are about what we might expect for that of $4f\,{}^3\Sigma$ or $4f\,{}^3\Pi$.

§ 4 THE SYSTEM ^{3}B → $2p\,{}^3\Pi$

What we have found of this with certainty is a v' progression and to all appearance a $v' = 0$ progression, the $v'' = 0$ band being much the strongest and the strength of the others falling away steadily as v'' increases from 0 to 3. In the $v'' = 0$ band, where there is only one known blend, the Q branch is the strongest and the P branch the weakest. The lines of this progression are set out in Table VII.

TABLE VII—LINES OF $^3B \rightarrow 2p\,^3\Pi$

The $v'' = 0$ *band*

∧	Q′1	24632·97 0 G 0 F 2·8 K.
0·00		
∨	P′2	24512·18 1*h* G 0 F.
∧	R1	24783·67 0*h* G 0/1 F 4·5 K.
+0·05		
×	Q2	24662·88 1 G 1 F 5·2 K.
−0·03		
∨	P3	24482·87 0 G 00 F 2·0 K.
∧	R′2	24837·69 *ab* G 00 F.
+0·01		
∨	Q′3	24657·77 0 G 1 F 3·1 K C++
	P′4	(24419·81) *ab* G *ab* F.
∧	R3	24878·53 0 G 1 F, also 1 → 1, $^3G \rightarrow 2p\,^3\Pi$, R′3.
−0·01		
∨	Q4	24640·87 0*a* G 1 F 3·4 K, also 0 → 2, $4d\,^1\Sigma \rightarrow 2p\,^1\Sigma$, R5 and 1 → 1, $5p\,^3\Pi \rightarrow 2s\,^3\Sigma$ R1.
	P5	(24346·67) *ab* G *ab* F.
		or
∧	R3	24889·98 2 G 1 F 5·6 K.
+0·03		
∨	Q4	24652·28 2 G 4 F 20·6 K, also 0 → 0, $^1N \rightarrow 2p\,^1\Sigma$, P6 and 1 → 1, $^3G \rightarrow 2p\,^3\Pi$, Q′4.
	P5	(24358·03) *ab* G *ab* F.
∧	R′4	24921·74 *ab* G 0 F.
−0·07		
∨	Q′5	24628·09 3 G 1 F 7·7 K.
	P′6	(24279·74) *ab* G *ab* F.

The $v'' = 0$ *band*—continued

∧	R5	24962·64 0*a* G *ab* F, also 1 → 1, $^3G \rightarrow 2p\,^3\Pi$, R2.
−0·02		
×	Q6	24615·06 00 G *ab* F 3·7 K.
+0·03		
∨	P7	24214·40 *ab* G 00 F.

The $v'' = 1$ *band*

∧	Q2	22329·78 5 G 3 F 21·6 K, also, 0 → 0, $4p\,^3\Pi \rightarrow 2s\,^3\Sigma$, R0 defect 0·16.
−0·01		
∨	P3	22158·45 4 G 3 F 31·5 K, also 0 → 2, $^1N \rightarrow 2p\,^1\Sigma$, P4, defect 0·12.
∧	R5	? 22663·18 *ab* G 0 F, defect 0·25
−0·16.		
∨	Q6	22331·59 *ab* G 0/1 F defect 0·16.

The $v'' = 2$ *band*

	Q2	20118·28 5 G 26·0 K, also 1 → 3, $3d\,^1\Pi_a \rightarrow 2p\,^1\Sigma$, P4 defect 0·06.
	Q6	20168·72 5 G 24·5 K, also 1 → 3, $3d\,^1\Pi_b \rightarrow 2p\,^1\Sigma$, Q4 defect 0·01.

The $v'' = 3$ *band*

	P3	17870·80 0 G, also 1 → 5, $3d\,^1\Pi_b \rightarrow 2p\,^1\Sigma$, Q5, defect 0·02.

The rotational structure of the initial state is shown in Table VIII. It is evidently strongly uncoupled and looks to be an even Π_b level. The lowest K = 1 level rests entirely on the single pair of Q′ 1 P′ 2 lines but the combination is good. Assuming the upper level of the progression to be the $v' = 0$ level, which is what it looks to be, the ν_0 of the 0 → 0 band is not very far from where we expect it for $5d\,{}^3\Pi_b \rightarrow 2p\,{}^3\Pi$, but it seems rather too low for this system.

The rotational structure as set out in Table VIII uses the lines R3 = 24878·53 and Q4 = 24640·87. These lines look much too weak for the rest of the band. The alternative lines R3 = 24889·98 and Q4 = 24652·28 have about the right intensities. On the other hand they make the K′ = 4 level appear to be about 12 wave-numbers too high. It seems that this level is abnormal either in intensity or position. Possibly the level may be split. A disadvantage of the stronger pair of lines is that the R3 line is given as more intense in Gale, Monk and Lee's than in Finkelnburg's tables. However, there does not seem to be much in this since Finkelnburg's eye estimates of the strength of these lines are confirmed by Kapuscinski and Eymers' intensity measurements.

TABLE VIII—ROTATIONAL STRUCTURE OF UPPER STATE OF ${}^3B \rightarrow 2p\,{}^3\Pi$

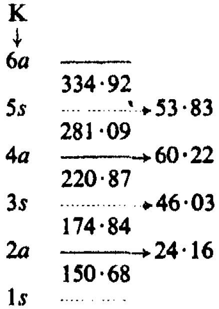

What are probably the lines of the $v' = 1$ progression of this system are given in Table IX. In this progression several of the combinations are poor and some of the intensities unexpected. However, the main band lies in a part of the spectrum which is unsatisfactory for observation and measurement and there seems to be some adequate reason for most of the discrepancies.

The rotational structure of the upper level is shown in Table X. This is evidently the continuation with v' increased by unity of the rotational structure of the level shown in Table VIII. If the progressions in Table VII and IX are really successive v' progressions of the same band system the initial vibrational intervals of the upper state are : at K = 1, 1417·58 ; at K = 2, 1399·46 ; at K = 3, 1392·74 ; at K = 4, 1383·96 ; at K = 5, 1369·78 ; at K = 6, 1353·63. It does not seem possible that these vibrational intervals could be associated with the two lowest vibrational levels of $5d\,{}^3\Pi_b$ which should continue the trend of $3d^3$, $4d^3$ towards the corresponding intervals of H_2+, the end of the nd^3 series.

TABLE IX—LINES OF ? $v' = 1$ PROGRESSION OF $^3B \to 2p\,^3\Pi$

The $v'' = 0$ *band*

∧	Q′1	26050·53 0*a* G 3 F.
−0·05		
∨	P′2	25929·79 0*ah* G 0/1 F.
∧	R1	26183·08 1 G 1 F, also ?? 0 → 0, $6p\,^3\Pi_a \to 2s\,^3\Sigma$, Q3.
−0·06		
×	Q2	26062·40 0 G 1 F.
+0·04		
∨	P3	25882·33 *ab* G 1 F.
∧	R′2	26230·66 *ab* G 0 F *r* D.
+0·22		
×	Q′3	26050·53 0*a* G 3 F.
+0·05		
∨	P′4	25812·55 *ab* G 00 F.
∧	R3	26261·82 1 G *ab* F.
−0·29		
×	Q4	26024·44 1*a* G 1 F, also 2 → 0, $3d\,^1\Pi_b \to 2p\,^1\Sigma$, Q7. Given in error as 26028·48 by Gale, Monk and Lee.
−1·22		
∨	P5	? 25731·42 *ab* G *ab* F *r* Tanaka.
∧	R′4	26291·66 *ab* G 0/1 F.
+0·18		
∨	Q′5	25997·76 0*h* G *ab* F, also 3 → 1, $4p\,^3\Pi_a \to 2s\,^3\Sigma$, Q1.
	P′6	(25649·52) *ab* G *ab* F.
∧	R5	26316·29 (?) G 2 F, mixed with 26316·55 (0*a*) G, 0 → 1, $4d\,^1\Delta_a \to 2p\,^1\Sigma$, P4.
+0·02		
×	Q6	25968·67 0 G 1 F 15·3 K, also 0 → 1, $4d\,^1\Pi_b \to 2p\,^1\Sigma$, Q3.
+0·01		
∨	P7	25568·03 1 G 2 F 8·2 K, also 0 → 1, $4d\,^1\Sigma \to 2p\,^1\Sigma$, P4.

The $v'' = 1$ *band*

R3	23937·51 *ab* G 00 F, defect (based on Q4 line) 0·06.
Q6	23685·24 *ab* G 0 F, defect 0·12

The $v'' = 2$ band

Q2	21517·59 *ab* G 0 F, defect 0·15.
P5	21252·59 *ab* G 00 F, defect (based on Q4 line) 0·04.

The $v'' = 3$ *band*

Q4	? 19443·68 *ab* G *ab* F *qd* Tanaka defect 0·38.

Possible alternative for K′ = 6 level.

The $v'' = 0$ *band*

∧	R5	(26321·53) *ab* G *ab* F, or covered by H_θ (= 26322·82 (2) F 29·9 K).
0		
×	Q6	25973·93 00 G *ab* F.
0·00		
∨	P7	(25573·30) *ab* G *ab* F.

The $v'' = 1$ *band*

Q6	23690·49 *ab* G 00 F, defect 0·13.

TABLE X—ROTATIONAL STRUCTURE OF THE UPPER LEVEL

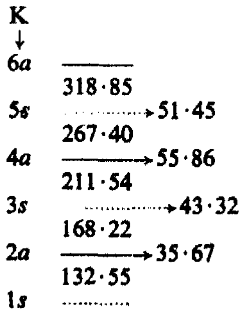

If these two progressions really belong to the same upper electronic state and the initial vibrational intervals are real it will be necessary to look for the interpretation of the initial state as some kind of an abnormal electronic state. The small initial vibrational intervals, which are consistent with the fact that the bands have more progressional development than is usual with bands ending on $2p\,^3\Pi$, suggest a state with a loose binding, indicating one which belongs to a series of which the limit at infinity is an unstable state. In favour of such an interpretation are (1) the detailed rotational structure is really a good deal different from what we should expect beforehand for $5d\,^3\Pi_b$, and (2) the absolute position seems somewhat lower than what we should expect for this state. It is possible that ^{3}B is the analogue in the triplet states of the singlet state ^{1}Q which it has been suggested* is the doubly excited state $2p\sigma\, 2p\pi\, ^1\Pi_g$. We shall show in a subsequent communication that ^{1}Q is a state with abnormally low vibrational intervals. ^{3}B has the opposite nuclear spin symmetry to that of ^{1}Q ; but if they are Π states either symmetry, or both, may occur. We shall return to the question of the electronic configuration of ^{3}B in § 6.

§ 5 THE SYSTEM $^3\mathrm{C} \rightarrow 2p\,^3\Pi$

Of this we have only found a single initial progression but it looks genuine enough. The Q branch is the weakest and may be entirely absent. There is not a lot to choose between the intensities of the R and P branches. The lines are set out in Table XI. There are, unfortunately, alternatives at each of the weak (s) $K = 3$ and $K = 5$ levels which makes the interpretation of the rotational structure correspondingly uncertain. There does not seem to be any decisive factor in favour of any of the alternatives and the rotational structures arising from the four possible combinations are set out in Table XII. On the whole A looks preferable to B and A and D is perhaps more likely than A and C.

From the fact that the upper state goes down to $2p\,^3\Pi$ together with the fact that its $K = 2$ level is an a level we can conclude that it is either an even Π_b level or an even Δ_b level. We have not been able to find any convincing evidence of the occurrence of a Q′ 1 P′ 2 combination, so that the $K = 1$ level is not demonstrably existent. If the $K = 1$ had no existence this would make ^{3}C a Δ level, but it would be very dangerous to draw this inference from the absence of the Q′ 1, P′ 2 combination in the present instance. Whichever of the possible alternatives are chosen the Q2 and Q′ 3 lines are definitely absent and we should therefore expect that Q′ 1 would be weaker than Q2 and so absent. Thus the K = 1 level could at the most be represented only by a weak P′ 2 line whose position is uncertain owing to the complicated rotational structure caused by uncoupling. There is, at present, no possibility of a confirmation of this P′ 2 line by combinations with non-diagonal bands because the *s* final vibrational intervals are unknown ; in any event we should expect the non-diagonal P′ 2 lines to be too weak to show up. Finally, if we compare ^{3}C with the other known strongly uncoupled Π_b and Δ_b states ($3d\,^3\Pi_b$, $3d\,^1\Pi_b$, $3d\,^3\Delta_b$, $3d\,^1\Delta_b$ given in R and D,

---

* "Molecular Hydrogen and its Spectrum," p. 314.

TABLE XI—THE LINES OF THE SYSTEM $^3\mathrm{C} \rightarrow 2p\,^3\Pi$

The v'' = 0 band

↑	R1	25248·16 0 G 0 F.
+0·05	Q2	(25127·40) *ab* G *ab* F.
↓	P3	24947·33 0 G 1 F.
↑	R′ 2	25291·62 0 G 0 F.
−0·03	Q′ 3	(25111·72) *ab* G *ab* F *A*.
↓	P′ 4	24873·81 0 G 0/1 F.
		or
↑	R′ 2	25302·13 1 G 0 F.
+0·02	Q′ 3	(25122·21) *ab* G *ab* F *B*.
↓	P′ 4	24884·27 00 G 0 F.
∧	R3	25327·97 1 G 2 F.
−0·11		
×	Q4	25090·41 *ab* G 0 F also 2 → 1 $3d\,^1\Delta_a \rightarrow 2p\,^1\Sigma$, R2
+0·09		
∨	P5	24796·08 3 G 1 F 9·8 K He 0.

The v'' = 0 band—continued

∧	R′ 4	25365·97 *ab* G 0 F.
+0·09		
×	Q′ 5	25072·16 0 G *ab* F *C*.
+0·02		
∨	P′ 6	24723·72 5 G 4 F 61·0 K, also 0 → 0, $3\,^1\mathrm{N} \rightarrow 2p\,^1\Sigma$, P4.
		or
↑	R′ 4	25364·07 *ab* G 00 F.
+0·02	Q′ 5	(25070·34) *ab* G *ab* F *D*.
↓	P′ 6	24721·91 *ab* G 00 F.
↑	R5	25404·80 1*a* G 2 F.
−0·08	Q6	(25057·24) *ab* G *ab* F.
↓	P7	24656·65 *ab* G 00 F.

The v'' — 1 band

↑	R1	22909·35 *ab* G 00F, defect 0·03.
+0·11		
↓	P3	22622·76 0 G 0 F, defect 0·03.
	Q6	22773·93 *ab* G 0 F, defect zero.

TABLE XII—POSSIBLE ALTERNATIVE ROTATIONAL STRUCTURES OF ^{3}C

K ↓	A and C	A and D	B and C	B and D
6*a*	———	———	———	———
	333·01	334·83	333·01	334·83
5*s*	⋯⋯→57·27	⋯⋯→60·95	⋯⋯→57·27	⋯⋯→60·95
	275·74	273·88	275·74	273·88
4*a*	———→59·36	———→57·50	———→69·84	———→67·98
	216·38	216·38	205·90	205·90
3*s*	⋯⋯→52·09	⋯⋯→52·09	⋯⋯→31·11	⋯⋯→31·11
	164·29	164·29	174·79	174·79
2*a*	———	———	———	———

Part II, Table IX, pp. 50, 51 : $4d\,{}^3\Pi_b$, $4d\,{}^1\Pi_b$, $4d\,{}^3\Delta_b$, $4d\,{}^1\Delta_b$ given* in R and D, Part III, Table VII, p. 53) the rotational structure looks as though ^{3}C might be either a Π_b or a Δ_b state with $n > 4$.

The ν_e of ^{3}C is quite close to that of the upper state ^{3}G which we saw in § 2 was probably $5d\,{}^3\Sigma_g$ or $5g\,{}^3\Sigma_g$. In neither case can the ν_e be measured with precision, owing to the very pronounced uncoupling effects. It is also possible that the analysis is being confused to a certain extent by an intermixture of closely lying levels belonging to different upper states. When one considers that some of the details of the $4d\,{}^1\Sigma\Pi\Delta$ states are not yet finally settled† although these states were discovered in 1928 or earlier‡; and in them the reality of the levels to be classified is established by long chains of progressional combinations, the progress we have made with these strongly uncoupled weak triplet 5 states with practically no strength off the diagonal seems almost surprising. It might, of course, turn out to be illusory, but we feel ourselves that we have made a substantial beginning with them.

§ 6 THE ELECTRONIC STRUCTURE OF ^{3}A, ^{3}B, ^{3}C AND ^{3}G

In concluding this paper we shall review some of the facts which bear on the electronic structure of the upper states of the four systems which have been described in §§ 2–5. Of these states we consider that ^{3}A is the most perplexing ; some of the difficulties in connection with it have been mentioned in § 3. There is one remarkable point, however, which has not been referred to. The state $4s\,{}^3\Sigma_g$ should exist and should go down to $2p\,{}^3\Pi_u$. We have spent some time looking for the $4s\,{}^3\Sigma \rightarrow 2p\,{}^3\Pi$ system and have been unable to find it. The remarkable thing is this. The ^{3}A state has all the properties we should expect the missing $4s\,{}^3\Sigma$ state to have except that it possesses one property which seems to be an absolute bar to its identification with $1s\sigma\,4s\sigma\,{}^3\Sigma_g$. This will be clearer after a study of Table XIII, which assembles the leading properties of all the known $s\Sigma$ states of H_2 with one electron excited and also those of the ion $1s\sigma\,{}^2\Sigma$ which is the end of all the series of states which have only one electron excited. The states ^{1}X, 3^1 O and 4^1 O may not be generally accepted as $1s\sigma\,2s\sigma\,{}^1\Sigma$, $1s\sigma\,3s\sigma\,{}^1\Sigma$ and $1s\sigma\,4s\sigma\,{}^1\Sigma$ but they have been put forward as the representatives of these states by one of us.[||]

---

* The lowest interval of $4d\,{}^3\Pi$ in this table is subject to the correction given in § 3 of Part I of the present series of papers.

† *Cf.* Richardson and Davidson, ' Proc. Roy. Soc.,' A, vol. 142, p. 70 (1933).

‡ Richardson, ' Proc. Roy. Soc.,' A, vol. 115, p. 528 (1927) ; Richardson and Davidson, ' Proc. Roy. Soc.,' A, vol. 123, p. 466 (1929).

If they are not, the only alternative seems to be to deny the existence of these theoretical singlet states. This is extremely improbable. In any event there is no doubt whatever about $2s\,^3\Sigma$ and no reasonable doubt about $3s\,^3\Sigma$. The approximate correctness of the values for the ground state of the molecular ion has now been confirmed in a great variety of ways[¶] from the properties of various excited states of H_2. The lowest K levels of ^3A for which vibrational intervals are available are at K = 2. These are not known for most of the other states. For $3s\,^3\Sigma$ the values given are the average of the values at K = 1 and K = 3, for ^1X the values are for K = 1 (the values for this state are not too certain as there is some doubt about the vibrational quantum numbering and also the $0 \rightarrow 0$ band is not very secure). For the ion the actual intervals are unknown ; the 1 − 0 interval is replaced by $\omega_0 - x\omega_0$ and $\Delta_2\nu$ by $2x\omega_0$. For $2s\,^3\Sigma\ \omega_0 - xw_0$ is about $0{\cdot}7w$ number below $\Delta_2\nu\,(1-0)$ at $K = 0$, $\Delta_2\,\nu\,(1-0)$ at $K = 1$ is about $3w$ numbers and at $K = 2$ about $10w$ numbers lower than this. These figures give a fair idea of the effect of K on the corresponding differences for the other states, apart from effects due to perturbations which seem rather common in $s\Sigma$ levels.

TABLE XIII—PROPERTIES OF VARIOUS $s\Sigma$ STATES

	$2s\,^3\Sigma$	$3s\,^3\Sigma$	^3A	^1X	$3\,^1O$	$4\,^1O$	$1s\sigma\,^2\Sigma$
Rydberg denominator	1·9333	2·94	3·943	2·18	3·07	3·95	∞
ν_0, below $1s\sigma\,^2\Sigma$......	29343	12645	7055	23055	11613	691_5	0
$\Delta_1\,\nu$, 1−0 interval at K = 2	2514·55	2261·97*	2225	2051·6†	2260	unknown	2173‡
Δ_1, ν, 2−1 interval, at K = 2	2378·80	2135·03*	2111	1809·7†	2062	,,	
Next difference $\Delta_2\nu$	135·75	126·94*	114	241·9†	198	,,	124§
$2B_0$	66·77	*ca.* $60{\cdot}_0$	*ca.* 58·2	?	59	*ca.* 60	58·2
Lowest K level and symmetry (*a* or *s*)	K = 0 (*s*)	K = 0 (*s*)	K = 0 (*a*) or K = 1 (*s*)	K = 0 (*s*)	K = 0 (*s*)	K = 0 (*s*)	

* Average of K = 1 and K = 3 intervals.

† K = 1 intervals (they may not be correct).

‡ Value of $\omega_0 - x\omega_0$.

§ Value of $2xw_0$.

[||] " Molecular Hydrogen and its Spectrum," pp. 302, 310 ff.

[¶] Some are mentioned in " Molecular Hydrogen and its Spectrum," pp. 153, 250, etc.

If we keep first to the triplet states we see that all the *numbers* in Table XIII point to $2s\,^3\Sigma$, $3s\,^3\Sigma$ and ^{3}A as being members of a series of which $1s\sigma\,^2\Sigma$ is the end. $\Delta_2\nu$ for ^{3}A looks rather low, but this might be due to small perturbations which seem to be present in some of the vibrational levels concerned. Anyhow it is not a very significant "constant." The values for ^{1}X, 3^1 O and 4^1 O are approaching those for $1s\sigma\,^2\Sigma$ in a different way, discussed in "Molecular Hydrogen and its Spectrum," p. 311. They are all states with some unusual features and ^{1}X is certainly very different from its opposite number in the triplet system, the very regular state $2s\,^3\Sigma$. We expect, however, that such differences between singlets and triplets will diminish with increasing principal quantum number n as both the singlet and triplet series terminate at the ion $1s\sigma\,^2\Sigma$. This is seen to be the case and at ^{3}A and 4^1 O the Rydberg denominators and the B_0's are almost identical. But there is something still more remarkable. Out of some sixty known electronic states of H_2, 4^1 O is the only one which had a rotational structure like that of ^{3}A.

So far, this looks like an overwhelming case for the identification of ^{3}A with $1s\sigma\,4s\sigma\,^3\Sigma_g$ but it is at once shattered when we look at the lowest row of Table XIII. This shows that the strong (a) levels are those with K even ; so that it has the wrong symmetry for an even Σ state. However, this may not be a miracle, after all ; although it has not hitherto been found in the H_2 spectrum. Let us reconsider the necessities of the case without paying too much attention to what we know already about the spectrum empirically.

In the first place ^{3}A must be an even level since it goes down to $1s\sigma\,2p\,^3\Pi$ which undoubtedly is an odd level. This means that the wave functions of the whole molecule ^{3}A must be even. Now these wave functions are products of a considerable number of factors of which the nuclear spin wave functions are one. Whether the strong (a) levels are those for K even or for K odd depends entirely on whether the nuclear wave functions are symmetric or anti-symmetric for the levels with odd K. If the a and s levels became interchanged without change in the symmetry of the wave functions of the whole molecule it means that the symmetry of the nuclear spin functions must have changed. The miracle that must happen then if ^{3}A is to be identified with an even Σ state like $1s\sigma\,4s\sigma\,^3\Sigma$ is that the nuclear spin functions of this state must have the opposite symmetry to what they have in all other known even Σ states of H_2. These include, at least, the following : $1s\sigma\,1s\sigma\,^1\Sigma$ (ground state), ^{1}X (? $1s\sigma\,2s\sigma\,^1\Sigma$), 3^1 O (? $1s\sigma\,3s\sigma\,^1\Sigma$), 4^1 O (? $1s\sigma\,4s\sigma\,^1\Sigma$), $1s\sigma\,3d\sigma\,^1\Sigma$, 3^1 K (? $2p\sigma\,2p\sigma\,^1\Sigma$), ^{1}L, ^{1}M (? $2p\pi\,2p\pi\,^1\Sigma$), ^{1}N (? $2p\sigma\,3p\sigma\,^1\Sigma$), 4^1 K (? $2p\sigma\,4p\sigma\,^1\Sigma$), $1s\sigma\,2s\sigma\,^3\Sigma$, $1s\sigma\,3s\sigma\,^3\Sigma$, $1s\sigma\,3d\sigma\,^3\Sigma$. $1s\sigma\,4d\sigma\,^3\Sigma$. While, so far as we are aware, there is nothing which makes such a state of affairs impossible, the fact that it is a unique occurrence makes it very desirable to search carefully for the possibility of interpreting ${}^3A$ as some kind of an even Π state. Since Π states, which are double, have in general both types of nuclear spin functions, success in this would, of course, remove the difficulty.

As has been pointed out in § 3 there is no possible even ${}^3\Pi$ state with a single excited electron which could have a Rydberg denominator as low as that of ${}^3A$. Such even ${}^3\Pi$ states are $1s\sigma\, 3d\ {}^3\Pi_{ab}$ and $1s\sigma\, 4d\ {}^3\Pi_{ab}$. These states are both well known and are different from ${}^3A$. The deepest even ${}^3\Pi$ states available are thus $1s\sigma\, 5d\pi\, {}^3\Pi_{ab}$ and $1s\sigma\, 5g\pi\, {}^3\Pi_{ab}$. It seems impossible that either of these could have a denominator so far from 5 as that of ${}^3A$. This is certainly true so far as $1s\sigma\, 5d\pi\, {}^3\Pi_{ab}$ is concerned, because the state $1s\sigma\, 4d\pi\, {}^3\Pi_{ab}$ has a denominator almost identical with that of ${}^3A$, and as the state $1s\sigma\, 3d\pi\, {}^3\Pi_{ab}$ has a denominator 1 lower than that of $1s\sigma\, 4d\pi\, {}^3\Pi_{ab}$ that of the next member of the series $1s\sigma\, nd\pi\, {}^3\Pi_{ab}$, at $n = 5$, must be very close to 1 higher than that of ${}^3A$. We shall see in a moment that the state ${}^3G$ is almost certainly either $1s\sigma\, 5d\sigma\, {}^3\Sigma$ or $1s\sigma\, 5g\pi\, {}^3\Pi_a$ and that ${}^3C$ is probably either $1s\sigma\, 5d\delta\, {}^3\Delta_b$ or, possibly, $1s\sigma\, 5d\pi\, {}^3\Pi_b$. We shall show in Part III that a new state called ${}^3F$ is undoubtedly the odd state $1s\sigma\, 5f\sigma\, {}^3\Sigma$. Every one of these states has a denominator very close to 5. All this makes it practically impossible that $1s\sigma\, 5g\pi\, {}^3\Pi$ can have a denominator less than 4. Similar arguments would apply with even greater force against the identification of ${}^3A$ with any possible state having $n > 5$. We are thus driven to the conclusion that ${}^3A$ cannot be any even ${}^3\Pi$ state with a single excited electron.

The next alternative is to suppose that ${}^3A$ is some kind of an abnormal state like the singlet states $3\,{}^1K$, ${}^1L$, ${}^1M$, ${}^1N$, etc. What we can then say about it depends on the attitude we adopt in regard to such states generally. A possible attitude is to say that they lie outside the scope of the present development of molecular theory. From that standpoint there is nothing more to be said. Such states might have almost any properties. In effect we are just adding an inconvenient triplet state to a collection of inexplicable states which happen to be well developed in the singlet spectrum.

The other attitude is to suppose that these abnormal states are states with both electrons excited. Reasons have been given* which make this rather plausible for the singlet states. On this view ${}^3A$ might be $2p\sigma\, np\pi\ {}^3\Pi_g$, $n = 4$ or 3. We shall see, however, that there is a stronger case for identifying ^{3}B with $2p\sigma\, np\pi\, {}^3\Pi_g$, $n = 5$ or 4 and the properties of ^{3}A and ^{3}B are so different that they can hardly be members of the same spectral series. There does not seem to be any other possibility for ^{3}A from this standpoint. It is therefore unlikely that ^{3}A is a state with two excited electrons.

---

* *Cf.* " Molecular Hydrogen and its Spectrum," chap. X.

Another possibility is that the $^3\mathrm{A} \rightarrow 2p\, {}^3\Pi$ system is just a collection of accidental coincidences. There is, however, so much of it and so much coherence about it that the odds against this must be very heavy. It might, of course, be a jumble of parts of more than one system. Such things have been found before and will no doubt be found again in the working out of this very complex spectrum. It does not, however, look to be a system which has gone wrong for that reason.

In order to form a judgment about the remaining states we have collected the leading properties of ^{3}A, ^{3}B, ^{3}C and ^{3}G in Table XIV. The case of ^{3}G has already been considered at some length in § 2 where we saw that it had the properties which we might reasonably anticipate for $1s\sigma\, 5d\sigma\, {}^3\Sigma_g$ or $1s\sigma\, 5g\sigma\, {}^3\Sigma_g$. The properties of the state $1s\sigma\, 5f\sigma\, {}^3\Sigma_u$ which we have now discovered (*cf.* Part III) throw some light on this question. This state which we call ^{3}F is more inverted than ^{3}G. Now when we consider typical states of the types $ns\, {}^3\Sigma$, $np\, {}^3\Sigma$, $nd\, {}^3\Sigma$, $nf\, {}^3\Sigma$ it appears that as 1 increases there is a general tendency for the rotational structure to become more irregular and for the lowest levels to become more inverted (as, in fact, one would expect from the general theory of uncoupling). Thus $1s\sigma\, 5g\sigma\, {}^3\Sigma$ should be more inverted than $1s\sigma\, 5f\sigma\, {}^3\Sigma$ and not less so. The rotational structure of ^{3}G is about what one might expect for $1s\sigma\, 5g\pi\, {}^3\Pi_a$ which is a possible interpretation of this experimental state if the P′ 1 lines do not belong to the bands. The existence of the state ^{3}C favours $1s\sigma\, 5g\pi\, {}^3\Pi_a$ as the more likely choice of these two for ^{3}G. On the face of it ^{3}C is an even $^3\Delta_b$ state with a rotational structure

TABLE XIV—PROPERTIES OF ^{3}A, ^{3}B, ^{3}C AND ^{3}G STATES

	^{3}A	^{3}B	^{3}C	^{3}G	$1s\sigma\, {}^2\Sigma$
Rydberg denominator	3·943	*ca.* 4·64	*ca.* 4·93	5·01	∞
ν_e, below $1s\sigma\, {}^2\Sigma$	7055	*ca.* 5114	*ca.* 4620	*ca.* 4302	0
$\Delta_1 \nu\,(1-0)$ interval, at K = 1	2225*	1417·68	unknown	2172·55	2173†
$2B_0$	58·2	*ca.* 60 ?	*ca.* 60	*ca.* 60	58·2
Lowest rotational level and symmetry (*s* or *a*)	K = 1 (*s*) or K = 0 (*a*)	K = 1 (*s*)	K = 2 (*a*)	K = 0 (*s*) ?	

* Interval K = 2.

† Value of $\omega_0 - x\omega_0$.

quite like that of the states $1s\sigma\, 4d\delta\, ^{1,3}\Delta_b$. It might, however, be a Π_b state with the lowest weak (s) $K = 1$ level undiscovered. It has every appearance of being a state with a single excited electron at principal quantum number 5. There are four possibilities here, namely, $1s\sigma\, 5d\delta\, ^3\Delta_b$ $1s\sigma\, 5g\delta\, ^3\Delta_b$, $1s\sigma\, 5d\pi\, ^3\Pi_b$ and $1s\sigma\, 5g\pi\, ^3\Pi_b$. However, in the four Σ, Π, Δ complexes which have previously been found in the H_2 spectrum the Σ state is always lowest and the Δ state highest. As the state ^3G lies higher than ^3C this would lead us to interpret it as $1s\sigma\, 5g\pi\, ^3\Pi_a$ and ^3C as $1s\sigma\, 5d\delta\, ^3\Delta_{bg}$ or, possibly, $1s\sigma\, 5d\pi\, ^3\Pi_{bg}$. However, the Rydberg denominator of ^3G is about right for $1s\sigma\, 5d\sigma\, ^3\Sigma$ in comparison with that of $1s\sigma\, 5f\sigma\, ^3\Sigma$ which is against this interpretation of ^3G as a $5g\, ^3\Pi_a$ state.

The whole question is quite difficult and it seems impossible to settle it definitely until more band systems in this region have been discovered. On the whole we are inclined to think that ^3G is $1s\sigma 5d\sigma ^3\Sigma$ and ^3C is $1s\sigma\, 5d\pi\, ^3\Pi_b$ although the denominator of ^3C is below that of ^3G. In the nd^3 complexes the (perturbed) denominator of Π_b is well above that of Σ at $n = 3$ but at $n = 4$ they are much closer together so that the trend indicates the possibility of a lower value for Π_b than for Σ at $n = 5$.

We now come to ^3B. The low $\Delta_1\, v$ interval at so high a denominator makes it unlikely that this is a state belonging to a series which terminates with the ion $1s\sigma\, ^2\Sigma$. This is also confirmed by the fact that the denominator is so far removed from an integer. The rotational structure also is not very like that of the Π_b levels of any of the known Σ, Π, Δ complexes. As a matter of fact the known H_2 state with the closest resemblance in vibrational and rotational structure to that of ^3B is the singlet state ^1Q. We have recently found the $v' = 0$ progression of $^1Q \rightarrow 2p\, ^1\Sigma$ and the progression originally given by Richardson and Davidson* now turns out to be the $v' = 1$ progression of this system. The new progression shows that the vibrational intervals of ^1Q are very low, about 730. The Rydberg denominator of ^1Q is about 2·86. It has been suggested by one of us that this state may be $2p\sigma\, 2p\pi\, ^1\Pi_g$. If ^3B is to be a $2p\sigma\, np\pi\, ^3\Pi$ state it would seem that n must be at least 4 as the denominator of ^3B is nearly two units higher than that of ^1Q and, in the states with one excited electron at any rate, triplet states are always deeper than the corresponding singlet states.

Much of the force of this argument about ^3B depends on the correctness of the $v' = 1$ progression which, as we have pointed out, has some doubtful elements in it. The $v' = 0$ progression alone might be interpreted as having the upper state $1s\sigma\, 5d\pi\, ^3\Pi_b$ but its denominator seems low for this. However, owing to the uncoupling perturbations the ν_e's of ^{3}B, ^{3}C and ^{3}G can only be estimated approximately and at such small values of ν_e the errors thus introduced may be affecting the denominators seriously.

---

* 'Proc. Roy. Soc.,' A, vol. 124, p. 69 (1929).

SUMMARY

This paper describes four new band systems which go down to the lowest triplet state $2p\,^3\Pi$ of H_2 from four hitherto undiscovered upper triplet states. These are called provisionally ^{3}A, ^{3}B, ^{3}C and ^{3}G. The constants and properties of the upper states are worked out and the possible electronic configurations considered. It seems fairly certain that ^{3}G is either $1s\sigma\, 5d\sigma\, ^3\Sigma_g$ or $1s\sigma\, 5g\pi\, ^3\Pi_a$ and ^{3}C $1s\sigma\, 5d\delta\, ^3\Delta_b$ or $1s\sigma\, 5d\pi\, ^3\Pi_b$. ^{3}B is probably an "abnormal" state of the type of ^{1}Q in the singlet systems. The interpretation of ^{3}A presents some difficulties which are discussed.

The Spectrum of H_2

Part III—New Bands and Band Systems ending on $2s\,^3\Sigma$ and an Extension of the Singlet System $^1Q \rightarrow 2p\,^1\Sigma$

By O. W. RICHARDSON, F.R.S., Yarrow Research Professor of the Royal
Society, and T. B. RYMER, B.A., King's College, London

(*Received July* 26, 1934)

§ 1—INTRODUCTION

In this paper we describe three new band systems ending on the lowest even triplet state $2s\,^3\Sigma$ of H_2 and coming from three hitherto undiscovered states which we call provisionally ^{3}D, ^{3}E, and ^{3}F. The main bands, which are all weak, lie in the yellow, blue, and violet respectively. We have found more of the system belonging to the isolated yellow band of Richardson and Das. This band ended on the $v'' = 1$ level of $2s\,^3\Sigma_g$. We now describe two other bands coming from the same electronic state at different vibrational levels and ending on $2s\,^3\Sigma$ at $v'' = 0$ and $v'' = 2$ respectively. All these band systems are of the type which consists practically of a sequence of bands along the diagonal axis. In addition, we describe the $v' = 0$ progression of the singlet system

${}^1Q \rightarrow 2p\,{}^1\Sigma$ of which Richardson and Davidson found only a single progression which now turns out to be the $v' = 1$ progression.

§ 2—A SYSTEM WHICH INCLUDES THE "YELLOW BAND"

The beginning of this system was published by Richardson and Das* in 1929 as "A New Band in the Yellow." A small change in it was subsequently proposed by Richardson† who suggested that it was a $1' \rightarrow 1''$ band and that the upper level might possibly be $1s\sigma\,4f\sigma\,{}^3\Sigma_u$ or $1s\sigma\,4f\pi\,{}^3\Pi_b$. The first of these alternatives is now excluded because we shall describe what we believe, on various grounds, to be the $4f\,{}^3\Sigma_u \rightarrow 2s\,{}^3\Sigma$ system in § 4. The known final rotational intervals of the Yellow Band show that its final level is the $v = 1$ level of $2s\,{}^3\Sigma$, so that it is a $v' \rightarrow 1''$ band of some system with the even $2s\,{}^3\Sigma$ state as the final electronic state. We have now found the $(v-1)' \rightarrow 0''$ and the $(v+1)' \rightarrow 2''$ bands of the same system and we find that there are no lines with any strength belonging to the bands of the system which lie off the axis of this sequence. We think that this is sufficient to establish it as a diagonal sequence on two grounds either of which would be adequate. In the first place band systems consisting of a single non-diagonal sequence do not exist, although systems which consist of practically nothing except a single line of bands strung along the diagonal axis are quite common in the H_2 spectrum. In the second place the existence of a band system consisting of a single sequence of bands off the diagonal axis would violate the general principles which govern the distribution of intensity in band systems. We conclude, therefore, that the old Yellow Band is a $1' \rightarrow 1''$ band and that the two new bands of the system we have found are the $0' \rightarrow 0''$ band and the $2' \rightarrow 2''$ band respectively.

The lines are set out, in the same form as that used formerly,‡ in Table I. As will be seen practically the whole of the strength is in the old $1 \rightarrow 1$ band. This was to be expected, as there is no group of unclassified lines left anywhere in the spectrum with the aggregate strength of those in this band. The poor combinations in the $0 \rightarrow 0$ band are probably adequately accounted for by the interferences with lines of other systems. The fact that R1 and P3 of the $0 \rightarrow 0$ band are He++ lines is a satisfactory feature as such lines are practically confined to the $0 \rightarrow 0$ bands in systems of this type. As may be seen from the well-developed

---

* 'Proc. Roy. Soc.,' A, vol. 125, p. 328 (1929).

† "Molecular Hydrogen and its Spectrum," p. 193.

‡ Richardson and Rymer, 'Proc. Roy. Soc.,' A, vol. 147, p. 24 (1934), referred to in this paper as Part I.

$1 \rightarrow 1$ band the R branch is stronger than the P branch, Q branches being necessarily absent if the upper state is a single state going down to the single state $2s\,{}^3\Sigma_g$.

TABLE I—LINES OF THE YELLOW BAND SYSTEM

The $0 \rightarrow 0$ *band.*		
∧	R0	17918·43 1G C++, also $1 \rightarrow 1$, ${}^3D \rightarrow 2s\,{}^3\Sigma$, R0.
0·15		
∨	P2	17719·08 1G 2·3K, also $0 \rightarrow 4$, $3\,{}^1O \rightarrow 2p\,{}^1\Sigma$, P4.
∧	R1	17949·95 2G 2·5K C+ He++, also ?$2 \rightarrow 1$, $3p\,{}^3\Pi_b \rightarrow 2s\,{}^3\Sigma$, P6.
0·07		
∨	P3	17619·11 1G 10·5K C++ He++
∧	R2	17981·37 0G
0·16		
∨	P4	17522·10 0G
The $1 \rightarrow 1$ *band*		
∧	R0	17778·92 4G 14·2 K, also ?$1 \rightarrow 0$, ${}^1N \rightarrow 2p\,{}^1\Pi$, Q3
0·01		
∨	P2	17589·17 3G 19·4K
∧	R1	17812·31 10G 57·8K L+
0·05		
∨	P3	17497·72 5G 33·5K
∧	R2	17837·29 3G 14·1K
0·10		
∨	P4	17400·48 1G
The $1 \rightarrow 1$ *band*—(continued)		
∧	R3	17866·95 0G
0·02		
∨	P5	17311·08 9G 37·0K L++ C++ also Q2 of $1 \rightarrow 1$, $3d\,{}^3\Delta_b \rightarrow 2p\,{}^3\Pi$
The $2 \rightarrow 2$ *band*		
∧	R0	17563·36 1*a*G 3·0K, also $2 \rightarrow 2$, ${}^3D \rightarrow 2s\,{}^3\Sigma$, R0
0·06		
∨	P2	17383·06 1G, also $2 \rightarrow 2$, ${}^3D \rightarrow 2s\,{}^3\Sigma$, P2
∧	R1	17594·32 0G
0·06		
∨	P3	17295·44 0G, also $0 \rightarrow 3$, ${}^1Q \rightarrow 2p\,{}^1\Sigma$, P3
∧	R2	17628·90 4G 13·0K, also $4 \rightarrow 3$, $3p\,{}^3\Pi_a \rightarrow 2s\,{}^3\Sigma$, Q3
0·05		
∨	P4	17213·82 0G C++, also $0 \rightarrow 0$, $3d\,{}^3\Delta_b \rightarrow 2p\,{}^3\Pi$, P′6 and $2 \rightarrow 2$, ${}^3D \rightarrow 2s\,{}^3\Sigma$, P3
∧	R3	17671·44 1G
0·11		
∨	P5	17143·53 0G C++

The rotational structure of the upper state at each of the vibrational levels $v' = 0$, 1, and 2 is shown in Table II. The intervals are extracted in the usual way from the line differences by making use of the accurately known and well-established rotational intervals of the final state $2s\,{}^3\Sigma$. This is a very regular state* and is single, so that the results can be given without the ambiguity which arises from the unknown doublet distance in the lowest final levels in the case of the upper states of systems which end on close double states like $2p\,{}^3\Pi_{ab}$. It is clear from Table II that the upper state has an irregular structure and is strongly uncoupled or perturbed. On the face of it, it is a Π_b state† as there is no convincing evidence of the existence of the K = 0 level. However, it would be difficult to be sure of the presence or absence of P1 lines with such an irregular rotational structure with the additional drawback of no possibility of confirmation by combinations with lines of bands off the diagonal axis ; so that the possibility of its being a Σ level could hardly be rejected on these grounds alone. We shall defer the further consideration of this question until the properties of another system in the same region of the spectrum have been considered in § 3.

---

* *Cf.* Richardson and Das, 'Proc. Roy. Soc.,' A, vol. 122, p. 688 (1929).

† So far as we are aware there is no clear statement in the literature as to when it is appropriate to use the symbol *b* rather than *a* in dealing with the components of double states like Π_{ab}, Δ_{ab}, etc. The convention always employed in papers on the

TABLE II—ROTATIONAL STRUCTURE OF UPPER STATE OF YELLOW BAND SYSTEM

At → K ↓	$\nu = 0$	$\nu = 1$	$\nu = 2$
4*a*		———	———
		217·89	221·44
3*s*	············	→ 66·49	············ → 66·83
	164·43	151·40	154·61
2*a*	——— → 66·33	——— → 54·60	——— → 63·41
	98·10	96·80	91·20
1*s*	············	············	············

The initial vibrational intervals got from equations of the type

$$\Delta\nu'(\mathrm{K}) = \Delta\nu''(\mathrm{K}+1) + \mathrm{P}(\mathrm{K}+1)(\overline{\nu+1} \rightarrow \overline{\nu+1}) - \mathrm{P}(\mathrm{K}+1)(\nu \rightarrow \nu),$$

and the known vibrational intervals $\Delta\nu''(\mathrm{K}+1)$ of $2s\,{}^3\Sigma$ are set out in Table III. The $1' - 0'$ intervals look rather high compared with $2' - 1'$ in comparison with most other H_2 systems. The security of

TABLE III—VIBRATIONAL INTERVALS OF UPPER STATE OF YELLOW BAND SYSTEM

$\Delta\nu$ ↓	K = 1	K = 2	K = 3	K = 4
1 – 0	2384·73	2383·45	2370·44	
2 – 1	2172·70	2167·13	2170·41	2173·99

H_2 spectrum is to use the symbol *b* for states for which the strong (*a*) levels have K even. This makes, for example, $\Pi_b \rightarrow \Sigma_g$ systems have bands with P and R branches only and $\Pi_b \rightarrow \Sigma_u$ systems Q branches only. It is, of course, the other way round with Π_a, Δ_a, etc. Whether this convention is the best one from a theoretical standpoint is open to question. Much could be said in favour of defining Π_b so that it had strong (*a*) levels for K even with even states and for K odd with odd states. Π_a, Δ_a, etc., would then always have the same type of symmetry in the rotational structure as the associated Σ state of any given complex. With this definition all ${}_b\Pi$, Δ_b, etc. $\rightarrow \Sigma_g$ or ${}_u$ systems would have Q branches only and all Π_a, Δ_a, etc. $\rightarrow \Sigma_g$ or ^{u} systems P and R branches only. However, as the system in vogue seems to have become established we shall continue to use it.

TABLE IV—THE LINES OF $^3\mathrm{D} \rightarrow 2s\,^3\Sigma$

The 0 → 0 *band*

?P1 18209·34 1G 2·8K

∧ R0 18229·78 1G
0·03
∨ P2 18030·31 0G 2·6K

∧ R1 18184·35 2G 3·2K
0·20
∨ P3 17853·78 1G 2·7K

∧ R2 18145·52 0*a*G
0·09
∨ P4 17686·18 0G, probably He+

∧ R3 (18116·24) mixed with 18115·94 8G 25·1K 3 → 2, $3p\,^3\Pi_b \rightarrow 2s\,^3\Sigma$, R0
0
∨ P5 17531·60 1G

The 0 → 2 *band*

R0 13317·3 3G, also ? 1 → 0, $^1\mathrm{X} \rightarrow 2p\,^1\Sigma$, P1, defect 0·1

The 1 → 0 *band*

P1 20426·30 (*r*) Tanaka, defect 0·22
P4 19873·74 9G 41·5K, also 0 → 4, $^1\mathrm{N} \rightarrow 2p\,^1\Sigma$, R0, defect 0·08
P5 19690·44 1G 7·8K, also 2 → 5, $3d\,^1\Sigma \rightarrow 2p\,^1\Sigma$, P1 defect 0·08

The 1 → 1 *band*

? P1 17905·45 0*a*G 2·1K

∧ R0 17918·43 1G C++, also 0 → 0, $^3\mathrm{Y} \rightarrow 2s\,^3\Sigma$, R0
0·13
∨ P2 17728·82 1G, also 0 → 3, $3d^1\Sigma \rightarrow 2p\,^1\Sigma$, P1

∧ R1 17867·99 0G C++
0·02
∨ P3 17553·43 1G C++

R2 (17818·73) *ab*
P4 17381·82 1G

∧ R3 17769·98 1G 2·9K
0·10
∨ P5 17214·23 0U G C++

The 1 → 3 *band*

R3 13162·9 00G, defect 0·1

The 2 → 0 *band*

∧ R0 22476·06 6G 4F 28·3K, also 0 → 0, $4d\,^3\Sigma \rightarrow 2p\,^3\Pi$, Q1, defect 0·12
0·23
∨ P2 22276·33 4G 5F 36·2K, also 2 → 4, $^1\mathrm{M} \rightarrow 2p\,^1\Sigma$, P3, defect 0·08

P3 22088·00 *ab*G 00F, defect 0·08
R2 22357·05 1G UF, also 0 → 0, $4d\,^3\Sigma \rightarrow 2p\,^3\Pi$, Q′ 2 and 0 → 0, $4d\,^3\Pi_b \rightarrow 2p\,^3\Pi$, P3, defect 0·11

The 2 → 1 *band*

P4 19405·75 (*rd*^{2}) Deodhar, defect 0·13
R3 19785·84 0G, defect 0·08

The 2 → 2 *band*

? P1 17555·59 0G

∧ R0 17563·36 1*a*G 3·0K, also 2 → 2, R0 of Yellow Band System
0·06
∨ P2 17383·06 1G, also 2 → 2, P2 of Yellow Band System

∧ R1 17512·41* 2G, C++
0·23
∨ P3 17213·82 0UG C++, also 0 → 0, $3d\,^3\Delta_b \rightarrow 2p\,^3\Pi$, P′ 6 and 2 → 2, $^3\mathrm{Y} \rightarrow 2s\,^3\Sigma$, P4

R2 17463·59 0G C++
P4 (17048·56) *ab*

∧ R3 17416·51 3G C+, also 2 → 2, $3d\,^3\Delta_b \rightarrow 2p\,^3\Pi$, R3
0·06
∨ P5 16888·55 0G

The 2 → 3 *band*

R2 15216·62 0*a*G, also 2 → 0, $3p\,^3\Sigma \rightarrow 2s\,^3\Sigma$, P4, defect 0·06

The 2 → 4 *band*

R0 13180·3 1G, also 1 → 1, $3d^1\Delta_a \rightarrow 2p\,^1\Pi$, Q3, defect 0·1 the 0 → 0 band is not as good as that of either the 1 → 1 band or the 2 → 2 band, but there do not appear to be any lines available which would give a more normal set of values for the 1′ — 0′ intervals.

---

* The wave number of this line is printed erroneously as 17512·71 in Gale, Monk, and Lee's Tables.

To determine the electronic frequency ν_0 of the system we may use the R0 line 17918·43 of the 0 → 0 band. F″ (0) is 8·35 and F′ (1) about 21 wave numbers. ν_0 is therefore about 17906 and the system lies about 11437 wave numbers below $1s\sigma\,{}^2\Sigma$, the ground state of the molecular ion. This corresponds to a Rydberg denominator 3·097. Even if the 0 → 0 band were wrong these figures would not be changed very much.

§ 3—THE SYSTEM ${}^3D \rightarrow 2s\,{}^3\Sigma$

This is a weak system, also with pronounced uncoupling, which lies in the same region as the one just described. The lines are set out in Table IV. Any strength there may be lies in three bands all on the diagonal axis at 0 → 0, 1 → 1, and 2 → 2. In the 2 → 2 band the R0 P2 lines are the same pair as those which occupy the same position in the 2 → 2 band of the Yellow System. However, the rotational structure of the upper state of the present system shows that the lines must be quite close to their assigned position and the fact that the R0 line is marked *a* by Gale, Monk, and Lee* is an indication that it is probably two lines.

TABLE V—ROTATIONAL STRUCTURE OF ${}^3D$

K ↓	$v = 0$		$v = 1$		$v = 2$	
4*a*						
	168·69		139·59		131·77	
3*s*		→ 74·68		→ 62·51		→ 60·69
	94·01		77·08		71·08	
2*a*		→ 72·66		→ 64·16		→ 61·64
	21·35		12·92		9·44	
1*s*		→ 67·55 (?)		→ 63·23 (?)		→ 61·97 (?) or 59·81 (?)
	−46·20 (?)		−50·31 (?)		−52·53 (?) or 50·37 (?)	
? 0*a*						

The rotational structure of the upper state is set out in Table V. There are no combinations to support the K = 0 levels at $v = 0$ and $v = 2$, but there happen to be unclassified lines, of which there are now few left in these parts of the spectrum, in Gale, Monk, and Lee's tables which continue the general rotational structure given by the other levels. The vibrational quantum numbers are settled by essentially the same arguments as those for the Yellow Band System ; there seems to be no need to repeat them. A possible variation in the $0 \rightarrow 0$ band would be to make P4 and P5 absent (the P lines seem to be weaker than the R lines at the two lower rotational levels) and to change R2 to 18140·90 (1) G also $1 \rightarrow 4$, ${}^3F \rightarrow 2s\,{}^3\Sigma$, R2 and R3 to 18097·31 (1) G 8·2 K. This would change the two upper rotational intervals at $v = 0$ to $K'(3) - K'(2) = 89{\cdot}38$ and $K'(4) - K'(3) = 154{\cdot}39$. This makes the rotational structure at $v' = 0$ closer to that at $v' = 1$ and 2. At $v' = 2$ P3 of the $1 \rightarrow 1$ band could be used as the P1 line of the $2 \rightarrow 2$ band giving for $K'(1) - K'(0)$ at $v' = 2$, $-50{\cdot}37$ instead of $-52{\cdot}53$.

---

* 'Astrophys. J.,' vol. 67, p. 89 (1928).

The vibrational intervals of the upper state, determined in the same way as for the Yellow System, are set out in Table VI. Where there are alternative values the first (upper) set correspond to the lines given in Table IV, the others to the alternative lines mentioned in the text. Here again the drop between the $1' - 0'$ and $2' - 1'$ intervals is rather unusually large, indicating an unusually large value of $x\omega_0$; but it is not so large as the corresponding drop in the upper state of the Yellow Band System. On the other hand, the intervals themselves are smaller, indicating a smaller value of ω_0, so that the factor x is not so very different for the upper states of the two systems.

TABLE VI—VIBRATIONAL INTERVALS OF ${}^3D$

Δv ↓	K = 0	K = 1	K = 2	K = 3	K = 4
1 − 0	2217·18	2213·02	2204·60	2187·70 or 2192·38	2158·67 or 2177·57
2 − 1	2035·26 or 2033·10	2033·12	2029·68	2023·73	2015·95

To determine the electronic frequency ν_0 of ${}^3D$ we have P1 of the $0 \rightarrow 0$ band $= 18209{\cdot}34$. Extrapolating $F'(0)$ as about -54 we have, since $F''(1) = 75{\cdot}01$, $\nu_0 =$ about 18338. The ${}^3D$ state thus lies about 11005 wave numbers below $1s\sigma\,{}^2\Sigma$, the ground state of the ion H_2+. This figure corresponds to a Rydberg denominator of 3·157.

It will be convenient at this stage to compare ${}^3D$ with the upper state of the Yellow System. Both states are close together on the frequency scale, ${}^3D$ being about 400 wave numbers higher, and their Rydberg denominators are a little above 3. Both exhibit marked uncoupling phenomena. Since both go down to $2s\,{}^3\Sigma_g$ they are both odd states. Apart from the reversal of the s and a symmetry for a given K due to this fact, ${}^3D$ has a rotational structure quite like that of $4d\,{}^3\Sigma_g$, and the upper state of the Yellow System one which is close to that of $4d\,{}^3\Pi_a$.* If these facts alone were to be taken into account we should assign them to a pair of odd states with a similar association to that between the two even states $4d\,{}^3\Sigma_g$ and $4d\,{}^3\Pi_a$. As their Rydberg denominators are between 3 and 3·2 it is natural to look for such a pair of states with principal quantum number $n = 3$. The only such odd triplet states with the single excited electron with $n = 3$ are $1s\sigma 3p\,\sigma\,{}^3\Sigma_u$ and $1s\sigma 3p\,\pi\,{}^3\Pi_{ab}$. These are already well known and quite different from the upper states of the systems now under consideration.

---

* *Cf.* Richardson and Davidson, 'Proc. Roy. Soc.,' A, vol. 142, p. 53 (1933).

We are thus led definitely to the conclusion that if these upper states are states with a single excited electron they must be states with $n > 3$. At $n = 4$, the odd triplet states available with one excited electron are $1s\sigma 4p\sigma\,{}^3\Sigma_u$, $1s\sigma 4p\pi\,{}^3\Pi_{ab}$, $1s\sigma 4f\sigma\,{}^3\Sigma_u$, $1s\sigma 4f\pi\,{}^3\Pi_{ab}$, $1s\sigma 4f\delta\,{}^3\Delta_{ab}$, and $1s\sigma 4f\phi\,{}^3\Phi_{ab}$. Of these $4p\,{}^3\Sigma_u$ and $4p\,{}^3\Pi_{ab}$ are well known and different from the states described here. It seems, then, that if they are states with one excited electron they should be $4f\,{}^3\Sigma_u$ and $4f\,{}^3\Pi_b$. There are, however, at least two serious objections to this classification. One is that the state which, both on the ground of its rotational structure and the presence of suitable P1 lines indicating the occurrence of the $K = 0$ level, should be the Σ level is higher than the state which on the corresponding grounds should be the Π level. Now in every securely established pair of $\Sigma\Pi$ states in the H_2 spectrum which belong to the same complex the Σ state is below the Π state. Thus $2p\,{}^1\Sigma$, $3d\,{}^1\Sigma$, $4d\,{}^1\Sigma$, $2p\,{}^3\Sigma$ (unstable state), $3p\,{}^3\Sigma$, $4p\,{}^3\Sigma$, $3d\,{}^3\Sigma$, and $4d\,{}^3\Sigma$ are each below $2p\,{}^1\Pi$, $3d\,{}^1\Pi$, $4d\,{}^1\Pi$, $2p\,{}^3\Pi$, $3p\,{}^3\Pi$, $4p\,{}^3\Pi$, $3d\,{}^3\Pi$, and $4d\,{}^3\Pi$ respectively. The other and more serious objection is the low value of the Rydberg denominators of the states. *A priori* we should expect these to be nearer 4 than 3 for $4f$ states.

The strength of these arguments is somewhat impaired by the marked perturbation of the states under consideration due to uncoupling. Nevertheless, we consider that they do constitute grave objections to classifying these states as $4f$ states. We think it more likely that they are states of abnormal type like ${}^1K$, ${}^1L$, ${}^1M$, etc., of which there are so many well-developed examples in the singlet system. This position will be strengthened by the consideration of two further systems ending on $2s\,{}^3\Sigma$ which are described in §§ 4 and 5.

§ 4—THE SYSTEM ${}^3E \rightarrow 2s\,{}^3\Sigma$

This is another weak system, in the blue region. It consists of two progressions, one ending on $v'' = 0, 1, 2,$ and 4, and the other ending on $v'' = 0, 1,$ and 2 of $2s\,{}^3\Sigma_g$. As the strength in the first progression lies in the $v'' = 0$ band and that in the second in the $v'' = 1$ band, we interpret these stronger bands as $0' \rightarrow 0''$ and $1' \rightarrow 1''$ bands respectively. This makes the system essentially a diagonal one like the two already described. There is, of course, no uncertainty in the vibrational quantum numbers of the final levels as these are settled by the known rotational and vibrational intervals of the final $2s\,{}^3\Sigma$ state. There is no reasonable alternative to the proposed initial vibrational numbering if we have found the main part of the system. It might, however, be necessary to change it in the unlikely event of there being some undiscovered part of the system lying in a relatively distant part of the spectrum.

The band lines are set out in Table VII. In contrast to the Yellow system the P branches are stronger than the R branches, in all the bands which are at all well developed. The reality of the $K = 0$ level of the upper state seems rather securely established, suitable P1 lines being found at the expected place in the $0 \rightarrow 0$, $0 \rightarrow 1$, $1 \rightarrow 1$, and $1 \rightarrow 2$ bands and these lines are confirmed by accurate combinations. The P1 line which constitutes the whole of the $1 \rightarrow 0$ band is doubtful, the combination being poor. The existence of these lines is important because they establish the upper state as a Σ state.

The rotational structure of the upper state is set out in Table VIII. The uncoupling effects are most pronounced, the extent of the inversion of the lowest rotational levels being greater than that for any state of H_2 which has hitherto been found. Thus at $v = 0$ the $K = 0$ level lies above the $K = 4$ level and the $K = 1$ level is well above the $K = 3$ level, whilst the $K = 2$ level is only a little below the $K = 3$ level. The degree of inversion is smaller, but still very striking at the $v = 1$ rotational levels. A similar tendency with increasing v is shown by the $3d\,{}^3\Sigma$* and the $4d\,{}^3\Sigma$† states.

As we have only found the $v' = 0$ and $v' = 1$ vibrational levels of the upper state we can only give the 1 — 0 vibrational intervals. These are : at $K = 0$, 2457·05 ; at $K = 1$, 2495·18 ; at $K = 2$, 2519·56 ; at $K = 3$, 2537·29 ; at $K = 4$, 2558·03. The average of these is higher than those of any previously known state of H_2 except the ground state $1s\sigma 1s\sigma\,{}^1\Sigma_g$, but they are not very different from the corresponding intervals of $2s\,{}^3\Sigma$.

Extrapolating F′ (0) as about −96 gives, from P(1) = 23228·36, ν_0 = about 23400. This makes ${}^3E$ lie about 5943 wave numbers below $1s\sigma\,{}^2\Sigma$. The Rydberg denominator corresponding to this figure is 4·296.

---

* Richardson and Davidson, 'Proc. Roy. Soc.,' A, vol. 140, p. 50 (1933).

† *Ibid.*, vol. 142, p. 53 (1933).

TABLE VII—THE LINES OF $^3E \rightarrow 2s\,^3\Sigma$

The $0 \rightarrow 0$ *band*

	? P1	23228·36 3G 00F 30·4K, also $2 \rightarrow 2$, $3\,^1K \rightarrow 2p\,^1\Sigma$, R0 and $0 \rightarrow 0$, $^1M \rightarrow 2p\,^1\Sigma$, R1
∧	R0	23170·37 *ab*G 00F
0·06		
∨	P2	22970·93 0G 00F 1·7K
∧	R1	23046·85 *ab*G 00F
0·08		
∨	P3	22716·16 0G 2F 4·2K, also $0 \rightarrow 1$, $^3F \rightarrow 2s\,^3\Sigma$, R0
∧	R2	22923·25 *ab*G 0F
0·03		
∨	P4	22463·85 0G 1F 3·2K, also $0 \rightarrow 0$, $4d\,^3\Pi_b \rightarrow 2p\,^3\Pi$, Q′ 3
∧	R3	22800·46 *ab*G 0F
0·02		
∨	P5	22215·80 1G 4F 3·5K C+

The $0 \rightarrow 1$ *band*

P1	20707·20 00G 00F, defect 0·09
R3	20295·69 0G 2·7K, also $0 \rightarrow 2$, $3\,^1O \rightarrow 2p\,^1\Sigma$, R1, defect 0·08

The $0 \rightarrow 2$ *band*

R2	18030·02 3G, also $3 \rightarrow 2$, $3d\,^3\Sigma \rightarrow 2p\,^3\Pi$, Q1, defect 0·12

The $0 \rightarrow 4$ *band*

R0	13874·6 1*c*G, defect 0·2

The $1 \rightarrow 0$ *band*

? P1	25685·20 *ab*G 00F, defect 0·21

The $1 \rightarrow 1$ *band*

	P1	23164·34 0G 0F
∧	R0	23141·25 *ab*G 00F
0·03		
∨	P2	22951·54 0*a*G 0/1F 2·0K
∧	R1	23045·38 *ab*G 00F
0·02		
∨	P3	22730·82 1G 2F 4·1K
∧	R2	22946·03 *ab*G 0/1F
0·02		
∨	P4	22509·10 2G 2F 8·6K, also $1 \rightarrow 1$, $3d\,^1\Sigma \rightarrow 2p\,^1\Sigma$, R0
∧	R3	22853·62 *ab*G 0F
0·05		
∨	P5	22297·72 1G 2F 2·3K
∧	R4	? 22763·69 1G 3F 7·3K, also $1 \rightarrow 1$, $3d\,^1\Sigma \rightarrow 2p\,^1\Sigma$, R0 *
?		
∨	P6	22092·40 0*a*G 1F *

The $1 \rightarrow 2$ *band*

	P1	20779·28 0G 0/1F, defect 0·06
∧	R0	? 20752·77 *ab*G 0F, defect 0·22
0·09		
∨	P2	20572·62 *ab*G 00F, defect 0·12
	P3	[20361·2] *ab*G Tanaka [ ], defect 0·2
	P4	20151·83 2G 15·0K, also $0 \rightarrow 2$, $3\,^1O \rightarrow 2p\,^1\Sigma$, P4, defect 0·21
	P5	19956·05 1G 9·2K L+, defect 0·04

* This final interval is uncertain.

TABLE VIII—ROTATIONAL STRUCTURE OF ^3E

K ↓	$v = 0$
4*a*	———
	75·20
3*s*	··········→65·93
	9·27
2*a*	———→66·09
	−56·82
1*s*	··········→67·78
	−124·60
0*a*	———

K ↓	$v = 1$
5*s*	
	158·02
4*a*	———→62·15
	95·87
3*s*	··········→68·88
	26·99
2*a*	———→59·46
	−32·47
1*s*	··········→54·01
	−86·48
0*a*	———

We shall postpone the further consideration of this state until the next system has been described.

§ 5—THE SYSTEM ^{3}F → 2*s* $^3\Sigma$

This is another weak system in the near ultra-violet in many respects similar to the last. We have found it at three initial vibrational levels which we identify as $v' = 0$, 1, and 2 mainly on the ground that this puts what strength there is along the diagonal axis, as in the preceding systems. The 1 → 1 and 2 → 2 bands show a tendency to be depressed in Finkelnburg's type of discharge as compared with Gale, Monk, and Lee's. There are five lines which are given by Gale, Monk, and Lee and which are absent from Finkelnburg's tables. Of these, three are strong enough to have been measured by Kapuscinski and Eymers. This represents an unusually large proportion of such lines. In fact, there are very few lines in Kapuscinski and Eymers' tables which are now unclassified. The fact that there are so many of their lines in the bands is definite evidence that they are genuine.

Another feature of these bands is that there is no clear indication of the usual tendency to enhancement in Finkelnburg's high temperature source, as compared with Gale, Monk, and Lee's, as the rotational quantum number of the band lines increases. A little consideration shows that this property is not surprising. Owing to the inversion of the lower rotational levels of the upper state, the whole of the levels of this state at a given vibrational quantum number are confined within a range of about 200 wave numbers ; so that the Boltzmann exp. $- E/kT$ factor cannot have much effect.

The lines are set out in Table IX. In the 0 → 0 and 2 → 2 bands the P1 lines are queried. Owing to the irregularity of the rotational structure it is impossible to say exactly where these lines should be, but it is unlikely that they are absent. There are, in fact, several unclassified lines which might be the P1 line of the 2 → 2 band, but the one chosen seems the most likely. There is a poor combination in the 2 → 2 band at the $K' = 4$ level, R3 − P5 having a defect of 0·29 compared with the standard value of this final difference. It is probable that one or both of these lines are blends. In the case of P5 this is supported by the fact that Finkelnburg's wave number for the line differs by 0·51 from Gale, Monk, and Lee's, and in a direction consistent with the fact that the lines of this band tend to be weakened under Finkelnburg's discharge conditions.

The rotational structure of the upper state is shown in Table X. It is of very similar type to that of ^{3}E. The inversion of the lower rotational

TABLE IX—THE LINES OF $^3F \rightarrow 2s\,^3\Sigma$

The 0 → 0 *band*

	? P1	25276·14	1G 2F 10·6K, also 1 → 1, $^1N \rightarrow 2p\,^1\Sigma$, P5
∧	R0	25240·38	1G 0/1F
0·03			
∨	P2	25040·91	*ab*G 4F
∧	R1	25126·97	1G 3F 9·6K, also 0 → 0, $^3G \rightarrow 2p\,^3\Pi$, R2
0·12			
∨	P3	24796·08	3G 1F 9·8K, also 0 → 0, $^3C \rightarrow 2p\,^3\Pi$, P5
∧	R2	25007·02	*ab*G 0F
0·15			
∨	P4	24547·74	0G 0F
∧	R3	24878·55	0G 1F, also 1 → 1, $^3G \rightarrow 2p\,^3\Pi$, R′3
0·08			
∨	P5	24293·83	*ab*G 0F

The 0 → 1 *band*

	R0	22716·18	0G 2F 4·2K, defect 0·12, also 0 → 0, $^3E \rightarrow 2s\,^3\Sigma$, P3
∧	R3	22373·67	2G 1F 4·4K, defect 0·03
0·20			
∨	P5	21817·62	00*a*G 0/1F, also 1 → 1, $4d\,^3\Sigma \rightarrow 2p\,^3\Pi$, Q5, defect 0·08

The 1 → 0 *band*

	P1	27693·46	*r* Deodhar, defect 0·24
	R0	27644·52	1G 2F, also 3 → 0, $3d\,^1\Pi_b \rightarrow 2p\,^1\Sigma$, Q1 and Q2, defect 0·01
	P2	(27445·11)	*ab*G *ab*F ?27444·03 (*rd*) Deodhar

The 1 → 1 *band*

	P1	25172·63	1G 2F
∧	R0	25120·19	1G 3F 10·5K
0·11			
∨	P2	24930·56	0G 0F, also ? 5 → 3, $4p\,^3\Pi \rightarrow 2s\,^3\Sigma$, Q1 and 1 → 1, $^3G \rightarrow 2p\,^3\Pi$, Q′2

The 1 → 1 *band*—(continued)

∧	R1	25003·91	1G 1F 8·7K
0·03			
∨	P3	24689·40	1G *ab*F 11·4K
∧	R2	24884·27	00G 0F
0·01			
∨	P4	24447·35	00*a*G 0F 4·6K
∧	R3	24761·87	0*a*G 00F
0·10			
∨	P5	24206·12	2G *ab*F 3·9K
	R4	?24638·48	1G 2F 15·5 K
	P6	(?23967·56)	*ab*G *ab*F Interval uncertain. Line may be covered by 23966·56 (10)G (8)F 137·0K

The 1 → 2 *band*

	R1	22618·93	1G 2F 6·4K, also 0 → 0, $4d\,^3\Pi_b \rightarrow 2p\,^3\Pi$, R′4, defect 0·14

The 1 → 3 *band*

	R3	20154·79	0G 3·7K, defect 0·10
	R4	20055·74	00G, defect 0·08

The 1 → 4 *band*

	P1	18410·59	0G 3·5K, defect 0·02
	P3	17973·40	1G 6·8K, also 1 → 6, $^1M \rightarrow 2p\,^1\Sigma$, R2, defect 0·01
	R2	18140·90	1G, defect 0·12

The 2 → 1 *band*

	P2	27162·34	1G 0F 9·9K, defect 0·13

The 2 → 2 *band*

	? P1	24961·24	00*a*G *ab*F
∧	R0	24964·06	0G 0/1F
0·15			
∨	P2	24783·67	0*h*G 0/1F 4·5K, also R1 of $v'' = 0$ band of $^3B \rightarrow 2p\,^3\Pi$
∧	R1	24891·16	1G 0/1F 5·2K
0·10			
∨	P3	24592·24	00G *ab*F

TABLE IX—(continued)

The 2 → 2 *band*—(continued)

∧	R2	24806·72 00*a*G 0F 2·4K
0·02		
∨	P4	24391·67 0*a*G 0F
∧	R3	24718·22 1G 1F 9·9K
0·29		
∨	P5	24190·49 0G 0F 2·8K
∧	R4	24629·74 00G *ab*F
0·11		
∨	P6	23992·92 00*a*G *ab*F 1·4K

The 2 → 3 *band*

P5	21980·26 *ab*G 00F, defect 0·16

The 2 → 4 *band*

R0	20580·93 *ab*G 00F, defect (with R0, 2 → 2) = 0·17 (with P2, 2 → 2) = 0·02
R1	20514·19 2G 20·0K, also 0 → 1, $3d\,{}^1\Pi_b \rightarrow 2p\,{}^1\Sigma$, Q1, defect 0·07

levels appears to be most pronounced at the $v = 1$ level where the K = 0 level is nearly as high as the K = 5 level. However, the more usual trend of diminishing inversion with increasing vibrational quantum number appears to be resumed at $v = 2$.

TABLE X—ROTATIONAL STRUCTURE OF ^{3}F

K ↓	$v = 0$	$v = 1$	$v = 2$
5*s*		··········	··········
		? 125·34	147·61
4*a*	———	———→ 59·39 (?)	———→ 57·13
	69·42	65·95	90·48
3*s*	··········→ 56·35	··········→ 59·27	··········→ 54·86
	13·07	6·68	35·62
2*a*	———→ 59·88	———→ 59·57	———→ 48·26
	−46·79	−52·89	−12·64
1*s*	··········→ 55·61 (?)	··········→ 62·86	··········→ 44·92 (?)
	−102·40 (?)	−115·75	−57·56 (?)
0*a*	———	———	———

The initial vibrational differences are set out in Table XI. The values for K = 0 are queried because the only P1 line of this system which is at all certain is that of the 1 → 1 band. However, even if the other P1 lines are wrong it is unlikely that they are far from the positions assigned to them. With these P1 lines the height of the K = 0 level above the rotationless state at $v = 0$, 1, and 2 extrapolates to −79, −90, and −49 respectively. The intervals between the rotationless states at $v = 0$, 1, and 2 are then 2428 and 2132, giving for the vibrational constants $\omega_0 = 2576$ and $\omega_0 x = 148$. Unless an irregularity in the K = 0 levels has vitiated the extrapolations, ω_0 has a considerably higher value than for any other known state in the H_2 spectrum except ^{3}E, $2s\,{}^3\Sigma$ and the ground state, whilst $\omega_0 x$ has the highest value of all the states. This seems consistent with the different degree of uncoupling shown by the different vibrational levels of ^{3}F, for if the vibrational intervals of the unperturbed ^{3}F level are considerably different from those of the levels perturbing it, the perturbations will differ greatly from one vibrational level to another. The unusual variation of the intervals as K increases is also due to uncoupling effects.

By an extrapolation from the wave number of the R0 line of the $0 \rightarrow 0$ band, similar to that described for $^3\mathrm{E} \rightarrow 2s\,^3\Sigma$, we find that the ^{3}F level lies about 3913 below that of $1s\sigma\,^2\Sigma$. This figure corresponds to a Rydberg denominator of 5·294.

TABLE XI—VIBRATIONAL INTERVALS OF ^{3}F

Δv ↓	K = 0	K = 1	K = 2	K = 3	K = 4	K = 5
1 − 0	2417·56 (?)	2404·17	2398·08	2391·70	2388·31	
2 − 1	2173·73 (?)	2232·03	2272·31	2301·32	2325·88	2348·32

§ 6—THE ELECTRONIC STRUCTURE OF ^{3}Y, ^{3}D, ^{3}E, AND ^{3}F

In order to attempt to arrive at some conclusion about the electronic configuration of the upper states of the four systems which have now been described we have set out the numerical values of their more important properties in Table XII, together with those of the ion $1s\sigma\,^2\Sigma$, the end of all the series $1s\sigma ns, p, d$, etc., Σ, Π, Δ, etc., which have a single excited electron. Owing to the pronounced uncoupling it is only possible to give rather rough values of such quantities as the Rydberg denominators, ν_e and B_0, but the values given are reliable enough to base some important conclusions on. The data for the upper state of the Yellow band system are given in the first column of figures under ^{3}Y and the others in the succeeding columns. The states ^{3}D, ^{3}E, and ^{3}F are all Σ states since $\Lambda = 0$, the lowest ($K = 0$) rotational levels being present. They are also all odd (Σ_u) states since they go down to the even $2s\,^3\Sigma_g$ level. This is also confirmed by their rotational structure, the even K levels being strong (*a*) levels in each case.

On a first glance at the numbers in Table XII one is tempted to make the three states ^{3}D, ^{3}E, and ^{3}F, which have a good deal of similarity to one another, into members of a series with a single excited electron like the well-known series such as $1s\sigma np\Pi\,^3\Pi$, $1s\sigma nd\,^3\Sigma$, etc. We have pointed out in § 3 that the lowest such state must have $n > 3$, which would identify ^{3}D with $1s\sigma\,4f\sigma\,^3\Sigma_u$. Some objections to this identification were pointed out in § 3. If it is also to be a member of a series which also includes ^{3}E and ^{3}F a further and quite serious objection emerges

TABLE XII

	^{3}Y	^{3}D	^{3}E	^{3}F	$1s\sigma\,^2\Sigma$
Rydberg denominator, about	3·097	3·157	4·296	5·294	∞
ν below $1s\sigma\,^2\Sigma$, about	11437	11005	5943	3913	0
Δ_1, $v = 1 - 0$ interval, at K = 0	—	2217·18	2457·05	2417·56 ?	—
Δ_1, $v = 2 - 1$ interval, at K = 0	—	2035·26	—	2173·73 ?	—
Δ_2, $v = (1 - 0) - (2 - 1)$, at K = 0	—	181·92	—	243·83 ?	—
Δ_1, $v = 1 - 0$ interval, at K = 1	2384·73	2213·02	2495·18	2404·17	2173*
Δ_1, $v = 2 - 1$ interval, at K = 1	2172·70	2033·12	—	2232·03	—
Δ_2, $v = (1 - 0) - (2 - 1)$, at K = 1	212·03	179·90	—	172·14	124†
$2B_e$, about	72	70	72	63	58·2
? Electronic structure	? $2p\sigma\, 3d\pi\, ^3\Pi_u$	? $2p\sigma\, 3d\sigma\, ^3\Sigma_u$	? $1s\sigma\, 4f\sigma\, ^3\Sigma_u$	? $1s\sigma\, 5f\sigma\, ^3\Sigma_u$	$1s\sigma\,^2\Sigma$
Lowest rotational level	K = 1 (*s*)	K = 0 (*a*)	K = 0 (*a*)	K = 0 (*a*)	—
Quantum number Λ	1	0	0	0	0

* Value of $\omega_0 - x\omega_e$.

† Value of $2x\omega_e$.

from Table XII. In this case ^3E is $1s\sigma\,5f\sigma\,{}^3\Sigma_u$ and ^3F is $1s\sigma\,6f\sigma\,{}^3\Sigma_u$. But with such a high principal quantum number as 6 it is extremely unlikely that the denominator would be as far from 6 as 5·294. Also the trend of the denominators from ^3E to ^3F suggests that this numbering is one unit too high. In addition the data do not represent a smooth series for ^3D, ^3E, ^3F, ..., $1s\sigma\,{}^2\Sigma$. In every instance either the values for ^3D are too low or those for ^3E too high to make a uniform series. Finally, whilst the states ^3E and ^3F are very much alike, for example in their rotational structure, ^3D is appreciably different from either. On these grounds we propose to reject this possible grouping.

There is a much stronger case to be made for identifying ^3E with $1s\sigma\,4f\sigma\,{}^3\Sigma_u$ and ^3F with $1s\sigma\,5f\sigma\,{}^3\Sigma_u$. It is practically certain that ^3F belongs to a state of some series of which $1s\sigma\,{}^2\Sigma$, the ground state of the molecular ion H_2+, is the limit. Such a high vibrational interval as 2404 would otherwise be incompatible with such a high Rydberg denominator as 5·3, since there is no excited state of the molecular ion which has a vibrational interval of even the same order of magnitude. All the numbers for ^3E, ^3F, and $1s\sigma\,{}^2\Sigma$ are such as are reasonable for such a series. Finally all the properties found for ^3E and ^3F are such as we should naturally expect for the states $1s\sigma\,4f\sigma\,{}^3\Sigma_u$ and $1s\sigma\,5f\sigma\,{}^3\Sigma_u$ respectively.

The adoption of ^3E as $1s\sigma\,4f\sigma\,{}^3\Sigma_u$ makes it necessary to reconsider the interpretation of ^3D and the nearby Π state ^3Y. It does not now seem possible to identify them with any orthodox state having a single excited electron owing to the fact that all such odd triplet levels at a comparable depth below $1s\sigma\,{}^2\Sigma$ are already known. It seems likely that they are abnormal levels of the type of ^1K, ^1L, ^1M, etc., in the singlet system. If these are levels with two excited electrons the most probable allocations are ^3Y as $2p\sigma\,3d\pi\,{}^3\Pi_u$ and ^3D as $2p\sigma\,3d\sigma\,{}^3\Sigma_u$ ($2p\sigma\,3s\sigma\,{}^3\Sigma_u$ seems less probable). This puts Π below Σ which is contrary to what happens in the singly excited states. However, it will be shown in § 7 that a state which one of us provisionally identified as $2p\sigma\,2p\pi\,{}^1\Pi_g$ is now found to lie below a state which was also identified provisionally at the same time as $2p\sigma\,2p\sigma\,{}^1\Sigma_g$. It seems undesirable to say much about such possibilities in the triplet system until the spectrum has been examined still more drastically, particularly as there are uncertain features in some of the bands of $^3Y \rightarrow 2s\,{}^3\Sigma$ and $^3D \rightarrow 2s\,{}^3\Sigma$. It is possible that further investigation may make some changes in the ^3Y and ^3D states, but it seems unlikely that they will be changed much.

At the same time we think that the following points ought to be mentioned in this connection : the $^3Y \rightarrow 2s\,{}^3\Sigma$ and $^3D \rightarrow 2s\,{}^3\Sigma$ systems are both characterized by being enhanced in the strongly condensed discharge. In this respect they differ from all other systems ending on $2s\,{}^3\Sigma$. In the ${}^3\mathrm{Y} \rightarrow 2s\,{}^3\Sigma$ system the following lines are given in Bay, Finkelnburg, and Steiner's* table : In the $0 \rightarrow 0$ band, R0 (also R0 of $1 \rightarrow 1$, ${}^3\mathrm{D} \rightarrow 2s\,{}^3\Sigma$), R1 (also P6 of $2 \rightarrow 1$, $3p\,{}^3\Pi \rightarrow 2s\,{}^3\Sigma$), P3. In the $2 \rightarrow 2$ band, P4 (also P′6 of $0 \rightarrow 0$, $3d\,{}^3\Delta_b \rightarrow 2p\,{}^3\Pi$ and P3 of $2 \rightarrow 2$, ${}^3\mathrm{D} \rightarrow 2s\,{}^3\Sigma$), P5. In the ${}^3\mathrm{D} \rightarrow 2s\,{}^3\Sigma$ system the enhancement in the strongly condensed discharge is even more evident, the following lines occurring in Bay, Finkelnburg, and Steiner's table : in the $1 \rightarrow 1$ band, R0 (also R0 of $0 \rightarrow 0$, ${}^3\mathrm{Y} \rightarrow 2s\,{}^3\Sigma$), R1, P3. In the $2 \rightarrow 2$ band, R1, P3 (also P′6 of $0 \rightarrow 0$, $3d\,{}^3\Delta_b \rightarrow 2p\,{}^3\Pi$ and P4 of $2 \rightarrow 2$, ${}^3\mathrm{Y} \rightarrow 2s\,{}^3\Sigma$), R2, R3 (also R3 of $2 \rightarrow 2$, $3d\,{}^3\Delta_b \rightarrow 2p\,{}^3\Pi$). In addition the P2 line of the $0 \rightarrow 0$ band is given by Merton and Barratt as enhanced in the condensed discharge.

The ${}^3\mathrm{Y} \rightarrow 2s\,{}^3\Sigma$ system therefore contains five lines (of which three are blends) and the ${}^3\mathrm{D} \rightarrow 2s\,{}^3\Sigma$ system no less than seven lines (of which only three are blends) which are enhanced in the strongly condensed discharge. This is remarkable in view of the fact that of the 58 lines in Bay, Finkelnburg and Steiner's table which have been classified only 20 do not belong to systems ending on $2p\,{}^3\Pi$ and of these only five belong to the very extensive previously discovered systems ending on $2s\,{}^3\Sigma$. It appears that the ${}^3\mathrm{D} \rightarrow 2s\,{}^3\Sigma$ and ${}^3\mathrm{Y} \rightarrow 2s\,{}^3\Sigma$ systems are favoured by rather vigorous excitation, which makes the more plausible their interpretation as systems having both electrons excited.

§ 7—THE SYSTEM ${}^1\mathrm{Q} \rightarrow 2p\,{}^1\Sigma$

This is one of the numerous abnormal systems in the singlet spectrum which were discovered by Richardson and Davidson† but they only found a single progression of it. Owing to the abnormal intensity distribution, a feature which is characteristic of these systems, it was uncertain whether it was a $v' = 0$ or a $v' = 1$ progression. We have now found another progression and on comparing the intenstiy distribution in the two there can be little doubt that the new one is the $v' = 0$ progression and the old one the $v' = 1$ progression. As some of the published data for the upper state ${}^1\mathrm{Q}$ were worked out on the tentative assumption that the old progression was a $v' = 0$ progression these will require modification.

---

* 'Z. phys. Chem.,' B, vol. 11, p. 351 (1930).

† 'Proc. Roy. Soc.,' A, vol. 124, p. 50, p. 69 (1929).

The band lines are set out in a rectangular v', v'' array in Table XIII. It will be seen that in the new progression the weakest band is the $v'' = 1$ band and in the old the $v'' = 2$ band. In fact, both these bands may be absent, each being represented only by a single line which is also a line of another system. It is usual for such features to move towards the right in such an array, *i.e.*, towards higher values of v'', as v' increases. This is an indication that the progressions belong to the same system. In the old progression too much of the strength lies in the $v'' = 0$ band for v' to be greater than 1; at any rate the intensity distribution would be without parallel in the whole H_2 spectrum if it did. We therefore conclude that the progressions have $v' = 0$ and $v' = 1$ respectively.

The rotational structure of the upper state is set out in Table XIV. There are alternative sets of lines at the $K' = 3$ level. The P4 lines originally assigned to the $v' = 1$ progression are the set in the bottom row of Table XIII. These lines and the corresponding P4 lines in the last row of the $v' = 0$ progression have the support of the combinations with the R2 lines of the $0' \rightarrow 0''$ and $1' \rightarrow 0''$ bands. If the upper set of P4 lines are chosen these R2 lines are not band lines. The lowest rows of P4 lines give the intervals 237·24 and 238·99. The others make the rotational structure look more regular. It seems likely that they are the ones which belong to this system and that the ones which give the R2 combinations are something else.

The ν_e of ^1Q lies about 13350 wave numbers below the level of the ion $1s\sigma\,^2\Sigma$. This corresponds to a Rydberg denominator 2·866. The old values, based on the assumption that the $v' = 1$ progression was the $v' = 0$ progression, were 12522 and 2·9595 respectively. The vibrational intervals of ^1Q are much lower than those of any other known state of H_2.

This strongly supports the view that ^1Q is a state with both electrons excited. It is improbable that with a denominator as low even as 2·866 a state belonging to a series ending with $1s\sigma\,^2\Sigma$ could have such small vibrational intervals.

As a matter of fact, we have recently found an even triplet Π state (^3B) which has unusually low vibrational intervals and also a rotational structure like that of ^1Q, particularly if the new P4 lines are chosen.* If ^1Q is $2p\sigma\, 2p\pi\, ^1\Pi_g$ as one of us† has suggested, and ^3B is $2p\sigma\, np\pi\, ^3\Pi$, then n must be at least 4, since the denominator of ^3B is nearly two units higher at 4·63 than that of ^1Q at 2·866 and so far, at any rate in the states

---

* This statement is subject to some reservations which we have given in Part II, p. 271.

† "Molecular Hydrogen and its Spectrum," p. 312.

TABLE XIII—THE LINES OF $^1Q \rightarrow 2p\,^1\Sigma$

The $v' = 0$ progression

$v'' \rightarrow$	0	1	2	3
R0	21183·67(1*a*)G 12·5K	—	18583·85(2)G 4·9K	(17337·14) interference
R2	21419·86(*ab*)G 00F	—	—	—
P2	21067·54(2)G 11·2K L+	—	18478·42(3)G 7·5K	17236·02(0)G
P3	21112·28(0*h*)G	19805·44(0*a*)G 4·2K*	18533·76(0)G 3·2K*	17295·44(0)G
P4	21153·00(1)G 8·3K	—	18587·77(5)G 6·7K*	17355·14(6)G 16·2K*
or				
P4	21197·95(0)G	—	18632·68(0*a*)G*	—

The $v' = 1$ progression.

$v'' \rightarrow$	0	1	2	3
R0	21922·71(2)G, 13·1K L++	—	19322·85(1)G 9·0K L+	18076·20(0)G
R2	22198·54(00)G*	—	—	—
P2	21806·54(5)G 54·3K L++ C−	20493·95(3)G 14·4K L++†	—	17975·00(3)G 11·8K He0
P3	21844·37(1)G 7·4K	20537·44(1*a*)G	—	18027·62(00)G
P4	21876·54(0)G†	—	—	18078·60(2)G 2·8K L+ He++
or				
P4	21931·77(4)G 25·4K*	20631·95(2)G 10·0K*	—	18134·00(1)G He++

* Blend.

† Doubtful line in another system.

TABLE XIV—Structure of the State ^1Q

Rotational structure				Vibrational intervals	
K ↓	$v' = 0$	K ↓	$v = 1$	K ↓	$\Delta_1 v = 1 - 0$
3*a*	———	3*a*	———	3	723·50 or 733·82
	192·40 or 237·24		183·71 or 238·99		
2*s*	·····→32·58 or 77·42	2*s*	·····→30·72 or 86·00	2	732·13
	159·82		152·99		
1*a*	———	1*a*	———	1	739·01

with only one excited electron, triplet states always lie below the corresponding singlet states. In that case there should be other $2p\sigma\, np\pi\, ^3\Pi$ states going down to $1s\sigma\, 2p\pi\, ^3\Pi$ and giving rise to systems in the measured part of the spectrum.

The following lines in the $^1Q \rightarrow 2p\, ^1\Sigma$ system are given by Brasefield* as enhanced in the electrodeless discharge : In the 0 → 0 band, P2 (?), P4, in the 0 → 2 band, P2. This enhancement in the electrodeless discharge,*† together with the weakness or absence of the 0 → 1 and 1 → 2 bands and the low value of B_0 (if the new alternative $K' = 3$ levels are chosen) marks off ^1Q as a state of the same type as ^1K, ^1L, etc., and confirms its interpretation as a state in which both electrons are excited.

Mecke's rule affords another confirmation of the view that ^1Q and ^3B are states of similar type in the singlet and triplet spectrum. In agreement with this rule, B_0/ω_0 has almost the same value for all states in the hydrogen molecule in which only one electron is excited. Of these more than 40 are known. The average value of B/ω_0 for all such states is 0·013. The abnormal, probably doubly excited levels, as might be expected, give different values for the constant. ^1Q and ^3B give the values 0·022 and 0·020 respectively for $B_0/(\omega_0 - \omega_0 x)$. The similarity of these two values, both of which are abnormal, suggests very strongly that ^3B and ^1Q are corresponding states.

SUMMARY

This paper describes three new band systems ending on $1s\sigma\, 2s\sigma\, ^3\Sigma$, the lowest even triplet state of H_2, and coming from three hitherto undiscovered upper states called provisionally ^3D, ^3E, and ^3F. It also describes bands coming from two new vibrational levels of the same state as the Yellow Band described by Richardson and Das and ending on $v'' = 0$ and $v'' = 2$ of $2s\, ^3\Sigma$ instead of $v'' = 1$ of $2s\, ^3\Sigma$. Finally an account is given of a new progression of the singlet system $^1Q \rightarrow 2p\, ^1\Sigma$. This

---

* 'Phys. Rev.,' vol. 33, p. 925 (1929).

† *Cf.* Richardson, "Molecular Hydrogen and its Spectrum," pp. 312, 321.

proves to be the $v' = 0$ progression and the one previously known is now shown to be the $v' = 1$ progression.

The band constants and the properties of the upper states are worked out and discussed. It is fairly certain that ^{3}E is $1s\sigma\, 4f\sigma\, ^3\Sigma_u$ and ^{3}F is $1s\sigma\, 5f\sigma\, ^3\Sigma_u$. The upper state of the Yellow Band System and ^{3}D are probably " abnormal " odd triplet states analogous to the " abnormal " states like ^{1}K, ^{1}L, etc., of which there are so many examples in the even singlet states of H_2.

The Determination of the Specific Heat of Gases at High Temperatures by the Sound Velocity Method

I—Carbon Monoxide

By G. G. Sherratt, B.A., and Ezer Griffiths, D.Sc., F.R.S., Physics Department, National Physical Laboratory

(*Received August* 20, 1934)

Introduction

The determination of the specific heats of gases at high temperatures is a problem of unusual difficulty and the attempts hitherto made to measure specific heats at temperatures exceeding 1200° C have been by the " explosion method."

This method involves the observation of transient phenomena and also the estimation of a relatively large radiation correction.

The " sound velocity " method is free from these limitations and the object of the present paper is to show how this method can be adapted for measurement with carbon monoxide up to temperatures of the order of 2000° C.

The two essentials are (*a*) the production of sound waves of definite frequency, and (*b*) the accurate measurement of temperature.

In the apparatus to be described sound waves of definite frequency were obtained from a rectangular block of quartz crystal vibrating piezo-electrically.

Temperatures were measured by means of a " disappearing filament " pyrometer.

Although many observers have used the sound velocity method at relatively low temperatures it does not appear to have been fully realized that measurements must be made using more than one frequency. Recent investigations, of which that of Pierce[*] on the velocity of sound in air and carbon dioxide at 0° C was the first, have proved that for any gas whose molecules have an appreciable internal energy there will be a frequency range or ranges over which sound dispersion will be in evidence. Hence it is essential that observations should be made with more than one frequency of sound.

The marked disagreement which is found between the values of the specific heats of gases at moderately high temperatures obtained by the sound velocity method and those calculated from band spectroscopic data is to be ascribed to the fact that account has not been taken of the disappearance from the expression for the adiabatic elasticity of part of the specific heat of the gas at certain frequencies. It is significant that the velocity of sound method using any one frequency has always given results which are lower than those calculated from band spectroscopic data.

In the experiments now to be described two frequencies have been employed in order that a correction can be made for possible sound dispersion.

DESCRIPTION OF APPARATUS

The apparatus consists essentially of a carbon tube which can be heated to a high temperature and in which a stationary train of sound waves can be set up from a quartz crystal vibrating piezo-electrically. A piston traverses the tube, its position being read on an accurately graduated steel rule. This piston functions as a reflector to set up the standing wave system in the tube, and the half wave-length is determined by recording the different positions of the reflector at which resonance occurs.

Resonance is detected by changes in the plate current of the oscillator maintaining the quartz crystal in vibration consequent upon the changes in the amplitude of vibration of the crystal which occur as the reflector is moved along the tube.

The temperature of the gas in the tube is determined by sighting an optical pyrometer of the "disappearing filament" type on to the face of the movable reflector. Fig. 1 gives the general lay-out of the apparatus.

The Carbon Tube Furnace—Since the half wave-length of sound in carbon monoxide at the lower frequency (8 kilocycles per second) is of the order of 6 cm at a temperature of 2000° C, it was necessary to use a long furnace to enable a uniformly heated region of at least 30 cm to be obtained.

---

[*] 'Proc. Amer. Acad. Arts Sci.,' vol. 60, p. 271 (1925).

The lower half of the furnace is shown in fig. 2, the upper half being similar in construction.

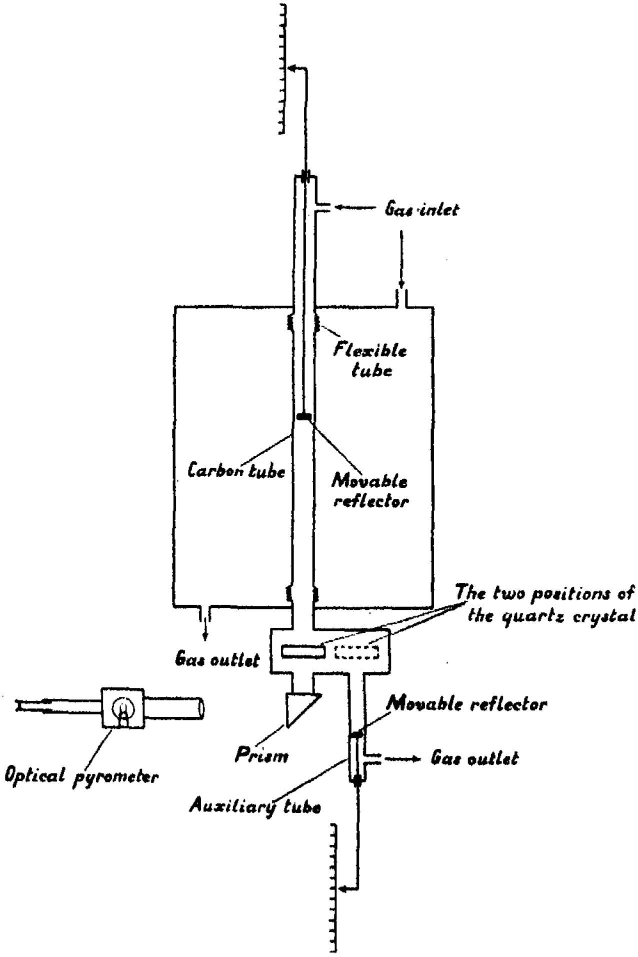

FIG. 1

The body of the furnace consists of a hollow iron cylinder, approximately 3 feet in length and of 1 foot internal diameter. It is provided with flanges at each end to which are bolted electrically insulated end-plates. The latter are in two portions, the centre portion being easily removable when it is desired to insert a new carbon tube into the furnace.

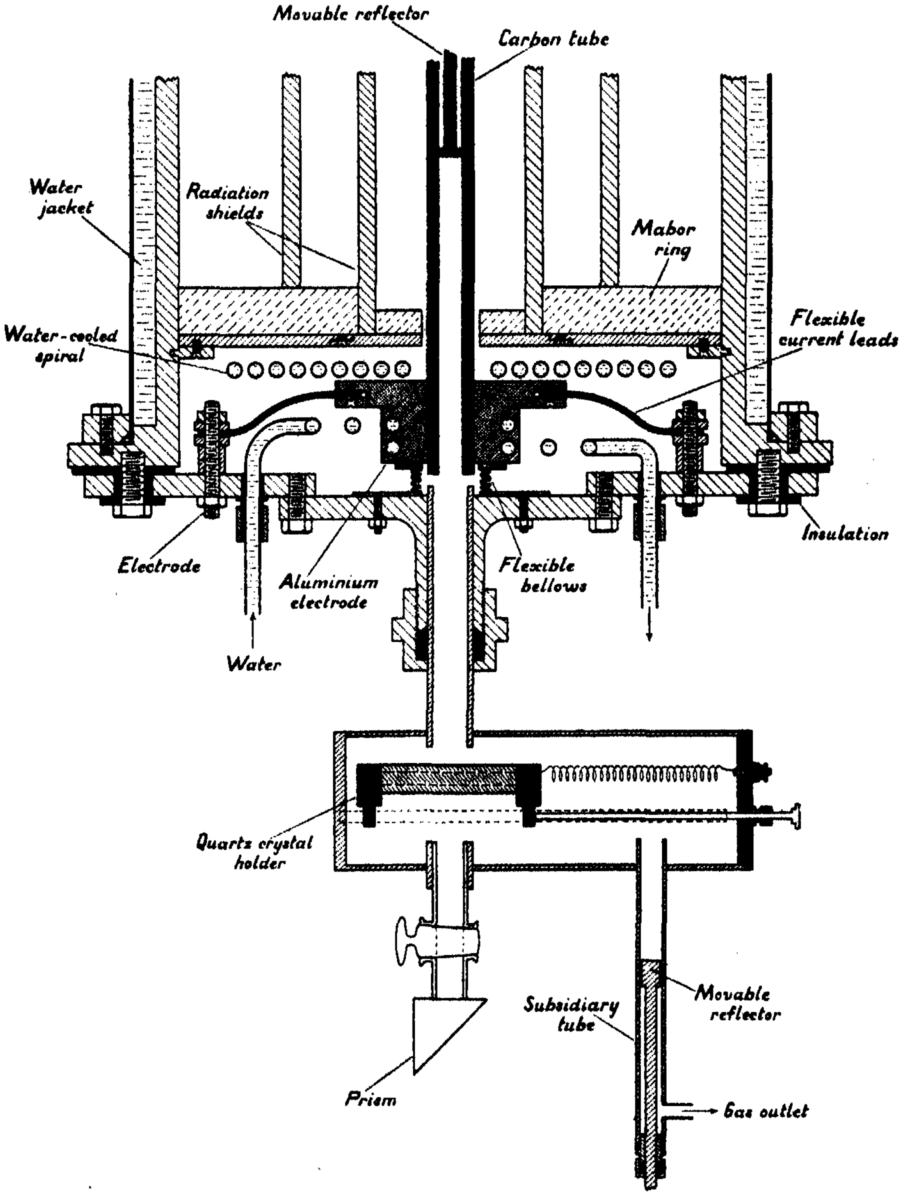
Movable reflector
Carbon tube
Water jacket
Radiation shields
Mabor ring
Water-cooled spiral
Flexible current leads
Electrode
Aluminium electrode
Flexible bellows
Insulation
Water
Quartz crystal holder
Subsidiary tube
Movable reflector
Prism
Gas outlet

FIG. 2

The thickness of the walls of the cylinder and of the end-plates is approximately ½ inch.

The weight of the body of the furnace is taken by a system of girders, the axis of the cylinder being vertical.

The cylindrical walls are water-cooled.

The carbon tube has a length of 3 feet, an approximate external diameter of 1 inch, and an approximate internal diameter of ½ inch. It is heated by the passage of an electric current and is supported by two electrode blocks of aluminium. Each electrode consists of two halves held together by means of screws and between each electrode and the tube is inserted a graphite sleeve split longitudinally to permit of compression on to the tube. The sleeve ensures good electrical and thermal contact when the electrode screws are tightened up.

The electrodes themselves are in turn supported by flexible spirals of copper tubing, through which a rapid stream of water is circulated for cooling purposes. The ends of the copper tubing are taken out of the furnace via packing glands in the furnace end-plates.

For the purpose of the electrical connection to the carbon tube, short lengths of studding pass through the end plates and support two brass rings with their planes perpendicular to the axis of the furnace. The rings are connected to the aluminium electrode by means of a network of copper braid which is quite flexible and does not subject the carbon tube to any constraint.

To diminish heat loss the central portion of the carbon tube is surrounded by two radiation shields of refractory material. They are supported by steel discs faced with " mabor " brick as shown in the figure.

As a protection from radiation, two closely wound copper spirals are inserted between the aluminium electrodes and the high temperature region. A rapid stream of water is circulated through these spirals.

To isolate the interior of the carbon tube from the body of the furnace, two flexible metal bellows are included between the ends of the tube and the end-plates of the furnace. This arrangement permits of a stream of gas being passed through the carbon tube independently of that circulating through the main body of the furnace. It will be observed that all connections to the carbon tube are made as flexible as possible to permit of its free expansion and contraction without restraint.

The upper half of the furnace is similar in construction to the lower half. In the packing gland on the top end-plate is held a length of 1-inch brass tubing. At the upper end of this tube is a second packing gland through which a movable piston passes. The piston is in two parts rigidly connected together but electrically insulated one from the other. The lower portion is of graphite rod ¼-inch in diameter having an enlarged end to act as a reflector for the sound waves. The upper portion consists of a steel rod of ⅜-inch diameter the upper end of which is attached to a vernier moving over an accurately graduated steel scale.

Sound Production—A single crystal of quartz is used for the production of the sound waves. It is in the form of a rectangular parallelopiped of dimensions $10 \times 1 \cdot 5 \times 1 \cdot 5$ cm the third axis being in the direction of the length and two of the longitudinal faces being at right angles to one of the electric axes. The crystal can be made to vibrate in either of two modes—the flexural mode and the longitudinal mode.

The arrangement of the electrodes for the former mode is described by Harrison.* It was found convenient to maintain the crystal in oscillation in this mode by connection to a modification of the Abraham-Block multivibrator.

For the longitudinal mode a simple one valve circuit sufficed. The frequencies in the two modes were measured in the Electrical Department of the Laboratory and found to be 7907·95 and 27422 cycles per second respectively. It was verified that no measurable change in the frequency is caused by changes in the acoustic load. The temperature coefficient of frequency is very small (a few parts in 10^6 per ° C).

The Crystal Enclosure—The enclosure containing the crystal is carried on a prolongation to the carbon tube. This consists of a short length of 1-inch external diameter brass tube which fits into the packing gland on the lower furnace end-plate and is terminated by a brass tubular box. Two steel rods are supported (parallel to the axis of the tubular crystal box), along which the crystal carriage slides. The other end of the crystal box is closed and made gas-tight by cementing on a thick brass end-plate. This end-plate carries the insulated terminals and a packing gland. The former are connected to the crystal electrodes and the packing-gland accommodates the brass rod by means of which the crystal carriage is moved. The crystal carriage has two alternative positions fixed by stops—one beneath the carbon tube and with the centre of the crystal in line with the axis of the tube : the other above a subsidiary tube. The latter tube, see fig. 2, is provided with a movable reflector to permit of sound velocity determinations being made on the gas which has passed through the carbon tube. Diametrically opposite and vertically beneath the brass prolongation tube from the furnace to the crystal box is fitted a short length of similar sized tubing into which is cemented a wide bore glass tap. On the lower end of the latter a right-angled prism is cemented. By this system an unobstructed line of sight is afforded for the optical pyrometer when focussed on to the reflector in the carbon tube. The tap is in the open position and the crystal carriage and crystal are withdrawn to the position over the subsidiary tube, when optical readings are being taken. The inclusion of the tap is to permit of the easy removal of the prism for cleaning without admitting an appreciable amount of air into the apparatus.

---

* ' Proc. Inst. Radio Engrs.,' vol. 15, p. 1040 (1927).

The Subsidiary Tube—The subsidiary tube was attached to the apparatus in order to be able to keep a continuous check on the purity of the gas which has passed through the carbon tube. As the gas leaves the carbon tube it passes down through the crystal box and into the subsidiary tube, leaving by a side tube.

The subsidiary tube is of brass and is provided with a short closely fitting brass cylinder which acts as a reflector of the sound waves emitted by the crystal when in position over the tube.

The reflector is moved by means of a brass rod which passes through a packing gland at the lower end of the tube and is attached to the carriage of a cathetometer. The total distance through which the reflector can be moved amounts to 18 cm.

The subsidiary tube is lagged to minimize the effect of changes in the temperature of the room.

Temperature Measurement—The temperature is measured by means of a calibrated " disappearing filament " pyrometer sighted through a right-angled prism, as previously described, on to the face of the reflector in the carbon tube.

In the preliminary experiments the pyrometer was sighted on the piston through the quartz crystal which has optically worked surfaces. Difficulties were encountered through dust settling on the crystal surfaces so the apparatus was modified to permit of direct sighting without the intermediary of the crystal.

In the modified arrangement there was an unobstructed path between the face of the reflector and the surface of the prism.

The only correction to the optical readings was that for absorption by the prism. This was determined in a series of separate experiments.

When the furnace was running at a steady temperature, it was found that the optical pyrometer readings remained constant as the face of the piston traversed a distance of about 30 cm in the central region of the furnace and the measurements of the half wave-lengths were restricted to this region.

Approximate calculations show that as the temperature gradient along the hot end of the graphite piston rod is small, the conduction of heat along the rod has a negligible effect on the temperature of the piston face.

APPARATUS FOR DETERMINATION OF THE COEFFICIENT OF EXPANSION OF GRAPHITE

It was necessary to apply a correction to the observed half wavelengths in the carbon tube on account of the thermal expansion of the graphite rod which constitutes the movable reflector. For the purpose of determining the coefficient of expansion, the rod was mounted in the apparatus shown in fig. 3. The apparatus consisted of a water-cooled vertical cylinder provided with a longitudinal window. The upper end of the rod was screwed into a graphite block fastened to the lid of the cylinder, the lower end being screwed into a small copper cylinder dipping into a water-cooled cup of mercury. The depth of immersion was adjusted so as to minimize the strain on the rod.

The rod was heated by the passage of an electric current and the mercury, which was electrically insulated from the body of the apparatus, formed one of the electrodes, the other being the lid of the cylinder. The enclosure was exhausted so as to prevent oxidation of the rod and to eliminate convection currents.

The distance between two selected points on the uniformly heated portion of the rod was measured by means of a cathetometer.

Temperature measurements were made by sighting on to the incandescent rod with a disappearing filament pyrometer.

PURITY OF GAS USED

The carbon monoxide for these experiments was supplied in cylinders by the Chemical Research Department. Several cylinders were used in the course of the investigation and the only impurity present in the gas was nitrogen. The percentage of the latter gas varied from 0·3 to 0·7 in the different cylinders.

As already stated, a continuous check can be kept on the state of purity of the gas in the carbon tube by sound velocity measurements in the auxiliary tube through which the gas passes on exit from the furnace. In addition to this physical check, samples of the gas were taken periodically and submitted for chemical analysis to the Chemistry Division of the Laboratory.

In the early experiments before the use of the corrugated end tubes to isolate the interior of the carbon tube from the body of the furnace, chemical analysis showed the presence of hydrogen in the gas issuing from the furnace. The source of this hydrogen has not been traced.

The difficulty was surmounted by the use of the above-mentioned device.

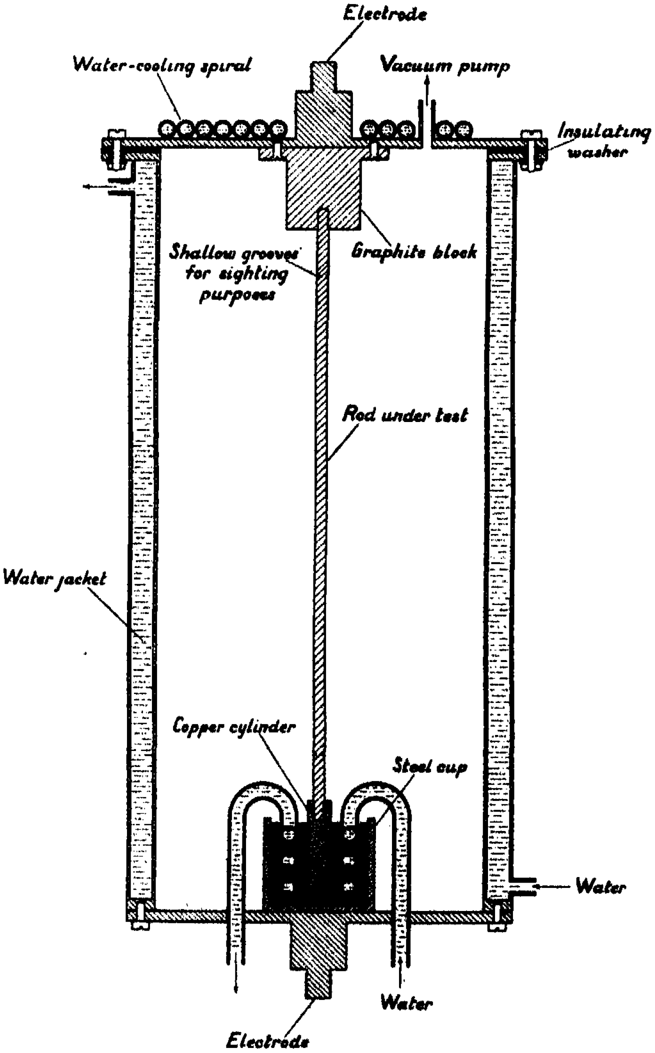

Fig. 3

EXPERIMENTAL DATA

The results for the two frequencies used are given in Tables I and II ; columns 1 and 2 give the half wave-length in the tube and the corresponding velocity in metres per second. Column 3 gives the mean apparent temperature in the region traversed by the movable reflector and column 4 gives the temperature after correction for the absorption of the prism.

TABLE I—FREQUENCY = 7908 CYCLES PER SECOND

Half wave-length in cm	Velocity in metres per sec	Mean apparent temperature °C	Corrected temperature °C
4.322	683·6	960	969
4·310	681·7	983	992
4·475	707·8	1025	1035
4·570	722·8	1065	1076
4·616	730·1	1103	1114
4·617	730·2	1107	1118
4·638	733·5	1110	1121
4·674	739·2	1158	1170
4·736	749·0	1175	1187
4·780	756·0	1211	1224
4·820	762·3	1222	1235
4·842	765·8	1240	1254
4·850	767·1	1260	1274
4·923	778·6	1292	1307
4·924	778·8	1288	1303
4·974	786·7	1334	1350
4·980	787·6	1338	1354
5·041	797·3	1396	1413
5·080	803·4	1389	1406
5·092	805·4	1414	1431
5·116	809·2	1440	1458
5·142	813·3	1444	1462
5·155	815·3	1464	1483
5·213	824·5	1493	1512
5·252	830·7	1531	1552
5·268	833·2	1539	1560
5·325	842·2	1593	1615
5·342	844·9	1599	1621
5·387	852·0	1624	1646
5·445	861·2	1671	1694
5·469	865·0	1700	1724
5·531	874·8	1736	1761
5·560	879·4	1781	1807
5·622	889·2	1781	1807
5·622	889·2	1835	1862

The velocities in the two tables are graphed in fig. 4.

The velocities at temperatures below 1000° C appear to be on the low side and have been ignored in smoothing the results. A possible explanation for this may lie in the fact that the equilibrium percentage of carbon dioxide in the presence of carbon increases rapidly as the temperature falls below 1000° C. The values given by Read and Wheeler* are 0·15% carbon dioxide at 1100° C, 0·59% at 1000° C, and 2·22% at 900° C. It is therefore conceivable that when the greater portion of the length of the tube is at a temperature between 900° and 1000° C sufficient carbon dioxide might be formed, in the short time that the gas takes to flow through the tube, to affect the results.

TABLE II—FREQUENCY = 27422 CYCLES PER SECOND

Half wave-length in cm	Velocity in metres per sec	Mean apparent temperature ° C	Corrected temperature ° C
1·321	724·7	1031	1041
1·343	736·6	1080	1091
1·366	749·1	1112	1124
1·401	768·4	1170	1182
1·443	791·4	1300	1315
1·476	809·5	1336	1352
1·486	815·0	1373	1390
1·534	841·3	1500	1519
1·566	858·9	1565	1586
1·604	879·9	1656	1678
1·605	880·1	1659	1681
1·639	899·0	1752	1777

CORRECTIONS

Corrections have to be applied to the velocities tabulated in the previous section for three reasons.

(1) The velocities are measured in a tube and, as is well known, the values so obtained are lower than the free-space velocities.

(2) The observed half wave-lengths require correction on account of the thermal expansion of the graphite rod forming the movable reflector.

(3) The carbon monoxide used in the experiment was not absolutely pure but contained from 0·3% to 0·7% of nitrogen.

The corrections may now be considered in greater detail.

(1) The question of the magnitude of the reduction in velocity below the free space value which should result from the passage of a sound wave through a tube was treated theoretically by Helmholtz and by Kirchhoff.

---

* 'J. Chem. Soc.,' vol. 97, p. 2178 (1910).

It should be noted that the theory deals only with plane waves and in the present work care has been taken to ensure that the frequencies used satisfy Rayleigh's condition for plane propagation.*

The Helmholtz-Kirchhoff equation connecting the observed velocity V of a sound wave of frequency n in a tube of radius r, with the free space velocity V_0, is

$$V = V_0 \left\{1 - \frac{c}{2r(\pi n)^{\frac{1}{2}}}\right\}$$

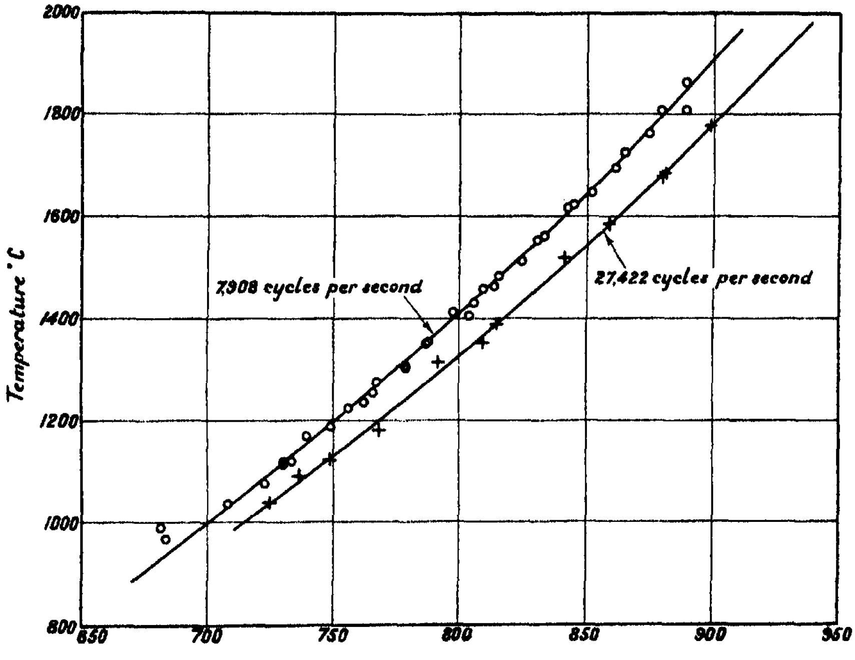

FIG. 4—Velocities in the carbon tube at frequencies of 7908 and 27422 cycles per sec

where c is the Kirchhoff constant given by

$$c = \mu^{\frac{1}{2}} + \left(\frac{\nu}{\gamma}\right)^{\frac{1}{2}} (\gamma - 1),$$

where μ = kinematic viscosity,
γ = ratio of the specific heats, and
ν = thermal diffusivity of the gas in the tube.

In a recent paper by Kaye and Sherratt† it was shown that the above equation was approximately true for smooth tubes, but gave too small a

---

* "Theory of Sound," vol. 2, p. 161.

† 'Proc. Roy. Soc.,' A, vol. 141, p. 123 (1933).

reduction in velocity with rough surfaced tubes in agreement with the general experience of observers.[*] It appeared that, when dealing with rough tubes a method of correction similar to that used by Dixon, Campbell, and Parker,[†] and by Partington and Shilling[‡] could be employed. This consists of writing the equation in the form

$$\mathrm{V} = \mathrm{V}_0\left(1 - \frac{kc}{2r\,(\pi n)^{\frac{1}{2}}}\right) = \mathrm{V}_0\,(1 - k_1\,c),$$

where k is a multiplying factor which must be found by experiment ; ($k > 1$ for rough tubes). The method of determining k is to perform sound velocity experiments in pure air at room temperature. The free space velocity in pure air is sufficiently accurately known, $\mathrm{V}_0 = 331 \cdot 6$ metres per second at a temperature of 0° C, to give reliable values of k. Actually, the quantity most easily dealt with is $k_1\,(= k/2r\,(\pi n)^{\frac{1}{2}})$, on account of the difficulty of making an accurate determination of the bore of a tube after it has been raised to a high temperature. This quantity shows an initial increase after a tube is first heated, but subsequently a slight but progressive decline sets in which continues until the tube burns out. The initial increase may be due to roughening of the wall of the tube and the final decrease to enlargement of the bore through loss of the material of the tube. The total range of variation is, however, small, and it is permissible to use the mean value for all the tubes in correcting the results. Taking the mean value $k_1 = k/2r\,(\pi n)^{\frac{1}{2}} = 0 \cdot 0051$ when $n = 7908$ cycles per second, the value for $n = 27422$ cycles per second works out to be $0 \cdot 0027$.

(2) The apparatus for the determination of the linear coefficient of thermal expansion of the graphite rod forming the movable reflector has already been described. The mean coefficient α_t over the range from room temperature to t° C varied in an approximately linear manner from $2 \cdot 15 \times 10^{-6}$ to $3 \cdot 5 \times 10^{-6}$ as t varied from 1000° C to 1800° C. The correction takes the form of a multiplying factor $\{1 + \alpha_t\,(t - t_0)\}$, where t_0 is the room temperature.

(3) The correction for the effect of the impurity present in the carbon monoxide, namely, 0·3% to 0·7% of nitrogen, turns out to be negligible since the two gases have almost exactly the same molecular weights and approximately the same specific heats.

---

[*] Schulze, 'Ann. Physik,' vol. 13, p. 1061 (1904).

[†] 'Proc. Roy. Soc.,' A, vol. 100, p. 1 (1921).

[‡] "The Specific Heats of Gases," p. 53 (London).

CORRECTED RESULTS

Tables III and IV contain smoothed values of the tube velocities as read off from fig. 4, at 200° C intervals, the velocities after correction for the thermal expansion of the rod carrying the movable reflector and the free space velocities derived therefrom by the application of the modified Helmholtz-Kirchhoff formula.

TABLE III—FREQUENCY 7908 CYCLES PER SEC. $k_1 = 0{\cdot}0051$

Temperature, ° C	1000	1200	1400	1600	1800
c = Kirchhoff's constant	1·792	1·997	2·188	2·368	2·533
Tube velocity in metres per sec, uncorrected	700·9	751·5	798·6	841·3	880·8
Tube velocity in metres per sec. corrected for the expansion of the rod carrying the reflector	702·5	753·7	801·8	845·7	886·4
Free space velocity in metres per sec	709·0	761·3	810·7	855·8	897·8
γ' the apparent ratio of the specific heats	1·329	1·324	1·322	1·316	1·309
C_v'/R	3·04	3·09	3·11	3·16	3·24

TABLE IV—FREQUENCY = 27422 CYCLES PER SEC. $k_1 = 0{\cdot}0027$

Temperature °C	1000	1200	1400	1600	1800
c = Kirchhoff's constant	1·792	1·997	2·188	2·368	2·533
Tube velocity in metres per sec, uncorrected	715·0	769·0	817·5	862·1	903·3
Tube velocity in metres per sec. corrected for the expansion of the rod carrying the reflector	716·6	771·2	820·7	866·5	909·0
Free space velocity in metres per sec	720·0	775·4	825·5	872·0	915·2
γ'' the apparent ratio of the specific heats	1·371	1·374	1·371	1·367	1·360
C_v''/R	2·69	2·67	2·69	2·72	2·78

The resulting values of γ' and γ'', the apparent ratios of the specific heats at the two frequencies, are also included together with C_v' and C_v'' —apparent specific heats at constant volume. The values of Kirchhoff's constant used in the tables are obtained by substituting in the formula previously given the values for the viscosity, density, and thermal conductivity given in the International Critical Tables.

The ratio of the specific heats is given by the formula

$$\gamma = \frac{V^2M}{RT},$$

where V is the corrected " free space " velocity in cm per sec, M is the molecular weight, R is the gas constant ($= 8 \cdot 315 \times 10^7$ ergs per gm mol) and T is the absolute temperature.

The correction necessary to the above formula for departure from the perfect gas laws is negligible since carbon monoxide, at the temperatures we are concerned with, is to all intents and purposes a perfect gas.

It is to be noted that the apparent specific heats are different at the two frequencies. An explanation of this phenomenon is to be found in a theory which has recently been put forward by Kneser.*

He found that the velocity of sound in carbon dioxide showed an increase over a certain frequency range. His explanation involved the supposition that the lag in the transfer of energy between a vibrational state of the carbon dioxide molecule and the other degrees of freedom may be much greater than would be expected from classical mechanics. In other words, as a sound wave of a frequency within the range over which the sound velocity showed an increase, passed through the gas, the gas could not be regarded as being in an equilibrium condition, due to the failure of part of the vibrational energy to follow the acoustic cycle. In fact, part of the vibrational energy had vanished from the expression for the adiabatic elasticity thus giving an increased sound velocity.

Kneser's theory led to the following formula :—

Apparent specific heat, derived from the velocity of sound data,

$$C_v' = \frac{C_v^2 + 4\pi^2 n^2 \beta^2 C_a^2}{C_v + 4\pi^2 n^2 \beta^2 C_a},$$

where

C_v = true specific heat,
n = frequency of the sound wave,
β = " period of relaxation " of the vibrational energy, and
C_a = specific heat of translation and rotation (= 5/2 R for a diatomic molecule such as we are dealing with at present).

Substituting in this equation the values of the apparent specific heats from Tables III and IV we have two equations at each temperature to determine β and C_v.

In Table V we give the values of β and of C_v thus obtained together with the theoretical values of C_v for the sake of comparison. The latter are given in columns 4–6, Table V. In column 4 the values are calculated from the Planck-Einstein function

$$\frac{C_{vib}}{R} = \left(\frac{h\nu}{kT}\right)^2 \frac{e^{h\nu/kT}}{(e^{h\nu/kT} - 1)^2},$$

---

* 'Ann. Physik,' vol. 11, p. 761 (1931).

where

C_{vib} is the vibrational specific heat of the gas,
h is Planck's constant,
k is Boltzmann's constant,
ν is the frequency of vibration of the atomic nuclei along the line joining them,
and T is the absolute temperature.

The value of $h\nu/k$ is taken as 3080.[*] The values in column 5 are based on equations given by Gordon and Barnes[†] in which the interaction terms in the expression for the rotational-vibrational energy states were taken into account.

The values in column 6 are based on calculations by Kassel.[‡]

TABLE V

		C_v/R			
Temperature °C	$\beta \times 10^5$ second	Experimental	Planck Einstein	Gordon and Barnes	Kassel
1000	1·0	3·147	3·127	3·150	3·135
1200	1·2	3·257	3·204	3·231	3·215
1400	1·15	3·261	3·260	3·291	3·273
1600	1·1	3·305	3·302	3·338	3·320
1800	1·0	3·368	3·334	3·376	3·354

DISSIPATION OF THE ENERGY OF THE SOUND WAVE IN THE GAS

The Kneser theory requires that for any frequency in the range over which the velocity of sound changes, there should be a considerable absorption of the energy of the sound wave, due to the irreversible heat transfer.

Concurrently with the half wave-length determinations which have already been described, measurements were made of the ratios of the galvanometer deflections at various nodes, in order to obtain such information about the sound absorption as was possible with the existing apparatus.

The energy of a sound wave passing through a tube is absorbed partly at the walls of the tube and partly in the gas contained in the tube. In the present case the former constitutes a considerable fraction of the total absorption.

---

[*] Mecke, 'Z. Physik,' vol. 42, p. 390 (1927).
[†] 'J. Chem. Phys.,' vol. 1, p. 297 (1933).
[‡] 'J. Chem. Phys.,' vol. 1, p. 576 (1933).

An estimate was made of the energy absorbed at the walls by application of the Helmholtz-Kirchhoff formula.* This estimate was only approximate as a correction of uncertain amount was necessary to the formula in order to take account of the roughness of the inner surface of the carbon tube. On subtraction of the estimated energy absorption at the walls from the observed absorption the remainder should represent the energy dissipated in the gas itself.

No agreement was found between the resulting sound absorption in the gas and that to be expected from Kneser's theory. Much weight is not to be attached to this as the discrepancy is in all probability due to some of the assumptions made and not to a failure of the theory. The latter would seem to be well supported by the velocity measurements which are of a much higher order of accuracy.

We desire to thank the Superintendent of the Physics Department for the facilities afforded for carrying out this investigation.

SUMMARY

The experiments recorded in this paper carry the determination of the specific heat of carbon monoxide by the sound velocity method up to a temperature of 1800° C.

By working with more than one frequency and correcting the data for the effect of frequency on the velocity of sound in the gas the specific heat in the temperature range 1000° to 1800° C is found to be in good agreement with that deduced from spectroscopic data.

Specific heats based on sound velocity measurements in various gases have not hitherto been found to be in accord even at moderately high temperatures with those obtained from spectroscopic data. It is probable, in the light of the present work, that the discrepancy is due to the fact that observers have based their conclusions on measurements made with a single frequency. From practical and theoretical considerations it is now known that the velocity of sound in a gas is not necessarily independent of the frequency. Corrections can be applied to the published values of specific heats of gases, at various temperatures, which are based on sound velocity measurements, when more accurate data become available as to the periods of relaxation of the vibrational specific heats of the different gases. There is every reason to believe that the discrepancy between the two sets of values will be greatly diminished.

---

* Rayleigh, "Theory of Sound," vol. 2, p. 325 ; see also Lichte, "Elekt. Nachr.-Techn.," vol. 4, p. 304 (1927) ; Tischner, "Elek. Nachr. Techn." vol. 7, p. 192 (1930).

On Active Chlorine

By E. J. B. WILLEY (Davy-Faraday Laboratory, Royal Institution, and Imperial Chemical Industries, Ltd.), and S. G. FOORD (Laboratory of Physical Chemistry, Cambridge)

(*Communicated by F. G. Donnan, F.R.S.—Received March* 28, 1934—*Revised July* 11, 1934)

Evidence has long been available that a modification of chlorine of abnormal chemical activity is produced by an electric discharge in this gas. The greater part of the earlier work was conducted under very badly defined experimental conditions which render the various researches difficult to correlate, but the properties of this " active chlorine " may be summarized as follows :—

(*a*) It possesses abnormal bleaching powers, and can react in the cold and the dark with acetic acid to form the monochlor derivative* ; with benzene it gives the hexachloride,† while with toluene the combination occurs mainly in the side chain.‡

(*b*) The yield of active gas is enhanced by irradiation of the discharge, by cooling, and by the presence of moisture.†

(*c*) It has a life period of at least 75 secs,‡ but is destroyed by heating, passage through water, and the action of another discharge ; it is not electrically charged and does not possess an abnormal density.§

(*d*) Since only very small changes in pressure follow passage of a discharge in a closed system containing chlorine, the active modification does not presumably represent an associated molecule such as Cl_3.‖ Reference may also be made to papers by Venkataramaiah¶ who gives a number of chemical reactions of chlorine activated in various ways, but his results must be treated with reserve (see Germann, *idem.*, p. 951).

In the present experiments we have endeavoured to repeat and extend the earlier studies under better defined conditions, and conclude that the phenomena are very probably due to a trace of atomic chlorine whose behaviour is markedly dependent upon the surface characteristics of the apparatus.

---

* Kellner, ' Deut. Reich. Patent,' No. 69780 (1892) ; ' Z. Elektrochem.,' vol. 8, p. 500 (1902).

† Russ, ' Ber. deuts. Chem. Ges.,' vol. 38, p. 1310 (1905).

‡ Schaum and Feller, ' Z. wiss. Photogr.,' vol. 23, p. 66 (1924).

§ Forster, ' Ber. deuts. chem. Ges.,' vol. 38, p. 1780 (1905).

‖ Vernon, ' Chem. News,' vol. 63, p. 67 (1891) ; Shenstone, ' J. Chem. Soc.,' vol. 71, p. 471 (1897) ; Briner and Durand, ' Z. Elektrochem.,' vol. 14, p. 706 (1908).

¶ ' J. Phys. Chem.,' vol. 27, pp. 74, 951 (1923).

EXPERIMENTAL

Pressure Change in Chlorine in the Silent Discharge—For this, the apparatus shown in fig. 1 was used. The discharge vessel was a Siemen's ozonizer of 2 mm annular space. Chlorine pressure was read upon a modified Bourdon gauge which departed from the usual form in having in place of the long indicator rod a short bar to whose end a galvanometer mirror was attached. Changes in the pressure of the system were read by the angular movement of the mirror, measured by a lamp and scale.

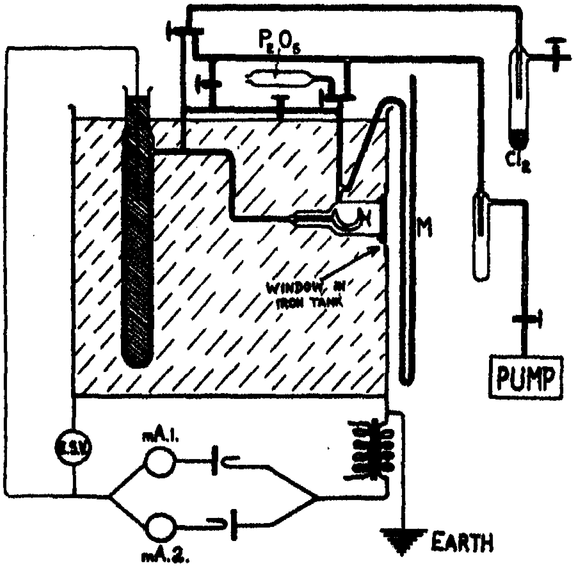

FIG. 1

— capillary ; ═ quill ; mA.1, mA.2 = milliammeters ; E.S.V. = Kelvin voltmeter.

This arrangement was much less subject to vibration than the older type, and a similar device has recently been adopted by Bodenstein for the construction of very small and compact manometers made in quartz. The discharge tube and pressure gauge were maintained in a thermostat. Chlorine from HCl and $KMnO_4$ was fractionated into the trap as shown, and then allowed to evaporate into the evacuated discharge vessel until the latter was filled to rather less than atmospheric pressure ; this having been several times repeated, the system was isolated by closing all taps. Although a pressure change of 1 : 5000 could have been measured, no contraction, due to an association, was observed when the gas was subjected to the silent discharge at (*a*) 50, and (*b*) 400 cycles, the applied voltage being varied from 4000 to 15,000 (*cf.* p. 312). A slight expansion of *ca.* 1 : 2000 was always observed on switching on the current, the initial pressure being immediately restored when the discharge was cut off. This slight expansion is in agreement with the observation of Vernon, but contrary to that of Shenstone. It may be due to the formation of a small stationary concentration of chlorine atoms, but in view of the uncertainty as to conditions in a silent discharge, and particularly as to temperature as understood in terms of the kinetic theory, this view cannot be adopted with any degree of confidence. When the voltage was sufficiently increased, brush discharges took place and a continual slow expansion set in, quantitatively attributable to a heating of the dilute acid forming the inner electrode.

We therefore conclude that any activation of chlorine in the silent discharge is not accompanied by a volume change of magnitude sufficient to be detected by the method used. It must not be assumed, however, that the formation of an associated molecule such as Cl_3 is ruled out, since in measurements of the degree of activation by benzene, to be described later, the amount of additional chlorination taking place corresponded under favourable conditions to about only 1 : 1000, which might conceivably be the result of chains initiated by Cl_3. The amount of active gas obtained was very much smaller than this when operating with the very pure chlorine used in the experiments just described. At present there is no definite evidence either for or against the formation of Cl_3 in this manner, but if it is present its concentration must be very small. It may here be mentioned that on passing oxygen through an ozonizer which had been used for discharges in chlorine, no ozone was formed until after several hours' running, showing that a trace of chlorine here exerts a very strong inhibitory action.

Attempts to Detect an Absorption Spectrum—With a view to the rapid detection and determination of active chlorine by a simple physical method, absorption spectra of chlorine in the unsparked and sparked condition were photographed for the range $\lambda = 5000$ to 2100 A. using a hydrogen tube and a Pointolite lamp as sources of continuous radiation. Experiments were made with silent and spark discharges at atmospheric and at 7 mm pressure, and a quartz absorption tube 150 cm long. No evidence of any absorption additional to that of ordinary chlorine was found.

Chemical Reactions—Two types of discharge were used, (*a*) a spark discharge between internally cooled electrodes, in a quartz vessel of the kind already described by one of us*; (*b*) a silent discharge in a Siemen's ozonizer; in this type the inner electrode was water-cooled when high currents were being passed. Alternating current was always used, and the silent discharge was supplied with 400 cycle current at 11,000 v. R.M.S.; this gave a minimum of brushing which might destroy the active chlorine first formed. The mean current under these conditions depended upon the material of the ozonizer walls, and was measured by moving-coil milliammeters in the two branches of a two-way rectifying circuit. Geometrically similar tubes of glass and quartz were used, and their characteristic curves are shown in fig. 2. Up to 8000–9000 v. capacitative current alone flows, giving the initial straight line through the origin, but at higher voltages a steeper line appears, indicating passage of energy into the gas; the tubes were always operated on this part of the curve. It is emphasized that the working potentials were the R.M.S. values, the maximum values being very much higher since the alternating current had a "peaky" wave of high form factor. It was found that comparatively large changes in the current brought about only small variations in the yields of active gas, and in view of the difficulty of comparing the activity from various tubes of differing surface

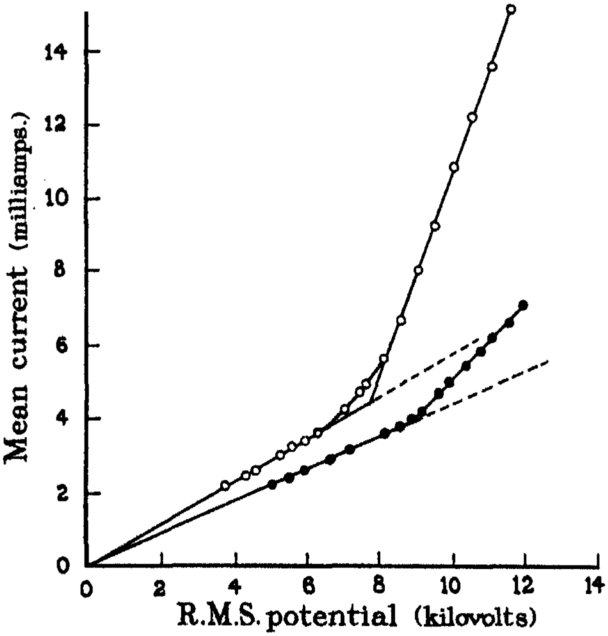

FIG. 2—○ Glass ozonizer; ● quartz ozonizer.

---

* Foord, 'Dissertation,' Univ. London, 1933.

materials, for simplicity and uniformity of working conditions the potential was held constant at 11,000 v. throughout.

The chlorine was taken direct from a cylinder and found by reaction with mercury to be of 99·98% purity. In all but the final series of runs, the gas was passed through a bubbler containing water to remove traces of ferric chloride said to be present, and then well dried by a long column of phosphorus pentoxide. It was later found that the supposition was not correct, and in the last series the bubbler was omitted; the effect of this is discussed elsewhere, in connection with the role of water vapour in the production of active chlorine.

The number of taps in circuit was reduced to a minimum of two ; these were lubricated with Apeizon L grease, which is only slowly attacked by chlorine, and forms solid products which do not pass on in the gas stream. The amounts of HCl formed with the grease were too small to interfere with the measurements.

From the discharge, the chlorine passed via capillary tubing, to apparatus for examination of its chemical activity. This consisted of two parallel circuits of two reaction vessels in series, which could be used alternately for continuous runs. (For details of technique, see Foord, *loc. cit.*)

In all experiments, the reaction vessels were kept in darkness. For gaseous reactions, the reagent was admitted through a side tube attached at a distance sufficient to prevent back-diffusion of the diluent gas into the discharge.

Determination of Combined Chlorine—For the determination of combined chlorine in organic liquids, the following methods were found most satisfactory.

(1) Reduction by sodium and alcohol, according to Stepanoff's method, followed by titration of the resulting sodium chloride with silver nitrate; the process as used was checked against monochlorbenzene.

(2) For substances which are not too vigorously oxidizable, the " combined " chlorine was converted into chromyl chloride and distilled into alkaline hydrogen peroxide, as described by Robertson* ; the analytical technique was checked against monochloracetic acid.

EXPERIMENTAL RESULTS

Tests of the reactivity were carried out with substances which are capable of only very slow reaction with ordinary chlorine, to overcome the difficulty of determining small differences between relatively large

* 'J. Chem. Soc.,' p. 902 (1915).

amounts of reaction. For quantitative work, benzene has been found to be the most satisfactory reagent, as was found by Russ, since its reaction with chlorine is very slow at room temperatures. As a result, the most useful and reliable data have been obtained with the aid of this substance, and are dealt with more fully.

A large number of the initial experiments were carried out with the spark discharge between carbon electrodes, but these are not always to be regarded as conclusive, owing to the formation of C_6Cl_6 by direct combination of the chlorine with the electrodes.* Although formed in small quantities only, crystals of this substance actually separated in some experiments, so that results exhibiting increased chlorination by the use of the spark could be attributed at least in part to the deposition of this compound in the reaction vessels. That the increased reactivity of the chlorine as observed was not entirely due to this cause was shown, in experiments on the chlorination of toluene, by precipitating most of the hexachlorobenzene with alcohol in the analytical processes. Owing to the contamination of the chlorine in this manner, and also by a small amount of HCl formed from hydrogen occluded on the carbon, results obtained with the silent discharge are to be regarded as more conclusive, since in the latter method there is unlikely to be any such possibility, which cannot be eliminated, of a reaction with the electrode materials.

For experiments with the silent discharge, a discharge tube of the Siemen's type was used. The approximate dimensions were overall diameter 4 cm, width of annular space 1·5 mm, axial length of annular space 30 cm. Geometrically similar discharge tubes, one of glass and one of quartz, were used in studying the effect of irradiation of the discharge, etc. In all experiments the annular space was shielded from extraneous light.

Reaction with Water—Chlorine from the spark discharge was led into water. A dense fume was formed in the reaction vessel, which tended to condense on subsequent parts of the apparatus ; this fume has not been examined in detail. After the experiment, dissolved chlorine was removed by adding excess of 5% potassium iodide solution, and then sodium thiosulphate until all free iodine was removed, the HCl formed in the reaction being estimated with N/50 sodium hydroxide solution. A three-fold increase in the amount of HCl was found, corresponding to the consumption of 0·1% of the chlorine passed.

A less marked but quite definite increase (50%) was observed when the silent discharge was used instead of the spark, corresponding to 0·02%

---

* See Bolton, ' Z. Elektrochem.,' vol. 9, p. 209 (1903).

of the chlorine passed. That this was not due to a silicon chloride formed by reaction of chlorine with the glass walls of the discharge vessel was shown by reproducing the experimental results using air charged with a trace of silicon tetrachloride vapour, the chloride which gives the greatest amount of HCl for a given deposit of silicic acid. For the formation of an equivalent amount of HCl, a thin gelatinous film of silicic acid was obtained with the $SiCl_4$ but none with the discharge experiment. The increased yield of hydrochloric acid may therefore be ascribed to a more reactive form of chlorine.

Reaction with Ferrous Salts—The oxidation, by chlorine, of aqueous ferrous chloride and ferrous sulphate solutions of approximately normal strength was measured with and without passage of a spark discharge through the gas. The amount of ferrous salt remaining was estimated with potassium permanganate for the sulphate, and for the chloride with potassium dichromate using potassium ferricyanide as external indicator. With the sulphate, the amount of chlorine reacting decreased from 5·6% to 5·0%. With ferrous chloride, no difference could be detected in the amount of oxidation. No explanation can as yet be offered why the oxidation of the sulphate should be affected and not that of the chloride, unless it be that the active chlorine can under some circumstances act as a reducing agent.

Aqueous Oxalic Acid—Ordinary chlorine reacts with oxalic acid according to the reaction : $(COOH)_2 + Cl_2 = 2CO_2 + 2HCl$. The amount of oxalic acid remaining after equal times of reaction with ordinary chlorine and with chlorine from the spark discharge was measured with potassium permanganate. No difference was observed in the two cases, but a small variation may well have been masked by the large amount of reaction occurring with ordinary chlorine.

Acetic Acid—Glacial acetic acid was treated in successive portions with ordinary and with sparked chlorine, and without removing dissolved gas the liquid was diluted and a portion used for estimating the total amount of chlorine, both free and combined present in solution ; Robertson's method was used for the analyses. An increased amount of reaction was obtained with the sparked chlorine, corresponding to combination by 0·8% of the chlorine passed, although the accuracy of this measurement was very low owing to the relatively large amount of free chlorine dissolved in the reagent.

Methane and Hydrogen—These gases were added to chlorine shortly after passage of the latter through a discharge, both spark and silent discharges being separately used. Experiments were made with moist and with dry chlorine. Differences in the amount of reaction were tested in two ways : (*a*) by observing the chlorine concentration photometrically with a photoelectric cell, by the method used for NO_2* ; (*b*) by absorbing in water the HCl formed, and determining it with standard alkali. Within the accuracy attainable no evidence of reaction could be found.

In the course of these experiments it was noted that a considerable quantity of methane dissolves unchanged in liquid chlorine at −80° C, which suggests a possible method for the separation of gases which are difficult to liquefy in the pure state.

Chlorination of Dyes—A number of experiments have been carried out using aqueous dye solutions in an apparatus of the type shown in fig. 3, with a view to determining whether active chlorine was capable of decolorizing them more rapidly than ordinary chlorine. The principle of the apparatus is seen from the diagram, the gas bubbling up through the liquid in the spiral passes off at the top, and at the same time causes a circulation of the dye solution through the side limb, which acts as an observation tube. The whole apparatus was painted black with the exception of the end windows of the latter part, so that chlorination could take place mainly in the dark while a continuous inspection of the colour was made. No dyes could be obtained which were fast to ordinary chlorine, so that comparative measurements of the rate of decolorizing had to be made. No difference was observed in the rate of decolorizing by ordinary and by sparked chlorine.

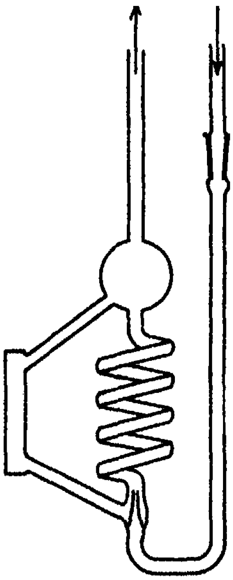
FIG. 3

Chlorination of Toluene—For studying the reaction with toluene, apparatus consisting of two parallel circuits of two reaction vessels in series was used. Chlorine from the discharge tube was bubbled through 20 cc of sulphur-free toluene in the first reaction vessel, and thence through 10 cc of water in the second to absorb any hydrochloric acid formed by substitutional chlorination of the toluene in the first vessel. Chlorine was passed at a rate generally standardized at 4 litres/hour, for a convenient time of experiment (usually 30 minutes), and then diverted through the second circuit of reaction vessels. A current of air was then passed at about 8 litres/hour through the first circuit for a period of 10 minutes, partly to remove some dissolved chlorine from the toluene, but primarily to carry over any dissolved hydrochloric acid from the toluene into the water in the second vessel. Blank experiments with toluene treated with gaseous HCl showed that the separation was satisfactorily effected.

---

* Willey and Foord, 'Proc. Roy. Soc.,' A, vol. 135, p. 166 (1932).

A difficulty introduced by interaction of toluene and dissolved chlorine was overcome by shaking the liquid, immediately after the experiment, with excess of sodium sulphite solution, which removed the whole of the free chlorine in a few seconds. HCl and SO_2 formed in this reaction were removed by repeated shaking with water in a separating funnel, and the *total* amount of combined chlorine in the residual liquid estimated by reduction with sodium and alcohol, without determination of the relative amounts of ring and side-chain chlorine.

The aqueous solution from the second vessel was treated as described on p. 314 to measure the amount of HCl present, except that the acid was titrated with N/10 alkali. Of the acid determined, only a very small amount was due to direct reaction between chlorine and the water, the remainder giving an approximate measure of the amount of substitutional chlorination of toluene which had taken place.

As the result of experiments with the spark discharge between carbon electrodes, it was found that no change occurred in the amount of substitutional chlorination, but a 10% increase in the total chlorination took place, corresponding to addition. That this increase was not due to a rise in the reaction temperature, produced by the heating effect of the discharge on the chlorine, was shown by measuring the temperature of the gas entering the reaction vessels. The temperature rise with the discharge was only 2° C. On raising the temperature of the gas by as much as 5° C, by means of a heating element, the temperature of the toluene remaining constant, no differences in the amount of chlorination could be observed with the gas at the two temperatures. A similar test was applied in the chlorination of benzene (*vide infra*). Since the spark was used in these experiments, the possibility that a considerable proportion of this increase was due to formation of C_6Cl_6 at the electrodes cannot be completely eliminated, but as previously shown the whole of the increase cannot be ascribed to this cause. The experiments would bear repetition with a silent discharge. A disadvantage attaching to the use of toluene for detecting active chlorine lies in the comparatively large amount of chlorination which occurs in blank experiments with the unsparked gas.

Chlorination of Benzene—According to Slator* the main reactions occurring with excess of chlorine in the presence of catalysts are :

$$C_6H_6 + Cl_2 = C_6H_5Cl + HCl \qquad (I)$$

$$C_6H_6 + 3Cl_2 = C_6H_6Cl_6 \qquad (II)$$

the relative extents of the two reactions being determined by the nature of the catalyst. No data are available on the reaction at room temperature in the dark and in the absence of catalysts, except that the reaction is very slow, but it may reasonably be supposed that the above reactions occur, the relative rates not being specified. The slowness of the reactions renders benzene a most suitable substance for the detection of active chlorine, as was found by Russ (*loc. cit.*).

In the present experiments, measurements were made of the substitution and addition which occurred, using essentially the same technique as was used for toluene. Benzene was found to dissolve even more chlorine than did toluene, *i.e.*, to the extent of about 20 times its own volume. Heat of solution of this chlorine, together with evaporation of the benzene, produced considerable variations of temperature of the reactants, but by standardization of experimental conditions, and the performance of duplicate measurements with and without activation of the chlorine, comparable conditions of experiment were obtained.

By estimation of the total chlorine and the HCl formed, a measure of the amounts of substitution and addition, *e.g.*, by reactions (I) and (II) was obtained. With the method used, the data for the two reactions could not be accurately correlated to determine their relative amounts, owing to the continuation of the chlorination of benzene vapour during passage of the gas from the first reaction vessel to the vessel containing water for absorbing the HCl. *Changes* in the amount of HCl formed could, however, be compared with the changes in overall combination, for the purpose of detecting chlorination by addition occurring simultaneously with substitutional chlorination, through the agency of the active gas.

With a spark discharge, increases were observed in both addition and substitution, but as the accuracy of the measurements was not high this result must only be regarded as qualitative. Quantitative results, though of smaller magnitude, were obtained by the use of a silent discharge. With non-activated chlorine, about 0·1% of the chlorine passed reacted with the benzene. On passage of the gas through a silent discharge in a glass ozonizer, a 50% increase in the amount of HCl formed was observed, corresponding to reaction by 0·05% of the chlorine passed if it is assumed that one molecule of Cl_2 gives one molecule of HCl. A somewhat larger increase in the total chlorination took place, showing the formation of an addition compound, such as $C_6H_6Cl_6$, the increase in which was the basis of Russ's method for detecting active chlorine. Actual separation of a white solid occurred on the entry tube to the reaction vessel where the gas first came into contact with the benzene ; this was probably benzene hexachloride, but was formed in quantities too small for confirmation of this by analysis. The accuracy of the above measurements was about 5–10% of their value, corresponding to 0·003% of the chlorine passed, higher precision being difficult to attain with such a small degree of chlorination.

---

* 'Trans. Chem. Soc.,' p. 729 (1903).

Definitely increased activity of the chlorine was thus observed, and could be ascribed to four possible causes : (*a*) formation of an active form of chlorine in the discharge; (*b*) a heating effect of the discharge, leading to increased rate of reaction; (*c*) combination of chlorine with impurity in the gas to form a chemically reactive compound; (*d*) combination of chlorine with the silica of the glass; (*b*) and (*d*) have been shown to be untenable. In view of the purity of the chlorine used, the effects, although small, were too large to be ascribed to (*c*), unless we postulate some form of cyclic reaction in which the reactive compound is regenerated. It would therefore appear that the effects are certainly attributable to active chlorine.

Owing to the long analytical processes involved in measuring the total chlorination, advantage was taken in later work of the parallelism between the increased total chlorination and the increased formation of HCl, and in investigations of further properties of active chlorine the activation has been measured solely in terms of the latter quantity. The comparatively large proportional effects observed in the chemical reaction with benzene rendered this reagent eminently suitable for determination of active chlorine.

For the sake of simplicity, and since experiments were carried out under standard conditions of time, flow-speed, and quantity of material, the observed activity will be expressed in terms of additional cc of N/10 acid formed in a discharge experiment. On this scale, 1·0 cc of acid corresponds to approximately 0·1% of the chlorine passed during an experiment, on the assumption already made (p. 318) as to the formation of HCl. It does not follow that it corresponds to the presence of 0·1% of active chlorine in the gas ; the actual value may be greater or less than this figure, according to whether partial reaction or a chain reaction occurs, but the scale adopted gives a convenient measure of the amount of active substance. In these experiments, the observed activity was of the order 1·0.

From a large number of experiments, the following conclusions were drawn :—

(*a*) Active chlorine reacts with benzene giving both substitution and addition compounds.

(*b*) Increase of the flow speed through the apparatus tends to increase the measured active chlorine concentration.

(*c*) Activated gas passed through a quartz tube acting as a time vessel showed a decrease in activity to one-third of the value obtained in the absence of the time vessel, the time of passage through the tube being 10 seconds.

(*b*) and (*c*) show that a slow decay occurs, at a rate which is much greater than that observed by Russ and by Schaum and Feller. This is ascribed to the use of a quartz time vessel, since, as will be shown later, the nature of the walls appears to play an important part in the decay of the activity.

EFFECT OF ADDED IMPURITIES

In the experiments so far described, the chlorine used was first bubbled through water, and then passed through a phosphorus pentoxide drying tube, before passage through the discharge. A disturbing factor which appeared towards the end of runs of 8 hours or more manifested itself in a falling off of the measured activity, the yield of active gas diminishing, fairly rapidly, to zero, but returning on discontinuing the experiments for some hours. It was therefore suspected that a small quantity of impurity was being introduced into the chlorine at the bubbler, which was capable of acting in a manner similar to that of a photogen by poisoning the walls with respect to a surface decay of active chlorine. The experiments with benzene were therefore repeated after removing the water bubbler from the circuit, and the observation was made that no activity was here acquired on passing the chlorine through a discharge in a glass ozonizer. It is therefore apparent that the active substance is either not produced at all or else undergoes a very rapid decay in the absence of a small quantity of impurity. The latter hypothesis is regarded as the more probable in view of the very small quantity of impurity required, and leads to the conclusion that the decay occurs by a wall process, an hypothesis which is supported by later experiments on the production of active chlorine in glass and in quartz discharge tubes.

Two explanations of these facts may be offered. Firstly it may be assumed that with the bubbler in circuit, a trace of water vapour remained in the gas after treatment with P_2O_5, and that this acted as the wall poison. This would explain the results obtained by Russ, who also found in his experiments that rigorous drying of the chlorine largely prevented its activation. On this theory, however, so long as any water remained in the bubbler, a constant activity should be observed in a continuous run of experiments over any length of time, which is contrary to the observations made in the present work. An alternative explanation, and one which is capable of accounting for the fatigue effect which occurs when using chlorine which has been passed through water, is that small amounts of impurity are formed by a slow reaction between chlorine and the water in the bubbler. This impurity is gradually swept away during the course of a long run until its concentration in the gas stream falls below the value required for effective poisoning of the walls for decomposition of active chlorine. The requisite concentration would be restored on arresting the flow of gas for a suitably long period of time. Such a slow reaction actually occurs, *i.e.*,

$$2HOCl \rightarrow 2HCl + O_2,$$

as a second stage following the reversible reaction :

$$Cl_2 + H_2O \rightleftharpoons HCl + HClO.$$

New substances produced are O_2, HCl, and HClO, and of these O_2 and HCl are impurities which comply with all the experimentally observed facts. It remains to examine the effect of adding these and other substances.

Oxygen—Small amounts of oxygen varying from 0·1% to 0·7% by volume were added to chlorine taken directly from the cylinder through a P_2O_5 tube. No increased reactivity towards benzene was observed on subjecting the gas to a silent discharge. By a process of elimination, therefore, it appears that a trace of HCl is the agent which has rendered the active chlorine comparatively stable. The complete proof of this would be to note the effect of adding HCl to the chlorine in an amount sufficiently small not to interfere appreciably with measurements of the HCl formed by the active gas. Unfortunately an opportunity for testing this did not arise owing to pressure of other experimental work, but if carried out would be of interest in settling this point. A serious objection to the theory that HCl acts as the stabilizing impurity is provided by the fact that in Russ's experiments the impurity could be progressively removed by increasing intimacy of contact with strong sulphuric acid, or by passage over P_2O_5; the latter observation is not substantiated by the present experiments, in which the same degree of activity was found whether the wet gas was passed through a P_2O_5 tube, or through a trap cooled to −20° C from which the chlorine presumably emerged with a water content intermediate between the partial pressure of water vapour over ice, 0·6 mm, and that over chlorine hydrate at this temperature. In view of the uncertainty of the nature of the stabilizing impurity, chlorine passed through water and then over P_2O_5 will be referred to in subsequent experiments as "moist chlorine." A tentative suggestion is that both HCl and water vapour play a part in the arrest of decay.

Nitrogen—No activity was obtained on passing a mixture of dry chlorine with up to 0·7% of nitrogen through a silent discharge.

Air—On adding air in small quantities up to 2% to dry chlorine, increased chlorination of benzene occurred by passage of the gas through a silent discharge, as shown by the following table :—

% Air	Activity
0·0	0·0 units
0·5	0·7
1·0	1·2
1·5	1·2
2·0	1·6 (Possible activity error = 0·1–0·2)

The increase was particularly marked with regard to the formation of white solid products on the entry tube to the reaction vessel. Sufficient of this solid was prepared in a long run to show qualitatively that it contained chlorine but no nitrogen, and hence was not a nitration product formed by the action of oxides of nitrogen. Previous experiments have shown that nitrogen and oxygen separately are incapable of producing any effect, the negative result with oxygen eliminating the important possibility that chlorine monoxide was formed in the discharge, and exercised its known property of reacting with benzene to form hexachlorobenzene.* The effect with air must therefore be due to a compound of nitrogen and oxygen, or of nitrogen, oxygen, and chlorine, formed in the discharge in necessarily quite small amounts owing to the initial small concentration of air. This being so, great care must be taken (as already emphasized) in assuming the effect to be due to active chlorine rather than to a simple chemical reaction involving the impurities. A more complete discussion of whether the increased reaction is actually due to active chlorine must be deferred until relevant experiments have been described dealing with the effect on the observed activity of irradiation of the chlorine with light.

---

* Scholl and Norr, 'Ber. deuts. chem. Ges.,' vol. 33, p. 725 (1900).

EFFECT OF IRRADIATION OF CHLORINE

The results of Russ indicated that increased yields of active chlorine were obtained by the simultaneous action of ultra-violet light and the discharge on chlorine, and it appeared desirable to examine these phenomena in greater detail.

Irradiation alone—Moist chlorine at a flow speed of 4 litres/hour was irradiated in a 10 cc quartz tube by the unscreened light from a horizontal mercury vapour lamp placed 3 inches away, and the resulting gas passed into benzene ; no additional reactivity appeared.

Irradiation before the Discharge—Moist chlorine was irradiated in the manner described above, and then passed through a silent discharge. The activity (1·1 units) of the resulting gas was the same whether the chlorine was previously irradiated or not.

Irradiation during the Discharge—In view of Russ's observations it appeared probable that much larger concentrations of active chlorine could be obtained by strong irradiation of the chlorine in the discharge. To carry out this process in the most effective manner, a special quartz mercury lamp was designed, being a modification of that due to Bovie* and described by Foord (*loc. cit.*). A particular feature of the lamp was its small overall diameter of 1 inch, arranged so that it could be slipped down bodily inside the Siemen's ozonizers used. As electrolyte for the inner electrode of the discharge tube, dilute sulphuric acid was used, and was kept cooled during operation by the water jacket of the mercury vapour lamp. By totally enclosing the lamp in this way, practically the whole of the available light was used for irradiating the chlorine in the annular discharge space. The efficiency of irradiation was still further increased by using mercury as the outer electrode to the discharge tube, the metallic surface reflecting transmitted light back through the chlorine.

Experiments were made using both glass and quartz ozonizers. With pure chlorine it had been observed that very little activity towards benzene was obtained with the normal dark discharge. No activity was obtained under similar conditions with the irradiated discharge. Using chlorine with 1% of air added, and the quartz ozonizer, the activity of 1·4 observed in the dark discharge was *not further increased* by irradiation of the discharge. These results are contrary to those of Russ.

---

* 'J. Amer. Chem. Soc.,' vol. 37, p. 1721 (1915).

Irradiation after the Discharge—In initial experiments using the moist gas, it will be remembered that the introduction of a 10 cc quartz tube produced a drop in the measured activity from 1·0 to 0·3, using a glass discharge tube. On irradiating the quartz tube with light from a mercury vapour lamp, an increase in the activity to 1·0, *i.e.*, to its original value, was observed. It appears that with the quartz tube the active chlorine is stabilized by the action of the light, since the light alone gave no evidence of producing activity. Furthermore, on using pure chlorine in a quartz discharge tube, in which no activity could be obtained, subsequent irradiation produced no effect.

On the other hand, activity equal to 2·0 was observed on passing a mixture of chlorine with 1% of air through a discharge in a quartz ozonizer, an activity which was not appreciably diminished on passing the gas from the discharge through a double-walled quartz time vessel of about 50 cc capacity, kept in the dark ; but in this case a *decrease* in the activity from 2·0 to 0·8 took place on irradiation.

DISCUSSION OF RESULTS

The stabilization of the activity produced in " moist " chlorine by the action of light (whether visible or ultra-violet has not been determined) at first led to the supposition that decay was prevented in the homogeneous phase by photochemically produced chlorine atoms, a possible mechanism being :

$$\mathrm{Cl}_a \rightleftharpoons \mathrm{Cl}_b + \mathrm{Cl}$$
$$\mathrm{Cl}_b \rightarrow \mathrm{Cl}_2,$$

where Cl_a = active chlorine and Cl_b = an intermediate body, when we take into account the non-production of active chlorine by the action of light alone. However, the reverse effect for chlorine with air as impurity (which will be called " photogenic " chlorine by analogy with the impurities required for production of active nitrogen) does not give support to this theory, if one assumes that the increased reactivity towards benzene is due to the same substance in each case. With photogenic chlorine it seems much more probable that the effect of the light is to initiate a photochemical reaction, which involves decomposition of the inhibitor.

For moist chlorine, a similar explanation might be given, assuming photochemical formation of an inhibitor ; it is difficult to imagine such a process taking place if the impurity in the chlorine is HCl alone. If water vapour is present, it appears quite possible that photochemical reaction with chlorine might produce a substance (*e.g.*, HOCl) capable of acting as a strong inhibitor. We have therefore to decide whether or no the activity observed in moist and in photogenic chlorine is due to reaction by the same compound.

The effects observed with photogenic chlorine may be discussed more fully. We have first to examine the possibility that the substance capable of such rapid reaction with benzene may be a known compound of nitrogen, oxygen, and chlorine, which is photochemically decomposed on irradiation, a possibility of particular importance in view of the experimentally observed fact that the decay process normally observed in moist chlorine is either entirely suppressed or rendered very slow in the case of photogenic chlorine by the presence of the impurity.

For the reason given previously, *i.e.*, non-production of activity in chlorine with added oxygen, the results cannot be explained on the assumption of the formation of a chlorine oxide. Nitrogen trichloride which might be formed, and is subject to photochemical decomposition, does not react with benzene* and is not produced by a discharge in mixtures of nitrogen and chlorine.† The known compounds of nitrogen, oxygen, and chlorine have been prepared, and their action on benzene studied to determine whether solid chlorination products were formed, as in discharge experiments. These will be dealt with in turn.

NOCl—This compound is photochemically decomposed below 6270 A.‡ but has been kept for a period of months in contact with benzene without any change taking place even in sunlight.§

$NOCl_2$—This is produced as an unstable intermediate compound in the formation of NOCl from nitric oxide and chlorine|| according to the mechanism :

$$NO + Cl_2 \rightleftharpoons NOCl_2$$
$$NOCl_2 + NO \rightarrow 2NOCl.$$

No data are given for a photochemical decomposition of $NOCl_2$, but

---

* Hentzschel, 'Ber. deuts. chem. Ges.,' vol. 30, p. 1434 (1897).

† Noyes, 'J. Amer. Chem. Soc.,' vol. 43, p. 1774 (1921).

‡ Bowen and Sharp, 'J. Chem. Soc.,' vol. 127, p. 1026 (1925).

§ Lynn and Arkley, 'J. Amer. Chem. Soc.,' vol. 45, p. 1045 (1923).

|| Trautz and Schluter, 'Z. anorg. Chem.,' vol. 136, p. 1 (1924).

it has a line absorption spectrum in the yellow and green. Its reactivity towards benzene was tested by passing a slow current of nitric oxide into a stream of chlorine, and, after passage through a time vessel, allowing the mixture to bubble through benzene. The volume of the time vessel and the gas flow speeds were so arranged that only about 50% of the NO had reacted on reaching the benzene, thus ensuring the presence of $NOCl_2$ in the gas at this point. No formation of solid chlorination products was observed in the benzene.

NO_2Cl—The method of preparation of NO_2Cl given by Hasenbach,[*] *i.e.*, strongly heating a mixture of NO_2 and Cl_2, appears doubtful, in view of the work of Schumacher and Sprenger[†] upon the thermal decomposition of this substance. NO_2Cl was therefore made according to the method given by the latter authors,[‡] *i.e.*, by preparing NOCl by interaction of NO and Cl_2, removing excess NO and chlorine by pumping and partial evaporation, and distilling several times in a current of ozonized oxygen, condensing each time in liquid ammonia. The resulting liquid containing both NOCl and NO_2Cl was allowed to evaporate, and the gas, consisting largely of NO_2Cl, passed into benzene. No solid chlorination products were obtained.

The oxychlorides N_2OCl_2 and N_2OCl recently postulated by Noyes[§] as intermediates in the reaction $NCl_3 + 3NO = 2NOCl + N_2O + Cl_2$ cannot very well be considered in view of the uncertainty as to their existence. It must therefore be concluded that the chlorinating properties of photogenic chlorine after passage through a discharge are not due to a known chemical compound.

Two alternative explanations of the experimental results may be offered. (*a*) A new compound of nitrogen, oxygen, and chlorine is formed in the discharge, capable of rapid reaction with benzene to form solid addition, and also substitution products, and which is subject to photochemical decomposition. (*b*) An active form of chlorine, together with a compound of nitrogen and oxygen, or of nitrogen, oxygen, and chlorine (not necessarily unknown) is formed in the discharge, the latter acting as an inhibitor to the decay of the active chlorine, and being at the same time subject to photochemical decomposition. On the existing evidence it is not possible to decide which of these alternatives is correct, although we favour the latter, and it would be of interest to investigate the stabilizing influence of the known oxides of nitrogen and nitrogen oxychlorides added in small amounts to the decaying active gas obtained with moist chlorine, just after passage of the latter through the discharge.

---

[*] 'J. Prakt. Chem.,' vol. 4, p. 1 (1871).

[†] 'Z. Elektrochem.,' vol. 35, p. 653 (1929).

[‡] 'Z. anorg. Chem.,' vol. 182, p. 139 (1929).

[§] 'J. Amer. Chem. Soc.,' vol. 52, p. 4298 (1930).

A point which weighs against the active chlorine theory of the activity of photogenic chlorine is the qualitative observation that rather more solid chlorination product for a given amount of substitution was found with photogenic chlorine than with moist chlorine, which tends to show that the chemical activity is not due to the same substance in each case. Furthermore, the slowness of decay in photogenic chlorine is not in agreement with the brief statement of Schaum and Feller that oxygen inhibits activation, but as this statement was not qualified, it cannot be considered as very definite. On the other hand, degrees of activity of approximately the same magnitude were obtained under similar conditions with both photogenic and moist chlorine, which is either a coincidence, or more probably evidence of a common origin of the activity in the two cases.

NATURE OF ACTIVE CHLORINE

On the evidence obtained in the present work, it is impossible to decide the structural nature of active chlorine, particularly as the experiments carried out may possibly be concerned with two reactive substances. It is of interest, however, to compare its properties with those of atomic chlorine, to obtain some idea as to whether the results obtained may be ascribed to the formation of that substance.

Decay of atomic chlorine by recombination to molecules occurs mainly as a wall reaction at low pressures. A similar wall decay is observed with active chlorine at high total gas pressures, but this decay is rendered very slow if " moist " chlorine is used. If it is assumed, with Russ, that water vapour is the stabilizing agent, this property of active chlorine is distinct from that of atomic chlorine, since,* according to Rodebush and Klingelhoeffer, water vapour has no effect on the initiation of reaction in hydrogen-chlorine mixtures by chlorine atoms. In the latter case, however, HCl would be present, and by poisoning the walls would render ineffective any other photogen (*e.g.*, water vapour).

The comparative inefficiency of the silent discharge for the production of chlorine atoms has been shown by Wendt, Landauer, and Ewing† in attempts to initiate the hydrogen-chlorine reaction, but it does not follow that the concentration of chlorine atoms is insufficient to lead to an appreciable amount of reaction with benzene, since reaction chains of the order of one million atoms in length have been observed in the photochlorination of benzene* which are presumably initiated by chlorine atoms. In addition, there is the significant fact that benzene hexachloride is the chief reaction product in both photochlorination of benzene and chlorination by the electrically activated gas.

---

* 'Proc. Nat. Acad. Sci.,' vol. 18, p. 531 (1932) ; 'J. Amer. Chem. Soc.,' vol. 55, p. 130 (1933).

† 'J. Amer. Chem. Soc.,' vol. 44, p. 2377 (1922).

As has been mentioned, at low pressures (0·1 mm Cl_2) recombination of atomic chlorine is mainly a wall reaction, and takes place with extreme rapidity. At higher pressures, diffusion to the walls becomes more difficult, and the possibility is introduced that in the high pressure experiments described in the present work sufficient chlorine atoms might survive to undergo an appreciable chemical reaction, particularly if a chain process is assumed. At the same time, the probability of recombination of atoms by 3-body collisions of two atoms and a molecule is very considerably increased. On the extreme assumption that all collisions of the type mentioned lead to destruction of the atoms, the probable atom concentration after passage through a delivery tube has been calculated in the Appendix, for the conditions obtaining (*a*) in experiments by Schwab and Friess† ; (*b*) in the present experiments at atmospheric pressure. The conclusion is reached that at low pressures recombination in the gas phase is always negligible compared with the wall recombination, and that at high pressures wall recombination is still the main factor governing the decay process. Furthermore, the concentration of atoms surviving passage through the delivery tube is sufficient to produce the observed benzene chlorination, if chains of moderate length are assumed to be propagated in the benzene.

The question of whether the active chlorine obtained with " moist " chlorine (which is presumably to be identified with that obtained by previous workers) is identical with atomic chlorine must therefore be left open until further data are available, but the balance of evidence suggests that they are probably basically the same.

APPENDIX

Recombination of Chlorine Atoms

1. *Wall Recombination*—According to Schwab and Friess,‡ chlorine atoms are destroyed after an average of 25 collisions with the vessel

---

* Bodenstein, 'Z. phys. Chem.,' vol. 85, p. 329 (1913).

† 'Naturwiss.,' p. 222 (1933) ; 'Z. Elektrochem.,' vol. 39, p. 586 (1933).

‡ 'Naturwiss.,' p. 222 (1933)

walls. Recombination must occur by reaction with an adsorbed chlorine atom layer in order to account for this small number of collisions together with the unimolecular nature of the destruction of the atomic chlorine. On the assumption that chlorine atoms are destroyed as a result of every collision with the walls, an approximate figure may be obtained for the relative number of chlorine atoms which are likely to survive passage through the delivery tube from the discharge to the reaction vessel.

In the absence of accurate data, and for the sake of simplicity, chlorine atoms will be assumed to have the same collision diameter as chlorine molecules, an assumption which does not introduce a very large error in the order of the result. Taking into account the fact that in viscous flow through tubes most of the gas moves in the neighbourhood of the axis, an estimate of the proportion of atoms emerging unchanged is obtained by calculating the fraction of atoms which do not diffuse through a distance greater than the radius of the tube.

A combination of Einstein's law of mean displacements with Meyer's approximate kinetic expression for the diffusion coefficient gives

$$\bar{x}^2 = \tfrac{2}{3}\,\bar{u}\lambda t,$$

where λ = mean free path, $\bar{u}$ = R.M.S. velocity, $\bar{x}$ = mean displacement. Hence the maximum R.M.S. velocity of an atom in order that it should pass through the delivery tube without collision with the walls, in time t is

$$u_{\text{max}} = \frac{3x^2}{2\lambda t},$$

where x = tube radius. Now

$$\lambda = \frac{1}{\sqrt{2}\pi\sigma^2 n}.$$

where n = number of molecules/cc. For chlorine atoms at atmospheric pressure, $\sigma = 1 \cdot 6 \,.\, 10^{-8}$ cm and $n = 2 \cdot 5 \,.\, 10^{19}$. Whence

$$u_{\text{max}} = \frac{3x^2}{7 \,.\, 10^{-6}\, t}.$$

The time of passage through the delivery tube is

$$t = \frac{\pi x^2 a}{\text{flow speed}},$$

where a = length of delivery tube. Substituting a = 25 cm, and flow speed = 1 cc/second, as used in practice, $t = 25\pi x^2$, therefore

$$u_{\text{max}} = 5 \cdot 5 \,.\, 10^2 \text{ cm/sec.}$$

This result is independent of the diameter of the delivery tube. Now

$$\bar{u} = \sqrt{\frac{3RT}{M}} = 4 \cdot 5 \,.\, 10^4$$

(M = mol. wt. = 35·5 for Cl atoms). Therefore

$$\frac{u_{\max}}{\bar{u}} = \frac{1}{80} = y \,.$$

It remains to calculate the fractional number of molecules which have a velocity less than 1/80th of the R.M.S. velocity. From Maxwell's law it can be shown that the fractional number of molecules with velocities less than $u_{\max}$ is given by

$$f = \frac{2}{\sqrt{\pi}} \left[\int_0^{x_0} e^{-x^2} dx - x_0 e^{-x_0^2} \right],$$

where $x_0^2 = \frac{u^2_{\max}}{\alpha^2}$ and $\alpha^2 = \frac{2}{3} \bar{u}^2$, *i.e.*, $x_0^2 = \frac{3}{2} y^2$.

Substituting for y, $x_0 = 0 \cdot 01531$, and for x_0 in the expression for f, and evaluating the integral above, we obtain $f = 2 \,.\, 10^{-6}$, *i.e.*, the atom concentration is reduced to $2 \,.\, 10^{-6}$ of its original value by wall recombination.

If it is assumed that in the chlorination of benzene by activated chlorine, as in the photochemical reaction, chains 10^6 atoms in length are initiated by chlorine atoms, and the experimental fact is further introduced that an additional fraction 10^{-4} of the modified gas reacted with the benzene, the increased chlorination might well be due to the presence of a fraction 10^{-10} of the total chlorine in the form of atoms. Since under the most favourable conditions for the destruction of atomic chlorine, the concentration only falls off by a fraction 10^{-6} during passage of the gas through the delivery tube, conversion of a fraction 10^{-4}, or 0·01% of the chlorine into atoms in the discharge should be sufficient to produce the observed effects. Dissociation of a larger percentage of chlorine would make the necessary chain length in the benzene much shorter.

2. *Recombination in the Gas Phase*—The rate of recombination of atoms by triple collisions between two atoms and a molecule will be determined, assuming all such collisions to be effective.

Let the mean velocity of an atom be u. The number of collisions/sec with another Cl atom = $\pi\sigma^2 un$, where n = number of atoms/cc. The number of collisions/sec with a Cl_2 molecule = $\pi\sigma^2 un'$, where n' = number of molecules/cc. The fraction of time spent by a Cl atom in contact with another atom is approximately given by

$$\frac{\sigma}{\lambda} = \pi\sigma^3 n\,,$$

since $\lambda = \frac{1}{\pi\sigma^2 n}$. Therefore, the number of triple collisions between two Cl atoms and a Cl_2 molecule/Cl atom/sec is

$$\begin{aligned} &\pi\sigma^2 u n' \pi\sigma^3 n \\ &= \pi^2\sigma^5 u n' n. \end{aligned}$$

The Cl_2 concentration changes very little owing to recombination of atoms, when their initial concentration is relatively small ; the concentration of atoms, however, falls off appreciably with time.

In time dt, the total number of such collisions/cc is

$$\tfrac{1}{2}\pi^2\sigma^5 u n' n^2 \,.\, dt = -\tfrac{1}{2}dn,$$

whence

$$-\frac{dn}{dt} = \pi^2\sigma^5 u n' n^2\,.$$

Integrating,

$$\frac{1}{n} - \frac{1}{n_0} = \pi^2\sigma^5 u n' t = \sqrt{2}\pi^2\sigma^5 \bar{u} n' t\,,$$

where n_0 = initial Cl concentration, $\bar{u}$ = R.M.S. velocity of the atoms.

(*a*) Application to data of Schwab and Friess (*loc. cit.*). Approximate data are :—

$t = 5 \,.\, 10^{-3}$ secs

$n' = 3 \,.\, 10^{15}$ (at 0·1 mm pressure)

$\sigma = 10^{-8}$

$\bar{u} = 4{\cdot}5 \,.\, 10^4$

$n_0 = 3 \,.\, 10^{14}$ (assuming 10% atoms to be present).

Then

$$\frac{1}{n} = \frac{1}{3\,.\,10^{14}} + \frac{1}{10^{21}}$$

which does not differ appreciably from $1/n_0$, *i.e.*, recombination in the gas phase is negligible.

(*b*) Application to present work. Approximate data are :—

$t = 2$ secs

$n' = 2{\cdot}5 \,.\, 10^{19}$ (Cl_2 at atmospheric pressure)

$\sigma = 10^{-8}$

$\bar{u} = 4{\cdot}5 \,.\, 10^4$

$n_0 = 2{\cdot}5 \,.\, 10^{17}$ (1% atoms assumed present).

Then

$$\frac{1}{n} = \frac{1}{2{\cdot}5 \, . \, 10^{17}} + \frac{310}{10^{17}},$$

or

$$n = 3 \, . \, 10^{14},$$

i.e., the atom concentration falls to 10^{-3} of its value, which is rather smaller than the effect produced by wall recombination.

These experiments were carried out in the Sir William Ramsay Laboratories, University College, London, in 1932, and we are glad to acknowledge our indebtedness to Professor F. G. Donnan, F.R.S., for the facilities extended to us. Our thanks are also due to Major F. A. Freeth, F.R.S., Mr. W. Rintoul, and Dr. E. H. Rodd for their interest in the work, and to Dr. O. L. Brady for his advice in the many analytical problems encountered.

The Catalytic Decomposition of Hydrogen Peroxide by Iron Salts*

By Fritz Haber and Joseph Weiss, The Chemical Laboratories, The University, Cambridge

(*Communicated by Sir William Pope, F.R.S.—Received May* 1, 1934)

[*Note by Dr. O. H. Wansbrough-Jones*—Shortly before Professor Haber died, he gave the manuscript of this paper to Professor Sir William Pope. The final revision for the press had not been made and in its original form the paper was not suitable for publication in an English journal. Considerable alterations in the wording have accordingly been made ; but, since Professor Haber had considered carefully how he wished to present the results embodied in it, the form and sequence of the paper remain unmodified.

The paper is, further, a sequel to some communications in German periodicals which may not be familiar to its readers. In an attempt to make it more quickly understandable, while keeping it as far as possible as it was left by Professor Haber, the following summary has been added.

---

* The manuscript of this paper was handed to me for communication by Professor Haber a few days before his death ; I have to thank Dr. O. H. Wansbrough-Jones for editing it.—W. J. P.

The catalytic decomposition of hydrogen peroxide by both ferrous and ferric salts is shown by the authors to be both a chain and a radical reaction, involving in its stages the radicals OH and HO_2 and the anion HO'_2. Varying concentrations of the reactants alter the length of the chains, and favour alternative means of terminating them, giving rise to various reaction products. To obtain quantitative results it is assumed that, to a first approximation, the concentration of the radicals remains stationary, and on this basis equations are derived from which the ratios of the various reaction products under different conditions may be arrived at.

The main stages of the reactions are set out in four equations ((1)–(4)) :—

$$Fe^{\cdot\cdot} + H_2O_2 = Fe^{\cdot\cdot\cdot} + OH' + OH \quad (1)$$

$$OH + H_2O_2 = H_2O + HO_2 \quad (2)$$

$$HO_2 + H_2O_2 = O_2 + H_2O + OH \quad (3)$$

$$OH + Fe^{\cdot\cdot} = Fe^{\cdot\cdot\cdot} + OH', \quad (4)$$

and inserting the appropriate reaction velocity constants, an equation (9') is obtained from which the ratio of the consumptions of hydrogen peroxide to ferrous ions may be expressed mathematically and to which experimental results adequately conform. More detailed consideration is then given to the effect of varying the acidity of the medium, and attention is called to the role played by the HO'_2 anion which enters into the reaction.

A large number of experiments are described and consideration of them shows that the main course of the reaction between H_2O_2 and $Fe^{\cdot\cdot}$ salts is described by the original equations ((1)–(4)), and that additional complications only come into being at the extreme ranges of the concentration ratios. To express their results the authors consistently use the value of the mean consumption ratio $\Delta H_2O_2/\Delta Fe^{\cdot\cdot}$ which they identify with the chain length, and study the variation of this ratio in different experimental conditions.

The effects of ferric salts are also described and largely elucidated. The effect of acidity is shown to be much more marked, and this is found to be due to the hydrogen peroxide no longer reacting as the uncharged molecule, as with ferrous salts, but rather as the ion HO'_2. The interplay between the reaction with ferrous and ferric salts is studied, and a remarkable result follows from an examination of the kinetic equations. By proper selection of the ratios of the concentrations of H_2O_2, $Fe^{\cdot\cdot\cdot}$ and $Fe^{\cdot\cdot}$ a sudden great increase in the rate of production of oxygen may be predicted and has been found experimentally. The chain mechanism proposed gives a simple rationale for this curious effect.

Finally, the authors consider the implications of their work in more general terms. They have had to assume that either chain or radical reactions are possible within the system with which they deal and moreover that one type may be changed easily to the other by a small alteration in the conditions. This suggestion gives an adequate explanation of the facts, and may, in their view, be a much more general phenomenon.]

In a preliminary paper* we discussed shortly the catalytic decomposition of neutral solutions of hydrogen peroxide in the presence of ferrous salts, and we showed that our results were not explicable by the earlier theory that the reaction took place through the interaction of six-valent iron-oxygen compounds with the hydrogen peroxide, but could be easily understood if the decomposition was actually a chain reaction whose course depended on the ratio of the concentrations of the reactants. Further experiments which we now describe have confirmed this latter view, and we also show that this theory serves to explain the catalytic decomposition of hydrogen peroxide, both by ferrous and ferric salts, in all important respects. To describe the decomposition by ferrous salts in acid and neutral solution a system of four equations is required, of which two ((2) and (3)) are the original Haber-Willstätter equations, the first (1) describes the process by means of which the chains are initiated, and the last (4) that by means of which they are broken. For the catalysis by ferric salts only one additional equation is required. The first four equations are :—

$$\mathrm{Fe^{\cdot\cdot} + H_2O_2 = Fe^{\cdot\cdot\cdot} + OH' + OH} \qquad k_1 \tag{1}$$

$$\mathrm{OH + H_2O_2 = H_2O + O_2H} \qquad k_2 \tag{2}$$

$$\mathrm{O_2H + H_2O_2 = O_2 + H_2O + OH} \qquad k_3 \tag{3}$$

$$\mathrm{OH + Fe^{\cdot\cdot} = Fe^{\cdot\cdot\cdot} + OH'} \qquad k_4 \tag{4}$$

By a neutral solution we mean one in which all the ferrous iron remains in solution while all ferric compounds have been precipitated. In the equations above $Fe^{\cdot\cdot}$ represents the total amount of dissolved bivalent iron, and if it be assumed that all the four processes are irreversible the rates of change of concentration of $Fe^{\cdot\cdot}$, H_2O_2, and the two radicals HO_2 and OH may be defined. Following the method of Bodenstein and Herzfeld $d(\mathrm{OH})/dt$ and $d(\mathrm{HO_2})/dt$ are set equal to zero ; that is to say, the concentrations of HO_2 and OH become stationary, and the relation between the radical concentrations and the hydrogen peroxide concentration when only the ferrous iron is considered is expressed by the equations :—

---

* Haber and Weiss, 'Naturwiss.,' vol. 20, p. 948 (1932).

$$(\mathrm{OH}) = \frac{k_1}{k_4}(\mathrm{H_2O_2}) \quad \text{and} \quad (\mathrm{HO_2}) = \frac{k_1k_2}{k_3k_4}(\mathrm{H_2O_2}) .$$

Thus the concentrations of the radicals appear to be directly proportional to the concentration of the hydrogen peroxide which naturally decreases throughout the reaction, and this result is clearly at variance with the assumption of stationary concentrations for these radicals; moreover, they must initially be zero and become zero again at the end of the reaction, but their extremely small value makes the assumption of invariability a sufficiently good approximation to account for all the chemical facts.

The kinetic equations for those substances whose concentrations alter during the reaction by amounts that can be detected by chemical means are given by

$$-\frac{d(\mathrm{H_2O_2})}{dt} = k_1(\mathrm{Fe^{\cdot\cdot}})(\mathrm{H_2O_2}) + 2\frac{k_1k_2}{k_4}(\mathrm{H_2O_2})^2 \tag{5}$$

$$\frac{d(\mathrm{O_2})}{dt} = \frac{k_1k_2}{k_4}(\mathrm{H_2O_2})^2 \tag{6}$$

$$-\frac{d(\mathrm{Fe^{\cdot\cdot}})}{dt} = 2k_1(\mathrm{Fe^{\cdot\cdot}})(\mathrm{H_2O_2}) \tag{7}$$

The fact is emphasized that the change in concentration of H_2O_2 cannot be represented by a simple equation of the first order.

In the simplest case it can be assumed that the concentration of hydrogen peroxide remains practically constant, so equation (7) may be integrated and the value of k_1 obtained, or its value may also be found from certain experiments in which the peroxide was decomposed without the liberation of oxygen. The latter reaction can be described simply by the stoichiometric relation

$$\mathrm{H_2O_2} + 2\mathrm{Fe^{\cdot\cdot}} = 2\mathrm{Fe^{\cdot\cdot\cdot}} + 2\mathrm{OH'}. \tag{8}$$

The situation is more complicated when, with varying concentrations of hydrogen peroxide, its consumption for each ferrous ion becomes greater than 0·5 ; (5) then must also be taken into account in addition to (7). Treating them as simultaneous differential equations, and dividing (5) by (7) we obtain the consumption ratios of the substances as

$$n = \frac{d(\mathrm{H_2O_2})}{d(\mathrm{Fe^{\cdot\cdot}})} = 0{\cdot}5 + \frac{k_2}{k_4}\cdot\frac{(\mathrm{H_2O_2})}{(\mathrm{Fe^{\cdot\cdot}})} . \tag{9}$$

This expression cannot generally be tested in its differential form, since only the mean consumption ratio $\bar{n}$ can be measured experimentally. Thus

$$\bar{n} = \frac{\Delta\,(H_2O_2)}{\Delta\,(Fe^{\cdot\cdot})} = \frac{\int_0^t \left[0\cdot5 + \frac{k_2}{k_4}\cdot\frac{(H_2O_2)}{(Fe^{\cdot\cdot})}\right]dt}{t}, \tag{9'}$$

and this cannot be integrated in the general case, but this difficulty should be overcome in order that the quantity k_2/k_4 which, together with k_1, determines the course of the reaction, may be evaluated. The quotient $d(H_2O_2)/d(Fe^{\cdot\cdot})$ in (9) is clearly a measure of the length of the reaction chain in the interval of time under consideration, since this chain length is measured by the number of molecules of oxygen appearing for each ferrous ion lost. Its value will change with time, and will evidently have a lower limit at 0·5, which value is attained with relatively small $(H_2O_2)/(Fe^{\cdot\cdot})$ ratios, so that (8) is applicable ; but no upper limit is given by the above system of equations though there is a very low concentration of ferrous salts at which the system becomes incomplete owing to the inadequacy of the single chain-breaking mechanism (4) in describing all the phenomena which then occur.

The four irreversible velocity expressions contain no terms in $H^{\cdot}$ or OH', so that the reaction velocity is independent of the acidity of the solution, and further since neither (3) nor (4) contains these terms the chain length is similarly independent. This fact that k_1 does not vary with the acidity has been confirmed experimentally, and forms the feature discriminating between catalysis by ferrous and ferric salts, but experiments also show that the chain length is not completely independent of the acidity, as strictly according to the equations (1) to (4) it should be. It was at first thought that this might be due to the hydrogen peroxide in equation (2) appearing actually as the anion HO'_2, but this supposition proved to be incorrect, for it was found that the equation

$$HO'_2 + OH = HO_2 + OH' \tag{2'}$$

did not give the correct variation of chain length with acidity, giving actually for the ferrous catalysts a much more marked variation of chain length with acidity than was observed. Thus (2) as originally written must be taken as correct, and to account for this discrepancy we must assume that (4) is not sufficient as it stands, but must be modified to include the fact that the breaking of the chains is favoured by an increase in acidity, and does not itself give all the forms of chain breaking. With sufficiently small concentrations of ferrous iron, other processes whose efficiencies depend on the p_H become important, and among the possible ones the following may first be considered

$$\text{Fe}^{\cdot\cdot} + \text{HO}_2 \rightarrow \text{Fe}^{\cdot\cdot\cdot} + \text{HO}'_2, \tag{10}$$

in which the anion HO'_2 is always present in the concentration given by the equation

$$\text{HO}'_2 + \text{H}^{\cdot} \rightleftharpoons \text{H}_2\text{O}_2, \tag{11}$$

with the equilibrium constant*

$$k_{20^{\circ}C} = \frac{(\text{H}^{\cdot})(\text{HO}'_2)}{(\text{H}_2\text{O}_2)} = 1 \cdot 2 \times 10^{-12}.$$

It would at first sight even seem possible to substitute this equation (10) for equation (4), but on closer examination it is found that the constant quantity 0·5 disappears from (9) and the important reaction (8) is no longer explained. Thus the process designated by (10) must be taking place as well as that of (4), and calculation on this basis shows that the constant 0·5 is retained and the explanation given above holds. Consequent on the introduction of the additional process (10) the consumption ratio n is no longer represented as a rigidly linear function of $(H_2O_2)/(Fe^{\cdot\cdot})$ but increases rather more slowly, especially in the region of small iron concentrations. Whether this actually occurs remains uncertain, for where the effect is expected to be marked the concentration of $Fe^{\cdot\cdot}$ is so small that exact measurements can no longer be made. On the other hand, the introduction of (10) does not explain the variation of chain length with acidity, since on this formulation the chain length should remain completely independent ; accordingly the introduction of (10) is presently to be avoided as an unnecessary complication, though it will be reconsidered in the second part of this paper.

That another chain breaking mechanism to supplement (4) is required is also clear from a consideration of the photochemical chains started by the formation of OH radicals†

$$\text{H}_2\text{O}_2 + h\nu \rightarrow 2\text{OH}.$$

These chains come to an end (in the absence of dissolved iron) after forming chains of medium length, and there can be no doubt that their termination then arises from the reciprocal destruction of two radicals. The same process would occur in ferrous ion catalysis when the ferrous ion concentration was so small that chain breaking by (4) was relatively infrequent.

---

* Joyner, ' Z. anorg. Chem.,' vol. 77, p. 103 (1912).

† Urey, Dawson, and Rice, ' J. Amer. Chem. Soc.,' vol. 51, p. 1371 (1929).

The experimental result that the photochemical decomposition of H_2O_2 proceeds more slowly as the acidity in the solution is increased* proves that this chain breaking process through the interaction of two radicals is favoured by the presence of H ion, and indeed the greater stability of acid solutions of hydrogen peroxide in the dark might well be attributed to the reciprocal removal of the two radicals under the influence of the low p_H. We think that the clearest example of such reciprocal action is to be found in the well-known formation of traces of ozone, whose presence is obvious from its smell, in the catalytic decomposition of H_2O_2. In this case the radical HO_2 may be responsible, by undergoing the reaction

$$HO_2 + HO_2 + H^{\cdot} = O_3 + H_2O + H^{\cdot}.$$

A quantitative proof of the breaking of the chains initiated by light through the interaction of two radicals is given by the fact that the velocity depends on the square root of the light intensity.† The unmistakable chain‡ character of the formation of oxygen from ozone and hydrogen peroxide falls into the same class,§ and the process

$$O_3 + H_2O \rightarrow H_2O_4 \rightleftharpoons 2HO_2,$$

may start the chain. The effect of acid in decreasing the speed‡ of this reaction as well as of the decomposition of ozone in aqueous solution is probably a similar phenomenon.||

Returning now to our study of the catalysis by ferrous salts, it seems that the simplest application of equations (1) to (4) lies in the explanation of the fact that very different mean consumption ratios can be obtained by suitable mixing of dilute ferrous solutions with dilute solutions of hydrogen peroxide. For this purpose ferrous sulphate solution is allowed to run slowly from the horizontal outlet of a burette which is being rapidly rotated about a vertical axis, into a large quantity of hydrogen peroxide solution of known concentration. Thus 50 cc of ferrous solution are rapidly driven through the outlet into 2 litres of hydrogen peroxide solution and quickly distributed throughout the whole bulk. Sufficient time is then allowed to elapse before titrating the solution, so that no

---

[*] Kornfeld, 'Z. wiss. Photogr.,' vol. 21, p. 66 (1921).

[†] Allmand and Style, 'J. Chem. Soc.,' p. 596 (1930).

[‡] Weiss (*in preparation*).

[§] Rothmund and Burgstaller, 'Monatsh. Chem.,' vol. 34, p. 665 (1913).

[||] Sennewald, 'Z. phys. Chem.,' A, vol. 164, p. 305 (1933).

further increase in this time produces any change in the observed composition, and the concentration of ferrous salt has been reduced to the limit of measurement. It is then strongly acidified to retard the decomposition of the unchanged hydrogen peroxide by the ferric iron now present and the residual hydrogen peroxide is finally estimated by titration with potassium permanganate, from which the average ratio $\bar{n}$ of H_2O_2 decomposed by each $Fe^{\cdot\cdot}$ can be evaluated. By this method we found that, contrary to the results of previous workers, a much higher value results for this ratio than that obtained when the solutions are mixed in a cruder manner, and further that the consumption ratio is far from attaining a value independent of the concentrations of either reactant.

TABLE I—CENTRIFUGAL EXPERIMENTS (IN NEUTRAL SOLUTION)

No.	$[H_2O_2]_0 \,.\, 10^3$ mols/ltr.	$[Fe^{\cdot\cdot}]_0 \,.\, 10^3$ mol/ltr. (entering solution)	$\bar{n} = \frac{\Delta H_2O_2}{\Delta Fe^{\cdot\cdot}}$
1	5·25	2·42	29·9
2	1·06	1·01	15·6
3	1·10	2·40	9·4
4	0·786	2·00	6·4
5	0·318	2·00	3·8
6	0·125	2·00	2·5

A different procedure, which had the advantage that the initial concentration ratio was better defined and that the rate of change could be determined for definite initial concentrations, gave important results. The second method was essentially this : one of the reacting solutions, normally the H_2O_2, was propelled in known quantity per unit time, in the form of a rapidly flowing turbulent stream, from an opening through an air space of varying length into a receiver. Before reaching the exit, the flowing stream took up the second reactant, also in known quantity per unit time, from a second co-axial tube, and with sufficient turbulence mixing by this arrangement was practically instantaneous so that the initial concentrations ($t = 0$) could be deduced accurately from the experimental data. The liquid was left in the receiver until increasing the time had again no effect on the results, and the mean consumption ratio was again obtained as in the former centrifugal experiments, but now for well-defined initial concentrations of the reactants. Two methods of titration were required to obtain the amount of the chain reaction which had taken place from the moment of mixing to the final time; firstly the streaming liquid was allowed to flow directly into a known excess of acid permanganate in the receiver so that the titration gave the sum of the H_2O_2 and $Fe^{\cdot\cdot}$ in the liquid, and secondly the permanganate was replaced by a strongly acid solution of the ferrous salt, by which means the unused H_2O_2 was rapidly destroyed according to (8). By this method the amount of reaction, according to the chain equations, which takes place in a time less than 1 second, may be found, but the time cannot be found with accuracy, though this difficulty can be overcome by varying the cross-sections of the turbulent stream. We have accordingly made two other series of experiments, " jet " experiments in which the liquid was forced from a glass jet of one square millimetre cross-section, and " pouring " experiments in which the liquid was poured all at once into a large funnel, and emerged from the opening into a wide vessel ; in both series of experiments the second reactant was again added through a narrow coaxial tube.

In the " pouring " experiments, 1 litre of the liquid was collected in the receiver in, at most, 2 seconds, and the reaction was stopped after a measured time t by adding 1 litre of the inhibiting liquid, either acid permanganate or ferrous sulphate, and ensuring rapid mixing by mechanical stirring. If the concentrations are such that the reaction is slow, the uncertainty in the measurement of the time of the reaction is ± 1 second, and is negligible, as may be seen from the values of t shown in Table II.

From the " pouring " experiments, the velocity constant k_1 may be deduced immediately ; from the " jet " experiments the reaction time may now be found, for the product k_1t is given accurately. The value of t found is of the order of $\frac{1}{2}$ second. From this we can obtain the initial value of the chain length in the jet experiments ; that is, for concentration ratios not far removed from the initial concentration ratios at $t = 0$, and we thus obtain the three quantities, the velocity constant k_1, the initial chain length, and finally the mean chain length throughout the complete reaction. The influence of temperature and acidity on these three quantities may also be determined separately.

Examining the results in more detail, we find in the " pouring " experiments that the consumption ratio is 0·5 as given by (8). The expression for the reaction velocity is then

$$-\frac{d(\mathrm{H_2O_2})}{dt} = -\tfrac{1}{2}\frac{(\mathrm{Fe}^{\cdot\cdot}}{dt} = k_1(\mathrm{Fe}^{\cdot\cdot})(\mathrm{H_2O_2}),$$

which may be integrated using the stoichiometrical relation (8) to give

$$k_1 = \frac{2\cdot3}{(\mathrm{H_2O_2})_0\, t}\log\frac{[\mathrm{Fe}^{\cdot\cdot}]_0\,[(\mathrm{H_2O_2})_0 - x/2]}{[\mathrm{H_2O_2}]_0\,[(\mathrm{Fe}^{\cdot\cdot})_0 - x]},$$

where x is the amount of iron used up in the time t. Table II summarizes these " pouring " experiments; average values for the three temperatures employed are given at the foot of the table, and from these the energy of activation has been found to be 8500 ± 500 cals. In agreement with the theory, the results in the table show that the velocity constant does not vary appreciably with the acidity.

TABLE II—POURING EXPERIMENTS

No.	$[H_2O_2]_0\ 10^4$ mol/ltr.	$[Fe^{\cdot\cdot}]\ .\ 10^4$ mol/ltr.	$[H^{\cdot}]\ .\ 10^2$ equiv./ltr.	Temp. °C	t sec.	Consumption ratio n_0	k_1
1	5·21	34·2	0·186	19·7	14	0·5	25
2	5·00	32·5	4·46	20·2	13	0·5	25·3
3	6·95	35·0	0·186	19·7	13·5	0·5	24·2
4	6·83	34·3	1·86	19·7	13·7	0·5	24·2
5	5·35	33·4	0·186	19·7	15	0·5	21·3
6	5·25	23·0	1·84	20	15	0·5	21·6
7	7·08	52·8	0·186	20	9	0·5	25·1
8	11·07	8·82	9·34	21	15·5	0·5	23·3
9	0·97	10·7	18·7	21	16	0·5	20·5
10	5·00	20·5	4·46	46·5	13	0·5	63·7
11	5·11	21·5	4·45	44·5	13	0·5	64·5
12	5·11	21·5	0·187	44	13	0·5	60·0
13	3·60	12·4	0·465	46	13	0·5	65·1
14	6·02	57·7	0·186	6	29	0·5	12·1
15	6·02	57·7	4·45	6	29	0·5	12·3
16	6·07	24·6	1·86	6	27	0·5	9·4
17	6·07	24·6	8·5	6	34	0·5	10·5

k_1 (6° C) = 11 ; k_1 (20° C) = 23 ; k_1 (45° C) = 63.

Table III gives the results of the " jet " experiments. Only the product k_1t can be obtained from this series, but its constancy is also a proof of the constancy of k_1, since the method of experiment involves no considerable change in the time t in the different experiments. The reaction times are calculated from the values of k_1 which had been determined previously, and the mean consumption ratios $\bar{n}$ which are also shown are seen to be definitely greater than the initial consumption ratios n_0 found from the much smaller times of flow in the " jet " experiments.

Equation (9) shows that when the consumption ratio differs at all from 0·5 the value of k_2/k_4 may be determined ; and this can be done from both series of experiments. We have not used the integrated form of the expression (9'), since we are considering those reactions in which the ratio is not much removed from 0·5 when an average value can be used without serious error. Table IV shows that $\bar{n}$ and hence k_2/k_4 is smaller, for short initial chain lengths only, as the acidity increases, but the influence of the acidity is relatively small, certainly far removed from simple proportionality. As has been stated above, we believe this result to be the consequence of the reaction between two radicals, an additional process that becomes the more important the greater the chain length and the acidity.

TABLE III—JET EXPERIMENTS

	$[H_2O_2]_0 . 10^4$ mols/ltr.	$[Fe^{\cdot\cdot}{}_0] . 10^4$ mols/ltr.	$H^{\cdot} . 10^2$ equiv./ltr.	Temp. ° C	t sec	$k_1 \times t$	Initial consumption ratio n_0	Mean consumption ratio $\bar{n}$
1	130·0	15·90	1·51	20	0·44	10·2	0·5	2·02
2	126·0	23·43	0·94	20	0·52	11·9	0·5	2·23
3	80·70	20·15	56·0	20	0·56	12·9	0·5	0·63
4	83·85	19·80	15·5	20	0·54	12·4	0·5	0·75
5	87·00	21·30	15·1	20	0·50	11·3	0·5	0·77
6	98·15	26·38	6·24	7	0·45	5·0	0·5	0·87
7	101·75	25·64	3·14	41	0·43	28·7	0·5	1·57
8	92·70	21·57	3·07	17	0·50	10·7	0·5	1·26

TABLE IV

No.	$[H_2O_2]_0 . 10$ mols/ltr.	$[Fe^{\cdot\cdot}] . 10^4$ mols/ltr.	$[H^{\cdot}] . 10^2$ equiv./ltr.	Temp. ° C	t sec	$\left(\frac{\Delta H_2O_2}{\Delta Fe^{\cdot\cdot}}\right)_t$	$\frac{k_2}{k_4} . 10^2$
1	67·5	16·9	0·47	20	4	0·68	2·8
2	65·6	15·2	0·47	20	4·8	0·66	2·3
3	20·65	13·6	0·47	20	12	0·60	2·7
4	11·20	8·82	0·47	21	14	0·56	3·7
5	10·97	10·7	0·19	21	15	0·56	3·7
6	55·0	17·2	4·46	20	4·8	0·555	1·2
7	21·2	10·0	4·46	20	12·2	0·565	1·7
8	82·85	21·7	0·15	20	0·5	0·625	3·0
9	98·75	16·2	$\sim 10^{-4}$ (neutral)	20	0·5	0·82	4·7
10	93·82	19·93	0·43	20	0·5	0·645	2·8
11	101·30	22·43	0·43	17	0·5	0·63	2·7

Nos. 1–7, jet experiments ; Nos. 8–11, pouring experiments.

Table V summarizes the results of experiments in which the time of observation has been extended so far that further increase had no effect. Pairs of comparable experiments with different acidities are shown together, and while no exact quantitative evaluation of the part played by the reciprocal action of the radicals in shortening the chains can be made, the effect of increasing the acidity in shortening the chain is clearly seen.

TABLE V

No.	$[H_2O_2]_0 \cdot 10^3$ mols/ltr.	$[FeSO_4]_0 \cdot 10^4$ mols/ltr.	$[H^{\cdot}] \cdot 10^3$ equiv/ltr.	$\frac{\Delta H_2O_2}{\Delta Fe^{\cdot\cdot}}$	Acidity ratio	Ratio of mean chain lengths
1	9·11	4·90	11·8	0·86	7·2	1·7
	8·90	5·00	85·0	0·50		
2	6·18	3·78	0·118	6·8	10	3·1
	6·32	3·65	1·18	2·2		
3	2·49	5·04	0·117	2·5	10	1·7
	2·47	5·05	1·17	1·5		
4	5·98	3·57	0·117	4·4	10	1·9
	6·82	3·39	1·18	2·3		
5	1·62	0·238	0·115	7·4	20	7·4
	1·61	0·243	2·31	1·0		
6	3·20	0·998	0·117	7·0	100	7·7
	3·15	0·990	11·7	0·9		
7	1·74	0·383	" neutral "	15·7	$\sim 10^4$	4·5
	1·72	0·268	0·57	3·5		

In Table VI are summarized a number of experimental results obtained at nearly constant p_H—a neutral solution. From these results it is possible to obtain an idea of the range of ferrous iron concentrations over which the mean chain length can be satisfactorily interpreted on the basis of equations (1) to (4), without taking the additional chain breaking mechan-

TABLE VI

No.	$[H_2O_2]_0 \cdot 10^3$ mols/ltr.	$[FeSO_4]_0 \cdot 10^4$ mols/ltr.	$\nu_0 \frac{[H_2O_2]_0}{[Fe^{\cdot\cdot}]_0}$	$\bar{n} = \frac{\Delta H_2O_2}{\Delta Fe^{\cdot\cdot}}$	f
1	10·1	0·384	262	23·5	$\sim 10^{-2}$
2	2·75	0·132	208	17·0	$\sim 10^{-2}$
3	2·81	0·138	203	16·3	$\sim 10^{-2}$
4	1·74	0·383	45	15·7	$\sim 10^{-2}$
5	3·00	1·08	28	14·7	$\sim 10^{-2}$
6	0·98	0·382	25	11·1	$\sim 10^{-2}$
7	0·72	0·340	21	6·8	$\sim 10^{-2}$
8	1·49	1·16	13	6·2	$\sim 10^{-2}$
9	0·48	0·333	15	5·7	$\sim 10^{-2}$
10	2·83	2·64	11	4·9	$\sim 10^{-2}$
11	4·68	4·81	10	4·3	$\sim 10^{-2}$
12	2·62	3·00	9	3·5	$\sim 10^{-2}$

isms into account. The ratio of the iron concentration after time t to the initial concentration may be denoted by f, so that

$$f = \frac{\mathrm{Fe}_t}{\mathrm{Fe}_0},$$

and from (7) it follows that

$$f = e^{-2k_1 (\mathrm{H_2O_2})_m t},$$

where $(H_2O_2)_m$ represents a mean value which does not differ seriously either from the initial value $(H_2O_2)_0$ or the final value $(H_2O_2)_t$, and is taken as constant from $t = 0$ to $t = t$. The differential equation (9′) can then be integrated for constant values of H_2O_2 between the limits Fe_0 and Fe_t, and the integral evaluated with the aid of the values for k_2/k_4 which we had previously determined. For the mean consumption ratio we then obtain

$$\bar{n} = 0{\cdot}5 + \frac{k_2}{k_4} \cdot \frac{1}{2k_1\, \mathrm{Fe}_0^{\cdot\cdot}\, t}\, [e^{-2k_1 (\mathrm{H_2O_2})_m t} - 1].$$

From this expression the fraction f may be determined, and we find that in all experiments in Table VI it is nearly 1%. Thus until this region is reached equations (1) to (4) are adequate, and it is only during the final 1% of the iron consumption that the additional chain breaking mechanisms play any appreciable part.

CATALYSIS BY FERRIC SALTS

In the preceding part of this paper, a description of the catalytic decomposition of hydrogen peroxide by ferrous salts has been given, and we now wish to discuss the relation of this reaction to the catalytic decomposition by the aid of ferric salts. There are two possibilities to be considered. If some ferrous salt is formed as an intermediate during the ferric iron catalysis, the equations developed above must find their place in the full description of the ferric iron catalysis ; since, in acid solution the only difference between the two cases will lie in the relative concentrations of the three reacting substances H_2O_2, $\mathrm{Fe}^{\cdot\cdot}$ and $\mathrm{Fe}^{\cdot\cdot\cdot}$. If, however, the ferric catalysis does not involve ferrous iron as an intermediary but rather proceeds through the iron being oxidized to a higher stage of valency, a new set of equations would have to be developed. The work of Bohnson and Robertson* might be interpreted as lending some support to this latter view, for their spectroscopic investigations of weakly acid solutions of ferric salts with hydrogen peroxide, in which some colour change is visible to the eye, were interpreted by them as showing the spectrum of ferric acid. We do not, however, regard this result as convincing for the experimental material seems insufficient to prove conclusively that the spectrum was really ferric acid, and despite numerous experiments of our own we have been unable to satisfy ourselves on this point. We do not propose to describe these spectroscopic investigations in detail for the presence of ferrous salts in the ferric iron catalysis of hydrogen peroxide in acid solution has been established by Kuhn and Wassermann,* and we have been able to extend and confirm their most important results; and thus in our consideration of the ferric catalysis we start with the assumption that the iron is present alternately in the ferric and ferrous forms. The view sometimes expressed in the literature that the rate of decomposition is the same both for ferrous and ferric salts is false for the experiments on which it is based have been made in acid solution with the addition of small amounts of ferric or ferrous salts, and when ferrous salt is used it is transformed almost entirely into ferric at the very beginning of the reaction, and the resulting slow catalysis by the ferric salt is naturally the same as if ferric salt had been added at the beginning in place of the ferrous.

---

* 'J. Amer. Chem. Soc.,' vol. 45, p. 2493 (1923).

Most of the results of previous workers gave the velocities of decomposition of hydrogen peroxide in solutions in which its concentration ranged from 10^{-1} to 10^{-3} mol/litre, in the presence of 10^{-2} to 10^{-3} mol/litre of iron and with acid concentrations corresponding to 10^{-1} to 10^{-3} equivalents per litre of free sulphuric acid. The use of weaker acid solutions is inadvisable since special complications due to the ferric iron no longer being present mainly in the form of ferric ions will then arise. Instead, most of the iron is present in the form of imperfectly known iron complexes as indicated by the difference in the colour of the solution from the plain yellow characteristic of ferric solutions in the region of acidity mentioned above.

It has been found that the rate of consumption of H_2O_2 is monomolecular with respect to itself, directly proportional to the total amount of iron in solution, and inversely proportional to the equivalent concentration of the added acid. Table VII gives a number of our own results, together with those of previous workers,† for the velocity constants of decomposition of H_2O_2 calculated from the equation

$$-\frac{d(H_2O_2)}{dt} = K\frac{(Fe^{\cdot\cdot\cdot})}{[H^{\cdot}]}[H_2O_2]. \tag{12}$$

---

[*] 'Liebigs Ann.,' vol. 503, p. 203 (1933).

[†] v. Bertalan, 'Z. phys. Chem.,' vol. 95, p. 338 (1920); Spitalsky and Petin, *ibid.*, vol. 113, p. 161 (1924); Bohnson and Robertson, *loc. cit.*

$Fe^{\cdots}$ represents the total amount of iron in solution expressed as mols/litre, and $H^{\cdot}$ is the equivalents per litre of added acid, in these experiments sulphuric.

TABLE VII

No.	$[Fe^{\cdots}] \,.\, 10^3$ mols/ltr.	$[H^{\cdot}] \,.\, 10^3$ equiv./ltr.	$\frac{[H^{\cdot}]}{[Fe^{\cdots}]}$	$2k_{10}K \frac{[Fe^{\cdots}]}{[H^{\cdot}]} 10^3$	$2k_{10} K \,.\, 10^5$
1	4·00	1·50	0·375	33·5	12·5
2	4·00	4·50	1·125	13·216	14·86
3	4·00	22·5	5·625	1·873	10·35
4	4·00	88·0	22·00	0·576	12·68
5	4·50	3·00	0·666	14·25	9·48
6	12·0	30·0	2·50	3·946	9·86
7	12·0	15·0	1·25	9·840	12·3
8	73·0	15·0	0·205	3·59	7.37
9	73·0	30·0	0·4105	26·5	10·88
10	73·0	150	2·055	7·48	15·35

$2k_{10}K$ (mean from our own experiments) .... $1{\cdot}16 \,.\, 10^{-4}$
$2k_{10}K$ (v. Bertalan) .... $1{\cdot}17 \,.\, 10^{-4}$
$2k_{10}K$ (Spitalsky and Petin)......................... $1{\cdot}19 \,.\, 10^{-4}$

The rate of reaction is inversely proportional to the acidity, and this is due to the fact that in contrast to the ferrous reaction the reactive state of the hydrogen peroxide is no longer H_2O_2 but is now the anion HO'_2, the concentration of which is related to that of the peroxide by (11). The variation with the total iron shows that in the stationary state only a small fraction of the iron is there as $Fe^{\cdot\cdot}$; and this must be so since the velocity of reaction of the ferric ion with the peroxide anion is very small compared with the corresponding reaction of $Fe^{\cdot\cdot}$ with H_2O_2. The primary process for the ferric ion is

$$Fe^{\cdots} + HO'_2 \rightarrow Fe^{\cdot\cdot} + HO_2, \tag{13}$$

and the velocity constant in (13) is related to k in (12) by the relation $k = 2k_{13}K$. The factor 2 comes in from the fact that in the stationary state

$$-\frac{d(H_2O_2)}{dt} = +2\frac{d(O_2)}{dt}.$$

From our own and other workers' results we find that $k_{13} = 6{\cdot}0 \times 10^7$ (secs. mol./litre) at 20° C.

The temperature coefficient determined by different observers gives a heat of activation of about 21000 cals. of which 8600 cals. is due to the heat of dissociation of H_2O_2, and the remaining part to the reaction (13), including the heat of dissociation of the ferric salt.

The combination of equation (13) with the four equations used to describe the ferrous ion catalysis leads to a surprising result. The production of oxygen through the interaction of the radical HO_2 with H_2O_2 necessitated the introduction of a term containing the square of the concentration of the peroxide in the expression for $d(H_2O_2)/dt$; but (12) shows that in the ferric catalysis only a term in the first power of the peroxide is required. Thus in the latter case the production of oxygen cannot proceed as a chain reaction if the chains are to be of appreciable length, and the radical HO_2 which we have recognized as the characteristic chain carrier in the ferrous catalysis must be able to disappear in the ferric ion catalysis without initiating or continuing any reaction chains. This process is the following

$$Fe^{\cdot\cdot\cdot} + HO_2 \rightarrow Fe^{\cdot\cdot} + O_2 + H^{\cdot}. \tag{14}$$

When the speed of this reaction (14) is greater than that of reaction (3) the chain reaction simply changes over to a reaction of radicals not involving chains. This may be important in view of the simple illustration it affords of the ease with which a radical reaction may change to a chain reaction and *vice versa* ; a very small variation of the conditions of the reaction being sufficient to effect this. In this reaction the rate of formation of oxygen, as given by the two equations (3) and (14), is evidently determined by two velocity constants, whose values lie sufficiently close together for either of the two reactions to predominate, the relative concentrations of H_2O_2 and $Fe^{\cdot\cdot\cdot}$ being the determining factor. Generally (14) is the dominant reaction, but alterations are possible which favour (3) to such an extent that chains appear; increase of H_2O_2 and decrease of $Fe^{\cdot\cdot\cdot}$ will cause this to happen, though there is a natural limit to the permissible decrease of $Fe^{\cdot\cdot\cdot}$ determined by a minimal amount being necessary to initiate the chains.

There is yet another way in which the HO_2 may disappear while the ferric reaction proceeds, namely, the reaction (10) which was omitted in the previous discussion as probably being unnecessary but not false. It now becomes important, and we see at once that since it is the inverse of (13)

$$Fe^{\cdot\cdot\cdot} + HO'_2 \underset{k_{10}}{\overset{k_{13}}{\rightleftharpoons}} Fe^{\cdot\cdot} + HO_2. \qquad \begin{cases} (13) \\ (10) \end{cases}$$

so long as reaction (10) proceeds with an appreciable velocity there will always be a certain amount of HO_2 which does not react according to (3) though it need not disappear according to the mechanism of (14). Examining this in further detail we see that if we wish to make reaction

(3) much the most important we must simultaneously keep the ferric ion concentration small in order to retard (14), and the H_2O_2 concentration large in order to favour (3), and also prevent the HO_2 from disappearing by means of reaction (10) with $Fe^{\cdot\cdot}$ without the production of oxygen. These three conditions occurring together should give the most favourable conditions for the production of oxygen from a chain reaction in the ferric catalysis. The concentration of H_2O_2 should be 1 mol/litre or more, that of the ferric ion small, as might be given by a very slightly dissociated complex salt such as the acetate or succinate; and there should also be a substance present in solution that will combine with the ferrous ion and keep its concentration low; these three conditions will reproduce the experiments of Kuhn and Wassermann (*loc. cit.*) and will give rise to a greatly accelerated production of oxygen. The reaction chains will be very long, and their termination due not to reaction (4) but to the interaction of two radicals. In these circumstances the rate of production of oxygen increases by about 100 times, a phenomenon termed by its discoverers the "Katalasestoss" and believed by them to be fundamentally a new kinetic effect, but it seems that the explanation given above is satisfactory and their view less probable. It may be mentioned that their method of minimizing the amount of ferrous ion is not a new one; it consists in the addition of $\gamma\gamma'$-dipyridyl, the action of which on mixtures of ferrous and ferric salts has been studied also by electrochemical methods by Friedheim and Michaelis.* This substance has been found to shift the potential so far to the side of the strong oxidizing materials that the development of the gaseous oxygen is a serious hindrance to the exact measurement of the electrode potential.

We have naturally tried to make a detailed analysis of the system obtained by combining all the relevant equations (1), (2), (3), (4), (10), (13), and (14), but the complicated expressions which result have proved to be of little value. The success attained previously in using the simple relationships (1) to (4) encouraged us to search for a simpler method of procedure, even at the risk of losing some of the completeness of the formulation. We have found that the (2), (3), (10), and (13) are adequate to explain the results, or, in other words, we make the assumption that the equilibrium expressed by (10) and (13) is readily established. Then the concentration of HO_2 can be derived with sufficient accuracy from the expression

$$[HO_2] = \frac{k_{13}}{k_{10}} \cdot \frac{[Fe^{\cdot\cdot\cdot}]}{[Fe^{\cdot\cdot}]} [HO'_2],$$

---

* 'J. Biol. Chem.,' vol. 91, p. 343 (1931).

and the kinetic equation corresponding to (3) may then be transformed to

$$\frac{d(O_2)}{dt} \sim k_3 \cdot \frac{k_{13}}{k_{10}} \frac{K}{[H^{\cdot}]} \frac{[Fe^{\cdots}]}{[Fe^{\cdot\cdot}]} [H_2O_2]^2. \tag{15}$$

Kuhn and Wassermann found that the rate of production of oxygen as proportional to the square of the concentration of the H_2O_2 and was retarded by increasing hydrogen ion concentration ; both these results are explained at once by the above expression (15), and in addition the action of diminishing $Fe^{\cdot\cdot}$ concentration is clear. Of the constants in this expression, $k_{13}/k_{10} = K_A$ deserves closer attention; k_{13} is known from our measurements to be $6 . 10^7$, and it is probable that the reverse process which is in the exothermic direction will have no heat of activation and since also it is a simple transfer of charge it is likely that k_{10} will be about 10^{11}, the normal value for reactions taking place at every collision; thus K_A will be about 10^{-3}. This result is of further interest, for we may express the reaction represented by (15) in the form

$$Fe^{\cdots} + \tfrac{1}{2}H_2 \rightleftharpoons Fe^{\cdot\cdot} + H^{\cdot}$$
$$HO_2 + \tfrac{1}{2}H_2 \rightleftharpoons HO'_2 + H^{\cdot}.$$

The first step will give the electrolytic potential of $Fe^{\cdots}/Fe^{\cdot\cdot}$ (known to be $+ 0{\cdot}75$ volt) ; the second the electrolytic potential HO_2/HO'_2 for which no value has so far been available but which from the value of K_A is now seen to be about $0{\cdot}58$ volt. This value is certainly not very exact, but it suffices to furnish an estimate of the four reduction potentials which govern the electrolytic reduction of O_2 to H_2O.

$$\begin{array}{ll} O_2 + H^{\cdot} + \varepsilon \rightleftharpoons O_2H & E_1 \\ O_2H + H^{\cdot} + \varepsilon \rightleftharpoons O_2H_2 & E_2 \\ O_2H_2 + H^{\cdot} + \varepsilon \rightleftharpoons OH_2 + OH & E_3 \\ OH + H^{\cdot} + \varepsilon \rightleftharpoons OH_2 & E_4 \end{array}$$

The sum of $E_1 + E_2 + E_3 + E_4$ will give the free energy of the reaction

$$O_2 + 4H^{\cdot} + 4\varepsilon \rightleftharpoons 2H_2O,$$

and so is numerically four times $1{\cdot}23$ volts. Now according to Lewis and Randall the sum $E_1 + E_2$ is equal to $1{\cdot}36$ volts, and from the value established above for the HO_2/HO'_2 potential and the known value of the dissociation constant of H_2O_2, the potential HO_2/H_2O_2 may be calculated. This sum $E_1 + E_2$ can be divided into the two parts

$$E_1 \sim 0{\cdot}08 \text{ volt}$$
$$E_2 \sim 1{\cdot}28 \text{ volts.}$$

$E_3 + E_4$ can also be divided into its two parts, for the equilibrium constant of the reaction

$$H_2O \rightleftharpoons OH + H$$

is fully known thermodynamically. Thus $E_4 = 2 \cdot 1$ volts and $E_3 \sim 1 \cdot 46$ volts, all values being measured against the hydrogen electrode. The total energy of $H + \frac{1}{2}H_2 = H_2 + 50$ k. cals. is almost the same as for the reaction $H + O_2 = HO_2$. The great difference between this value and the much larger value for $H + HO_2 = H_2O_2$ is due to the fact that the double bond in the oxygen molecule must be opened to produce the first product HO_2 but is already open for the second step to proceed.

There are many other allied processes with a direct bearing on the explanations given above. Thus in our preliminary paper we have already discussed the catalysis by iodine ions, a subject on which we have made many experiments, and in this paper we have referred both to the photochemical catalysis and to the catalytic decomposition of H_2O_2 by ozone, but we do not wish to enter here upon a detailed consideration of these much more complicated processes. The points which we wish to stress are the existence and the importance of the radicals HO_2 and OH in the decomposition of hydrogen peroxide, and the easy change from the radical to the chain or from the chain to the radical reaction.

The promoting action of copper salts in the homogeneous decomposition of hydrogen peroxide in the presence of ferric salts has been studied by Bohnson and Robertson,* and we believe that their results are fully explicable in terms of the theory given above. We hold that the action of the cupric ion is analogous to that of the ferric. The promoting action then comes about through the reaction

$$Cu^{\cdot} + Fe^{\cdot\cdot\cdot} \rightleftharpoons Cu^{\cdot\cdot} + Fe^{\cdot\cdot}$$

The heterogeneous decomposition of hydrogen peroxide is closely connected to the homogeneous catalysis. We have found that according to the experimental conditions, polarization of a cathode of amalgamated platinum in sulphuric acid and hydrogen peroxide solutions may lead to the direct reduction of H_2O_2 without the production of any gas, the production of hydrogen alone, of oxygen and hydrogen simultaneously or of oxygen alone. In suitable conditions the last process may occur as a chain reaction, sixteen times as much oxygen being produced as the Faraday equivalent. We propose to discuss this in a later paper.

---

* 'J. Amer. Chem. Soc.,' vol. 45, p. 2512 (1923).

The single basic idea inherent in the foregoing theory is that the hydrogen peroxide molecule is never simultaneously attacked by two monovalent reagents, nor by a bivalent reagent, whether the material is oxidized to oxygen or reduced to water; instead there is monovalent change transforming the peroxide into one of the radicals HO_2 or OH. This is true of the chemical, photochemical, and electrochemical processes. These radicals may then produce oxygen or water in a second step, or they may take part in the chain reaction by further reaction with hydrogen peroxide to water and oxygen and reproduce themselves according to the equations

$$OH + H_2O_2 = H_2O + O_2H \quad (2)$$

$$O_2H + H_2O_2 = O_2 + H_2O + OH. \quad (3)$$

It may be that the easy change from radical to chain reactions, exemplified by this detailed study of the action of ferrous and ferric salts, will prove to be a result of more general value. The conception of chain reactions has influenced the general standpoint of chemists, and there now exists the danger of overlooking the main point that the progress of the reaction through the radicals is the primary process, and the formation of chains by these radicals an interesting but secondary phenomenon. The idea of the reaction progressing through radicals is less new than that of chain reactions, but it often seems that all its implications are not fully accepted. It may be worth emphasizing that the difficulties encountered in the interpretation of single steps in a reaction, whether a chain reaction or a radical reaction, become the less the more numerous the experimentally measurable relationships between the variable factors and the products of the reaction. The more various and complicated are the experimental changes which may be produced and studied in a reaction system the more certain is it that an explanation covering all of them will be actually correct. Thus in our work, the phenomenon of " Katalasestoss " at first sight incompatible with our general knowledge of reactions, becomes finally the best piece of evidence in favour of the system of interactions which we have developed.

Some General Properties of the Formulæ of the Magneto-Ionic Theory

By H. G. BOOKER, B.A., Christ's College, Cambridge

(*Communicated by E. V. Appleton, F.R.S.—Received May* 23, 1934)

§ 1—INTRODUCTION

Appleton's magneto-ionic theory* of the propagation of wireless waves in the ionosphere has been discussed by several authors,† usually for the case when incidence is vertical and damping due to electronic collisions is neglected. Two salient features of the theory which appear upon the removal of these restrictions are described in the present paper. In sections 3, 4, and 5 the effect of collisional friction on vertical propagation is examined and the nature of the transition from longitudinal to transverse propagation is described. Curves are drawn (in section 5) showing this transition when there is a small constant value of friction and the Lorentz polarization term is neglected. In some respects this part of the paper resembles the treatment in a recent paper by Taylor,‡ but there appears to be a difference between her conclusions and ours. In section 6 the further complication of oblique incidence is considered with particular reference to the relation between the polarizations of downcoming magneto-ionic components.

A description of the relation between the complex polarization and the elliptical polarization which it represents is included in section 4.

§ 2—APPLETON'S THEORY

We employ the following notation which is almost identical with that of Appleton :—

c = velocity of electromagnetic waves *in vacuo*.

m = mass of an electron.

e = charge on an electron (e.s.u). e is negative for negative electrons.

N = electron density.

H = imposed magnetic field (gauss).

---

* Appleton, 'J. Inst. Elec. Engs.,' vol. 71, p. 642 (1932).

† Taylor, 'Proc. Phys. Soc.,' vol. 45, p. 245 (1933) ; Ratcliffe, 'Wireless Engineer,' vol. 10, p. 354 (1933).

‡ 'Proc. Phys. Soc.,' vol. 46, p. 408 (1934).

H_L = component of magnetic field along the positive direction of propagation.

H_T = component of magnetic field perpendicular to the direction of propagation.

$p = 2\pi \times$ frequency of wave.

$p_H = \left|\frac{eH}{mc}\right| = 2\pi \times$ the magneto-ionic frequency.

ν = the frequency of electronic collisons (which determines the effective damping forces).

$$x = \frac{4\pi N e^2}{m p^2}.$$

$$y = \frac{p_H}{p} = \left|\frac{eH}{mcp}\right|.$$

$$y_L = \frac{eH_L}{mcp}.$$

$$y_T = \frac{eH_T}{mcp}.$$

$$z = \frac{\nu}{p}.$$

l = the "Lorentz term" which has sometimes been assumed to be equal to 0, and sometimes to $\frac{1}{3}$.*

Q = the complex polarization, defined as the ratio of the component of the complex magnetic field *of the wave* in the direction of H_T to the component at right angles to H_T. If the positive direction of the latter component is taken to be that which is related to H_T and the positive direction of propagation by the right-hand rule, then the polarization is left-handed, linear, or right-handed about the positive direction of propagation according as $I(Q) \gtreqless 0$.

μ = the refractive index.

κ = the absorption coefficient.

$$\chi = \frac{c\kappa}{p}.$$

$q = \mu - i\chi$ = the complex refractive index.

θ = angle between the direction of propagation and the direction of the imposed magnetic field.

$$\zeta = \left[y_L^2 + \left\{\frac{\frac{1}{2}y_T^2}{1-(1-l)\,x-iz}\right\}^2\right]^{\frac{1}{2}},$$ a two-valued function.

---

* See Darwin, 'Proc. Roy. Soc.,' A, vol. 146, p. 17 (1934).

h = height above the surface of the earth.

h_0 = height at which $x = \frac{1}{1-l}$. This height depends on the frequency of the wave.

The propagation of a plane monochromatic electromagnetic wave through a homogeneous ionized medium under the influence of a superimposed magnetic field is described by means of its complex polarization and refractive index, and the above-mentioned theory of Appleton gives expressions for these quantities in terms of the physical constants of the medium, the direction of propagation, and the frequency of the wave. These formulæ are

$$\left\{\begin{aligned} \mathrm{Q} &= -\frac{i}{y_{\mathrm{L}}}\left\{\zeta - \frac{\frac{1}{2}y_{\mathrm{T}}^2}{1-(1-l)\,x-iz}\right\} && (1)\\ q^2 &= 1 - \frac{x}{1+lx-iz+iy_{\mathrm{L}}\mathrm{Q}}\,. && (2)\end{aligned}\right.$$

Q is two-valued, because ζ is two-valued ; the two values refer to the two types of wave which can be propagated without change of form in the medium. For a given value of Q, there are two values of q ; it is physically obvious, however, that one of these values of q must lie in the fourth quadrant of the complex plane, and that only this value is of interest.

The simplest admissible picture of the ionosphere is one in which N and ν are functions only of the height h above the earth's surface, N increasing from a small value and ν decreasing from a large value as h increases from zero. We assume that a wave travelling into the ionosphere is split into two waves (called its magneto-ionic components), which are propagated *independently*,* and that the propagation may be adequately described by formulæ (1) and (2) in which x and z are now regarded as functions of h. We shall start by assuming vertical propagation of the waves, so that y_{L} and y_{T} are independent of h. We shall, however, arrange the work so that this assumption is as unessential as possible in order to facilitate the subsequent removal of this restriction.

§ 3—THE ζ-PLANE

At the transmitter the complex quantity ζ is represented in the complex plane by a pair of points, the join of which is bisected by the origin, and these two points correspond to the two magneto-ionic components, into which the transmitted wave is split. As h increases from zero these points describe continuous curves, and, for vertical propagation, the two points remain symmetrical with respect to the origin for the same value of h. We proceed to investigate the general properties of these curves. Special difficulty will arise under conditions when a determination of ζ approaches the origin because this point is a branch point of the function. ζ may be written in the form

---

* See Försterling and Lassen, 'Ann. Physik,' vol. 18, p. 26 (1933).

$$\zeta = \left[y_L{}^2 + \frac{y_T{}^4}{4} \frac{\{1-(1-l)\,x\}^2 - z^2}{[\{1-(1-l)\,x\}^2 + z^2]^2} + i\,\frac{y_T{}^4}{2} \frac{\{1-(1-l)\,x\}\,z}{[\{1-(1-l)\,x\}^2 + z^2]^2} \right],$$

from which it follows that the necessary and sufficient conditions that $\zeta = 0$ are

$$x = \frac{1}{1-l}, \quad \left| \frac{y_T{}^2}{2zy_L} \right| = 1.$$

Suppose that $x \ll 1$ at $h = 0$ and that, for the particular frequency under consideration, x increases to the value $\dfrac{1}{1-l}$ as h increases to h_0. The values of functions of h at $h = h_0$ will be denoted by a suffix 0.

First let us consider the situation in the ζ^2-plane. $I(\zeta^2) \gtreqless 0$ according as $x \lesseqgtr \dfrac{1}{1-l}$. Also when $x = \dfrac{1}{1-l}$, $R(\zeta^2) \lesseqgtr 0$ according as $\left|\dfrac{y_T{}^2}{2zy_L}\right| \lesseqgtr 1$. Hence as h increases through h_0 the curve representing ζ^2 for a particular magneto-ionic component crosses the real axis from above to below, and the crossing point is to the right or left of the origin according as $\left|\dfrac{y_T{}^2}{2zy_L}\right|_0 \lessgtr 1$ for that magneto-ionic component. For vertical propagation $\left|\dfrac{y_T{}^2}{2zy_L}\right|_0$ has the same value for the two magneto-ionic components and this value is independent of whether the wave is ascending into the ionosphere or returning from it. If $\left|\dfrac{y_T{}^2}{2zy_L}\right|_0 = 1$, then the curve crosses the real axis at the origin, and in this case we shall require to know the angle, $2\phi \left(0 \leqslant \phi \leqslant \dfrac{\pi}{2}\right)$, at which the curve cuts the real axis (see fig. 1).

$$\begin{aligned} 2\phi &= \lim_{h\to h_0} \arg \zeta^2 \\ &= \lim_{h\to h_0} \tan^{-1} \frac{2y_T{}^4\,\{1-(1-l)\,x\}z}{4y_L{}^2\,[\{1-(1-l)\,x\}^2+z^2]^2 + y_T{}^4\,[\{1-(1-l)\,x\}^2 - z^2]}. \end{aligned}$$

Since $\left|\frac{y_T^2}{2zy_L}\right|_0 = 1$ the fraction on the right-hand side becomes indeterminate at $h = h_0$, but its limit may be evaluated by differentiating top and bottom separately. Using a dash to denote differentiation with respect to h,

$$2\phi = \tan^{-1}\frac{(1-l)\,y_{T0}^4\,x'_0}{2z_0\,y^3_{T0}\,y'_{T0} - 4z_0^3\,y_{L0}\,y'_{L0} - y^4_{T0}\,z'_0}$$

$$= \tan^{-1}\left\{\frac{4\pi(1-l)\,e^2}{mp}\,\frac{p_H^2\sin^3\theta_0 \,.\, N'_0}{2\nu_0 p_H^2\sin^2\theta_0\cos\theta_0\theta'_0 + 4\nu_0^3\cos\theta_0\theta'_0 - p_H^2\sin^3\theta_0\nu'_0}\right\}. \quad (3)$$

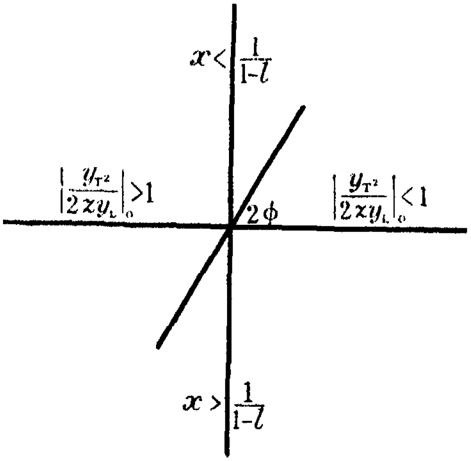
$x < \frac{1}{1-l}$
$\left|\frac{y_{T^2}}{2zy_L}\right|_0 > 1$
2ϕ
$\left|\frac{y_{T^2}}{2zy_L}\right|_0 < 1$
$x > \frac{1}{1-l}$

FIG. 1—ζ^2-plane. (y_{T^2} should read y_T^2)

For vertical propagation we have to put y'_L, y'_T, and θ' zero, so that

$$2\phi = \tan^{-1}\left\{p\left(-\frac{1}{N}\frac{dN}{d\nu}\right)_0\right\}.$$

If in addition ν does not vary with height then $\phi = \frac{\pi}{4}$.

The curve representing ζ as a function of h is obtained from the ζ^2-curve by taking the square root in the complex plane (see fig. 2). If $h < h_0$ ζ lies in the first or third quadrants; if $h > h_0$ ζ lies in the second or fourth quadrants. The ζ-curve has two branches corresponding to the two magneto-ionic components ; one of these starts at $h = 0$ in the first quadrant and will be called branch 1, while the other starts in the third quadrant and will be called branch 2. The magneto-ionic components corresponding to branches 1 and 2 will be called waves 1 and 2 respectively.

Consider branch 1. As h increases through h_0 branch 1 passes from the first quadrant to the fourth or second quadrant according as $\left|\frac{y_T^2}{2zy_L}\right|_0 \lessgtr 1$. If $\left|\frac{y_T^2}{2zy_L}\right|_0 = 1$ the representative point in the ζ-plane approaches the origin from a direction determined by the angle ϕ (see fig. 2). If $\left|\frac{y_T^2}{2zy_L}\right|_0$ is very near 1, then the representative point is deflected through a right-angle by the origin, to left or right depending on the sign of $\left|\frac{y_T^2}{2zy_L}\right|_0 - 1$. Corresponding remarks may be made about branch 2 of the ζ-curve; for vertical propagation the two branches are symmetrical with respect to the origin.

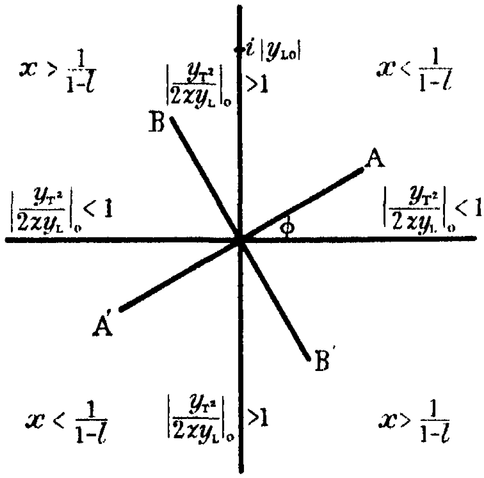
$x > \frac{1}{1-l}$
$\left|\frac{y_{T^2}}{2zy_L}\right|_0 > 1$
$i\,|y_{Lo}|$
$x < \frac{1}{1-l}$
B
A
$\left|\frac{y_{T^2}}{2zy_L}\right|_0 < 1$
ϕ
$\left|\frac{y_{T^2}}{2zy_L}\right|_0 < 1$
A′
B′
$x < \frac{1}{1-l}$
$\left|\frac{y_{T^2}}{2zy_L}\right|_0 > 1$
$x > \frac{1}{1-l}$

FIG. 2—ζ-plane. (y_{T^2} should read y_T^2)

It is sometimes convenient to denote by ζ_+ that determination of ζ which has its real part positive, or more strictly for which $-\frac{\pi}{2} < \arg \zeta \leqslant \frac{\pi}{2}$. Thus, if for one of the magneto-ionic components under some particular circumstances R (ζ) happens to be negative, we write

$$\zeta = -\zeta_+:$$

ζ_+ is then the value of ζ for the other magneto-ionic component at the same height provided propagation is vertical. At the transmitter wave 1 is given by $\zeta = +\zeta_+$ and wave 2 by $\zeta = -\zeta_+$, by definition, and this remains true so long as $h \leqslant h_0$. In the region $h > h_0$ wave 1 is given by $\zeta = \pm\zeta_+$ according as $\left|\frac{y_T^2}{2zy_L}\right|_0 \lessgtr 1$, while wave 2 is given by $\zeta = \mp \zeta_+$ according as $\left|\dfrac{y_T^2}{2zy_L}\right|_0 \lessgtr 1$. The different behaviour at the height h_0 according as $\left|\dfrac{y_T^2}{2zy_L}\right|_0 \lessgtr 1$ was first pointed out by Appleton and Builder,* who suggested that propagation in the neighbourhood of the height h_0 should be called quasi-longitudinal if $\left|\dfrac{y_T^2}{2zy_L}\right|_0 < 1$ and quasi-transverse if $\left|\dfrac{y_T^2}{2zy_L}\right|_0 > 1$.

We proceed to consider the conditions which exist in the neighbourhood of the height h_0 when $\left|\dfrac{y_T^2}{2zy_L}\right|_0$ is near 1. We have already examined the situation in the ζ-plane and we have to translate these results into terms of polarization and refractive index by means of formulæ (1) and (2). Now the scale of variation of h along a ζ-curve when the latter passes near the origin is large, because $\dfrac{d\zeta}{dh}$ contains the factor $\dfrac{1}{\zeta}$, and so for studying the variation of Q and q near $h = h_0$ when $\left|\dfrac{y_T^2}{2zy_L}\right|_0$ is near 1 we may give the quantities other than ζ in formulæ (1) and (2) their values at $h = h_0$ and replace $\dfrac{y_{T0}^2}{2z_0}$ by $|y_{L0}|$. We thus obtain

$$\begin{cases} \mathrm{Q} = -\dfrac{i}{y_{L0}}(\zeta - i\,|y_{L0}|) & (4) \\ q^2 = 1 - \dfrac{1}{1 - (1 - l)(iz_0 - iy_{L0}\,\mathrm{Q})}. & (5) \end{cases}$$

§ 4—THE Q-PLANE. (POLARIZATION)

Before proceeding to a discussion of equation (4) it may not be out of place to make some general remarks concerning the relation between the complex quantity Q and the polarization ellipse which it represents. Fig. 3 shows the wave-front of an approaching wave and H_T is the component of the earth's magnetic field transverse to the direction of propagation. The complex polarization Q is defined to be the ratio of the y-component to the x-component of the complex magnetic field of the wave. Fig. 4 shows the complex plane representing Q. Points above the real axis correspond to ellipses described in a direction left-handed about the positive direction of propagation, while points below the real axis correspond to right-handed rotation. Points on the real axis correspond to linear polarization. Points to the right of the imaginary axis correspond to ellipses whose major axes lie in the first and third quadrants of fig. 3, while points to the left of the imaginary axis correspond to ellipses whose major axes lie in the second and fourth quadrants. The origin corresponds to linear polarization perpendicular to H_T, the points ± 1 to linear polarization at 45° to H_T, and the point

---

* 'Proc. Phys. Soc.,' vol. 45, p. 208 (1933).

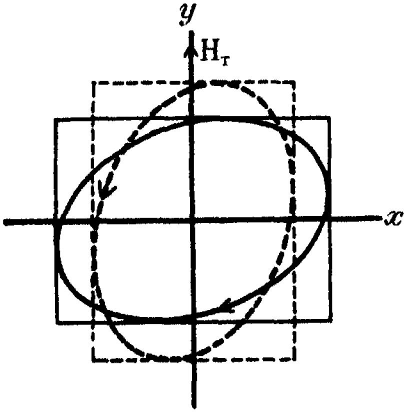

FIG. 3—Polarization ellipses (wave approaching)

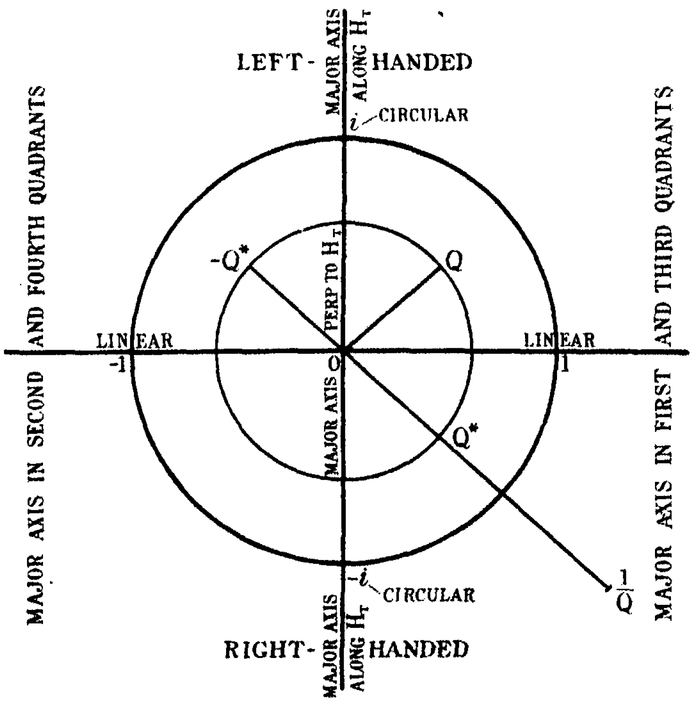

FIG. 4—Q-plane, general survey

at infinity to linear polarization along H_T. Points on the imaginary axis correspond to ellipses having their major axes perpendicular or parallel to H_T; for points between $\pm i$ the major axis is perpendicular to H_T and for points outside this interval the major axis is parallel to H_T. The points $\pm i$ correspond to circular polarizations. The distance of a point from the origin is the ratio of the sides of the rectangle within which the ellipse is inscribed (side parallel to H_T/ side perpendicular to H_T, see fig. 3). Thus all points on a circle, with centre the origin, represent ellipses inscribed in the same rectangle; the points where the circle cuts the real axis give the diagonal linear polarizations, and the points where it cuts the imaginary axis give the symmetrical elliptical polarizations.

Suppose that Q represents a certain polarization. Then the complex conjugate Q^* represents the same ellipse described in the opposite direction. $-Q^*$ represents the ellipse obtained by reflecting the given one in the x or y-axis of fig. 3, the direction of rotation remaining unaltered. $1/Q$ is obtained by inverting in the complex plane with respect to the unit circle and reflecting in the real axis. The polarization represented by $1/Q$ is obtained by rotating the given ellipse through a right angle, reflecting in a co-ordinate axis, and reversing the direction of description. The dotted ellipse in fig. 3 is obtained from the other ellipse in this way, and so the two types of polarization indicated are such that the product of their complex polarizations is unity. It is well known (and is easily verified) that, for the same values of N, ν, H, and θ the product of the two values of Q given by (1) is unity and so the two corresponding polarizations are related as in fig. 3. This is precisely the relation between the polarizations of the two magneto-ionic components at a given height for vertical propagation.

The variation of the polarization at the height h_0 with the value of $\left|\frac{y_T^2}{2zy_L}\right|_0$ is easily followed out in fig. 4 by putting $x = \frac{1}{1-l}$ in equation (1). As $\left|\frac{y_T^2}{2zy_L}\right|_0$ decreases from ∞ to 1 one determination of Q moves from the centre to the circumference of the unit circle along a real radius, while the other (reciprocal) determination moves down the real axis from infinity to the same point. As $\left|\frac{y_T^2}{2zy_L}\right|_0$ decreases from 1 to 0, the two determinations of Q move in opposite directions round the circumference of the unit circle until they meet the imaginary axis. In this interval the ellipses are inscribed in a square, and (for the same values of y_L and y_T) are identical but described in opposite directions.

The evolution of the polarization ellipses when $x = \frac{1}{1-l}$ as $\left|\frac{y_T^2}{2zy_L}\right|_0$ decreases from ∞ to 0 is shown in fig. 5.

After this general survey of the Q-plane we return to the consideration of the variation near the height h_0 of the polarization of a magneto-ionic component when $\left|\frac{y_T^2}{2zy_L}\right|_0$ is near 1. The quantity $\zeta - i\,|y_{L0}|$ in equation (4) is obtained from fig. 2 by transferring the origin to the point $i\,|y_{L0}|$. Q is then obtained by multiplying the unit by $|y_{L0}|$ and rotating the figure about the (new) origin through a right angle. The rotation is anti-clockwise or clockwise according as $y_{L0} <$ or > 0, *i.e.*, according as $eH_{L0} <$ or > 0. Fig. 6 shows Q for the two cases ; the lettering corresponds to fig. 2.

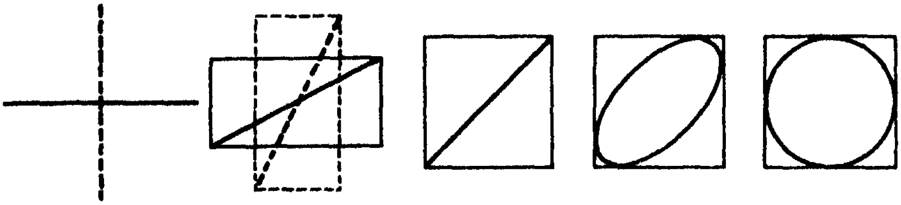

$\left|\frac{y_{T'}}{2zy_L}\right|_0 \gg 1$ $\left|\frac{y_{T'}}{2zy_L}\right|_0 > 1$ $\left|\frac{y_{T'}}{2zy_L}\right|_0 = 1$ (Identical linear polarizations) $\left|\frac{y_{T'}}{2zy_L}\right|_0 < 1$ (Identical ellipses, opposite rotations) $\left|\frac{y_{T'}}{2zy_L}\right|_0 \ll 1$

FIG. 5—Polarization when $x = \frac{1}{1-l}$. ($y_{T'}$ should read y_T^2)

Whether the magneto-ionic component is wave 1 or wave 2, Q does not or does cross the real axis according as $\left|\frac{y_T^2}{2zy_L}\right|_0 \lessgtr 1$. Hence if $\left|\frac{y_T^2}{2zy_L}\right|_0$ is slightly less than 1 the polarization ellipse of the wave becomes very narrow as h approaches h_0 and opens out again as h recedes from h_0, the direction of rotation in the ellipse being unchanged. If, on the other hand, $\left|\frac{y_T^2}{2zy_L}\right|_0$ is slightly greater than 1, the polarization ellipse of the wave narrows down to a straight line at $h = h_0$ and then opens out into an ellipse again, the direction of rotation in the ellipse being reversed. If $\left|\frac{y_T^2}{2zy_L}\right|_0 = 1$, the polarization of the wave becomes linear at 45° to the direction of H_T as h approaches h_0, and then the wave splits into two waves ; for each of these two waves the polarization ellipse opens out from a straight line and the directions of rotation in the two ellipses are opposite. Provided propagation is vertical both magneto-ionic components are resplit at $h = h_0$ in this case and the types of propagation experienced by the two parts of each component above the height h_0 are the same for wave 1 as for wave 2 ; there are, in fact, two fundamental modes of propagation above the height h_0, but each contains energy derived from both the incident magneto-ionic components. Physically it is unlikely that a wave would be able to undergo the rapid variation of polarization near $h = h_0$ indicated by the theory in this case.

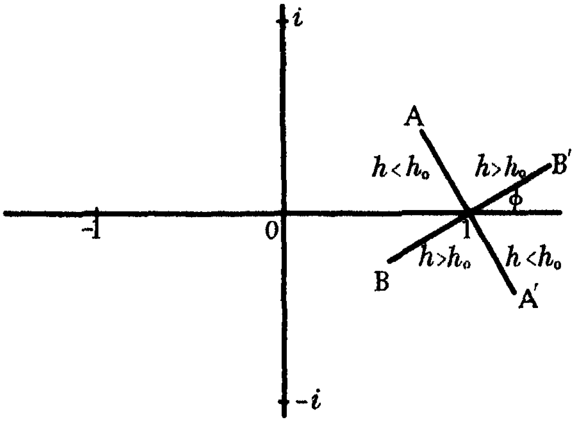

FIG. 6a—Q-plane, $eH_{L0} < 0$.

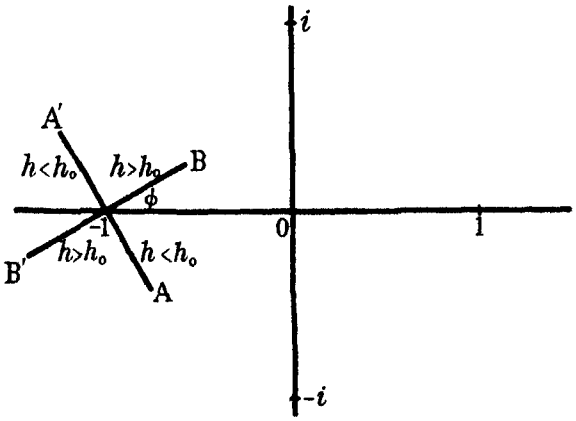

FIG. 6b—Q-plane, $eH_{L0} > 0$.

§ 5—THE Q-PLANE (REFRACTIVE INDEX AND ABSORPTION COEFFICIENT)

The behaviour of q near $h = h_0$ when $\left|\frac{y_T^2}{2zy_L}\right|_0$ is near 1 is obtained direct from that of ζ by means of the formula

$$q^2 = 1 - \frac{1}{1 - i(1-l)(z_0 + |y_{L0}|) + (1-l)\zeta}, \tag{6}$$

which is obtained by substituting for Q from equation (4) into equation (5). For short write

$$a = 1 - i(1 - l)(z_0 + |y_{L,0}|) \qquad (7)$$

$$w = (1 - l)\,\zeta$$

so that equation (6) becomes

$$q^2 = 1 - \frac{1}{w + a}. \qquad (8)$$

a satisfies $-\frac{\pi}{2} < \arg a < 0$. The w-curves are identical with the ζ-curves except for a possible change of scale.

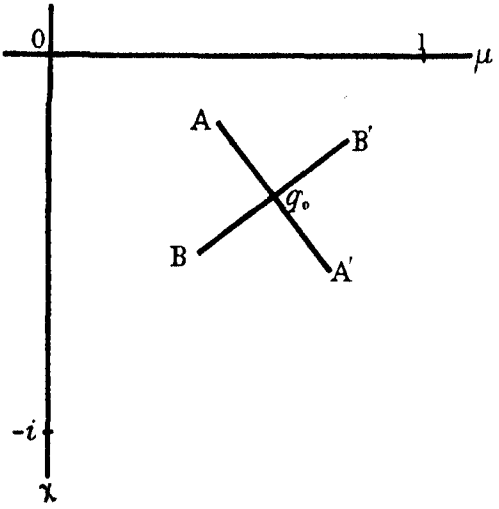

FIG. 7—q-plane

To obtain q from w we transfer the origin to the point $-a$, invert with respect to the unit circle, reflect in the imaginary axis, transfer the origin to the point -1 and take the square root. The restriction on the value of arg a restricts the point $q_0 = \left(1 - \frac{1}{a}\right)^{\frac{1}{2}}$ to the second or fourth quadrants, and we are only interested in the latter quadrant. The effect is to transform fig. 2 into some such fig. as 7, from which can be read off the nature of the transition which would take place at $h = h_0$ in the (μ, h) and (χ, h) curves were circumstances to change in such a way that $\left|\frac{y_T^2}{2zy_L}\right|_0$ passed through 1. Remembering how distended is the scale of h along the curve in the complex plane under these conditions, we see that the transition in the (μ, h) and (χ, h) curves must be of the type shown in fig. 8, in which μ or χ is supposed to increase upwards and h to the right.

The interpretation to be given to fig. 8 depends on the particular case under consideration. Suppose, for instance, that the lines AA′, BB′ turn out to have an orientation in the q-plane such as that shown in fig. 7, that we are dealing with wave 1 and that it is approaching the height h_0 from below. Then the representative point in the q-plane is approaching q_0 in the direction Aq_0 and is deflected to the left or right according as $\left|\frac{y_T^2}{2zy_L}\right|_0$ is slightly less or slightly greater than 1. As $\left|\frac{y_T^2}{2zy_L}\right|_0$ increases through 1 the (μ, h) curve changes from type $f'f$ to type $d'c'$, while the (χ, h) curve changes from type $d'c'$ to type $f'f$. For vertical propagation the (μ, h) curve for wave 2 at the same time changes from type aa' to type cd, while the (χ, h) curve changes from type cd to type aa'.

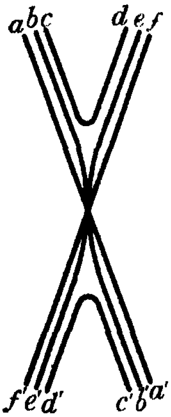

FIG. 8—(μ, h) and (χ, h) transition curves

The interpretation of fig. 8 depends on the orientation of the lines AA′, BB′ in the q-plane, as this interpretation changes whenever they rotate through a configuration parallel to the real and imaginary axes. Now the orientation of these lines in the q-plane is determined by the amount of anti-clockwise rotation which they have received as a result of transformation from the ζ-plane to the q-plane, and this is $\arg \frac{dq}{dw}$ evaluated at $w = 0$.

From equation (8)

$$2q\frac{dq}{dw} = \frac{1}{(w + a)^2},$$

therefore

$$\arg q + \arg \frac{dq}{dw} = -2 \arg (w + a). \tag{9}$$

In this we have to put $w = 0$; the value of $\arg q$ at $w = 0$ is, from equation (8),

$$\begin{aligned} \arg q_0 &= \tfrac{1}{2} \arg\left(1 - \frac{1}{a}\right) \\ &= \tfrac{1}{2} \arg (a - 1) - \tfrac{1}{2} \arg a. \\ &= -\frac{\pi}{4} - \tfrac{1}{2} \arg a \end{aligned} \tag{10}$$

from equation (7). It is important that this value of arg q_0 be used, and not the value which differs from it by π, because we are interested in the determination of q which lies in the fourth quadrant. From equations (9) and (10) the required value of $\arg \frac{dq}{dw}$ is

$$\left(\arg \frac{dq}{dw}\right)_0 = \frac{\pi}{4} - \tfrac{3}{2} \arg a. \tag{11}$$

Hence the angle between the direction of A′A in the q-plane and the positive direction of the real axis is

$$\psi = \frac{\pi}{4} + \phi - \tfrac{3}{2} \arg a. \tag{12}$$

Since $0 \leqslant \phi \leqslant \frac{\pi}{2}$ and $-\frac{\pi}{2} < \arg a < 0$, it follows that $\frac{\pi}{4} < \psi < \frac{3\pi}{2}$.

Other things being equal, the intepretation of fig. 8 does not alter so long as ψ remains in one of the intervals $\left(\frac{\pi}{4}, \frac{\pi}{2}\right)$, $\left(\frac{\pi}{2}, \pi\right)$, $\left(\pi, \frac{3\pi}{2}\right)$, but changes if ψ passes through either of the values $\frac{\pi}{2}$ or π. These critical cases are, according to equation (12), given by

$$-\arg a = \frac{\pi}{6} - \tfrac{2}{3}\phi \text{ or } \frac{\pi}{2} - \tfrac{2}{3}\phi.$$

Using (7) and writing $t = \tan \frac{2\phi}{3}$ these conditions become

$$(1 - l)(z_0 + |y_{L0}|) = \frac{1 - \sqrt{3}t}{\sqrt{3} + t} \text{ or } \frac{1}{t}.$$

The intervals

$$\frac{\pi}{4} < \psi < \frac{\pi}{2},$$

$$\frac{\pi}{2} < \psi < \pi,$$

$$\pi < \psi < \frac{3\pi}{2},$$

correspond respectively to

$$(1 - l)(z_0 + |y_{L0}|) < \frac{1 - \sqrt{3}t}{\sqrt{3} + t},$$

$$\frac{1 - \sqrt{3}t}{\sqrt{3} + t} < (1 - l)(z_0 + |y_{L0}|) < \frac{1}{t},$$

$$\frac{1}{t} < (1 - l)(z_0 + |y_{L0}|),$$

or

$$p > (1-l)\frac{\sqrt{3}+t}{1-\sqrt{3}t}(\nu_0+p_{\mathrm{H}}\,|\cos\theta_0|),$$

$$(1-l)\frac{\sqrt{3}+t}{1-\sqrt{3}t}(\nu_0+p_{\mathrm{H}}\,|\cos\theta_0|) > p > (1-l)\,t\,(\nu_0+p_{\mathrm{H}}\,|\cos\theta_0|),$$

$$(1-l)\,t\,(\nu_0+p_{\mathrm{H}}\,|\cos\theta_0|) > p.$$

With the help of the relation

$$\left|\frac{y_{\mathrm{T}}^2}{2zy_{\mathrm{L}}}\right|_0 = 1,$$

which may be written

$$\nu_0 = \tfrac{1}{2}\frac{\sin^2\theta_0}{|\cos\theta_0|}p_{\mathrm{H}},$$

these inequalities become respectively

$$p > \frac{1-l}{2}\,\frac{\sqrt{3}+t}{1-\sqrt{3}t}\,\frac{1+\cos^2\theta_0}{|\cos\theta_0|}p_{\mathrm{H}}$$

$$\frac{1-l}{2}\,\frac{\sqrt{3}+t}{1-\sqrt{3}t}\,\frac{1+\cos^2\theta_0}{|\cos\theta_0|}p_{\mathrm{H}} > p > \frac{1-l}{2}\,t\,\frac{1+\cos^2\theta_0}{|\cos\theta_0|}p_{\mathrm{H}}$$

$$\frac{1-l}{2}\,t\,\frac{1+\cos^2\theta_0}{|\cos\theta_0|}p_{\mathrm{H}} > p.$$

Let us define an angle Θ, lying between 0 and $\pi/2$, by means of the equation

$$\nu_0 = \tfrac{1}{2}\frac{\sin^2\Theta}{\cos\Theta}p_{\mathrm{H}}. \tag{13}$$

If, at the height h_0, a magneto-ionic component is such that $0 \leqslant \theta_0 < \Theta$ or $\pi - \Theta < \theta_0 \leqslant \pi$, then its propagation at this height is quasi-longitudinal, whereas, if it is such that $\Theta < \theta_0 < \pi - \Theta$, then its propagation at this height is quasi-transverse. The nature of the transition which takes place in the (μ, h) and (χ, h) curves as θ_0 passes through either of the values Θ or $\pi - \Theta$ is obtained from fig. 8 and depends on the orientation of the lines AA′, BB′ in the q-plane ; this orientation is given by

$$\left.\begin{array}{l} \frac{\pi}{4} < \psi < \frac{\pi}{2} \\[1em] \frac{\pi}{2} < \psi < \pi \\[1em] \text{or} \qquad \pi < \psi < \frac{3\pi}{2} \end{array}\right\} \tag{14}$$

according as

$$\left.\begin{aligned} & p > \frac{1-l}{2}\,\frac{\sqrt{3}+t}{1-\sqrt{3}t}\,\frac{1+\cos^2\Theta}{\cos\Theta}\,p_H \\ \frac{1-l}{2}\,\frac{\sqrt{3}+t}{1-\sqrt{3}t}\,\frac{1+\cos^2\Theta}{\cos\Theta}\,p_H > {} & p > \frac{1-l}{2}\,t\,\frac{1+\cos^2\Theta}{\cos\Theta}\,p_H \\ \text{or}\quad \frac{1-l}{2}\,t\,\frac{1+\cos^2\Theta}{\cos\Theta}\,p_H > {} & p, \end{aligned}\right\} \quad (15)$$

In interpreting these inequalities it must be remembered that, in general, t is a function of p. From equation (3) t is given by

$$t = \tan\tfrac{1}{3}\tan^{-1}\left\{\frac{4\pi(1-l)e^2}{mp}\,\frac{p_H^2\sin^3\Theta\,.\,N'_0}{2\nu_0 p_H^2\sin^2\Theta\cos\Theta\,\theta'_0+4\nu_0^3\cos\Theta\,\theta'_0-p_H^2\sin^3\Theta\,\nu'_0}\right\} \quad (16)$$

and for vertical propagation θ'_0 is zero.

If we now suppose, in addition to vertical propagation, that ν does not vary with height, then $\theta' = \nu' = 0$ and so from (16) $t = 1/\sqrt{3}$, independent of p; the first of the inequalities (15) therefore disappears. The orientation of the lines AA′, BB′ in the q-plane is now given by

$$\frac{\pi}{2} < \psi < \pi \quad \text{or} \quad \pi < \psi < \frac{3\pi}{2},$$

according as

$$p \gtrless \frac{1-l}{2\sqrt{3}}\,\frac{1+\cos^2\Theta}{\cos\Theta}\,p_H = p_1 \quad \text{(say)}.$$

Suppose we are drawing the (μ, h) and (χ, h) curves for various values of θ. Then the nature of the transition which takes place at $h = h_0$ as θ passes through the value Θ (or $\pi - \Theta$) is of type A or type B, fig. 9, according as $p \gtrless p_1$; the continuous curve denotes wave 1, and the dotted curve wave 2.

Let us further suppose that ν is sufficiently small, so that we can estimate the (μ, h) and (χ, h) curves, for the cases $\theta = 0$, π, or θ lying definitely between Θ and $\pi - \Theta$, from the curves for $\nu = 0$ by the method of "rounding off corners." We know the behaviour of the curves near $h = h_0$ when θ is near Θ or $\pi - \Theta$, and since Θ is small because ν is small, as shown by equation (13), we may write $\cos\Theta = 1$ and so $p_1 = \dfrac{1-l}{\sqrt{3}}p_H$. The sort of curve obtained in this way is shown in figs. 10 to 15 in which the continuous curve denotes wave 1 and the dotted curve denotes wave 2, and it is supposed that $l = 0$. If $\left|\frac{y_T^2}{2zy_L}\right| = 1$, each magneto-ionic component passing the height h_0 is resplit. The faint curves denote the two types of propagation which are possible above the height h_0 in this case ; as already pointed out each of these two fundamental modes will contain energy derived from both the incident magneto-ionic components. We notice how, for heights greater than h_0, the magneto-ionic components exchange their types of propagation via a splitting process as $\left|\frac{y_T^2}{2zy_L}\right|$ passes through the value 1.

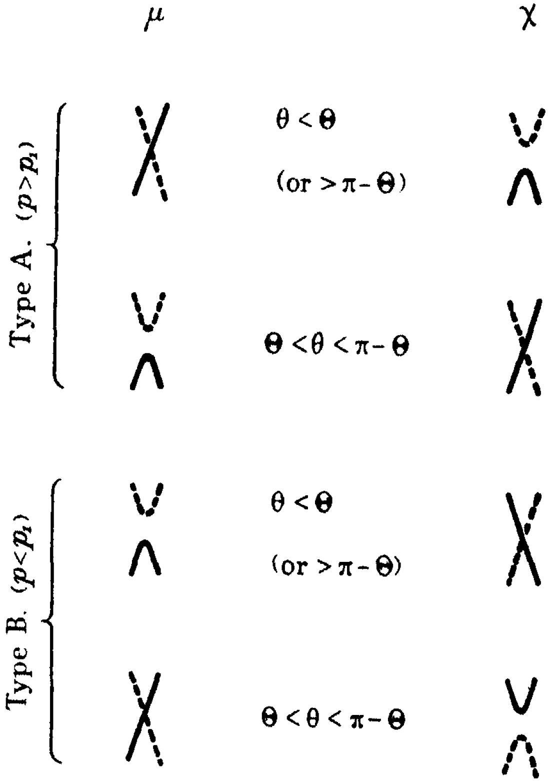

FIG. 9—(μ, h) and (χ, h) transition curves for vertical incidence and constant friction

We may suppose that each magneto-ionic component is reflected when the absolute value of its complex refractive index becomes sufficiently small, and that its polarization relative to the *upward vertical* is preserved. Each magneto-ionic component then retraces on its downward journey the same (μ, h) and (χ, h) curves as it traversed on its upward journey, while

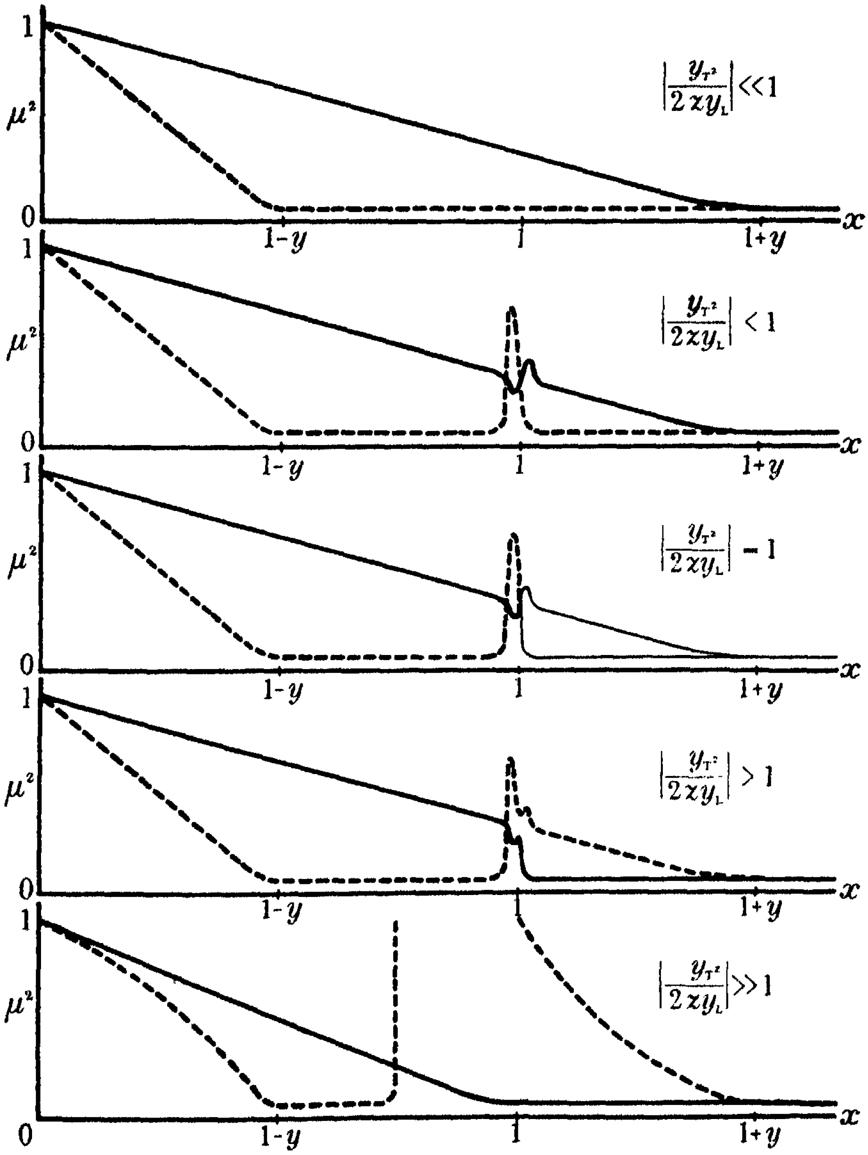

FIG. 10—Form of (μ^2, x) curves for various θ, $p > p_H$, vertical incidence, small constant friction, $l = 0$. (y_{T^2} should read y_T^2)

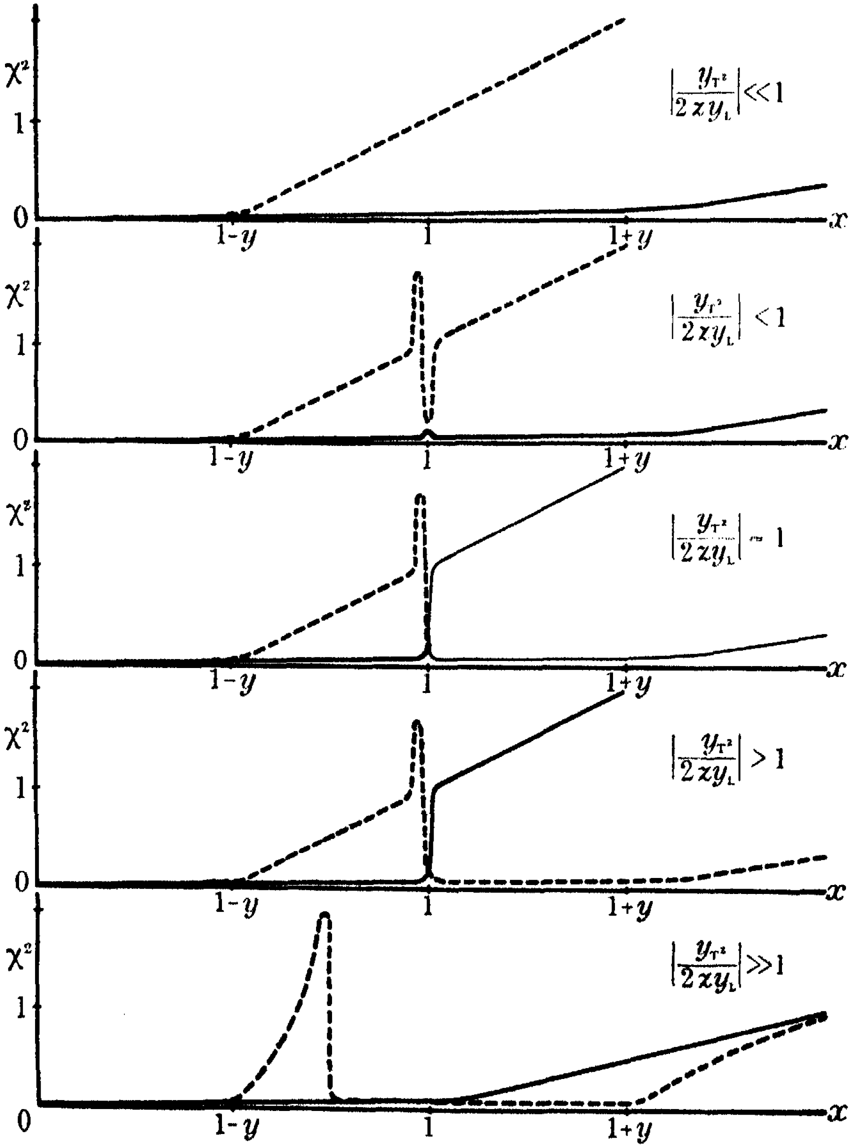

Fig. 11—Form of (χ^2, x) curves for various θ, $p > p_H$, vertical incidence, small constant friction $l = 0$. (y_{T^2} should read y_T^2)

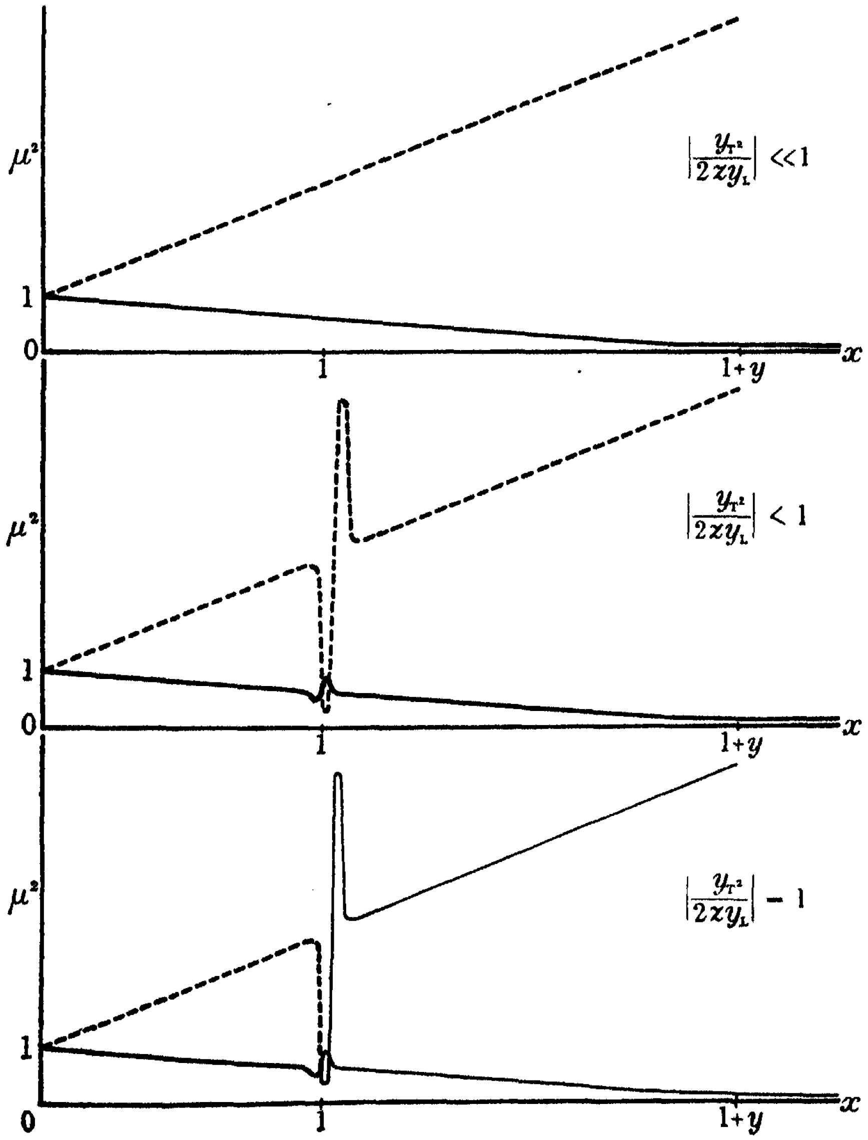

FIG. 12—Form of (μ^2, x) curves for various θ, $p_H > p > \frac{p_H}{\sqrt{3}}$(approx.), vertical incidence, small constant friction, $l = 0$. (y_{T^2} should read $y_T{}^2$)

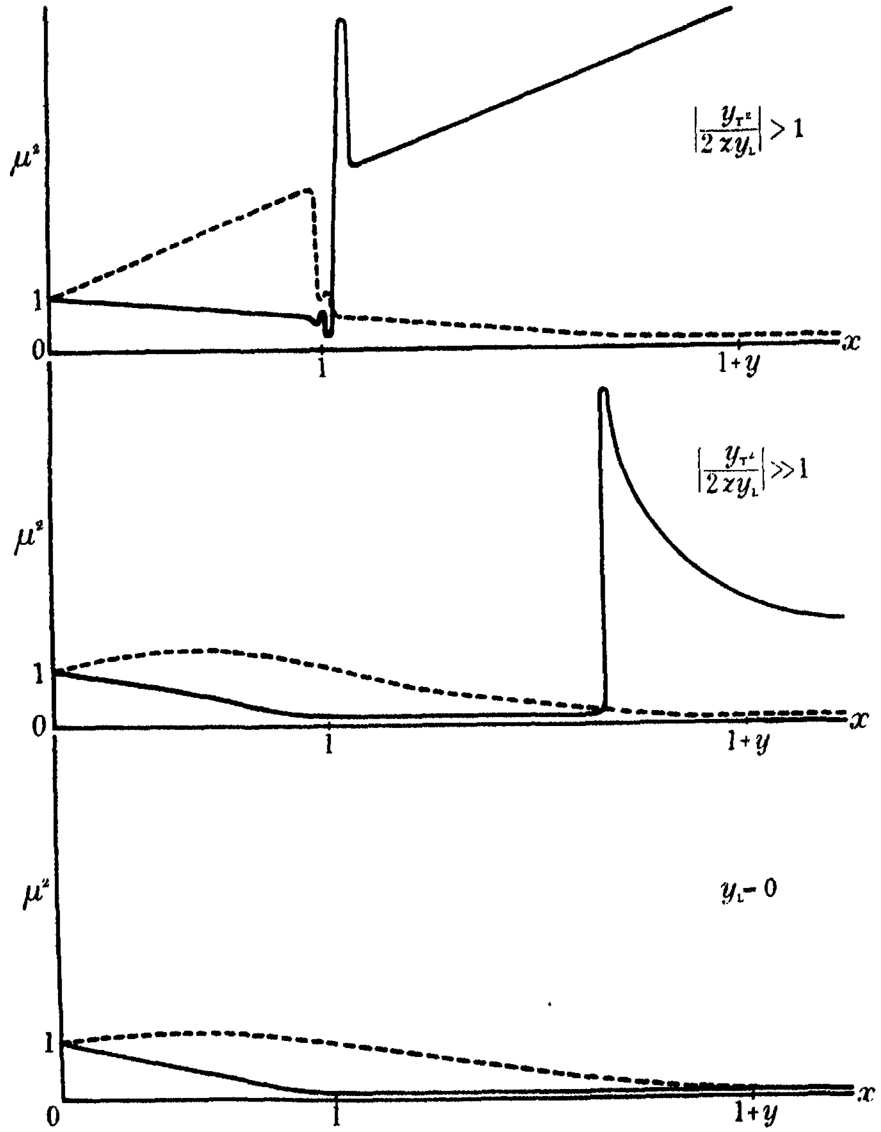

FIG. 12—(continued)

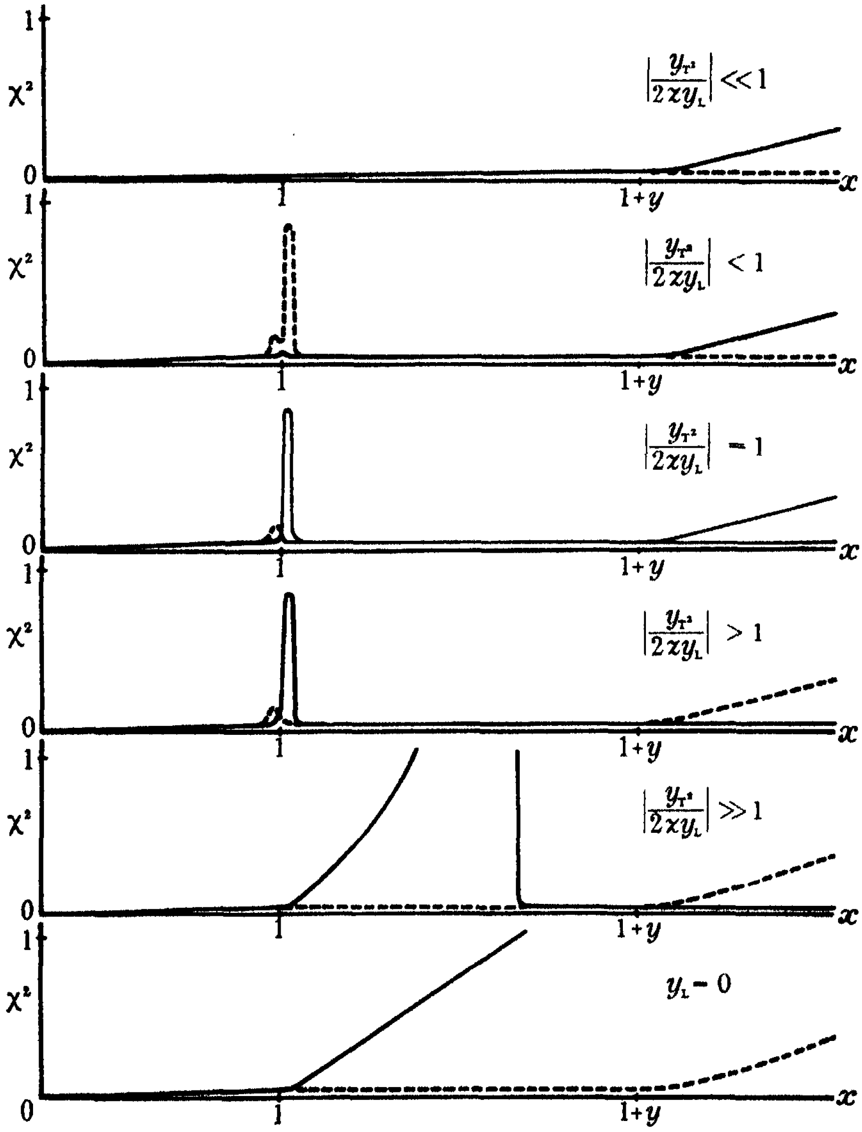

FIG. 13—Form of (χ^2, x) curves for various θ, $p_H > p > \frac{p_H}{\sqrt{3}}$ (approx.), vertical incidence, small constant friction, $l = 0$. ($y_{T'}$ should read $y_T{}^2$)

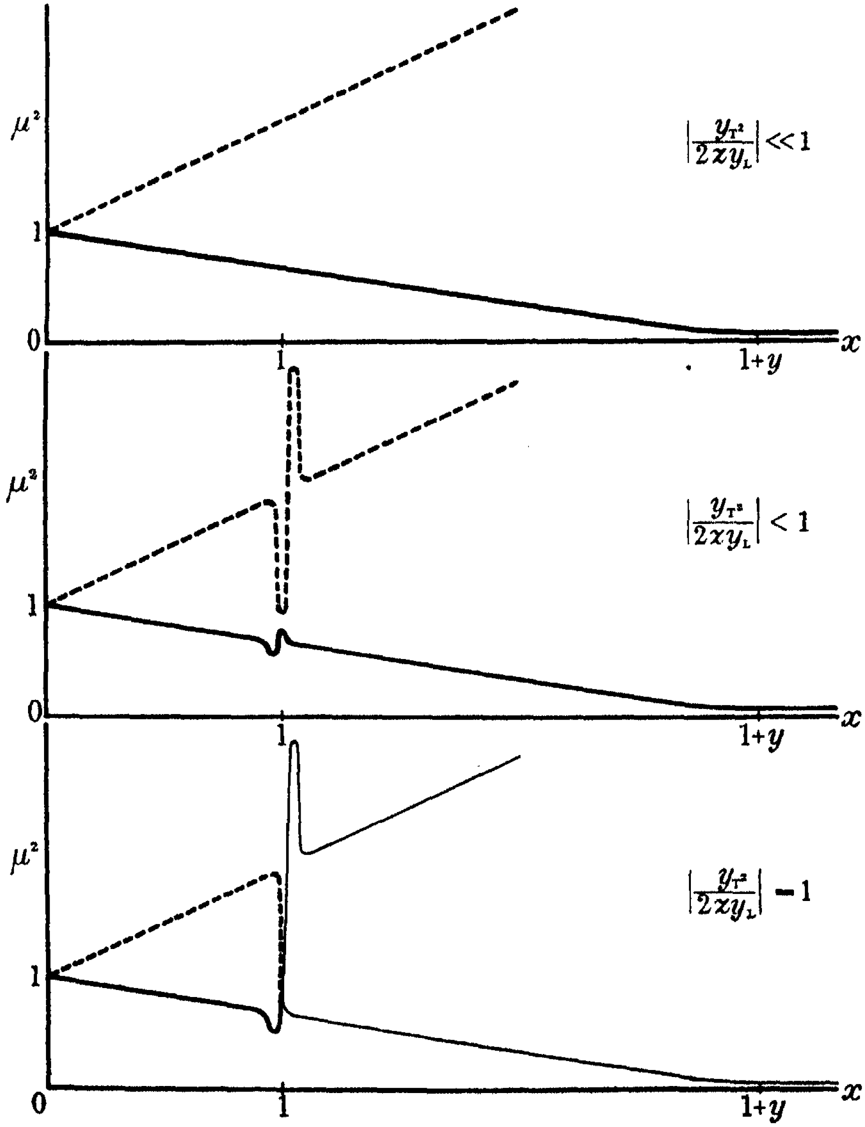

FIG. 14—Form of (μ^2, x) curves for various θ, $p < \frac{p_{\parallel}}{\sqrt{3}}$ (approx.), vertical incidence, small constant friction, $l = 0$. (y_{T^2} should read $y_T{}^2$)

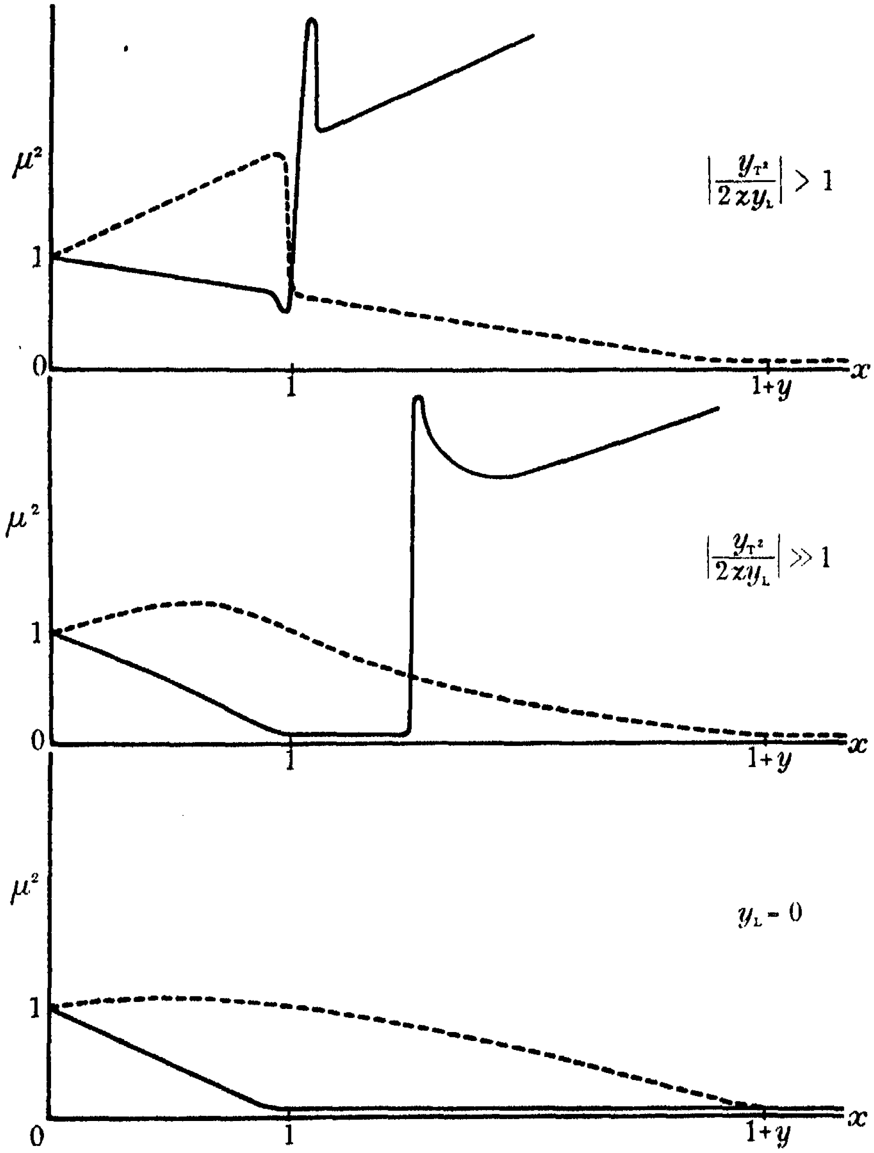

FIG. 14—(continued)

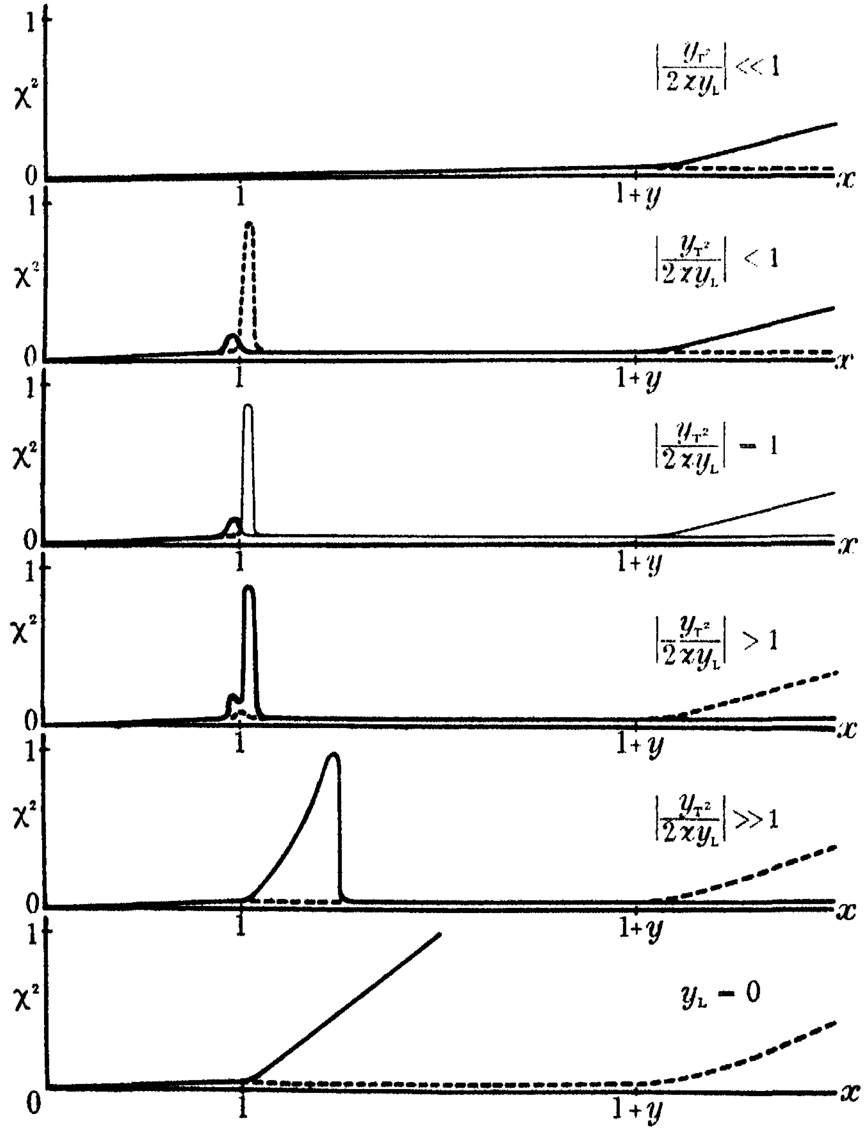

FIG. 15—Form of (χ^2, x) curves for various θ, $p < \frac{p_H}{\sqrt{3}}$ (approx.), vertical incidence, small constant friction, $l = 0$. (y_{T^2} should read $y_T{}^2$)

its polarization at any height referred to the upward vertical is the same on the downward journey as it was on the upward journey. When $\left|\frac{y_T^2}{2zy_L}\right|_0 = 1$ each part of each magneto-ionic component reflected above $h = h_0$ is again resplit on its downward journey and multiple echos would thereby be produced.

§ 6—GENERALIZATION TO OBLIQUE INCIDENCE

We now turn to consider the general case of propagation via the ionosphere between two non-coincident points on the earth's surface (assumed flat). In this case the direction of propagation varies throughout the trajectory so that y_L and y_T are functions of h. Moreover, the paths of the two magneto-ionic components are not in general the same, so that y_L and y_T are different functions of h for the two components. We assume that, for each magneto-ionic component, y_L and y_T are *known* functions of h. A wave travelling into the ionosphere is bent back towards the earth when its refractive index becomes sufficiently small. Thus, for each magneto-ionic component, y_L and y_T are two-valued functions of h, one value referring to the upward journey into the ionosphere and the other value referring to the return journey. The highest point of a trajectory is referred to as a point of reflection.

With the exception of the statements referring explicitly to vertical propagation, the above assumptions permit the application of a great deal of the foregoing discussion to the general case, provided due care is exercised. The definitions of waves 1 and 2 are still suitable, and, at the transmitter, the join of the corresponding points in the ζ-plane is still (practically speaking) bisected by the origin. But, with increase of height, the two points in the ζ-plane *do not remain symmetrical* with respect to the origin for the same value of h because the components follow different paths. In applying the foregoing arguments, then, we must consider each magneto-ionic component on its own merits. We must remember that the values of $\left|\frac{y_T^2}{2zy_L}\right|_0$ for the two components are not, in general, the same, and that if $\left|\frac{y_T^2}{2zy_L}\right|_0 = 1$ for one component then $\left|\frac{y_T^2}{2zy_L}\right|_0 \neq 1$ for the other component. We must remember, too, that the parameter h along a branch of the ζ-curve increases from zero to a certain value (h_1 for branch 1 and h_2 for branch 2, h_1 and h_2 being the heights of reflection of waves 1 and 2 respectively) and then returns to zero, and that the value of $\left|\frac{y_T^2}{2zy_L}\right|_0$ for a particular magneto-ionic component on its downward journey may be very different from the value on its upward journey. Of course, it is quite possible for a component to be reflected before it reaches the height h_0.

Consider branch 1 of the ζ-curve (fig. 2). If $h_1 < h_0$ the representative point never leaves the first quadrant either on the upward or downward journey. If, however, $h_1 > h_0$, then, as h increases through h_0 branch 1 passes from the first quadrant to the fourth or second quadrant according as $\left|\frac{y_T^2}{2zy_L}\right|_0 \lessgtr 1$ for wave 1 on the upward journey. As h decreases through h_0 branch 1 returns to the first quadrant or passes on to the third quadrant according as $\left|\frac{y_T^2}{2zy_L}\right|_0 - 1$ has the same or the opposite signs on the upward and downward journeys for wave 1. Corresponding remarks may be made about branch 2 of the ζ-curve.

We notice that, subject to the assumption that it is possible for a magneto-ionic component to be reflected at a height greater than h_0 in such a way that $\left|\frac{y_T^2}{2zy_L}\right|_0 - 1$ has opposite signs on the upward and downward journeys, it is possible for the representative point in the ζ-plane to terminate at $h = 0$ in the quadrant opposite to that in which it started at $h = 0$. It is also possible for both branch 1 and branch 2 of the ζ-curve to terminate in the same quadrant, although they necessarily start in opposite quadrants. (Consider, for example, a case in which $h_2 < h_0$, but $h_1 > h_0$ and $\left|\frac{y_T^2}{2zy_L}\right|_0 - 1$ has opposite signs on the upward and downward journeys for wave 1.)

The argument may be put in terms of ambiguous signs as follows. At the transmitter wave 1 is given by $\zeta = +\zeta_+$ and wave 2 by $\zeta = -\zeta_+$ and this remains true in the whole of the region $h \leqslant h_0$ on the upward journey. If either wave is reflected in the region $h \leqslant h_0$, then ζ is given for that wave on its downward journey by the same sign as on its upward journey. If, however, wave 1 is reflected in the region $h > h_0$, then, for this wave in this region, $\zeta = \pm\zeta_+$ according as $\left|\frac{y_T^2}{2zy_L}\right|_0 \lessgtr 1$ for wave 1 on the upward journey. Similarly, if wave 2 is reflected in the region $h > h_0$, then, for this wave in this region, $\zeta = \mp\zeta_+$ according as $\left|\frac{y_T^2}{2zy_L}\right|_0 \lessgtr 1$ for wave 2 on the upward journey. If either wave is reflected at a height greater than h_0, then, in the region $h \leqslant h_0$ on the downward journey, ζ is given by the same sign as or the opposite sign to what it was on the upward journey in this region according as $\left|\frac{y_T^2}{2zy_L}\right|_0 - 1$ for the wave in question has the same or the opposite signs on the upward and downward journeys.

It is possible that, for the same magneto-ionic component, ζ is given by one sign at the transmitter and the opposite sign at the receiver ; it is also possible that, at the receiver, both magneto-ionic components are given by the same sign. For a particular magneto-ionic component, ζ is given by the same sign at the receiver as at the transmitter if and only if either (i) it is reflected in the region $h < h_0$, or (ii) $\left|\frac{y_T^2}{2zy_L}\right|_0 - 1$ has the same sign on the downward journey as it had on the upward journey for that magneto-ionic component. One or other of these conditions is always satisfied at practically *vertical* incidence.

The names of the magneto-ionic components may now receive attention. Consider the special case in which the direction of propagation is vertical and the applied magnetic field is horizontal. In the region $h < h_0$ the determination of ζ which lies in the first quadrant of the complex plane is

$$\zeta = \frac{\frac{1}{2}y_T^2}{1-(1-l)\,x-iz}$$

and from formulæ (1) and (2) the corresponding complex refractive index is given by

$$q^2 = 1 - \frac{x}{1+lx-iz}.$$

In this case the propagation of the magneto-ionic component for which ζ lies in the first quadrant in the region $h < h_0$ is unaffected by the imposed magnetic field. For this reason it has become common, even in the general case, to call the component for which ζ lies in the first quadrant in the region $h < h_0$ the "ordinary wave" and the component for which ζ lies in the third quadrant in the region $h < h_0$ the "extraordinary wave."

We have seen, however, that it is possible for a branch of the ζ-curve to originate at $h = 0$ in the first quadrant and terminate at $h = 0$ in the third quadrant, or vice versa. In such a case the same magneto-ionic component would be classed as "ordinary" at the transmitter and "extraordinary" at the receiver, or vice versa. We have seen, too, that it is possible for both branches of the ζ-curve to terminate at $h = 0$ in the same quadrant (first or third). In this case the magneto-ionic components would be classed both " ordinary " or both " extraordinary " at the receiver.

In terms of ambiguous signs, a magneto-ionic component is described as " ordinary " or " extraordinary " in the region $h < h_0$ according as $\zeta = +\zeta_+$ or $-\zeta_+$. But we have seen that, for the same magneto-ionic component, ζ can be given by one sign at the transmitter and the opposite sign at the receiver, and that both magneto-ionic components can be given by the same sign at the receiver.

The nomenclature " ordinary " and " extraordinary " does not therefore appear to be convenient in general. This nomenclature is, however, satisfactory in the case of practically vertical incidence because then each branch of the ζ-curve terminates in the quadrant in which it originated ; in this case wave 1 can be called " ordinary " and wave 2 " extraordinary." We shall continue to describe the waves by the numbers 1 and 2 as already defined.

The nature of the transition which takes place at the height h_0 in the polarization, (μ, h) and (χ, h) curves when $\left|\frac{y_T^2}{2zy_L}\right|_0$ passes through 1 for one of the magneto-ionic components is the same as at vertical incidence, but the transition in general only takes place for one component at a time and then only on one or other of the two passages of the component through the height h_0. The details can easily be worked out as for vertical incidence.

The relation between the direction of rotation in an elliptically-polarized magneto-ionic component at the receiver and its direction at the transmitter depends, of course, on the number of reversals of direction of rotation which take place en route. When reflection takes place at a height greater than h_0, reversal can take place at $h = h_0$, either on the upward or downward journeys, or both ; reversal does or does not take place according as $\left|\frac{y_T^2}{2zy_L}\right|_0 \gtrless 1$ for the component under consideration. Reversal will also take place at a point where the direction of propagation is momentarily transverse to the earth's magnetic field, provided y_L then changes sign; the condition for the existence of such a point is that the initial angle of incidence should be less than the angle made with the horizontal by the component of the earth's magnetic field in the plane of propagation. Reversal cannot take place at any point other than those already mentioned because the sign of the real part of

$$\zeta - \frac{\frac{1}{2}y_T^2}{1 - (1 - l)\,x - iz}$$

is determined by the sign of the real part of ζ, and so Q cannot become real except at these points.

The initial direction of rotation for wave 1 is left-handed or right-handed according as $eH_L <$ or > 0 at the transmitter ; the reverse is true of wave 2. The final directions of rotation depend on the conditions experienced by the waves in the ionosphere. As an example, suppose that the conditions indicated in fig. 16 are possible, wave 2 being reflected below $h = h_0$, and wave 1 above $h = h_0$ in such a way that $\left|\frac{y_T^2}{2zy_L}\right|_0 < 1$ on the upward journey and > 1 on the downward journey. The directions of rotation are indicated by the letters R (right) and L (left) on the assumption that e is negative; P denotes plane-polarization. It is seen that the final polarizations of *both* magneto-ionic components are right-handed in this case.

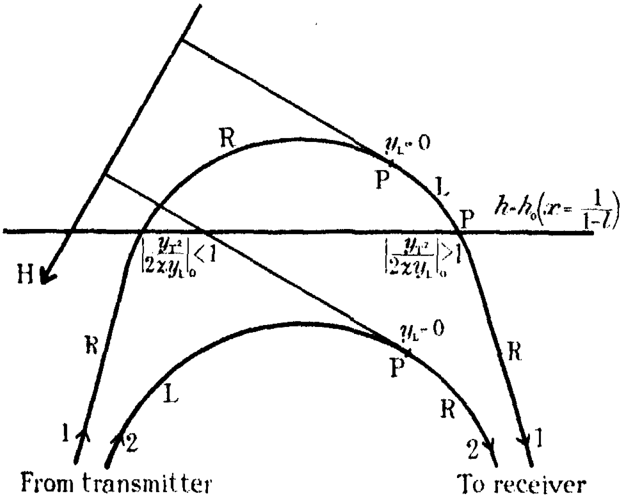
R
$y_L = 0$
P
L
P
$h = h_0\left(x = \frac{1}{1-l}\right)$
$\left|\frac{y_{T^2}}{2xy_L}\right|_0 < 1$
$\left|\frac{y_{T^2}}{2xy_L}\right|_0 > 1$
H
R
$y_L = 0$
P
R
L
R
1
2
2
1
From transmitter
To receiver

FIG. 16. (y_{T^2} should read y_T^2)

§ 7—SUMMARY

A discussion is given of some general features of the magneto-ionic theory which appear when collisional friction is taken into account and incidence is not necessarily vertical. The nature of the transition from longitudinal to transverse propagation is described. It is shown that, at the height where $N = \frac{mp^2}{4\pi(1-l)e^2}$, the direction of rotation in the polarization ellipse of a magneto-ionic component does or does not reverse according as $\nu \lessgtr \frac{1}{2}\frac{\sin^2\theta}{|\cos\theta|}p_H$ at this height, and that in the intermediate case the component resplits. Curves are drawn showing the general nature of the variation of μ and ck/p with height at vertical incidence when there is a small constant value of friction and the Lorentz polarization term is neglected. When incidence is oblique the magneto-ionic components follow different paths, and it is shown that the names " ordinary " and " extraordinary " are in general unsuitable. Although the directions of rotation in the polarization ellipses of the magneto-ionic components are necessarily opposite at the transmitter they may be the same at the receiver. Reversal of direction of rotation can only take place at the height already mentioned or at a height where propagation is transverse to the earth's magnetic field.

Pressure and the Water Relations of Proteins
I—Isoelectric Gelatin Gels

By D. JORDAN LLOYD and T. MORAN, Laboratories of the British Leather Manufacturers' Research Association and Low Temperature Research Station, Cambridge

(*Communicated by Dr. R. H. Pickard, F.R.S.—Received June* 4, 1934)

Recent work on the structure of fibre proteins, as deduced from X-ray analysis, suggests that the bound water or water of hydration of proteins cannot be regarded as being simply a complete shell of water around the protein molecule or micelle. It seems much more probable that the water is localized around definite points and in a recent paper* one of us has suggested two possible mechanisms of hydration.

Katz,† Svedberg,‡ Rosenbaum§ and others have followed the thermal, vapour pressure and volume changes when a dried protein takes up water. Their work also suggests that the linkages or orientating forces holding water to the protein are not uniform in strength. More recent work on the freezing of gelatin gels which is discussed later in this paper has confirmed this and given figures for the amounts of water held by the gelatin at different activities of the water.*

---

* Jordan Lloyd and Phillips, 'Trans. Faraday Soc.,' vol. 29, p. 132 (1932).

† 'Kolloid chem. Beih.,' vol. 9, p. 1 (1917).

‡ 'J. Amer. Chem. Soc.,' vol. 46, p. 2673 (1924).

§ 'Kolloid chem. Beih.,' vol. 6, p. 177 (1914).

The object of the present work was to obtain a measure of the forces holding the separate increments of water to the gelatin molecule. Posnjak† showed that when a dry colloid takes up water to form a gel a swelling pressure is developed, the magnitude of which depends upon the amount of water already taken up by the colloid. Alternatively, if a pressure is applied greater than the swelling pressure, water will be forced out of the gel and a fresh equilibrium set up. Posnjak examined the effects of small pressures (up to 60 lb. per sq inch) ; in the present work pressures up to 48,000 lb. per sq inch have been investigated.

The results obtained by Posnjak differ widely from those obtained in the present work (see fig. 2). He allowed the gelatin to take up water under a series of controlled external pressures and measured the swelling by the volume attained at equilibrium. The pressures measured by him are therefore the pressures at any stage of swelling at which further entry of water is prevented. The pressures measured by us are those necessary to drive out water already present in the system. At equilibrium, however, the two methods should give identical results. Posnjak used commercial gelatin and points out himself that there was considerable leakage of gelatin through the pores of the diaphragm of his apparatus. We have used a highly purified gelatin and in our experiments the expressed water was free from any dissolved protein. These facts are therefore probably sufficient to account for the discrepancy between the two sets of results.

APPARATUS AND METHODS

The essential part of the apparatus consists of a steel cup A (about 200 cc in volume) with plunger B and a push-on base C with channels draining into an outlet tube T, fig. 1, *a*. The gel under investigation—usually about 60 gm—was placed inside a piece of canvas, 8 in. × 8 in., which had been impregnated with collodion and soaked in running water for several days to remove traces of ether. The "parcel" of gel was then placed in the cup and pressure applied to the head of the plunger.

For pressures up to about 2000 lb. per sq inch the press shown in fig. 1, *b* was employed. This and the cup and plunger were made by Mr. Barker, of the Cambridge University Engineering Laboratory. The press consists of a calibrated spring S which can be compressed by a central screw operated by the handle H. The spring is compressed and then released to the desired length L (corresponding to a definite pressure).

---

* Moran, 'Proc. Roy. Soc.,' A, vol. 112, p. 30 (1926), *ibid.*, vol. 135, p. 411 (1932).

† 'Kolloid chem. Beih.,' vol. 3, p. 417 (1912).

In actual practice the pressure on the plunger was applied in stages of approximately 100 lb. per sq inch per hour. As the pressure was increased water drained out of the tap T and, apart from one or two of the earlier experiments, equilibrium was attained only when the water expressed did not exceed 0·1 cc in the final 24 hours. As the water drained away the length of the spring was re-adjusted so that the pressure remained constant throughout each experiment. For the higher pressures the same cup and plunger was used in a Tangye hydraulic press.

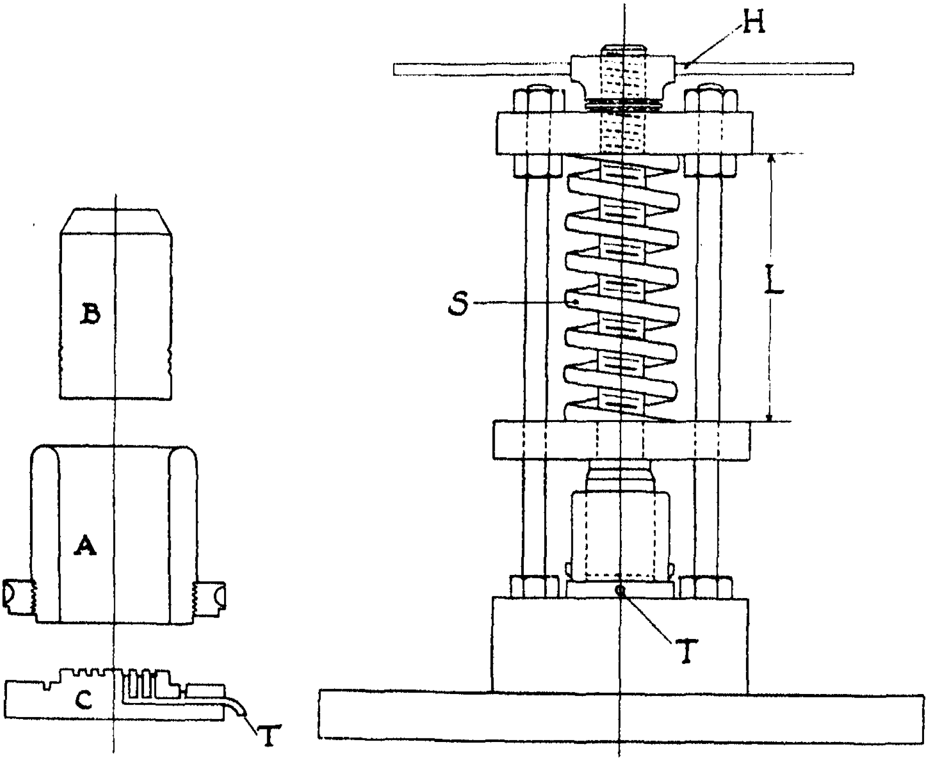

(*a*) Fig. 1 (*b*)

The press in fig. 1, *b* gave pressures which could be recorded with an accuracy between 2·5 and 5% ; with the Tangye press there was frequently a "slip" or loss of pressure so that it had to be adjusted every few hours, but the maximum pressure could be registered with an accuracy of about 4%.

The gelatin used in all the experiments was prepared from Coignet Gold Label gelatin either by washing in acid and salt and dialysing till free from chlorides* or by soaking in water, adding hydrochloric acid until a p_H of 4 was obtained and electro-dialysing until the conductivity had become vanishingly small. At this stage the gelatin in 2% solution sets rapidly to an opaque white gel. The ash content is of the order of 0·02% of the dry weight. Repeated observations showed that when soaked in water this gelatin gave a p_H of 5·1 to the water.

The purified gelatin was dried to approximately 16% water content and stored for use in the dry state. In most of the experiments the dry gelatin was placed in distilled water and allowed to swell to near equilibrium before being placed in the press (water-swollen gels). In a few experiments weighed amounts of gelatin were dissolved in known volumes of warm water and the gels were left to set at 0° for 24 hours (heated gels).

The concentration of the gel at the beginning and end of every experiment was determined by taking the dry weight (after drying at 103° C). In the early experiments a few nitrogen determinations were made, but as the amount of nitrogen in the expressed fluid was too small to be detected, this procedure was abandoned as unnecessary. The expressed fluid was tested for dissolved protein, but gave only negative tests. A measured volume was taken in every experiment and evaporated to dryness. Generally about 3 parts in 10,000 of dry solids was recovered, consisting probably only of traces of grease and rust from the press. It may therefore be assumed that all colloidal matter was held back by the collodion membrane.

EXPERIMENTAL RESULTS

In the present work only isoelectric gelatin has been examined.

Three variables were examined : (1) pressure, (2) temperature, (3) the initial concentration of the gel.

THE EFFECT OF VARYING THE PRESSURE

Table I and figs. 2 and 3 show the results obtained after submitting gels to different pressures until equilibrium had been obtained. In fig. 2 pressure is measured on an arithmetic scale and the results obtained by Posnjak at the comparatively low pressures which he used are recorded. In fig. 3 the pressures are recorded on a logarithmic scale. Fig. 3 includes

---

* Jordan Lloyd and Pleass, 'Biochem. J.,' vol. 14, p. 1352 (1927).

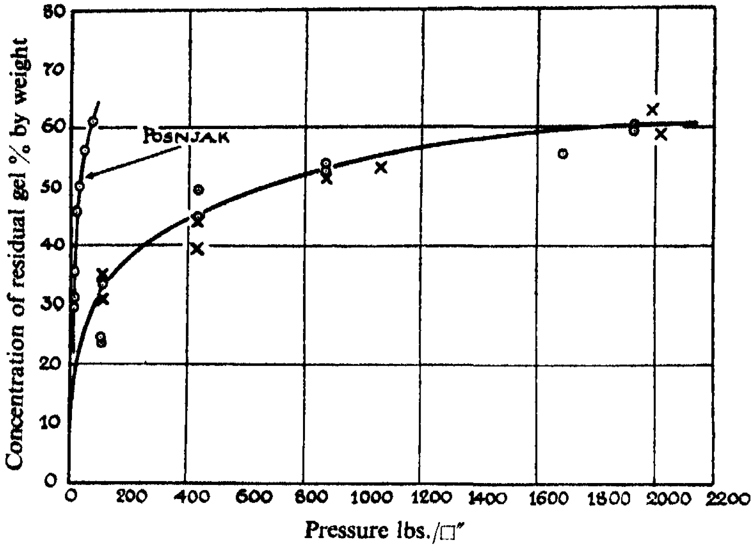

FIG. 2—⊙, Room temperature = 20° ± 2° C ; ×, 0° C

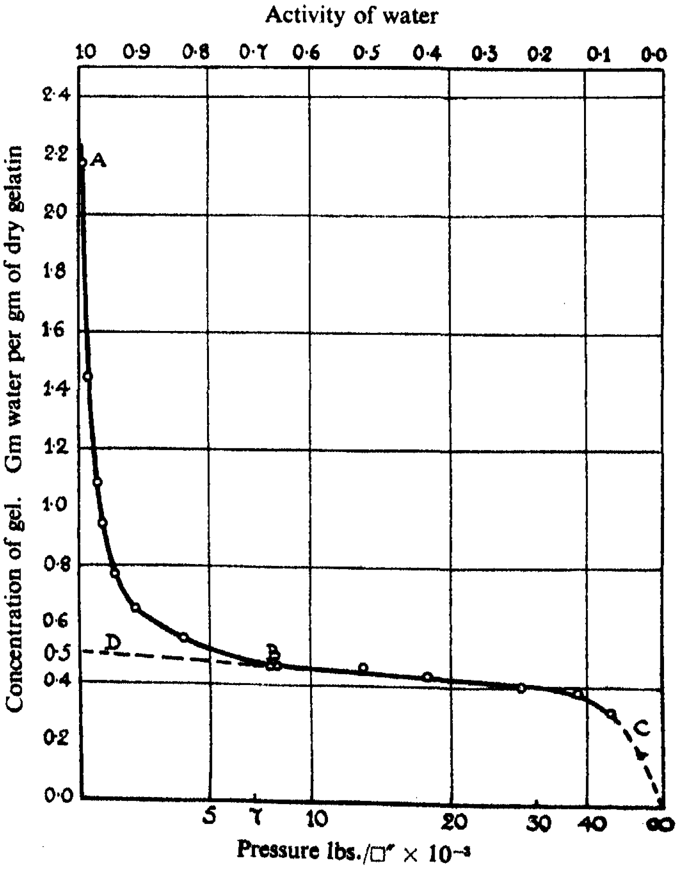

FIG. 3

TABLE I—WATER-SWOLLEN GELS

Temp.	Conc. of original gel	p_H	Pressure lb. per sq in	Time applied (days)	Conc. of residual gel	% solids in expressate
Room	10	5·1	111	9	24·75	0·0285
Room	10	5·1	111	5	33·6	0·018
0°	16	5·0	111	4	31·1	0·042
0°	17·8	—	111	4	35·1	0·029
Room	10·7	—	444	3	45·0	0·045
Room	10·1	5·0	444	3	49·4	0·034
0°	16·2	5·3	444	3	44·5	0·044
0°	11·85	—	444	7	39·1	0·027
Room	—	5·15	888	2	52·8	0·029
Room	—	5·1	888	3	54·2	0·036
0°	—	—	888	8	51·6	0·042
0°	13·6	—	1067	10	53·3	0·033
Room	5·9	5·9	1692	1	55·5	—
Room	10·9	—	1930	2	60·5	0·053
Room	—	5·25	1930	4	59·7	0·022
0°	16·8	5·0	2016	4	59·0	0·035
0°	17·2	6·1	1990	18	63·3	0·033
Room	7·7	—	8300	4	68·3	0·015
Room	—	—	13300	4	68·3	0·026
Room	9·4	—	18300	6	69·9	0·073
Room	7·8	—	28300	6	71·5	0·018
Room	11·3	—	38300	6	72·6	0·024
Room	11·8	—	48300	4	75·8	0·027
			Heated Gels			
0°	4·5	—	2066	6	47·9	0·057
0°	4·5	—	2066	6	57·8	0·048
0°	5·6	—	2066	9	56·5	0·034
0°	6·2	—	2066	6	46·0	0·024
0°	6·3	—	2066	7	57·2	0·029
0°	13·9	—	2066	6	60·2	0·027
0°	20·0	—	2066	6	62·5	0·050
0°	41·4	—	2066	6	62·6	0·057

fig. 2, together with the results obtained at the higher pressures. In this figure the concentration of gel is expressed as grams of water per gram of dry gelatin. The amount of water at equilibrium in the compressed gel falls with increasing pressure, rapidly at first and more slowly later. After about 8000 lb. per sq inch the amount of water falls only slowly with increasing pressure. At very high pressures, however (more than 38,000 lb. per sq inch), there is further marked loss of water.

THE EFFECT OF VARYING THE TEMPERATURE

A number of experiments were carried out at 0° and the remainder at room temperature, 20° ± 2°. Table I and fig. 2 show that the effect of temperature on the pressure-concentration curve is within the experimental error of the method. This is discussed later.

THE EFFECT OF VARYING THE INITIAL CONCENTRATION OF THE GEL

An isoelectric gel of concentration 10% can be regarded as an equilibrium system under a pressure of one atmosphere.* Weaker gels contract when immersed in water. Stronger gels take up water. Accordingly a number of gels were made by dissolving the gelatin in warm water and allowing to set at 0° for 24 hours. The gels were then all put under the same pressure of 2066 lb. per sq inch, the pressure being applied at 0°. The experimental results are shown in Table I (heated gels). The results suggest that the effect of pressure on gels weaker than 10% is different from that on stronger gels. It should be pointed out, however, that the experimental error is increased with decreasing initial concentration because of the smaller mass of gelatin and the correspondingly smaller bulk of gel remaining in the press at the end of the experiment. On the whole, however, the weaker gels seemed to hold part at least of their water content with stronger forces than the more concentrated gels.

DISCUSSION

The experimental results confirm the suggestion that the water in gelatin gels is to be regarded as existing in at least two states : (1) Loosely bound water, which can be removed completely by a pressure of 8000 lb. per sq inch, by freezing to about 20° – (Moran, *loc. cit.*, 1932) or by evaporation in an atmosphere in which the pressure of water vapour is such that its ratio (*h*) to the vapour pressure at saturation is approx. 0·5 (Katz, *loc. cit.*), and (2) closely bound water which is not removed under any of these conditions. Pressures between 8000 and 38,000 lb. per sq inch remove only a comparatively small fraction of the closely bound water, but as the pressure is still further increased this water is removed in increasing amounts.

The relation between (*h*), which gives a measure of the activity of the water in the gel, and the swelling pressure, P, has been investigated thermodynamically by Katz (*loc. cit.*). He showed that the following equation should hold for gelatin swelling in water:—

---

* Jordan Lloyd, 'Biochem. J.,' vol. 25, p. 1580, 1931 ; Kunitz, 'J. Gen. Physiol.,' vol. 12, p. 289 (1928).

$$P = -\frac{RT}{MV_0}\log h, \tag{1}$$

where P is the swelling pressure,

M is the molecular weight of water = 18,
V_0 is the specific volume of water,
h is the ratio of the vapour pressure of the water in the gel to the vapour pressure of pure water, *i.e.*, the activity of the water in the gel,
R is the gas constant,
T is the absolute temperature.

In this equation no allowance is made for the contraction in the system when gelatin is allowed to swell in water or for the changes in V_0 with pressure.

The implications of equation (1) are these. Consider a pressure P giving at equilibrium a gel of concentration C containing water at an activity α ($= h$). The effect of P when it is being applied is to increase α to unity thereby effecting an equilibrium between the gel under pressure and the activity of pure water under atmospheric pressure. On this basis equation (1) can also be derived from the fundamental equation for the effect of pressure on the activity of water in a solution.* This is

$$\left(\frac{\partial \ln \alpha}{\partial P}\right)_T = \frac{V}{RT}, \tag{2}$$

where V is the molal volume of water in the solution or gel. Assuming V to be independent of pressure, equation (2) can be integrated to give equation (1).

Lewis and Randall suggest methods for an exact solution of equation (2) where data are available for the changes in V with P. Such data, however, are not available for gelatin gels. Equation (1) therefore has been used in its uncorrected form although it is likely that at the very high pressures a certain degree of error is involved.† Equation (1) is identical with the equation relating osmotic pressure to vapour pressure in those cases where the perfect gas laws apply to the vapour and changes in V_0 with pressure are negligible. There is therefore a certain similarity between swelling pressure and osmotic pressure although the exact kinetic mechanism of swelling pressure is still obscure. Sackur* (1910) has shown that in the osmotic pressure results obtained by Berkeley and Hartley† for sugar solution, changes in V_0 up to 133·7 atmospheres (1950 lb. per sq inch) at least can be neglected.

---

* Lewis and Randall, 'Thermodynamics,' McGraw Hill Book Co. (1923).

† Taking the value for the compressibility of pure water (26×10^{-6} per atmosphere) and assuming the change in V to be directly proportional to the pressure, equation (2) shows that at 28,300, 38,300, and 48,300 lbs. per sq inch the activities of the water in the gel are 0·251, 0·156, and 0·097 instead of 0·242, 0·146, and 0·088, the values obtained using equation (1) (*cf.* Table 3).

The relationship between concentration of gel and activity of the water in the gel, as calculated from equation (1), is shown in fig. 3.

The relationship between activity of water and concentration of gel has also been investigated by determining the concentration of gelatin gel remaining unfrozen at different temperatures (Moran, *loc. cit.* 1932). According to Lewis and Randall the activity of the water in the unfrozen gel at a reference temperature T″ is given by the equation

$$\log_{10} a_{\mathrm{H_2O}} + 0{\cdot}004211\,\theta + 0{\cdot}0000022\,\theta^2 = x, \tag{3}$$

where θ is the difference between 273° and the equilibrium temperature of the gel (T′) and x is given by the equation

$$x = -\,\overline{\mathrm{L}}_{1\,(\mathrm{T}'')}\,\frac{\mathrm{T}''-\mathrm{T}'}{2{\cdot}303\,\mathrm{R}\mathrm{T}''\mathrm{T}'} + (\bar{c}_{p_1} - \bar{c}^{\circ}_{p_1})\left(\mathrm{T}''\,\frac{\mathrm{T}''-\mathrm{T}'}{2{\cdot}303\,\mathrm{R}\mathrm{T}''\mathrm{T}'} - \frac{1}{\mathrm{R}}\log\frac{\mathrm{T}''}{\mathrm{T}'}\right). \tag{4}$$

where $\overline{\mathrm{L}}_1$ is the relative partial molal heat content of water in the gel at a temperature T″ and is assumed to be a linear function of temperature, $\bar{c}_{p_1}$ and $\bar{c}^{\circ}_{p_1}$ are the partial molal heat capacities of the water in the gel and in pure water respectively at T″. If the heat of dilution of a particular gel is small, x can be equated to zero., *i.e.*, the activity of the water in a particular gel is independent of temperature.

Table II, columns 2 and 3, gives the observed concentrations of gel in equilibrium with ice at the temperatures in column 1. The actual values vary slightly for different samples of gelatin (Moran, *loc. cit.*, 1932), but the values in Table II were determined for the stock of gelatin used in the present experiments. According to Rosenbaum (*loc. cit.*) the heat of dilution of gels of concentration <66·6% is negligible and in column 4 are shown the corresponding activities of water in the gel using equation (3) and putting $x = 0$. By substituting these activities for (*h*) in equation (1) it is possible to calculate the corresponding swelling

---

* 'Z. Phys. Chem.,' vol. 70, p. 477 (1910).

† 'Phil. Trans.,' A, vol. 206, p. 481 (1906).

TABLE II

1	2	3	4	5	6	7
	Conc. (observed), Freezing exps.		Activity of water	Calc. pressure Lb./sq in	Conc. at calc. pressure. Pressure exps.	
Temp. °C.	Gelatin % of gel	Gm water per gm gelatin			Gelatin % of gel	Gm water per gm gelatin
− 0·5	40·9	1·44	0·995	100·7	31·5	2·17
− 1·5	50·4	0·98	0·986	279	41·0	1·44
− 3	57·3	0·75	0·971	585	48·0	1·08
− 4	58·6	0·71	0·962	768	52·0	0·92
− 6	61·75	0·62	0·943	1166	56·5	0·77
−10	64·2	0·56	0·907	1940	60·5	0·65
−20	66·6	0·50	0·822	3893	64·6	0·55
−40	66·6	0·50	0·673	7867	68·3	0·46
−45	66·6	0·50	0·64	8866	68·3	0·46

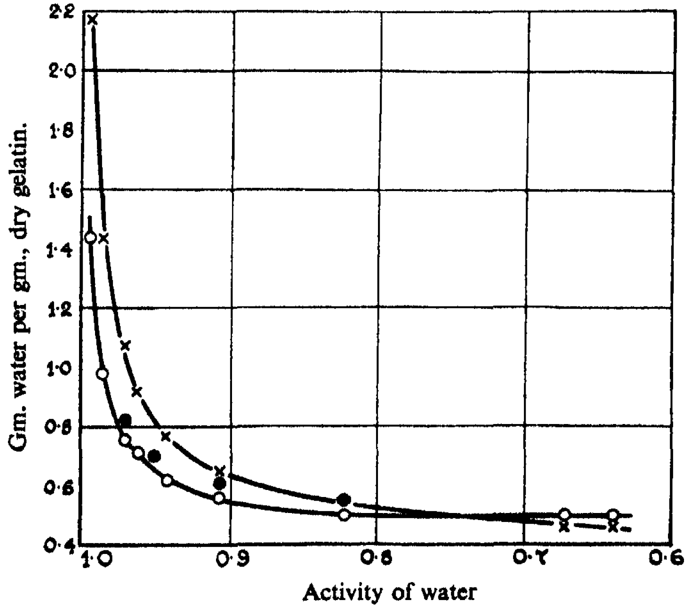

FIG. 4—× Pressure (D. J. L. and T. M.) ; ○ Freezing (T. M.) ; ● Heat capacity (W. F. H. and J. H. M.).

pressures. These pressures are given in column 5, while in columns 6 and 7 are given the corresponding concentrations of the gels read off from figs. 2 and 3. Fig. 4 shows the relationship between the activity of water and the concentrations of the gel expressed as grams of water per gram of gelatin, both from the freezing and the pressure data. Considering the experimental difficulties in the pressure method, particularly at low pressures, the agreement between the two curves is satisfactory.

There is a tendency for somewhat lower concentrations of gel to be observed in the pressure experiments at the higher activities of water (corresponding to the lower pressures) than in the freezing experiments, but it is believed that this is due to the difficulty of obtaining equilibrium values at low pressures even though several days were allowed. The fact that the curves in fig. 4 cross suggests that any resistance to pressure offered by the gel framework is small, although it is probable from the known structure of the gelatin molecule* that such a pressure does exist.

Fig. 4 also shows the values obtained by Hampton and Mennie† for the bound water of gelatin using a calorimetric method. Figs. 3 and 4 therefore confirm that the water binding capacity of gelatin in isoelectric gels is a function of the activity of the water in the gel.

TABLE III

Pressure (observed) lb/sq cm	Activity of water	Conc. of gel (observed)		Calc. equivalent freezing temperature ($x = 0$)	Corrected freezing temperature ($x \neq 0$)
		%gel	Gm water per gm gelatin		
8,300	0·658	68·3	0·46	− 43° C.	− 73° C.
13,300	0·513	68·3	0·46	− 67° C.	− 94° C.
18,300	0·398	69·9	0·43	− 94° C.	− 109° C.
28,300	0·242	71·5	0·40	− 135° C.	− 130° C.
38,300	0·146	72·6	0·38	− 211° C.	− 146° C.
48,300	0·088	75·8	0·32	− 223° C.	− 158° C.

The freezing experiments were carried out with great difficulty down to temperatures as low as − 45° C. No significant difference was observed in the equilibrium concentration of gel at − 20° and − 45° C. and, in fact, the average of the results at each temperature was the same. By the pressure method it is possible to study indirectly the effects of much lower temperatures on the water holding capacity of gelatin. In Table III are shown the observed equilibrium concentrations of gel at the higher pressures, also the corresponding activity of water calculated from equation (1). From equation (3) it is possible to calculate the freezing temperature corresponding to a given activity of water and column 5 gives the calculated temperatures assuming $x = 0$. It has been shown, however, both by Rosenbaum and by Moran that in gels with a greater concentration than 66% x cannot be taken as 0. The data available for gelatin gels are not sufficient to permit of a precise solution of equation (3). If, however, the empirical equation found by Katz to apply to the data of Rosenbaum is extended to include the lower concentrations in Table III it would appear that $\bar{L}_1$ in this range is approximately $-$ 1000 cals. at 0° C. Similarly an average value for $\bar{c}_{p_1} - \bar{c}^{\circ}_{p_1}$ is 13 cals.* The final column of Table III shows the calculated freezing temperatures using these figures. It is clear that very low temperatures are required to remove, by freezing, the more firmly bound water of gelatin.

---

* Astbury and Atkin, 'Nature,' vol. 132 p. 348 (1933).

† 'Can. J. Res.,' vol. 7, p. 187 (1932).

The fact that no appreciable difference could be detected between the effects of pressure on gel concentration at 0° and 20° C is readily understood from an examination of equation (1). For example, increasing T from 273° to 293° increases the calculated values of h at 2000 lb. per sq in. by 0·006, which is too small to show any marked difference in the equilibrium concentration of gel.

The water attached to the gelatin molecule can roughly be divided into two classes, one which can be removed at comparatively high activities of water (1 to 0·7)—AB in fig. 3—the other, much more resistant, the greater portion of which is removed only at low activities ($<$ 0·2), *cf.* DBC in fig. 3.

GELS CONTAINING 0·0 TO 0·5 GRAMS WATER PER GRAM OF GELATIN

The whole of the water in these gels is in chemical combination with the protein (Moran, *loc. cit.*, 1932).

The hydration of proteins can occur by the formation of a co-ordinate link between a water molecule and certain groups in the protein structure for instance, the positively charged basic groups of the proteins readily accept a pair of electrons from the oxygen of a water molecule on to one (or more) of the hydrogen atoms.

Conversely the negatively charged acidic groups of the proteins readily donate a pair of electrons from the singly bound oxygen atom to the hydrogen of a water molecule.

Neutral groups, such as OH, NH_2, NH, COOH, can similarly form co-ordinate links with water molecules either by the donation or the acceptance of a pair of electrons. The formation of a co-ordinate link would be expected to show the usual characteristics of chemical change, namely, heat changes (commonly evolution of heat) and considerable resistance to changes in physical conditions such as temperature, etc. It should be noticed, however, that there is no way of constructing a co-ordinate link between a protein molecule and a water molecule except by donating a pair of electrons on to a chemically combined hydrogen atom. Since this already carries two electrons in its sheath, and is in a stable condition, the link formed by making an outer sheath of four electrons will not be very resistant if compared with those links where the donation of two electrons leads to the completion of an electron sheath. Water co-ordinately bound to the protein molecule would be expected to show a considerable but not extreme resistance to, say, the forces of evaporation. Katz's data on the vapour pressure isotherm of a gelatin gel show that this actually is the case.

---

* Mennie, 'Can. J. Res.,' vol. 7, p. 178 (1932).

The complete constitution of the gelatin molecule has recently been calculated by Atkin,* using the analytical data of Dakin and Van Slyke. Reference to his figures will show that in a gelatin molecule, with molecular weight 34,500, formed by the condensation of 360 amino-acid residues, there will be about 200 points on the side chains where co-ordinate links with water molecules are possible. If the carbonyl and amino groups of the condensed amino acid residues of the molecular backbone are in the open form (Jordan Lloyd and Phillips, *loc. cit.*), then there are a further 700 (about) possible points of co-ordination. If, however, these are in the form of closed rings then the co-ordination will be limited to the side chains. The latter form is the more likely, and Astbury and Woods† have recently shown from the evidence of X-ray analysis that the hydration of protein molecules starts at the side chains.

The experimental data given here and previously show that 1 gram of dry gelatin carries 0·5 grams of closely bound water. One molecule of gelatin (mol wt. 34,500) is therefore closely bound to 960 water molecules, a figure very close to the calculated number of possible co-ordination centres.

GELS CONTAINING 0·5 OR MORE GRAMS OF WATER PER GRAM OF GELATIN

The bound water in these gels in excess of the first 0·5 grams is probably held by the formation of multi-molecular films of oriented water dipoles round charged centres such as occur in the acidic and basic side chains of the protein zwitterion. Water held in this way would be in a state of dynamic equilibrium such as occurs with any electrolytic solution. Furthermore, it would be expected that much of this water would be free to dissolve crystalloids and in that sense be little different from ordinary free water in bulk. An examination of the bound water of gelatin in gels containing neutral salts indicates that this is so (Moran, *loc. cit.*, 1932). The work of Brooks* is also indirect evidence. After allowing for the water necessary to dissolve the salts in muscle he arrived at a low figure (0·3 grams) for the bound water of the proteins of muscle even at an activity of water of 0·994.

---

* 'J. Int. Soc. Leather Tr. Chem.,' vol. 17, p. 575 (1933).

† 'Nature,' vol. 127, p. 663 (1931).

We should like to thank Mr. F. C. Barrett for his assistance in the experimental work and Mr. V. Parsons for preparing the isoelectric gelatin.

SUMMARY

1. When isoelectric gelatin gel is placed under pressure, pure water is squeezed out of the gel. The concentration of the residual gel is a function of the pressure.

2. The thermodynamic equation of Katz for swelling pressures has been applied to the results ; the relationship between concentration of gel and activity of water in the gel as deduced from the pressure data is similar to that obtained from an analysis of the freezing point-concentration curve of gelatin gel.

3. The water attached to the gelatin molecule can be regarded as being divided into two classes, one firmly held, the bulk of which is removed only at low activities ($< 0\cdot2$) and the other present only at high activities ($> 0\cdot7$).

4. It would appear that most of the firmly bound water of gelatin is unfrozen at temperatures above − 105° C.

5. The possible nature of the forces holding the two types of water to the protein molecule is discussed.

---

* 'Proc. Roy. Soc.,' B, vol. 114, p. 258.

Applications of the Bloch Theory to the Study of Alloys and of the Properties of Bismuth

By H. JONES, H. H. Wills Physical Laboratory, University of Bristol

(*Communicated by A. M. Tyndall, F.R.S.—Received July* 27, 1934)

INTRODUCTION

In recent years many binary alloys have been examined by means of X-rays and their structures have been determined at various compositions. It has been shown in this way that a pure phase consists of a single structure, whilst in the regions of mixed phases the alloy forms a simple mixture of two crystal types. Sometimes the range of composition of a pure phase is extremely narrow, as, for example, in the ϵ-phase of the Cu–Sn alloy. The composition within this phase corresponds almost exactly with the formula Cu_3Sn. Examples of this kind have naturally led to the conception of intermolecular compounds, and, since the formation of a compound in chemistry is described in terms of valency bonds, it is natural that in the existing literature attempts to discuss the reason for the formation of various phases, and the properties of the alloys in these phases, have been based mainly upon the conception of the homopolar bond.[*] It does not seem, however, that this conception is very successful in the interpretation of the formation and properties of metallic alloys. It is advantageous therefore to attempt an examination of alloys from the standpoint of the Bloch model.[†]

In Bloch's theory a stationary state of an electron in a crystal is specified by the three components of a vector $\mathbf{k}$ which may be regarded as the average momentum associated with the state; $\mathbf{k}$ is not, however, the average velocity times the mass of the electron, but is defined in such a way that the rate of change of $\mathbf{k}$ is proportional to the external force acting on the electron.[‡] Since the difference in $\mathbf{k}$ between two successive stationary states is in general exceedingly small, the vector $\mathbf{k}$ may be regarded as varying continuously from state to state. It is now a well-known result of the theory that the energy of a state is not a continuous function of position in **k** space, but is discontinuous across certain planes. The positions of these planes are determined by the crystal symmetry of the metal, and they divide **k** space into the various " Brillouin zones."

---

[*] Bernal, 'Trans. Faraday Soc.,' vol. 25, p. 367 (1929).

[†] 'Z. Physik,' vol. 52, p. 555 (1928). See also the account by Sommerfeld and Bethe in the 'Handbuch d. Physik,' vol. 24/2 (1934).

[‡] Sommerfeld and Bethe, *loc. cit.*; Jones and Zener, 'Proc. Roy. Soc.,' A, vol. 144, p. 101 (1934).

In this paper two classes of alloys will be considered: in Part I binary alloys which form ε- and η-phases both having a close-packed hexagonal structure are treated on the lines of the author's previous paper* on the γ-phase; and in Part II alloys formed of bismuth with small concentrations of other metals in solid solution are considered. The pure metal bismuth is also considered, and a general explanation of its structure is given.

PART I

1—*The Variation of the Lattice Parameters of the ε- and η-Phases with the Composition in the* Cu–Zn *Alloy*

Owen and Pickup† have made a very accurate determination of the two lattice parameters, *a* and *c*, of the Cu–Zn system in the hexagonal ε- and η-phases. These two phases are both hexagonal close-packed, and differ only in the *c/a* ratio (Table I). The ε-phase begins at 78·6 atomic per cent. Zn, and ends at 86·8, whilst the η-phase begins at 97·3 and goes directly into pure zinc. The region between 86·8 and 97·3 atomic per cent. zinc is a region of mixed crystals each type of which has a composition corresponding to the boundaries of the phases.

The variation of the lattice parameters with composition throughout the ε- and η-phases is summarized in Table I. Within a single phase experiment shows that the parameters vary linearly with the composition.

TABLE I—SHOWING THE CRYSTAL PARAMETERS, *a* AND *c*, IN A

		a	*c*	*c/a*
ε-phase	beginning	2·730	4·286	1·570
	end	2·760	4·289	1·554
η-phase	beginning	2·674	4·823	1·804
	end	2·659	4·935	1·856
Ideal close-packed hexagonal structure.		—	—	$\sqrt{\frac{8}{3}} = 1{\cdot}63$

In general in passing from one phase to another neighbouring phase there is a complete change in the structural type, *e.g.*, to the immediate left (copper rich side) of the ε-phase with the hexagonal close-packed structure, there lies the γ-phase with the complicated cubic structure. The phase change which we are concerned with here is of a much simpler kind, *being merely a discontinuous change in the values of the lattice* parameters, the structural type remaining unaltered.

---

* 'Proc. Roy. Soc.,' A, vol. 141, p. 225 (1934).

† 'Proc. Roy. Soc.,' A, vol. 140, p. 179 (1933).

2—*The Form of the First Brillouin Zone for the Hexagonal Close-packed Structure*

The method of construction of the Brillouin zones has been described before,* and we shall therefore merely give the results for the particular structures considered. The vector $\mathbf{k}$ specifying a stationary state is more precisely defined by means of the Bloch wave function of the electron in that state, namely,

$$\psi_{\mathbf{k}} = u_{\mathbf{k}}(\mathbf{r})\, e^{2\pi i(\mathbf{k},\,\mathbf{r})}, \tag{1}$$

$\mathbf{k}$ is thus the reciprocal of a length. In the special case of free electrons $u(\mathbf{r})$ is merely a constant and the energy associated with a state $\mathbf{k}$ is

$$E_{\mathbf{k}}{}^{0} = \frac{h^2}{2m} k^2. \tag{2}$$

If $E_{\mathbf{k}}{}^{0}$ is measured in volts, and $\mathbf{k}$ in reciprocal Angstrom units, this relation becomes $E_{\mathbf{k}}{}^{0} = 150k^2$. The number of states per cc per unit volume of $\mathbf{k}$ space is $2 \,.\, 10^{24}$, or, otherwise expressed, the density of states per atom is 2τ, where τ is the atomic volume measured in cubic A.

A hexagonal close-packed lattice can be formed by four interpenetrating simple orthorhombic lattices suitably displaced relative to each other. Using this fact, we may expand the potential at any point in the lattice in the form

$$V = \Sigma_n A\ \{1 + e^{-\pi i(n_1+n_2)}\}\{1 + e^{-\pi i(n_1+\frac{1}{3}n_2+n_3)}\}\, e^{-2\pi i\left(\frac{n_1}{a}x + \frac{n_2}{\sqrt{3}\,.\,a}y + \frac{n_3}{c}z\right)}, \tag{3}$$

from which the equations to the planes of energy discontinuity are at once found to be

$$\frac{n_1}{a}k_x + \frac{n_2}{\sqrt{3}\,.\,a}k_y + \frac{n_3}{c}k_z = \tfrac{1}{2}\left\{\left(\frac{n_1}{a}\right)^2 + \tfrac{1}{3}\left(\frac{n_2}{a}\right)^2 + \left(\frac{n_3}{c}\right)^2\right\}, \tag{4}$$

where n_1, n_2, n_3 are zero, positive, or negative integers. Not every plane given by (4) corresponds to a finite energy discontinuity, but only those for which the factor

$$\{1 + e^{-\pi i(n_1+n_2)}\}\{1 + e^{-\pi i(n_1+\frac{1}{3}n_2+n_3)}\},$$

is different from zero.

---

* Sommerfeld and Bethe (*loc. cit.*) ; Jones (*loc. cit.*).

The shape of the first zone, *i.e.*, the first region in **k** space about the origin in which the energy is continuous from point to point is shown in fig. 1. The number n of states per atom, contained within this first zone is easily shown to be

$$n = 2 - \tfrac{3}{4}\left(\frac{a}{c}\right)^2\left(1 - \tfrac{1}{4}\left(\frac{a}{c}\right)^2\right). \tag{5}$$

Beyond each of the faces marked A in fig. 1 there is a small region bounded by planes of energy discontinuity as indicated in the figure. The number of states per atom contained within these six small regions plus the number of states per atom contained within the inner zone amounts to exactly 2. A curious feature of the Brillouin zones for the hexagonal close-packed structure is that the energy gap between the inner zone and the next outer one vanishes along the lines such as PQ and QR, but at no other points over the surfaces A. A general proof is given in Appendix I for a two-dimensional hexagonal lattice.

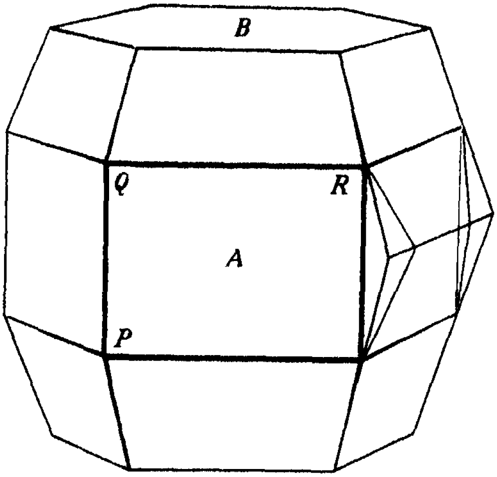

FIG. 1—The first Brillouin zone for a hexagonal close-packed structure. The principal axis of the hexagonal lattice corresponds with the axis of symmetry of the zone.

At the beginning of the ε-phase in the Cu–Zn alloy we have, according to (5), $n = 1\cdot727$. The number of electrons per atom to be distributed within the Brillouin zones is determined by the composition of the alloy; each zinc atom contributes 2, each copper atom 1. The composition at the beginning of the ε-phase shows that there are 1·786 electrons per atom. Hence even at the beginning of the ε-phase electrons must overlap into the second zone. The points at which this overlap occurs can easily be found. The value of **k** at the point A at the beginning of the ε-phase is $a/\sqrt{3} = 0\cdot2103$ reciprocal A, and the corresponding *free* electron energy is by (2) $E_A{}^0 = 6\cdot63$ volts. At the point B the value of **k** is $1/c = 0\cdot2329$ reciprocal A and the free electron energy is $E_B{}^0 = 8\cdot13$ volts. Thus at the beginning of the ε-phase the overlap into the second zone will occur at the points similarly situated to A. As the zinc concentration increases through the ε-phase the value of a increases whilst c remains practically constant. Hence at the end of the ε-phase, *i.e.*, at the zinc rich boundary, the energy of a state at the point A will be even lower relative to the energy of a state at the point B than at the beginning of the phase. Thus we may conclude that throughout the ε-phase the small amount of overlap into the second zone which occurs will take place at the points A. This conclusion is verified by consideration given later.

At the beginning of the η-phase the value of **k** at the points A is 0·2159 reciprocal A, and the energy $E_A{}^0 = 6\cdot99$ volts, whilst **k** at the points B is 0·2073 reciprocal A and the energy $E_B{}^0 = 6\cdot45$ volts. On passing from the beginning of the η-phase to pure zinc the energy associated with the points B decreases, whilst that associated with the points A increases, and therefore throughout this phase $E_A{}^0 > E_B{}^0$. The number of states per atom included within the first zone at the beginning of the η-phase is 1·79, whilst from the composition one finds that there are 1·97 loosely bound electrons per atom ; the least possible overlap is therefore 0·18 electrons per atom, which is much greater than the corresponding quantity for the ε-phase. We conclude therefore that in the η-phase overlap occurs into the second zone both at the points A and B.

3—*Internal Stresses arising from a given Electron Distribution in* **k** *Space*

It will now be shown how the results of Owen and Pickup's experiments (Table I) may be interpreted. We shall show that as a result of the foregoing conclusions (viz., that during the ε-phase the overlap into the second zone occurs only at points A, whilst in the η-phase the overlap occurs at both the points A and B), it is possible to estimate the rate of change of the lattice parameters with the composition, and that these estimates are in fair agreement with the experimental results obtained by X-ray analysis. Any change in the composition of the alloy changes the number of loosely bound electrons per atom, and it is only this effect which we consider.

First we calculate the internal stress in the crystal due to a small number of electrons lying beyond a plane of energy discontinuity. In fig. 2 let O be the origin of **k** space, and PQ a section of a plane of discontinuity which is perpendicular to the line OA. Let S be a section of a surface of constant energy which encloses between itself and the plane n states per atom. The total energy per atom corresponding to the states between S and PQ is

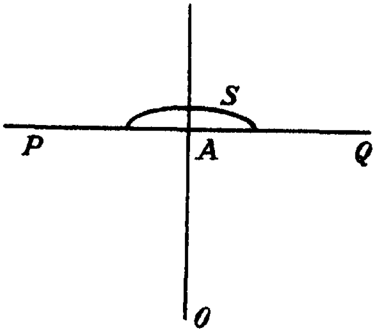

FIG. 2

$$U = 2\tau \int E(\mathbf{k})\, dv,$$

where dv represents an element of volume in **k** space, and τ is the atomic volume. The value of **k** at the point A will be inversely proportional to the lattice parameter in the corresponding direction in the crystal, *e.g.*, the point B in fig. 1, has a value of **k** equal to $1/c$. Thus if the crystal is given a strain $\delta\varepsilon$, the component of **k** parallel to OA will change by an amount $-k\delta\varepsilon$. The surface S will change to some slightly different surface S′. If the number of states per atom enclosed between the surface, and the plane of energy discontinuity is kept constant during the strain, then

$$\frac{\partial U}{\partial \varepsilon} = 2\tau \int \frac{\partial E}{\partial \varepsilon}\, dv. \tag{6}$$

If σ is the stress in dynes per sq cm which produces the strain ε, equation (6) may be written

$$\tau\sigma = -n\,\overline{\frac{\partial E}{\partial \varepsilon}}, \tag{7}$$

where $\overline{\partial E/\partial \varepsilon}$ is the average value of $\partial E/\partial \varepsilon$ taken over the n states between S and the plane PQ. To find an approximate value for this quantity we consider the case of free electrons

$$\frac{\partial E^\circ}{\partial \varepsilon} = -k\frac{\partial E^\circ}{\partial k} = -2E^\circ. \tag{8}$$

The approximation involved in substituting $-2\mathrm{E}$ for $\partial\mathrm{E}/\partial\varepsilon$ is that the change in the width of the energy discontinuity under the strain is negligible in comparison with the change in the mean position of the energy discontinuity. Thus the stress σ produced in a crystal by n electrons per atom lying in a small region beyond a plane of discontinuity acts in a direction perpendicular to the plane and is given approximately by

$$\sigma = \frac{2n}{\tau}\,\bar{\mathrm{E}}, \tag{9}$$

where $\bar{\mathrm{E}}$ is the mean value of the energy, and τ the atomic volume.

We apply this result to find the change in the lattice parameters in the η-phase for a small change in the composition. Let n_1 and n_2 be the number of electrons per atom which lie in the second zone just beyond the points B and A respectively (fig. 1). If n_1 is increased by δn_1, the increase in the z component of the internal stress is given by

$$\delta\sigma_z = \frac{2\bar{\mathrm{E}}_1}{\tau}\,\delta n_1. \tag{10}$$

In the case of a uniform lateral stress acting in all directions at right angles to the z axis

$$\frac{\partial \mathrm{U}}{\partial \varepsilon_x} = -2\sigma_x, \tag{11}$$

where ε_x is the strain in the direction of the x axis, and $\sigma_x = \sigma_y$ the corresponding value of the stress. Hence applying (11) to find the change in the stress σ_x due to a change δn_2 in the number of electrons lying outside the points A we find

$$\delta\sigma_x = \frac{\bar{\mathrm{E}}_2}{\tau}\,\delta n_2.$$

Hence, if we know the elastic constants of the crystal, we can write down the changes in the strains due to that change δn in the number of electrons per atom which corresponds to a definite change of composition

$$\left.\begin{aligned}\frac{\delta\varepsilon_x}{\delta n} &= \frac{1}{\tau}(\mathrm{S}_{11}+\mathrm{S}_{12})\,\bar{\mathrm{E}}_2\,\frac{\delta n_2}{\delta n} + \frac{2}{\tau}\,\mathrm{S}_{13}\,\bar{\mathrm{E}}_1\,\frac{\delta n_1}{\delta n}\\ \frac{\delta\varepsilon_z}{\delta n} &= \frac{2}{\tau}\,\mathrm{S}_{13}\,\bar{\mathrm{E}}_2\,\frac{\delta n_2}{\delta n} + \frac{2}{\tau}\,\mathrm{S}_{33}\,\bar{\mathrm{E}}_1\,\frac{\delta n_1}{\delta n}\end{aligned}\right\}. \tag{12}$$

Since in the η-phase the alloy contains over 97% Zn we may take as the values of the elastic constants those measured by Bridgman* for pure zinc crystals. $S_{11} = 8 \cdot 23 \,.\, 10^{-13}$, $S_{12} = 0 \cdot 34 \,.\, 10^{-13}$, $S_{13} = -6 \cdot 64 \,.\, 10^{-13}$, $S_{33} = 26 \cdot 38 \,.\, 10^{-13}$ cm^2/dynes. The values of $\bar{E}_1$ and $\bar{E}_2$ must both be in the neighbourhood of 7 volts, and $\tau = 14 \cdot 98 \,.\, 10^{-24}$ cc. Hence substituting these values in (12) we find

---

* 'Proc. Nat. Acad. Sci. Wash.,' vol. 10, p. 411 (1924).

$$\frac{\delta\varepsilon_x}{\delta n} = 0 \cdot 63 \frac{\delta n_2}{\delta n} - 0 \cdot 98 \frac{\delta n_1}{\delta n}$$

$$\frac{\delta\varepsilon_z}{\delta n} = -0 \cdot 98 \frac{\delta n_2}{\delta n} + 3 \cdot 9 \frac{\delta n_1}{\delta n}.$$

Estimates of $\delta n_1/\delta n$ and $\delta n_2/\delta n$ obtained from a perturbation calculation which is given briefly in Appendix II shows that these quantities are not very different from each other. If we put each equal to $\frac{1}{2}$, we obtain $\delta\varepsilon_x/\delta n = -0 \cdot 18$ and $\delta\varepsilon_z/\delta n = 1 \cdot 5$. From Table I we can find the observed rate of change of a and c with composition, and therefore the observed values of $\delta\varepsilon_x/\delta n$ and $\delta\varepsilon_z/\delta n$. These are found to be $-0 \cdot 22$ and $+0 \cdot 91$ respectively.

The corresponding formulæ giving the change of strain with composition for the ε-phase, is obtained from those for the η-phase by merely putting $\frac{\delta n_1}{\delta n} = 0$. The elastic constants are not known for the ε-phase, but one sees that $\delta\varepsilon_x/\delta n$ is essentially positive which agrees with experiment, whilst $\delta\varepsilon_z/\delta n$ is negative according to the formula but is practically zero according to the measurements.

TABLE II

Alloy	c/a observed	Number of states per atom in the inner zone calculated from (5)	Number of electrons per atom at beginning of ε-phase (observed)
Cu–Zn	1·570	1·727	1·786
Cu–Sn	1·571	1·727	1·75
Ag–Zn	1·581	1·730	1·715
Ag–Cd	1·581	1·730	1·671
Au–Zn	1·558	1·723	1·863
Au–Hg	1·646	1·749	1·75
Fe–Zn	1·607	1·738	1·74

From these considerations of the Cu–Zn system, we may conclude that in any binary alloy a phase which gives the characteristic ε-structure will have such a composition that the number of valency electrons per atom at the beginning of the phase will be very closely equal to the number of states per atom of the inner zone given by formula (5). Table II shows the type of agreement obtained. The fact that the composition of the ε-phase invariably corresponds to approximately 1·75 valency electrons per atom was first noticed by Hume-Rothery and constitutes one of his well-known empirical rules. The numbers of valency electrons per atom assumed to obtain column 3 are as follows : Cu 1, Ag 1, Au 1, Zn 2, Cd 2, Hg 2, Sn 4, Fe 0. The range of homogeneity of a phase, it is seen, is determined by the range in the number of valency electrons per atom for which the structure is stable. Hence the range of the ε-phase in Cu–Sn will be only one-third of the range in Cu–Zn, since each atom of tin supplies three extra electrons per atom, whilst Zn supplies only 1. This conclusion is in fair agreement with the observations, but, of course, other factors such as the size of the ion must also play an important part in determining the range of homogeneity of the ε-phase.

PART II

4—*The Form of the Brillouin Zones for the Bismuth Structure*

The bismuth atom contains five electrons external to a closed shell. In the solid state, the bismuth structure is based upon a rhombohedral lattice with two atoms per unit cell. The potential at any point in the lattice may therefore be expressed in the form

$$V = \Sigma_n V_n \{1 + e^{-4\pi i u (n_1+n_2+n_3)}\} e^{-\frac{2\pi i}{a}(n_1 x' + n_2 y' + n_3 z')}, \tag{13}$$

where x', y', z' are the oblique co-ordinates associated with the rhombohedral lattice, a is the lattice constant, and u the parameter specifying the distance between the two atoms of the unit cell. n_1, n_2, n_3 are zero, positive, or negative integers.

It is most convenient to express the equations to the planes of energy discontinuity in **k** space in rectangular co-ordinates in which the k_z axis corresponds to the trigonal axis of the rhombohedral lattice. The equations are readily found to be

$$(2n_1-n_2-n_3)\,k_x + \sqrt{3}\,(n_2-n_3)\,k_y + (n_1+n_2+n_3)\sqrt{2}\sqrt{\frac{1-\cos\alpha}{1+2\cos\alpha}}\,.\,k_z$$
$$+\frac{\sqrt{6}}{2a}\,\frac{\{(n_1^2+n_2^2+n_3^2)(1+\cos\alpha)-2\cos\alpha\,(n_1n_2+n_2n_3+n_3n_1)\}}{(1+2\cos\alpha)\sqrt{(1-\cos\alpha)}}=0. \tag{14}$$

The equations of these planes take a symmetrical form if expressed in oblique co-ordinates k'_x, k'_y, k'_z, whose axes are parallel to the axes of the co-ordinates x', y', z'. For bismuth $\alpha = 57° \; 16'$, $a = 4{\cdot}74$ A, $u = 0{\cdot}237$.

By analogy with the explanation of the large diamagnetism of alloys in the γ-phase, recently given by the author (*loc. cit.*), one would expect that a Brillouin zone exists in bismuth containing just five electrons per atom. This will not, of course, be the lowest, *i.e.*, it will include sub-zones ; but its boundaries will be strongly reflecting planes. Such a zone may be found, and its form is shown in fig. 3. The sides parallel to the trigonal axis are formed by the planes $\{1\bar{1}0\}$, the three top planes are the planes $\{\bar{2}\bar{2}\bar{1}\}$, and the three bottom ones $\{221\}$. The volume of the zone is independent of the precise value of α.

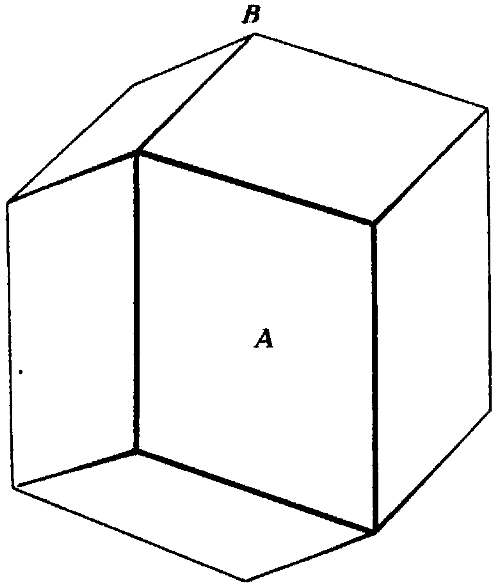

Fig. 3—The Brillouin zone for the bismuth structure which contains five states per atom. The principal axis of the lattice corresponds to the axis of symmetry of the zone.

The energy discontinuity across a plane given by equation (14) is proportional to the factor

$$S_{n_1 n_2 n_3} = \left|1 + e^{-4\pi i u (n_1+n_2+n_3)}\right| = 2 \cos 2\pi u \,(n_1 + n_2 + n_3).$$

One sees therefore that if u were equal to one-quarter the discontinuity across the planes $\{221\}$ would vanish since S_{221} would be zero. The value of S_{221} for the metals Bi, Sb, As, are respectively 0·7942, 1·0180, 1·3690. For the $\{1\bar{1}0\}$ planes $S_{1\bar{1}0} = 2$ in each case.

In the following sections, from a consideration of physical properties, we shall see that in bismuth the zone shown in fig. 3 must be almost exactly filled by the five outer electrons of the bismuth atom. It is then easy to interpret the fact that bismuth does not form an exact co-ordination lattice, which would occur if u were equal to $\frac{1}{4}$; the small difference between the value 0·237 of u for bismuth and the value $\frac{1}{4}$ produces the rather large energy gap ($S_{221} = 0{\cdot}7942$) over the {221} planes, and therefore depresses the total energy of the electrons.

5—*Alloys of Bismuth which retain the Bismuth Structure*

The elements Sn, Pb, Te, Se, dissolve in bismuth to the extent of two or three atomic per cent, forming solid solutions. If larger amounts of these elements are added, the alloy passes into a mixed crystal region. The number of electrons per atom outside a closed shell for Sn and Pb is 4, and for Te and Se 6. Thus adding small quantities of Pb or Sn lowers the number of electrons per atom in the alloy, whilst adding Te or Se increases the number per atom.

The mean temperature coefficient of the electrical resistance between 0° and 30° C has been measured for the alloys Bi–Sn.[*] For pure bismuth the temperature coefficient is, of course, positive, the resistance increasing with the temperature. A concentration of 0·13% Sn, however, causes the temperature coefficient to become negative. A similar result has been obtained by Thomas and Evans,[†] who find that small amounts of Pb in bismuth give rise to a negative temperature coefficient of the resistance. The significance of a negative temperature coefficient of the electrical resistance, which is the characteristic of electronic semi-conductors, can be seen as follows.[‡] Let E_2 be the lowest energy state in the second zone, and E_s the energy at the surface of the Fermi distribution at the absolute zero of temperature. We consider three possibilities : (1) $E_2 - E_s \gg kT$, (2) $E_2 - E_s \ll kT$, (3) $E_2 - E_s \sim kT$, where T is of the order of magnitude of the temperature at which the resistance measurements are made. In the first two cases the temperature coefficient of the resistance will be positive ; the first case would correspond to metals like the alkalis, the second to divalent metals. In the third case as the temperature is raised there is a flow of electrons from the inner to the outer zone, which increases the effective number of electrons taking part in the conduction and therefore leads to a decrease in the resistance with increasing temperature. From this result we conclude that adding 0·13% Sn to bismuth reduces the number of valency electrons per atom to such an extent that all the electrons which overlap into the second zone in pure bismuth are removed. Hence the number of electrons in the outer zone in pure bismuth must be less than 0·0013 per atom.

---

[*] Ufford, ' Proc. Amer. Acad. Sci.,' vol. 63 (1928).

[†] ' Phil. Mag.,' vol. 16, p. 329 (1933).

[‡] *Cf.* Wilson, ' Proc. Roy. Soc.,' A, vol. 133, p. 458 (1931).

Referring to the details of the Brillouin zone which contains five electrons per atom one sees that the overlap which occurs must take place over the planes $\{1\bar{1}0\}$ at the points marked A. In the immediate neighbourhood of the points A the energy surfaces must approximate to a family of ellipsoids, since, if the energy is expanded as a function of the co-ordinates referred to A as origin, only even powers of the co-ordinates can occur by symmetry. As there are five states per atom in the Brillouin zone, and just five electrons per atom in pure bismuth, it follows that inside the inner zone there must be a number of vacant places, the number per atom being equal to the overlap into the outer zone. A perturbation calculation shows that the surface of the Fermi distribution inside the inner zone will consist of two closed regions, each having a flattened shape in the direction of the principal axis and having trigonal symmetry about it.

6—*The Diamagnetic Properties of the Solid Solutions of* Sn, Pb, Te, Se, *in Bismuth*

According to the theory of Peierls,* the most important contribution to the diamagnetic susceptibility of a metal is given by the formula

$$\chi = -\tfrac{2}{3}\left(\frac{e}{4\pi c}\right)^2 \frac{1}{h^2}\iint \frac{1}{|\mathrm{grad}_k\,\mathrm{E}|}\left\{\frac{\partial^2\mathrm{E}}{\partial k_x^2}\frac{\partial^2\mathrm{E}}{\partial k_y^2} - \left(\frac{\partial^2\mathrm{E}}{\partial k_x\,\partial k_y}\right)^2\right\} d\mathrm{S}, \qquad (15)$$

where the integration is taken over the surface of the Fermi distribution, but not along a boundary where the electron distribution touches a plane of energy discontinuity. The susceptibility given by this expression depends essentially therefore on the crystal structure of the metal, since this determines the nature of the surface separating the occupied and unoccupied states. The fact that the mass susceptibility of pure bismuth at room temperature parallel to the principal axis is $-1{\cdot}035\,.\,10^{-6}$ whilst for molten bismuth it is only $-0{\cdot}08\,.\,10^{-6}$ shows that the diamagnetism of bismuth is intimately connected with the structure.

For entirely free electrons (15) reduces to a formula first given by Landau, and if one applies this to bismuth one finds for the mass susceptibility $\chi = -0{\cdot}039\,.\,10^{-6}$ which is about 25 times too small to agree with experiment.

---

* 'Z. Physik,' vol. 80, p. 763 (1933).

It is only in the simplest cases that the integral (15) can be evaluated without immense labour. It is interesting to find the diamagnetic susceptibility in the special case when the energy surfaces form a family of similar ellipsoids, as they do, for example, just beyond a plane of energy discontinuity in the way indicated in fig. 2. Let

$$E = \frac{h^2}{2m}\{\alpha_1 k_x^2 + \alpha_2 k_y^2 + \alpha_3 k_z^2\}. \tag{16}$$

One then finds for the volume susceptibility in the direction parallel to the z axis

$$\kappa_z = -0\cdot1222\sqrt{E}\sqrt{\frac{\alpha_1\alpha_2}{\alpha_3}}\,10^{-6}, \tag{17}$$

where E is the energy in volts according to (16) of the ellipsoid which bounds the occupied states. Thus the susceptibility of a number of electrons for which the bounding surface in **k** space is a prolate spheroid will be large parallel to the axis of symmetry, and small at right angles to it. On the other hand, a part of the surface of the Fermi distribution which forms an oblate spheroid will lead to a small susceptibility along the axis, and a large one at right angles to it.

According to a formula obtained in a previous paper (Jones, *loc. cit.*) the value of α_1 just beyond a plane of energy discontinuity which lies perpendicular to the k_x axis is given by

$$\alpha_1 = 1 + \frac{4E^0}{\Delta E}, \tag{18}$$

where E^0 is the energy of a free electron at the point in **k** space considered, and ΔE is the energy gap across the plane of discontinuity. The length of the perpendicular from the origin to the points marked A in fig. 3 is $k = 0\cdot220$, and therefore by (2) $E^0 = 7\cdot27$ volts. Hence, if we assume a value for the energy gap of the order of 1 volt, we find that α_1 is of the order 30.

When the number of electrons per atom which lie in the outer zone, and therefore in the region of **k** space where the energy surfaces approximate to a family of ellipsoids, is given, there exists a relation between the value of E in (17) and the parameters α_1, α_2, α_3. If τ be the atomic volume, the number of states per atom n enclosed within the surface E is

$$n = \frac{8\pi\tau}{3}\left(\frac{2mE}{h^2}\right)^{3/2}\frac{1}{\sqrt{(\alpha_1\alpha_2\alpha_3)}}. \tag{19}$$

We have seen that the number of electrons per atom in the outer zone in pure bismuth is approximately 0·0013. Reference to fig. 3 shows that the second zone will contain three separate regions in which the energy surfaces are ellipsoids. There are, of course, six separate regions in the second zone, but these are to be taken in pairs so that the surface of the Fermi distribution in any one of these three regions forms a complete ellipsoid. Hence in each ellipsoid there are about 0·0004 electrons per atom. With this value, and substituting known constants we obtain from (17) and (19)

$$\chi_z 10^6 = -0\cdot00173 \left\{\frac{(\alpha_1\alpha_2)^2}{\alpha_3}\right\}^{1/3},$$

where χ_z is the susceptibility per gram in the direction of the z axis. Thus the mass susceptibility of Bi parallel to the principal axis $\chi_{\parallel}$ will be given approximately by $3\chi_z$, since the contribution arising from the surface of the Fermi distribution inside the inner zone will be small, as already explained, and so may be neglected in this rough calculation. Hence

$$-\chi_{\parallel} 10^6 = 0\cdot0052 \left\{\frac{(\alpha_1\alpha_2)^2}{\alpha_3}\right\}^{1/3}. \qquad (20)$$

The shape of the Brillouin zone indicates that α_3 will be small of order of magnitude unity, whilst α_1 and α_2 will be large, *e.g.*, 30 or 40. From which it follows that $-\chi_{\parallel} 10^6$ is of the order 1, agreeing with experiment.

It should be noticed that for a given number of electrons per atom the parameters α_1, α_2, α_3 are definitely limited, because grad_k E should at no point in **k** space have a greater value than that corresponding to free electrons at that point. A conclusion which is easily understood by reference to fig. 3 of a previous paper (Jones, *loc. cit.*).

These considerations show that in bismuth the susceptibility $\chi_{\parallel}$ arises mainly from those electrons which lie in the second zone, *i.e.*, about the points A, whilst the susceptibility perpendicular to the principal axis $\chi_{\perp}$ arises mainly from those parts of the surface of the Fermi distribution which lie inside the first zone, since these surfaces must behave like oblate spheroids with their axes parallel to the principal axis. Hence we conclude that *if* the number of electrons per atom is decreased the quantity $\chi_{\perp}/\chi_{\parallel}$ will increase, whilst if the number of electrons per atom is increased $\chi_{\perp}/\chi_{\parallel}$ will decrease.

Goetz and Focke* have measured $\chi_{\perp}/\chi_{\parallel}$, which they call the magnetic anisotropy, for the solid solutions of Sn, Pb, Te, Se in bismuth for different concentrations of the solute elements. Examples of their results for Sn and Te taken at room temperature are given in Table III.

---

* 'Phys. Rev.,' vol. 45, p. 170 (1934).

Pb behaves quite similarly to Sn, and Se to Te. These results agree very well with the theoretical expectations, since addition of Sn and Pb decreases the number of electrons per atom, whilst Te and Se increases the number per atom.

TABLE III

Atomic per cent Sn	$\chi_\perp/\chi_\parallel$	Atomic per cent Te	$\chi_\perp/\chi_\parallel$
0·01	1·470	0·01	1·329
0·03	1·570	0·03	1·197
0·09	1·803	0·09	0·903
0·81	2·965	0·27	0·697
2·43	4·655		

7—*The Magnitude of the Electrical Conductivity of Bismuth*

The result that the number of electrons in the outer Brillouin zone in bismuth is extremely small might lead one to suppose that these considerations would give an electrical conductivity far too small to agree with observation. A simple consideration in this section shows that, in fact, no difficulties of this kind arise.

Let f_0 be the Fermi distribution function when the metal is in equilibrium in the absence of an electric field. Let f be some other function which differs slightly from f_0. Then if

$$\frac{\partial}{\partial t}(f-f_0) = -\frac{f-f_0}{\lambda},$$

λ is defined as a time of relaxation. If f be taken as the Fermi function when the metal is in equilibrium under the action of an electric field F applied in the direction of the x axis, then according to a well-known procedure one finds

$$f = f_0 - \frac{Fe}{h}\lambda\frac{\partial E}{\partial k_x}\frac{\partial f_0}{\partial E},$$

which leads at once to the expression for the conductivity

$$\sigma = \frac{2e^2}{h^2}\iiint \lambda\left(\frac{\partial E}{\partial k_x}\right)^2 \frac{\partial f}{\partial E}\, dk_x dk_y dk_z\ .$$

Assuming λ to be a function of the energy only, and taking E as given by equation (16), one finds

$$\sigma = \frac{e^2 n\lambda\alpha_1}{m}. \tag{21}$$

Here n is the number of electrons per cc which lie in those regions of **k** space where the energy surfaces may be approximately represented by (16); that is to say, for bismuth the number of electrons per cc which lie in the second zone. Of course, since the inner zone is not completely filled, it also will contribute to the conductivity, but for the present purpose this contribution may be neglected. If equation (21) is applied to free electrons ($\alpha_1 = 1$), and if a mean free path l is introduced in place of λ by means of the equation $\lambda = l/\bar{v}$ where $\bar{v}$ is the mean velocity at the surface of the Fermi distribution, then Sommerfeld's well-known formula is obtained.

Using the known values for the conductivities we may compare the mean times of relaxation for the metals silver and bismuth

$$\frac{\lambda_{\mathrm{Ag}}}{\lambda_{\mathrm{Bi}}} = \frac{\sigma_{\mathrm{Ag}} n_{\mathrm{Bi}} \alpha_1}{\sigma_{\mathrm{Bi}} n_{\mathrm{Ag}}}.$$

With the results $n_{\mathrm{Bi}}\tau_{\mathrm{Bi}} = 0{\cdot}0013$, $\alpha_1 = 30$, $n_{\mathrm{Ag}}\tau_{\mathrm{Ag}} = 1$, $\sigma_{\mathrm{Ag}} = 6{\cdot}6710^5$, $\sigma_{\mathrm{Bi}} = 0{\cdot}926 \,.\, 10^4$, it follows that $\lambda_{\mathrm{Ag}}/\lambda_{\mathrm{Bi}} = 1{\cdot}4$. Thus it is seen that the distribution of the electrons amongst the Brillouin zones deduced and employed in the previous sections is not incompatible with the observed electrical conductivity of bismuth.

8—*Magnetostriction*

The magnetostriction of single crystals of bismuth has been investigated thoroughly by Kapitza.* His results may be most conveniently expressed as a relation between the change of the magnetic susceptibility in a given direction in the crystal and the strain in that direction. If κ is the volume susceptibility, and ε the strain, both in the direction of the principal axis, the experiments yield a relation

$$-\kappa\, 10^6 = 4{\cdot}75 + 8{\cdot}85\,(1 - 38{\cdot}68\,\varepsilon), \tag{22}$$

which shows that, as the length of the crystal in the direction of the principal axis is increased, the diamagnetic susceptibility in that direction decreases.

On the basis of the foregoing considerations, it is easy to calculate the change in the magnetic susceptibility parallel to the principal axis due to a strain in the same direction. When the crystal is elongated parallel to the trigonal axis, the point B of fig. 3 moves closer to the origin, which means that the figure becomes more symmetrical ; the number of the electrons in the outer zone is therefore reduced, thereby reducing the susceptibility $\chi_{\parallel}$.

---

* 'Proc. Roy. Soc.,' A, vol. 135, p. 537 (1932).

If we differentiate equation (17) with respect to ε we find

$$\frac{d}{d\varepsilon}(-\kappa_2\,10^6) = \frac{0\cdot 0611}{\sqrt{\mathrm{E}}}\sqrt{\frac{\alpha_1\alpha_2}{\alpha_3}}\frac{d\mathrm{E}}{d\varepsilon}\,. \tag{23}$$

Since the energy over the surface of the Fermi distribution is the same both for those parts of it which lie in the inner zone and those parts which lie in the outer zone, it follows that $d\mathrm{E}/d\varepsilon$ is equal to the rate of change of the energy at the surface of the Fermi distribution in the inner zone with respect to the strain.

It is due to this change of energy in the inner zone that the number of electrons diminishes in the outer zone. Hence using the values of α_1, α_2, α_3, required to give the right order of magnitude to $\chi_{\parallel}$, and the value of E given by (19) we obtain

$$\frac{d}{d\varepsilon}(-\kappa_{\parallel}\,10^6) = 13\left(\frac{d\mathrm{E}}{d\varepsilon}\right)_i, \tag{24}$$

where the subscript i denotes that E now refers to the surface of the Fermi distribution in the inner zone, expressed in volts, and $\kappa_{\parallel}$ is the total susceptibility due to the three separate regions in the outer zone, see § 6. $(d\mathrm{E}/d\varepsilon)_i$ may be estimated in the way explained in § 3, equation (8). The value of the energy at the surface of the Fermi distribution is in general found to be within a few per cent equal to the value given by the simple Sommerfeld free electron theory.* For Bi the free electron model gives 9·9 volts. Hence equation (24) shows that $\frac{d}{d\varepsilon}(-\kappa\,10^6) = -260$ whilst experiment gives $-342\cdot 3$ according to equation (22).

For the change in $\chi_{\perp}$ with the strain perpendicular to the principal axis it is impossible to make even rough calculations since the form of the energy surfaces near the surface of the Fermi distribution in the inner zone, which is mainly responsible for $\chi_{\perp}$ is not known. It is clear, however, that in this case one would expect the strain to increase $\chi_{\perp}$.

It is a pleasure to express my thanks to Professor N. F. Mott for many discussions and for his assistance in preparing this paper for publication.

---

* O'Bryan and Skinner, 'Phys. Rev.,' vol. 45, p. 379 (1934).

SUMMARY

The Bloch model is applied to binary alloys in the ε- and η-phases (Part I) and to bismuth and to some of its alloys (Part II). In Part I a qualitative explanation is given of the variations of the crystal parameters within these phases observed by Owen and Pickup, and also of the electron-atom ratio at which the ε-phase begins (Hume-Rothery's rule). In Part II a Brillouin zone is found for bismuth containing five electrons per atom. The theory shows why bismuth does not form of a co-ordination lattice. The conductivity of alloys of Bi Sn and Bi Pb are considered ; the observed variation with composition leads to a determination of the "overlap" of the Fermi surface into the second zone. From this the diamagnetism of pure bismuth and of Bi Sn, Bi Te alloys are deduced, as is also the magnetostriction, in good agreement with experiment. The theory gives a value of the conductivity in agreement with experiment.

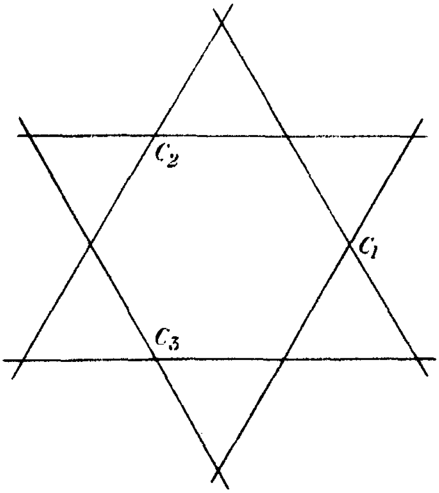

FIG. 4

APPENDIX I

It is sufficient to consider the simple case of a two-dimensional hexagonal lattice, for which the potential may be expressed in the form

$$V = \Sigma_n V_n e^{-\frac{2\pi i}{a}\left(n_1 x + \frac{n_2}{\sqrt{3}} y\right)}, \qquad (1.1)$$

where a is the distance between nearest atoms.

Since the potential is a real quantity and is unchanged by a reflection in the origin, it follows that the coefficients V_n are real. Fig. 4 shows the first few Brillouin zones for this case. The free electron wave functions for the three combining states C_1, C_2, C_3 in the figure are :

$$\left.\begin{aligned} \psi_1 &= e^{2\pi i \frac{2}{3a} x} \\ \psi_2 &= e^{2\pi i \left(-\frac{1}{3a} x + \frac{1}{\sqrt{3}a} y\right)} \\ \psi_3 &= e^{2\pi i \left(-\frac{1}{3a} x - \frac{1}{\sqrt{3}a} y\right)} \end{aligned}\right\}, \tag{1.2}$$

and the secular equation for the energies at these points is :

$$\begin{vmatrix} E_C^0 - E & \beta & \beta \\ \beta & E_C^0 - E & \beta \\ \beta & \beta & E_C^0 - E \end{vmatrix} = 0, \tag{1.3}$$

where $\beta = V_{-11} = V_{-1-1} = V_{0-2}$. These Fourier coefficients of V must be equal by symmetry. The roots of (1.3) are

$$\left.\begin{aligned} E_1 &= E_C^0 + 2\beta \\ \left.\begin{matrix} E_2 \\ E_3 \end{matrix}\right\} &= E_C^0 - \beta \end{aligned}\right\}, \tag{1.4}$$

and the zero order wave functions are

$$\left.\begin{aligned} \Psi_1 &= \psi_1 + \psi_2 + \psi_3 \\ \Psi_2 &= \psi_1 + \omega^2 \psi_2 + \omega \psi_3 \\ \Psi_3 &= \psi_1 + \omega \psi_2 + \omega^2 \psi_3 \end{aligned}\right\}, \tag{1.5}$$

where ω is a cube root of unity.

Let R be an operator representing a rotation through an angle $\frac{2}{3}\pi$. Then $R\psi_1 = \psi_2$, $R\psi_2 = \psi_3$ and

$$R\Psi_1 = \Psi_1, \qquad R\Psi_2 = \omega\Psi_2, \qquad R\Psi_3 = \omega^2\Psi_3.$$

Since the potential is invariant under R it follows that the only functions which will combine with Ψ_1, Ψ_2, Ψ_3 under the action of V are functions which have respectively the same symmetries. We have therefore three sets of states which are mutually non-combining. The wave functions may be written $\Psi_1(n)$, $\Psi_2(n)$, $\Psi_3(n)$, where n specifies the different states in one set. Thus, for example,

$$\Psi_1(n) = \psi_1(n) + \psi_2(n) + \psi_3(n),$$

where $\psi_1(n)$ is the free electron wave function associated with a point in the reciprocal lattice which combines with C_1. $\psi_2(n)$ and $\psi_3(n)$ are obtained from $\psi_1(\mathbf{n})$ by operating with R and R^2 respectively. The matrix elements of V with respect to the wave functions $\Psi_1(\mathbf{n})$, etc., may be expressed as follows :

$$\tfrac{1}{3}(\Psi^*_1(\mathbf{n}), V\Psi_1(\mathbf{m})) = (\psi^*_1(\mathbf{n}), V\psi_2(\mathbf{m})) + (\psi^*_1(\mathbf{n}), V\psi_3(\mathbf{m})) \qquad (1.6)$$

$$\tfrac{1}{3}(\Psi^*_2(\mathbf{n}), V\Psi_2(\mathbf{m})) = \omega^2(\psi^*_1(\mathbf{n}), V\psi_2(\mathbf{m})) + \omega(\psi^*_1(\mathbf{n}), V\psi_3(\mathbf{m})) \qquad (1.7)$$

$$\tfrac{1}{3}(\Psi^*_3(\mathbf{n}), V\Psi_2(\mathbf{m})) = \omega(\psi^*_1(\mathbf{n}), V\psi_2(\mathbf{m})) + \omega^2(\psi^*_1(\mathbf{n}), V\psi_3(\mathbf{m})). \qquad (1.8)$$

Since the Fourier coefficients of the potential are real all the terms $(\psi^*_1(\mathbf{n}), V\psi_2(\mathbf{m}))$, etc., are real. Thus (1.7) is the complex conjugate of (1.8), and therefore the energies E_2 and E_3 are equal, not only to the first order, but exactly.

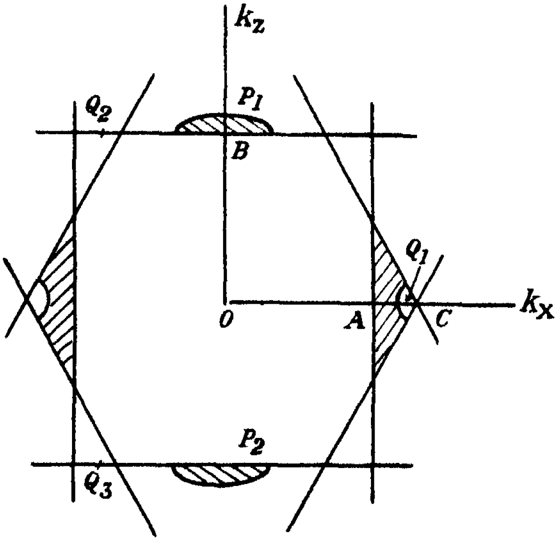

FIG. 5

APPENDIX II

Fig. 5 represents a section of the Brillouin zone shown in fig. 1 in the $k_y = 0$ plane. The energies of the states at the points P_1 and P_2 are given by the roots of the equation

$$\begin{vmatrix} E_{P_1}{}^0 - E, & V_{00-2} \\ V_{002} \quad , & E_{P_2}{}^0 - E \end{vmatrix} = 0 , \qquad (2.1)$$

where V_{002} and V_{00-2} are the Fourier coefficients of the potential V

$$V = \Sigma_n V_n e^{-2\pi i\left(\frac{n_1}{a}x + \frac{n_2}{\sqrt{2}a}y + \frac{n_3}{c}z\right)}. \qquad (2.2)$$

If ξ, η, ζ are the co-ordinates of a point in **k** space referred to B as origin, the energy surfaces in the second zone in the neighbourhood of B are given by

$$E_1 = \frac{h^2}{2m}\left\{\frac{1}{c^2} + \xi^2 + \eta^2 + \zeta^2 + \frac{2}{c}\sqrt{\zeta^2 + (\gamma/c)^2}\right\}, \tag{2.3}$$

where $\gamma = \Delta E_1/4E_B{}^0$ and $\Delta E_1 = 2\,|V_{002}|$ is the energy gap across the planes {002}. Let ζ_0 be the value of ζ at the point where one of the surfaces (2.3) cuts the ζ axis. The number of states per atom enclosed within this surface, and the plane of energy discontinuity is given by the equation

$$n_1 = \pi\sqrt{3}a^2c\left\{\tfrac{2}{3}\,\zeta_0{}^3 + \frac{\zeta_0}{c}\sqrt{\zeta_0{}^2 + (\gamma/c)^2} - \frac{\gamma^2}{c^2}\sinh^{-1}\frac{c\zeta_0}{\gamma}\right\}, \tag{2.4}$$

and the energy of the enclosing surface which cuts the axis in the point ζ_0 is

$$E_1 = \frac{h^2}{2m}\left\{\frac{1}{c^2} + \zeta_0{}^2 + \frac{2}{c}\sqrt{\zeta_0{}^2 + (\gamma/c)^2}\right\}. \tag{2.5}$$

Hence from (2.4) and (2.5)

$$\frac{dE_1}{dn_1} = \frac{\sqrt{3}}{4\pi}\,\frac{h}{mc^3}\,\frac{1}{\zeta_0}. \tag{2.6}$$

Thus by means of (2.6) and (2.4) dE_1/dn_1 may be evaluated as a function of n_1 when the value of γ is known. Curve 1, fig. 6, shows dE_1/dn_1 plotted against n_1 where the energy gap ΔE_1 has been assumed to have a value 3 volts.

In a similar manner one can obtain the energy in the neighbourhood of the point C along the line OC. The state Q_1 combines with the states Q_2 and Q_3 leading to the following equation for the energy

$$\begin{vmatrix} E_{Q_1}{}^0 - E, & V_{0-2-1}\,, & V_{0-21} \\ V^*_{0-2-1}, & E_{Q_2}{}^0 - E, & V_{00-2} \\ V^*_{0-21}\,, & V^*_{00-2}\,, & E_{Q_3}{}^0 - E \end{vmatrix} = 0.$$

This determinant factorizes and one finds for the energy in the second zone at the point Q_1

$$E_2 = \frac{h^2}{2m}\{(k_c - \xi_0)^2 + 2\xi_0{}^2\sin\theta\} + \frac{\Delta E_1}{4}\left\{1 - \left[\left(1 + \frac{4h^2}{m}\,\xi_0{}^2\sin^2\theta\right)^2 + 6\left(\frac{\Delta E_2}{\Delta E_1}\right)^2\right]^{\frac{1}{2}}\right\}, \tag{2.7}$$

where ξ_0 is the co-ordinate of Q_1 referred to C as origin, and $k_c = OC$, and ΔE_2, which is equal to $2\,|\,V_{021}\,|$, is the energy gap across the planes

{021} and θ is the angle which the perpendicular to the {021} planes makes with the k_2 axis, and is given by

$$\sin\theta = \left(1 + \tfrac{3}{4}\left(\frac{a}{c}\right)^2\right)^{-\frac{1}{2}}.$$

According to a formula given by the author in a previous paper (*loc. cit.*) the energy discontinuity, obtained by a first order perturbation calculation, across any plane is approximately inversely proportional to the square of the perpendicular from the origin to the plane. To this approximation therefore

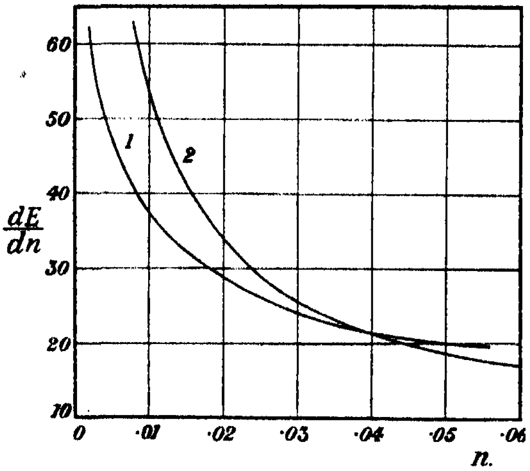

FIG. 6—Curve (1) represents dE_1/dn_1 plotted against n_1, and curve (2) dE_2/dn_2 plotted against n_2, both E_1 and E_2 are expressed in volts

$$\frac{\Delta E_1}{\Delta E_2} = \tfrac{1}{4} + \tfrac{1}{3}\frac{c^2}{a^2}.$$

The energy surfaces close to the points C in the second zone are approximately cylindrical; if one makes the approximation of supposing them to be exactly cylindrical, then the number of unoccupied states per atom is given by the formula

$$n_2 = \frac{2\theta c}{\sqrt{3}\, a \sin^4\theta}\,\frac{\xi_0^2}{k_c^2}\left\{1 - \tfrac{3}{4}\left(\frac{a}{c}\right)^2 + \frac{2\xi_0}{3k_c \sin^2\theta}\right\}.$$

Hence from equations (2.7) and (2.8) the values of dE_2/dn_2 for different values of n_2 can be calculated ; the result is shown in curve 2, fig. 6. The ratio $\frac{\delta n_1}{\delta n} : \frac{\delta n_2}{\delta n}$ (*cf.* § 3) is equal to the ratio $\frac{dE_2}{dn_2} : \frac{dE_1}{dn_1}$ and is therefore not very different from unity when the number of electrons per atom in the second zone beyond the point B lies between 0·02 and 0·05.

The Behaviour of Electrolytes in Mixed Solvents

VI—The Electrical Conductivities of some Salts in Water-Ethyl Alcohol Solutions

By L. C. CONNELL, R. T. HAMILTON, and J. A. V. BUTLER, University of Edinburgh

(*Communicated by J. Kendall, F.R.S.—Received June* 22, 1934)

Extensive measurements of the conductivities of salts in mixed solvents have been made by Jones and his co-workers.* Although they were neither sufficiently accurate, nor carried to a sufficiently low concentration to define the limiting conductivities at infinite dilution, these measurements give a good idea of the general nature of the phenomena which are to be observed in mixed solvents. For salts which are strong electrolytes in both pure solvents, a close parallelism was generally found between the conductivities and the fluidity of the solvents, but with others, particularly salts of cobalt, nickel, copper, etc., which frequently have very small conductivities in non-aqueous media, the matter appears to be complicated by changes in the degree of dissociation. Apart from this, a considerable amount of work has been done on acids in water-alcoholic solvents,† and on the effect of the addition of small quantities of water to dilute solutions of electrolytes in various solvents.‡ It is found that in hydroxylic and similar solvents the conductivity of strong acids is decreased by the addition of water to a much greater extent than can be accounted for by the change of viscosity, but with other strong uni-univalent salts the effect is of the same order as the viscosity change. This, no doubt, arises from the different mechanism of migration, and can be explained qualitatively at least in terms of recent theories of the mobility of the hydrogen ion.§ On the other hand, if the solute is a weak electrolyte in the non-aqueous solvent the addition of water may cause a large increase of conductivity by increasing the degree of dissociation.[*]

---

* 'Publ. Carneg. Inst.,' 80 and 180.

† Goldschmidt, 'Z. phys. Chem.,' vol. 89, p. 131 (1914); Goldschmidt and Dahll, *ibid.*, vol. 114, p. 1 (1925); Goldschmidt and Aarflot, *ibid.*, vol. 122, p. 371 (1926).

‡ Ulich, 'Z. angew. Chem.,' vol. 41, p. 1141 (1928); Murray, Rust, and Hartley, 'Proc. Roy. Soc.,' A, vol. 126, p. 84 (1929); Hughes and Hartley, 'Phil. Mag.' (7), vol. 15, p. 610 (1933).

§ Hückel, 'Z. Electrochem.,' vol. 34, p. 546 (1920); Bernal and Fowler, 'J. Chem. Phys.,' vol. 1, p. 515 (1933).

Although numerous measurements have been made of the effect of small additions of water to non-aqueous solutions, and a few of the addition of non-electrolytes to aqueous solutions of salts, in no case have measurements been made over the whole range of mixed solvents with sufficient accuracy to determine the conductivities at infinite dilution. We have therefore determined the conductivities at small concentrations in a series of mixtures of water and ethyl alcohol of lithium chloride and potassium iodide, two salts which are strong electrolytes in both of the pure solvents and have derived the equivalent conductivities at infinite dilution. We have also examined the behaviour in these solvents of zinc chloride, a salt which is a strong electrolyte in water and a very weak electrolyte in ethyl alcohol.

EXPERIMENTAL METHODS

Apparatus—The conductivity cell was of the type described by Hartley and Barratt[†] of Pyrex glass, with lightly platinized electrodes approximately 4 cm^2 in area and 1 cm apart. The cell constant, determined at 25° using the potassium chloride solution recommended by Parker and Parker,[‡] was 0·08971. Redeterminations during the investigation showed no appreciable change. A second cell having a cell constant about 10 times as great was used with the stronger zinc chloride solutions.

The resistance bridge was a length of constantan wire stretched over a metre scale, with two similar 50 ω end coils, the resistances of which were found to be equivalent to 573·1 and 572·6 average cm of the bridge wire. The effective length of the bridge, in terms of the average cm of the bridge wire, was thus 1245·7 cm. The bridge wire itself was carefully calibrated with known resistances. The ultimate resistance standards were obtained from a non-inductive box by Tinsley containing 100–11000 ω. The source of the alternating current was a Cambridge valve oscillator, used at a constant frequency of 1000 ~. In order to balance the capacity of the conductivity cell, a variable condenser was connected in parallel with the standard resistance, and adjusted to give the minimum sound in the telephones. A two-valve amplifier was used to increase the sensitiveness of the latter, and except with very high cell resistances the sound minimum did not extend over more than a fraction of a millimetre, and measurements of the same resistance at different parts of the bridge differed by less than 0·1%. The bridge connections were of stout tinned copper wire, of negligible resistance, and the leads to the cell of constantan wire, the resistance of which was determined and subtracted from the cell resistance. The cell was immersed in a thermostat at 25 ± 0·01°, and the room temperature kept at about 20°.

---

[*] *E.g.*, Goldschmidt, 'Z. phys. Chem.,' vol. 91, p. 46 (1916).

[†] 'J. Chem. Soc.,' p. 789 (1913).

[‡] 'J. Amer. Chem. Soc.,' vol. 46, p. 312 (1923).

Materials—Conductivity water was prepared by redistilling the laboratory distilled water from a 5-litre Pyrex flask, through an eight-bulb Pyrex fractionating column, in a stream of CO_2-free air, the first fractions being rejected. A good quality ($0 \cdot 5$–$0 \cdot 7 \times 10^6$ mhos) water was readily obtained by this simple method. Ethyl alcohol was purified and dried as previously described,* and preserved out of contact with the carbon dioxide of the atmosphere.

Lithium chloride was prepared by recrystallizing the Kahlbaum pure reagent from dry alcohol and dried in a stream of hydrogen at 200° C. Zinc chloride was prepared as described in Part IV.† The other salts used were twice recrystallized from conductivity water and dried to constant weight at a suitable temperature. The potassium chloride was heated to dull redness for 20 minutes before use.

Procedure—A weighed quantity of the solvent was placed in the cell and its resistance determined. Small additions of a salt solution of suitable concentration in the same solvent were then made from a weight pipette, and the resistance determined after each addition. With mixed solvents, the appropriate quantities of alcohol and water were weighed into the conductivity cell and a quantity of the mixed solvent then withdrawn for the preparation of the salt solution. Precautions were taken during the transfers to prevent the absorption of atmospheric carbon dioxide. All concentrations were determined by weighing. The volume concentrations were calculated from the densities of the mixed solvents, obtained by interpolation from 'International Critical Tables,' vol. 3, assuming that the small amounts of salts added do not appreciably change the density.

VISCOSITY OF WATER-ALCOHOL SOLUTIONS

The viscosity of water-alcohol solutions has been determined at 25° by Dunstan and Thole.‡ The solutions measured are, however, somewhat widely spaced and do not permit accurate interpolation. We therefore determined the viscosities of some additional solutions, mostly at lower concentrations of alcohol. The viscosimeter was of the type described by Washburn and Williams,* consisting of a bulb of about 10 cc capacity, a capillary U-tube 0·02–0·03 cm in diameter and 20 cm long, opening into a large flat bulb 6 cm high and 8 cm across. The relative viscosities of two liquids, when the time of flow is sufficiently long, are given by

---

* 'Proc. Roy. Soc.,' A, vol. 125, p. 694 (1929).

† *Ibid.*, A, vol. 138, p. 450 (1932).

‡ 'J. Chem. Soc.,' vol. 93, p. 1556 (1909). *Cf.* Bingham, White, Thomas, and Cadwell, 'Z. phys. Chem.,' vol. 83, p. 641 (1913).

$$\frac{\eta}{\eta_0} = \frac{t\,(\mathrm{D} - \lambda)}{t_0\,(\mathrm{D}_0 - \lambda)} \,.\, \mathrm{P},$$

where t, t_0 are the times, D, D_0 the densities of the liquids, and λ the density of air. The factor P, determined by calibrating the viscosimeter with water and alcohol, was 1·0028. The values obtained, which are in reasonable agreement with the curves of Dunstan and Thole, are given in Table I.

TABLE I—Viscosity of some Alcohol-Water Solutions

Mols % alcohol	D_4^{25}	t (secs)	η^{25}
0·0	0·9971	684·9	0·00891
1·48	0·9875	770·1	0·01027
4·78	0·9784	1090·2	0·01394
8·23	0·9683	1306·5	0·01712
9·56	0·9669	1412·5	0·01793
11·29	0·9597	1532·5	0·01990
12·69	0·9543	1606·5	0·02075
15·29	0·9479	1802·2	0·02240
25·33	0·9178	1997·0	0·02391
49·91	0·8597	1759·2	0·01980
69·54	0·8257	1469·9	0·01592
100·00	0·7851	1072·2	0·01101

CONDUCTIVITIES OF SOME ALKALI HALIDES IN WATER-ALCOHOL MIXTURES

The measurements with these salts are given in Table II. Here k is the specific conductivity of the solvent in reciprocal megohms, which is subtracted from the conductivity of the solution ; c the concentration of the salt in gm-equivalents per litre, and Λ_c the equivalent conductivity. The Kohlrausch equation ($\Lambda_c = \Lambda_0 - x\sqrt{c}$) holds for the salts investigated in the mixed solvents as well as in water and alcohol. The limiting conductivity Λ_0 was determined by extrapolating the $\Lambda_c - \sqrt{c}$ curve to

---

* 'J. Amer. Chem. Soc.,' vol. 35, p. 737 (1913).

TABLE II—Electrical Conductivities of Salts in Water-Alcohol Solvents

1—Lithium chloride

Water

$k = 1·01$

$\Lambda_0 = 115·05$

$x = 100$

$\sqrt{c} \times 10^2$	Λ_c	Λ_c (calc.)
0·8412	116·25	114·21
1·210	113·88	113·84
2·436	112·23	112·61
3·907	111·13	111·14
5·327	109·69	109·72
6·518	108·55	108·53

2·17 mols % alcohol

$k = 1·01$

$\Lambda_0 = 92·97$

$x = 67$

$\sqrt{c} \times 10^2$	Λ_c	Λ_c (calc.)
0·9378	92·83	92·34
1·706	91·87	91·83
2·466	91·41	91·34
3·563	90·57	90·59
4·305	90·03	90·09
5·467	89·37	89·32
6·407	88·72	88·68

10·83 mols % alcohol

$k = 0·41$

$\Lambda_0 = 53·48$

$x = 42$

$\sqrt{c} \times 10^2$	Λ_c	Λ_c (calc.)
0·9166	53·15	53·10
1·893	52·72	52·68
2·533	52·14	52·42
3·455	52·11	52·03
4·595	51·54	51·55
6·313	50·92	50·83
7·575	50·35	50·30

17·19 mols % alcohol

$k = 0·50$

$\Lambda_0 = 44·11$

$x = 46$

$\sqrt{c} \times 10^2$	Λ_c	Λ_c (calc.)
0·8772	44·65	43·71
1·425	43·50	43·45
2·473	43·04	42·97
3·032	42·68	42·71
3·821	42·26	42·35
5·319	41·71	41·66
6·333	41·51	41·20

46·87 mols % alcohol

$k = 0·19$

$\Lambda_0 = 37·20$

$x = 65$

$\sqrt{c} \times 10^2$	Λ_c	Λ_c (calc.)
0·9563	36·89	36·58
1·489	36·37	36·23
2·358	35·72	35·67
3·109	35·22	35·18
4·006	34·62	34·60
4·625	34·24	34·19
5·281	33·84	33·77

93·55 mols % alcohol

$k = 0·028$

$\Lambda_0 = 38·41$

$x = 138$

$\sqrt{c} \times 10^2$	Λ_c	Λ_c (calc.)
0·8565	37·97	38·23
1·725	36·12	36·02
2·735	34·52	34·64
3·677	33·13	33·34
4·466	33·11	32·24
5·268	31·19	31·22

100 mols % alcohol : $k = 0·053$, $\Lambda_0 = 38·99$, $x = 145$

$\sqrt{c} \times 10^2$	Λ_c	Λ_c (calc.)	$\sqrt{c} \times 10^2$	Λ_c	Λ_c (calc.)
0·756	38·05	37·90	2·740	35·06	35·03
1·142	37·49	37·34	3·410	34·03	34·04
1·401	36·97	36·96	3·918	33·24	33·31
2·053	36·14	36·01			

TABLE II—(continued)

2—Potassium iodide

Water : k = 1·086, Λ_0 = 151·05, x = 100

$\sqrt{c} \times 10^2$	Λ_c	Λ_c (calc.)	$\sqrt{c} \times 10^2$	Λ_c	Λ_c (calc.)
1·122	149·96	149·93	3·815	147·49	147·24
1·608	149·40	149·44	4·704	146·09	146·35
2·447	148·57	148·60	5·420	145·51	145·63

2·92 mols % alcohol

k = 0·55

Λ_0 = 123·73

x = 101

$\sqrt{c} \times 10^2$	Λ_c	Λ_c (calc.)
1·284	122·68	122·44
1·969	121·97	121·74
2·769	120·69	120·93
3·461	119·95	120·24
4·015	119·42	119·66
4·832	119·36	118·85

6·83 mols % alcohol

k = 0·33

Λ_0 = 93·67

x = 57

$\sqrt{c} \times 10^2$	Λ_c	Λ_c (calc.)
0·8378	92·51	93·19
1·406	92·86	92·87
1·962	92·60	92·55
2·707	92·24	92·13
3·375	91·92	91·75
4·388	91·27	91·17
5·171	90·69	90·72

22·70 mols % alcohol

k = 0·292

Λ_0 = 55·05

x = 43

$\sqrt{c} \times 10^2$	Λ_c	Λ_c (calc.)
1·387	54·49	54·45
2·195	54·09	54·11
3·016	53·85	53·75
3·814	53·33	53·41
4·692	52·95	53·03
5·976	52·51	52·47

44·63 mols % alcohol

k = 0·192

Λ_0 = 48·12

x = 72

$\sqrt{c} \times 10^2$	Λ_c	Λ_c (calc.)
1·288	47·31	47·19
1·995	46·73	46·64
2·671	46·34	46·20
3·394	45·73	45·68
4·114	45·35	45·16
4·915	44·99	44·58
5·850	44·36	43·90

75·50 mols % alcohol

k = 0·119

Λ_0 = 49·15

x = 134

$\sqrt{c} \times 10^2$	Λ_c	Λ_c (calc.)
1·054	(46·11)	—
1·461	47·33	47·20
2·116	46·37	46·31
3·277	44·78	44·76
4·336	43·49	43·34
5·388	42·29	41·93

100 mols % alcohol

k = 0·065

Λ_0 = 50·72

x = 210

$\sqrt{c} \times 10^2$	Λ_c	Λ_c (calc.)
1·392	48·03	47·80
1·717	47·23	47·11
2·229	46·21	46·03
2·686	45·21	45·08
3·306	43·82	43·77
5·166	40·28	39·86

TABLE II—(continued)

3—Other salts

NaCl in 1·86 mols % alcohol k = 0·70 Λ_0 = 107·0 x = 85		NaI in 2·61 mols % alcohol k = 0·50 Λ_0 = 99·9 x = 61	
$\sqrt{c} \times 10^2$	Λ_c	$\sqrt{c} \times 10^2$	Λ_c
1·119	106·3	0·897	(98·30)
1·610	105·6	1·969	98·81
2·213	104·9	2·675	98·23
3·230	104·4	3·976	97·53
4·103	103·4	4·830	96·96
4·665	103·0		
5·653	102·3		

zero concentration. The values of Λ_0 and x so obtained are given at the head of each section of the table, and the calculated values of Λ_c show that these constants are capable of reproducing the experimental figures with considerable accuracy, except in the case of a few of the most dilute solutions.

DISCUSSION

We shall consider first the variation of the Λ_0 values with the solvent composition. In fig. 1, Λ_0 and $1/\eta$ are plotted against the molar fraction of alcohol, and it can be seen that the conductivities follow approximately the same course as the fluidity curve up to about 20 mols % alcohol, but in greater proportions of alcohol there is a steadily increasing divergence between the two. Taking no account, for the moment, of the minor divergences of the initial parts of the curves we see that the mobilities of ions at infinite dilution run parallel with the fluidity of the solvent in small proportions of alcohol, while in solvents containing more than 20 mols % alcohol these quantities differ to a steadily increasing extent.

Walden has shown* that for large organic ions in different solvents the ratio of the ionic mobility at infinite dilution (l_0) and the fluidity of the solvent (ϕ) is nearly constant. That this does not hold for the simple inorganic ions is evident from the following values of ($l_0\eta$) at 25°.†

---

* 'Z. phys. Chem.,' vol. 55, p. 207 (1906); vol. 78, p. 257 (1912); Walden and Ulich, *ibid.*, vol. 107, p. 219 (1923).

† Barak and Hartley, *ibid.*, A, vol. 165, p. 290 (1933).

	Water	MeOH	EtOH
Li^+	0·36	0·22	0·16
K^+	0·67	0·30	0·24
Cl^-	0·69	0·29	0·26
I^-	0·68	0·33	0·31

These differences have generally been attributed to the differences of the solvation of the ions in the various solvents. The measurements given above confirm this view, for the steady fall of the ratio of the conductivity to the fluidity begins at about the same point as that at which, as has been shown by measurements of the molar refractivities and partial molar volumes of salts in these solvents,* the solvation of the ions by alcohol molecules begins to take place.

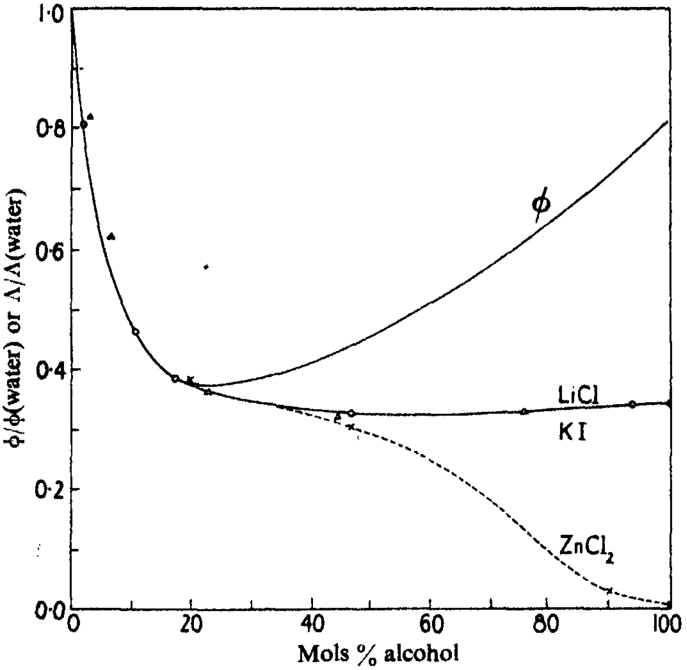

FIG. 1—Relative fluidities and equivalent conductivities in water-alcohol solvents. —⊙— $\Lambda_0/(\Lambda_0)$*water* for LiCl ; —×— $\Lambda/(\Lambda)$*water* for $ZnCl_2$ at $c = 0\cdot0004$; —△— $\Lambda_0/(\Lambda_0)$*water* for KI ; ϕ curve of fluidity relative to water.

The nature of the divergence of the mobilities and the fluidity of the solvents is better shown by the values of $\Lambda_0\eta/(\Lambda_0\eta)_{water}$ which are given in Table III. With lithium chloride this ratio remains nearly constant

---

[*] Butler and Lees, ' Proc. Roy. Soc.,' A, vol. 131, p. 382 (1931).

up to 20 mols % alcohol, but with potassium iodide it is markedly increased by the first additions of alcohol. That is, in this case the mobilities of the ions are decreased to a smaller extent by the addition of alcohol than the decrease of the fluidity of the solvent. Some isolated measurements were made with other salts to see how this effect varies with the nature of the salt. From the results, which are shown on a larger scale in the inset diagram, fig. 2, it can be seen that the initial rise in the ratio $\Lambda_0\eta/(\Lambda_0\eta)_{\text{water}}$ is for different ions in the order $K^+ > Na^+ > Li^+$, while iodides and chlorides have about the same effect.

TABLE III—Variation of Λ_0 with Viscosity of Solvent

Salt	Mols % alcohol	Λ_0	η	$\Lambda_0\eta/(\Lambda_0\eta)_{\text{water}}$
LiCl	0·00	115·05	0·00891	1·0000
	2·17	92·97	0·01110	1·007
	10·83	53·48	0·01935	1·009
	17·19	44·11	0·02318	0·9974
	46·87	37·20	0·02050	0·7437
	93·55	38·41	0·01187	0·4447
	100·00	38·99	0·01101	0·4187
KI	0·00	151·65	0·00891	1·000
	2·92	123·73	0·01190	1·095
	6·83	93·67	0·01582	1·110
	22·70	55·05	0·02309	0·946
	44·63	48·12	0·02098	0·749
	75·50	49·15	0·01490	0·543
	100·00	50·72	0·01101	0·414
NaCl..........	1·86	107·02	0·01082	1·027
NaI	2·61	99·93	0·01161	1·022

An effect of this kind might be expected on the grounds that (1) the frictional resistance between an ion, which is solvated entirely by water, and the mixed solvent will be less than that which corresponds with the bulk viscosity of the latter ; (2) the viscosity of the solvent outside the solvation sphere may also be less than that at a distance from the ion on account of the salting-out of alcohol molecules in this region. Discussing the proportionality between the conductivities of salts and the fluidity of the solvent, on the basis of the scanty measurements made in dilute solutions of non-electrolytes, Kraus has pointed out* that the deviation is greater the greater the molecular weight of the non-electrolyte. Since substances of high molecular weight are salted-out to a greater extent, this indicates that (2) may be the correct explanation. It is not clear, however, why the effect with potassium is greater than that with sodium, and lithium, since the usual order of magnitude of the salting-out produced by salts of these ions is the reverse. No information is available as to the actual salting-out order in alcoholic solutions.

---

* 'The properties of electrically conducting systems' (Chemical Catalogue Co.) p. 121 (1922).

While Λ_0 is determined by the properties of the solvent in the immediate vicinity of the ions, the slope x of the $\Lambda_c - \sqrt{c}$ curves, which depends on the mean properties of the solvent between the ions, should be comparatively uninfluenced by the interaction of the ions and neighbouring solvent molecules. According to Onsager's theory* the value of x for a uni-univalent electrolyte is given by

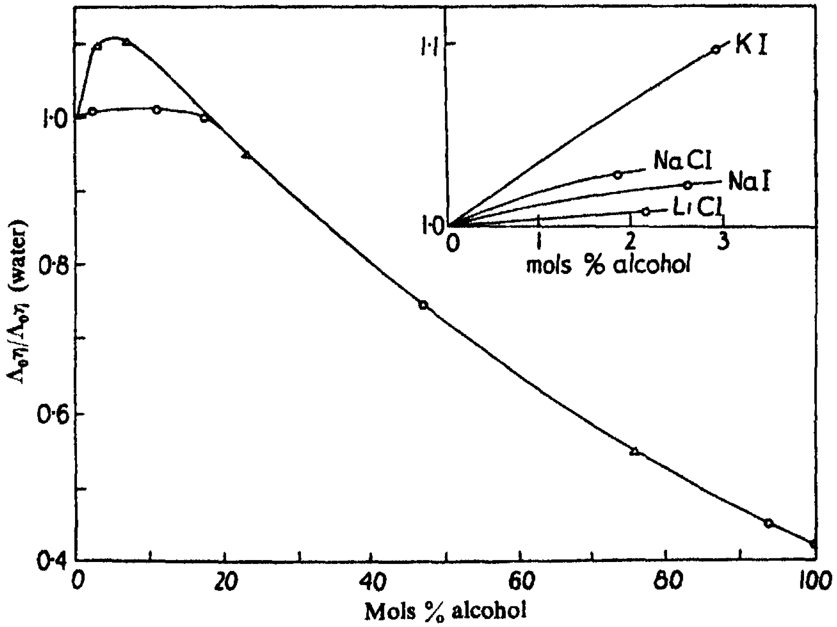

FIG. 2—Variation of $\Lambda_0\eta/(\Lambda_0\eta)$*water* with composition of solvent. —⊙— LiCl; —△— KI.

$$x = \sqrt{2}\left(\frac{5 \cdot 78 \times 10^5\,\Lambda_0}{(\mathrm{DT})^{3/2}} + \frac{58 \cdot 0}{(\mathrm{DT})^{1/2}\,\eta}\right),$$

where D is the dielectric constant and η the viscosity of the medium. The values of x calculated by this equation, using the dielectric constants of alcoholic solutions determined by Åkerlöf,† are given in Table IV.

---

* 'Phys. Z.,' vol. 27, p. 388 (1926); vol. 28, p. 277 (1927).

† 'J. Amer. Chem. Soc.,' vol. 54, p. 4125 (1930).

The positive deviation between the observed and the calculated slopes in the pure solvents, which is particularly great for potassium iodide in ethyl alcohol, has usually been regarded as due to ion-association. It can be seen that the deviation is less in the mixed solvents, and becomes negative in the region of 10–20 mols % alcohol.

TABLE IV

Salt	Mols % alcohol	x (obs.)	x (calc.)	Δ (%)
LiCl	0·00	100	86·5	+16
	2·17	67	72	−7
	10·83	42	47	−11
	17·19	46	43	+7
	46·87	65	62	+5
	93·55	138	128	+8
	100·00	145	139	+4
KI	0·00	100	95	+5
	6·83	57	61	−7
	22·70	43	51	−16
	44·63	72	67	+7
	75·50	134	111	+21
	100·0	210	152	+38

On the whole Onsager's equation applies more exactly in the mixed than in the pure solvents, and if a positive deviation is rightly taken as evidence of ion association, it may be concluded that the mixed solvents are better ionizing media than the pure solvents, or more especially, than ethyl alcohol.

CONDUCTIVITY OF ZINC CHLORIDE IN WATER, ETHYL ALCOHOL, AND THEIR MIXTURES

Zinc chloride is a very weak electrolyte in ethyl alcoholic solution, and the range of mixed solvents between water and the alcohol should show every variety of behaviour from the completely dissociated to the nearly undissociated salt. The experimental measurements, which were carried to greater concentrations than in the previous salts studied, are given in Table V. In water its behavior is that of a typical strong electrolyte. The initial slope of the $\Lambda_c - \sqrt{c}$ curve is 175, in good agreement with that calculated by Onsager's equation (172), for dissociation as $ZnCl_2 = Zn^{++} + 2Cl^-$. Even at concentrations up to $c = 1$ there is no sign of incomplete dissociation, for the slope x decreases

TABLE V—Conductivities of Zinc Chloride in Water-Alcohol Mixtures

Water		19·64 mols % alcohol		46·62 mols % alcohol	
$k = 0{\cdot}99$		$k = 0{\cdot}47$		$k = 0{\cdot}21$	
$\sqrt{c} \times 10^2$	Λ_c	$\sqrt{c} \times 10^2$	Λ_c	$\sqrt{c} \times 10^2$	Λ_c
1·765	122·8	1·298	47·05	1·393	37·96
3·209	119·8	2·111	46·55	2·738	34·77
5·640	116·5	3·585	45·42	3·799	31·42
7·243	115·4	4·883	44·40	6·052	25·35
8·633	114·3	6·066	43·39	8·194	20·84
10·22	112·8	7·617	42·09	9·972	17·98
		8·431	41·50	11·52	16·06
$k = 1{\cdot}10$		13·26	37·38	25·59	7·16
		26·28	29·85	36·00	5·44
12·58	110·3	43·47	22·14	54·20	4·08
17·80	105·4	63·65	16·19	78·91	3·39
25·17	99·47	96·21	11·14	119·0	2·85
31·87	94·92				
50·43	85·19				
55·60	82·55				
71·32	74·69				
100·8	60·91				
122·8	51·25				

89·92 mols % alcohol			100 mols % alcohol		
$k = 0{\cdot}076$			$k = 0{\cdot}029$		
$\sqrt{c} \times 10^2$	Λ_0	k_1	$\sqrt{c} \times 10^2$	Λ_0	k_1
1·834	4·10	$1{\cdot}54 \times 10^{-6}$	1·329	0·90	$3{\cdot}96 \times 10^{-8}$
3·067	2·47	1·50	1·888	0·63	3·70
5·142	1·70	1·95	2·839	0·43	3·82
6·825	1·34	2·13	4·299	0·29	4·02
8·511	1·13	2·34	5·591	0·26	5·42
10·48	0·95	2·50	6·871	0·217	5·90
11·66	0·88	2·63	7·723	0·197	6·17
20·87	0·59	3·81	14·55	0·130	9·1
34·30	0·49	7·05	22·88	0·111	—
49·23	0·46	—	34·33	0·106	—
74·08	0·45	—	50·98	0·109	—
99·84	0·46	—	71·54	0·120	—

steadily in the more concentrated solutions, as is also the case with the strong uni-univalent electrolytes.

It can be seen in fig. 1, which shows the curve of $\Lambda/(\Lambda)_w$ at $c = 0{\cdot}0004$, that in very dilute solutions the change of conductivity produced by the addition of alcohol is at first of the same order as the fluidity change, and the conductivity relative to water follows the same course as that observed with lithium chloride and potassium iodide to about 40 mols %

alcohol. Beyond this, it falls below the values of the uni-univalent salts and becomes very small in pure alcohol. Assuming that the Λ_c values for the completely dissociated electrolyte follow a similar course to those of the uni-univalent salts, we see that at $c = 0{\cdot}0004$ the degree of dissociation remains practically unity until 40 mols % alcohol are present, and from this point it decreases rapidly to about 1% in pure alcohol.

In the solution containing 20 mols % alcohol, the initial slope of the $\Lambda_c - \sqrt{c}$ curve (81) is of the same magnitude as that which is to be expected on Onsager's theory, for complete dissociation ; although data is lacking for a precise calculation. However, the experimental slope (275) in the 46·6% alcohol is much greater than that given by Onsager's theory and it is evident that although the salt is largely dissociated at $c = 0{\cdot}0004$, the degree of dissociation decreases rapidly with growing concentration. From these considerations and from the form of the conductivity curves for constant concentrations of zinc chloride, fig. 3, it may be concluded that in the more concentrated solutions ($c = 0{\cdot}01 - 0{\cdot}5$), alcohol depresses the degree of dissociation when present in comparatively small proportion.

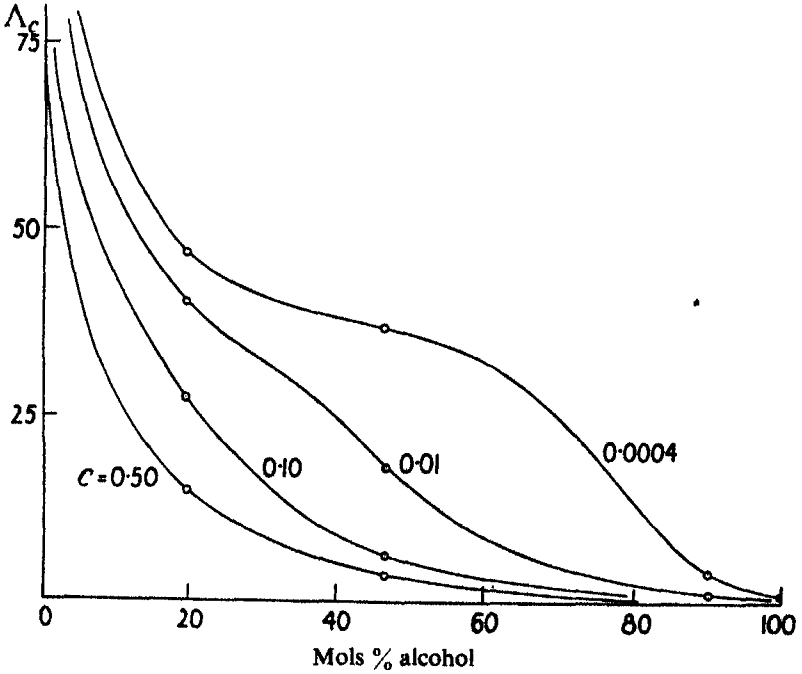

FIG. 3—Equivalent conductivities of zinc chloride in water-alcohol mixtures.

In both 90% and 100% alcohol the change of conductivity with concentration is not greatly different from that of a weak ***uni-univalent*** electrolyte as is shown by the Ostwald dissociation constants ($k_1 = \alpha^2 c/(1 - \alpha)$, where $\alpha = \Lambda_c/\Lambda_0$) given in Table V, which were calculated on the assumption that $\Lambda_0 = 45$ in 100% alcohol and 44 in 90% alcohol. These values, in fact, increase linearly with $\sqrt{c}$ and, extrapolating to zero concentration, we find that in 100% alcohol, $k_1 = 3 \cdot 8 \times 10^{-8}$, in 90% alcohol, $k_1 = 1 \cdot 6 \times 10^{-6}$, *i.e.*, the dissociation constant is increased about 40 times by the presence of 10 mols % water.* Goldschmidt† found that with weak acids in alcohol the dissociation constant was increased about 120 times by the same proportion of water. Comparatively small amounts of water thus have a smaller effect on the dissociation of zinc chloride than on that of weak acids, but since zinc chloride becomes a comparatively strong electrolyte when 50 mols % water are present it is evident that with further additions the effect is relatively greater. From this we can draw the conclusion that the effect of water on the dissociation increases with a higher power of its concentration with zinc chloride than with weak acids, so that more molecules of water are concerned in the dissociation process of the former.

Zinc chloride has been considered in some detail because, so far as can be judged from the limited information available, it is typical of a considerable group of salts, including the halides of cadmium and mercury and probably also to some extent those of (divalent) copper, cobalt, iron, nickel, etc. Some of these salts are incompletely dissociated in aqueous solution, but they all appear to be considerably weaker electrolytes in alcoholic solution. Since some of these salts readily give rise to complex ions, it is necessary to consider whether this occurs to any appreciable extent in the zinc chloride solutions. If k_3 is the equilibrium constant of the reaction

$$2ZnCl_2 = ZnCl_3^- + ZnCl^+, \qquad (\gamma)$$

and k_1 the primary dissociation constant of zinc chloride, as

$$ZnCl_2 = ZnCl^+ + Cl^-, \qquad (\alpha)$$

---

* If different values of Λ_0 (within reasonable limits) are used, a similar variation of K_0 with concentration is obtained. The conclusion that zinc chloride dissociates almost entirely as a uni-univalent electrolyte is thus not a consequence of a particular choice of Λ_0. The actual values of the dissociation constants obtained here and below do, however, depend on the values of Λ_0 assumed. The values given are estimates based on what appear to be the most probable values of the ionic mobilities.

† 'Z. phys. Chem.,' vol. 91, p. 46 (1916).

it can be shown that to a first approximation, assuming that the ions Zn^{++} and $ZnCl_4^{=}$ are not present in appreciable concentrations, and that the mobilities of the ions Cl^- and $ZnCl_3^-$ are not greatly different, the molecular conductivity of zinc chloride is

$$\Lambda_c = (\Lambda^0_{ZnCl^+} + \Lambda^0_{ZnCl_3^-})\sqrt{k_3 + (k_1/c)},$$

where c is the total concentration of zinc chloride. When k_3 is much greater than k_1/c, the conductivity is therefore entirely determined by the reaction (1) and is independent of the concentration. This appears to be so at large concentrations of zinc chloride in 90 and 100% alcohol, for in these solvents (Table V) Λ_c reaches a nearly constant value* from which an estimate of k_3 can be made. Taking $(\Lambda^0_{ZnCl^+} + \Lambda^0_{ZnCl_3^-})$ as 50 in both solutions, we find for 100% alcohol, $k_3 = 1 \cdot 6 \times 10^{-5}$; for 90% alcohol, $k_3 = 3 \times 10^{-4}$.

A confirmation of the former value has been obtained by Mr. W. J. C. Orr, in this laboratory, by measurements of the conductivities of alcoholic solutions containing lithium chloride at a constant and zinc chloride at a variable concentration. In these solutions the dissociation of zinc chloride is largely repressed by the added chloride, and the conductivity is determined by the equilibrium

$$ZnCl_3^- = ZnCl_2 + Cl^-, \qquad (\beta)$$

The conductivity of the lithium chloride solution is increased a little by the addition of zinc chloride, owing to the replacement of Cl^- by $ZnCl_3^-$ ions, which have a slightly greater mobility. It was found that with $c\,(LiCl) = 9 \cdot 6 \times 10^{-3}$, half the total increase occurred when $c\,(ZnCl_2) = 6 \times 10^{-3}$. From this it follows that the primary dissociation constant of $ZnCl_3^-$ is about $k_2 = 1 \cdot 5 \times 10^{-3}$; and therefore $k_3 = k_1/k_2 = 2 \times 10^{-5}$, which agrees with the previous estimate. It thus appears to be possible to determine by these methods the dissociation constants of undissociated molecules and complex ions in salt solutions which are not dissociated to a considerable extent.

We are grateful to the Department of Industrial and Scientific Research for the award of a maintenance grant (1930–1932) to R. T. H. which enabled him to take part in this work. We thank the Committee of the Moray Fund for a grant which enabled us to construct the valve amplifier, and to Imperial Chemical Industries, Ltd., for their grant.

---

* The values given in Table V are equivalent conductivities and must be doubled for this purpose.

SUMMARY

1. The electrical conductivities of lithium chloride, potassium iodide, and zinc chloride have been determined in a series of water-ethyl alcohol solutions.

2. The equivalent conductivities at infinite dilution of the first two salts, which are strong electrolytes in both pure solvents, have been determined. The change of Λ_0 is approximately proportional to the fluidity of the solvent until about 20 mols % of alcohol are present. The solvation of the ions by alcohol molecules begins here and gives rise in greater proportions of alcohol to a steadily increasing divergence between the two. The Kohlrausch equation $\Lambda = \Lambda_0 - x\sqrt{c}$ is obeyed in all the solvents, and the values of x show on the whole a better agreement with Onsager's equation in the mixed than in the pure solvents.

3. Zinc chloride is apparently completely dissociated in water even at high concentrations, while in ethyl alcohol its behaviour is not far different from that of a weak uni-univalent electrolyte having a dissociation constant, $K_0 = 4 \times 10^{-8}$. In the mixed solvents at low concentrations ($c = 4 \times 10^{-4}$) the degree of dissociation remains unity until about 40 mols % alcohol are present and then falls rapidly to comparatively small values, but at greater concentrations the alcohol begins to reduce the degree of dissociation when present in smaller proportions. An estimate of the extent of complex ion formation in the alcoholic solutions is made.

Absorption Bands of HCN in the Photographic Infra-red

By G. HERZBERG and J. W. T. SPINKS, Physikalisches Institut, Technische Hochschule, Darmstadt, Germany

(*Communicated by A. J. Allmand, F.R.S.—Received June* 25, 1934)

[PLATE 1]

The infra-red absorption spectrum of HCN has previously been investigated photographically by Badger and Binder.* Since their publication, plates have become available which are sensitive much further into the infra-red. The most recent Agfa plates have their maximum of sensitivity at 10600 A and have been used by us as far as 12300 A† with a tungsten lamp or even 12900 A‡ with the sun. We have now used these plates to investigate the infra-red absorption spectrum of HCN up to 12300 A. While Badger and Binder found only two very weak bands at 7912 and 8563 A we have found two rather strong bands at 10385 A and 11645 A which could be accurately measured and analysed.§ In addition we have found an interesting pressure effect on the line width.

The whole infra-red spectrum of this molecule and the vibrational energy scheme has recently been discussed by Adel and Barker‖ who have also measured several new bands in the far infra-red.

EXPERIMENTAL

A glass tube 2 m long and 45 mm diameter with plane glass windows fused on was used for most of the experiments. For one experiment a tube 40 cm long was also used. The tubes were filled with HCN gas from a tube containing pure liquid HCN, and then sealed off.

Light was passed from a tungsten lamp twice through the tube and fell on the slit of the 3 m grating spectrograph. The first order was used

---

* 'Phys. Rev.,' vol. 37, p. 800 (1931).

† Herzberg and Spinks, 'Z. Physik,' vol. 89, p. 474, (1934).

‡ Herzberg, 'Nature,' vol. 133, p. 759 (1934).

§ With ordinary infra-red methods and rather low dispersion Brackett and Liddel ('Smithonian Inst.,' vol. 85, No. 5, 1931) had already observed these bands.

‖ 'Phys. Rev.,' vol. 45, p. 277 (1934).

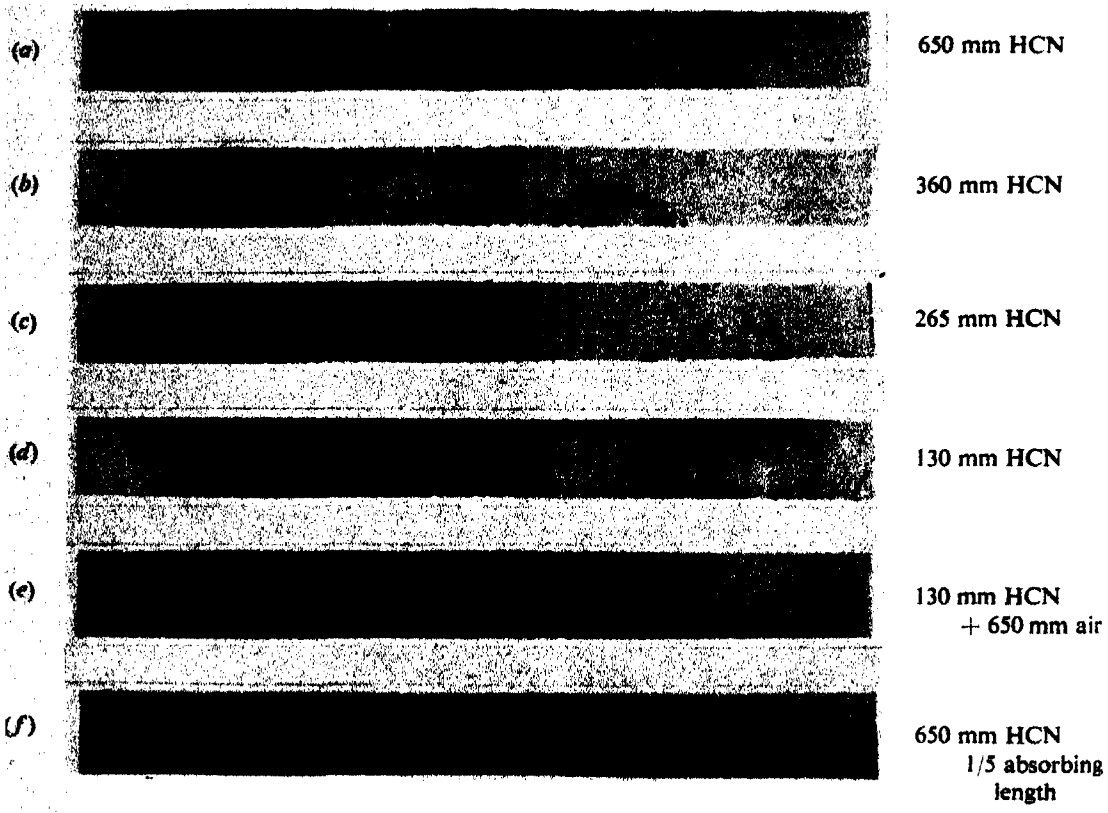

FIG. 1—HCN-band at 1·04 μ

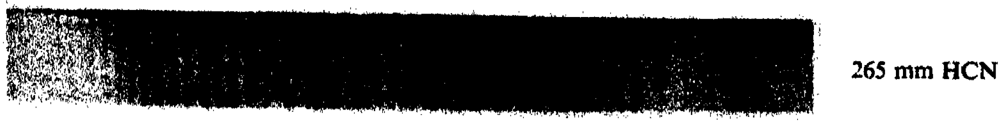

FIG. 2—HCN-band at 1·16 μ

giving a dispersion of 5·4 A mm. A slit width of 0·05 mm was used throughout. Measurements were made in the usual manner.†

ROTATIONAL STRUCTURE

Spectrograms of the two new bands at 1·04 μ and 1·16 μ respectively are given in figs. 1 and 2, Plate 1. Table I contains the wave numbers of the band lines. The 1·04 μ band was measured on a spectrogram at low pressure where the lines are quite sharp (*cf.* below) so that the measurements are rather accurate (mean error about ± 0·015 cm^{-1}) whereas the 1·16 μ band could only be measured on a spectrogram taken at an intermediate pressure where the lines are broader and the measurements less accurate (mean error ± 0·05 cm^{-1}). Therefore one

TABLE I—HCN BANDS AT 1·04 μ AND 1·16 μ

	ν_0 = 9627·04 cm^{-1}		ν_0 = 8585·6 cm^{-1}	
J	R(J)	P(J)	R(J)	P(J)
0	9629·935	—	—	—
1	32·761	9624·108	8591·32	—
2	35·521	21·073	94·10	8579·55
3	38·250	17·962	96·81	76·59
4	40·887	14·773	99·41	73·40
5	43·440	11·608	8602·03	70·16
6	45·889	08·354	04·51	66·90
7	48·349	04·983	07·00	63·62
8	50·728	01·594	09·38	60·22
9	53·056	9598·088	11·72	56·73
10	55·289	94·574	13·98	53·32
11	57·482	90·956	16·21	49·69
12	59·595	87·344	18·32	46·05
13	61·680	83·588	20·49	42·39
14	63·634	79·820	22·48	38·64
15	65·531	75·959	24·48	34·79
16	67·395	72·054	26·34	31·01*
17	69·179	68·069	28·20	26·93*
18	70·937	64·034	29·96	23·11*
19	72·566	59·936	31·71	19·06*
20	74·117	55·778	33·28	
21	75·695	51·645	34·98	
22	77·067	47·194*	36·70	
23	78·521	42·963*	37·93*	

* Means very weak lines difficult to locate under the microscope and therefore less accurate than the others.

---

† *Cf. e.g.*, Herzberg and Spinks, ' Z. Physik,' vol. 89, p. 474 (1934).

more figure is given for the lines of the 1·04 μ band than for those of the 1·16 μ band. The accuracy given above is only relative. Because of a possible shift between iron arc comparison spectrum and HCN spectrum the absolute accuracy is somewhat less. Therefore for the ν_0-values the last figure has been dropped.*

As the bands have simple P- and R-branches it is at once evident that the molecule HCN must be linear, a conclusion already reached by Badger and Binder (*loc. cit.*). So the simple relations valid for diatomic molecules can be applied. The rotational constants B for the three vibrational levels involved follow from the combination differences

$$\Delta_2F'' = R(J-1) - P(J+1)$$
$$\Delta_2F' = R(J) - P(J).$$

These are tabulated in Table II for the two bands. As will be seen the Δ_2F'' values for the two bands agree within ± 0·08 cm^{-1} or even less, *i.e.*, within the experimental error,† whereas the Δ_2F' values show a very slight difference.

For the rigid rotator Δ_2F should be a strictly linear function of J. That this is not the case is seen in fig. 3 where the differences of the observed Δ_2F'' values for the more accurately measured 1·04 μ band are plotted against $4B(J + 1/2)$ with $4B = 5{\cdot}9$. The deviation from a straight line can be completely accounted for by the introduction of the rotational constant D in the expression for the rotational energy

$$F(J) = BJ(J+1) - DJ^2(J+1)^2$$

which accounts for the stretching caused by centrifugal force.

A D value of $3{\cdot}63 \,.\, 10^{-6}$ cm^{-1} is empirically found which may be used for all three vibrational states.‡ For diatomic molecules the rotational constant D is usually accurately determined by Kratzer's theoretical relation $D = 4B^3/\omega^2$. It is, however, not at once possible to apply this relation to polyatomic molecules because of the ambiguity in ω. Still it seems evident that by inserting into this formula the frequency of a vibration which in one half period produces a displacement

---

* For the 1·16 μ bands the temperature of the grating unfortunately was not constant so that the shift for this band might be appreciable. Because of lack of time the exposure could not be repeated.

† Only the differences calculated from the very weak lines marked by * in Table I show slightly larger deviations.

‡ This seems to be the first time that the effect of stretching has been calculated for a polyatomic molecule, *cf.* also Hersberg and Spinks Z. Physik, vol. 91, p. 386 (1934).

TABLE II—COMBINATION DIFFERENCES

J	$\Delta_2F''(J) = R(J-1) - P(J+1)$		$\Delta_2F'(J) = R(J) - P(J)$	
	Band 1·04 μ	Band 1·16 μ	Band 1·04 μ	Band 1·16 μ
1	8·862	—	8·653	—
2	14·799	14·73	14·448	14·55
3	20·748	20·70	20·288	20·22
4	26·642	26·65	26·114	26·01
5	32·533	32·51	31·832	31·87
6	38·457	38·41	37·535	37·61
7	44·295	44·29	43·366	43·38
8	50·261	50·27	49·134	49·16
9	56·154	56·06	54·968	54·99
10	62·100	62·02	60·715	60·66
11	67·945	67·93	66·526	66·52
12	73·894	73·82	72·251	72·27
13	79·775	79·68	78·092	78·10
14	85·721	85·70	83·814	83·84
15	91·584	91·47	89·572	89·69
16	97·462	97·55	95·341	95·33
17	103·361	103·23	101·110	101·27
18	109·243	109·14	106·903	106·85
19	115·159		112·630	112·65
20	120·921		118·339	
21	126·923		124·050	
22	132·732		129·873	
23			135·558	

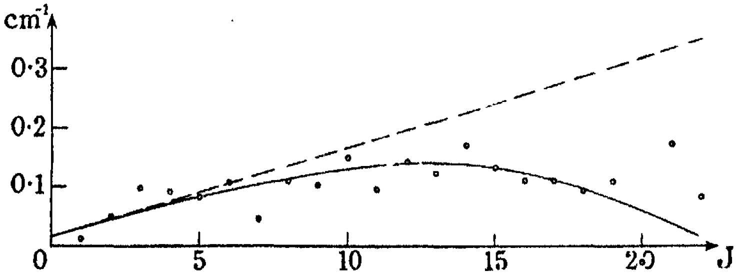

FIG. 3—Deviation of Δ_2F'' values from $5{\cdot}9\,(J + \frac{1}{2})^2$

of the nuclei in the same sense as the centrifugal force (*i.e.*, away from the centre of gravity) one should get at least a lower limit for D. This indeed occurs with HCN. $\nu_1 = 2090$ (*i.e.*, the CN vibration) gives $D = 3{\cdot}0\,.\,10^{-6}$ cm^{-1}. The difference is to be explained by the fact that the H atom is relatively more strongly displaced towards larger distances from the centre of gravity by the centrifugal force than by the CN vibration, so that on the whole the stretching effect (D) is larger than that given by Kratzer's formula.*

With the above D value the rotational constants B may be derived more accurately than was formerly possible.

The B-values obtained from the Δ_2F values in the usual manner have been corrected slightly by calculating the branches and altering the constants until there remained no systematic differences.† The final rotational constants are given in Table III. The resulting value for the moment of inertia in the lowest state I_0 is also included. (For explanation of the v numbering *cf.* below.)

TABLE III—ROTATIONAL CONSTANTS

v_1	v_2	v_3	B (cm^{-1})	D (cm^{-1})	
0	0	0	$1{\cdot}4789_0$		
1	0	2	$1{\cdot}4482_0$		
0	0	3	$1{\cdot}4467_2$	$3{\cdot}63 \,.\, 10^{-6}$	
1	0	3	$1{\cdot}437$		Badger and Binder
0	0	4	$1{\cdot}435$		

$\alpha_1 = 0{\cdot}00924$ cm^{-1}
$\alpha_3 = 0{\cdot}01073$ cm^{-1}
$I_0 = 18{\cdot}703 \,.\, 10^{-40}$ g cm^2

The B values for the excited vibrational levels are appreciably different from that of the ground state. The generalization for the case of linear polyatomic molecules of the formula $B_v = B_e - \alpha(v + 1/2)$ valid for diatomic molecules obviously is

$$B = B_e - \Sigma\alpha_i (v_i + 1/2).$$

For HCN the values of α_1 and α_3 can accordingly be calculated from the data obtained (*cf.* Table III). But as α_2 is unknown an accurate value for B_e and consequently also I_e cannot be given.

From the value I_0 or I_e unambiguous values for both the CN and CH distances cannot be determined. However, in a forthcoming paper‡ we have investigated the infra-red spectrum of C_2HD and by comparison with C_2H_2 have obtained unambiguous values for the internuclear distances in C_2H_2. Supposing that the CH distance thus obtained is the same in HCN one gets for the CN distance 1·154 A. In Table IV these internuclear distances are compared with those of the free radicals. It is seen that the distances are smaller in saturated molecules than in the free radicals as might be expected.

---

* A rough calculation shows that the difference can, in fact, be explained in this way.

† Evidently the lines themselves are more accurate than the Δ_2F values.

‡ Herzberg, Patat and Spinks, Z. Physik. (*in the press*).

A really unambiguous determination of the internuclear distances in HCN can only be made by investigating DCN, an investigation we are preparing to do. It will thus be possible to decide whether the CH distance is really the same in HCN and C_2H_2 or how large the difference is.

TABLE IV—INTERNUCLEAR DISTANCES IN C_2H_2 AND HCN COMPARED WITH THOSE IN DIATOMIC RADICALS

	C_2H_2 ; HCN	Radical
r_{C-C}	1·204 A	1·311 A
r_{C-H}	1·057 A	1·132 A
r_{C-N}	1·154 A	1·171 A

All numbers are r_0 values, not r_e values.

VIBRATIONAL STRUCTURE

The origins of the two bands have been calculated from the branches to be 9227·04 and 8585·6 cm^{-1}, the first of which should be accurate within $\pm 0{\cdot}05\ \text{cm}^{-1}$ whereas the latter may be wrong by about $\pm 0{\cdot}2\ \text{cm}^{-1}$. As can easily be seen from Adel and Barker's scheme these bands are the combinations of the vibrationless state with the $v_1 = 0$, $v_2 = 0$, $v_3 = 3$, and the $v_1 = 1$, $v_2 = 0$, $v_3 = 2$ states where the indices 1, 2, 3 mean the CN vibration (2089), the transverse vibration (712) and the CH vibration (3313) respectively.*

The above ν_0 values do not agree very well with the formula given by Adel and Barker, the deviation being $-3{\cdot}86$ for the first and $+3{\cdot}6$ cm^{-1} for the second band. On the assumption of a formula

$$G_v = w_1v_1 + w_2v_2 + w_3v_3 + x_{11}v_1^2 + x_{22}v_2^2 + x_{33}v_3^2 + x_{ll}l^2 \\ + x_{12}v_1v_2 + x_{23}v_2v_3 + x_{13}v_1v_3$$

it seems impossible to represent all the available data.† It is either necessary to include higher terms (v^3) or to assume that perturbations occur in the upper level of the new bands or certain other levels. Further data on HCN must be awaited before an accurate formula can be given.

---

* The absence of any Q branch in both bands proves that at any rate the quantum number for the rotation round the axis of symmetry l must be zero in all states involved.

† Unless it is assumed that the far infra-red ν_0 data are wrong by as much as several cm^{-1}.

BROADENING OF THE HCN LINES BY PRESSURE

Mecke has already noted that in several cases, NH_3, CH_3Cl, HCN, the infra-red absorption lines are rather diffuse whereas in others they are quite sharp (H_2O, CH_4, etc.). It seems clear to us that for NH_3, CH_3Cl, HCN the diffuseness cannot be due to anything other than pressure broadening, vibrational predissociation* being excluded from energetical grounds.

This interpretation of the diffuseness has been completely confirmed by us for HCN. In figs. 1*a*–1*d*, Plate 1, spectrograms of the HCN band at 1·04 μ are reproduced at different pressures. It will be seen that the lines are very sharp at 130 mm pressure ; in fact, as sharp as may be expected from the slit width used, whereas at 650 mm they are extremely diffuse. In order to get a correct idea of the amount of broadening, in fig. 1*f*, Plate 1, is given a spectrogram taken at ∼650 mm but with only 80 cm absorbing length so that the product $p \,.\, l$ is the same as for spectrogram fig. 1*d*, where the pressure is only 130 mm (l = 400 cm). So the number of absorbing molecules is the same. In spectrogram fig. 1*f*, the lines are very faint because of the large broadening. Only by using higher pressure with constant absorbing length is it possible to observe the same number of lines as at low pressure.

From spectrogram fig. 1*a* it will also be seen that the higher rotation lines are comparatively sharper than those of lower rotation.

We have further investigated the influence of the pressure of a foreign gas (air) on the line width of the HCN lines. Fig. 1*e*, Plate 1, gives the spectrogram obtained with HCN of 130 mm and 630 mm of air. This has to be compared with spectrograms, figs. 1*d* and 1*f*, for which the number of absorbing HCN molecules is the same. Though there is a definite broadening effect of air on the HCN lines it is very much smaller than the influence of the HCN molecules on one another.

Pressure broadening of spectral lines has already been thoroughly investigated by a great number of workers.† In the far infra-red Hettner and his co-workers‡ have completed a number of investigations. They found in this region Lorentz collision broadening to be the only reason for broadening to occur. The broadening was found to be of the same order of magnitude if caused by different gases including the absorbing gas (mostly HCl) itself, though individual differences were present. The broadening in 1 atmosphere of HCN is, however, considerably larger than that in 1 atmosphere of HCl as can be seen by a comparison of the spectrograms shown here with that of the second overtone of HCl recently obtained by us.* It is also considerably larger than the broadening of HCN lines by 1 atmosphere of air (spectrogram, fig. 1*e*). It therefore seems certain that the effect observed cannot be pure Lorentz collision broadening. It must be connected with *a strong interaction of the* HCN *molecules at rather large distances*. That this interaction cannot be due only to the strong dipole moment of HCN is shown by the fact that H_2O and HCl do not exhibit this strong broadening. It seems that a further necessary condition for the effect to occur is that the molecule be rather easily deformable as shown by a small vibration frequency, the lowest frequency of HCN being 713 cm^{-1} whereas that of H_2O is ~ 1600 cm^{-1}, that of HCl ~ 3000 cm^{-1}.

---

* Herzberg, 'Ergebn. exakt. Naturwiss.,' vol. 10, p. 207 (1931).

† *Cf.* the summary of Weiszkopf, 'Phys. Z.,' vol. 34, p. 1 (1933).

‡ Hettner, 'Phys. Z.,' vol. 27, p. 787 (1926) ; Kuszmann, 'Z. Physik,' vol. 48, p. 831 (1928) ; Becker, *ibid.*, vol. 59, p. 583 (1930) ; Lasareff, *ibid.*, vol. 64, p. 598 (1930) ; Kühne, *ibid.*, vol. 84, p. 722 (1933) ; Grasse, *ibid.*, vol. 89, p. 261 (1934).

In this connection it seems significant that the broadening decreases with increasing rotation. This means that the interaction of two HCN molecules decreases with increasing rotation, *i.e.*, that HCN is stabilized by rotation. A dependence of the broadening on the rotational quantum number is to be expected for an intermolecular Stark effect. But this effect should be proportional to $1/J^3$ whereas it really decreases much more slowly. Therefore the broadening also cannot be explained as a pure intermolecular Stark effect.

Further experiments are necessary to obtain a fuller understanding of this strong interaction of HCN molecules. It is planned first to investigate the influence of HCl on HCN and on C_2H_2 in order to decide whether a foreign dipole gas may cause a similar strong broadening effect. It is hoped thereby to obtain more information on these intermolecular forces.

In conclusion, it is a pleasure to acknowledge the kindness with which the firm " Agfa " placed their new infra-red plates at our disposal. We further have to thank the Helmholtz-Gesellschaft and the Hochschulgesellschaft, Darmstadt, for financial aid. We are greatly indebted to Professor H. Rau for his kind interest and for placing every facility at our disposal.

SUMMARY

Two strong absorption bands of HCN at 1·04 μ and 1·16 μ have been photographed with high dispersion and analysed. The rotational

---

* Herzberg and Spinks, 'Z. Physik,' vol. 89, p. 474 (1934).

constants and the moment of inertia of HCN in its lowest state is derived therefrom with considerable accuracy ($I_0 = 18 \cdot 703 . 10^{-40}$ gm cm^2). The internuclear distances are calculated from I_0 on the assumption that the CH distance is the same as in C_2H_2. They are smaller than those in the free diatomic radicals. The effect of stretching of the HCN molecule by centrifugal force is considered.

The positions of the different bands of HCN cannot be represented by a simple formula including only quadratic terms.

The line width of the HCN lines increases rapidly with pressure. An equal amount of air produces far less broadening than HCN itself. The broadening is smaller for higher rotational lines. It seems probable that the broadening in this and other cases of infra-red spectra is due to a strong intermolecular interaction and not to a pure Lorentz collision broadening.

The Low Energy β-Rays of Radium E

By H. O. W. RICHARDSON, Bedford College, London

(*Communicated by C. D. Ellis, F.R.S.—Received June* 29, 1934)

[PLATE 2]

The object of this work was to obtain information about the shape of the low energy end of the continuous β-ray spectrum of radium E, an element convenient because of its negligible γ-ray emission. The failure of theory to explain the continuous spectrum makes it of interest to obtain all possible experimental information, and although much is now known about the high energy part of the curve, the low energy region has remained obscure owing to certain experimental difficulties. The chief of these has been the contamination of the low energy end of the curve by rays reflected with unknown energy loss from the material on which the radioactive body was deposited.

This effect can be eliminated by mounting it on sufficiently thin metal leaf so that no particles can be reflected with appreciable loss of energy. Such a source would be too weak to use in a magnetic spectrograph, and the method therefore adopted in this work was to mount it in a Wilson expansion chamber and take stereoscopic photographs from which the ranges of any slow tracks formed could be measured, a method already used by the writer for radium D.*

---

* 'Proc. Roy. Soc.,' A, vol. 133, p. 367 (1931).

The fact that ranges are measured restricts the method to rays between about 9 and 65 electron-kilovolts energy, as the end points of faster rays would lie outside the chamber.

By using, as before, gas mixtures of three different stopping-powers, it is possible to cover conveniently that region of energy. Each gas mixture will give a fairly complete registration of tracks of about 2·5 cm range, but various factors will reduce the numbers of tracks which are much longer or shorter. In order to allow for these selective effects three corrections were applied which extend the region over which each gas mixture can give an undistorted representation of the energy distribution.

A useful feature of the method is that by counting the number of α-tracks present it is possible to obtain an absolute value for the number of β-ray disintegrations photographed. This can be done because the rate of growth of the succeeding α-ray element polonium is a measure of the quantity of its parent body, radium E. Having thus calculated the number of disintegrations represented by each set of measurements it is possible to combine the resulting energy distributions on the same scale and obtain a mean distribution curve as in fig. 2.

An interesting feature of the results, well shown in fig. 3, is the surprisingly large number of low energy particles found. These occur in an energy region where secondary electrons are to be expected due to branching of the primary rays in passing through the mounting foil.

An attempt has been made to carry through a detailed calculation of the number of secondary electrons, and while this calculation suggests that most of the observed electrons with energies below 15 electron kilovolts may arise in this way, it fails to account for more than a small fraction of the number found at about 60 electron kilovolts.

Two conclusions seem possible, either that the distribution curve does have a hitherto unsuspected maximum near this point, or that the result of the calculation is in error. It seems unlikely that any such error can be attributed to the approximations used so that if the second conclusion were true, it appears to require that the available information on branching is incorrect.

A point of some interest is that these slow electrons are definitely present whatever their origin, and that if their origin is secondary they should be still more prominent in experiments with the radioactive material mounted on supports thicker than the metal leaf used here.

EXPERIMENTAL METHOD

A standard expansion chamber was used about 17 cm in diameter and 6 cm high. The photographs were taken with a double camera on

Imperial Eclipse soft plates, and the necessary illumination was obtained by discharging a 1/10 mfd condenser charged to 20 kv through two quartz mercury lamps with reflectors placed behind them. A clearing potential of 100 volts was maintained between the roof and the piston together with a vertical magnetic field of about 200 gauss, which incidentally showed that the electrons observed were negatively charged.

The activated foil was held vertically near the centre of the chamber and was enclosed by a box-like aluminium shutter fixed to the piston of the chamber. This shutter shielded the source until the piston had fallen through about half its stroke and thus prevented the rays from crossing the chamber until near the end of the expansion, thereby greatly reducing the number of "old" diffused ions present. Without the shutter the background of cloud due to these old ions made work impossible except with very weak sources.

The photographs, Plate 2, were measured by the method of Nuttall and Williams.* The chief source of inaccuracy in the range measurements was due to the difficulty of determining the point on the source from which a track started because the eddying and the great number of tracks there made it impossible to trace the tracks right up to their origins.

The direct distance from source to end of all slow tracks was also measured together with the lengths of those portions of α-tracks lying clearly in view. These data were used subsequently in calculating the corrections. Care was taken to reject tracks produced by branching of fast rays in the gas in the chamber, a branch being detected as a track not traceable back to the source and starting at nearly 90° to the fast primary ray producing it. The latter ray would normally be invisible, but its direction could be inferred. Of course, a branch produced in or very near the foil is indistinguishable from a primary ray.

In activating the sources certain conditions of purity had to be fulfilled. First, as most of the β-radiation of Ra D falls within the region investigated, the sources must be free from that element. Second, it is advisable that very little polonium be present when the source is first prepared in order to avoid confusion by the α-tracks and to facilitate the deduction of the number of disintegrations. The following method was used :

1—Ra (E + F) was obtained by kathodic deposition on platinum at very low current density from a solution of Ra (D + E + F) in N/10 HNO_3.

2—The Ra E was dissolved off the kathode in HCl which was then diluted to N/2 and any Ra F was removed by introducing a piece of silver for one hour.

---

* 'Phil. Mag.,' vol. 2, p. 1109 (1926).

3—The solution was diluted to N/10 and electrolysed for four hours in the presence of $PbCl_2$.

4—The wire kathode with its deposit of Ra E was then dipped into a drop of N/10 HCl placed centrally on the Au or Ag leaf and the activity was transferred from the wire by electrolysis.

In the case of Ag leaf the drop was removed, but with Au it was allowed to evaporate to dryness and replaced by distilled water which was then removed. This removed any hygroscopic matter which could encourage condensation on the source. Further, to ensure dryness, the temperature of the source was always maintained slightly higher than that of the floor of the chamber.

THE ANALYSIS OF THE EXPERIMENTAL MEASUREMENTS

1—*Calculation of the Energies of the Tracks*—When the chamber contained hydrogen the energy of each measured track was calculated from the range using the Thomson-Whiddington relation $E = 24330 \left(\frac{n_1}{n_2} . R\right)^{\frac{1}{2}}$ electron volts, R being the measured range in cm, n_1 the number of extranuclear electrons per cc in the gas in the chamber at the end of the expansion and n_2 that in 1 cc of oxygen at 0° C and 760 mm. In the other gas mixtures the stopping power was mainly due to oxygen and the results of Williams* were used : $E = 24600 \left(\frac{n_1}{n_2} . R\right)^{\cdot 65}$.

Each track was then allotted to its place in one of the energy distributions.

2—*Corrections to the Distributions*—It is evident that corrections will be necessary if these distributions are to give an undistorted picture of the β-ray emission of Ra E, because there are several factors at work which will cause the loss of more tracks of one range than of another.

The general effect of the corrections applied can be seen from fig. 1.

The most important source of selection was that tracks were only photographed if they lay within a horizontal layer about 2 cm deep and 12 cm across. In the case of Ra D this layer effect was corrected by a formula based on the solid angle available, but in the present case it was found better to use an experimental derivation for the correction. In the hydrogen photographs the registration layer was traversed by long α-tracks with random directions and it was possible to survey the boundaries of the layer by measuring the length of each α-track that clearly lay within it with visibility comparable with that needed to show the presence of the end of a β-track.

---

* 'Proc. Roy. Soc.,' A, vol. 130, p. 310 (1931).

By deducing the correcting factor from the distribution of these visible parts of the α-tracks it was possible to allow for the ending of the layer at the side of the chamber and it was also found that the layer became distinctly shallower near the shutter.

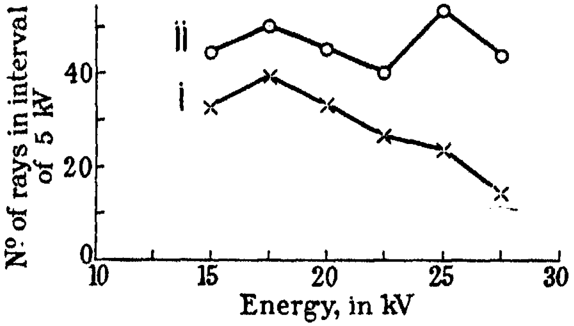

Fig. 1—Curve I, the energy distribution of the measured tracks in the O series ; II, curve I corrected for selective effects.

A second selective effect was due to the destruction of portions of the longer tracks by confusion with other tracks. The number of tracks rendered unmeasurable in this way varied considerably in the different series so that in order to make the various series comparable and to allow for the fact that long rather than short tracks were destroyed, it was necessary to apply a correction. This was done by comparing the distribution curve of the straight start-to-end distances for the spoilt tracks with that for the measurable tracks and thus finding the fraction of tracks spoilt at different distances, care being taken not to include branches starting in the gas. The values of this correcting factor are given in Table I.

A third correction of much less magnitude was applied to allow for the loss of short tracks due to the presence of an irregular volume around the source in which few tracks formed. The length of the gap in every track where it crossed this volume was measured and from the distributions of these lengths it was possible to correct roughly for the short tracks lost inside the irregular volume. This correction, like the preceding one, had the effect of increasing the similarity in the shapes of the various distributions.

3—*The Number of Disintegrations*—In order to combine the distributions from the various series of experiments the number of disintegrations which each represented was calculated from the rate of growth of the number of polonium α-particles observed. It was assumed that the time interval per expansion in which the end part of a β-ray would form a sharp track equalled that in which a sharp α-track would form. The most probable direction of error in this assumption is to reduce the interval for β-rays which would cause the number of low energy rays in relation to the whole spectrum to be even larger than is shown in fig. 3. It was necessary to allow for the variation of the time interval with the composition of the gas in the chamber. This was obtained from the numbers of α-tracks which gave 1 : 1·38 : 1·67 as the ratio of the time intervals in (91% $H_2 + O_2$), (59·5% $H_2 + O_2$) and oxygen alone.

TABLE I

Series of tracks	Straight start-to-end length in cm	Factor to correct destruction
O	all lengths	×1·0
T	<2·0	×1·0
	>2·0	×1·4
Q	<2·1	×1·0
	>2·1	×1·25
R1—5	<2·0	×1·0
	>2·0	×1·6
	>5·5	×2·0
R6—9	<2·2	×1·0
	>2·2	×1·33
R10—17	<2·1	×1·0
	>2·1	×1·2
	>2·3	×1·5
	>2·5	×2·0

4—*The Experimental Results*—The corrected distributions are shown in fig. 2, each point giving the number of rays lying within an energy interval of 5 kilovolts for hydrogen tracks and 10 kilovolts for the others. The distributions are arranged to represent equal numbers of disintegrations except for the T series which is fitted arbitrarily. The number written against each point is the number of measured tracks on which it is based and gives the weight allotted to it in the weighted means, curve I.

From the α-ray data the number of low energy β-rays between 20 and 60 kilovolts energy is estimated to be about 0·08 per disintegration. This number is surprisingly large when viewed in conjunction with the previously accepted energy distribution. This is shown in fig. 3, in which both distributions are drawn to the same scale. The ordinate at 60 kv is about six times what might have been expected.

It must be emphasized that this result is based on the α-tracks observed which give an absolute value to the number of disintegrations recorded in the photographs.

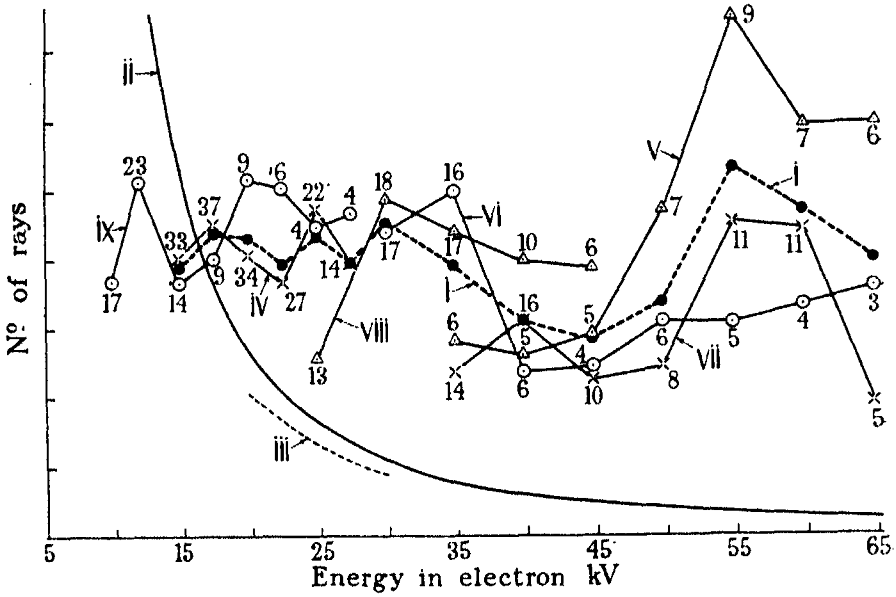

FIG. 2—Curve I : The final distribution of weighted means ; curve II : the estimated distribution of the secondary branch electrons ; curve III : curve II corrected for energy losses in the foil ; curve IV : the O series, 100 tracks in 91% hydrogen, Ag source ; curve V : the Q series, 23 tracks in oxygen, Au source ; curve VI : the T series, 42 tracks in oxygen, Ag source ; curve VII : series R1–5, 44 tracks in oxygen, Au source ; curve VIII : series R6–9, 41 tracks in 59·5% hydrogen, Au source ; curve IX : series R10–17, 50 tracks in 91% hydrogen, Au source.

THE ORIGIN OF THE SLOW ELECTRONS

In discussing these results the most natural initial assumption is that the energy distribution of Ra E descends smoothly to the origin from its maximum at 300 kv, in which case most of the slow electrons must be attributable either to contamination with radium D or to some secondary origin.

The first explanation was carefully tested by rephotographing the sources after a sufficient time had elapsed for the radium E to decay almost completely. Any remaining β-radiation must then be due to

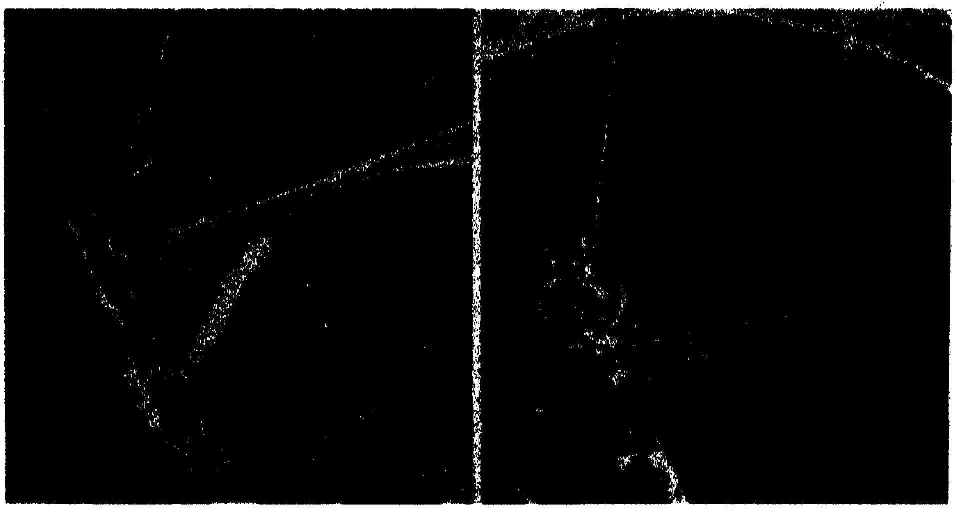

a *b*

a and *b*—O series (91% Hydrogen).
Each shows β-tracks of low energy coming from the source

c

c—T series (Oxygen)

contamination of the source or chamber. Several β-tracks were found but as very few of them started from the source, the final conclusion drawn from such tests was that the fraction of tracks due to Ra D must be less than about 1/8 at 30 kv. In any case, Ra D could not account for the tracks found about 45 kv, which must have some other origin.

In order to test the second explanation of a secondary origin, a calculation was made on the basis of the available information on the branching of β-ray tracks. For example, it has been shown* that a β-ray of 500 kv energy passing through oxygen ejects approximately one branch electron with an energy exceeding 20 kv in every 50 cm of path. As already stated, a branch track starting in the metal leaf or very close to its surface will be indistinguishable from a primary track of low energy.

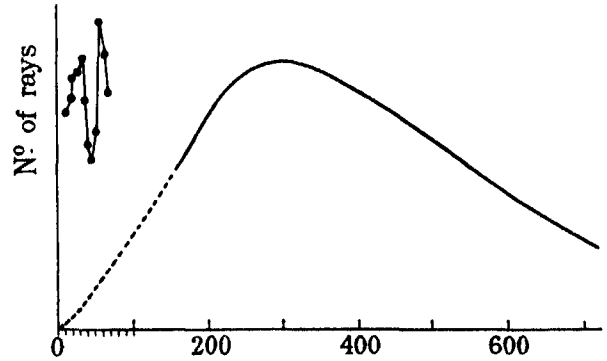

Fig. 3

The number of such branches to be expected was calculated using the formula, based on classical mechanics, for the number of branches per cm of path with energy between Q and Q + *d*Q.

$$\phi\,(\mathrm{Q})\,d\mathrm{Q} = \frac{2\pi e^4 n}{mv^2}\left(1 + \tfrac{4}{3}\,\frac{\varepsilon}{\mathrm{Q}}\right)\frac{d\mathrm{Q}}{\mathrm{Q}^2},$$

where n is the number of extranuclear electrons of charge e and mass m per cc in the medium traversed, and ε is their average kinetic energy. v is the velocity of the primary particle. In the region of Q considered, ε/Q is small and ε was taken as the mean binding energy. An average value of $1/v^2$ was obtained from the accepted energy distribution of Ra E. The results of Williams and Terroux* show that for branches in oxygen the experimental results gave $\phi\,(\mathrm{Q})$ about double that given by the classical formula, so in the present case the calculated values were also doubled. To apply the formula the average distance traversed by the primary rays in the foil must be calculated. This distance is limited by the effect of scattering which was allowed for in the following way.

---

* Williams and Terroux, 'Proc. Roy. Soc.,' A, vol. 126, p. 289 (1930).

Let fig. 4 (*a*) represent a normal cross-section through the foil.

Consider a particle starting at O and entering the foil in the direction OA. With no scattering OA would be the path of the particle and the average value of *r* over all values of θ would be infinite. Scattering prevents this by making the average distance traversed by particles starting along such a path as OB less than OB, and the more the scattering the less the average path. As the calculation was intended to give an upper limit for the number of branches a high value for the velocity of the particles, $v/c = 0 \cdot 92$, was taken with consequent small scattering. The scattering process was represented by a simplified model. Only angles between the ray and the surface of the foil were considered, bending in planes parallel to the surface being irrelevant. After travelling a distance Δ each ray was assumed to make a collision and divide into two equal forks making angles of ψ with the previous direction.

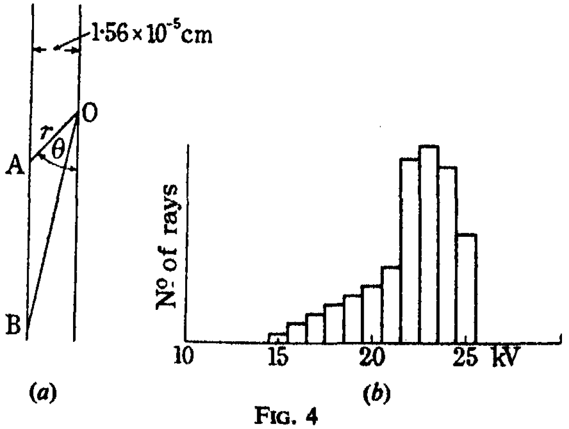

(*a*) (*b*)

FIG. 4

The value chosen for Δ was $1 \cdot 56 \times 10^{-5}$ cm (*i.e.*, the thickness of the foil) which gave $\psi = 5 \cdot 9°$. The relation between ψ and Δ was such that, after enough subdividing to allow of statistical analysis, the distribution curve of the angular deviations of the components of the scattered beam would be the same as that given by Bothe's* formula for multiple scattering with the same value of *x*,

$$\lambda^2 = \pi N x\, a^2 Z^2 \,.\, 4 \cdot 8,$$

---

[*] 'Z. Physik,' vol. 13, p. 368 (1923).

where $a = 2e^2\ mv^2$, x is the distance traversed in the scattering medium, N is the number of scattering nuclei per cc of charge Ze, while e, m and v apply to the β-ray.

Three values of θ, 2·95°, 5·9° and 17·7° were taken in turn and the paths of the fanlike scattered beams calculated. This was done by a method using a symbol to represent each component of the beam. The emergence of a component from the foil was known by certain indices passing limiting values.

The method can be applied to any angle of incidence or shape of scatterer and it avoids the scattering back of particles which have once emerged from the scatterer.

For each of the three values of θ the fractions of the beam leaving the foil between the nth and $n + 1$th collisions were found and were plotted against n. As $n\Delta$ is the path in the foil it was possible to obtain its average value for each of the angles of incidence.

TABLE II—The effect of scattering in the foil

Angle of incidence θ	2·9°	5·9°	17·7°
Value of r	19·8 Δ	10·25 Δ	3·28 Δ
Mean path in foil	6·55 Δ	7·05 Δ	4·04 Δ
Fraction of beam left in foil after 14th collision	8·15%	7·0%	1·8%

The results are shown in Table II from which it appears that the mean path has a maximum of about 7 Δ and is much less than OA for small values of θ, but slightly larger for large values.

To obtain an upper limit to the mean path for all angles of incidence it was therefore assumed that from $\theta = 0$ to $\theta = \sin^{-1} 1/7$ the average path had the constant value 7 Δ and from $\theta = \sin^{-1} 1/7$ to $\theta = 90°$ it equalled the radius vector r.

Remembering that Δ equals the thickness of the foil, $r = \Delta/\sin\theta$, and the average path in the foil of all the rays which enter it, $\bar{r}$, may be expressed as the sum of the two terms corresponding to the two ranges of θ.

$$\begin{aligned}\bar{r} &= \Delta\,.\int_{\sin^{-1} 1/7}^{\pi/2} \cot\theta\,.\,d\theta + 7\,\Delta \int_0^{\sin^{-1} 1/7} \cos\theta\,.\,d\theta \\ &= \Delta\,(\log_e 7 + 1) \\ &= 2{\cdot}95\ \Delta\ \text{cm.}\end{aligned}$$

To convert this from gold to oxygen it was multiplied by the ratio of the numbers of extranuclear electrons per cc giving 0·501 cm of oxygen as the mean equivalent path in the foil of those β-rays which enter it.

To get their number from the α-particle data an addition of 45% was made to allow for the non-registration of α-rays emitted in a vertical direction. Assuming that one β-ray in every two disintegrations enters the foil, curve II in fig. 2 was obtained.

This curve cannot be expected to give the observed energies of the branch tracks because of the ordinary straggling of the ranges and because of energy losses in escaping from the foil. It is important to see if these effects are such as to increase the resemblance between the theoretical and experimental curves and a rough calculation was therefore made of the energy losses in the foil of branches of 25 kv initial energy. The origins of the branches were assumed to be distributed isotropically in the foil and the average rate of emergence of nine typical elementary beams was obtained, each beam being calculated by the scattering model previously described.

The result is shown by the curve in fig. 4 (*b*), giving the observed energy distribution of the 25 kv branches on emergence. Curve III, fig. 2, represents curve II after correction for these energy losses using the simplifying assumption that the width of the loss distribution in fig. 4 (*b*), remained constant over the region considered.

This is roughly true because, although low energy rays lose more energy per cm, their paths in the foil are shorter than those of faster tracks because they are scattered out more rapidly.

Though curve III may be expected to coincide with curve II at high energies while diverging more at low energies, it is evident that this flattening is quite inadequate to bring its shape into line with that of the experimental curve. A calculation of the effect of straggling showed that it was negligible in the region of 25 kv.

CONCLUSION

It is evidently possible to attribute most of the tracks below 15 kv to a secondary source which means that the nuclear continuous spectrum possibly reaches zero intensity at or just before the origin.

While some doubt exists as to the absolute magnitude of the energy distribution of the secondary electrons it must be emphasized that its shape can be predicted with more certainty and that it differs considerably from that of the experimental curve. It would be necessary to increase the ordinates of curve III by a factor of 3 at 25 kv and by one of 10 to 15 at 60 kv. In general, the approximations made were such as to exaggerate the absolute magnitude of the number of secondary electrons predicted, but even if the result is in error far more electrons of low than of high energy are to be expected in contrast to the fairly uniform distribution actually found.

It is therefore considered that the existing theory of close collisions between electrons fails to give a satisfactory explanation of the results, so that while it is unwise to draw a final conclusion, there appears to be evidence that Ra E emits a group of low energy β-rays of about 0·08 per disintegration.

THE EFFECT OF THE ATOMIC NUMBER OF THE MOUNTING MATERIAL

Since the above conclusion was reached it was decided for the following reasons to take further photographs with sources mounted on films of lower atomic number. Bothe (*loc. cit.*) using Ra E β-rays, has reported that gold foils give more low energy secondary electrons than aluminium foils of similar stopping power, while Langstroth* has recently found many more secondaries scattered back from Al than from celluloid films. His films were bombarded with electrons of 20 to 12 kv energies.

If some new effect associated with heavy atoms is present it might account for the low energy electrons in the present results, though an excessive production of secondaries cannot be explained on the classical theory of electron collisions.†

Photographs were therefore taken, first, with a source on a celluloid film of about 3×10^{-5} gm/cm², in oxygen and, second, on paper of $2 \cdot 1 \times 10^{-3}$ gm/cm² using alcohol instead of water in oxygen and in $O_2 + H_2$. The emission of low energy rays appeared to be just as copious as it was with the mountings of large atomic number. The investigation is being continued by another method. I wish to thank Mrs. A. Leigh-Smith for her assistance in preparing the pure Ra E and the celluloid films for this part of the work.

I wish to thank Dr. C. D. Ellis for suggesting the problem and for his valued advice, Dr. J. Chadwick for providing some radium D, and Professors E. V. Appleton and W. Wilson for providing facilities in their laboratories.

SUMMARY

By measuring the ranges of the β-rays from Ra E in an expansion chamber an energy distribution curve has been obtained extending from

---

* 'Proc. Roy. Soc.,' A, vol. 140, p. 159 (1933).

† Thomas, 'Proc. Camb. Phil. Soc.,' vol. 23, p. 829 (1927); Webster, Hanson and Duveneck, 'Phys. Rev.,' vol. 43, p. 384 (1933).

10 to 65 kv. The absolute number of disintegrations represented by the curve is obtained from the growth of the succeeding α-ray body. The curve fails to fit the accepted energy distribution for Ra E.

To attempt to account for this a calculation has been made of the energy distribution of secondary electrons due to branching of the primary rays which is to be expected. This distribution fails to agree in shape and in magnitude with the experimental curve and it is concluded either that the available data on branching are inadequate or that a group of low energy particles is emitted by Ra E.

The Oxygen Afterglow

By Eric M. Stoddart, The Sir William Ramsay Laboratories of Inorganic and Physical Chemistry, University College, London

(*Communicated by F. G. Donnan, F.R.S.—Received June* 29, 1934)

Thomson,* during an investigation of electrodeless discharges through various gases at low pressures, found that oxygen possessed a glow resembling a yellow fog, which persisted some considerable time after the electrical discharge had been interrupted. A similar phenomenon with nitrogen has been thoroughly investigated, although the oxygen afterglow has aroused but little interest. Herzberg† made a careful study of the conditions necessary for the appearance of an afterglow in oxygen-nitrogen mixtures. He showed that when the mixed gases were admitted into a well baked out vessel and electrically excited, no afterglow was produced; this was obtained only when the surfaces of the vessel were covered with a poisoning material, such as water vapour. It is of interest to note that Herzberg was unable to obtain any afterglow in oxygen free from nitrogen, even in a vessel with poisoned surfaces; addition of 2% or more of nitrogen to the oxygen was essential for an afterglow to be observed.

Lewis‡ also investigated the effect of surface conditions on both nitrogen and oxygen afterglows. His results substantiate those of Herzberg in as much that no afterglow was obtained in vessels with

---

* 'Phil. Mag.,' vol. 32, p. 321 (1891).

† 'Ann. Physik,' vol. 84, p. 553 (1927) ; 'Z. Physik,' vol. 46, p. 878 (1928).

‡ 'J. Amer. Chem. Soc.,' vol. 51, p. 654 (1929).

" clean " surfaces, but, on the other hand, he found that an afterglow could be obtained in pure oxygen when water vapour at −60° C ($8 \cdot 10^{-3}$ mm) was admitted to the gas, the surfaces of the containing vessel thereby being poisoned.

In an investigation of the hydroxyl radicle, the present author found that when damp oxygen was streamed through a discharge tube fitted with aluminium electrodes, the intensity of the afterglow was at a maximum when the amount of water vapour in the gas phase was at a minimum, provided that the surfaces of the system remained poisoned. Excess water vapour quenched the afterglow with the production of free hydroxyl. It was decided to extend this work and to determine the effect of various gaseous impurities upon the production of the oxygen afterglow, with a view to identify the emitter of the radiation.

ELECTRODELESS DISCHARGES

The experiments about to be described were all conducted with high frequency electrodeless discharges, thereby eliminating the contaminating influence of metal electrodes on the gas. In the earlier experiments, a coil of 15 turns of 18 S.W.G. copper wire wrapped round the observation tube was connected (via two condensers of 0·005 mf) to the output terminals of a 0·75 KVA transformer, giving a maximum voltage output of 8000 A.C. volts, which had a spark-gap shunted across the output terminals. Such an arrangement was similar to that used by Lewis (*loc. cit.*). In later experiments, a valve oscillatory circuit was used, employing a Marconi-Osram transmitting valve (D.E.T. 1) which gave a maximum output of 35 watts with an anode voltage of 1000 volts. The circuit was of the usual simple type, employing Gambrell coils B_1, E_1 and F in the grid, plate and output circuits respectively. The grid circuit was also tuned with a small condenser. Two insulated strips of thin lead foil wrapped round the observation tube and pasted in position, were connected to the terminals of the output coil. In operation, this arrangement was as satisfactory as the transformer method as well as being much more convenient.

The apparatus was constructed in soft soda glass and after treatment with hot chromic-nitric acid, was thoroughly washed with tap water followed by distilled water. After being dried in a steam oven, it was all assembled in the manner shown in fig. 1. The system was evacuated by a Leybold two-stage metal mercury vapour pump (type G) backed by a Hyvac pump. Mercury vapour was excluded from the apparatus by a large liquid air trap. After a preliminary pumping, the apparatus was baked out for many hours with a soft blowpipe flame, which raised its temperature to just below softening point for the glass, the surfaces of the system thus being freed from any extraneous gas which might have caused some unforeseen phenomenon. During this process, the platinum wire enclosed in the bulb K and the silver wire in the tube C were electrically heated to a dull white heat. In this manner, it was found possible to maintain for as long as it was required, a vacuum of less than 10^{-3} mm, but the pumping and baking were continued for over a fortnight, at the end of which time, little or no green fluorescence could be observed on the glass surfaces when a Tesla coil was brought close to the apparatus in the dark. Taps 1, 2, and 7 were then closed against the tubes A, B, and N, the side arms of which were opened for the introduction of A.R. potassium permanganate, pure sodium azide and A.R. cadmium carbonate, respectively. After the side arms had been re-sealed, the tubes were separately evacuated to 10^{-6} mm again. Since these experiments depend upon the gases employed being extremely pure, the preparation of each gas will be described in turn.

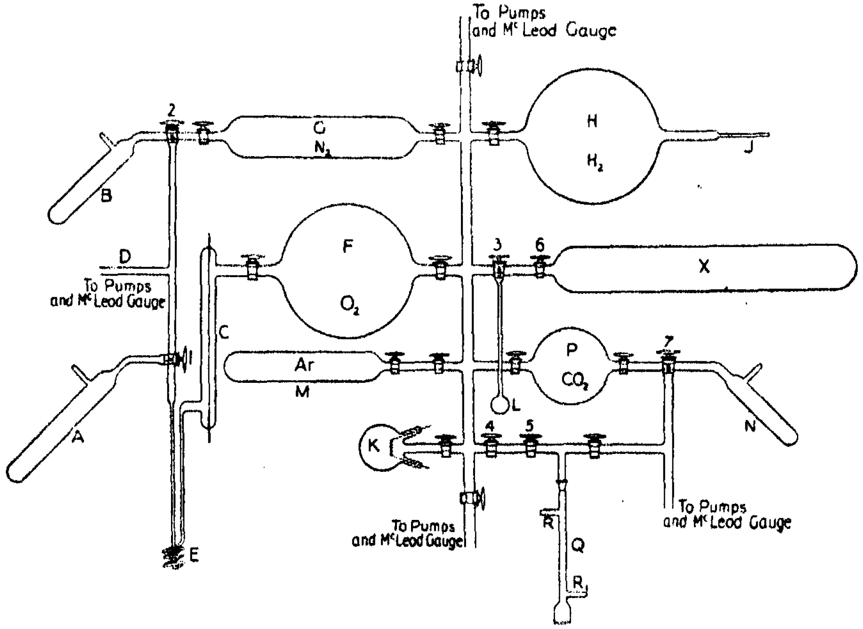
To Pumps and M^c Leod Gauge
2
G
N_2
H
H_2
J
B
D
To Pumps and M^c Leod Gauge
F
O_2
3
6
X
C
1
Ar
M
P
CO_2
7
L
A
K
4
5
N
To Pumps and M^c Leod Gauge
R
Q
R_1
To Pumps and M^c Leod Gauge
E

FIG. 1

Oxygen—The 44 S.W.G. pure silver wire, a foot in length, supported axially in the tube C by means of stout copper-clad lead in wires had been previously de-gassed. The wire was electrically exploded, thereby coating the inner walls of the tube C with pure silver in a very active state.

Since potassium permanganate decomposes at about 300° C in a vacuum, the expelled oxygen may be expected to contain certain contaminating gases driven off from the hot glass and the heated crystal surfaces. Consequently, two-thirds of the permanganate was decomposed, the expelled oxygen being pumped away through the tube D and not being allowed to enter the main apparatus. It was considered that such treatment would leave a little permanganate capable of evolving oxygen with a high degree of purity. The only conceivable impurities which might be present in the remaining oxygen are carbon dioxide and chlorine.

Tap 1 was turned so as to allow the remaining oxygen to be driven through the coil E immersed in liquid air, then, via the tube C, into the 4-litre storage bulb F. The permanganate was so slowly decomposed that no solid material was ever carried forward by the gas stream into the main apparatus. The oxygen in the storage bulb was allowed to remain for several hours in contact with the cold coil E and the silvered tube C, any trace of carbon dioxide was thus removed by the cold coil and any chlorine or similar chemical substance by the silvered tube.

Nitrogen—Sodium azide with a high degree of purity is obtainable and decomposes *in vacuo* at about 300° C, giving extremely pure nitrogen.* The source of the present nitrogen was the sodium azide in the tube B, two-thirds of which was decomposed thermally, the expelled gases being removed via the tube D. The remaining material was decomposed as required and the nitrogen stored in the 2-litre container G.

Hydrogen—This was required for the preparation of pure water necessary for poisoning purposes. The 4-litre bulb H was fitted with a palladium diffusion tube J, which was tested for leaks by impinging a small carbon monoxide flame on to it. The Tesla coil and McLeod gauge did not reveal the admittance of any gas. Hydrogen was admitted to the bulb through the palladium as required.

Water—This was required for poisoning the surfaces of the observation tube. Since it is difficult to prepare pure water by distillation processes and to transfer it to such a system without the risk of contamination, it was decided to synthesize it from the pure oxygen and hydrogen *in situ*, thereby eliminating impurities other than compounds of oxygen and hydrogen. The gases in their respective containers were allowed to mix and were fired by the electrical heating of the platinum filament in the bulb K, the water produced being condensed in the bulb L cooled in liquid air. Manipulation of the tap 3 served to isolate the bulb L from the rest of the system. About 0·2 cc of water was produced and stored in this fashion. The excess gases were removed from the apparatus by the pumps.

---

* Tiede, 'Ber. deuts. chem. Ges.,' vol. 49, p. 1742 (1916).

Argon—Preliminary experiments showed that ordinary cylinder oxygen possessed an intense afterglow in a simple discharge tube. Since argon is a common impurity of cylinder oxygen, it was thought that it may have considerable influence on the production of an afterglow in pure oxygen. Therefore, spectrally pure argon was obtained in the container M from The British Oxygen Co. Ltd., and attached to the apparatus as indicated.

Carbon Dioxide—This was prepared by heating A.R. cadmium carbonate which decomposes *in vacuo* at quite a low temperature. It was therefore better suited for the present purpose than other carbonates. The material was contained in the tube N, and a considerable portion of it decomposed before any of the forthcoming gas was stored in the bulb P.

Spectral Analysis of the Gases—A sample of each gas was separately admitted to the quartz tube Q, the taps 4 and 5 being used for suitable adjustment of the pressure. The gas was excited electrodelessly by the valve oscillator, the external electrodes being wrapped round the side arms R, R_1 of the quartz tube, and the emission spectrographically examined. The oxygen was found free from nitrogen, and *vice versa*; the hydrogen showed no foreign lines, and mercury vapour from the pumps and McLeod gauge was always absent. Such gases were used throughout the investigation, fresh samples always being subjected to the test. Whenever impurities were detected, that particular sample of gas was discarded, its container baked out, and a fresh quantity prepared.

Any of the gases could be admitted to the observation tube X via the taps 3 and 6, the volume between the latter (8 cc) being used for dosing purposes. The gases could thereby be mixed in any desired ratio, provided their initial pressures in their respective holders had been previously determined with the McLeod gauge. The observation tube X was 2½ inches in diameter and 3 feet long.

Pure oxygen was admitted to the baked out clean observation tube at a series of pressures between 0·08 and 0·42 mm but no afterglow was visually detectable on excitation of the gas. This was in agreement with the previous observations of Lewis and Herzberg (*loc. cit.*).

The pressure of oxygen in the observation tube was then adjusted to 0·16 mm, the pressure, according to Lewis, of maximum duration of the afterglow. The water in the bulb L was cooled with melting chloroform (—62° C) and the tap 3 adjusted so as to admit water vapour at this temperature to the oxygen in the tube. In view of the observations of Lewis, the afterglow should have been at once observable, but strangely enough, this was not so. After 12 hours, the oxygen was still glowless. Spectroscopical analysis of the gas revealed the prominent Balmer lines and the principal hydroxyl bands, so that it is clear that the absence of the afterglow is in no way due to lack of water vapour present in the gas phase required for the poisoning of the walls. Nevertheless, water vapour at (*a*) liquid air temperature, (*b*) —80° C, (*c*) —40° C, (*d*) —22° C, and (*e*) 0° C was also tried with variation of the oxygen pressure between 0·1 mm and 0·3 mm. The oxygen was always glowless.

These results may be explained by assuming that the nature of the glass walls is altered on baking in such a way that they refuse to re-adsorb water vapour from the gas phase, thereby leaving the surfaces " clean " so that the afterglow cannot be observed. Such an explanation, although contrary to the accepted conceptions of surface phenomena, was tested in the following manner.

A 4-litre bulb with a small side arm was substituted for the observation tube. The bulb was baked out and evacuated for 8 hours at 400° C. Water from the main apparatus was distilled into the side arm of the bulb cooled in liquid air, and this was followed by oxygen at 0·16 mm pressure. The bulb was then separated from the rest of the system, and it was noted that the oxygen was again glowless. The water present in the side arm was allowed to heat up to room temperature, the pressure in the bulb, due to water vapour, rising to such an extent that no discharge would pass through the gas. This water vapour could be removed from the gas phase by various refrigerants and the oxygen tested for an afterglow whenever desired. Although the bulb was kept for over six months the oxygen remained glowless. It is quite inconceivable that the glass surfaces could be so altered on baking as to refuse to re-adsorb water vapour at several millimetres pressure over such a long period.

In order finally to settle the problem an observation tube pumped out for 100 hours without any baking at all was employed for the experiment. The surfaces were poisoned in the customary manner and the oxygen pressure varied over the usual range, but the oxygen remained glowless.

The experiment was repeated in unbaked and baked bulbs of Pyrex and quartz, but no afterglow was ever observed.

The effect of the addition of various gases to the oxygen was then investigated. Mixtures of oxygen and nitrogen have often been described as possessing a powerful afterglow* in vessels with poisoned walls, although most workers have employed ordinary electrode discharge tubes for this type of experiment, thereby contaminating their gases with unknown gaseous impurities from the metal electrodes, and casting considerable doubt upon the validity of their observations. Incidentally, Herzberg reported that oxygen required the presence of 2% or more of nitrogen for it to possess an afterglow.

Pure oxygen at 0·16 mm was admitted in the usual manner to the observation tube, the surfaces of which had been previously poisoned with water vapour at −62° C. The tube system up to the tap 6 was then exhausted and filled with nitrogen at known pressure. Varying quantities of this nitrogen could then be admitted to the oxygen via the dosing tube, but the oxygen remained glowless even when as much as 40% nitrogen was present. The initial oxygen pressure was also varied without success, experiments being tried with 0·12 mm, 0·23 mm, and 0·35 mm of oxygen. Similar experiments were performed dosing the oxygen with hydrogen, argon and carbon dioxide in turn, but all such attempts to produce an afterglow were abortive.

It may be noted in passing that no stray discharges, causing an experimental difficulty often met with in dealing with high frequency discharge currents, were ever noticeable in these investigations. This may have been largely due to the fact that the sole metal parts of the apparatus *i.e.*, the silver wire and the platinum wire, were at a considerable distance from the discharge and also separated from it by taps, thereby rendering it impossible for the high frequency current to find a passage to earth through the apparatus.

It is well known that oxygen in a simple electrode discharge tube with poisoned surfaces readily shows an afterglow on excitation, and, since the work just described gives results opposed to this general idea, it was decided to re-investigate carefully the phenomenon in an electrode discharge tube employing gases purified as for the experiments above.

---

* Wrede, 'Z. Physik,' vol. 54, p. 53 (1929).

ELECTRODE DISCHARGES

It is well known that oxygen is dissociated in an electrical discharge with the production of considerable concentration of the atomic form, which possesses powerful oxidizing properties. Copeland[*] found it necessary to use moist oxygen for this dissociation, the water vapour being required for poisoning the surfaces of the system, thereby minimizing the wall re-combination of the atoms. It is under such conditions that oxygen generally shows its afterglow best. It seemed clear that if the experiments described in the previous section had to be repeated in an electrode discharge tube, the metal electrodes of the latter would have to be constructed so as to facilitate their de-gassing. Discharge tubes are usually made in such a way that the electrodes remain as cool as possible, any tendency for the electrodes to sputter, which would lead to the destruction of any active body produced by the discharge, being thus prevented. Such a tube would be of little use in the present instance.

Thin sheet aluminium was employed for the manufacture of the electrodes, these being ¾ inch in diameter and 1½ inches long, supported on stout copper-clad wires leading through the glass. The tube was of the simple straight type, 2 feet in length and 1½ inches in diameter; the electrode chambers being 2 inches in diameter and thereby thermally insulating the electrodes as well as possible. This discharge tube was substituted for the observation tube, fig. 1, and was exhausted for half an hour. Pure oxygen was then admitted at a series of pressures between 0·1 and 0·5 mm, the electrical excitation employed being the high frequency discharge, the A.C. high voltage discharge and the condensed A.C. high voltage discharge. Intense afterglows were always obtained, and the duration of an afterglow was little affected by the type of discharge used. The following table gives the times of duration of the afterglow, measured visually with a stop watch, under the various conditions.

	0·12 mm	0·16 mm	0·24 mm	0·32 mm	0·48 mm
	secs.	secs.	secs.	secs.	secs.
High frequency	6	10	10	9	7
A.C. uncondensed	8	14	11	9	7
A.C. condensed	8	12	14	10	9

The electrodes were de-gassed in the following simple, though effective, manner. Pure oxygen at a pressure of 0·5 mm was admitted to the discharge tube and a heavy current passed through the gas, thus causing the electrodes and the walls of the tube to become heated with evolution of their adsorbed gases. The tube was evacuated whilst the discharge current was being passed, and it was not until 20 minutes later that the discharge current ceased owing to the complete evacuation of the tube. When the current ceased more oxygen was admitted, and the process was repeated several times. In this way, the tube was so thoroughly cleaned out that pure oxygen admitted to the tube remained spectrally free from nitrogen over a period of several hours. Incidentally, the process had the effect of baking the walls of the tube, which were left in a "clean" condition.

---

[*] 'Phys. Rev.,' vol. 36, p. 1221 (1930).

Pure oxygen was admitted to the tube at a series of pressures between 0·1 mm and 0·4 mm, but no afterglow was detectable on excitation of the gas. The walls of the tube were then poisoned in the usual manner, water vapour at (*a*) −80° C, (*b*) −62° C, (*c*) −40° C, (*d*) −22° C, and (*e*) 0° C being employed, but the oxygen remained glowless. Additions of argon, carbon dioxide and hydrogen were also tried, but without restoration of the glow. Such results conform with those described in the previous section.

However, the addition of nitrogen produced interesting results. On addition of 1% nitrogen to glowless oxygen contained in the tube with poisoned surfaces, an intense afterglow of long duration was easily obtainable. This restoration of the glow by the addition of pure nitrogen was observed over the usual range of pressures.

Extremely small quantities of nitrogen were found capable of restoring the glow to pure oxygen, as the following experiment shows. The surface gases were removed from the platinum wire in the bulb K by electrical heating *in vacuo*, after which, pure nitrogen at 1 cm pressure was admitted to the bulb and allowed to remain there overnight. The nitrogen was pumped away, and the bulb put into communication with the discharge tube containing glowless oxygen at 0·2 mm, the surfaces of the tube being poisoned as usual. The oxygen remained glowless so long as the platinum wire was not electrically heated, in which case, the glow was restored by the small quantity of adsorbed nitrogen liberated from the heated surface of the platinum. The oxygen remained glowless when the experiment was repeated with the platinum wire free from all adsorbed gases, or, when it was allowed to adsorb hydrogen, argon or carbon dioxide.

THE ROLE OF NITRIC OXIDE

Restoration of the afterglow by the addition of nitrogen to glowless oxygen in electrode discharge tubes is of interest since the phenomenon cannot be observed when electrodeless tubes are employed. The presence or absence of metal in the gas appears to be an important factor in these experiments. The fact that nitrogen is essential for the appearance of the afterglow at all, at once suggests that the phenomenon is the same chemiluminescence observed by Strutt* when nitric oxide and ozone are allowed to react together. If this is so, then absence of an afterglow in oxygen containing nitrogen in electrodeless discharges may be due to absence of the formation of ozone, nitric oxide or both. The formation of ozone has often been noticed in electrodeless discharges through oxygen, but it is of interest to note that the formation of nitric oxide in a discharge through oxygen-nitrogen mixtures is known to be dependent upon the nature of the surfaces of the electrodes.† Thus it is quite conceivable that the electrodeless discharge employed throughout the present work may not have been capable of synthesizing nitric oxide from a mixture of oxygen and nitrogen, thereby accounting for the non-appearance of the afterglow in these experiments. The following experiments will show that this is indeed the explanation.

An electrodeless discharge was passed through pure oxygen containing 2% nitrogen, the discharge tube being in communication with a trap cooled in CO_2-ether. Any nitric oxide produced by the discharge would be condensed in the trap as nitrogen peroxide, but none was ever chemically detectable. On repetition of the experiment with an electrode discharge tube, a strong afterglow was observed in all parts of the apparatus, even remote from the path of the exciting discharge, but, after a short time, the afterglow became less intense and finally almost disappeared. Addition of further small quantities of nitrogen restored the afterglow, which, again almost disappeared after a short time. It seemed as though some product, essential for the existence of the afterglow, was being removed in the cooled trap, and this indeed occurred, the produce being chemically identified as nitrogen peroxide. It may be noted in passing, that ozone, nitric oxide or nitrous oxide are not condensable at −80° C.‡

A large decrease in pressure was always noted in these experiments, and after the discharge had been passed for a long time, it was sometimes possible to decrease the pressure to such an extent that the discharge ceased to pass. The gas in the tube could be recovered by removing the cooling mixture and warming the trap. A similar instance of this extraordinary self-evacuation was noticed by Lewis (*loc. cit.*) in connection with the nitrogen afterglow. The phenomenon did not appear to be the usual " clean up " effect observed in discharge tubes, and was probably due to adsorption of the gas on the cooled nitrogen peroxide surfaces, since the gas could be recovered on warming the cooled trap. Moreover, the phenomenon did not occur in electrodeless discharges.

---

* 'Proc. Phys. Soc.,' vol. 23, p. 66 (1910).

† Briner, Corbaz and Wakker, 'Helv. Chim. Acta.,' vol. 14, p. 1307 (1931).

‡ *Cf.* Majewska and Bernhardt, 'Z. Physik,' vol. 48, p. 137 (1928).

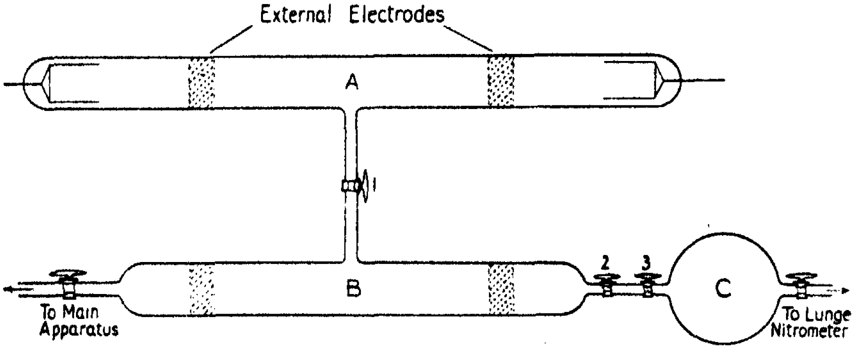

FIG. 2

The following further experiments were devised which show that the oxygen afterglow and the nitric oxide-ozone chemiluminescence are one and the same phenomenon. The discharge tube A, fig. 2, with aluminium electrodes was connected via a stop cock 1 to the simple electrodeless tube B which was employed in place of the observation tube X, fig. 1. Tap 2 was closed and the two discharge tubes baked and pumped out, the electrodes of tube A being thoroughly de-gassed by the passage of a heavy discharge current. The surfaces of the tubes were poisoned with water vapour and oxygen containing 1% nitrogen at 0·18 mm admitted to both tubes, which were then separated from each other by tap 1. Both tubes were electrodelessly excited at the same time, the distance between the external electrodes being the same in both cases. An afterglow of long duration was obtained in tube A but no afterglow was obtained in tube B, although when tap 1 was opened, both tubes possessed an afterglow. It is clear that since the same gas supply and mode of excitation were used in each case, the presence of metal was the deciding factor for the appearance of the afterglow.

It has been shown that absence of an afterglow in the electrodeless experiments was due to the lack of formation of nitric oxide. Consequently, the effect of the addition of small quantities of nitric oxide to such discharges through oxygen might be expected to lead to restoration of the afterglow. Bulb C was filled with pure nitric oxide from a Lunge nitrometer connected to tap 4, and the pressure of the gas in the bulb was reduced to about ½ cm in order to facilitate subsequent manipulations. The tubes A and B were thoroughly evacuated and pure oxygen at a suitable pressure admitted to both, after the walls had been poisoned in the usual way. Tap 1 was closed and the oxygen found to be glowless in both cases, owing to the absence of nitrogen. On admitting a small quantity of nitric oxide to the tube B, whilst the gas was being electrically excited, an intense flash of an afterglow was obtained throughout the entire length of the tube. This was the first case observed of an afterglow in an electrodeless tube without metal being present.

Lewis (*loc. cit.*) stated that an afterglow could be obtained in pure oxygen, but it is of interest to note that his apparatus had been previously used in a similar investigation of the nitrogen afterglow. In the light of the present work, it may be assumed that spectrally small quantities of nitrogen were liberated from the walls of his apparatus during the oxygen experiments, and nitric oxide was synthesized during the passage of the discharge, giving rise to an afterglow in what was presumably pure oxygen. It is peculiar that his electrodeless discharge should produce nitric oxide, but it is possible that he had stray discharges present which would lead to such a synthesis. One of the features of the present work was the designing of the apparatus in such a way as to avoid all such stray discharges.

A critical examination of the evidence leads to the conclusion that the afterglow of oxygen is only obtained under conditions favourable to the formation of nitric oxide in a discharge through oxygen containing traces of nitrogen.

THE AFTERGLOW SPECTRUM

Strutt (*loc. cit.*) described the chemiluminescence of the reaction between nitric oxide and ozone as being a continuous spectrum from 4200 A to 6700 A. The air afterglow and the oxygen afterglow have the same spectrum, but it was always doubtful whether or not the oxygen afterglow was due to the same emitter as the nitric oxide-ozone reaction. The present work leaves little doubt that this is so.

Electrolytic oxygen was passed through a water bubbler and a trap cooled to −78° C, streamed through a pressure reducing valve into an electrode discharge tube, and excited by a high voltage transformer; the glowing gas was drawn away from the discharge in the customary fashion by pumps. The spectrum of the afterglow was photographed through a quartz window by means of a Hilger constant deviation spectrograph. Exposures of 36 hours were made on Ilford Hypersensitive Panchromatic plates and it was of interest to observe that the spectrum was not strictly continuous. It consisted of 28 or 30 very weak diffuse bands spaced at equal intervals over the range 4200 A to 6700 A. It is quite impossible to produce a print from the plate owing to the lack of contrast of such high-speed plates. It is interesting to note that the nitric oxide bands were always absent, although it has been shown that its presence is essential for the afterglow. The hydroxyl band was observed in emission when larger quantities of water vapour were allowed to stream into the discharge tube with the oxygen.

Since no oxygen bands are present in the emission, the afterglow cannot be due to recombination of oxygen atoms, as in the nitrogen afterglow. Since the emission is only observed in presence of nitric oxide, it would appear that the emitter is some high oxide of nitrogen. The weak diffuse bands throughout the entire spectrum bring to mind the predissociation phenomenon with polyatomic molecules.

In its interaction with water vapour, the glowing gas is able to dissociate the water molecule with production of an unexcited hydrogen atom and an excited hydroxyl molecule. This requires very much more energy than the gas would be expected to possess with a limiting emission of 4200 A. In all probability, this dissociation effect is due to recombination of oxygen atoms which are known to be present in the chemically active gas. These oxygen atoms will also combine with oxygen molecules to form the ozone which is another constituent of the gas, although the oxygen atoms will mainly disappear owing to wall recombination with each other, since termolecular collisions are rare at these low pressures.

The author wishes to record his thanks to Professor F. G. Donnan, C.B.E., F.R.S., for the interest with which he has followed this work.

SUMMARY AND CONCLUSIONS

Pure oxygen is glowless in " clean " and " poisoned " vessels when excited electrodelessly. Addition of various gases, including nitrogen, does not restore the afterglow.

Pure oxygen is glowless in ordinary discharge tubes provided the electrodes are thoroughly de-gassed. Addition of various gases showed that only nitrogen was able to restore the glow.

Ordinary electrode discharges through oxygen-nitrogen mixtures readily synthesized nitric oxide, whereas the synthesis did not take place if electrodeless discharges were employed.

Addition of nitric oxide to an electrodeless discharge through pure oxygen produced an afterglow.

Glowing oxygen could be rendered glowless by trapping some active constituent from the gas at −80° C. This constituent was found to be nitrogen peroxide.

The afterglow spectrum has been carefully examined and found to consist of weak diffuse bands from 4200 A to 6700 A.

It is concluded that the oxygen afterglow is due to the same emitter as present in the nitric oxide-ozone reaction.

The Reflection of X-Rays from Powdered Anthracene

By B. WHEELER ROBINSON, The Davy Faraday Laboratory, The Royal Institution, London

(*Communicated by Sir William Bragg, O.M., F.R.S.—Received July* 3, 1934)

1—INTRODUCTION

In a previous communication* the author has described absolute measurements of the intensity of reflection of X-rays from the (001) planes of single crystals of anthracene. According to these measurements, the structure factor was slightly greater for the wave-length 0·709 A than it was for the wave-length 1·539 A. Such a difference has no theoretical basis, and it is important to determine whether it has a real existence.

The most uncertain factor in these measurements appeared to be the application of the correction for absorption and extinction to the single crystal, particularly with the softer radiation; and it seemed worth while to attempt to overcome this difficulty by the substitution of a powder for the single crystal. Using a block of powdered particles, the conditions are much nearer the ideal from the theoretical point of view; the block can be given a definite geometrical shape, and the effects of absorption and primary and secondary extinction can be exactly estimated.

---

* 'Proc. Roy. Soc.,' A, vol. 142, p. 422 (1933).

If for example, fig. 1, a parallel beam of monochromatic X-rays defined by a stop S is incident normally on a uniform block of powder of thickness T, the total X-ray intensity C diffracted in a cone of semi-angle 2θ can be written down immediately in terms of W the mass per unit area of the powder, M the total energy of the beam emerging from the block, F the structure factor of the reflecting planes of the crystal lattice, and known constants. The absorption coefficient of the rays in the block enters only as a small correction term, if the angle 2θ is small. It is not necessary to know the area of cross-section of the beam, nor need the X-ray intensity be uniform over this cross-section. Consequently the measurement of the structure-factor is in essentials a simple one, involving only the comparison of two X-ray beams C and M, and the weighing of a given volume of the powder.

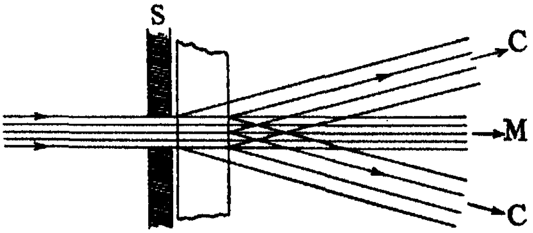

FIG. 1

A further great advantage of this method of measurement is that the effects of primary extinction on the observed intensity, which were disregarded in the earlier measurements, can be limited to a known amount. For particles of anthracene of average size 1 μ and for $\lambda = 0 \cdot 709$ A, the Darwin primary extinction factor is about $0 \cdot 96$; *i.e.*, not more than 2% error would arise from this cause in the calculation of the structure factor. Havighurst* concluded that the effective size of the particles of a powder of rock-salt was much less for this purpose than their physical dimensions ; if, as seems reasonable, the same is true for the soft and often very imperfect crystals of anthracene, we can entirely neglect the effects of primary extinction for a powder of particles of size the order of 1 μ.

On the other hand, if we abandon the single crystal in favour of the powder, we meet with fresh experimental difficulties, of which the chief is the question of intensity. Also, even slight compression of the powder produces marked orientation of the component crystals, and so leads to fictitious intensity measurements.

---

* 'Phys. Rev.,' vol. 28, p. 882 (1926).

2—APPARATUS

The X-ray source, spectrometer and ionization current amplifier, were in all essentials the same as those previously described (*loc. cit.*). The ionization chamber was rebuilt to adapt it for the measurement of the complete cone of diffracted radiation. The steel electrode was mounted centrally behind a large window of cellophane backed with aluminium foil in the front of the chamber, whose walls were of thin steel tube. A series of annular diaphragms could be mounted with their centres on the axis of the chamber; these diaphragms were made of brass, the central portion being positioned with three fine wires. An allowance for the effect of these wires in obstructing the passage of rays to the chamber could easily be made. The whole chamber with its amplifier could be slid parallel to its axis, which was adjusted to be in the plane of the incident X-rays and at right angles to the axis of the spectrometer.

A set of series-parallel resistances controlled the galvanometer sensitivity over a wide range, and the intensity of the main beam was reduced by the use of a spinning sector disc, which gave a reduction of about 50 : 1. The disc was 25 cm in diameter, and this reduction factor could be found fairly accurately by geometrical measurement. Over the apertures of the disc absorbing screens could be placed which reduced the beam in a known ratio (of the order of 6 : 1); these screens were of glass, celluloid or aluminium. The effect of the screens could be measured directly in terms of the shunts, and that of the spinning disc in terms of the screen and shunts together: intercomparisons were made until confidence was gained in the separate or combined use of each of these three methods of reducing the apparent intensity of the beam.

3—EXPERIMENTAL PROCEDURE

The Powder—It was found that by long-continued grinding of small quantities of anthracene in an agate mortar a powder was obtained whose particles had a size of from 5 μ to 1 μ as measured under the microscope. A more uniform powder could be prepared by precipitation from solution. A hot fairly concentrated solution of anthracene in either alcohol or acetone was quickly mixed with an excess of hot water; the anthracene was precipitated immediately as a flocculent precipitate which was washed and dried in a vacuum desiccator. This procedure gave a remarkably uniform powder whose particles were usually between 1 and 2 μ in size; the exact value seemed to depend partly on the temperature of precipitation. Kahlbaum's "research" grade material was employed in the preparation of the powder.

During the measurement the powder was contained in a small metal press, by which it could be given a definite volume, that either of a cylinder or of a rectangular prism, fig. 2. After a very gentle compression to the required shape, the sides A or the plunger and plate B could be removed, leaving the powder block still supported at the sides but accessible to the X-rays. After the measurement the mass of powder could be carefully pushed out into a weighed watch-glass for the determination of its density.

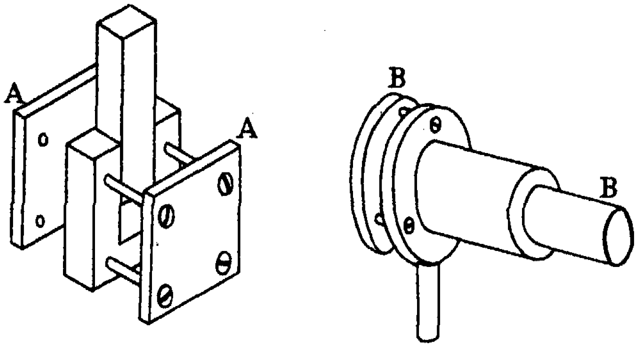

FIG. 2

Procedure—Fig. 3 shows the general arrangement of the apparatus. C is the monochromatizing crystal; the beam is defined by the circular apertures X, Y, of about 1 mm diameter, between which the spinning disc D revolves. P is the powder block, S a small stop carried on a fine wire and adjusted to absorb as much as possible of the main beam after its passage through the powder; thereby diminishing the general scattering from the air in front of the powder (which might easily become comparable with the powder scattering which we wish to measure). This stop is carried on a swinging arm so that it can be removed during the

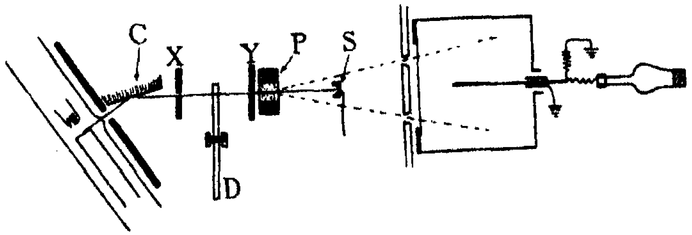

FIG. 3

measurement of the main beam. Both the stop and the second of the apertures Y are adjustable by screw motions in three dimensions.

A set of four annular diaphragms is used for each measurement, of radii so adjusted, fig. 4, that if, for example, C is positioned to include all the diffracted energy from the (001) planes, A and B should give no intensity (since their apertures lie wholly outside or inside that of C) while D, which is slightly larger than C, should give the same reading, as a check on the proper adjustment of C. Actually, of course, the inner and outer diaphragms will always give a measureable background ionization current due to general scattering from the air, slits, etc.; the amount of this background was usually about one-tenth of the reading given by the ring itself, and its average value, after correction for the relative area of the different diaphragms, was subtracted from the observed reading of C.

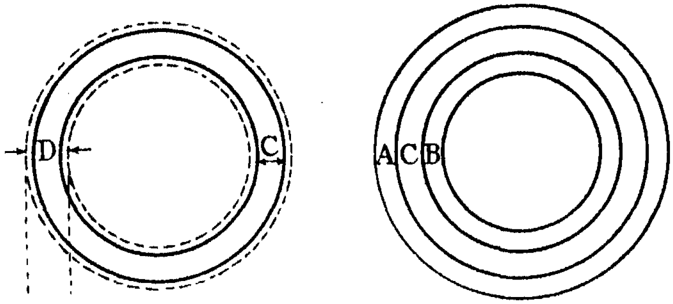

FIG. 4

Having secured a proper adjustment of the diaphragms, and observed the ionization current corresponding to each of them, the centre stop is removed, the chamber swung through an angle 2θ, the disc and absorber brought into action, and the intensity of the main beam through the powder recorded. A further measure of the same beam is made with the powder removed, from which σ, the transmission of the powder, may be found if necessary. The pellet of powder, whose dimensions are known from those of the container, is carefully pushed out on to a watch-glass and weighed; hence the density is calculable. The measurement is now complete. In practice for each pellet the main beam and the ring intensity are each measured three or four times alternately, as a check on the constancy of emission of the X-ray tube.

Calculation of the Results—The powder scattering formula as usually quoted* is:—

$$C/I_0 = Q \, . \, p/2 \cos 2\theta \, . \, V.$$

---

[*] Darwin, 'Phil. Mag.,' vol. 27, p. 675 (1914).

Here C is the total intensity diffracted in a cone of semi-angle 2θ, V the volume of the element of powder, I_0 the primary intensity per unit area at the powder, while Q has its usual meaning, involving the structure factor F and known constants. In our case p, the number of positions in which a given set of planes can contribute to the total intensity, is 2.

Consider now a block of powder of thickness t, with an incident beam of total intensity M, an emergent beam of intensity M/σ. Also let μ_0 be the linear absorption coefficient of the radiation in compressed anthracene powder of maximal density ρ_0 (the actual density of any sample will, of course, be some less value ρ and its absorption coefficient will be μ). Then by integrating the diffracted intensity over the thickness of the block and over the cross-section of the beam, we obtain the following expressions for the total diffracted intensity:—

$$C = Q \,.\, M \log_{10} \sigma \,.\, 2{\cdot}303 \cos 2\theta \,.\, \frac{1}{\mu_0} \qquad \text{(i)}$$

$$C = Q \,.\, MW \,.\, \cos 2\theta \,.\, \frac{1}{\rho_0}. \qquad \text{(ii)}$$

To find Q, using either of these expressions, we have to measure the diffracted energy in the cone C and M, the main beam energy which traverses the powder; (i) requires in addition the measurement of σ, the transmission of the powder, and (ii) the measurement of W, the weight of powder per unit area. Formula (i) is the easier to apply, since the measurement of σ is quickly carried out without removing the powder from the holder; but it suffers from the disadvantage that a small error in σ, if this quantity is nearly unity, *i.e.*, if the powder block is not very thick, is very serious in the final results. In consequence the measurements were mostly made using formula (ii), involving a separate weighing of the powder, which is assumed to be of uniform density throughout the block. This assumption is easily checked by using a narrow X-ray beam and moving the powder block about in it, the transmitted intensity being observed meanwhile.

These formulæ have been calculated on the assumption that the path of each ray in the block is equal to the thickness of the block. This assumption is not, of course, true, and it is necessary to evaluate a correction for the oblique paths of the rays. The calculation is simply performed, and the result is that the observed intensity of the cone must be multiplied by the factor $1/\{1 - \frac{1}{2}\mu t (\sec \theta - 1)\}$ to make the formula applicable (in this calculation 2θ is supposed to be small). For anthracene (001) the value of this correction is only $0{\cdot}998$ for Cu Kα and

0·9998 for Mo Kα, even assuming that the thickness t and the absorption μ of the block is the maximum which was ever used in these experiments.

Non-monochromatism of the Beam—A more awkward correction is that due to the presence of unwanted radiation of half the proper wave-length in the " monochromatic " beam derived from the analysing crystal. This effect was discussed in the work with single crystals, and there allowance was made for it by analysing the beam with a large rock-salt crystal. In the present experiments a different monochromator arrangement had been adopted, and it was necessary to make a re-determination of the percentage of this unwanted radiation in the beam. This was done by an absorption method, leading to the figures 0·5% $\lambda/2$ radiation for the molybdenum target, and 0·4% for the copper target.

The presence of $\lambda/2$ in the main beam affects the measurements in several ways: thus (*a*) the transmitted beam will appear to be too strong in relation to the scattered ring, as the $\lambda/2$ which it contains makes no contribution to this ring; (*b*) superposed on the ring will be some energy representing the reflection of the $\lambda/2$ radiation by those planes in the crystal which have about half the spacing of the (001) planes. For anthracene there is a small group of such planes, including the (002) and the very strong (110), the reflection of $\lambda/2$ from which will pass through the annular slit and be recorded in the ionization apparatus; (*c*) a further error will be caused in the apparent values of the absorption both of the powder block and also of the screens used to reduce the intensity of the primary beam ; owing to the presence of the $\lambda/2$ radiation these values will appear too low. A detailed calculation was made of these effects, allowing also for the fact that the absorption of both radiations in the ionization chamber is not necessarily complete; the errors are to a certain extent self-cancelling, and the final result was that, for x per cent. of $\lambda/2$ radiation in the main beam, the observed ring intensity must be increased by a factor of $0{\cdot}6x\%$ for the copper target and $0{\cdot}33x\%$ for the molybdenum target.

As a further measure of safety, in the later measurements the pressure of absorbing gas in the ionization chamber (argon or methyl bromide) was chosen so as to give only 85% of the complete absorption of the λ radiation; we may calculate approximately that in this case only 20% of the $\lambda/2$ radiation will be absorbed in the same chamber, *i.e.*, the chamber will be very inefficient for this wave-length. This device is equivalent to the reduction of the proportion of $\lambda/2$ radiation in the main beam, at the expense of a small diminution of its intensity.

The Measurement of μ_0—In the formula (i) we need to know the value of the linear absorption of the anthracene powder at maximum density. This was found experimentally, by preparing pellets of the fine powder by compression in a hydraulic press with pressures of the order of 40 tons per square inch. The thickness of the pellet, ranging from ½ to 5 mm, was measured with a micrometer, and its absorption was found on the ionization apparatus. The density was determined (*a*) from the weight and dimensions, (*b*) by weighing in water. The results shown in Table I were obtained ; using the copper target ($\lambda = 1 \cdot 539$ A).

TABLE I

Thickness mm	Density	Direction	Absorption Cofficient (corrected to density $\rho_0 = 1 \cdot 258$)
3·04	1·222	A	0·547
2·01	1·222	B	0·552
1·23	1·244	A	0·553
1·00	1·210	B	0·558

In Table I A indicates that the direction of X-rays in the measurement was parallel to the direction of compression, and B that it was at right angles to it. It will be seen that the high degree of orientation, which must have been present in these compressed blocks, has made no great difference to the value of the absorption coefficient. Taking the mean of these results, this value is 0·553 per mm, and is definitely higher than the value (0·503, *loc. cit.*) previously adopted as the result of measurements of single crystals. A further pellet was made from roughly powdered anthracene taken from the stock bottle, without the process of precipitation to give the fine powder; this pellet gave for μ_0 the value 0·508, agreeing with the single-crystal value. This discrepancy in the values of μ_0, which much exceeds the probable experimental error, will be further investigated.

Orientation of the Powder—Mention has already been made of the difficulties which may arise due to orientation of the anthracene powder, the crystals of which are in the form of thin plates. It was found that if the degree of compression was such as to give a fairly hard block, which could be handled without a supporting framework, considerable orientation effects were present. The figures in Table II illustrate this effect; a given mass of powder was enclosed in a circular press and the diffraction measured with increasing compression, *i.e.*, diminishing thickness of the slab.

If there were no orientation, the figures in the last column should, of course, remain constant.

Consequently it was necessary to make all the measurements at the minimum possible degree of compression.

After making the pellet its uniformity could be checked in the X-ray beam; with fairly thick pellets, 3–4 mm, it was not found difficult to produce uniform density. The surface of the pellets, though possessing quite a good plane surface, would crumble immediately if touched.

TABLE II

Thickness (mass constant) cm	$C/M \log_{10} \sigma$ arbitrary units
0·485	3·20
0·395	3·00
0·345	2·79
0·235	2·24
0·185	1·76

In the results listed in the next section, Table III, the symbols A or B indicate, as in the previous section, the direction of the X-ray beam in relation to the direction of motion of the plunger in the process of forming the pellet. From the fact that there is no significant difference between the A and the B results, we may infer that orientation effects are absent ; since any orientation would have the result of increasing the B figures and diminishing the A ones.

4—FINAL RESULTS

After the preliminary measurements had been made, three series of figures were taken on various samples of powder, the first with the copper target and the calculation with formula (i) above, the second and third using formula (ii) and with molybdenum and copper targets respectively. Each of these figures represents a separate self-contained determination, being the average of several measurements on a given pellet. The particular sample of powder, the thickness of the pellet, and the particular absorber used in the main beam measurement, were varied from time to time in the endeavour to eliminate systematic errors.

The results obtained are shown in Table III.

TABLE III

1 Formula (i), $\lambda = 1{\cdot}539$ A

Thickness mm	Direction	$\text{Log}_{10}\,\sigma$	C/M $\log_{10}\sigma$
1·5	B	0·150	3·31
1·5	B	0·210	3·26
—	A	0·319	3·20
2·0	B	0·268	3·38
2·0	B	0·276	3·38
2·0	B	0·259	3·48
—	A	0·152	3·19
—	A	0·245	3·16

2 Formula (ii), $\lambda = 0{\cdot}709$ A

Thickness mm	Direction	Wt/unit area	C/MW
5·7	A	0·2083	4225
6·8	A	0·2028	4220
6·1	B	0·1381	4250
6·1	B	0·2588	4260
6·1	B	0·1917	4610
6·1	B	0·2020	4710
7·5	A	0·1751	4255
4·5	A	0·3062	4380

3 Formula (ii), $\lambda = 1{\cdot}539$ A

Thickness mm	Direction	Wt/unit area	C/MW
2·0	B	0·0966	911
2·0	B	0·0600	899
4·2	A	0·1109	867
3·1	A	0·0855	849
6·1	B	0·1732	827
6·1	B	0·1883	825
6·1	B	0·1780	859
6·1	B	0·1659	824
2·0	B	0·0444	880
5·4	A	0·1340	860

From the average values of the last columns of this table, after applying the appropriate factors, we obtain values for Q, and hence, since $Q \propto F^2$, for the structure factor F. The results are :—

1. ($\lambda = 1{\cdot}539$ A) $F = 34{\cdot}2 \pm 0{\cdot}14$
2. ($\lambda = 0{\cdot}709$ A) $F = 33{\cdot}9 \pm 0{\cdot}18$
3. ($\lambda = 1{\cdot}539$ A) $F = 34{\cdot}8 \pm 0{\cdot}13$.

The probable errors are here calculated from the spread of the figures in the last columns of Table III, which should, of course, be constant. Giving equal weights to each of these three results, and making an allowance for the possible errors in the calibration of the apparatus (galvanometer shunts, spinning disc, etc.) the final result is :

$$F(001) = 34 \cdot 3 \pm 0 \cdot 3.$$

In these calculations the corrections for the crosswires on the aperture systems were of the order of 2%, and those due to the presence of $\lambda/2$ radiation of the order of 0·3%. The values for the constants of anthracene were taken as in the previous work.

Discussion—We see that as a result of these powder measurements the previous discrepancy which was found in the single crystal measurements between the F values as determined with the two radiations has disappeared, and the value of F itself appears to be higher. It is tempting to ascribe this increase to the previous effects of primary extinction in the single crystals; it will be remembered that no attempt was made to allow for this effect. An obvious extension of the work would be to make a series of measurements on powders of gradually increasing grain size; if this explanation is correct, a gradual fall in the value of F should appear with increasing size. Though with the larger powders further difficulties in regard to orientation may be expected, experiments on these lines will be undertaken. The original discrepancy which led to the making of these powder measurements is presumably due to an incomplete application of the absorption and secondary extinction corrections to the results with copper radiation and single crystals. It is interesting to note that the final result of the present work, F = 34·3, gives good agreement with the figure (F = 34·0) assumed by Robertson for this constant in his work on the structure of anthracene.* His value was deduced from an extrapolation of the graphite scattering curves of Bernal, Ponte and Lonsdale.†

In conclusion, my thanks are due to Sir William Bragg and to the Managers of the Royal Institution for the opportunity of carrying out this work, and to my assistant Mr. R. Dawton for his continuous help.

SUMMARY

Previous measurements by the author of the F(001) value for single crystals of anthracene showed a discrepancy between the values obtained

---

* 'Proc. Roy. Soc.,' A, vol. 140, p. 79 (1933).

† *Cf.* Proc. Roy. Soc. A,, vol. 123, p. 499 (1929).

with two different X-ray wave-lengths. Measurements with powdered crystals are more satisfactory in that absorption and extinction effects can be accurately estimated; the technique of making such measurements with anthracene is described, and the results give the same value for either wave-length, the value being somewhat higher than that previously found (34·3 as against 30·5 and 32·8).

The Principle of Least Action in Milne's Kinematical Relativity

By A. G. Walker, Ph.D., Senior Scholar of Merton, and Senior Mathematical Scholar of the University of Oxford

(*Communicated by E. A. Milne, F.R.S.—Received July* 7, 1934)

1—Introduction

In a recent paper,[*] Professor Milne has obtained a gravitational field with non-zero density of matter in flat space-time, the field in question being appropriate to the whole cosmos. It was obtained, without recourse to a formal theory of gravitation, by constructing a system of particles in motion satisfying Einstein's cosmological principle applied to a set of fundamental observers in uniform relative motion: the result was a set of motions and a particle-density distribution which would be described in the same way by each one of the fundamental observers. This method of obtaining a gravitational field is fundamentally different from Einstein's, the applicability being dependent upon explicit recognition of the principle[†] that "an observer can either (*a*) select any one of the spaces of pure geometry presented to him by the mathematician, use it in order to describe the phenomena of nature, and then infer the laws obeyed by natural phenomena in this space; or alternatively (*b*) posit beforehand the laws of nature he wishes to see obeyed and then determine the space in which, in consequence, he must embed the phenomena he describes." Einstein's theory of gravitation consists essentially in obtaining a metric ds^2 such that a free particle obeys the law of nature $\delta \int ds = 0$, and is an example of alternative (*b*). The gravitational field for the system described above begins by selecting Euclidean space and Newtonian time for any one observer, the different observers' spaces and times being connected by Lorentz transformations, and then determines the laws of motion in this space ; it is an example of alternative (*a*). The laws of motion were obtained as formulæ for the components of acceleration of a free particle as functions of the seven variables, t, x, y, z, u, v, w, reckoned from defined zeros.

---

[*] 'Z. Astrophys.,' vol. 6, pp. 1, 95 (1933).

[†] Milne, *loc. cit.*, p. 29.

The alternative procedures have been recently stated very clearly by Milner. He wrote*: " Two courses are open to us. (1) We can modify the geometry assumed in the relation $ds^2 = \sum_{i=1}^{4} (dx^i)^2$ so that a mathematically straight track (*i.e.*, its length obeys a stationary principle) still continues to represent the non-uniform motion of a particle; this is the method of general relativity. (2) We can retain the four-fold with unaltered geometry and specify a curved track which represents the observed motion by weighting each element of its length so that the integral weighted length between two points is stationary; this is the method of ' least action.' Both these methods of describing the motions of bodies must be considered equally logical when one remembers that a manifold (even when it is called ' space-time ') is not the actual world, but a mental concept, in which real phenomena are represented symbolically."

Milne has recently† solved a more fundamental problem, and has found *the equations of motion of a free test-particle in the presence of a simple kinematical system.* Referring to an observer attached to a particle of this system, the set of particles constituting a simple kinematical system are distributed with particle density n given by

$$n\,dx\,dy\,dz = \frac{\mathrm{B}t\,dx\,dy\,dz}{c^3\{t^2 - (x^2+y^2+z^2)/c^2\}^2} \qquad (1)$$

and move with the velocity components

$$u = x/t, \qquad v = y/t, \qquad w = z/t, \qquad (2)$$

where B is a pure constant specifying the system, and t, x, y, z are the co-ordinates of any event in the experience of the observer at the origin.

---

* ' Proc. Roy. Soc.,' A, vol. 139, p. 349 (1933).

† Lecture before the London Mathematical Society: " World-gravitation by Kinematic Methods," May 17, 1934. Professor Milne has kindly given me access to the text of the lecture, which is in course of publication.

Milne found that, in the presence of this system, the motion of a free particle passing through the point (x, y, z) at epoch t with velocity components (u, v, w) is of the form

$$\frac{du}{dt} = (x - ut)\frac{\mathrm{Y}}{\mathrm{X}}\,\mathrm{G}(\xi), \qquad u = \frac{dx}{dt}, \tag{3}$$

etc., where

$$\mathrm{X} = t^2 - \Sigma x^2/c^2, \quad \mathrm{Y} = 1 - \Sigma u^2/c^2, \quad \mathrm{Z} = t - \Sigma xu/c^2; \quad \xi = \mathrm{Z}^2/\mathrm{XY}, \tag{4}$$

and $\mathrm{G}(\xi)$ is not further determined by the arguments used.

The general kinematical system first proposed by Milne may now be constructed by the addition of a statistical system of particles to the above simple system, distributed and moving in such a way that the set of motions and the density distribution would be described in the same way by each one of the fundamental observers attached to the particles of the simple system. It is to be observed that the equations of motion of a particle of the general system have the same form* as the equations of motion (3) of a test-particle in the presence of the simple system. The form of $\mathrm{G}(\xi)$ is, however, different, and for the general system, it is to be expected that $\mathrm{G}(\xi)$ is arbitrary, thus allowing for the existence of a variety of such systems.

The equations of motion of a particle in the field of the simple kinematical system were originally obtained by a transformation method; the object of this paper is to show how, following Milner, these equations can be expressed under the form of the principle of least action. That is to say, we shall find the weighting factor W such that the equation $\delta \int \mathrm{W}ds = 0$, where $ds^2 = dt^2 - \Sigma dx^2/c^2$, reproduces Milne's equations of motion. Substituting any appropriate form of $\mathrm{G}(\xi)$ in W, we at once have an equation giving the equations of motion of a particle of the general kinematical system, so that, when W is found for the simple system, we shall have solved the problem for the general system.

It is very satisfactory in itself to show that the free particles of Milne's structure obey a law of nature which can be described in the form of a principle of least action, but the results of this paper are of further interest when we come to consider the form of Wds. Milner has recently† pointed out that as soon as the weighting factor is found for a particular metrical geometry, the corresponding factor can at once be found for any other geometry, any given event being described by the same co-ordinates

---

[*] Milne, *loc. cit.*, p. 56.

[†] 'Nature,' vol. 133, p. 830 (1934).

in all such spaces. In particular, the space in which the free paths are geodesics, or curves of stationary length, must have the metric $d\sigma^2 = W^2 ds^2$. If, therefore, $d\sigma^2$ is a quadratic in the co-ordinate differentials, the geometry is Riemannian, and the system of particles is a kinematical system of general relativity. If, however, W cannot be chosen so that $d\sigma^2$ is a quadratic in the differentials, the given system is not included in the systems described by the methods of general relativity.* We shall show by this method that Milne's system is fundamentally different from that of general relativity.

2—DETERMINATION OF THE WEIGHTING FACTOR

The equations of motion of a free particle in the field of a simple kinematical system are the equations (3). These equations are invariant under a transformation from the fundamental particle at the origin to any other given or fundamental particle of the system, Y and Z are covariant, and X and ξ are invariant. A particular form of this transformation is when the given fundamental particle has velocity components (v, o, o) in which case we have the Lorentz transformation

$$t' = \beta(t - vx/c^2), \quad x' = \beta(x - vt), \quad y' = y, \quad z' = z;$$
$$\beta = (1 - v^2/c^2)^{-1/2}.$$

The following identities will be required. Writing

$$\chi = G(\xi)\, Y/X, \tag{5}$$

then from (3) and (4) we have

$$\frac{dX}{dt} = 2Z, \qquad \frac{dY}{dt} = 2\chi(Z - tY) \tag{6}$$

$$\frac{dZ}{dt} = Y + \chi(X - tZ) \tag{7}$$

$$\frac{d\xi}{dt} = -2(\xi - 1)\frac{Z}{X}\left(1 + \frac{X}{Y}\chi\right). \tag{8}$$

If the paths satisfy a principle of least action, there must exist a function W of t, x, y, z, u, v, w, such that equations (3) are given by

$$\delta \int W ds = 0, \tag{9}$$

---

* In general relativity it is assumed that the paths of freely moving particles can be represented by the geodesics in a Riemannian space.

where

$$ds^2 = dt^2 - \Sigma dx^2/c^2 \tag{10}$$

and the integral is taken between two arbitrary field events. As *ds* and equations (3) are invariant in form under transformations from one observer to another, W can depend only on the two invariants X, ξ.

By (10) and (4)

$$ds/dt = \mathrm{Y}^{\frac{1}{2}} = \mathrm{Z}\mathrm{X}^{-\frac{1}{2}}\xi^{-\frac{1}{2}},$$

whence, writing

$$\mathrm{W}(\mathrm{X}, \xi) = \mathrm{X}^{\frac{1}{2}}\xi^{\frac{1}{2}}\mathrm{V}(\mathrm{X}, \xi), \tag{11}$$

V is required to satisfy

$$\delta \int \mathrm{ZV}\, dt = 0. \tag{12}$$

Varying x, y, z as functions of t, (12) leads to the Lagrangian equations

$$\frac{d}{dt}\left\{\frac{\partial}{\partial u}(\mathrm{ZV})\right\} - \frac{\partial}{\partial x}(\mathrm{ZV}) = 0, \tag{13}$$

etc., and V must be such that the equations resulting from (13) are equivalent to (3).

Writing

$$\mathrm{A} = \frac{\mathrm{Z}}{\mathrm{Y}}\xi\frac{\partial \mathrm{V}}{\partial \xi}, \tag{14}$$

$$\mathrm{B} = \xi\frac{\partial \mathrm{V}}{\partial \xi} + \tfrac{1}{2}\mathrm{V} = \frac{\mathrm{Y}}{\mathrm{Z}}\mathrm{A} + \tfrac{1}{2}\mathrm{V}, \tag{15}$$

we have identically, by (4),

$$\frac{c^2}{2}\frac{\partial}{\partial x}(\mathrm{ZV}) = -\mathrm{B}u + \left(\frac{\mathrm{Y}}{\mathrm{X}}\mathrm{A} - \mathrm{Z}\frac{\partial \mathrm{V}}{\partial \mathrm{X}}\right)x,$$

$$\frac{c^2}{2}\frac{\partial}{\partial u}(\mathrm{ZV}) = \mathrm{A}u - \mathrm{B}x,$$

etc. Hence by (3) and (5),

$$\frac{c^2}{2}\frac{d}{dt}\left\{\frac{\partial}{\partial u}(\mathrm{ZV})\right\} = \left(\frac{d\mathrm{A}}{dt} - \mathrm{B} - \mathrm{A}t\chi\right)u - \left(\frac{d\mathrm{B}}{dt} - \mathrm{A}\chi\right)x,$$

etc., and equations (13) become

$$\left(\frac{d\mathrm{A}}{dt} - \mathrm{A}t\chi\right)u - \left\{\frac{d\mathrm{B}}{dt} + \left(\frac{\mathrm{Y}}{\mathrm{X}} - \chi\right)\mathrm{A} - \mathrm{Z}\frac{\partial \mathrm{V}}{\partial \mathrm{X}}\right\}x = 0, \tag{16}$$

etc. We have, by (15), (14), and (6),

$$\frac{dB}{dt}+\left(\frac{Y}{X}-\chi\right)A-Z\frac{\partial V}{\partial X}=\frac{Y}{X}\left(\frac{dA}{dt}-At\chi\right).$$

Hence equations (16) become

$$\left(u-\frac{Y}{Z}x\right)\left(\frac{dA}{dt}-At\chi\right)=0,$$

etc., and these equations are satisfied only if $u=xY/Z$, etc., or if $dA/dt=At\chi$. The first alternative at once gives $u=x/t$, etc., which are the equations of motion (2) of particles of the given kinematical system. The form of $V(X, \xi)$ for the general motion of a free particle must accordingly be given by

$$dA/dt=At\chi. \tag{17}$$

We define $\phi(X, \xi)$ by

$$\phi(X, \xi)=\log(X\xi^2\,\partial V/\partial\xi). \tag{18}$$

Then (14) becomes $A=Z^{-1}\exp.\,\phi$, and (17) becomes

$$t\chi=\frac{d}{dt}(\log A)=\frac{d\phi}{dt}-\frac{1}{Z}\frac{dZ}{dt},$$

i.e.,

$$t\chi=\frac{\partial\phi}{\partial X}\frac{dX}{dt}+\frac{\partial\phi}{\partial\xi}\frac{d\xi}{dt}-\frac{1}{Z}\frac{dZ}{dt}. \tag{19}$$

Substituting from (5), (6), (7), and (8), equation (19) becomes

$$\frac{X}{1+G(\xi)}\frac{\partial\phi}{\partial X}-(\xi-1)\frac{\partial\phi}{\partial\xi}=\frac{1}{2\xi}, \tag{20}$$

a partial differential equation in X and ξ only, defining the function ϕ we are seeking. This equation can be integrated at once, and the general solution can be written in the form

$$\phi=\log\left[\Theta\{X\theta(\xi)\}(\xi-1)^{-\frac{1}{2}}\xi^{\frac{1}{2}}\right]\;:\;\theta(\xi)=\exp\int^{\xi}\frac{d\xi}{(\xi-1)\{1+G(\xi)\}}, \tag{21}$$

where Θ is an arbitrary function of its argument. Substituting (21) in (18), we find that V is given by

$$\frac{\partial V}{\partial\xi}=X^{-1}\,\Theta\{X\theta(\xi)\}(\xi-1)^{-1/2}\xi^{-3/2},$$

whence, from (11), the weighting factor W is

$$\mathrm{W} = \mathrm{X}^{-\frac{1}{2}}\xi^{\frac{1}{2}} \int_{f(\mathrm{X})}^{\xi} \Theta\{\mathrm{X}\theta(\xi)\}\,(\xi - 1)^{-1/2}\,\xi^{-3/2}\,d\xi, \tag{22}$$

where Θ, f are arbitrary functions and $\theta(\xi)$ is given by

$$\theta(\xi) = \exp \int_{\infty}^{\xi} \frac{d\xi}{(\xi - 1)\,\{1 + \mathrm{G}(\xi)\}}, \tag{23}$$

X remaining constant in the integration in (22). The lower limit of the integral in (23) may be any arbitrary constant, but this does not affect the form of W as Θ is arbitrary. Milne has shown, in his unpublished work, that $\mathrm{G}(\xi)$ must be such that $\theta(\xi)$ converges as $\xi \to \infty$.

3—REPRODUCTION OF THE EQUATIONS OF MOTION

We have now shown that if there exists a weighting factor $\mathrm{W}(\mathrm{X}, \xi)$, it must be of the form (22), and it can now be verified that $\delta\int \mathrm{W}\,ds = 0$ does, in fact, reproduce Milne's equations of motion except in the degenerate case $\Theta \equiv \text{const.}$

In the notation of § 2,

$$\mathrm{A} = \mathrm{X}^{-\frac{1}{2}}\mathrm{Y}^{-\frac{1}{2}}\,(\xi - 1)^{-\frac{1}{2}}\Theta\{\mathrm{X}\theta(\xi)\}, \tag{24}$$

and equations (13) become

$$\mathrm{A}\frac{du}{dt} = \left(\frac{\mathrm{Y}}{\mathrm{Z}}\frac{d\mathrm{A}}{dt} + \frac{\mathrm{A}}{2\mathrm{Z}}\frac{d\mathrm{Y}}{dt}\right)x - \frac{d\mathrm{A}}{dt}u,$$

etc. We can therefore write

$$du/dt = \mathrm{P}x - \mathrm{Q}u, \tag{25}$$

etc., where

$$\mathrm{P} = \frac{\mathrm{Y}}{\mathrm{ZA}}\frac{d\mathrm{A}}{dt} + \frac{1}{2\mathrm{Z}}\frac{d\mathrm{Y}}{dt}, \qquad \mathrm{Q} = \frac{1}{\mathrm{A}}\frac{d\mathrm{A}}{dt}. \tag{26}$$

Hence, by (4) and (25),

$$\mathrm{P} - \frac{\mathrm{Y}}{\mathrm{Z}}\mathrm{Q} = \frac{1}{2\mathrm{Z}}\frac{d\mathrm{Y}}{dt} = -\frac{\mathrm{P}}{\mathrm{Z}}(t - \mathrm{Z}) + \frac{\mathrm{Q}}{\mathrm{Z}}(1 - \mathrm{Y}),$$

i.e.,

$$\mathrm{Q} = t\mathrm{P}. \tag{27}$$

From (4), (25), and (27),

$$\left.\begin{aligned} \frac{dX}{dt} = 2Z, \quad \frac{dY}{dt} = 2P\,(Z - tY), \quad \frac{dZ}{dt} = Y + P\,(X - tZ) \\ \frac{d\xi}{dt} = -\frac{2Z}{X}(\xi - 1)\left(1 + \frac{X}{Y}P\right) \end{aligned}\right\}. \tag{28}$$

From (26) and (24),

$$P = \frac{Y}{Z}\left[-\frac{1}{2X}\frac{dX}{dt} - \frac{1}{2Y}\frac{dY}{dt} - \frac{1}{2\,(\xi - 1)}\frac{d\xi}{dt} + \frac{\Theta'}{\Theta}\left\{\theta(\xi)\frac{dX}{dt} + \theta'(\xi)\,X\,\frac{d\xi}{dt}\right\}\right] + \frac{1}{2Z}\frac{dY}{dt}.$$

Hence, by (28),

$$0 = 2Y\left\{\theta(\xi) - (\xi - 1)\left(1 + \frac{X}{Y}\,P\right)\theta'(\xi)\right\}\frac{\Theta'}{\Theta}. \tag{29}$$

This equation is satisfied identically if $\Theta \equiv$ const., in which case the paths are indeterminate except for the fact that du/dt is of the form $P\,(x - ut)$; $W ds$ is therefore degenerate. For any other form of Θ, (29) gives

$$P = \frac{Y}{X}\left\{1 + \frac{1}{(\xi - 1)\,\theta'/\theta}\right\} = \frac{Y}{X}G(\xi)$$

by (23), and equations (25) reduce to the form (3). Hence, *the equations of motion can be expressed in the form* (9) *where* W *is given by* (22) *and* (23), *and* Θ *and* f *are arbitrary functions of their arguments, the case* $\Theta \equiv$ *const. being excluded.*

4

It is usually required in a kinematical theory that the light paths shall be tracks of zero action, and we can show that this determines the lower limit of the integral in (22). For Milne has shown* that particles of speed c require for their specification an additional parameter which can be identified with a frequency, and so are indistinguishable from photons, and further that tracks of particles possessing the constant speed c exist and are straight lines, *i.e.*, are given by

$$u,\ v,\ w = \text{const.}, \qquad \Sigma u^2 = c^2. \tag{30}$$

We therefore conclude that the light paths are those given by equations

---

* *Loc. cit.*, Part III, p. 83.

(30). Along such a path, $Y = 0$ and hence ξ is infinite. We have in general

$$Wds = WY^{1/2}\,dt = WZX^{-1/2}\,\xi^{-1/2}\,dt,$$

and hence, from (22), as $\xi \rightarrow \infty$, $Wds \rightarrow 0$ only if $f \equiv \infty$.

Again, from (23), $\theta(\xi) \sim 1$ as $\xi \rightarrow \infty$, so that, putting $f \equiv \infty$ in (22), we have for ξ large

$$W \sim X^{-1/2}\,\Theta(X)\,\xi^{1/2} \int_{\infty}^{\xi} \frac{d\xi}{\xi^2},$$

i.e.,

$$W \sim -\,X^{-1/2}\,\Theta(X)\,\xi^{-1/2}.$$

Hence, as $\xi \rightarrow \infty$,

$$Wds \sim ZX^{-1}\,\Theta(X)\,\xi^{-1}\,dt \rightarrow 0. \tag{31}$$

It follows that *in order that the tracks of zero action shall be light paths, it is necessary and sufficient that* $f \equiv \infty$ *in* (22).

If action is defined so that the above condition is satisfied, the light paths are members of the system of free paths and are tracks of zero action. This corresponds to that axiom of general relativity which states that light paths are null geodesics.

5

We observe that any arbitrary function $W(X, \xi)$ will not, when $\int Wds$ is minimalized, necessarily give a system of paths in accordance with the principles of relativity, for when f, Θ, and θ are eliminated from (22), there remains a partial differential equation for W which must be satisfied by all possible fields. For *any* $W(X, \xi)$, it can easily be verified that the equations of motion take the form

$$\frac{du}{dt} = (x - ut)\,\frac{Y}{X}\,H,$$

etc., where H is given by W and may depend on both X and ξ. Such equations, certainly, satisfy the analytical conditions given by the principles of relativity, but the case when H involves X is excluded by a consideration of the physical dimensions of the argument of H.

If $\Theta(x)$ is chosen to be of the form x^{n+1} and $f \equiv$ const., then by (22), W has the form $X^n\,\Phi(\xi)$. Conversely, if W is given to be of the form $X^n\,\Phi(\xi)$, the above conditions are satisfied by W, and $\theta(\xi)$ and hence

$G(\xi)$ can at once be found by writing $\Theta(x) \equiv x^{n+\frac{1}{2}}$. Hence, *for any arbitrary function* Φ *the paths defined by*

$$\delta \int X^n \, \Phi(\xi) \, ds = 0 \tag{32}$$

constitute a system in accordance with the principles of relativity.

In classical mechanics, the dimensions of action are ML^2T^{-1}, and to conform with classical mechanics W must therefore have dimensions ML^2T^{-2}. Hence, choosing $f \equiv \infty$ as in § 4, we see from (22) that $\Theta(x)$ must be of the form $\alpha mc^2 x^{\frac{1}{2}}$, where α is a pure constant and m is the mass of a free particle, and we have

$$W = \alpha c^2 \xi^{\frac{1}{2}} \int_{\xi}^{\infty} m \, \{\theta(\xi)\}^{1/2} \, (\xi - 1)^{-1/2} \, \xi^{-3/2} \, d\xi. \tag{33}$$

This, therefore, is the form of W for which action has the physical dimensions of the action of classical mechanics. We observe that W does not involve X.

6

It may be of interest to examine the degenerate case $\Theta \equiv$ const. in the general solution (22). When $\Theta \equiv 0$, $W ds$ has the form $2g(X)\, Z\, dt$, which can be written $g(X)\, dX$. Hence $W.ds$ is a perfect differential, and this case is therefore trivial.

When $\Theta \equiv$ const. $= \frac{1}{2}R$, f can be chosen so that (22) becomes

$$W = RX^{-\frac{1}{2}} \, (\xi - 1)^{\frac{1}{2}}. \tag{34}$$

We see, from (4), that $W^2 \, ds^2$ is now a quadratic in the differentials dt, dx, ..., and $d\sigma^2 = W^2 \, ds^2$ is therefore the metric of a Riemannian space, the geodesics of which correspond to the free paths we are considering. Writing

$$\lambda = x/ct, \quad \mu = y/ct, \quad \nu = z/ct, \tag{35}$$

this metric becomes

$$d\sigma^2 = R^2 \left[\frac{\Sigma \, d\lambda^2}{1 - \Sigma\lambda^2} + \frac{(\Sigma \lambda \, d\lambda)^2}{(1 - \Sigma\lambda^2)^2} \right], \tag{36}$$

so that the space is only one of three dimensions, one set of co-ordinates being λ, μ, ν for which the metric is (36). Now it can easily be verified that the form (36) is the metric of the hypersphere

$$t^2 - \Sigma x^2/c^2 = R^2$$

embedded in the flat space

$$ds^2 = dt^2 - \Sigma \, dx^2/c^2,$$

and also, from (35), the point (λ, μ, ν) is the radial projection on this hypersphere of the point (t, x, y, z). Hence, the paths of free particles project radially into geodesics of a hypersphere about the origin, which means simply that each path lies in a two-dimensional plane through the origin of space-time, *i.e.*, that each trajectory in the observer's 3-space lies in a plane passing through him.

7—MILNE'S SYSTEM AND GENERAL RELATIVITY

It was indicated in § 1 that as soon as Wds is known, we can determine whether the system of paths we have been considering is the kinematical system resulting from any other theory, whatever geometry is used as a means of reference. When a space V_4 is used in relativity, it is such that there is a (1, 1) correspondence between the physical events and the points of V_4, a point being described by a set of co-ordinate values. If therefore two spaces V_4, V'_4 are used to describe the same physical system, there must be a (1, 1) correspondence between the points of V_4, V'_4, *i.e.*, a (1, 1) transformation of co-ordinates. The path of a free particle is a sequence of events, to which, therefore, there corresponds a curve in V_4 and another in V'_4, the one transforming into the other by the above transformation. These results are independent of any metrical properties of V_4, V'_4, the spaces being treated merely as point sets.

If V_4 is a metrical space, of linear element ds, and if the physical system obeys a principle of least action, there exists a weighting factor W, a function of the eight variables (x), (dx), homogeneous of zero degree in (dx), such that the curves of V_4 corresponding to the free paths are given by $\delta \int W ds = 0$. If ds' is the linear element of V'_4, these equations, under the above transformation, can be written $\delta \int W' ds' = 0$, where W' is determined by ds, ds', and W. In particular, we can choose a space V''_4, co-ordinates (x), such that the linear element is $ds'' = W ds$, and in this space, the curves corresponding to the free paths are the geodesics, or curves of stationary length. In general, W is not completely determined by the physical system, so that there is a variety of spaces V''_4 satisfying this condition.

In general relativity, the space chosen is Riemannian, and events are assumed to be so ordered that the curves corresponding to free paths are the geodesics. The equations are therefore $\delta \int d\sigma = 0$, where $d\sigma^2$ is a quadratic in the co-ordinate differentials. Any point transformation will leave this property unaltered, whence, if a given physical system is equivalent to a kinematical system of general relativity, and if the events are described by points (x) of a space V_4, linear element ds, there must exist a weighting factor W such that W^2ds^2 is a quadratic in the differentials (dx). If this is satisfied, the space with linear element $d\sigma = Wds$ is Riemannian and is such that the geodesics correspond to free paths, *i.e.*, the above condition is necessary and sufficient.

We see, therefore, that Milne's system is equivalent to a kinematical system of general relativity only if the arbitrary functions Θ, f, in (20) can be chosen so that W^2ds^2 is a quadratic in the differentials dt, dx, ... It can easily be verified that, except for the degenerate case $\Theta \equiv$ const., this is only satisfied when $G(\xi) \equiv a\xi + b$ so that, in general, *Milne's system is fundamentally different from that of general relativity.* This at once answers in the negative the question whether one can be transformed into the other. It should be noted that the comparison can be made by using only the kinematical aspects of the system; it has not been necessary to introduce the field equations of general relativity.

The above conclusion is important, for several writers, when criticizing Milne's theory, assume that his free particles can be described by the geodesics of a Riemannian space, *i.e.*, correspond to the free particles of general relativity. For example, McVittie writes,* in a recent paper, " . . . it is difficult to believe that our non-fundamental particles are any other than the particles of Milne's statistical theory." In a paper now being prepared by the author, a more detailed comparison is made between the two kinematical systems. The system of general relativity is referred to co-ordinates defined by observations in such a way that they agree with Milne's co-ordinates† t, x, y, z, and the equations of motion corresponding to the geodesics are found in terms of these co-ordinates. The difference in form between these equations and equations (1) is interesting, it is the replacement $G(\xi)$ by $G(X)$. The new form, which corresponds to a weighting factor $W(X)$, satisfies the analytical conditions given by the principles of relativity and the only argument against this form is one based on physical dimensions.

8—CONCLUSIONS

In conclusion, we observe that, in general, $d\sigma = Wds$ is homogeneous of the first degree in dt, dx, . . , but $d\sigma^2$ is not a quadratic in the differentials, so that the space with linear element $d\sigma$ is a *Finsler* space. Several writers* have considered the geometry of such spaces, and many well-known features of Riemannian spaces have been generalized to Finsler spaces. It would seem, therefore, that if we wish to describe in terms of geometry, all phenomena included in some generalization of Milne's model, we must use Finsler geometry the free paths being geodesics and the light paths null geodesics.

---

* 'Mon. Not. R. Astr. Soc.,' vol. 94, p. 482 (1934). See also Robertson, 'Rev. Mod. Phys.,' vol. 5, p. 83 (1933).

† In his forthcoming work, Milne defines these co-ordinates from observations.

I am greatly indebted to Professor E. A. Milne, who proposed the problem of finding the weighting factor for his kinematical system, and who has assisted me considerably in the preparation of the earlier part of this paper.

9—SUMMARY

It is shown that the equations of motion of free particles in Milne's kinematical system can be expressed under the form of the principle of least action, and the general form of the appropriate weighting factor is found. Particular forms of the general solution are discussed, and it is finally shown that Milne's kinematical system cannot be equivalent to any kinematical system of general relativity.

---

* *Cf.* Synge, 'Trans. Amer. Math. Soc.,' vol. 27, p. 61 (1925). This paper contains the important references to other papers on Finsler geometry.

The Structure of Surface Films

XXI—Surface Potentials of Dibasic Esters, Alcohols, Aldoximes, and Ketones

By N. K. ADAM, J. F. DANIELLI, and J. B. HARDING

From the Sir William Ramsay Laboratories of Inorganic and Physical Chemistry, University College, London, and Imperial Chemical Industries, Ltd.

(*Communicated by F. G. Donnan, F.R.S.—Received July* 12, 1934—*Revised July* 27, 1934)

The object of this work was to obtain further information on several points affecting the dependence of surface potentials of unimolecular films on water surfaces, on the constitution and orientation of the molecules in the films. Measurements on the dibasic esters were expected to throw light on the relation between surface potential and density of packing of molecules in films of " gaseous " type; the measurements on alcohols, aldoximes, and methyl ketones were undertaken primarily in order to obtain values for the surface potentials produced by the polar groups in these compounds, which could be compared with the potentials found with derivatives of the sterols, in which the same polar groups are attached to a complex ring system, instead of to an aliphatic straight carbon chain.

The surface potential ΔV is the change in contact potential between the aqueous solution on which the film is spread, and air, caused by the presence of the surface film. The simplest basis of comparison is the quantity μ given by the equation

$$\Delta V = 4\pi n \mu,$$

n being the number of molecules per square centimetre of the films. If the dipoles of the film molecules were arranged as a parallel plate condenser in the surface, $K\mu \cos \theta$ would be the dipole moment of the molecules, θ being the angle at which these dipoles are inclined to the vertical, and K the dielectric constant of the surface film. θ is in general unknown; but by comparison of the highest values of μ obtained, with the values for the dipole moments of various polar groups in organic molecules obtained by other methods, it may be concluded that the value of K in the surface films is usually of the order 5 to 10.

ETHYL ESTERS

Figs. 1 to 4 show the values of the surface pressure, F, the surface potential, ΔV, and μ as ordinates.* For the dibasic esters, which are gaseous films over much of the region investigated, the abscissæ are the values of n, the number of molecules per sq cm, areas per molecule being indicated at the top of the figure; also the product of surface pressure and area FA is plotted as ordinates, as this quantity indicates very simply the degree of departure of the films from the perfect "gaseous" state. A perfect gaseous film, in which no appreciable lateral attraction existed between the molecules of the films, and where these molecules occupied an infinitesimal fraction of the space available in the surface, would have a constant value of FA, equal to kT, where k is the Boltzmann gas constant. kT has the value of 400, very nearly, at room temperature, when A is expressed in square Angström units; therefore a perfect gaseous film should be represented in fig. 1 by a horizontal straight line at FA = 400.

For the dibasic esters, the values of F at low pressures (areas greater than about 200 sq A) are taken from the earlier work of Adam and Jessop† and the values at higher pressures include some new determinations. The somewhat "smoothed" dotted curves given represent a mean of the two sets of results, discrepancies in the values of FA amounting at most to 70 (at the highest values of n only) having been found. As the general trend of the two sets of results was the same, and is all that is of importance for the discussion in this paper, it was not thought necessary to investigate these discrepancies accurately. The FA curves show that both the esters, with 11 and with 16 CH_2 groups in the chains, form gaseous films at areas greater than about 140 sq A.

The 11 CH_2 ester is one of the most perfect gaseous films ever found; it approaches closely to the theoretical value of 400 at the greatest areas; shows a slight dip in FA due to lateral adhesions as the area is diminished; and a steady considerable rise in FA as the area is diminished below 180 sq A, undoubtedly due to the fact that the molecules occupy so large a fraction of the total area of the surface, lying flat, that the "b" correction of Van der Waals becomes very large. The 16 CH_2 ester shows a second fall in FA, noticeable below 140 sq A, due to the lateral adhesions between the molecules causing aggregation into the condensed state; this is clearly shown in the F — A curves published by Adam and Jessop* in 1926.

---

* The experimental methods used here are fully described in earlier publications; see "The Physics and Chemistry of Surfaces," p. 38 (1930); Adam and Harding, 'Proc. Roy. Soc.,' A, vol. 138, p. 411 (1932); 'Trans. Faraday Soc.,' vol. 29, p. 837 (1933).

† 'Proc. Roy. Soc.,' A, vol. 112, p. 376 (1926).

The surface potential ($\Delta V - n$) curves for both esters are accurately straight lines, passing through the origin, at all areas above 140 sq A ; they indicate constant values of μ, $12 \cdot 0 \times 10^{-19}$ e.s.u. for the 11 CH_2 and $11 \cdot 2 \times 10^{-19}$ for the 16 CH_2 ester. These appear to be the highest values of μ yet reported; they apply, of course, to two polar groups, but the half value, for one group, of nearly 6×10^{-19}, is quite unusually large.

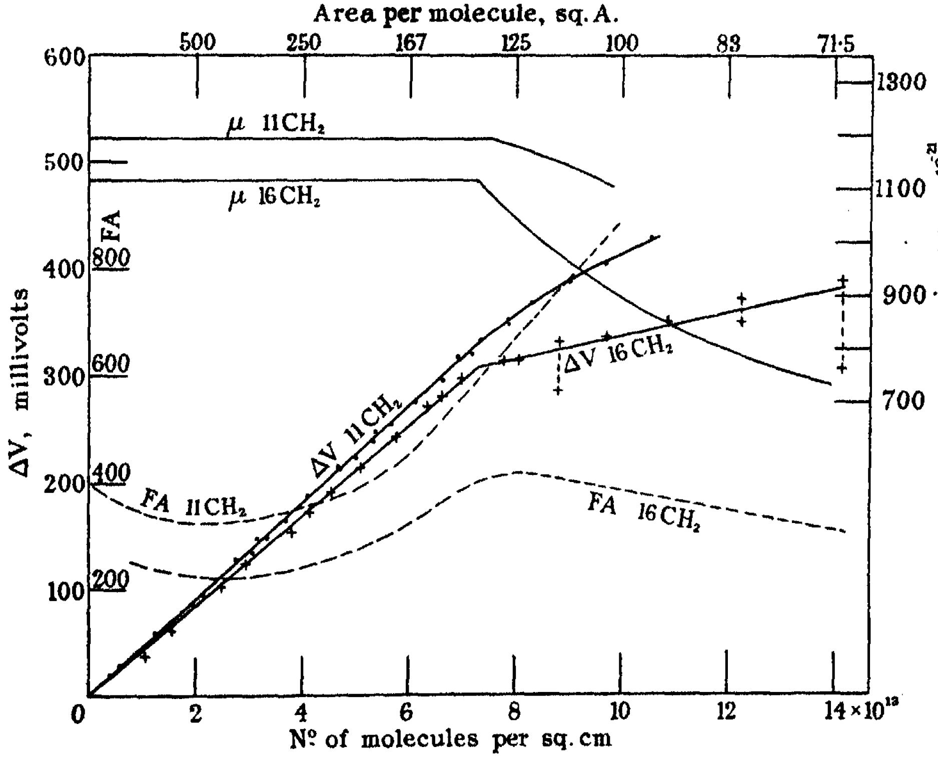

FIG. 1—Dibasic esters $C_2H_5OOC.(CH_2)_n.COOC_2H_5$

In the gaseous region, about 140 sq A, the films showed a potential constant within 5 millivolts in different parts.

At about 140 sq A the 16 CH_2 ester begins to condense. The $\Delta V - n$ curve changes direction abruptly and μ decreases. Further, large fluctuations in potential appear, up to 80 millivolts, indicating that the film is not homogeneous; there is thus no doubt at all that the transition to the condensed film occurs with two kinds of film present, in islands large enough to be distinguished by the movement of the polonium electrode at a height of 1 or 2 mm above the surface. The 11 CH_2 ester also shows a change of direction in the $\Delta V - n$ curve at about the same area, but the film was found to be collapsing here.

---

* *Loc. cit.*, fig. 1.

In the condensed state, it has long been known that these molecules stand on one end, with one polar group in the water and one away from the surface. We have examined longer chain members of the series, with 20 and 32 CH_2 groups, both of which were condensed films. For these μ was only about $3 \cdot 4 \times 10^{-19}$ e.s.u.

It is interesting to compare these values for μ with those found with long chain esters containing only one $COOC_2H_5$ group at the end. Schulman and Hughes* found with ethyl myristate, which is a vapour expanded film having a considerable amount of lateral adhesion between the molecules, though not enough to render the film coherent, a $\Delta V - n$ curve passing through the origin, and linear down to areas about 50 sq A; this indicates a constant value of μ, $4 \cdot 3 \times 10^{-19}$. We have examined two condensed monobasic ethyl esters, ethyl eicosoate and behenate; these showed μ $1 \cdot 89$ and $1 \cdot 68 \times 10^{-19}$ respectively.

The main conclusion to be drawn from these results is that, in gaseous films, μ does not depend on the closeness of packing of the molecules, provided that their orientation is not forcibly changed by crowding to the stage at which tilting occurs. Two of us† found a similar constancy of μ in gaseous films of œstrin derivatives, though the range of areas was there much smaller. This proves that the crowding of the dipoles of the molecules in the film does not affect the dielectric constant of the film, at any rate down to packings at which the average area is 70 sq A. It is rather more difficult to be certain that μ is not affected by simple crowding down to smaller areas, because in all films of smaller area there is a likelihood that re-orientation may occur on compression, so that any effect of crowding might easily be masked; but the frequency with which constant, or nearly constant, values of μ occur through all the changes down to 25 sq A, including many cases of transition to the condensed state, in the work on expanded films of Schulman and Rideal, Schulman and Hughes, and ourselves, makes it probable that any changes which are found down to 25 sq A are due to re-orientation of the axis of the dipole rather than to effects of crowding.

---

* 'Proc. Roy. Soc.,' A, vol. 138, p. 434 (1932).

† Adam, Danielli, Marrian and Haslewood, 'Biochem. J.,' vol. 26, p. 1233 (1932).

The changes in μ as the molecules tilt away from the horizontal are rather remarkable; μ falls steadily from about 12 to 13·4 × 10^{-19} e.s.u., the value when the molecules are upright with one end only in the water. Schulman and Hughes' value for the single $COOC_2H_5$ group in the vapour expanded state is about 75% of half the value for our two similar groups in the gaseous state; this difference is probably outside experimental error and may be due to the molecules not lying quite flat in the vapour expanded film. Since μ falls as the molecule stands more upright, the axis of the dipoles is probably inclined at a steep angle to the length of the molecule; but the results may be much complicated by changes of position of the atoms in the end group, through rotation about linkages. It is surprising that the value of μ for the dibasic esters in the condensed state, when the area is only about 20 sq A, so that the molecules are certainly standing on end with one polar group up and the other down, should be so nearly double that with a single polar group. Some mutual neutralization of the effects of the two groups would not have been improbable in this position; it must be remembered, however, that there are probably more water molecules round the lower group than round the upper, which would produce a larger " dielectric constant " in the region of the low polar group; again, internal rotation in the upper end group, under the influence of the stray field of the surface, may have completely changed its orientation to the surface and its resultant moment. The small area excludes the possibility of these dibasic molecules forming hoops, with each end in the water and the chain humped up in the middle.

ALCOHOLS

Fig. 2 shows the surface pressure F, surface potential ΔV, and μ, plotted against areas per molecule, for films of the liquid expanded and condensed types. μ changes little with change of tilt of the molecules as a whole; it actually changes most in the less compressed region of the condensed curves. The surface pressure results confirm the earlier work of Adam and Dyer* and the values of ΔV agree fairly well with those of Schulman and Hughes† as regards order of magnitude; we cannot, however, follow the films to areas much less than 20 sq A as they appear to have done, and suggest that some of their results are on partially collapsed films.

---

* 'Proc. Roy. Soc.,' A, vol. 101, p. 461 (1922) ; *ibid.*, vol. 106, p. 695 (1924).

† *Ibid.*, vol. 138, p. 446 (1932).

ALDOXIMES

The specimens were from the collection of the late Dr. Le Sueur. The surface pressure results agree satisfactorily with those of Adam.* μ is of the order 3×10^{-19} and changes very little as the expanded film is compressed into the condensed state. We could detect no fluctuations in surface potential greater than 4 millivolts during the transition from expanded to condensed state, in spite of the sharp break in the surface pressure curve. As, however, μ changes so little between the expanded and condensed states, the absence of fluctuations in potential does not show that the transition occurs without the co-existence of two types of film.

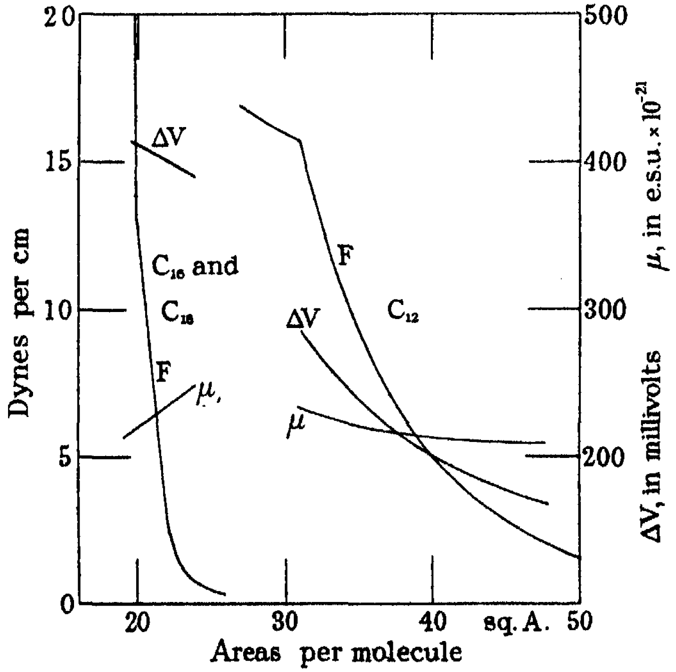

FIG. 2—Alcohols

METHYL KETONES

Two methyl ketones, with chains of 17 and 13 carbon atoms, gave the results in fig. 4. The surface pressures agree with those of Adam and Jessop.† μ falls by some 30% from the expanded to the condensed states, but we did not find fluctuation in the surface potential in the transition region, nor any discontinuity in the $\Delta V - A$ curve to correspond with that in the surface pressure curve. Between 60 and 90 sq A, the 13 carbon chain ketone showed fluctuations in potential of about 20 millivolts; this film was found earlier to be of the vapour expanded type, but it would appear from these fluctuations that there is sufficient lateral adhesion to form reasonably large islands of fairly coherent film. Heptadecyl methyl ketone gave large fluctuations at areas greater than 22 sq A indicating islands of condensed film in equilibrium with a few molecules entering a very small surface vapour pressure.

---

* 'Proc. Roy. Soc.,' A, vol. 103, pp. 691, 694 (1923).

† *Ibid.*, vol. 112, p. 370 (1926).

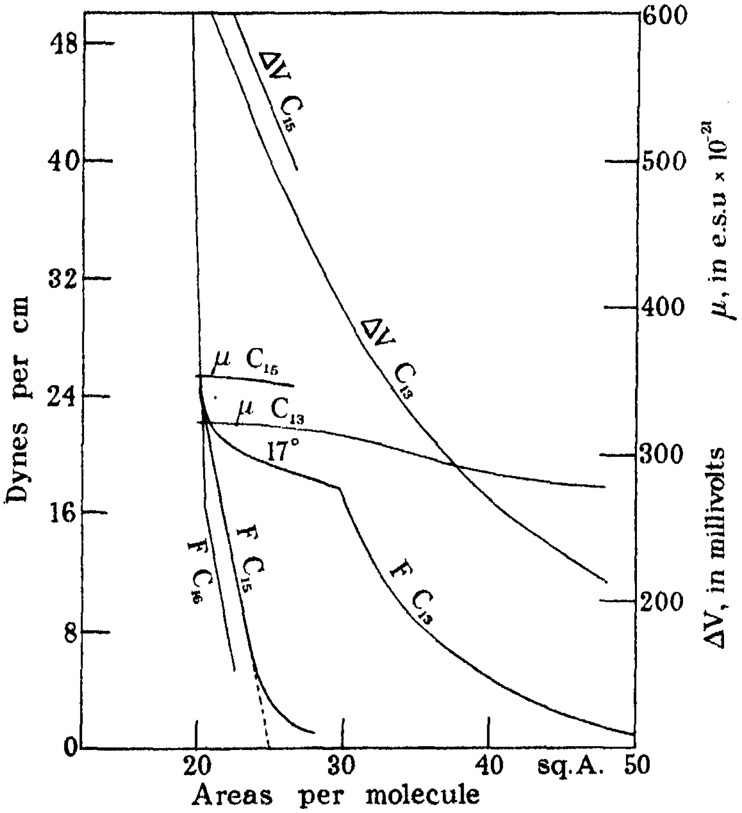

FIG. 3—Aldoximes

STEARONE

An attempt was made to spread stearone, $C_{17}H_{35}$. CO . $C_{17}H_{35}$; but it was found to give a scarcely perceptible surface pressure; dark ground illumination with the cardioid condenser confirmed that it was scarcely spread at all.

These last three groups of compounds also indicate that there is no systematic effect on μ, due to interaction between the dipoles when the molecules are crowded together. Such slight changes as do occur in μ between the expanded and condensed states may easily be accounted for by slight re-orientation of the axis of the dipoles, as the molecules are crowded; but the re-orientation is never through a large angle. There is, of course, an extensive re-arrangement of chains during this transition.

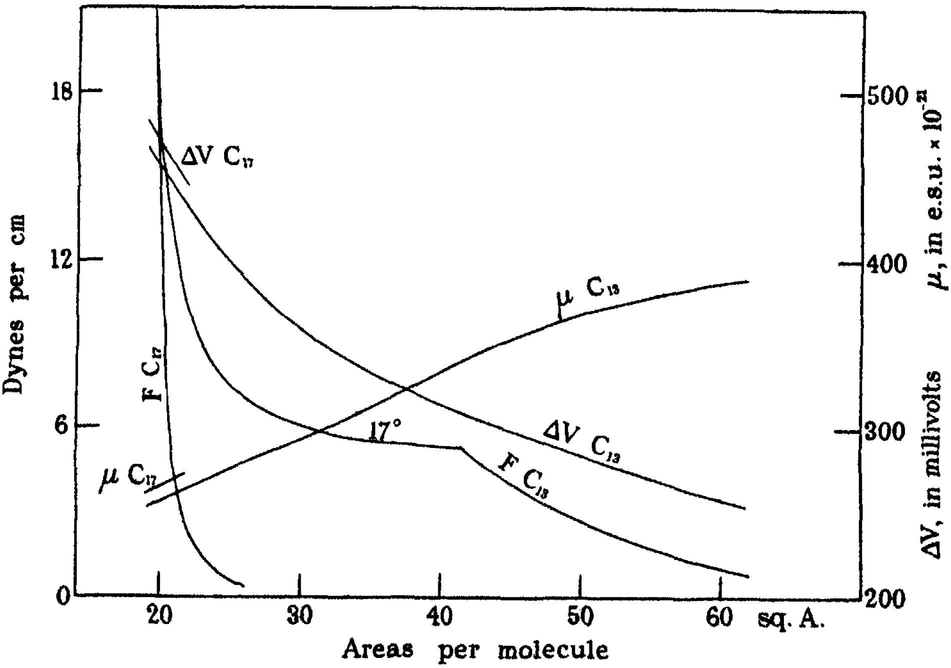

Fig. 4—Methyl Ketones

One of us* suggested that in the liquid expanded state the chains are whipping about, vibrating in an irregular manner owing to the flexibility of the chains. Langmuir's recent beautiful theory,† which treats the liquid expanded films as having an upper and a lower interface, with a liquid layer between, has really developed this idea of chaotic motions of the hydrocarbon chains in a quantitative form, since for the hydrocarbon portion of a monomolecular film to be a liquid, the chains must be in chaotic motion. Langmuir's theory provides what was lacking before,

* "The Physics and Chemistry of Surfaces," p. 74 (1930).

† 'J. Chem. Phys.,' vol. 1, p. 756 (1933).

a reason why the liquid expanded films are coherent in spite of the oscillation of the molecules; there is still much cohesion between the chains, just as in liquid hydrocarbons. The conclusion to be drawn from all the work on surface potentials of expanded films is that, although the oscillations of the chains may be considerably restricted as the available space on the surface is diminished, there is no necessary re-orientation of the end groups, as the molecules come closer together. In fact, the chains and end groups of the molecules appear to behave to a large extent independently of each other, in the expanded type of film.

In general, the values of μ here found for hydroxyl, carbonyl, and oxime groups attached to aliphatic chains are decidedly lower than for similar groups attached to a sterol skeleton. One of us (J. F. D.) has found the following unpublished values for μ, with groups attached to a sterol ring-system : secondary alcohol, 4·15 ; ketone, 10·9 ; ketoxime, $7 \cdot 2 \times 10^{-19}$ e.s.u.

Our thanks are due to the Government Grant Committee of the Royal Society for defraying part of the cost of the apparatus; also to the Department of Scientific and Industrial Research for personal grants to two of us (J. F. D. and J. B. H.).

SUMMARY

Surface potential measurements on spread films of molecules with two ethyl ester groups, at opposite ends of a long chain, show a constant value of μ, *i.e.*, inappreciable interaction between the dipoles of the end groups, so long as the molecules remain flat and the films are gaseous. μ is much larger for these groups when the molecules lie flat than when standing on end.

With alcohols, methyl ketones, and aldoximes, μ does not change much during transition from the expanded state to the condensed, indicating that the orientation of the end groups to the surface remains nearly unchanged. μ is usually smaller for a given end group attached to aliphatic chains than to a sterol skeleton.

The Magnetic Moment of the Nucleus of Cæsium

By D. A. JACKSON, Clarendon Laboratory, Oxford

(*Communicated by F. A. Lindemann, F.R.S.—Received July* 13, 1934)

INTRODUCTION

In a previous paper[*] the author investigated the structure of the lines of the principal series of cæsium, and was able to deduce an approximate value for the magnetic moment of the nucleus. This was the first attempt to measure a nuclear magnetic moment; a simple theory was used, requiring a knowledge of the hyperfine structure of the P levels; these could not be observed directly, but their value was estimated from differences in the separations of the hyperfine doublets of the principal series.

In the meanwhile, Fermi and Segrè[†] and Goudsmid,[‡] developing the author's theory by wave mechanical methods, found more exact formulæ for calculating the nuclear magnetic moment from the structure of the P levels, and also for evaluating this quantity from the hyperfine structure of the S level.

In view of this work, a complete resolution of the hyperfine structure of the P levels in addition to that of the S level was very desirable, for it would enable a comparison to be made between the values of the nuclear magnetic moment given by the hyperfine structures of the various levels. It was possible to measure directly the separation of the two hyperfine structure levels of the $6\,{}^2P_{1/2}$ level by observation of the first three members of the diffuse series, which were found to be very close doublets and also from the separations of the components of the line $6\,S_{1/2}-6\,{}^2P_{1/2}$ which was resolved into all the four components required by theory. The observed structure of this line also gave directly the separation of the hyperfine structure of the term $6\,S_{1/2}$. It was also possible to calculate with a considerable degree of accuracy the total hyperfine structure separations of the terms $6\,{}^2P_{3/2}$, $7\,{}^2P_{1/2}$, and $7\,{}^2P_{3/2}$ from measurements of the separations of blends. The value of the magnetic moment of the nucleus could therefore be calculated from the hyperfine structure of five different terms; with the appropriate relativity corrections, all the terms investigated give the same value for the nuclear magnetic moment, within the limits of experimental accuracy; the mean value is 2·75/1838 Bohr magneton.

---

[*] D. A. Jackson, 'Proc. Roy. Soc.,' A, vol. 121, p. 432 (1928).

[†] 'Z. Physik,' vol. 82, p. 729 (1933).

[‡] 'Phys. Rev.,' vol. 43, p. 636 (1933).

EXPERIMENTAL

I. *The light source*—The most important of the lines to be investigated were in the infra-red, possessing wave-lengths between 8500 A and 9000 A. Even the fastest infra-red sensitive plates are relatively very slow when exposed to light of these wave-lengths, so that it was necessary to use a very intense light source. On the other hand, it was essential for the vapour pressure of the cæsium to be extremely low, and for the thickness of the radiating layer to be small ; for the resonance lines, which were being investigated, are very easily self-reversed. If the depth of the radiating layer is 5 mm the vapour pressure of cæsium must not exceed 1/1000 mm. Accordingly the light source used was a discharge tube containing helium at about 3 mm pressure, and a small quantity of cæsium. The tube was excited by external electrodes which were connected to a high frequency oscillator, capable of an output of ½ k.w. The lower half of the discharge tube (the tube being used in a vertical position) was immersed in an oil bath, the temperature of which was between 90° C and 100° C. The heat generated by the discharge prevented the condensation of metal in the capillary, so that the vapour pressure of the radiating cæsium was that corresponding to a temperature between 90° and 100° C ; that is, about 1/2000 mm of mercury. Under these conditions self-reversal was entirely absent, although the intensity of the cæsium lines was very great. The reason for this is that the high frequency discharge in helium produces a very great number of electrons with sufficient energy to excite cæsium atoms; so that, although the vapour pressure of cæsium is extremely low, the intensity of the radiated light is very great, the proportion of excited atoms being very much greater than it would be under other conditions of excitation.

The discharge tube was used also in an alternative method. A small quantity of cæsium metal was allowed to run into the capillary, and the tube was excited in a horizontal position, a strong current of air being direct on to it in order to cool it. The degree of cooling and the magnitude of the current in the discharge tube (which caused the capillary to become hot) were so adjusted that the relative intensitites of the lines cæsium 4555 and helium 4480 were about 1 : 5. This corresponds to the relative intensities when the vapour pressure of cæsium is about 1/2000 mm of mercury. Under these conditions the lines were free from self-reversal. Nevertheless, by causing a small increase in the vapour pressure of cæsium (by slightly increasing the current through the discharge tube, while the current of air used for cooling remained constant) it was possible to cause the components of the resonance lines to self-reverse. The two observed components of the line 8590 each reversed, under suitable conditions, two self-reversed lines being observed, giving the appearance of four components. At slightly higher vapour pressures all four components of the line 8900 also self-reversed; four self-reversed components were observed, the line appearing under these conditions to possess eight components. The very high resolving power of the étalon (arising from the great reflecting power of silver for light of long wavelength) rendered the observation of this detail possible. This possibility of causing close doublets to self-reverse is of the greatest value when resonance lines are under investigation; it shows that the very close doublets observed are true structures, and not themselves self-reversal.

II. *The Spectrograph*—The spectrograph used was of the simplest orm, consisting of a slit and collimator, a dense glass prism and a camera. The objectives of the collimator and the camera were quartz, rock-salt quartz triplets, of 5 cm diameter and 150 cm focal length. In each of the achromats the quartz lens on one side of the central rocksalt lens was made of right-handed crystalline quartz, while the other quartz component was made of left-handed quartz ; the curvatures were so calculated that at any point on the objective the thickness of the first quartz lens was exactly equal to that of the second. In this way all possibility of the double refraction of quartz giving rise to a doubling of the image is avoided; the principle being the same as that of the Cornu prism. The high resolving power instrument used was a Fabry-Perot étalon; the plates were silvered by evaporation of silver wire from a tungsten filament in a very high vacuum. The degree of silvering was controlled by measurement of the deflection of a galvanometer connected to a copper-copper oxide photocell, the plates being so arranged in the silver evaporator that a beam of light could be passed through them, and the intensity of the transmitted light measured during the course of the silvering. The most favourable results were obtained when the transmission of light by one plate was about 10%. (This is a mean value for the range of wave-lengths for which the photocell was most sensitive, the light source being a tungsten filament cinema projection lamp; the transmission for infra-red radiation was probably considerably less, the reflecting power of silver being greatest for long wave-lengths.)

The étalon was introduced between the collimator objective and the prism; the separations of the plates of the étalon used being 1 cm, 2½ cm and 4 cm. With the longest path, particularly, this method of using the étalon is very advantageous. The angular separation of the fringes is very small and unless an objective of long focus is used, it is difficult to avoid loss of resolving power, on account of the small scale of the fringes. In this arrangement the objective forming the image of the fringe system is the camera lens, with a focal length of 150 cm. It would be extremely inconvenient to use an objective of this focus to project an image of the fringes on to the slit, and moreover would involve a loss of about 10 or 15% of the light. For hyperfine structure investigations the internal mounting of the étalon is, therefore, unquestionably superior to the external, the only disadvantage being that a spectrograph of the Littrow type, with its relative compactness and optical simplicity, cannot be used.

The lines $6\,S_{1/2} - 6\,{}^2P_{1/2}$ (8943) and $6\,S_{1/2} - 6\,{}^2P_{3/2}$ (8521) and $6\,{}^2P_{1/2} - 4\,{}^2D_{3/2}$ (8761) were photographed on Eastman mesocyanine stained plates. The plates were hypersensitized immediately before use by bathing them in a bath containing 4% solution of commercial liquid ammonia (0·880) at a temperature of 15° C. The sensitivity of the plates is increased four or five times by this process; and if they are dried very quickly after bathing (the warm air current given by a hair drier was found very satisfactory as it dried the plates completely in about five minutes) there is very little general chemical fog. The exposures required by the lines 8521, 8943, and 8761 were respectively about fifteen minutes, forty-five minutes, and two and a half hours. The lines $6\,{}^2P_{1/2} - 5{}^2D_{3/2}$ (6723) and $6\,{}^2P_{1/2} - 6\,{}^2D_{3/2}$ (6010) were photographed on Ilford hypersensitive panchromatic plates and required about eight minutes and fifteen minutes exposure respectively. This shows how very much more sensitive these plates are for these wave-lengths than the infra-red sensitive plates are in the infra-red; for although these lines are considerably weaker than the line 8761, they require between one-tenth and one-twentieth of the exposure.

All of these lines were examined with étalons of 10 mm, 25 mm, and 40 mm plate separation. With the shortest path, only the resonance lines showed structure. Both of these appeared to be doublets; the separation of the components of the longer wave-length line being 0·315 cm^{-1} and that of the two components of the other line 0·294 cm^{-1}. The étalon of 25 mm plate separation showed the three lines 8761, 6723, and 6010 to be very close doublets, with separations of rather less than 0·04 cm^{-1}, the component of longer wave-length being the stronger.

The line 8943 was resolved into four components by the 25 mm étalon, the two components observed with the 10 mm étalon being found to be very close doublets of unequal intensity, and about 0·04 cm^{-1} separation. The line 8521 was still found to be a doublet, but the components were observed to be broad, their half value width being about 0·025 cm^{-1}.

The lines $6\,S_{1/2} - 7\,^2P_{1/2}$ (4593) and $6\,S_{1/2} - 7\,^2P_{3/2}$ (4555) were examined with a glass Lummer Gehrcke plate, described in an earlier paper by the author. The pressure of cæsium vapour in the capillary was very low, the discharge tube being used in the vertical position with the lower end at a temperature of about 90° C. Under these conditions the effect of self-absorption on the relative intensities of the components is almost entirely eliminated. Both of the lines were observed to possess two components with separations of 0·309 cm^{-1} and 0·301 cm^{-1} respectively. These figures are the mean of over twenty measurements, each line being photographed on four independent plates, and about seven fringes measured in each plate. The accuracy of the determinations of these separations is about 0·001 cm^{-1}.

The following table contains the observed hyperfine structures of all the lines investigated. The components are arranged in order of increasing frequency and decreasing wave-length.

TABLE OF RESULTS

Line	Position of components in cm^{-1}		Intensities
$6\,S_{1/2} - 6\,^2P_{1/2}$	0·000	± 0·001	3
(8943)	0·039		2
	0·305		1
	0·344		3
$6\,S_{1/2} - 6\,^2P_{3/2}$	0·000	± 0·001	5
(8521)	0·295		4
$6\,^2P_{1/2} - 4\,^2D_{3/2}$	0·000	± 0·002	4
(8761)	0·036		3
$6\,^2P_{1/2} - 5\,^2D_{3/2}$	0·000	± 0·005	4
(6723)	0·036		3
$6\,^2P_{1/2} - 6\,^2D_{3/2}$	0·00	± 0·01	4
(6010)	0·04		3
$6\,S_{1/2} - 7\,^2P_{1/2}$	0·000	± 0·001	1·27
(4593)	0·309		1
$6\,S_{1/2} - 7\,^2P_{3/2}$	0·000	± 0·001	1·26
(4555)	0·301		1

Hyperfine Structure of the Terms

From the observed hyperfine structures of the lines the structures of the terms involved can also be determined.

The structure of the terms $6\,S_{1/2}$ and $6\,^2P_{1/2}$ can be found from the observed structure of the line $6\,S_{1/2} - 6\,^2P_{1/2}$ (8943). This line possesses four components, at positions 0·000, 0·039, 0·305, and 0·344 cm^{-1}. This structure is explained perfectly by assuming that the $6\,S_{1/2}$ and $6\,^2P_{1/2}$ levels are both double, with separations of 0·304 cm^{-1} and 0·040 cm^{-1} respectively; the greater separation is ascribed to the $6\,S_{1/2}$ level because a separation of about 0·3 cm^{-1} is common to all the lines of the principal series, and a separation of about 0·04 cm^{-1} is found in all the lines of the diffuse series which involve the term $6\,P_{1/2}$.

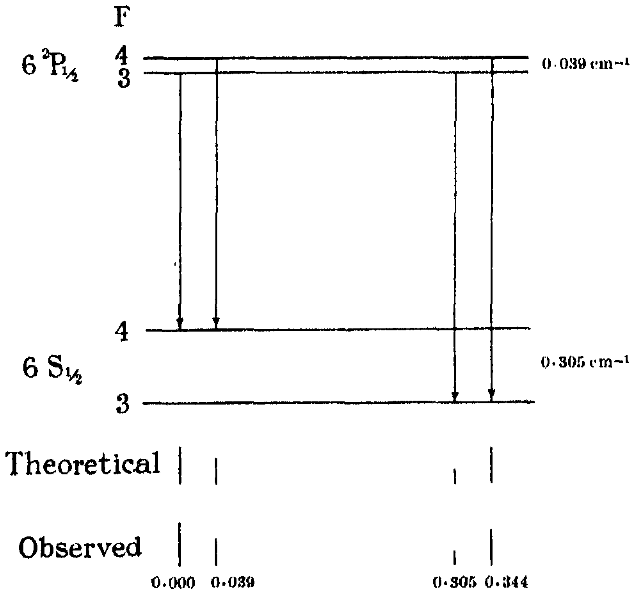

FIG. 1—$6\,S_{1/2} - 6^2P_{1/2}$ (8943 A)

The transitions are shown in fig. 1. The numbers to the left of the hyperfine structure levels represent the value of the quantum number F $(\vec{J} + \vec{I})$; the value of I, the quantum number of the nuclear spin, was found in a previous paper by the author* to be 7/2, and J is equal to ½ in both terms; accordingly F has the value 4 or 3.

The observed doublet structure of the three lines 8761, 6723, and 6010 is also in agreement with the above determined structure of the term

* D. A. Jackson, 'Proc. Roy. Soc.,' A, vol. 145, p. 455 (1934).

$6\,^2P_{1/2}$. The measurement of the separations of the components of the lines 6723 and 6010 was difficult because the lines were only just resolved (for a given separation in cm^{-1}, as the wave-length of the line decreases, an increasingly higher resolving power is required for resolution, while the possible resolving power determined by the Doppler width of the lines is independent of the wave-length); the slight discrepancy between the observed value is within the limits of error. For the line 8761 ($6\,^2P_{1/2} - 4\,^2D_{3/2}$) the difference between the observed separation and the separation of the $6\,^2P_{1/2}$ level found from the structure of the line 8943 is possibly 0·002 cm^{-1} beyond the limit of error. This could be explained by ascribing to the $4\,^2D_{3/2}$ term an unresolved structure of about 0·004 cm^{-1} total separation. This is of the order of magnitude which would be expected, the multiplet separation of the terms $6\,^2P_{1/2}$ and $6\,^2P_{3/2}$ being about ten times greater than that of the terms $4\,^2D_{3/2}$ and $4\,^2D_{5/2}$.

Although it was not possible completely to resolve the line 8521 ($6\,S_{1/2} - 6\,^2P_{3/2}$), the separation of the hyperfine structure of the term $6\,^2P_{3/2}$ can be calculated with a high degree of accuracy from the observed doublet separation of the hyperfine structure of this line and the value of the separation of the two hyperfine structure components of the term $6\,S_{1/2}$, which was found by direct measurement of the four completely resolved components of the line 8943 ($6\,S_{1/2} - 6\,^2P_{1/2}$).

The value of I,* the nuclear spin, is known to be 7/2 ; the term $6\,P_{3/2}$ accordingly possesses four hyperfine structure levels, the quantum numbers, F, of which are 5, 4, 3, and 2. The term $6\,S_{1/2}$ possesses two levels with F equal to 4 and 3. Fig. 2 shows the transitions between these levels.

Now the separation observed experimentally is that between the centre of gravity of the three lines *a*, *b*, and *c*, and the three lines *d*, *e*, and *f*.

The intensity ratios of these four components are

$$a;\ b;\ c;\ d;\ e;\ f\ ::\ 21 : 63 : 132 : 60 : 63 : 45$$

so that if the separations between the levels 5 and 4, 4 and 3, and 3 and 2 of the $6\,^2P_{3/2}$ term are respectively z, y, and x, and the separation of the two components of the term $6\,S_{1/2}$ is X, then the position of the centre of gravity of the three lines *a*, *b*, and *c* is equal to

$$\frac{21\,x + 63\,(x + y) + 132\,(x + y + z)}{216} = x + 0{\cdot}89y + 0{\cdot}59z$$

---

* D. A. Jackson, *loc. cit.*

and the position of the centre of gravity of the three lines *d*, *e*, and *f* is

$$\frac{60\,\mathrm{X} + 63\,(\mathrm{X} + x) + 45\,(\mathrm{X} + x + y)}{168} = \mathrm{X} + 0{\cdot}64x + 0{\cdot}27y.$$

The difference in the position of the centre of gravity of the lines *d*, *e*, and *f* and that of the lines *a*, *b*, and *c* is equal to the observed doublet separation. This has the value 0·295 cm, and the value of X, the hyperfine structure of the 6 $\mathrm{S}_{1/2}$ term, is 0·305, so that

$$0{\cdot}305 - 0{\cdot}295 = 0{\cdot}010 = 0{\cdot}36x + 0{\cdot}62y + 0{\cdot}59z.$$

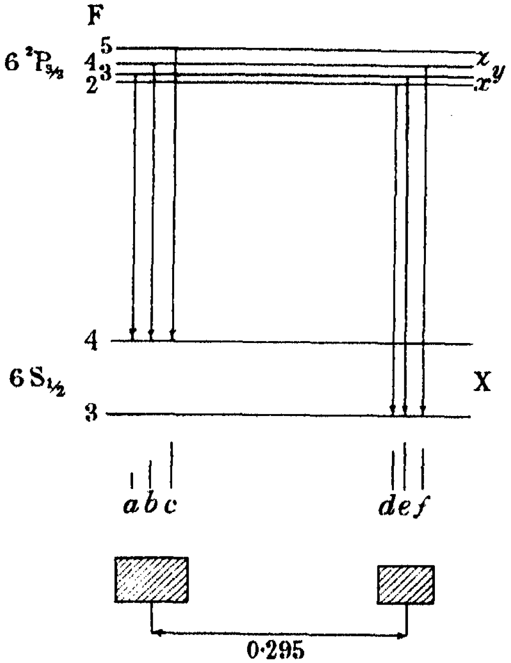

Fig. 2—6 $\mathrm{S}_{1/2}$ — 6 $^2\mathrm{P}_{3/2}$ (8521 A)

But the ratio of the separations *x*, *y*, and *z* is 3 : 4 : 5 so that

$$\begin{aligned} &0{\cdot}36x + 0{\cdot}62y + 0{\cdot}59z \\ &= \left(\frac{0{\cdot}36 \times 3}{12} + \frac{0{\cdot}62 \times 4}{12} + \frac{0{\cdot}59 \times 5}{12}\right)(x + y + z) \\ &= 0{\cdot}55\,(x + y + z).^{*} \end{aligned}$$

---

[*] [*Note added in proof*, *October* 5, 1934—It can be shown by this method that the observed hyperfine doublet separation of the components of a $\mathrm{S}_{1/2} - {}^2\mathrm{P}_{3/2}$ line when the hyperfine structure of the $\mathrm{S}_{1/2}$ term only is resolved, is equal to $\delta\mathrm{S}_{1/2} - \frac{5}{9}\,\delta\,{}^2\mathrm{P}_{3/2}$ ($\delta\mathrm{S}_{1/2}$ being the separation of the hyperfine structure levels of the $\mathrm{S}_{1/2}$ term and $\delta\,{}^2\mathrm{P}_{3/2}$ being the total separation of the hyperfine structure levels of the $\delta\,{}^2\mathrm{P}_{3/2}$ term) for any half integral value of I.]

Accordingly the value of the total hyperfine structure separation $(x+y+z)$ of the $6\,^2P_{1/2}$ level is equal to $\frac{0\cdot010}{0\cdot55} = 0\cdot018$ cm^{-1}. The accuracy of this figure is about $\pm\ 0\cdot004$ cm^{-1}. The widths of the two lines forming this observed doublet were measured. The line consisting of a blend of the components a, b, and c had a width of $0\cdot032$ cm^{-1}; while the width of the other observed line (a blend of the components d, e, and f) was $0\cdot028$ cm^{-1}. Now the width $0\cdot032$ cm^{-1} is equal to the sum of the separations y and z and the Doppler width of a simple line; this is equal to $0\cdot018$ cm^{-1}. The value of $y + z$ is therefore $0\cdot014$ cm^{-1}; but $y + z$ is equal to $9/12\ (x + y + z)$, the total separation of the term $6\,^2P_{3/2}$; the latter is therefore equal to $0\cdot018$ cm^{-1}. The quantity $0\cdot028$ cm^{-1} is equal to the sum of the separations x and y, and the Doppler width; $x + y$ is therefore equal to $0\cdot010$ cm^{-1}, and as this is equal to $7/12\ (x + y + z)$ the total separation is equal to $0\cdot017$ cm^{-1}. The values found in this way for the total separation of the term $6\,^2P_{3/2}$ are therefore in very good agreement with the value ($0\cdot018$ cm^{-1}) found above.

The total separation of the hyperfine structure of the term $7\,^2P_{3/2}$ can be calculated from the observed hyperfine structure doublet separation of the line $6\,S_{1/2} - 7\,^2P_{3/2}$. The structure of this term is exactly similar to that of the term $6\,^2P_{3/2}$ except that the separations are all proportionally smaller. The value of the total separation is now given by

$$0\cdot305 - 0\cdot301 = 0\cdot004 = 0\cdot55\ (x + y + z)$$

The total separation, $x + y + z$, of the term $7\,^2P_{3/2}$ is therefore equal to $\frac{0\cdot004}{0\cdot55} = 0\cdot007$ cm^{-1}. The accuracy of this figure is about $\pm\ 0\cdot004$ cm^{-1}.

The structure of the term $7\,^2P_{1/2}$ could not be directly observed by a complete resolution of the line 4593 ($6\,S_{1/2} - 7\,^2P_{1/2}$) into all four components, as was possible for the term $6\,^2P_{1/2}$ in the line 8943; for the line 4593 could only be resolved into two components. It can, however, be calculated from the observed separation of these two components; this was found to be $0\cdot308$ cm^{-1}.

The line consists of four components; the positions of these components being o, x, X and X $+\ x$ where x is the separation of the two hyperfine structure levels of the term $7\,^2P_{1/2}$ and X is the separation of the two hyperfine structure levels of the term $6\,S_{1/2}$. The intensity ratios of these four components are $3 : 2\cdot14 : 1 : 3$, the value of the nuclear spin quantum number being $7/2$.

In the observed structure o and x are unresolved, as are also X and $X + x$; the doublet separation found being that between the centre of gravity of o and x and the centre of gravity of X and $X + x$.

The position of the centre of gravity of o and x is

$$\frac{0 + 2 \cdot 14x}{5 \cdot 14} = 0 \cdot 42x,$$

while that of X and $X + x$ is

$$\frac{X + 3\,(X + x)}{4} = X + 0 \cdot 75x.$$

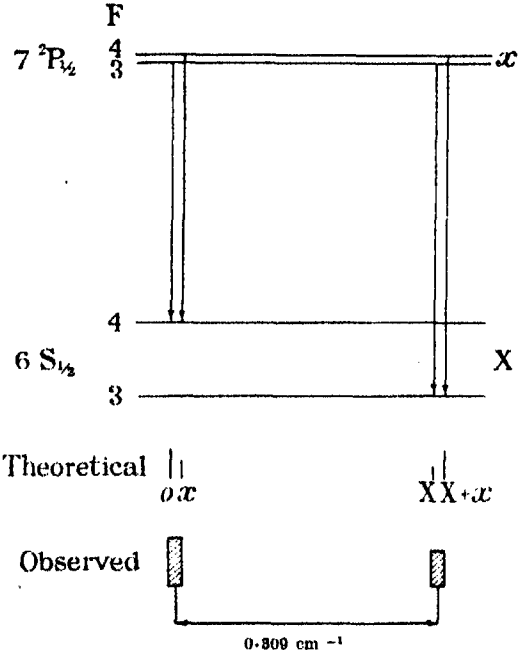

FIG. 3—$6\,S_{1/2} - 7\,^2P_{1/2}$ (4593 A).

The separation of the two observed components of the line is therefore

$$X + 0 \cdot 75x - 0 \cdot 42x = X + 0 \cdot 33x.^*$$

But the value of X (the separation of the two hyperfine structure levels of the term $6\,S_{1/2}$) is known to be $0 \cdot 305 \pm 0 \cdot 001$ cm^{-1}; and that of

---

* [*Note added in proof, October* 5, 1934—It can be shown by his method that the observed hyperfine doublet separation of a $S_{1/2} - {}^2P_{1/2}$ line when the hyperfine structure of the $S_{1/2}$ term only is resolved, is equal to $\delta\,S_{1/2} + \frac{1}{2}\,\delta\,{}^2P_{1/2}$ ($\delta S_{1/2}$ being the separation of the hyperfine structure levels of the $S_{1/2}$ term and $\delta\,{}^2P_{1/2}$ being the separation of the hyperfine structure of the ${}^2P_{1/2}$ level) for any half integral value of I.]

$X + 0\cdot33x$ (the separation of the two observed components of 4593) is $0\cdot309 \pm 0\cdot001$ cm^{-1}; the value of x, the separation of the two hyperfine structure levels of $7\,{}^2P_{1/2}$ therefore has the value $0\cdot012 \pm 0\cdot006$ cm^{-1}.

Table II contains the structures of the terms.

TABLE II

Term	Total separation of hyperfine structure	Term	Total separation of hyperfine structure
$6\,S_{1/2}$	$0\cdot305 \pm 0\cdot001$ cm^{-1}	$7\,{}^2P_{1/2}$	$0\cdot012 \pm 0\cdot006$ cm^{-1}
$6\,{}^2P_{1/2}$	$0\cdot039 \pm 0\cdot002$ cm^{-1}	$7\,{}^2P_{3/2}$	$0\cdot007 \pm 0\cdot004$ cm^{-1}
$6\,{}^2P_{3/2}$	$0\cdot018 \pm 0\cdot004$ cm^{-1}		

Of these values the first two are found by direct measurement of completely resolved structures; the others are obtained by calculation from the observed separations of blends; the value for the term $6\,{}^2P_{3/2}$ is obtained also by measurement of the width of the two observed blends which comprise the line $6\,S_{1/2} - 6\,{}^2P_{3/2}$.

CALCULATION OF THE MAGNETIC MOMENT OF THE NUCLEUS

The magnetic moment of the nucleus can be calculated approximately without the aid of wave-mechanical methods from the hyperfine structure of the P and P terms of a single electron spectrum. It was shown by the author in an earlier work* that

$$\frac{\mu_n}{\mu_e} = \tfrac{1}{2}Z\frac{\delta P}{\Delta P},$$

where μ_n and μ_e are the magnetic moments of the nucleus and electron respectively,

Z is the atomic number of the atom,

δP is the mean of the total hyperfine structure separations of the terms ${}^2P_{1/2}$ and ${}^2P_{3/2}$,

ΔP is the multiplet separation of the terms ${}^2P_{1/2}$ and ${}^2P_{3/2}$.

The values of δP and ΔP for the 6P terms are $0\cdot028 \pm 0\cdot003$ cm^{-1} and 554 cm^{-1}; this gives a value $3\cdot4 \pm 0\cdot4/1838$ Bohr magneton for the nuclear magnetic moment of cæsium. The corresponding value for the 7 P terms are $0\cdot009$ and $0\cdot004$ cm and 181 cm, giving the value $3\cdot1/1838$ magneton. These values are rather higher than that given ($2\cdot8/1838$) by the wave-mechanical calculations, with relativity corrections, but for so simple a theory the accuracy is good.

---

* D. A. Jackson, 'Proc. Roy. Soc.,' A, vol. 121, p. 432 (1928).

Goudsmid[*] and Fermi and Segré,[†] using wave-mechanical methods of calculation, have found more exact formulæ for deriving the value of the nuclear magnetic moment from the hyperfine structure and the multiplet structure of P terms, and also from the hyperfine structure of S terms. These formulæ contain relativity corrections. The formula for P terms of a single electron arc spectrum is

$$\mu = \mathrm{I} \,.\, \frac{a}{\Delta \mathrm{P}} \,.\, \mathrm{Z}\,(l + \tfrac{1}{2})\,\frac{j(j+1)}{l\,(l+1)} \,.\, \frac{\lambda\,(l, \mathrm{Z})}{\kappa\,(l, \mathrm{Z})},$$

where

I = quantum number of nuclear spin,

a = interval factor of hyperfine structure,

$\Delta\mathrm{P}$ = multiplet separation of $^2\mathrm{P}_{1/2}$ and $^2\mathrm{P}_{3/2}$ terms,

Z = atomic number,

$\lambda\,(l, \mathrm{Z})$ = relativity correction for multiplet separation,

$\kappa\,(l, \mathrm{Z})$ = relativity correction for hyperfine structure.

The interval factor a is a function of the hyperfine structure separation and the nuclear spin ; it is equal to the separation between two adjacent hyperfine structure levels divided by the quantum number F of the upper level. From this it follows that it is equal to the total hyperfine structure separation $\delta\nu$ divided by the sum of the F numbers of all the hyperfine structure levels except the lowest. For a $^2\mathrm{P}_{1/2}$ term a is therefore $\delta\nu/\mathrm{I} + \tfrac{1}{2}$ and for a $^2\mathrm{P}_{3/2}$ term $\delta\nu/(\mathrm{I} + 3/2) + (\mathrm{I} + \tfrac{1}{2}) + (\mathrm{I} - \tfrac{1}{2})$. For $\mathrm{I} = 7/2$ these are respectively $\delta\nu/4$ and $\delta\nu/12$.

The relativity corrections are functions of the atomic number becoming greater as the atomic number is increased. For $^2\mathrm{P}_{1/2}$ and $^2\mathrm{P}_{3/2}$ the multiplet relativity corrections are 1·05 and the hyperfine structure corrections respectively 1·30 and 1·05.

For an S term of a single electron arc spectrum the formula is

$$\mu = \mathrm{I} \,.\, \frac{3a}{8\mathrm{R}\alpha^2} \,.\, \frac{n_0^{\,3}}{\mathrm{Z}} \,.\, \frac{1}{\kappa\,(\frac{1}{2}, \mathrm{Z})},$$

where α is Sommerfeld's relativity constant, R is Rydberg's constant, and n_0 is the effective quantum number of the term ; the other symbols have the same meaning as in the formula for P terms. The relativity correction, $\kappa\,({}_{1/2}, \mathrm{Z})$ has the value 1·37 for cæsium. Table III gives the values of the nuclear magnetic moment derived by these formulæ from the hyperfine structure of the five terms which were investigated.

---

[*] 'Phys. Rev.,' vol. 43, p. 636 (1933).

[†] 'Z. Physik,' vol. 82, p. 729 (1933).

TABLE III

Term	Total hyperfine structure separation (cm^{-1})	Magnetic moment of nucleus $\left(\frac{\text{Bohr magneton}}{1838}\right)$	g (I) value
$6\,S_{1/2}$	$0{\cdot}305 \pm 0{\cdot}001$	$2{\cdot}73 \pm 0{\cdot}01$	$0{\cdot}78 \pm 0{\cdot}01$
$6\,^2P_{1/2}$	$0{\cdot}039 \pm 0{\cdot}002$	$2{\cdot}8 \pm 0{\cdot}2$	$0{\cdot}80 \pm 0{\cdot}06$
$6\,^2P_{3/2}$	$0{\cdot}018 \pm 0{\cdot}004$	$3{\cdot}2 \pm 0{\cdot}7$	$0{\cdot}9 \pm 0{\cdot}2$
$7\,^2P_{1/2}$	$0{\cdot}012 \pm 0{\cdot}006$	$2{\cdot}6 \pm 1$	$0{\cdot}75 \pm 0{\cdot}3$
$7\,^2P_{3/2}$	$0{\cdot}007 \pm 0{\cdot}004$	$3{\cdot}8 \pm 2$	$1{\cdot}0 \pm 0{\cdot}5$

The first three terms, $6\,S_{1/2}$, $6\,^2P_{1/2}$, and $6\,^2P_{3/2}$, are seen to give values of the nuclear magnetic moment which are in excellent agreement, the small differences being well within the experimental limits of accuracy. The hyperfine structure of the last two terms was only determined approximately, and again the differences are within the range of the experimental accuracy. From the experimental point of view the term $6\,S_{1/2}$ is the most suitable for the calculation of the magnetic moment of the nucleus, the hyperfine structure of this term being very much greater than that of any other term in the spectrum, and consequently known with the highest accuracy. Assuming the theoretical formula to be correct the value of μ is $2{\cdot}73 \pm {\cdot}01/1838$ magneton; it is not, however, certain that the formula for an S term can be relied on to this accuracy. The hyperfine structure of the terms $6\,^2P_{1/2}$ and $6\,^2P_{3/2}$ were also found with a fair degree of accuracy, although very much less than that for the $6\,S_{1/2}$ term. The corresponding values of μ are $2{\cdot}8 \pm 0{\cdot}2/1838$ and $3{\cdot}2 \pm 0{\cdot}7/1838$ magneton, respectively. The formulæ from which these values are calculated are certainly reliable to the limits of accuracy required by the experimental data (about 5%); the relativity corrections are not great, and the multiplet separation is only 554 cm. These formulæ become unreliable only when the relativity correction becomes great (here it is $1{\cdot}30$ for the $6\,^2P_{1/2}$ term and $1{\cdot}05$ for the $6\,^2P_{3/2}$ term), or when the multiplet separation is so great that the orbits of the $6\,^2P_{1/2}$ and $6\,^2P_{3/2}$ terms are very different, as in the atoms indium and thallium.

The value $2{\cdot}8 \pm 0{\cdot}2/1838$ is theoretically the most reliable, although the value $2{\cdot}73 \pm 0{\cdot}01/1838$ has a much higher accuracy if the formula for an $S_{1/2}$ term is not in error. The mean of these two values, $2{\cdot}75/1838$ magneton can be regarded as the most probable value for the nuclear magnetic moment of cæsium, the accuracy being about 5%. The corresponding value of g (I), the ratio of the magnetic moment (measured in units of 1/1838 magneton), to the mechanical moment is $0 \cdot 79 \pm 0 \cdot 02$.

SUMMARY

The hyperfine structure of five terms in the arc spectrum of cæsium was investigated. Using the formulæ of Goudsmid and of Fermi and Segré, values of the nuclear magnetic moment, which were in agreement within the limits of experimental accuracy, were found from all five terms; the mean value given by the most accurately known terms is 2·75/1838 magneton, with a probable error of less than 5%; or if the formula for calculating the magnetic moment from the $S_{1/2}$ term is accurate the probable error is less than 1%.

Spectrum of the Flame of Ethylene

By W. M. VAIDYA, B.Sc., Research Student, Imperial College

(*Communicated by A. Fowler, F.R.S.—Received July* 17, 1934)

[PLATE 3]

INTRODUCTORY

In the course of a detailed examination of the spectra of the flames of carbon compounds, which was undertaken at the suggestion of Professor A. Fowler, it has been found that the flame of ethylene shows, in addition to the familiar bands of C_2, CH and HO, a system of bands which has not previously been adequately described. These bands occur feebly in the ordinary Bunsen flame, as noted by Rassweiler and Withrow,* and with greater intensity in the flame of ether, as shown in a photograph by Emeléus.† Other flames which exhibit these bands have also been found in the course of the present investigation, but as the bands appear to have their greatest intensity in ethylene, they may conveniently be called the "ethylene flame bands" for the purposes of the present paper. The bands are degraded to the red, and have been observed to extend from λ 4100 to λ 2500.

---

* 'Indus. and Eng. Chem.,' vol. 29, p. 529 (1932).

† 'J. Chem. Soc.,' p. 2948 (1926).

EXPERIMENTAL PROCEDURE

For the production of the bands under the most favourable conditions, it was necessary to use a Smithells' flame separator to divide the inner and outer cones. The separator employed, fig. 1, consisted of two concentric tubes, F and G, the inner tube, F, being mounted on the outer nozzle, D, of a two-way blow-pipe. The inner tube was made of Pyrex, 15 cm in length and 1·2 cm in diameter, while the outer one—12 cm long and 1·5 cm in diameter—was made of quartz so as to permit observations in the ultra-violet. The inlet A was connected to a cylinder of ethylene gas (rated 100% pure), the arrangement being such that the gas could then pass through the outer nozzle, D. Through the inner nozzle, E, could be passed air blown through the other inlet, B, by an electric blower. In the absence of air, the gas burnt with a smoky flame on the outer tube, G. When air was blown through, the flame became non-luminous, and, with suitable adjustment of air and gas supply by the handle, C, the inner cone was clearly developed. Then, on sliding the inner tube of the separator about 4 cm below the top of the outer tube, the cones were completely separated, the inner cone burning steadily on the inner tube. Under these conditions the inner cone was about 2 cm high, and was of greenish colour.

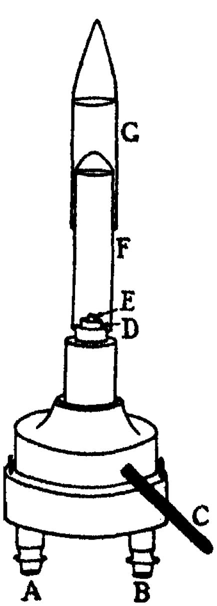

FIG. 1

Exposures of long duration, up to 150 hours, were necessary to give fair intensity in photographs of the ethylene flame bands with this simple arrangement. After considerable experimenting, however, it was found possible to increase the intensity by making the inner tube of the separator of a wide fish-tail form so as to increase the thickness of the flame presented to the spectrograph. To increase the intensity still further, a concave mirror was placed behind the flame to reflect the light from the back of the flame. Under these conditions the spectrum could be satisfactorily photographed with exposures of 50 hours.

An important change in the spectrum was found when the mode of burning the ethylene gas was varied. If the bands occurring in the separated inner cone be regarded as the normal ethylene flame bands and designated by the letter A, this change may be described as the appearance of additional bands in the ultra-violet, which may conveniently be designated by the letter B. These extra bands are also degraded towards the red, and have a general resemblance to the A bands, with which they are intermingled. The B bands were developed in several modified flames, as will now be described.

(i) In the experiments in which the inner tube of the flame separator was of fish-tail form, it was found that while the A bands appeared alone when the constriction was rather wide, both A and B bands appeared when it was sufficiently narrowed.

(ii) When ethylene was burnt with air in a two-way blow-pipe, the bright but diffuse bluish-green cone at the mouth of the inner tube gave the normal A bands, as in the inner cone of a separated flame. On blowing hydrogen instead of air, however, in just sufficient quantity to make the flame non-luminous, the inner cone became fainter and the B bands made their appearance. The bluish-green appearance was restricted to the rim of the outer nozzle, and it was therefore necessary to clamp the blow-pipe horizontally in order to allow the image of the rim to lie along the slit of the spectrograph. With excess of hydrogen the bluish-green cone tended to bulge outwards, and was also more sharply defined, but the ethylene bands became less intense, and it was difficult to determine whether the B bands were present or not. The intensity of the HO bands, however, increased considerably.

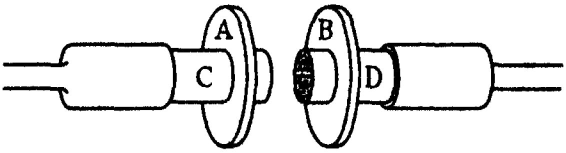

FIG. 2

(iii) The B bands also appeared when ethylene was burnt between two opposing multiple capillary tubes of silica glass (C and D of fig. 2), so that the flame fed by ethylene passing through one of the tubes was met by streams of air blown through the narrow channels of the other. A thin flat flame of bluish-green colour and considerable intensity was then produced, and its spectrum showed both the A and B sets of bands. Silica discs, A, B, mounted on the tubes, were useful to produce intimate mixing of gas and air, and to prevent the flame from projecting behind the vertical plane of the tubes.*

---

* The author is indebted to Mr. Lamont, of Professor Bone's laboratory, for suggesting the multiple jet arrangement, which has been successfully used by him in high pressure research work.

Of these three sources yielding the B bands, (iii) was found to be most convenient, because the manipulation was quite simple, and the quantity of gas burnt was relatively small. In this source the bands were relatively bright, but the individual bands did not extend so far from their respective heads as they did in (i). In (i) a considerable quantity of gas was consumed, and there was the added disadvantage that the gas and air supply had to be constantly regulated. With (ii) some difficulty was experienced in adjusting the quantity of hydrogen to the precise amount necessary for the production of the B bands. In all the experiments which developed the B bands, the A bands appeared with diminished intensity as compared with their appearance in the normal ethylene flame.

Some attempts have been made to obtain brighter sources of the bands in experiments on discharges through various carbon compounds in vacuum tubes, but so far without success.

In the first instance, photographs of the flame-spectra were taken with a small quartz spectrograph (Hilger, E 31), and these were, in fact, finally used for wave-lengths lower than λ 3100. The comparison spectrum in this case was that of the copper arc. For higher wave-lengths, the E 2 quartz spectrograph was used with the iron arc as the source of reference lines.

DESCRIPTION OF THE SPECTRUM

When produced with the aid of a Smithells' separator, the spectrum of the inner cone includes strong bands of C_2, CH, and HO, and the fainter bands which have been provisionally designated the normal ethylene flame bands. Some of the fainter hydrocarbon bands are also present.

The ethylene flame bands extend from λ 4100 to about λ 2500, and although the heads are somewhat diffuse, the bands are clearly degraded towards the red. With the dispersion employed, there were no distinct signs of resolution of the structure of the individual bands. The general appearance of the bands will be gathered from the photograph reproduced in fig. 3 *c*, Plate 3. Some of the bands which might be expected to be present from the vibrational analysis are obscured by the CH and HO bands; by comparison with the HO bands given by anoxy-hydrogen flame, fig. 3 *a*, however, it was possible to identify a few heads superposed on the HO spectrum. The bands thus recognized were λ 3014·8, λ 2948·2, and λ 2858·0.

The extra bands, B, which appear in the modified flames which have been described, are similar in appearance to the normal A bands, as will be seen from fig. 3 *d* and fig. 4 *b*.

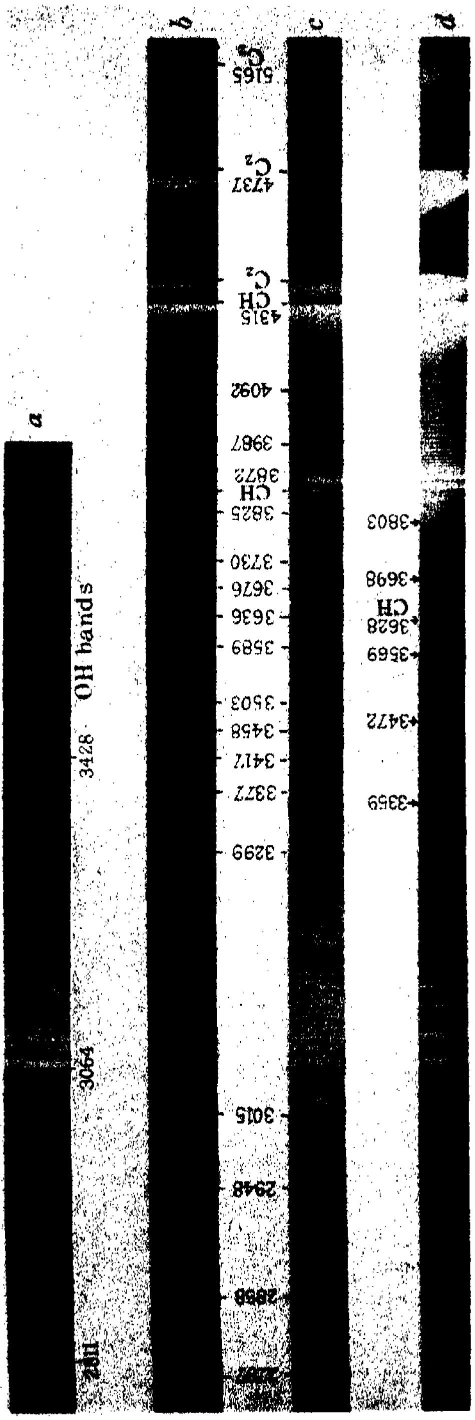
a
b
c
d
OH bands
5165 C₂
4737 C₂
4315 CH C₂
4092
3987
3872 CH
3825
3730
3676
3636
3589
3503
3458
3417
3372
3299
3015
2948
2858
3428
3064
3803
3698
3628 CH
3569
3472
3369

FIG. 3

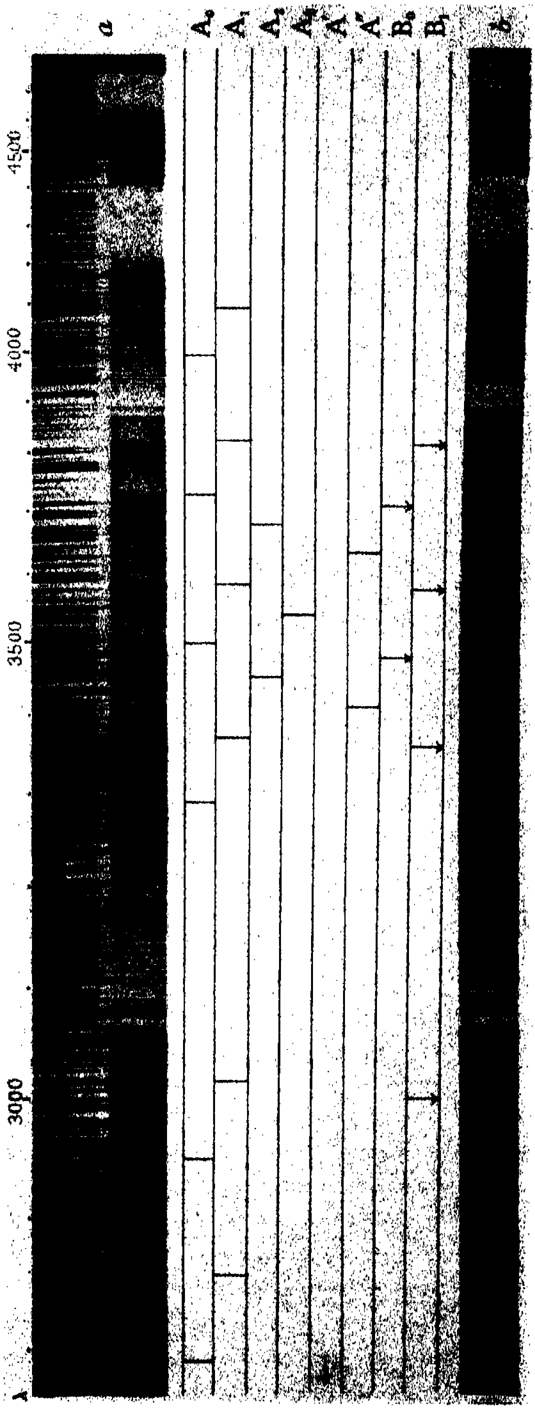
a
A₀
A₁
A₂
A₃
A'
A''
B₀
B₁
b
4500
4000
3500
3000
λ

FIG. 4

Wave-lengths of Ethylene Flame Bands

The results of the measurements are collected in Table I. Under the heading "intensity," *a* and *b* refer respectively to the normal ethylene flame, in which the A bands occur alone, and the modified flame in which the B bands appear and the A bands are reduced in intensity. The progressions to which the various bands appear to belong are indicated in the last column and also in fig. 4. In addition to the bands tabulated, there were indications of several fainter bands which, however, were unsuitable for satisfactory measurement.

Table I—"Ethylene Flame" Bands.

	Intensity			Progression		Intensity			Progression
λ	*a*	*b*	ν*		λ	*a*	*b*	ν	
4092·0	3	1	24431	A_1	3001·5	—	2	33307	B_1
3987·5	2	—	25071	A_0	2948·2	7	3	33909	A_0
3824·9	4	2	26137	A_1	2858·0	6	2	34979	A_1
3802·7	—	2	26290	B_1	2797·1	5	2	35741	A_0
3730·5	5	3	26798	A_0	2780·4	—	2	35955	(B)
3697·7	—	4	27036	B_0	2774·6	1	—	36031	A_2
3676·0	1	—	27196	A_2	2751·5	4	2	36333	A'
3635·6	3	1	27498	A''	2716·0	5	2	36808	A_1
3588·6	8	4	27858	A_1	2704·5	—	1	36964	B_1
3569·2	—	3	28010	B_1	2672·3	1	1	37410	
3539·9	2	—	28241	A_3	2658·8	4	3	37600	A_0
3502·7	8	4	28541	A_0	2640·5	1	—	37860	A_2
3472·5	0	5	28789	B_0	2618·0	3	—	38186	A'
3458·4	1	—	28907	A_2	2585·5	3	—	38666	A_1
3417·4	3	1	29254	A''	2550·3	2	1	39199	(A)
3377·4	10	5	29600	A_1	2532·4	2	1	39476	A_0
3359·0	—	5	29762	B_1	2517·5	1	?	39710	A_2
3299·2	10	5	30302	A_0	2495·0	1	?	40068	A'
3014·8	8	3	33160	A_1					

Measurements of the heads of the bands were always somewhat difficult on account of their diffuse appearance.

Analysis of the Bands

The majority of the normal ethylene flame bands (Group A) can be arranged in the usual way in a v' v''* scheme, such as is considered appropriate for the spectrum of a diatomic molecule. This is shown in Table II, where the v', v'' progressions are indicated by A_0, A_1, A_2, and A_3 for convenience of reference. Two partial progressions of A bands which do not form part of this scheme, but appear to have the same v'' separations, have been designated A′ and A″, and are shown in the lower part of the table.

---

* The Greek ν should not be confused with the Italic v of this font.

The B bands can also be arranged in progressions. One of them, designated B_0, appears to run parallel to A_0, at a distance of about 240 units of wave-number, while the other, B_1, similarly runs parallel to A_1, at a distance of about 154 units. Additional bands which might be expected in these progressions are, unfortunately, obscured by bands of HO and CH.

The intensity distribution among the A_0–A_3 bands is such that the Condon parabola is widely open, as would be expected from the large differences between $\Delta\nu''$ and $\Delta\nu'$.

The assignment of quantum numbers ν', ν'', in Table II is merely provisional. By analogy with other band spectra, however, it is not improbable that the progression A_0 has $\nu' = 0$, but the ν'' values are little more than guesses, and are subject to correction when further facts about the bands become available.

THE EMITTER OF THE BANDS

The separations of successive bands shown in Table II do not appear to be related to any of the known separations in the spectra of the diatomic molecules C_2, CH, and HO which accompany the bands in question in hydrocarbon flames, nor to those which have been found in the spectrum of CO. For this reason, and in view of the superposition of other band progressions on those which have been designated A_0–A_3, it seems probable that the ethylene flame bands have their origin in molecules of greater complexity. The analysis of the spectrum, however, as well as the theory of the spectra of polyatomic molecules, is not yet sufficiently complete to give any definite indication as to the nature of such molecules.

Comparison with the known spectrum of formaldehyde, which has been found by chemical methods to occur in the oxidation of hydrocarbons, has also been unfruitful. Formaldehyde yields a definite absorption spectrum of bands in the ultra-violet, but the analysis of these by Henri and Schou* reveals nothing in common with that of the ethylene flame bands. The same applies to comparisons with the fluorescence bands of formaldehyde, as obtained by Herzberg and Franz,† and by Gradstein.‡

* ‘Z. Physik,’ vol. 49, p. 774 (1928).

† ‘Z. Physik,’ vol. 76, p. 720 (1932).

‡ ‘Z. phys. Chem.,’ B, vol. 22, p. 384 (1933).

TABLE II—ANALYSIS OF ETHYLENE FLAME BANDS

v' \ v''	3		4		5		6		7	8		9		10		11		12		
0	39476 (2)	*1876*	37600 (3)	*1859*	35741 (5)	*1832*	33909 (7)		*	30302 (10)	*1761*	28541 (8)	*1743*	26798 (5)	*1727*	25071 (2)			A_0	
												248		*238*					B_0	
							*		*	*		28789 (5)	*1762*	27036 (4)		†				
			1066		*1067*		*1070*					*1059*		*1060*		*1066*				*1063*
1			38666 (3)	*1858*	36808 (5)	*1829*	34979 (6)	*1819*	33160 (8)	*		29600 (10)	*1742*	27858 (8)	*1721*	26137 (4)	*1706*	24431 (3)	A_1	
					156				*147*			*162*		*152*		*153*			B_1	
					36964 (1)		*		33307 (2)	*		29762 (5)	*1752*	28010 (3)	*1720*	26290 (2)				
			1044		*1052*		*1052*							*1049*		*1059*				*1051*
2			39710 (1)	*1850*	37860 (1)	*1829*	36031 (1)							28907 (1)	*1711*	27196 (1)			A_2	
																1045				*1045*
3																28241 (1)			A_3	
	40068 (1)	*1882*	38186 (3)	*1853*	36333 (4)														A′	
												29254 (3)	*1756*	27498 (3)					A″	

Not included above—

		Int.		
λ 2780·4 =	ν 35955	—	2	B
2672·3 =	37410	1	1	
2550·3 =	39199	2	1	A

* Obscured by bands of HO.
† Obscured by CH band.

As the spectrum is not very complex in appearance, Professor Fowler has suggested that the A and B bands may originate in molecules of HCO. It has been found that molecules having the same number of external electrons have certain similarities in their spectra, as expressed in Mecke's principle of isosterism.[*] If this be applicable to the spectrum under discussion, the spectrum of HCO would be expected to show some similarity to that of NO, since each of these molecules has 15 external electrons, and the substitution of CH for N in NO involves only a small change of mass. It is actually found that the vibrational constants of the ethylene flame bands A_0–A_3 are not very different from those of the β-bands of NO. For the NO bands, the double heads were found by Johnson and Jenkins[†] to be represented approximately by the formula

$$\nu = \left.\begin{matrix}45394\cdot6\\45485\cdot0\end{matrix}\right\} + (1029\,v' - 7\cdot5\,v'^2) - (1889\cdot05\,v'' - 13\cdot96\,v''^2)$$

For the ethylene flame bands $A_0 - A_3$, with the numbering shown in Table II, the corresponding formula is approximately

$$\nu = 45255 + (1072\,v' - 6\,v'^2) - (1960\,v'' - 11\cdot4\,v''^2).$$

The greatest uncertainty in connection with this formula is that of the limiting term 45255, which depends on the somewhat arbitrary values assigned to v''; small variations in the latter, however, do not greatly affect the other constants.

The similarity of the constants of the two formulæ is very striking, and lends considerable weight to the suggestion that the ethylene flame bands are to be attributed to HCO. Further support for this suggestion is provided by chemical considerations. If it be supposed that the O_2 molecule is directly incorporated in the ethylene molecule by collision, as can happen according to the "peroxidation theory" of hydrocarbon combustion,[‡] and such oxygenated molecule decomposes, HCO molecules could be produced. Thus

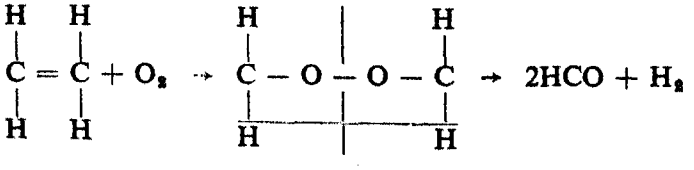

$$\mathrm{H_2C{=}CH_2 + O_2 \rightarrow H_2C{-}O{-}O{-}CH_2 \rightarrow 2HCO + H_2}$$

It is recognized, however, that further evidence is desirable as to the precise origin of these bands. Owing to the very long exposures necessary for obtaining photographs of fair intensity, even with instruments of moderate dispersion, it is considered impracticable to use greater dispersion for purposes of rotational analysis. Attempts to obtain further experimental evidence as to the molecule which gives rise to the ethylene flame bands are still in progress.

---

[*] 'Trans. Faraday Soc.,' vol. 30, p. 200 (1934).

[†] 'Phil. Mag.,' vol. 2, p. 621 (1926).

[‡] *E.g.*, H. L. Callendar, 'Engineering,' vol. 123, pp. 147, 182, 210 (1927).

In conclusion, the author has great pleasure in expressing his sincere thanks to Professor Fowler for his valuable guidance during the course of this research. He is also grateful to the High Commissioner for India for a grant which enabled him to complete the paper.

SUMMARY

The inner cone of the flame of ethylene burning in a Smithells' flame separator has been found to yield a number of faint bands which have hitherto received little attention. The conditions for the occurrence of these bands have been investigated, and a table of their wave-lengths is given. The emitter of the bands is not precisely known, but there is reason to believe that they may be due to HCO. Support for this suggestion is given by a preliminary vibrational analysis and by chemical considerations.

DESCRIPTION OF PLATE

All the photographs were taken on Hilger's quartz spectrograph E 2.

FIG. 3—(*a*) Oxy-hydrogen flame showing HO bands.
 (*b*) Meker burner, showing the A group of ethylene flame bands.
 (*c*) Inner cone of ethylene in flame-separator, showing the A bands.
 (*d*) Flame of ethylene in multiple-jet burner, showing A and B groups of bands, and also some of the fainter CH bands.

FIG. 4—(*a*) Inner cone of ethylene flame, showing the various progressions in A bands. Iron arc comparison.
 (*b*) Flame of ethylene in multiple-jet burner, showing the progressions in B bands.

On the Quantization of the New Field Equations I

By M. Born and L. Infeld[†]

(*Communicated by P. A. M. Dirac, F.R.S.—Received July* 19, 1934)

§ 1. INTRODUCTION

The new field theory has been developed in two papers.[‡] The first, quoted as I, contains not only a classical treatment, but also an attempt at quantization; the second, quoted as II, a new foundation based on the relativity principle and a more complete representation of the classical consequences.

We have tried to work out the quantum ideas laid down in I, but have met great difficulties and have therefore tried another way.

The method of quantization developed in this paper has some points in common with the method of Heisenberg and Pauli, but differs from it in essential points. Heisenberg and Pauli worked out a general formalism of quantization of a continuous medium and applied it afterwards to the Maxwell field of radiation and to the Dirac field of matter, adding simply the Hamiltonians of the field and mass points. This dualistic standpoint meets with the well-known difficulties connected with the formulation of the commutation rules of the potential vector and specially with the appearance of the infinite self-energy.

The unitarian standpoint represented in this paper takes, as classical equations which are to be quantized, the equations of the new field theory developed in I and II.

Our quantization method has, however, in common with that of Heisenberg and Pauli, the commutation rules for the field strengths, which form the starting point for our further considerations.

But the commutation rules induce us to change the appearance of the new field equations (without changing their content); there is no use of electrodynamic potentials. In this way we avoid the above-mentioned difficulties of the other theory.

[†] Research Fellow of the Rockefeller Foundation.

[‡] Born, 'Proc. Roy. Soc.,' A, vol. 143, p. 410 (1934), quoted as I ; Born and Infeld, 'Proc. Roy. Soc.,' A, vol. 144, p. 425 (1934), quoted as II.

§ 2. A NEW FORM OF THE CLASSICAL FIELD EQUATIONS

In the mechanics of mass points the equations of motion can be derived from different variation principles of the form $\delta \int F\,dt = 0$. We shall call F the action function. Corresponding to the choice of variables, F is called the Lagrangian L or the Hamiltonian H, and the latter is identical with the total energy.

In the new field theory the field equations can also be derived from a variation principle $\delta \int F\,dx\,dy\,dz\,dt = 0$. The action function F has been given in I and II in two forms which, in analogy with the theory of the mass point, we have called the Lagrangian L and the Hamiltonian H; neither of them is identical with the energy-density (this being the component T_{44} of the energy-momentum-tensor).

In quantum mechanics it is an important point that the two notions of action function and energy coincide. Therefore we have tried to transform the field theory in such a way that the energy-density plays the role of the action function. The new equations are identical with the old for a given co-ordinate system, but do not allow of a covariant space-time formulation. This is connected with the fact that in the quantum theory the time plays an essentially different role from that of the space co-ordinates.

We intend to repeat here briefly those of the formulæ quoted in II, which will form the starting point of our considerations. They are in the first place the electrodynamical equations,† (taking $c = 1$) :

$$\frac{\partial \mathbf{D}}{\partial t} = \operatorname{rot} \mathbf{H}; \qquad \frac{\partial \mathbf{B}}{\partial t} = -\operatorname{rot} \mathbf{E}; \tag{2.1}$$

$$\operatorname{div} \mathbf{D} = 0; \qquad \operatorname{div} \mathbf{B} = 0. \tag{2.2}$$

The four-space vectors $\mathbf{E}$, $\mathbf{B}$ and $\mathbf{D}$, $\mathbf{H}$ form two anti-symmetrical tensors f_{kl} and p_{kl} in the four dimensional world. Two of the four-space vectors are independent, the other two are functions of them. We have, however, some liberty in the choice of which ones we take as independent vectors. In principle there are four possible standpoints.‡

---

† II, p. 437.

‡ Very similar to the four possibilities of representation of thermodynamics by potentials. The connection between these functions is given in both cases by Legendre transformations.

Standpoints 1: **E**, **B** *are chosen as independent variables*, **D**, **H** *as functions of them.*—The latter ones can be derived from *one* function, the Lagrangian L (**E**, **B**)[†]

$$\mathbf{D} = -\frac{\partial L}{\partial \mathbf{E}}; \quad \mathbf{H} = \frac{\partial L}{\partial \mathbf{B}}. \tag{2.3}$$

This standpoint was the original basis of the new field theory. The Lagrangian L had there the following form :

$$L = \sqrt{1 + \mathbf{B}^2 - \mathbf{E}^2 - (\mathbf{E} \cdot \mathbf{B})^2} - 1 \tag{2.4}$$

Later we shall need the expressions for the momentum-energy-tensor-density, quoted from II[‡] :

$$4\pi\mathbf{S} = -T_{4k} = (\mathbf{D} \times \mathbf{B}) \tag{2.5}$$

$$4\pi U = T_{44} = L + (\mathbf{D} \cdot \mathbf{E}). \tag{2.6}$$

All these equations are contained in paper II, with the one alteration, that here we set $c = 1$ and $b = 1$, *i.e.*, the time and the field-components are to be measured in the natural units.

Standpoint 2 : **D**, **H** *are chosen as independent variables*, **E**, **B** *as functions of them.* The roles played by **E**, **B** and **D**, **H** are, therefore, interchanged. The action function is here the Hamiltonian. This standpoint has also been treated in paper II.[§] It will not concern us here.

Standpoint 3 : **D**, **B** *are chosen as independent variables*, **E**, **H** *as functions of them.* This means that we split up the anti-symmetrical tensors **E**, **B** and **D**, **H**. The advantage of this step will become clear if we regard the energy-density U as function of **D**, **B** and calculate its derivatives. We have from (2.6) :

$$4\pi\, dU = dL + \mathbf{D} \cdot d\mathbf{E} + \mathbf{E} \cdot d\mathbf{D},$$

and from (2.3) :

$$dL = -\mathbf{D} \cdot d\mathbf{E} + \mathbf{H} \cdot d\mathbf{B},$$

therefore

$$4\pi\, dU = \mathbf{E} \cdot d\mathbf{D} + \mathbf{H} \cdot d\mathbf{B},$$

or

$$\mathbf{E} = 4\pi \frac{\partial U}{\partial \mathbf{D}}; \quad \mathbf{H} = 4\pi \frac{\partial U}{\partial \mathbf{B}}. \tag{2.7}$$

We see that from this standpoint the energy-density U plays a similar role as the Lagrangian L from the standpoint 1.

[†] II, p. 437. There was a mistake of sign ; compare appendix.

[‡] II, p. 438.

[§] II, § 4.

Our electrodynamical equations (2.1) can now be written in the following form:

$$\frac{1}{4\pi}\frac{\partial \mathbf{D}}{\partial t} = \operatorname{rot}\frac{\partial \mathrm{U}}{\partial \mathbf{B}}; \quad \frac{1}{4\pi}\frac{\partial \mathbf{B}}{\partial t} = -\operatorname{rot}\frac{\partial \mathrm{U}}{\partial \mathbf{D}}. \tag{2.1A}$$

This formulation of classical electrodynamics will be the starting point of our further considerations.

It would also be possible to work with

Standpoint 4 : **E**, **H** *are chosen as independent variables*, **D**, **B** *as functions of them.* This standpoint will not concern us here, because it cannot be used in our quantization method. The reason for this is the form of the commutation laws which contain **D**, **B** (§ 3) ; besides, these vectors appear in Maxwell's equations differentiated with respect to time. One avoids formal difficulties by taking **D**, **B** as the fundamental quantities.

As the further developments in this paper are essentially based on standpoint 3, we want to determine U as a function of **D**, **B**, if L is given as function of **E**, **B** by (2.4). The calculation is given in the Appendix. If we denote

$$\mathrm{R} = (\mathbf{D}\,.\,\mathbf{B}), \tag{2.8}$$

the result is :

$$4\pi \mathrm{U} = \sqrt{(1+\mathbf{D}^2)(1+\mathbf{B}^2) - \mathrm{R}^2} - 1 \tag{2.9}$$

The momentum-density **S** has already been expressed in terms of **D**, **B** in (2.5).

Applying our fundamental equation (2.7) to (2.9) we obtain :

$$\left.\begin{aligned} \mathbf{E} &= \frac{\mathbf{D}(1+\mathbf{B}^2) - \mathbf{B}\mathrm{R}}{\sqrt{(1+\mathbf{D}^2)(1+\mathbf{B}^2) - \mathrm{R}^2}} \\ \mathbf{H} &= \frac{\mathbf{B}(1+\mathbf{D}^2) - \mathbf{D}\mathrm{R}}{\sqrt{(1+\mathbf{D}^2)(1+\mathbf{B}^2) - \mathrm{R}^2}} \end{aligned}\right\}. \tag{2.7A}$$

For

$$4\pi \mathrm{U} = \tfrac{1}{2}(\mathbf{B}^2 + \mathbf{D}^2),$$

the equations (2.1A) go over in Maxwell's equations and if U has the form (2.9), we obtain the electrodynamic equations of the new field theory. Their properties have been discussed in I and II.

We can also write U in another form:

$$\begin{aligned} 4\pi \mathrm{U} &= \sqrt{1 + \mathbf{B}^2 + \mathbf{D}^2 + (\mathbf{B}\times\mathbf{D})^2} - 1 \\ &= \sqrt{1 + \mathbf{B}^2 + \mathbf{D}^2 + (4\pi)^2\mathbf{S}^2} - 1, \end{aligned} \tag{2.10}$$

which shows distinctly that U must always be positive.

By integrating (2.5) and (2.6) over the whole space we can get the total energy and momentum:

$$4\pi\mathfrak{p} = 4\pi\int \mathfrak{S}\,dv = \int (\mathbf{D}\times\mathbf{B})\,dv \tag{2.11}$$

$$4\pi \mathrm{W} = 4\pi\int \mathrm{U}\,dv = \int \{\sqrt{1+\mathbf{B}^2+\mathbf{D}^2+(4\pi)^2\mathfrak{S}^2}-1\}\,dv \tag{2.12}$$

($\mathfrak{p}$ is a space vector and W a scalar).

We consider here, as well as later in quantum mechanics, our system as isolated. This is always possible for a limited time by taking the boundary surface far enough away.

It follows from the conservation laws for the energy-momentum-tensor† that $\mathfrak{p}$ and W do not depend on time:

$$\frac{\partial\mathfrak{p}}{\partial t} = 0; \qquad \frac{\partial \mathrm{W}}{\partial t} = 0. \tag{2.13}$$

According to the theory of relativity

$$p_1,\, p_2,\, p_3,\, \mathrm{W} \tag{2.14}$$

is a space-time-vector‡ and therefore

$$\mathrm{W}^2 - p^2 \tag{2.15}$$

is invariant with respect to Lorentz transformations. We shall show that the total momentum-energy-vector has a time character, *i.e.*, we shall prove that (2.15) is always positive. We get from (2.10):

$$(4\pi\,|\,\mathrm{U}\,|+1)^2 = 1+\mathbf{B}^2+\mathbf{D}^2+(4\pi)^2\,|\,\mathfrak{S}^2\,|. \tag{2.16}$$

We have denoted here by $|\,\mathrm{U}\,|$ and $|\,\mathfrak{S}\,|$ the absolute values of U and $\mathfrak{S}$. They are

$$|\,\mathrm{U}\,| = \mathrm{U}; \quad |\,\mathfrak{S}\,| = \sqrt{\mathfrak{S}^2} = 4\pi\,|\,\mathbf{B}\,|\,.\,|\,\mathbf{D}\,|\,.\,|\sin(\mathbf{B},\mathbf{D})\,|.$$

The following inequality is always fulfilled:

$$\mathbf{B}^2+\mathbf{D}^2 \geqslant 2\,|\,\mathbf{B}\,|\,.\,|\,\mathbf{D}\,|\,.\,|\sin(\mathbf{B},\mathbf{D})\,| = 8\pi\,|\,\mathfrak{S}\,|. \tag{2.17}$$

It follows from this equation and (2.16):

$$(1+4\pi\,|\,\mathrm{U}\,|)^2 \geqslant 1+8\pi\,|\,\mathfrak{S}\,|+(4\pi)^2\,|\,\mathfrak{S}\,|^2 = (1+4\pi\,|\,\mathfrak{S}\,|)^2. \tag{2.18}$$

---

† II, § 3.

‡ Pauli, "Relativitätstheorie," pp. 641, 683.

We have therefore:

$$U \geqslant |\mathfrak{S}|, \quad \text{or} \quad U^2 \geqslant \mathfrak{S}^2. \tag{2.19}$$

It follows from (2.19) with respect to the known properties of the integrals :

$$W \geqslant |\mathfrak{p}|, \tag{2.20}$$

which means that (2.15) is not negative or—in other words—that (2.14) is a vector of a time-character (and a zero-vector in the limiting case $W = |\mathfrak{p}|$). Therefore the quantity m_0 defined by

$$W^2 - \mathfrak{p}^2 = m_0^2 \tag{2.21}$$

is real; we regard m_0 as the rest-mass of the whole system.

It follows from the time-character of the total energy-momentum-vector that there always exists a co-ordinate system—say Σ_0—in which $\mathfrak{p} = 0$. In this co-ordinate system we have for the total energy W_0 :

$$W_0 = m_0.$$

As an example of a field with a non-vanishing rest-mass we can take the static central symmetric solution given in I and II. For this solution $\mathfrak{p}$ vanishes and W is finite. Identifying W with the energy of the electron we found[†] (in the usual units) that

$$m_0c^2 = W = \frac{e^2}{r_0} 1\cdot2361, \tag{2.22}$$

where m_0 is the mass of the electron, e is elementary charge and r_0 the radius of the electron.[‡] The equation (2.22) allowed us to calculate r_0 and we found that

$$r_0 = 1\cdot2361 \frac{e^2}{m_0c^2} = 2\cdot28 \,.\, 10^{-13} \text{ cm}. \tag{2.23}$$

In any arbitrary co-ordinate system Σ the energy and the momentum of the electron are connected by (2.21), where m_0 (or m_0c^2) is given by (2.22)

We are now able to generalize the equation (2.21) (in the same manner as we have done in II), if an external field is acting.[§] For this purpose let us assume that the external field has, in the chosen co-ordinate system, an *electrostatic* character, and that this field is, in a region surrounding the system considered, say the electron, *very small* compared with the proper field of the system. We denote the proper field of the system (electron) by $\mathbf{D}^{(0)}$ assuming that in the chosen co-ordinate system the system (electron) is at rest and that therefore its magnetic field $\mathbf{B}^{(0)}$ vanishes. We denote the external electrostatic field by

---

[†] II, p. 446.

[‡] In this theory there is only one absolute length defined, which we like to call "electronic radius." It is probable that this is also the real radius of action of the proton (in spite of its big mass).

[§] II, p. 445.

$$\mathbf{D}^{(e)} = \mathbf{E}^{(e)} = -\operatorname{grad} \phi \tag{2.24}$$

where ϕ is the potential of the external field. We have, therefore, in the first approximation for the whole field $\mathbf{D}$:

$$\mathbf{D} = \mathbf{D}^{(o)} + \mathbf{D}^{(e)} \tag{2.25}$$

and expanding W we get:

$$\begin{aligned} 4\pi \mathrm{W} &= 4\pi \int \mathrm{U}\, dv = 4\pi \int \mathrm{U}^{(o)}\, dv + 4\pi \int \left\{ \left(\frac{\partial \mathrm{U}}{\partial \mathbf{D}} \right)_{\mathbf{D}^{(\ )}} . \, \mathbf{D}^{(e)} \right\} dv \\ &= 4\pi\, \mathrm{W}^{(o)} - \int (\mathbf{E}^{(o)} . \operatorname{grad} \phi)\, dv = 4\pi\, \mathrm{W}^{(o)} + \int (\phi . \operatorname{div} \mathbf{E}^{(o)})\, dv. \end{aligned} \tag{2.26}$$

We know that $\frac{1}{4\pi}$ div. $\mathbf{E}^{(o)}$ is the "free-charge-density" of the electron,† *i.e.*,

$$\operatorname{div} \mathbf{E}^{(o)} = 4\pi\rho \tag{2.27}$$

and therefore

$$\mathrm{W} = \mathrm{W}^{(o)} + \int \rho \phi\, dv. \tag{2.28}$$

If the external potential is essentially constant in a region surrounding the system (electron), we get instead of (2.28)

$$\mathrm{W}^{(o)} = \mathrm{W} + e\phi. \tag{2.29}$$

The equation holds in the chosen co-ordinate system in which the electron is at rest. In an arbitrary co-ordinate system we have therefore

$$\mathrm{W}^{(0)} = \mathrm{W} + e\phi; \qquad \mathbf{p}^{(0)} = \mathbf{p} + \mathbf{A}e, \tag{2.30}$$

where $\mathbf{A}$ is the vector-potential. If therefore an external field is acting, we get instead of (2.21) the following equation:

$$(\mathrm{W} + e\phi)^2 - (\mathbf{p} + e\mathbf{A})^2 = m_0{}^2 \tag{2.31}$$

provided that the formulated assumptions are fulfilled and that we can assume the superposition of the $\mathbf{D}^{(0)}$ and $\mathbf{D}^{(e)}$ according to (2.25).

---

† II, p. 444.

§ 3. THE COMMUTATION RULES FOR THE FUNDAMENTAL VARIABLES AND THE NATURAL UNITS

We repeat the definition of the two kinds.of field tensors:

$$\mathbf{B} \rightarrow f^{*14}, f^{*24}, f^{*34}; \qquad \mathbf{E} \rightarrow f^{*23}, f^{*31}, f^{*12} \tag{3.1}$$

$$\mathbf{H} \rightarrow p_{23}, p_{31}, p_{12}; \qquad \mathbf{D} \rightarrow p_{14}, p_{24}, p_{34}. \tag{3.2}$$

The tensors $f_{\lambda\nu}$ (*i.e.*, **B**, **E**) and $p_{\lambda\nu}$ (*i.e.*, **H**, **D**) can be derived from four-dimensional vector-potentials. It is not possible to do this for the variables **B**, **D** as they belong to different tensors. Therefore in formulating the commutation rules we shall use not the vector-potentials, but the variables **B**, **D**, directly. We shall regard **B**, **D** as *q*-functions of the space-time-variables which will be regarded as *c*-numbers. We shall simply transfer the commutation laws of Heisenberg and Pauli to the case, when **B**, **D** represent the field strengths. The justification of our assumption lies in the consequences which we shall draw from them. It will be shown that the commutation rules, together with the definition of the time-derivative, lead us to the equations of the new field theory.

The *commutation laws* are in conventional units†:

$$\text{(I)} \quad \left\{ \begin{array}{ll} [\mathrm{B}_k, \bar{\mathrm{B}}_l] = 0; \qquad [\mathrm{D}_k, \bar{\mathrm{D}}_l] = 0 & (3.3) \\ [\mathrm{D}_1, \bar{\mathrm{B}}_2] = -[\mathrm{B}_1, \bar{\mathrm{D}}_2] = 4\pi c\,\delta(x-\bar{x})\,\delta(y-\bar{y})\,\delta'(z-\bar{z}) & (3.4) \\ [\mathrm{D}_1, \bar{\mathrm{B}}_3] = -[\mathrm{B}_1, \bar{\mathrm{D}}_3] = -4\pi c\,\delta(x-\bar{x})\,\delta'(y-\bar{y})\,\delta(z-\bar{z}) & (3.5) \\ [\mathrm{D}_2, \bar{\mathrm{B}}_3] = -[\mathrm{B}_3, \bar{\mathrm{D}}_2] = 4\pi c\,\delta'(x-\bar{x})\,\delta(y-\bar{y})\,\delta(z-\bar{z}) & (3.6) \\ [\mathrm{D}_k, \bar{\mathrm{B}}_k] = [\mathrm{B}_k, \bar{\mathrm{D}}_k] = 0; \qquad k, l = 1, 2, 3. & (3.7) \end{array} \right.$$

The equations (I) need some explanation.

The symbol [F, L] denotes

$$\frac{\hbar}{i}[\mathrm{F}, \bar{\mathrm{L}}] = \mathrm{F}(x, y, z, t) \,.\, \mathrm{L}(\bar{x}, \bar{y}, \bar{z}, t) - \mathrm{L}(\bar{x}, \bar{y}, \bar{z}, t)\,\mathrm{F}(x, y, z, t). \tag{3.8}$$

$[\mathrm{F}, \bar{\mathrm{L}}]$ is to be taken for different space points, but for *the same time*. $\hbar$ denotes Planck's constant divided by 2π and c is the velocity of light.

---

† Heisenberg and Pauli, 'Z. Phys.,' vol. 56, p. 25 (1929).

δ are the known Dirac-functions and, as we shall often make use of them, we repeat briefly their properties†:

$$\int_{-\infty}^{+\infty} \delta(x)\,\delta(y)\,\delta(z)\,dx\,dy\,dz = 1, \tag{3.9}$$

$$\int_{-\infty}^{+\infty} f(x, y, z)\,\delta'(x)\,\delta(y)\,\delta(z)\,dx\,dy\,dz = -\left(\frac{\partial f}{\partial x}\right)_{x=y=z=0}, \tag{3.10}$$

$$\left.\begin{array}{ll} \delta'(x) = -\dfrac{\delta(x)}{x}; & \delta''(x) = -\dfrac{2\delta'(x)}{x} \\ \delta(x) = \delta(-x); & \delta'(x) = -\delta'(-x) \\ x\,\delta(x)\,\delta(y)\,\delta(z) = 0; & x\,\delta(x)\,\delta'(y)\,\delta(z) = 0, \text{ etc.} \end{array}\right\} . \tag{3.11}$$

The equations (I) are formulated in the conventional units. According to (3.8) [**B**, **D**] has the dimensions of cm^{-4}. The Dirac-function $\delta(x)$ has the dimension cm^{-1} and $\delta'(x)$ the dimension cm^{-2} as follows from (3.9) and (3.11). The dimensions on both sides in (I) are therefore the same. But there is a discrepancy between the units used in the equations of the new field theory in § 2 and the units used in equations (I). The former equations are expressed in the natural units of the field strength, *i.e.*, the field strength is measured by the field inside the electron having the value b which represents the upper limit of the field strength in the static case. If we also want to express (I) in the natural units, we have to divide both sides by‡:

$$b^2 = e^2/r_0^4. \tag{3.12}$$

If we take as an example the equation (3.4) of (I), we get

$$\mathbf{B}_1\,\overline{\mathbf{D}}_2 - \overline{\mathbf{D}}_2\,\mathbf{B}_1\,4\pi\frac{\hbar c}{ie^2}(r_0\,\delta(x-\overline{x}))\,(r_0\,\delta(y-\overline{y}))\,(r_0^2\,\delta'(z-\overline{z})), \tag{3.13}$$

$r_0\,\delta(x)$ and $r_0^2\,\delta'(x)$ are dimensionless. We see, therefore, *how the idea of the finite radius comes*, automatically, *into the principal equations* (I). As

$$\frac{e^2}{\hbar c} = \alpha = \frac{1}{137,1} \tag{3.14}$$

is the fine structure constant, we find in (3.13) the numerical factor

$$\frac{4\pi}{\alpha} = 4\pi\,.\,137,1 = 1722. \tag{3.15}$$

---

† Dirac, " The principles of quantum mechanics," Oxford, p. 63 (1930).

‡ II, p. 446.

Now the right-hand term of the commutation laws has the coefficient αr_0^4, where α has the value (3.14), independent of any choice of units. Therefore we are induced to assume the natural unit of length r_0 which we, of course, take as 1. Then in our *natural system of units*, where $b = 1$, it follows, from $e^2 = b^2 r_0^4$, that $e = 1$. We have therefore in natural units:

$$r_0 = 1;\quad c = 1;\quad e = 1;\quad b = 1. \tag{3.16}$$

From

$$m_0 c^2 = 1{,}2361,$$

we get for the mass of the electron in the natural units

$$m_0 = 1{,}2361 \tag{3.17}$$

and from (3.14) it follows for $\hbar$ in the same units:

$$\hbar = 137{,}1. \tag{3.18}$$

The commutation rules (written in the natural units and with $\frac{1}{id}[\mathrm{F}, \bar{\mathrm{L}}] = \mathrm{F}\,\bar{\mathrm{L}} - \bar{\mathrm{L}}\,\mathrm{F}$) take, therefore, the following form:

$$(\mathrm{I_A})\left\{\begin{array}{ll} [\mathrm{B}_k, \bar{\mathrm{B}}_l] = [\mathrm{D}_k, \bar{\mathrm{D}}_l] = 0 & (3.3\mathrm{A}) \\ [\mathrm{D}_1, \bar{\mathrm{B}}_2] = -[\mathrm{B}_1, \bar{\mathrm{D}}_2] = 4\pi \frac{\partial}{\partial z}\,\delta(\mathbf{r} - \bar{\mathbf{r}}) & (3.4\mathrm{A}) \\ [\mathrm{D}_k, \bar{\mathrm{B}}_k] = [\mathrm{B}_k, \bar{\mathrm{D}}_k] = 0 & (3.7\mathrm{A}) \\ \delta(\mathbf{r} - \bar{\mathbf{r}}) = \delta(x - \bar{x})\,\delta(y - \bar{y})\,\delta(z - \bar{z}) & (3.19) \end{array}\right.$$

It can easily be proved, that if $\bar{\mathrm{F}}$ is a function of $\mathbf{D}(\bar{x}, \bar{y}, \bar{z}, t)$, $\mathbf{B}(\bar{x}, \bar{y}, \bar{z}, t)$ (provided that $\bar{\mathrm{F}}$ can be expanded in a power series in the components $\mathbf{B}$, $\mathbf{D}$) we have :

$$\left.\begin{array}{l} [\mathrm{D}_1, \bar{\mathrm{F}}] = 4\pi\left(\dfrac{\partial\bar{\mathrm{F}}}{\partial\mathrm{B}_2}\dfrac{\partial}{\partial z}\,\delta(\mathbf{r} - \bar{\mathbf{r}}) - \dfrac{\partial\bar{\mathrm{F}}}{\partial\mathrm{B}_3}\dfrac{\partial}{\partial y}\,\delta(\mathbf{r} - \bar{\mathbf{r}})\right) \\ [\mathrm{B}_1, \bar{\mathrm{F}}] = -4\pi\left(\dfrac{\partial\bar{\mathrm{F}}}{\partial\mathrm{D}_2}\dfrac{\partial}{\partial z}\,\delta(\mathbf{r} - \bar{\mathbf{r}}) - \dfrac{\partial\bar{\mathrm{F}}}{\partial\mathrm{D}_3}\dfrac{\partial}{\partial y}\,\delta(\mathbf{r} - \bar{\mathbf{r}})\right) \end{array}\right\}, \tag{3.20}$$

and similarly for the other components of $\mathbf{D}$ and $\mathbf{B}$.

§ 4. THE TIME-DERIVATIVE AND THE FIELD EQUATIONS

In § 2 we have quoted the expressions of the momentum- and energy-density as functions of $\mathbf{B}$ and $\mathbf{D}$. In natural units we have

$$4\pi\,\mathfrak{S} = (\mathbf{D} \times \mathbf{B}), \tag{2.5A}$$

$$4\pi\mathrm{U} = \sqrt{1 + \mathbf{B}^2 + \mathbf{D}^2 + 4\pi^2\mathfrak{S}^2} - 1. \tag{2.10A}$$

Let us now consider the expressions for $\mathfrak{S}$ and U (for the case) when **B** and **D** are *q*-numbers. As the values of $\mathfrak{S}$ and U depend on the order of **B** and **D** in the products, we have to symmetrize the functions $\mathfrak{S}$ and U. This is easily done for $\mathfrak{S}$:

$$4\pi\mathfrak{S} = \tfrac{1}{2}\{(\mathbf{D} \times \mathbf{B}) - (\mathbf{B} \times \mathbf{D})\}. \tag{4.1}$$

The function under the square root in (2.10A) will also be symmetrized, if we substitute for $\mathfrak{S}$ the expression (4.1). Introducing

$$Z = \mathbf{B}^2 + \mathbf{D}^2 + 8\pi^2\{(\mathbf{D} \times \mathbf{B}) - (\mathbf{B} \times \mathbf{D})\}^2, \tag{4.2}$$

where

$$Z(\mathbf{B}, \mathbf{D}) = Z(\mathbf{D}, \mathbf{B}), \tag{4.3}$$

we have

$$4\pi U = \sqrt{1 + Z} - 1. \tag{4.4}$$

The expression $\sqrt{1 + Z}$ denotes here a power series of the function Z:

$$\sqrt{1 + Z} = 1 + \tfrac{1}{2}Z - \tfrac{1}{8}Z^2 + \tfrac{1}{32}Z^3 \ldots \tag{4.5}$$

We see that U is also symmetrical in **B** and **D** :

$$U(\mathbf{B}, \mathbf{D}) = U(\mathbf{D}, \mathbf{B}). \tag{4.6}$$

The expression (4.2) for Z is not the only one which fufils the condition (4.3) of symmetry and gives, in the limiting case when **B** and **D** are *c*-functions the classical value for U. We see indeed that if

$$Z = \mathbf{B}^2 + \mathbf{D}^2 + \tfrac{1}{2}\mathbf{B}^2\mathbf{D}^2 + \tfrac{1}{2}\mathbf{D}^2\mathbf{B}^2 - R^2, \tag{4.7}$$

we get, when **B** commutes with **D**, the expression (2.10) for U, and U in this case also fulfils the condition (4.6). It seems impossible to decide now, without solving any special problems, which of the admissible expressions of U has to be used.

In the following calculations we shall not consider any special form of U. They are all valid if U is an arbitrary symmetrical function in **B** and **D**, provided that it can be developed in a power series.

We denote by W (as before) the space integral of U, *i.e.*, the total energy:

$$W = \int U\, dv. \tag{4.8}$$

Let us now introduce the *time derivative* of our fundamental variables by the following *definition*:

$$\text{(II)} \quad \left\{ \begin{aligned} \dot{\mathbf{D}}_k &= \frac{\partial \mathbf{D}_k}{\partial t} = -[W, \mathbf{D}_k], && (4.9) \\ \dot{\mathbf{B}}_k &= \frac{\partial \mathbf{B}_k}{\partial t} = -[W, \mathbf{B}_k]. && (4.10) \end{aligned} \right.$$

We shall calculate for example $\dot{D}_1$. We find:

$$-[W, D_1] = -i\alpha \int (UD_1 - D_1U)\,dv = \int [D_1U]\,dv. \tag{4.11}$$

In view of (3.20) we get

$$\left.\begin{aligned}\dot{D}_1 = 4\pi \int \frac{\partial U}{\partial B_2}\,\delta(x-\bar{x})\,\delta(y-\bar{y})\,\delta'(z-\bar{z})\,d\bar{x}\,d\bar{y}\,d\bar{z}\\ -4\pi \int \frac{\partial U}{\partial B_3}\,\delta(x-\bar{x})\,\delta'(y-\bar{y})\,\delta(z-\bar{z})\,d\bar{x}\,d\bar{y}\,d\bar{z}\end{aligned}\right\}. \tag{4.12}$$

According to (3.10) we can write this equation:

$$\frac{1}{4\pi}\dot{D}_1 = \frac{\partial}{\partial y}\left(\frac{\partial U}{\partial B_3}\right) - \frac{\partial}{\partial z}\left(\frac{\partial U}{\partial B_2}\right). \tag{4.13}$$

Calculating in the same way D_2, D_3 and B_k, we get finally

$$\dot{\mathbf{D}} = \operatorname{rot}\mathbf{H}; \quad \dot{\mathbf{B}} = -\operatorname{rot}\mathbf{E}, \tag{4.14}$$

where

$$\mathbf{H} = 4\pi\frac{\partial U}{\partial \mathbf{B}}; \quad \mathbf{E} = 4\pi\frac{\partial U}{\partial \mathbf{D}}. \tag{2.7}$$

The last equations are identical in form with (2.1A), *i.e.*, with the field equations of the new field theory.

We see, therefore, that if U has the form (2.10) the formulated commutation rules together with the definition of the time derivatives lead us to the equations of the new field theory, whereas it would lead us to Maxwell's equations, if U were to have the form :

$$U = \frac{1}{8\pi}(\mathbf{B}^2 + \mathbf{D}^2).$$

The Maxwell expression for U can also be regarded here as the limiting case for very small **B** and **D**. But the assumption of very small **B** and **D** means (from the unitarian standpoint) absence of matter.

The definition of the time derivative given in (II) will allow us to find the time derivatives of an arbitrary function F of the fundamental variables **B**, **D**, provided that F can be expanded in a power series. Taking as an example B_kD_l we can easily prove :

$$\frac{\partial}{\partial t}(B_kD_l) = B_k\dot{D}_l + \dot{B}_kD_l. \tag{4.15}$$

The right-hand side of (4.15) gives according to (II):

$$- i\alpha\,(B_k W D_l - B_k D_l W) - i\alpha\,(W B_k D_l - B_k D_l W)$$

$$= - i\alpha\,(W\,B_k D_l - B_k D_l W). \tag{4.16}$$

Therefore:

$$- [W, B_k\, D_l] = B_k\, \dot{D}_l + \dot{B}_k\, D_l = \frac{\partial}{\partial t}(B_k\, D_l). \tag{4.17}$$

For an arbitrary function F (**B**, **D**) we have:

$$- [W, F] = \frac{\partial F}{\partial t} = \sum_{k=1}^{3} \frac{\partial f}{\partial B_k}\, \dot{B}_k + \sum_{k=1}^{3} \frac{\partial f}{\partial D_k}\, \dot{D}_k. \tag{4.18}$$

But it is important to pay attention to the order of the *q*-numbers. B_k or D_k is to be inserted where B_k or D_k was before the differentiation (as for example in (4.15)).

Applying the definition of the time derivative to the function W itself we find:

$$\left.\begin{aligned} \dot{W} &= - [W, W] = 0 \\ W &= \text{const.} \end{aligned}\right\}. \tag{4.19}$$

The last equation expresses the law of conservation of the energy.

The quantities $[D_k, \bar{B}_l]$ are *c*-numbers, as follows from the commutation rules. They commute, therefore, with W or, in other words, their time derivative vanishes. It is, therefore, enough to suppose that the commutation rules are valid for $t = 0$. From

$$\frac{\partial}{\partial t}[D_k, \bar{B}_l] = 0 \tag{4.20}$$

follows their validity for any time.

§ 5. THE DIVERGENCE EQUATIONS AND THE SPACE DERIVATIVE

We have stated in § 4 that the commutation rules (I), together with the definition of the time derivative, lead us to the equations of the new field theory. But in this way we have obtained only the equations (4.14), corresponding to (2.1) in § 2, and not the equations (2.2), *i.e.*,

$$\operatorname{div} D = 0; \qquad \operatorname{div} B = 0. \tag{2.2}$$

Our scheme of equations consisting of (I) and (II) is, therefore, not complete. We shall show that it is possible to formulate, with help of the commutation rules alone, supplementary equations for **B** and **D** which are entirely equivalent to (2.2).

For this purpose we shall have to introduce the vector **p**, *i.e.*, the total momentum of the field. **p** is connected with **S** in the same way as W with U:

$$\mathbf{p} = \int \mathbf{S}\, dv = \frac{1}{8\pi} \int \{(\mathbf{D} \times \mathbf{B}) - (\mathbf{B} \times \mathrm{D})\}\, dv. \tag{5.1}$$

We are now able to formulate our supplementary equations with the help of the vector **p**. They have the form:

$$\text{(III)} \quad \begin{cases} [p_1, \mathrm{D}_1] + [p_2, \mathrm{D}_2] + [p_3, \mathrm{D}_3] = \sum\limits_{k=1}^{3} [p_k, \mathrm{D}_k] = 0 & (5.2) \\ [p_1, \mathrm{B}_1] + [p_2, \mathrm{B}_2] + [p_3, \mathrm{B}_3] = \sum\limits_{k=1}^{3} [p_k, \mathrm{B}_k] = 0 & (5.3) \end{cases}$$

To prove the equivalence of (III) and (2.2) we have to calculate $[p_k, \mathrm{D}_k]$ and $[p_k, \mathrm{B}_k]$. Beginning with $[p_1, \mathrm{D}_1]$ we find :

$$[p_1, \mathrm{D}_1] = - [\mathrm{D}_1, p_1] = - \int [\mathrm{D}_1, \mathrm{S}_1]\, d\bar{x}\, d\bar{y}\, d\bar{z}. \tag{5.4}$$

Since we have (3.20) and (4.1), we find:

$$[p_1, \mathrm{D}_1] = \int \{\mathrm{D}_3 \delta(x - \bar{x})\, \delta(y - \bar{y})\, \delta'(z - \bar{z}) + \mathrm{D}_2\, \delta(x - \bar{x})\, \delta'(y - \bar{y})\, \delta(z - \bar{z})\}\, d\bar{x}\, d\bar{y}\, d\bar{z},$$

and according to (3.10) we get:

$$- [p_1, \mathrm{D}_1] = \frac{\partial \mathrm{D}_2}{\partial y} + \frac{\partial \mathrm{D}_3}{\partial z}. \tag{5.5}$$

Similarly:

$$- [p_2, \mathrm{D}_2] = \frac{\partial \mathrm{D}_1}{\partial x} + \frac{\partial \mathrm{D}_3}{\partial z} \tag{5.6}$$

$$- [p_3, \mathrm{D}_3] = \frac{\partial \mathrm{D}_1}{\partial x} + \frac{\partial \mathrm{D}_2}{\partial y}. \tag{5.7}$$

From the last three equations it follows immediately that

$$- \sum_{k=1}^{3} [p_k, \mathrm{D}_k] = 2 \operatorname{div} \mathbf{D}, \tag{5.8}$$

and in the same way we find that

$$- \sum_{k=1}^{3} [p_k, \mathrm{B}_k] = 2 \operatorname{div} \mathbf{B}. \tag{5.9}$$

Our supplementary equations (III) are therefore completely equivalent to the field equations (2.2). Our scheme of equations contains the commutation rules (I), the definition of the time derivative (II) and the supplementary conditions (III) for the fundamental variables.

If we take α not as a numerical number but as a parameter, we get in the limiting case of

$$\frac{1}{\alpha} \to 0$$

from our scheme of equations the classical equations of the new field theory. The quantities which characterize the field become *c*-numbers, and (4.14) and (2.2) are our field equations connecting *c*-functions.

We are now able to express the space derivatives with the help of the commutation rules. It can be shown that:

$$\left.\begin{aligned} [p_l, \mathrm{D}_k] &= \frac{\partial \mathrm{D}_k}{\partial x^l} \\ [p_l, \mathrm{B}_k] &= \frac{\partial \mathrm{B}_k}{\partial x^l} \\ x^1 = x, \quad x^2 &= y, \quad x^3 = z \end{aligned}\right\} . \tag{5.10}$$

This is immediately evident for $k = l$ because of ((5.5)–(5.7)) since $\operatorname{div} \mathbf{B}$ and $\operatorname{div} \mathbf{D}$ vanishes. It can also be proved if $k \neq l$. We shall take as an example $[p_2, \mathrm{D}_1]$.

$$[p_2, \mathrm{D}_1] = -\int [\mathrm{D}_1, \mathrm{S}_2]\, dv =$$

$$-\int \{\mathrm{D}_1\, \delta(x - \bar{x})\, \delta'(y - \bar{y})\, \delta(z - \bar{z})\}\, d\bar{x}\, d\bar{y}\, d\bar{z} = \frac{\partial \mathrm{D}_1}{\partial y} = \frac{\partial \mathrm{D}_1}{\partial x^2} . \tag{5.11}$$

In a similar way we could prove the validity of all other equations contained in (5.10).

The equations (5.10) can easily be generalized for an arbitrary function F of the fundamental variables **B**, **D** provided that F can be expanded in a power series. For example, we can easily prove for $\mathrm{B}_k \mathrm{D}_l$ that:

$$[p_s, \mathrm{B}_k \mathrm{D}_l] = \frac{\partial \mathrm{B}_k}{\partial x^s} \mathrm{D}_l + \mathrm{B}_k \frac{\partial \mathrm{D}_l}{\partial x^s} . \tag{5.12}$$

The right side of (5.12) gives according to (5.10):

$$\left.\begin{aligned} i\alpha (p_s \mathrm{B}_k \mathrm{D}_l - \mathrm{B}_k p_s \mathrm{D}_l) + i\alpha (\mathrm{B}_k p_s \mathrm{D}_l - \mathrm{B}_k \mathrm{D}_l p_s) \\ = i\alpha (p_s \mathrm{B}_k \mathrm{D}_l - \mathrm{B}_k \mathrm{D}_l p_s) \end{aligned}\right\} . \tag{5.13}$$

Therefore

$$[p_s, \mathbf{B}_k \mathbf{D}_l] = \frac{\partial}{\partial x^s}(\mathbf{B}_k \mathbf{D}_l). \tag{51.4}$$

For an arbitrary function F (**B**, **D**) we have:

$$[p_s, \mathrm{F}(\mathbf{B}, \mathbf{D})] = \frac{\partial \mathrm{F}(\mathbf{B}, \mathbf{D})}{\partial x^s} = \sum_{k=1}^{3} \frac{\partial \mathrm{F}}{\partial \mathbf{B}_k} \frac{\partial \mathbf{B}_k}{\partial x^s} + \sum_{k=1}^{3} \frac{\partial \mathrm{F}}{\partial \mathbf{D}_k} \frac{\partial \mathbf{D}_k}{\partial x^s}; \tag{5.15}$$

$\left(\frac{\partial \mathbf{B}_k}{\partial x^s}\right.$ or $\frac{\partial \mathbf{D}_k}{\partial x^s}$ is to put on that place where $\mathbf{B}_k$ or $\mathbf{D}_k$ was before the differentiation.$\left.\right)$

Applying (5.15) to the functions p_k themselves we find as p_k does not depend on the space variables:

$$[p_k, p_s] = 0. \tag{5.16}$$

The vector $\mathbf{p}\,(p_1, p_2, p_3)$ commutes not only with itself but also with W since W does not depend on x, y, z. We have, therefore,

$$[p_s, \mathrm{W}] = \frac{\partial \mathrm{W}}{\partial x^s} = 0, \tag{5.17}$$

but because of (4.18) and (5.17) we find also

$$[p_s, \mathrm{W}] = \frac{\partial p_s}{\partial t} = 0,$$

therefore

$$\dot{p}_1 = \dot{p}_2 = \dot{p}_3 = 0; \qquad p_k = \text{constant}. \tag{5.18}$$

The equations (5.18) together with (4.19) express the law of the conservation of momentum and energy.

The results which have been attained here will allow us to express the quantized field equations of the new field theory *i.e.*, (4.14) and (2.2) merely with the help of the commutation rules. This follows immediately since the field equations contain time and space derivatives and since we are able, as we have shown in the last two sections, to express the time as well as the space derivatives with the help of the commutation rules. Using the four-dimensional space-time-notation we are able to do so in a symmetrical and simple form.

We can express the field **B**, **D** as well as **H**, **E** with the help of the antisymmetrical tensor f^{*kl} and p_{kl}, using the notation of (3.1) and (3.2). The field equations (4.14) and (2.2) take the form[†]

$$\left.\begin{array}{c} \displaystyle\sum_{\lambda=1}^{4} \frac{\partial f^{*\rho\lambda}}{\partial x^\lambda} = 0; \qquad \sum_{\lambda=1}^{4} \frac{\partial p^{\rho\lambda}}{\partial x^\lambda} = 0 \\ x^1 = x; \quad x^2 = y; \quad x^3 = z; \quad x^4 = t \end{array}\right\}. \tag{5.19}$$

[†] II., p. 433.

(The rule for raising and lowering the indices is very simple. This operation on the index 4 does not change the value of the tensor component and on one of the indices 1, 2, 3 changes only its sign.) We shall introduce further :

$$t_{4\lambda} = \int \mathrm{T}_{4\lambda}^{\cdot\cdot} dv = \begin{cases} -4\pi p_\lambda & \text{if } \lambda = 1, 2, 3, \\ 4\pi \mathrm{W} & \text{if } \lambda = 4. \end{cases}$$

The equations (5.19) can, therefore, be written:

$$\sum_{\lambda=1}^{4} [t_{4\lambda}, f^{*\rho\lambda}] = 0; \qquad \sum_{\lambda=1}^{4} [t_{4\lambda}, p^{\rho\lambda}] = 0. \tag{5.19A}$$

The Lorentz-invariance of (5.19A) is evident because of the space-time-vector character of $t_{4\lambda}$.

§ 6. THE LORENTZ TRANSFORMATIONS AND THE COMMUTATION RULES

The commutation rules are formulated in a given co-ordinate system Σ for two different space points and for the same time t. We have now to answer the following question : Are the commutation rules valid in $\bar{\Sigma}$, if they are valid in Σ, provided that Σ and $\bar{\Sigma}$ are connected by a Lorentz transformation ? We shall prove that this is in fact so.

Let us denote by

$$x^1, x^2, x^3, x^4 - x, y, z, t \tag{6.1}$$

the co-ordinates of the world points in the co-ordinate system Σ and by

$$\bar{x}^1, \bar{x}^2, \bar{x}^3, \bar{x}^4 - \bar{x}, \bar{y}, \bar{z}, \bar{t} \tag{6.2}$$

the co-ordinates of the world points in the co-ordinate system $\bar{\Sigma}$. We shall consider only the infinitesimally small transformation from Σ to $\bar{\Sigma}$:

$$\bar{x}^\mu = \delta_\nu^\mu x^\nu + \varepsilon_{\nu}^{\cdot\mu} x^\nu. \tag{6.3}$$

The *Greek* indices take all values from 1 to 4 and we shall use here the convention that one has to sum up from 1 to 4 over any index which appears twice. The rule of raising and lowering the indices was explained before. δ_ν^μ has the value:

$$\delta_\nu^\mu = \begin{cases} 1 & \text{if } \mu = \nu \\ 0 & \text{if } \mu \neq \nu. \end{cases} \tag{6.4}$$

$\varepsilon_{\nu}^{\cdot\mu}$ is an infinitesimally small coefficient. The dot in $\varepsilon_{\nu}^{\cdot\mu}$ denotes the order of the indices. For example:

$$\varepsilon_{2}^{\cdot 3} = -\varepsilon^{23}; \qquad \varepsilon_{43} = \varepsilon^{4}_{\cdot 3} = -\varepsilon^{43} \tag{6.5}$$

In consequence we shall neglect in all the following calculations the expressions in which the products of two $\varepsilon_{\nu}{}^{\cdot\mu}$ appear.

We find from (6.3):

$$x^{\mu} = (\delta_{\nu}{}^{\mu} - \varepsilon_{\nu}{}^{\cdot\mu})\,\overline{x}^{\nu}. \tag{6.3A}$$

From the invariance of $x^{\nu}x_{\nu}$ follows

$$\varepsilon_{\rho\nu} = -\,\varepsilon_{\nu\rho}. \tag{6.6}$$

$\varepsilon_{\rho\nu}$ vanishes, therefore, if $\rho = \nu$.

All results which we shall obtain, assuming an infinitesimally small transformation, are also valid for a finite transformation because of the group character of the Lorentz transformations.

In § 3 we formulated the commutation rules, *i.e.*, the value of the expressions:

$$[\mathrm{D}_k, \mathrm{D}'_l]\,; \qquad [\mathrm{B}_k, \mathrm{B}'_l]\,; \qquad [\mathrm{D}_k, \mathrm{B}'_l]. \tag{6.7}$$

The dash on D'_l, B'_l denotes that these quantities are to be taken for a different space-point from D_k, B_k, but for the same time. The expressions in (6.7) can be written also in a space-time symbolism:

$$[p^{k4}, p'^{l4}]\,; \quad [f^{*k4}, f'^{*l4}]\,; \quad -\,[p^{k4}, f'^{*l4}] \qquad k, l = 1, 2, 3. \tag{6.7A}$$

The *Latin* indices which we shall use in this section can take only the values from 1 to 3. One has to sum up from 1 to 3 if the *Latin* index appears twice.

Let us take as an example one of the expressions in (6.7A), *i.e.*,

$$[\mathrm{D}_k, \mathrm{B}'_l] \rightarrow -\,[p^{k4}, f'^{*l4}]. \tag{6.8}$$

We shall consider the change which this expression undergoes by an infinitesimally small Lorentz transformation, and we shall prove the invariance of (6.8). The invariance proof for the remaining expressions in (6.7) is quite similar, but simpler, since the other two expressions in (6.7) always vanish. We shall, therefore, omit here the proof of the invariance for $[\mathrm{D}_k, \mathrm{D}'_l]$ and $[\mathrm{B}_k, \mathrm{B}'_l]$.

As we know, p^{k4} and f'^{*l4} are to be taken for the same time. We consider the value of (6.8) in the following world points:

$$(\mathrm{P}_0):\ 0, 0, 0, 0\,; \qquad (\mathrm{P}):\ x, y, z, 0. \tag{6.9}$$

The choice of $t = 0$ does not imply any restriction. We know (§ 3) that the commutation rules are always valid if they are valid for $t = 0$. We denote:

$$p_0{}^{k4} = p^{k4}(0, 0, 0, 0)\,; \qquad f^{*k4} = f^{*k4}(x, y, z, 0). \tag{6.10}$$

In the co-ordinate system Σ, the expression (6.8), for the chosen two space points, takes the form:

$$[D_{0k}, B_l] = [p_0^{k4}, f^{*l4}]. \tag{6.8A}$$

We shall now go over from the co-ordinate system Σ to $\bar{\Sigma}$. We shall do so in two steps:

1. We can find $\bar{p}_0^{k4}$ and $\bar{p}^{l4}$ from the transformation rules for tensors. We have:

$$\text{In } \Sigma\text{: } p_0^{k4}\,(0, 0, 0, 0); \qquad \text{in } \bar{\Sigma}\text{: } \bar{p}_0^{k4}\,(0, 0, 0, 0)$$

$$\text{In } \Sigma\text{: } f^{*l4}\,(x^1, x^2, x^3, 0); \quad \text{in } \bar{\Sigma}\text{: } \bar{f}^{*l4}\,(\bar{x}^1, \bar{x}^2, \bar{x}^3, \bar{x}^4).$$

The world point P_0 in (6.9) has the same co-ordinates in Σ and $\bar{\Sigma}$. For the world point P we have :

$$\bar{x}^k = x^k + \varepsilon_{s}^{\cdot k} x^s; \qquad \bar{x}^4 = \varepsilon^{r4}_{\cdot} x^r \tag{6.11}$$

$$x^k = \bar{x}^k - \varepsilon_{r}^{\cdot k}\bar{x}^r - \varepsilon_{4}^{\cdot k}\bar{x}^4; \qquad x^4 = 0. \tag{6.11A}$$

We see, therefore, that the two world points which have the same time in Σ, have different times in $\bar{\Sigma}$.

2. Our commutation rules are defined only for the same time in the functions p^{k4}, f^{*l4}. To find the commutation rules in $\bar{\Sigma}$ we have to choose two world points with the same time in $\bar{\Sigma}$, *i.e.*,

$$(P_0)\ 0, 0, 0, 0; \qquad (P)\ \bar{x}^1, \bar{x}^2, \bar{x}^3, 0.$$

The second step of our calculations will consist, therefore, in changing the world point

$$(P)\text{: } \bar{x}^1, \bar{x}^2, \bar{x}^3, \bar{x}^4 \text{ into } (\bar{P})\text{: } \bar{x}^1, \bar{x}^2, \bar{x}^3, 0.$$

Let us begin with the *first* step and calculate $\bar{p}_0^{k4}$ and $\bar{f}^{*l4}$.

We find that:

$$\begin{aligned}\bar{p}_0^{k4} &= (\delta_\nu^{k} + \varepsilon_{\nu}^{\cdot k})(\delta_\rho^{4} + \varepsilon_{\rho}^{\cdot 4})\, p_0^{\nu\rho} \\ &= p_0^{k4} + p_0^{\nu 4}\varepsilon_{\nu}^{\cdot k} + p_0^{k\nu}\varepsilon_{\nu}^{\cdot 4},\end{aligned} \tag{6.12}$$

and similarly $\bar{f}^{*k4}$. Therefore, in view of (6.6):

$$\begin{aligned}-[\bar{p}_0^{s4}, \bar{f}^{*k4}] = &-[p_0^{s4}, f^{*k4}] - \varepsilon_{a}^{\cdot s}[p_0^{a4}, f^{*k4}] \\ &- \varepsilon_{a}^{\cdot k}[p_0^{s4}, f^{*a4}] - \varepsilon_{r}^{\cdot 4}\{[p_0^{sr}, f^{*k4}] + [p_0^{s4}, f^{*kr}]\}.\end{aligned} \tag{6.13}$$

To simplify the further calculations we shall consider only one of the equations (6.13), *i.e.*, for

$$s = 1; \quad k = 2.$$

The invariance proof for the rest of the equations (6.13) is quite similar and especially simple if $s = k$.

We shall begin with the calculation of the first three expressions on the right-hand side in (6.13), *i.e.*,

$$-[p_0{}^{14}, f^{*24}] - \varepsilon_{a}^{\cdot 1}[p_0{}^{a4}, f^{*24}] - \varepsilon_{a}^{\cdot 2}[p_0{}^{14}. f^{*a4}], \tag{6.14}$$

or in the space-vector notation:

$$[\mathrm{D}_{01}, \mathrm{B}_2] + \varepsilon_{a}^{\cdot 1}[\mathrm{D}_{0a}, \mathrm{B}_2] + \varepsilon_{a}^{\cdot 2}[\mathrm{D}_{01}, \mathrm{B}_a]. \tag{6.15}$$

The second and third expression in (6.15) vanish if a is either 1 or 2 (because of (6.6) and (3.7)). We have, therefore:

$$[\mathrm{D}_{01}, \mathrm{B}_2] + \varepsilon_{3}^{\cdot 1}[\mathrm{D}_{03}, \mathrm{B}_2] + \varepsilon_{3}^{\cdot 2}[\mathrm{D}_{01}, \mathrm{B}_3]. \tag{6.14A}$$

From (I) and (3.11) we get for (6.14A) :

$$-4\pi\{\delta(x)\,\delta(y)\,\delta'(z) - \varepsilon^{3}_{\cdot 1}\,\delta'(x)\,\delta(y)\,\delta(z) - \varepsilon^{3}_{\cdot 2}\,\delta(x)\,\delta'(y)\,\delta(z)\}. \tag{6.15}$$

It follows from (6.11) and (3.11) that this expression (6.15) is equal to

$$-4\pi\,(\delta(\bar{x})\,\delta(\bar{y})\,\delta(\bar{z})). \tag{6.16}$$

We can write, therefore, our equation (6.13) for $s = 1$, $k = 2$, in the following form:

$$[\bar{\mathrm{D}}_{01}, \bar{\mathrm{B}}_2] = -4\pi\,\delta(\bar{x})\,\delta(\bar{y})\,\delta(\bar{z}) - \varepsilon_{r}^{\cdot 4}\,\{[p_0{}^{1r}, f^{*24}] + [p_0{}^{14}, f^{*2r}]\}. \tag{6.17}$$

We now have to make the *second* step consisting of the changing of the world points. We have on the left-hand side in (6.17) the world points:

$$(\mathrm{P}_0):\ 0, 0, 0, 0;\quad (\mathrm{P}):\ \bar{x}, \bar{y}, \bar{z}, \bar{t}.$$

We have to change these world points into:

$$(\mathrm{P}_0):\ 0, 0, 0, 0;\quad (\mathrm{P}):\ \bar{x}, \bar{y}, \bar{z}, \bar{0}, \tag{6.18}$$

using the relation

$$\begin{aligned} f(t) &= f_{t=0} + \left(\frac{\partial f}{\partial t}\right)_{t=0} \bar{t} \\ &= f_{t=0} + \frac{\partial f}{\partial t}\,\varepsilon_{r}^{\cdot 4} x^{r}. \end{aligned} \tag{6.19}$$

We denote by

$$\frac{1}{i\alpha}\,[\mathrm{D}_{01}, \mathrm{B}_2]_0$$

the value of $D_{01}B_2 - B_2D_{01}$ for the world points (6.18). We have from (6.19) :

$$[\bar{D}_{01}, \bar{B}_2] = [\bar{D}_{01}, \bar{B}_2]_0 + \left[D_{01}, \frac{\partial B_2}{\partial t}\right] \varepsilon_r{}^{;4} x^r. \tag{6.20}$$

From (6.17) and (6.20) we get:

$$\begin{aligned}[\bar{D}_{01}, \bar{B}_2]_0 = &- 4\pi\, \delta(\bar{x})\, \delta(\bar{y})\, \delta'(\bar{z}) \\ &- \left\{x^r \left[D_{01}, \frac{\partial B_2}{\partial t}\right] + [p_0{}^{1r}, f^{*24}] + [p_0{}^{14}, f^{*2r}]\right\} \varepsilon_r{}^{;4}.\end{aligned} \tag{6.21}$$

The invariance of the commutation rules will be proved for $[D_{01}\ B_2]$, if we show that the coefficient of $\varepsilon_r{}^{;4}$ vanishes for $r = 1, 2, 3$. We shall show it only when $r = 3$, because for $r = 1$, or 2, the calculations are quite similar, but more simple. We have, therefore, to calculate the coefficient of $\varepsilon_r{}^{;4}$, namely,

$$[p_0{}^{13}, f^{*24}] + [p_0{}^{14}, f^{*23}] + z\left[D_{01}, \frac{\partial B_2}{\partial t}\right]. \tag{6.22}$$

We begin with the first expression:

$$[p_0{}^{13}, f^{*24}] = -[H_{02}, B_2] = [B_2, H_{02}]. \tag{6.23}$$

With respect to (2.7), (3.1), (3.2) and (3.20) we have:

$$\begin{aligned}[p_0{}^{13}, f^{*24}] = [B_2, H_{02}] = (4\pi)^2 \Big\{&\frac{\partial^2 U}{\partial D_1\, \partial B_2}\, \delta(x)\, \delta(y)\, \delta'(z) \\ &- \frac{\partial^2 U}{\partial D_3\, \partial B_2}\, \delta'(x)\, \delta(y)\, \delta(z)\Big\}.\end{aligned} \tag{6.24}$$

Similarly we have for the second expression in (6.22):

$$\begin{aligned}[p_0{}^{14}, f^{*23}] = -[D_{01}, E_1] = (4\pi)^2 \Big\{&\frac{\partial^2 U}{\partial B_2\, \partial D_1}\, \delta(x)\, \delta(y)\, \delta'(z) \\ &- \frac{\partial^2 U}{\partial B_3\, \partial D_1}\, \delta(x)\, \delta'(y)\, \delta(z)\Big\}.\end{aligned} \tag{6.25}$$

The calculation of the third and last expression in (6.22) is a little more difficult. On account of (4.14), we have :

$$z\left[D_{01}, \frac{\partial B_2}{\partial t}\right] = z\left[D_{01}, \frac{\partial E_3}{\partial x}\right] - z\left[D_{01}, \frac{\partial E_1}{\partial z}\right]. \tag{6.26}$$

We begin with the first expression on the right side in (6.26). We are only interested in the calculation of the limiting case $x, y, z \to 0$, because for $r \neq 0$ all expressions in (6.22) vanish and contribute nothing to (6.21). We have:

$$z\left[D_{01}, \frac{\partial E_3}{\partial x}\right] = z \frac{\partial}{\partial x}[D_{01}, E_3]$$

$$= -(4\pi)^2 z \frac{\partial}{\partial x}\left\{\frac{\partial^2 U}{\partial B_2\, \partial D_3}\, \delta(x)\,\delta(y)\,\delta'(z) - \frac{\partial^2 U}{\partial B_3\, \partial D_3}\, \delta(x)\,\delta'(y)\,\delta(z)\right\}. \tag{6.27}$$

For $x, y, z \to 0$ we have using (3.11):

$$z\left[D_{01}, \frac{\partial E_3}{\partial x}\right] = (4\pi)^2 \left\{\frac{\partial^2 U}{\partial B_2\, \partial D_3}\, \delta'(x)\,\delta(y)\,\delta(z) - z\frac{\partial}{\partial x}\left(\frac{\partial^2 U}{\partial B_2 \partial D_3}\right) \delta(x)\,\delta(y)\,\delta'(z)\right\}. \tag{6.28}$$

We shall now calculate the second expression in (6.26):

$$-z\left[D_{01}, \frac{\partial E_1}{\partial z}\right] = -z\frac{\partial}{\partial z}[D_{01}, E_1]$$

$$= (4\pi)^2 z \frac{\partial}{\partial z}\left\{\frac{\partial^2 U}{\partial B_2\, \partial D_1}\, \delta(x)\,\delta(y)\,\delta'(z) - \frac{\partial^2 U}{\partial B_3\, \partial D_1}\, \delta(x)\,\delta'(y)\,\delta(z)\right\}. \tag{6.29}$$

In the limiting case $x, y, z, \to 0$ we find because of (3.11):

$$-z\left[D_{01}\cdot \frac{\partial E_1}{\partial z}\right] = (4\pi)^2 \left\{\frac{\partial^2 U}{\partial B_3\, \partial D_1}\, \delta(x)\,\delta'(y)\,\delta(z) - 2\frac{\partial^2 U}{\partial B_2\, \partial D_1}\, \delta(x)\,\delta(y)\,\delta'(z) + z\frac{\partial}{\partial z}\left(\frac{\partial^2 U}{\partial B_2\, \partial D_1}\right) \delta(x)\,\delta(y)\,\delta'(z)\right\}. \tag{6.30}$$

Adding (6.28) and (6.30) we get for $x, y, z, \to 0$:

$$z\left[D_{01}, \frac{\partial B_2}{\partial t}\right] = (4\pi)^2 \left\{\frac{\partial^2 U}{\partial B_2\, \partial D_3}\, \delta'(x)\,\delta(y)\,\delta(z) - 2\frac{\partial^2 U}{\partial B_2\, \partial D_1}\, \partial(x)\,\delta(y)\,\delta'(z) + \frac{\partial^2 U}{\partial B_3\, \partial D_1}\, \delta(x)\,\delta'(y)\,\delta(z)\right\}. \tag{6.31}$$

In (6.31) we have omitted the expression

$$(4\pi)^2 \left\{ z \frac{\partial}{\partial z} \left(\frac{\partial^2 U}{\partial B_2 \, \partial D_1} \right) - z \frac{\partial}{\partial x} \left(\frac{\partial^2 U}{\partial B_2 \, \partial D_4} \right) \right\} \delta(x) \, \delta(y) \, \delta'(z), \quad (6.32)$$

because it gives no contribution to (6.31). Indeed we see that the coefficient of $\delta(x) \, \delta(y) \, \delta'(z)$ vanishes for $x, y, z \to 0$, provided that $\frac{\partial^2 U}{\partial B_k \, \partial D_l}$ is continuous in the zero point.

In (6.24), (6.25) and (6.31) we have written all of the three expressions which appear in (6.22). We see immediately that the sum of these three expressions gives zero. The coefficient in (6.21) therefore vanishes for $r = 3$ and so the same holds for $r = 1$ and $r = 2$. We have in (6.21) :

$$[\bar{D}_1 (0, 0, 0, 0), \bar{B}_2 (\bar{x}, \bar{y}, \bar{z}, 0)] = - 4\pi \, \delta(\bar{x}) \, \delta(\bar{y}) \, \delta'(\bar{z}),$$

and this is exactly one of our commutation rules in the co-ordinate system $\bar{\Sigma}$. We have therefore proved that our scheme of equations is Lorentz invariant.

APPENDIX[†]

Starting from the Lagrangian

$$L = \sqrt{1 + \mathbf{B}^2 - \mathbf{E}^2 - G^2} - 1, \qquad (a)$$

where

$$G = (\mathbf{E} \, . \, \mathbf{B}), \qquad (b)$$

we want to express the energy-density

$$4\pi U = L + (\mathbf{D} \, . \, \mathbf{E}) \qquad (c)$$

as function of **D** and **B**.

We get from (2.3):

$$\mathbf{D} = - \frac{\partial L}{\partial \mathbf{E}} = \frac{\mathbf{E} + \mathbf{B} G}{\sqrt{1 + \mathbf{B}^2 - \mathbf{E}^2 - G^2}}, \text{‡} \qquad (d)$$

therefore

$$(\mathbf{D} \, . \, \mathbf{E}) = \frac{\mathbf{E}^2 + G^2}{\sqrt{1 + \mathbf{B}^2 - \mathbf{E}^2 - G^2}},$$

[†] This Appendix is chiefly due to Mr. P. Weiss who has also kindly helped us in our whole work.

[‡] There is a misprint in II, p. 437, (3.3A) II should read

$$D = - b^2 \frac{\partial L}{\partial \mathbf{E}} = \frac{\mathbf{E} + G\mathbf{B}}{\sqrt{1 + F - G^2}}$$

instead of

$$D = b^2 \frac{\partial L}{\partial \mathbf{E}} = \frac{\mathbf{E} - G\mathbf{B}}{\sqrt{1 + F - G^2}}.$$

and from (*c*) using (*a*):

$$4\pi U = \sqrt{1 + \mathbf{B}^2 - \mathbf{E}^2 - G^2} + \frac{\mathbf{E}^2 + G^2}{\sqrt{1 + \mathbf{B}^2 - \mathbf{E}^2 - G^2}} - 1$$

$$4\pi U = \frac{1 + \mathbf{B}^2}{\sqrt{1 + \mathbf{B}^2 - \mathbf{E}^2 - G^2}} - 1. \tag{e}$$

We now denote

$$R = (\mathbf{D} \, . \, \mathbf{B}) \tag{f}$$

and obtain for R from (*d*):

$$R = \frac{G\,(1 + \mathbf{B}^2)}{\sqrt{1 + \mathbf{B}^2 - \mathbf{E}^2 - G^2}}. \tag{g}$$

From (*g*) and (*e*) it follows:

$$4\pi U = \frac{R}{G} - 1. \tag{h}$$

Now we have only to express G in terms of **D** and **B**. For this purpose we write first (*d*) in the following form :

$$\mathbf{D} = \frac{\mathbf{E} + \mathbf{B}G}{1 + \mathbf{B}^2} \cdot \frac{1 + \mathbf{B}^2}{\sqrt{1 + \mathbf{B}^2 - \mathbf{E}^2 - G^2}},$$

and because of (*g*):

$$\mathbf{D} = \frac{\mathbf{E} + \mathbf{B}G}{1 + \mathbf{B}^2} \cdot \frac{R}{G}. \tag{i}$$

Now we solve (*g*) and (*i*) with respect to G by eliminating **E**.

Squaring (*g*) gives:

$$R^2\mathbf{E}^2 + \{R^2 + (1 + \mathbf{B}^2)^2\}\,G^2 = R^2\,(1 + \mathbf{B}^2) \tag{j}$$

Squaring (*i*) gives:

$$R^2\mathbf{E}^2 = \{\mathbf{D}^2\,(1 + \mathbf{B}^2)^2 - R^2\,(2 + \mathbf{B}^2)\}\,G^2 \tag{k}$$

From (*j*) and (*k*) follows:

$$\{(1 + \mathbf{D}^2)\,(1 + \mathbf{B}^2)^2 - R^2\,(1 + \mathbf{B}^2)\}\,G^2 = R^2\,(1 + \mathbf{B}^2)$$

or

$$G = \frac{R}{\sqrt{(1 + \mathbf{D}^2)\,(1 + \mathbf{B}^2) - R^2}}. \tag{l}$$

Introduction of (*l*) into (*h*) gives:

$$4\pi U = \sqrt{(1 + \mathbf{D}^2)\,(1 + \mathbf{B}^2) - R^2} - 1. \tag{m}$$

SUMMARY

The new field theory uses the primary field vectors **E**, **B** and derives secondary field vectors **D**, **H** by differentiating the Lagrangian L (**E**, **B**), with respect to **E**, **B**. If one gives up the invariant form (*i.e.*, the four-dimensional tensor notation) one can introduce other pairs of primary variables, altogether in four ways : **E**, **B**—**D**, **H**—**E**, **H**—**D**, **B** ; and in each case there exists an action function, from which the complementary pair can be derived by differentiation. The most important case is the last one; for the action function U (**D**, **B**) is just the energy-density. Using this representation it is possible to formulate the quantum laws of the field. The components of **D**, **B** have to be considered as q-numbers, being functions of x, y, z, t and satisfying the same commutation laws as have been used by Heisenberg and Pauli.

The field equations can be written without any space or time derivatives, only by means of commutators connecting the field vectors with the total energy and the total momentum. The relativistic invariance of the commutation laws which is not immediately evident can be proved by a direct application of the method of infinitesimal transformation.

These results show that the new field equations allow a coherent unitarian quantum theory of matter and field to be formulated.

The Mean Lives of Excited Hydrogen Atoms

By J. H. E. Griffiths

(*Communicated by F. A. Lindemann, F.R.S.—Received July* 27, 1934)

A method of determining directly the mean lives of excited atoms was described in detail in a previous paper.* This method employs a Kerr cell operated by a high frequency oscillator which is also used to run a Geissler tube. With the electrical arrangement used, a minimum of light should pass through the Kerr cell system if light were emitted instantaneously. Owing to the finite time that the atoms remain in the excited state, there is a lag between the current in the discharge tube and the emission of light. By increasing the distance that the light travels before reaching the cell a point may be found where a maximum of light passes the cell, from which the lag may be determined. This is directly connected with the mean life of the state. In the previous paper results for neon were given and the present paper deals with the application of this method to hydrogen.

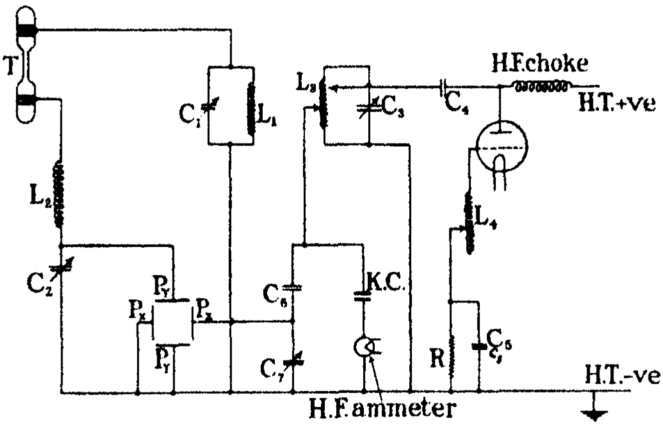

FIG. 1.

Fig. 1 shows the electrical arrangement used. This is essentially the same as that used for neon, except that a cathode ray oscillograph is used to determine the phase difference between the potential on the Kerr cell and the current in the discharge tube. Thus the deflector plates P_x give deflections proportional to the voltage on the Kerr cell K.C. while the plates Py give deflections proportional to the voltage on C_2 and therefore in phase quadrature with the current through the discharge tube. L_1C_1 is a tuned circuit which picks up energy from the oscillator and by tuning this, the oscillograph figure may be made a straight line. When this is so the current through the discharge tube is 90° out of phase with the voltage on the Kerr cell. L_2C_2 forms a series tuned circuit of low impedance, and the variable condenser C_7 gives a means of making the two deflections equal. The oscillograph can be set for linearity within an accuracy of $\frac{1}{2}°$ which is of the same order as the accuracy of the experiment. A correction has to be applied for the time that the electrons take to travel between the plates of the oscillograph. Thus when the same oscillating voltage is applied to the two pairs of plates, the oscillograph figure is not a straight line, but shows an apparent phase difference, owing to the fact that one pair of plates acts on the electron beam sooner than the other pair. With the oscillograph used, this time was $1 \cdot 5 \,.\, 10^{-9}$ secs, or at a wave-length of 60 metres a phase angle of 2·7°. This must be added to the observed lag.

---

* 'Proc. Roy. Soc.,' A, vol. 143, p. 588 (1934).

The optical system was the same as before. Several photographs of the spectrum were made on the same plate with the second nicol prism rotated through different angles from its crossed position. Hence the angle δ at which the two images are of equal intensity was determined. A curve was then constructed of the value of the angle δ for different lengths of the light path from the tube to the Kerr cell. The position of the maximum of this curve gives the lag between the emission of the light and the current in the tube. It was shown in the previous paper that this lag α is connected with the average life of the atom by the relation

$$\tan 2\alpha = 2\omega\tau, \qquad (1)$$

where α is the lag expressed as a phase angle, τ is the average life of the state and $\omega/2\pi$ is the frequency of the oscillations employed.

For hydrogen the discharge tube was filled with water vapour. This was in equilibrium with a sulphuric acid solution of known strength maintained at a constant temperature. This gives a means of keeping the pressure constant at a known value.

THE THEORETICAL VALUES FOR HYDROGEN

The theoretical values for hydrogen have been evaluated by Sugiura* by means of Schrödinger's wave mechanics. These are given in Table I.

---

* 'Sci. Pap. Inst. phys. chem. Res., Tokyo,' No. 193 (1929).

$A_{j,k}$ is the transition probability for the transition for the state j to k, the sum $\sum_k A_{j,k}$ is taken over all states k to which transitions are possible and the average life τ is then given by

$$\tau = \frac{1}{\sum_k A_{j,k}}. \tag{2}$$

Saha and Banerji* give a formula for the transition probabilities, derived by means of Dirac's mechanics, which takes into account the spin of the electron. However, for states with the same value of n and l, the sum of the transition probabilities given by this formula is the same as the value given by Sugiura and hence the lives are the same. This is a theoretical expression of the Dorgelo sum rule for the intensities of a normal multiplet. The fifth column gives values of $A_{j,k}g_j$ for transitions giving rise to components of H_α and H_β, g_j being the statistical weight of the state j. These are required later and are proportional to the intensity of the component. In the present case the components are unresolved and an average value must be found.

TABLE I

n, l	n, l—n', l'	$A_{j,k} \times 10^{-8}$ secs^{-1}	$\sum_k A_{j,k} \times 10^{-8}$	$A_{j,k}g_j \times 10^{-8}$	τ_j secs.
2, 1	2, 1—1, 0	6·10	6·10	—	1·64 . 10^{-9}
3, 0	3, 0—2, 1	0·0615	0·0615	0·0615	1·625 . 10^{-7}
3, 1	3, 1—1, 0 3, 1—2, 0	1·629 0·219	1·848	0·657	5·41 . 10^{-9}
3, 2	3, 2—2, 1	0·629	0·629	3·145	1·59 . 10^{-8}
4, 0	4, 0—2, 1 4, 0—3, 1	0·0251 0·0178	0·0429	0·0251	2·33 . 10^{-7}
4, 1	4, 1—1, 0 4, 1—2, 0 4, 1—3, 0 4, 1—3, 2	0·664 0·0941 0·0298 0·0034	0·791	0·2823	1·264 . 10^{-8}
4, 2	4, 2—2, 1 4, 2—3, 1	0·2008 0·0685	0·269	1·004	3·71 . 10^{-8}
4, 3	4, 3—3, 2	0·134	0·134	—	7·46 . 10^{-8}

---

* 'Z. Physik,' vol. 68, p. 704 (1931).

The relation between the observed lag and the life of the state may be found in a similar manner to that used in the previous paper. It was shown there that the rate of excitation could be taken proportional to

$$(a_0 + a_1 \cos 2\theta), \tag{3}$$

where $\theta = \omega t$.

Assuming that atoms are excited to the different states at a rate proportional to the statistical weight of the state, we have for any one state j

$$\frac{dn}{d\theta} + k_j n = g_j (a_0 + a_1 \cos 2\theta), \tag{4}$$

where $k_j = 1/\omega\tau_j$.

The number of atoms in the state j at any moment is given by the solution of equation (4). Since we are dealing with a steady state the complementary function vanishes and the solution becomes :—

$$n = g_j \left\{\frac{a_0}{k_j} + a_1 \frac{2 \sin 2\theta + k_j \cos 2\theta}{(4 + k_j^2)}\right\} = g_j \,\mathrm{F}(\theta, k_j). \tag{5}$$

The intensity of light emitted by transitions from the state j is proportional to

$$g_j \sum_k \mathrm{A}_{j,k} \,.\, \mathrm{F}(\theta, k_j), \tag{6}$$

where the sum is taken over all states k to which transitions occur giving rise to the line being investigated.

The total light being emitted is proportional to

$$\sum_j g_j \,.\, \mathrm{F}(\theta, k_j) \,.\, \mathrm{A}_j, \tag{7}$$

where A_j is written for $\sum\limits_k \mathrm{A}_{j,k}$.

If we then carry through the analysis for the Kerr cell in a similar manner to that used for a single state, we obtain an equation connecting the k's with the value of α at the maximum or minimum of the experimental curve :—

$$\sum_j g_j \,.\, \mathrm{A}_j \,.\, \frac{2 \cos 2\alpha - k_j \sin 2\alpha}{(4 + k_j^2)} = 0 \tag{8}$$

or

$$\tan 2\alpha = \frac{2 \sum\limits_j \dfrac{\mathrm{A}_j \cdot g_j}{(4 + k_j^2)}}{\sum\limits_j \dfrac{\mathrm{A}_j \cdot g_j k_j}{(4 + k_j^2)}} = 2\omega\tau. \tag{9}$$

This relation gives a means of comparing the theoretically determined values of k_j and A_j with the experimentally determined value of τ, which can be considered as a mean or effective value of the life. For a single state this reduces to equation (1) τ being then equal to $1/\omega k$.

RESULTS

Measurements were made on H_α and H_β at a wave-length of 60 metres and over a range of water vapour pressures up to 2·5 mm of Hg. Fig. 2 shows the values of $1/\tau$ for H_β at different pressures, the experimental errors being indicated by vertical lines. Extrapolation of this to zero pressure gives a value of τ of $3{\cdot}1 \pm 0{\cdot}5 \,.\, 10^{-8}$ secs and from a similar curve for H_α a value of $1{\cdot}75 \pm 0{\cdot}3 \,.\, 10^{-8}$ secs. These compare with the theoretical values $3{\cdot}13 \,.\, 10^{-8}$ secs and $1{\cdot}52 \,.\, 10^{-8}$ secs respectively calculated by means of (9).

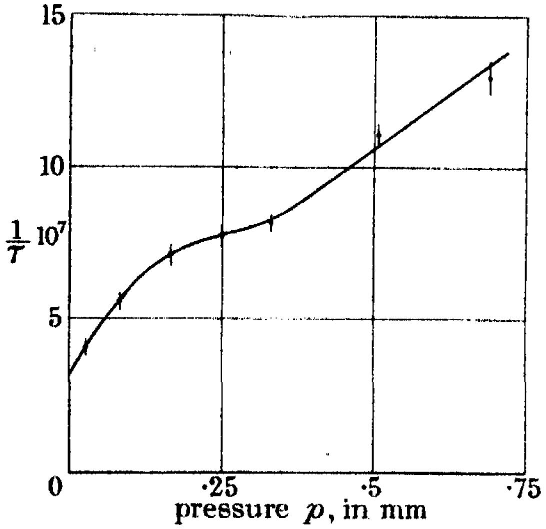

FIG. 2

That the experimental value for H_α is slightly high may be due to a certain amount of repopulation from higher levels, but the difference is not greater than the experimental error.

This agreement seems to confirm the assumption that all states with the same main quantum number have the same probability of excitation. For if this were not so one would expect the states 3, 1 and 4, 1 from which transitions to the ground state are possible to have a higher probability of excitation than the others. The measured lives would then be considerably shorter.

DETERMINATION OF COLLISION RADII

Fig. 2 shows that with increasing pressure the life of the state decreases. From this may be found the probability that a collision will result in the atom leaving the state. This may be expressed as a collision radius σ which is defined as the average distance between the centres of the colliding molecules for collisions effecting transitions from that state. For a single state this may be found as follows :—

If τ is the natural life of the state and P*dt* is the probability that an atom will leave the state as a result of a collision during an interval *dt*, the total probability that an atom will leave the state in unit time is

$$\frac{1}{\tau} + \mathrm{P},$$

and the life of the state will then be given by τ_p, where

$$\frac{1}{\tau_p} = \frac{1}{\tau} + \mathrm{P}. \tag{10}$$

The probability P is inversely proportional to the time between collisions of the excited atom with quenching atoms and should therefore be proportional to the pressure. A graph of $1/\tau_p$ against P should therefore be a straight line. The point where this cuts the axis of $p = 0$ gives the natural life and the slope gives the quenching efficiency.

If we put $\mathrm{P} = \mathrm{K}p$ we find from kinetic theory considerations that

$$\mathrm{K} = \frac{2\mathrm{N}\sigma^2}{\rho} \sqrt{2\pi \mathrm{RT}\left(\frac{1}{\mathrm{M}_1} + \frac{1}{\mathrm{M}_2}\right)}, \tag{11}$$

where R is the gas constant, N the number of colliding molecules per cc and M_1 and M_2 the masses of the colliding molecules. If p is the vapour pressure of the water in mm of Hg in equilibrium with the sulphuric acid and T is the absolute temperature of the gas in the discharge tube

$$\mathrm{N} = 9{\cdot}74 \,.\, 10^{18} \,.\, \rho/\mathrm{T},$$

whence

$$\sigma^2 = 6{\cdot}17 \,.\, 10^{23} \,.\, \mathrm{K}. \tag{12}$$

T was estimated as 800° A since the tube was of Pyrex glass and the sodium lines occasionally appeared in the discharge. However, an error of 100° in this will only produce an error of 3½% in the value of σ. For hydrogen a straight line is not obtained, this being due to the fact that we have here a set of states very close together producing a number of unresolved lines. Collisions may occur effecting transitions out of this set, or transitions between members of the set.

At zero pressure the life should be given by (9), but since the energy differences between members of the same set of states is extremely small for hydrogen, it seems at first sight possible that, even at low pressures, the probability of transitions between members of the same set of states might be very large.

Let us consider the limiting case where this probability is infinitely large compared with the probability of transitions out of this set of states whether due to emission of light or to collisions. Under these conditions the set of states will behave like a single state. A graph of $1/\tau_p$ against p should again give a straight line, but the intercept with the axis of $p = 0$ will not necessarily be given by (9). We can find the value of τ under these conditions by considering an assembly of N atoms, the number in a state s being $n \,.\, g_s$ such that

$$\mathrm{N} = \sum_s n \,.\, g_s, \tag{13}$$

since the number of atoms in a state at any moment will be proportional to the statistical weight g_s of that state.

The total number of atoms making the transitions from the set of states in unit time is

$$\sum_s ng_s \,.\, \mathrm{Q}_s, \tag{14}$$

where Q_s is the total probability of an atom leaving the state s.

The probability of an atom leaving the set of states in unit time is then

$$\frac{\sum_s ng_s \,.\, \mathrm{Q}_s}{\mathrm{N}} = \frac{\sum_s g_s\mathrm{Q}_s}{\sum_s g_s} = \frac{1}{\tau}, \tag{15}$$

Q_s includes collision transitions and emission transitions, *i.e.*,

$$\mathrm{Q}_s = \mathrm{P}_s + \mathrm{A}_s,$$

where A_s is the sum of the Einstein transition probabilities. At low pressures where P_s may be negligible and yet the condition still hold we find for the theoretical value of $1/\tau$ for H_α and H_β the values $9 \cdot 72 \,.\, 10^7$ and $2 \cdot 94 \,.\, 10^7$ respectively.

That the experimental values agree with equation (9) rather than (15) seems to show that the probability of collisions effecting transitions between members of the same set of states is not very much greater than that of collisions effecting transitions out of the set of states. The difference in values is most marked in the case of H_α. On the other hand, the fact that the graph of $1/\tau_p$ against p is not a straight line shows that these transitions do take place.

At higher pressures the graph for H_β has been drawn as a straight line, but owing to the small values of τ the experimental error becomes rather large and it is not possible to say whether this is so.

Taking the slope of this line we obtain a value for σ of $9{\cdot}5 \,.\, 10^{-8}$ cm for H_β and similarly for H_α we obtain $\sigma = 6{\cdot}57 \,.\, 10^{-8}$ cm.

The radius of a water molecule can be taken as approximately $2{\cdot}0 \,.\, 10^{-8}$ cm and if we add to this the radii of the 3rd and 4th Bohr orbits we obtain values for σ of $6{\cdot}77$ and $10{\cdot}5 \,.\, 10^{-8}$ cm for H_α and H_β respectively in agreement with the experimental values given above. This assumes that the charge distribution in the excited states is spherically symmetrical, whereas this is only so for one state. An average value might be found, but the added complication is too great and the accuracy of the results does not warrant it. The most interesting point is the difference between the values for H_α and H_β, showing the effectively larger radius of the 4 quantum state. The figures also show that water vapour is a very effective quenching agent.

It was found that the discharge did not run well below a pressure of about 0·08 mm and therefore helium at a pressure of 1·3 mm was admitted and the water vapour pressure kept at 0·025 mm. That this gave a point which, as can be seen from fig. 2 agrees with the other points, shows that helium has no quenching effect.

It is hoped to continue the work on other radiating atoms and other collision processes.

The wave-length measurements were made by a wave meter accurate to 0·1% for which I am indebted to the Government Grant Committee of the Royal Society.

In conclusion, I would like to thank Professor Lindemann for his constant help and advice throughout the research.

SUMMARY

The average lives of the excited states of hydrogen have been measured using a method described in a previous paper. The values found were $1{\cdot}75 \pm 0{\cdot}3 \,.\, 10^{-8}$ secs for H_α and $3{\cdot}1 \pm 0{\cdot}5 \,.\, 10^{-8}$ secs for H_β as compared with the theoretical values of $1{\cdot}52 \,.\, 10^{-8}$ secs and $3{\cdot}13 \,.\, 10^{-8}$ secs for H_α and H_β respectively.

The decrease of life with increasing water vapour pressure was used to find the effective collision radius for quenching collisions between excited hydrogen atoms and water molecules. This was found to be $6 \cdot 57 . 10^{-8}$ cm and $9 \cdot 5 . 10^{-8}$ cm for H_α and H_β respectively. This is almost exactly the same as the kinetic theory collision distance, taking the Bohr theory radius as the size of the hydrogen atom. It was shown that helium has no quenching effect.

Slow Oxidations at High Pressures

I—Methane and Ethane, II—Methyl Alcohol, Ethyl Alcohol, Acetaldehyde, and Acetic Acid

By D. M. Newitt and P. Szego, High Pressure Gas Research Laboratories of the Imperial College of Science and Technology, London

(*Communicated by W. A. Bone, F.R.S., Received August* 1, 1934)

1—Introduction

In two recent papers* from these laboratories it was shown that when methane- and ethane-oxygen mixtures containing excess of the hydrocarbon react at high pressure various liquid products can be isolated. For methane-oxygen mixtures methyl alcohol and water are found, and for ethane-oxygen mixtures ethyl alcohol, acetaldehyde, methyl alcohol, acetic acid, formic acid, and water. These products being important for the light they throw on the mechanism of hydrocarbon combustion and because they suggest means for using waste hydrocarbon gases, further experiments have now been made with the object of finding the order of their formation and the optimum condition for their survival.

The method employed in the work referred to consisted in introducing the previously mixed and compressed hydrocarbon-oxygen (10 : 1) mixture into a reaction chamber maintained at a suitable temperature and removing and cooling the products as soon as the greater part of the free oxygen had been consumed. In such circumstances there ensues a competition for oxygen between the unburnt hydrocarbon and all the intermediate products present in the system and the proportions in which they survive will depend *inter alia* upon their relative rates of oxidation and/or thermal decomposition. It was found, for example, that in the oxidation of an 8 : 1 methane-oxygen mixture at 100 atmospheres pressure and 341° C 22·3% of the methane burnt was recoverable in the products as methyl alcohol, and a further 0·75% as formaldehyde, whilst with a 9 : 1 ethane-oxygen mixture at 100 atmospheres and 272° C the corresponding figures were 36·5% of ethyl alcohol and 8·0% of acetaldehyde.

---

* 'Proc. Roy. Soc.,' A, vol. 134, p. 59, and vol. 140, p. 426.

In the further experiments, now recorded, it has been found possible, by employing hydrocarbon-oxygen mixtures containing not more than 5% of oxygen and a flow method in which the gaseous medium was made to pass rapidly at 50 atmospheres pressure through a reaction zone maintained at some suitable temperature between 340° and 430°, so to adjust the rate of flow as to increase largely the proportion of the primary product (alcohol) surviving, until with methane it corresponded to just over 50% and with ethane to 62·6% of the hydrocarbon burnt.

Additional evidence supporting the hydroxylation theory of hydrocarbon combustion has also been obtained by studying the slow oxidation and thermal decompositions of each of the principal intermediate oxidation products of ethane at appropriate temperatures and pressures.

2—The Slow Oxidation of Methane and Ethane in a Flow System at High Pressures

Experimental

Method—The apparatus, shown diagrammatically in fig. 1, consisted of two storage cylinders A and B containing the hydrocarbon-oxygen mixture previously compressed to a pressure considerably higher than the proposed reaction pressure. These were connected by a capillary steel pipe line with a pre-heating coil P and an electrically heated steel reaction tube T. The reaction tube had a free cross sectional area of ·7 sq mm and was heated over a length of 20 cm. The gases and vapours leaving the tube were passed through a steel coil S, cooled in an ice-salt freezing mixture, a water scrubber R_1 surrounded by ice cold water and through the reducing valve V to a second scrubber R_2. The residual gas after passing through a gas meter M was collected in a calibrated gas holder of 10 cub. ft. capacity.

The rate of flow was maintained constant during an experiment by setting the valve V and periodically adjusting the valves on the storage cylinders so that the pressure in the system as indicated by the gauge G remained substantially constant. In all experiments using ethane-oxygen mixtures it was found necessary to heat externally all valves and constrictions in the system to prevent condensation of the hydrocarbon.

During a run in which the reaction temperature and the rate of flow had remained constant, the composition of gas samples taken at V_1 showed satisfactory agreement. Samples from beyond the gas meter varied slightly in carbon dioxide content owing to partial removal of this gas by the scrubber.

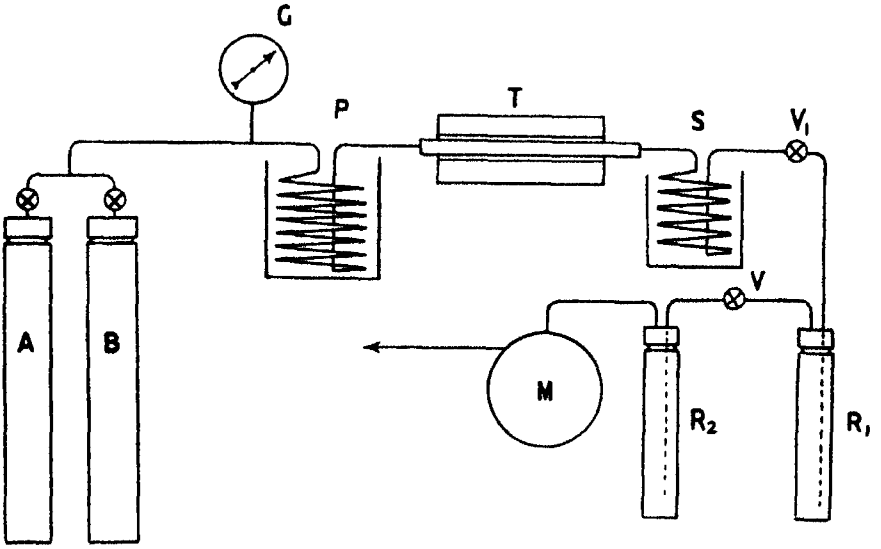

FIG. 1

The principal difficulty in such small scale flow experiments is to maintain constant temperature conditions ; for unless the pre-heater is kept at a suitable temperature, varying with the rate of flow, the reaction tube may be cooled or heated by the gas stream; and since the reaction is strongly exothermic, ignition may occur in the latter event. Indeed it was only by employing low concentrations of oxygen that satisfactorily constant temperature conditions could be maintained throughout a long run.

Results

(A) *Methane*—In two series of experiments at 50 atmospheres pressure with methane-oxygen-nitrogen mixtures of composition $CH_4 = 90$, $O_2 = 3$, $N_2 = 7\%$ and $CH_4 = 90$, $O_2 = 5$, and $N_2 = 5\%$, respectively, the rates of flow were so adjusted that the reaction time varied between 5 seconds and 30 seconds each experiment being continued until approximately 75 litres of gas had passed through the system. The alcohol and aldehyde contents of the products are given in Table I.

TABLE I

Initial mixture	Initial temp. of reaction tube °C	Rise of temp. °C	Duration of heating secs.	Percentage of methane burnt surviving as	
				CH_3OH	H . CHO
(1) $CH_4 = 90$	430	5	5	51	4·1
$O_2 = 3$	430	5	7	49	3·2
$N_2 = 7$	410	15	10	43	3·2
100·0	400	28	20	12	2·16
(2) $CH_4 = 90$	410	35	5	29·0	1·4
$O_2 = 5$	410	46	7	18·0	0·9
$N_2 = 5$	400	75	30	3·0	1·0
100·0					

No formic acid survived and the gaseous products consisted of the two oxides of carbon, in the approximate ratio $CO/CO_2 = 1 : 1$, hydrogen being absent.

It will be seen that in the first series very rapid rates of flow accompanied by correspondingly rapid cooling of the products resulted in as much as 51% of the methane burnt appearing as methyl alcohol, and 4·1% only as formaldehyde, in the surviving products. As the rate of flow was reduced the oxidation proceeded further with the formation of increasing amounts of oxides of carbon and steam.

When the oxygen content of the reacting gases was raised from 3 to 5% (Series 2) the amount of alcohol surviving in the products even under the most favourable conditions was only 29%.

On comparing the alcohol and aldehyde figures in the two series it will be seen that the former increased rapidly with increase in the rate of flow, a result that accords with the view that methyl alcohol is the initial product of the combustion.

(B) *Ethane*—In Table II are summarized the results of a similar series of oxidation experiments with ethane at 340°–360° and 50 atmospheres pressure, the composition of the mixture employed being $C_2H_6 = 90$, $O_2 = 3$, and $N_2 = 7\%$. Here again rapid rates of flow favoured the survival of ethyl alcohol; thus, for example, with the most rapid flow

TABLE II—THE SLOW OXIDATION OF ETHANE AT 50 ATMOSPHERES PRESSURE. REACTING MEDIUM : $C_2H_6 = 90, O_2 = 3, N_2 = 7\%$

Initial temp. of reaction tube, ° C	Temp. rise ° C	Duration of heating, secs	Products as percentages of the carbon of the ethane burnt							Total carbon accounted for, %
			$C_2H_5 . OH$	$CH_3 . CHO$	$CH_3 . OH$	$CH_3 . COOH$	CH_4	CO	CO_2	
360	11	4	62·6	4·8	Trace	1·1	9·3	9·2	4·7	91·7
360	22	7	47·4	6·2	2·5	2·9	10·1	11·5	15·8	96·4
340	54	20	14·5	4·9	7·8	2·1	13·6	20·2	26·8	89·9

no less than 62·6% of the carbon of the ethane burnt survived as alcohol, and only 4·8% as acetaldehyde. It is also noteworthy that four-fifths of the remaining gaseous products in this experiment consisted of methane and carbon monoxide, which are products of the thermal decomposition of acetaldehyde. It would therefore appear that about 90% of the carbon of the ethane burnt was accounted for as ethyl alcohol, acetaldehyde, and the thermal decomposition products of the latter.

For the purpose of comparison the percentage distribution of carbon burnt in the products from the reaction of a $C_2H_6 = 72 \cdot 0$, $O_2 = 9 \cdot 9$, $N_2 = 18 \cdot 1\%$ medium at 50 atmospheres pressure in a static system maintained at 290° C is given below :—

Ethyl alcohol ..	23·9	Formaldehyde ..	0·3	Carbon monoxide	23·8
Acetaldehyde ..	4·9	Acetic acid ..	2·9		
Methyl alcohol..	16·1	Formic acid ..	0·2	Carbon dioxide	25·0
		Ethyl acetate ..	3·7		

It was shown in the previous paper (*loc. cit.*) that the formation of these compounds could be represented, according to the hydroxylation theory, by the following scheme :

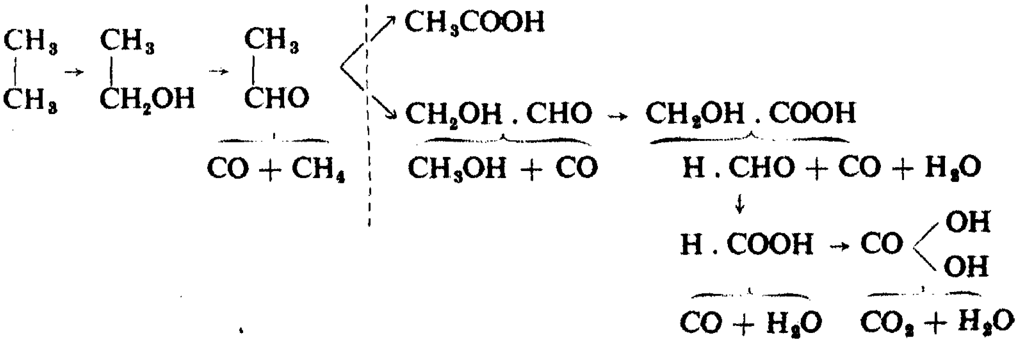

$$\begin{array}{l} \begin{array}{c} CH_3 \\ | \\ CH_3 \end{array} \rightarrow \begin{array}{c} CH_3 \\ | \\ CH_2OH \end{array} \rightarrow \underbrace{\begin{array}{c} CH_3 \\ | \\ CHO \end{array}}_{CO + CH_4} \left< \begin{array}{l} \nearrow CH_3COOH \\ \searrow \underbrace{CH_2OH . CHO}_{CH_3OH + CO} \rightarrow \underbrace{CH_2OH . COOH}_{H . CHO + CO + H_2O} \end{array} \right. \\ \qquad\qquad\qquad\qquad\qquad\qquad\qquad\qquad\qquad H . CHO \downarrow \\ \qquad\qquad\qquad\qquad\qquad\qquad\qquad\qquad\qquad \underbrace{H . COOH}_{CO + H_2O} \rightarrow \underbrace{CO \left< \begin{array}{l} OH \\ OH \end{array} \right.}_{CO_2 + H_2O} \end{array}$$

It can now be seen that by rapid cooling in the present flow experiments the oxidation of ethane has been substantially arrested at the second stage, all the products to the right of the dotted line being either absent or present in very small quantities.

3—The Slow Oxidation of Ethyl Alcohol, Methyl Alcohol, Acetaldehyde, and Acetic Acid at High Pressures

The principal intermediate products of the slow oxidation of ethane have been oxidized separately in a static system at temperatures and pressures corresponding to those employed in the original hydrocarbon experiments. The apparatus employed and the procedure have been described in previous papers (*loc. cit.*); briefly the method consisted in forcing measured quantities of the reactants under pressure into a closed steel vessel maintained at the desired temperature and removing and cooling the products as soon as nearly all the free oxygen had been consumed. As some simultaneous thermal decomposition might take place blank experiments were also carried out with the combustible alone.

(A) *Ethyl Alcohol*

(i) *Thermal Decomposition*—The products from experiments in which the alcohol at 25 atmospheres was maintained for 2 hours at 250° and 350° C respectively, showed that it underwent simultaneous decomposition to acetaldehyde and hydrogen and to ethylene and steam, thus:

$$CH_3CH_2OH = CH_3 . CHO + H_2$$

and

$$CH_3CH_2OH = CH_2 : CH_2 + H_2O$$

and subsequently that secondary reactions occurred resulting in the production of ethane by the hydrogenation of ethylene, ethyl acetate by condensation of acetaldehyde, and methane and carbon monoxide by decomposition of acetaldehyde.

Of the alcohol decomposed at 250°, 39·2% was accounted for as acetaldehyde and a further 21·7 as ethyl acetate; at 350° the corresponding figures were 14·4% of acetaldehyde and 3·3% of ethyl acetate. The gaseous products had the following composition:—

	At 250°	At 350°
Carbon dioxide	25·0	21·1
Ethylene	5·4	23·0
Carbon monoxide	5·4	10·1
Hydrogen	60·4	29·8
Methane	3·0	8·8
Ethane	0·8	7·2
	100·0	100·0

At both temperatures the decomposition also resulted in the formation of small quantities of a brown oil which appeared to be a polymerization product of ethylene.

(ii) *Oxidation*—Two series of experiments were carried out at pressures of 50 and 100 atmospheres, respectively, with mixtures containing usually less oxygen than that required for complete combustion of the alcohol. Using nitrogen as a diluent the relative partial pressure of the two reactants were varied in each series, the total pressure being maintained constant. In general, oxidation proceeded slowly without any well-defined induction period or appreciable temperature rise. The products consisted of acetaldehyde and formaldehyde, methyl alcohol, ethyl acetate, acetic and formic acids, water and the two oxides of carbon. In a few experiments in which the reaction proceeded rapidly with a considerable temperature rise methane, hydrogen, and ethylene were also found in the gaseous products.

The results of the two series are summarized in Table III. Attention may be directed to the following features:—

(1) As the alcohol-oxygen ratio was progressively diminished from 5 : 1 to 1 : 5, the total pressure and reaction temperature being maintained substantially constant, the proportion of the carbon of the alcohol burnt appearing in the liquid products decreased from 83% to 13·7%. The principal product from the 5 : 1 alcohol-oxygen mixture was acetaldehyde; ethyl acetate and acetic acid were present to the extent of 17·1 and 1·4% respectively whilst methyl alcohol was absent. On increasing the partial pressure of oxygen, there was a sharp fall in the amount of acetaldehyde surviving and methyl alcohol appeared in the products in considerable quantities.

(2) The quantity of ethyl acetate surviving remained fairly constant over a wide range of mixture composition, and only when a large excess of oxygen was present did it undergo further oxidation.

(3) The complete absence of hydrogen and ethylene in the products from seven out of ten of the experiments suggests that except in special circumstances the alcohol was not undergoing rapid thermal decomposition and it therefore seems probable that the acetaldehyde was formed almost entirely as the result of oxidation.

The experiments at 100 atmospheres showed similar variations of the products with mixture composition. The formation of ethyl acetate, however, appeared to be favourably influenced by pressure, and even when the ratio of alcohol to oxygen was 1 : 2, upwards of 19% of it survived.

(B) *Methyl Alcohol*

(i) *Thermal Decomposition*—More than 20 years ago Bone and Davies* found that when methyl alcohol at ordinary pressures was heated in

---

* 'Trans. Chem. Soc.,' vol. 105, p. 1691 (1914).

TABLE III—THE SLOW OXIDATION OF ETHYL ALCOHOL

Products as percentages of the carbon or hydrogen of the alcohol burnt or decomposed

Partial pressures of reactants		Initial temp. °C	Duration of expt. mins.	$CH_3.CHO$	$CH_3.COOH$	$CH_3.COOC_2H_5$	$CH_3.OH$	$H.CHO$	$H.COOH$	CO_2	CO	CH_4	C_2H_4	H_2
$C_2H_5\,OH$	O_2													
				Pressure = 50 atmospheres, diluent = nitrogen										
5	1	280	60	64·3	1·4	17·1	—	—	0·3	3·8	13·2	—	—	—
10	5	280	123	18·0	4·4	26·3	16·9	0·8	1·1	23·2	9·0	—	—	—
5	5	280	137	12·2	0·6	25·1	9·4	0·1	0·4	45·1	6·7	—	—	—
2·5	5	280	60	10·5	1·2	20·9	5·3	—	0·3	28·3	26·5	6·6	—	6·6
1	5	280	60	4·4	0·6	5·3	3·0	0·4	—	86·1	—	—	—	—
10	5	322	30	0·3	—	—	0·2	—	0·1	14·1	62·5	20·4	2·6	—
				Pressure = 100 atmospheres, diluent = nitrogen										
20	4	261	78	32·8	0·8	39·9	7·5	—	0·5	5·1	13·6	—	—	—
20	10	261	120	20·7	2·4	36·2	13·5	0·2	0·3	20·4	3·6	2·6	—	—
10	10	261	180	10·4	1·4	35·6	8·2	—	0·4	27·6	12·5	—	—	—
5	10	261	142	3·4	1·7	19·4	4·3	Trace	0·3	63·0	7·9	—	—	—

a closed porcelain vessel to temperatures between 650° and 900° C it decomposed in two ways, thus :

$$CH_3OH = :CH_2 + H_2O \qquad (1)$$
$$CH_3OH = \underbrace{HCHO}_{H_2 + CO} + H_2 \qquad (2)$$

the $:CH_2$ residue from (1) being subsequently hydrogenated to methane by hydrogen liberated in (2). At 650° C the final gaseous products contained $CO = 33 \cdot 0$, $H_2 = 55 \cdot 75$, and $CH_4 = 11 \cdot 25\%$, showing that about one-fourth of the alcohol had decomposed according to (1).

We have found that when heated in a steel vessel at 25 atmospheres it decomposes quite readily at 350° C and slowly at 280° C, the products containing, in addition to the gases already mentioned, considerable quantities of carbon dioxide as well as some methyl formate. The results of these experiments are given in Table IV.

TABLE IV—THE THERMAL DECOMPOSITION OF METHYL ALCOHOL AT 25 ATMOSPHER AND TEMPERATURES BETWEEN 279·5° AND 355° C.

Temp. °C	Duration of expt. hours	Composition of products—per cent. by volume					
		H . CHO	H . COOCH$_3$	H$_2$	CO	CH$_4$	CO$_2$
279·5	12	0·6	3·9	61·5	9·7	10·2	14·1
301·0	3	0·4	2·2	60·2	10·5	12·3	14·4
355·0	2	0·5	1·5	55·5	11·1	15·6	15·8

It will be seen that while at 25 atmospheres decomposition took place substantially in accordance with equations (1) and (2), secondary reactions (probably catalysed by the steel walls of the vessel) exerted a considerable influence on the composition of the products. In this connection the comparatively small amount of carbon monoxide formed and the occurrence of upwards of 14% of carbon dioxide suggests that the "water-gas" equilibrium has been established.

(ii) *Oxidation*—Two series of experiments (*a*) and (*b*) were carried out with a 2 : 1 alcohol-oxygen mixture diluted with nitrogen at pressures of 50 and 100 atmospheres, respectively. In series (*a*) the partial pressure of alcohol was kept constant throughout at 10 atmospheres, the reaction temperature being varied between 251·5 and 325·5° C, and in series (*b*) at 20 atmospheres, the temperature range being 244°–254° C.

The products consisted of formaldehyde, methyl formate, and formic acid (included together in Table V), water, the two oxides of carbon and hydrogen. Methane was only found in one experiment (at 100 atmospheres) in which the reaction was very rapid and accompanied by a considerable rise in temperature.

From the results, summarized in Table V, it will be seen that at both pressures only small quantities of formaldehyde, formic acid, and methyl formate survived, the greater part of the carbon of the alcohol burnt appearing as oxides of carbon. At the lower reaction temperatures, *i.e.*, 251·5° in series (*a*) and 244° in series (*b*), oxidation proceeded slowly and the gaseous products consisted almost entirely of carbon dioxide. As the temperature was progressively increased, carbon monoxide and hydrogen appeared in comparatively large quantities and in proportions such as would result from the thermal decomposition of formaldehyde.

TABLE V—THE SLOW OXIDATION OF METHYL ALCOHOL. REACTING MEDIUM: $CH_3 . OH = 20,\ O_2 = 10,\ N_2 = 70\%$.

Initial temp. °C	Duration of expt. mins.	Products as percentages of the carbon or hydrogen of the alcohol burnt or decomposed					
		H . CHO	H . COOH and H . COOCH$_3$	CO_2	CO	CH_4	H_2
			Series (*a*). Pressure = 50 atmospheres				
251·5	120	0·80	1·60	97·5	—	—	—
265·0	<5	1·25	3·90	24·2	70·8	—	35·4
276·0	<5	0·95	1·85	32·8	64·3	—	29·4
282·0	<5	0·45	2·80	37·6	57·3	—	49·0
325·5	<5	0·35	1·20	42·2	56·4	—	37·2
			Series (*b*). Pressure = 100 atmospheres				
244·0	134	0·35	0·55	99·1	—	—	—
247·0	90	0·55	0·55	89·0	10·0	—	—
254·0	<5	0·90	0·85	12·6	79·3	6·7	60·5

(C) *Acetaldehyde*

(i) *Thermal Decomposition*—When a 1 : 4 aldehyde-nitrogen mixture at 50 atmospheres was subjected to prolonged heating at 130° C the only detectable products of thermal change were crotonaldehyde and water.* At 210° some direct decomposition to carbon monoxide and methane occurred together with the formation of vinyl alcohol,† ethylene oxide, and ethyl acetate. On raising the temperature to 282° decomposition proceeded rapidly accompanied by the formation of increased amounts of ethyl acetate and crotonaldehyde.

---

* Bone and Smith (' J. Chem. Soc.,' vol. 87, p. 915 (1905)) detected crotonaldehyde in the products obtained by passing undiluted acetaldehyde vapour at atmospheric pressure over porous porcelain heated to 450°–500° C.

† Identified by means of its double compound with mercuric oxychloride.

The effect of temperature (at 50 atmospheres pressure) may therefore be summarized as (*a*) an aldol condensation, with subsequent splitting off of water to give crotonaldehyde; (*b*) internal molecular rearrangement giving vinyl alcohol and ethylene oxide; (*c*) condensation to ethyl acetate, and (*d*) direct decomposition to carbon monoxide and methane.

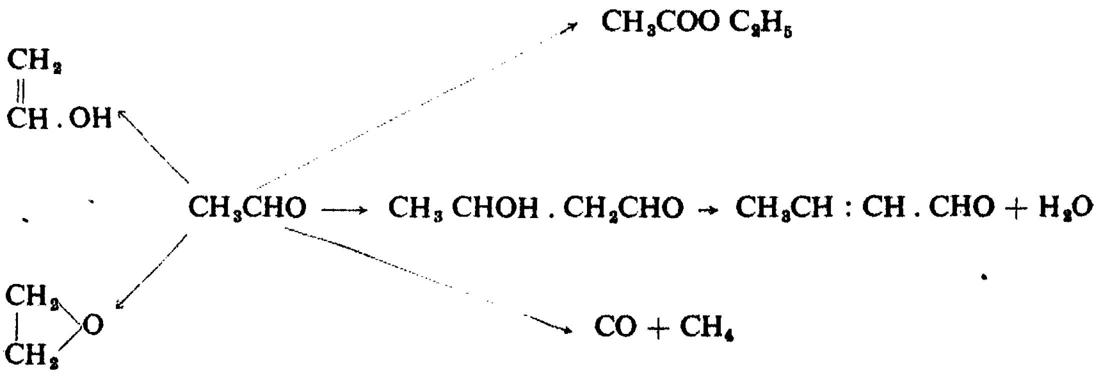

(ii) *Oxidation*—In order to study the oxidation under conditions comparable with those existing during the slow combustion of ethane low partial pressures of aldehyde with nitrogen as diluent were employed. Using a $CH_3CHO = 10$, $O_2 = 5$, and $N_2 = 85\%$ mixture at 50 atmospheres, experiments were carried out over a sufficiently wide temperature range to include both slow and rapid rates of reaction.

The results, Table VI, show that whilst at low temperatures acetic acid was the principal product of combustion, further oxidation took place as the temperature was raised giving methyl alcohol and the two

TABLE VI—PRODUCTS FROM THE OXIDATION OF ACETALDEHYDE AT TEMPERATURES BETWEEN 27° AND 269° C AND AT PRESSURES OF 50 ATMOSPHERES

Initial mixture $CH_3CHO = 10$, $O_2 = 5$, and $N_2 = 85\%$

Temperature °C	Products as percentages of the carbon of the acetaldehyde oxidized or decomposed					
	$CH_3.COOH$	Total peroxides	CH_3OH	CO_2	CO	CH_4
27	92·5	5·7	1·0	—	—	—
49	84·3	4·5	2·7	2·9	—	—
94	57·5	Nil	4·7	8·1	13·0	7·5
269	8·0	Nil	2·6	13·4	52·9	20·6

oxides of carbon. Above 94° the carbon monoxide and methane contents of the products indicated that thermal decomposition of the aldehyde was taking place. In addition to acetic acid small quantities of peroxides (diacetyl peroxide and peracetic acid) were found in the products of the low temperature oxidation but not above 94°. In view of the suggestion that a peroxide is the primary product of hydrocarbon oxidation it should be noted that in our experiments no peroxides whatever were found in the products of the slow oxidation of methane, ethane, methyl alcohol, or ethyl alcohol and that in the case of aldehyde they could only be detected during the slow oxidation at temperatures below 100°.

In addition to the products included in Table VI, identification tests were made for the following substances with results as recorded :—

Vinyl alcohol, formaldehyde, methyl acetate	Present in small quantities at all temperatures.
Glycollic and formic acid	Present in small quantities at and above 49°.
Crotonaldehyde, crotonic acid, ethylene oxide	Present in small quantities at and above 94°.
Oxalic acid, acetone, glycollic aldehyde, glyoxal	Absent.

(D) *Acetic Acid*

(i) *Thermal Decomposition*—Owing to the highly corrosive action of hot acetic acid vapour even on the most resistant nickel-chromium alloy steels, its thermal decomposition could not satisfactorily be studied at high pressures with the apparatus available. Experiments were therefore carried out at atmospheric pressure in a silica vessel of 500 cc capacity, connected to a mercury manometer and heated in an electric furnace.

At 442° C decomposition was found to take place slowly, the ratio of final to initial pressure after 1 hour being 1·22. The gaseous products were : carbon dioxide = 45·6, carbon monoxide = 27·5, ethylene = 6·8, and methane = 12·4%. In addition methyl acetate, acetone, and traces of acetic anhydride were found. These products indicated that decomposition was taking place in two ways, thus:

$$CH_3COOH = CH_3OH + CO \qquad (1)$$

$$CH_3COOH = H_2O + (CH_3CO)_2O \rightarrow \underbrace{CH_3 . CO . CH_3}_{CH_4 + CO + \frac{1}{2}C_2H_4} + CO_2 \qquad (2)$$

the methyl alcohol formed in (1) combining with excess of acetic acid to give methyl acetate.

(ii) *Oxidation*—Although the vapour phase oxidation of acetaldehyde to acetic acid now forms the basis of a manufacturing process little systematic work appears to have been done upon the further oxidation of the acetic acid.

We have therefore carried out experiments with various acetic acid-oxygen mixtures (*a*) in a silica vessel of 500 cc capacity at reduced pressures, and (*b*) in a nickel-chromium alloy steel vessel at 50 atmospheres pressure in order to elucidate the mechanism of its combustion.

Experiments at Reduced Pressure—The experimental method consisted in introducing successively known amounts of the acid and oxygen into the previously evacuated vessel, maintained at a suitable high temperature, and following the progress of the reaction by pressure-time observations. The reaction was usually allowed to go to completion, but was sometimes arrested at an earlier stage by plunging the hot vessel into a freezing mixture; the cooled products were then withdrawn and analysed.

General Features of the Oxidation—The oxidation could conveniently be followed manometrically over the temperature range 426°–486°C at pressures of 200 mm or thereabouts. In such circumstances it was predominantly homogeneous and proceeded slowly to completion without any marked induction period. Pressure-time curves for three representative experiments with mixtures having acetic acid: oxygen ratios of 0·8, 2·9 and 4·1 : 1 and reacting at 442° C are given in fig. 2.

The products of the oxidation consisted of the two oxides of carbon, methane, and steam together with quantities of methyl acetate and acetone too small to be estimated with accuracy. Analyses of the residual gases from the reaction of a 1 : 1 acid-oxygen mixture at 426°, 458°, and 485° and 200 mm pressure are given below.

Reaction temperature °C	Gaseous products %		
	CO_2	CO	CH_4
486	54·4	41·8	3·8
458	51·6	41·9	6·5
426	54·2	38·0	7·8

The Influence of Acetic Acid Concentration on the Velocity of the Reaction—Two series of experiments (I and II) at 442° were carried out, the partial pressure of oxygen being maintained constant at 45 mm and 135 mm, respectively, whilst the pressure of acetic acid was varied over a wide range. From the times of half change for the different mixtures, Table VII, it can be seen that the velocity of oxidation increased rapidly with the acid concentration. Also the order of the reaction with respect to acetic acid was found to vary with its concentration for low partial pressures of oxygen (Series I) and to be approximately second order for high partial pressures (Series II).

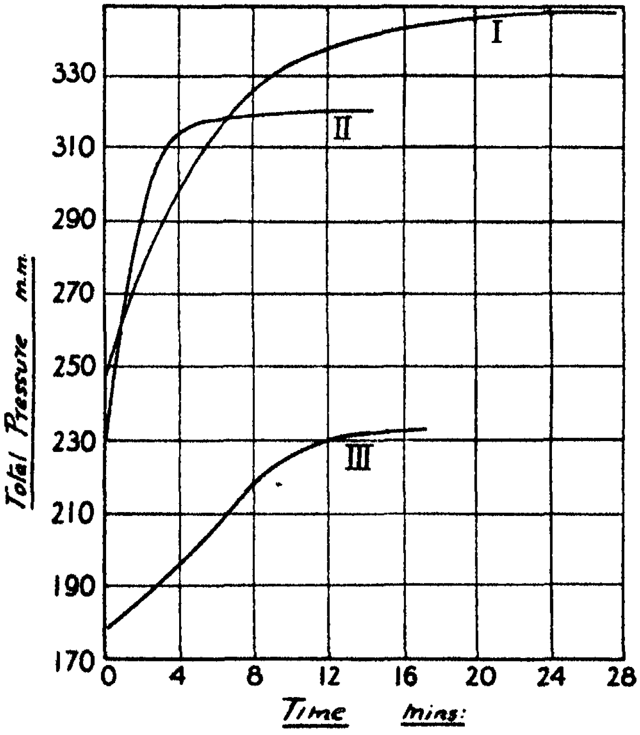

I P_{O_2} = 135 mm. P_{Ac} = 109 mm.
II P_{O_2} = 45 mm. P_{Ac} = 185 mm.
III P_{2} = 45 mm. P_{Ac} = 131 mm. Temperatures = 442°C.

FIG. 2

TABLE VII

Series I—Reaction temperature = 442° C. Partial pressure of oxygen = 45 mm.

Partial pressure of acetic acid, mm	43	57	85	139	157
Time of half change, min.........	16·0	13·75	7·0	2·8	1·2

Series II—Reaction temperature = 442° C. Partial pressure of oxygen = 135 mm.

Partial pressure of acetic acid, mm.	46	65	99	144	222
Time of half change, min.........	7·7	6·9	4·1	3·35	1·9

Experiments at High Pressures—It was found that at 50 atmospheres acetic acid could be oxidized readily at 300° C and we were therefore able to carry out a number of experiments in the steel reaction vessel at this temperature without undue corrosion taking place.* An initial mixture containing acetic acid = 20, oxygen = 10, and nitrogen = 70% undergoing reaction at 50 atmospheres and 290°, yielded products of the following composition :—

Products—percentages of the carbon of the acid consumed

Acetone	10·3	Carbon dioxide	52·5
Methyl acetate and methyl alcohol	19·0	Carbon monoxide	2·2
Glycollic acid	10·0	Glyoxylic acid	1·0
Formic acid	4·0	Acetic anhydride	Not estimated

Omitting those substances resulting from thermal decomposition of the acid, the formation of the remainder can satisfactorily be accounted for as the result of successive hydroxylations and decompositions, thus:

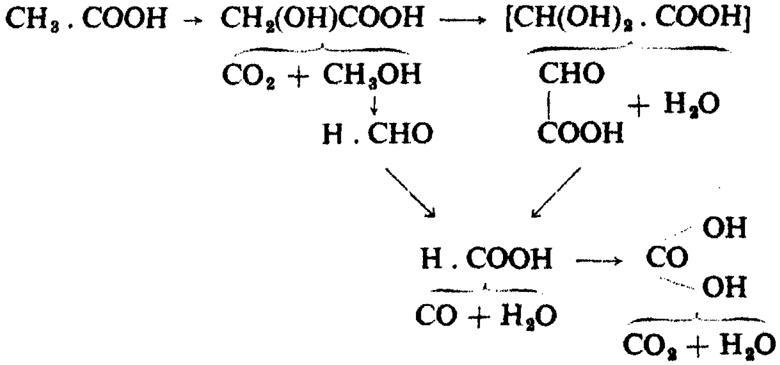

It will be noted that all the substances formed during the oxidation of acetaldehyde at temperatures above 100° are present in the products of acetic acid oxidation and it is therefore reasonable to infer that acetic acid is the initial hydroxylation product of the aldehyde molecule. This being so it is possible to simplify the scheme given on p. 560 for the slow combustion of ethane by introducing acetic acid as a link in the direct sequence of hydroxylations immediately following acetaldehyde, thus:

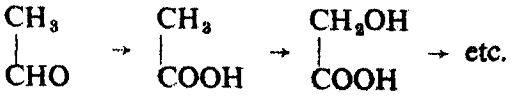

$$\begin{matrix}CH_3\\|\\CHO\end{matrix} \rightarrow \begin{matrix}CH_3\\|\\COOH\end{matrix} \rightarrow \begin{matrix}CH_2OH\\|\\COOH\end{matrix} \rightarrow \text{etc.}$$

---

* After such an experiment the walls of the vessel were found to have suffered slight local attack with the formation of nickel and iron compounds of peroxidic character.

In conclusion, we desire to acknowledge the assistance given by Messrs. A. H. Boultbee and I. B. Stuart in carrying out the experiments on the decomposition of methyl alcohol and the oxidation of acetic acid, respectively.

4—SUMMARY

When methane and ethane are oxidized at 50 atmospheres pressure in a flow system in which the reacting medium can be rapidly cooled, the reaction is partially arrested at an early stage so that large quantities of the primary product (methyl or ethyl alcohol) survive in the products. In one experiment, for example, with a $C_2H_6 = 90$, $O_2 = 3$, $N_2 = 7\%$ medium reacting at 360° C, no less than 62·6% of the carbon of the ethane burnt appeared as ethyl alcohol in the products, without any trace of peroxidation.

The thermal decomposition and slow oxidation of ethyl alcohol, methyl alcohol, acetaldehyde, and acetic acid have been studied under similar conditions of temperature and pressure to those employed in the oxidation of ethane, and it has been shown that, in each reaction, the products are such as would result from an hydroxylation mechanism of combustion.

The oxidation of acetic acid at reduced pressures, in a silica vessel, is predominantly a homogeneous reaction, of variable order with respect to acetic acid concentration. At temperatures between 426° and 486° C and pressures of about 200 mm it proceeds uniformly without any marked induction period, the products consisting of the two oxides of carbon, methane, steam, and traces of methyl acetate and acetone.

The Upper Limits of the Continuous β-Ray Spectra of Thorium C and C″

By W. J. HENDERSON, M.A., Trinity College, Cambridge, 1851 Exhibitioner, Queen's University, Kingston, Canada

(*Communicated by C. D. Ellis, F.R.S.—Received August* 8, 1934)

§ 1—INTRODUCTION

It is well known that the disintegration electrons from a radioactive body are distributed over a wide range of velocities, and that a characteristic feature of this distribution is that there is an upper energy limit above which no electrons are emitted. The accurate determination of these upper limits and the corresponding maximum energy of the β-rays has become of much importance in connection with special theories which have been advanced to explain the nature of the β-ray disintegration.

Numerous experiments have been done to find these upper limits or end points. Most of the existing data are based on range measurements in which the energy of the fastest β-rays from a source is deduced from their range. The chief advantage of the method is that it can be carried out with weak or rapidly decaying sources; the great disadvantage is that owing to the scattering suffered by the β-particles, the range found by experiment is an indefinite quantity and has no simple relation to the maximum energy of the β-particles. Because of this fact range methods, while frequently giving results in general agreement with magnetic analysis, are not capable of leading to accurate results for the upper limits. There remain two other methods of analysis, the magnetic spectrograph and the expansion chamber. The latter as used by Terroux and Alexander* gives a higher upper limit than other methods. For radium E Terroux† reported a tail extending to 3,000,000 volts, while other methods give an end point at about 1,070,000 volts. Champion,‡ in repeating Terroux's experiments, emphasized the precautions that must be taken in interpreting the experimental material. To eliminate the effect of scattering he was forced to adopt a criterion that a particle would be counted only if it had an undisturbed track greater than a certain length. The cloud-chamber method, while applicable to very weak sources, must be used with great care, and cannot give an accurate value of the end point without taking a very large number of photographs.

---

* 'Proc. Camb. Phil. Soc.,' vol. 28, p. 115 (1932).

† 'Proc. Roy. Soc.,' A, vol. 131, p. 90 (1931).

‡ 'Proc. Roy. Soc.,' A, vol. 134, p. 672 (1932).

The magnetic spectrograph, adopted in these experiments, is the most convenient method for determining the end points. The β-rays are focussed by allowing them to traverse a semi-circle in a uniform magnetic field and their intensity measured with some form of sensitive detector. The only existing data concerning the end points of the thorium bodies by this method are those of Gurney* on thorium C and thorium B. As a β-particle detector Gurney used a Faraday cylinder whose sensitivity to β-rays is so low that only by using wide slits and large sources could he explore the region of the end points. In order to deal with relatively weak sources and also bodies such as thorium C″, which have a short period, a much more sensitive detector is necessary. The obvious choice is some form of counter, but at once the difficulty of the γ-ray effect presents itself. This effect unfortunately remains practically constant throughout the spectrum and therefore becomes more and more important as the end of the spectrum is approached and the β-ray effect gradually vanishes. Even when the γ-rays are absorbed by as much lead as is practical the β-rays near the end point are much less than the effect of the γ-rays. For the present experiments a form of coincidence counter has therefore been constructed which makes it possible to use the great sensitivity of counting methods in spite of the γ-rays.

The method of detecting cosmic ray particles by the coincident discharges of two Geiger-Müller counters is well known. Discharges in one counter caused by particles which do not pass through the second counter are not recorded, except as " accidental coincidences." Theoretically the number of accidental coincidences is given by $2N_1N_2T$, where N_1 and N_2 are the number of discharges per minute in each individual counter and T the resolving time of the recording circuit. The resolving time can easily be made 1/1000 sec and if there are 100 independent discharges in each counter the number of accidental coincidences is one in every three minutes. If now discrete particles are made to pass through both counters, each one will be recorded as a coincidence.

When coincidence counting is applied to counting β-rays in the presence of γ-rays, such conditions cannot be realized. In order to allow the β-particles to pass through both counters, they must be placed very close together and without any appreciable absorbing material between them. This greatly increases the chance of a secondary particle, produced by γ-rays, passing through both counters and being recorded as a coincidence. It was found that the coincidence method reduced the effect of the γ-rays by a factor of about 25, and this allowed accurate measurements of the β-rays in the region of the end point with a 1·5 mg source of thorium (B + C + C″). Due to the high sensitivity of the arrangement to β-rays, the high energy β-ray lines of thorium C″ were detected. These lines appear beyond the end of the continuous spectrum and are due to the internal conversion of the $2 \cdot 62 \times 10^6$ volt γ-ray. Their total intensity is only 2·5 electrons per 1000 thorium C atoms disintegrating, and hitherto they have only been detected photographically.

---

* 'Proc. Roy. Soc.,' A, vol. 112, p. 380 (1926).

The measurements with the coincidence counter lead to accurate values for the upper limits of thorium C and thorium C″. These quantities are of considerable importance in view of recent suggestions regarding the energy balance around the thorium C branches. This is discussed more fully in § 4 where it is shown that the maximum energies liberated in the two branches of thorium C balance, in agreement with the prediction of Ellis and Mott.*

§ 2—EXPERIMENTAL

The two counters were mounted on an insulating strip in an airtight metal container, which was evacuated to the desired pressure and sealed off. The β-rays entered the counters through a mica window, equivalent in stopping power to 1·5 cm of air, in the bottom of the container. It was also found necessary to put a thin sheet of mica between the counters to prevent one setting off the other by ultra-violet light produced during the discharge.

The complete spectograph is shown in fig. 1. The radius of curvature was made relatively large (*i.e.*, about 9 cm), to reduce still further the effect of the γ-rays. The brass box B was completely lined with aluminium 3 mm thick to reduce secondary electron emission. The counter container was set in a brass ring on the top of the box, the joint being made airtight with plasticene. The source at S was placed under a brass cap also made airtight with plasticene. In the work with thorium C″ the source was kept outside the box, since owing to the rapid decay, it had to be changed very frequently. The slit A was then covered with thin mica (1 cm air equivalent). The measurements with thorium (B + C + C″) sources were done both with and without this mica, and no difference in the shape of the upper part of the spectrum could be detected.

---

* 'Proc. Roy. Soc.,' A, vol. 141, p. 502 (1933).

The defining slit is at C, its width was calculated so that the maximum of a line would be fully developed. The β-rays could be completely cut off by a shutter T, allowing for the determination of the inevitable effect of the γ-rays and other stray effects. To make certain that no β-rays entered the counter except those coming directly from the source, a system of aluminium baffles C_1, C_2, etc., 3 mm thick were placed as shown. Slits were cut in these to limit the beam to one slightly greater than that defined by the slit C. This construction makes it very improbable that a β-ray once scattered from the beam can return and be recorded with the wrong energy. At one stage of the experiments it was thought that β-rays slower than those being focussed were entering the counter through small angle scattering from the aluminium on the lower surface of the shielding lead. The surface was therefore altered from the usual shape to that shown. It was designed to act as a trap and prevent slow β-rays which might be scattered from the surface between the baffles from passing through the remaining defining slits. It was found that

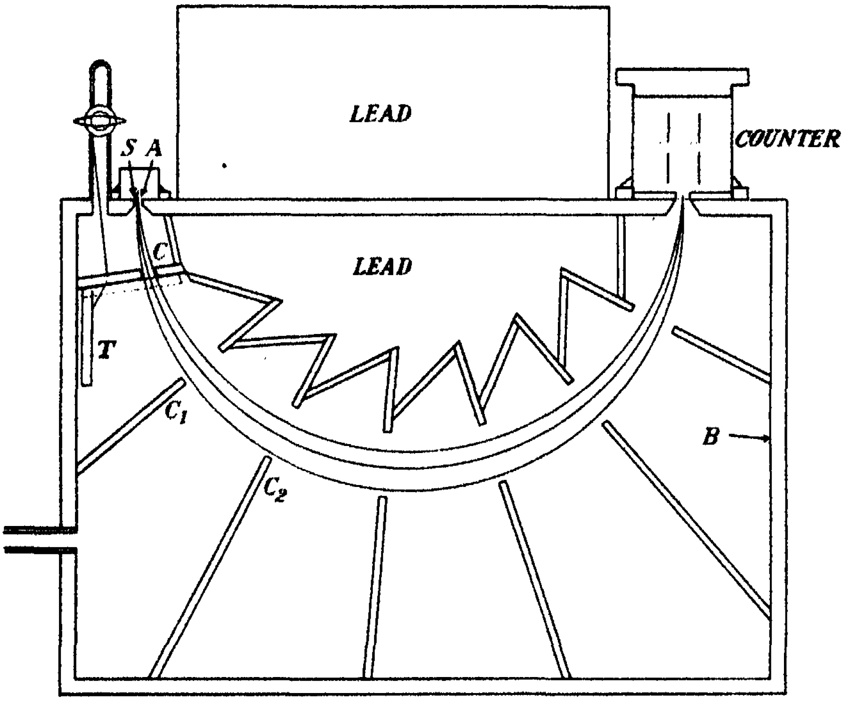

FIG. 1.

the alteration made no detectable difference to the value found for the upper limit. The whole apparatus was made airtight and then maintained at the pressure given by a Hyvac oil-pump running continually.

Coincidences of the two counters were isolated by the circuit developed by Rossi and recorded with a thyratron and telephone counting meter. For each setting of the field, readings were taken with the shutter closed and open. The difference between these two readings is taken as the β-ray intensity.

Some actual measurements near the end point of the thorium C spectrum will show the advantage of the coincidence arrangement. The counters were each 1 cm long and 1 cm in diameter. The kicks in a single counter due to the natural effect and γ-rays from a 1·5 mg (γ-ray equivalent) source passing through the lead screens were about 65 per minute; this gave about two coincidences per minute. The number of coincidences due to both γ- and β-rays was between 7 and 8 per minute. With the coincidence counter the presence of β-rays is quite definite, while with a single counter it is very difficult to detect such a small number of β-rays in the presence of the much more intense γ-ray effect. At first sight it might appear that the large number of γ-ray coincidences was due to low resolving power of the amplifier which was in fact about 10^{-3} sec. With this value of the resolving power and 65 kicks per minute in each counter, the number of casual coincidences should be $V = 2N_1N_2T = 0\cdot14$ per minute. Most of the γ-ray coincidences observed were therefore not casual but real coincidences caused by the passage of a secondary electron through both counters. This effect is increased by having the counters close together and with the ends open to allow the passage of the β-rays.

For measurements on the upper energy limit of thorium C a source of thorium (B + C + C″) was used. The active deposit was collected on a polished non-magnetic steel plate 8 mm by 3 mm by exposure to the emanation. The source was placed in the apparatus in the usual way so the β-rays left at almost grazing incidence. The thorium C″ was collected on a similar source plate by recoil from thorium (B + C + C″). Since the half period of thorium C″ is 3·2 minutes, the source had to be changed every 8 to 10 minutes. Two similar source plates were used, and while one was in the apparatus the other was being activated. That the recoil sources were free from contamination from the parent source was shown by the fact that they decayed with a 3·2 minute half period and after 20–25 minutes no β-rays at all could be detected. With each source a count was taken at a standard value of the field. When all readings had been corrected for decay, these counts were used to bring the different readings to the same source strength.

The hard γ-rays from a source of thorium (B + C + C″) are all known to come from thorium C″. At first it was hoped that this fact could be used to find how much of the β-radiation from a thorium (B + C + C″) source was due to the thorium C″ by finding the relation between the hard γ-rays and the β-ray counts with a thorium C″ source. The γ-rays were filtered through 4 mm of lead and measured with an ordinary β-ray electroscope. The γ : β relation was found by alternately measuring the γ-rays with the electroscope and counting the β-rays in the spectrograph. With the thorium C″ sources a fairly consistent β : γ ratio was found for different sources on similar source plates. Different thorium (B + C + C″) sources, however, did not give consistent results, presumably owing to uneven distribution of the active deposit. When the approximate value of the β : γ ratio was used to express the thorium C″ and the thorium (B + C + C″) curves for equal hard γ-ray intensities about the same number of electrons was found in the line appearing above the end of the spectrum in both sets of curves. This line is known to be due to thorium C″, and results from the internal conversion of the 2·62 million volt γ-ray from the decaying thorium C″ nucleus.

§ 3—RESULTS

The experimental results for the thorium (B + C + C″) and thorium C″ sources are shown in fig. 2 ; the ordinates are particles per minute per milligram γ-ray activity. To obtain the true distribution with Hρ the ordinates must be divided by H. It is seen that the curves descend sharply in the region below the end point and then flatten out into a faint background, on which a line appears superimposed. The curves then descend to the zero axis and for greater fields no β-particles could be detected. The line appears for both sources, and it is undoubtedly that reported by Black* and Ellis†. Thorium C″ emits a γ-ray about 1 quantum per atom of $2 \cdot 62 \times 10^6$ volts energy, and Ellis has found lines at Hρ 10,000, 10,250, and 10,300 due to the interval conversion of this γ-ray in the K.L.M. levels of the parent atom. According to Ellis, the intensity of these lines is about 2·5 electrons per 1000 thorium C″ atoms disintegrating. Owing to a wide slit at the counter, the lines are not resolved, but using Ellis' values of Hρ and relative intensity 5 : 1 : 0·2 for the K.L.M. lines the form of the line expected for this apparatus is very close to that found. For example, assuming a reasonable extrapolation of the background through the line, it is found that particles in the line are first detected at Hρ 10,280 in good agreement with the highest energy line found by Ellis. The mean value for the main line calculated from the value of the field when the whole of the line first enters the counter and that at which it begins to leave gives a value of

---

* 'Proc. Roy. Soc.,' A, vol. 109, p. 166 (1925).

† *Ibid.*, vol. 138, p. 318 (1932).

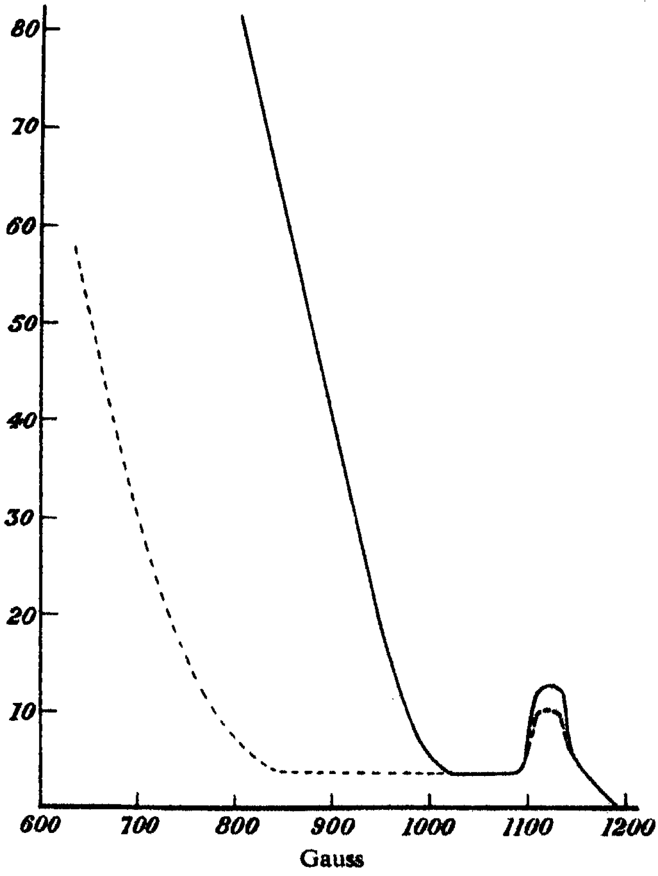

FIG. 2—Th C ——— ; Th C″ ----

Hρ 9990. While no accurate estimate of the absolute intensity of the line can be made from the present measurements an approximate curve taken down to Hρ 2000 shows the intensity is of the right order, but too high. With the present apparatus the β-rays have to pass through mica and air equal in all to about 3 cm of air before they can be recorded. This will seriously cut down the low velocity rays and lead to an underestimation of the number of β-particles in the continuous spectrum. It is hoped very soon to reduce the amount of matter traversed so as to examine the main body of the spectrum, and to arrive at the absolute intensity of the line.

The portion in both curves lying between the end point and the line is attributed to recoil and photoelectrons from the $2\cdot62 \times 10^6$ volt γ-ray. This γ-radiation will produce recoil electrons up to Hρ 9500 in the forward direction and photoelectrons up to Hρ 10,000. Check experiments in which the source slit was covered with lead sufficient to stop the fastest β-rays were carried out. It was found that a measurable background of secondary electrons from the lead did exist and was of the same order of intensity as that found with the bare source. With the bare source the background is presumably due to recoil electrons from the slit edges and material near the source.

To obtain a value for the end points of the spectra, it remains to decide just where the spectrum curve joins the background. This cannot be done with high accuracy, but since the curve falls steeply, fairly narrow limits can be assigned for the end points. There is a slight tail caused by the passage of the final rays across the counter slit and the end point is only reached when the inside ray from the source falls on the inside edge of the counter slit. Therefore, to obtain the Hρ value for the end point, the minimum radius of curvature—that is, the half distance between the inside of the source and the inside edge of the counter slit—must be used ; this was 8·86 cm.

The limits which can be assigned from the curve for the end point of thorium C are H = 1015 gauss and H = 1025 gauss with a most probable value of H = 1020 gauss. The corresponding best value of Hρ is $8\cdot86 \times 1020 = 9040$ or $2\cdot25 \times 10^6$ volts.

From the thorium C'' spectum curve limits of H = 839 gauss and H = 855 gauss can be assigned. The best value for the end point is $8\cdot86 \times 847 =$ Hρ 7500 or $1\cdot795 \times 10^6$ volts.

Apart from estimating the critical point from the experimental curve the main source of error in the value found is the measurement of the magnetic field H. The field was measured with a flux meter and search coil. The fluxmeter was subsequently calibrated against a standard Duddell mutual inductance. The search coil consisted of 30 turns of wire wound on an accurately turned marble cylinder and was kindly lent to the writer by Dr. C. D. Ellis. It was found that the field settings were reproducible within the experimental error which was about 1 part in 250. The field was also examined for homogeneity using a small search coil at various points along the path traversed by the β-particles. It was found that a correction had to be added to the value of the field owing to slight inhomogeneities near the ends of the path. This correction has been applied according to the analysis given by Hartree* and amounted to 0·58%. It is felt that the final absolute values for the magnetic field are not in error by more than ½%. Taking the intervals decided upon above and considering the possible errors in H, the values given for the upper limits should be correct to ± 1·5%.

The only previous values for the upper limits by magnetic focussing are those of Gurney (*loc. cit.*) whose curve shows a value of $H\rho$ 8860 and Madgwick† who used an ionization chamber and found $H\rho$ 8800 for the end point of the spectrum of thorium C + C″. Chalmers‡ has determined the end points of thorium C and thorium C″ continuous spectra by the range method and found $H\rho$ 9100 and $H\rho$ 7800 respectively. Sargent§ by a similar method found $H\rho$ 7550 as the end point of the thorium C″ spectrum. Terroux and Alexander‖ obtained a value of $H\rho$ 9400 for the end point of the thorium C″ spectrum using an expansion chamber, but all the evidence now indicates that these values are too high. Wang¶ has recently made a thorough study of the main portion of the β-ray spectra of the thorium bodies using a single counter as detector. For the reasons pointed out above he was not able to investigate the end points in detail.

§ 4—DISCUSSION

It is now well established from γ-ray energies and the fine structure of α-rays that the radioactive nuclei in these cases exist in quantized states. A recent theory due to Ellis and Mott** considers that the nucleus may also be quantized for the β-ray disintegrations. On this theory the maximum energy of the β-rays emitted is given by the difference in binding energies of the parent and product nuclei allowance being made for the γ-ray excitation when it occurs. The difference between the maximum energy and the energy of β-particles of lower velocity must simply disappear or an alternative is the emission of a neutron.

In support of their theory Ellis and Mott suggested that the maximum energies liberated in the two branches of thorium C should be equal.

---

[*] 'Proc. Camb. Phil. Soc.,' vol. 21, p. 746 (1923).

[†] 'Proc. Camb. Phil. Soc.,' vol. 23, p. 982 (1927).

[‡] *Ibid.*, vol. 25, p. 331 (1929).

[§] 'Proc. Roy. Soc.,' A., vol. 139, p. 659 (1932).

[‖] 'Proc. Camb. Phil. Soc.,' vol. 28, p. 115 (1932).

[¶] 'Z. Physik,' vol. 87, p. 633 (1934).

[**] 'Proc. Roy. Soc.,' A, vol. 141, p. 502 (1933).

Beck* working from a definite hypothesis about the disintegration has arrived at the same conclusion. From the data then available Ellis and Mott found that the maximum energies balanced approximately. A definite conclusion could not be drawn because of the lack of precise data about the upper limits. The present experiments give these data and the results are in complete agreement with the suggestion of Ellis and Mott.

Thorium C disintegrates in the following way :—

$$\begin{tikzcd}
 & \mathrm{ThC}' \arrow[dr, "\alpha"] & \\
\mathrm{ThC} \arrow[ur, "\beta"] \arrow[dr, "\alpha"'] & & \mathrm{ThP}b \\
 & \mathrm{ThC}'' \arrow[ur, "\beta"'] &
\end{tikzcd}$$

The energy of the α particles from thorium C′ is $8{\cdot}95 \times 10^6$ volts and the upper limit found for thorium C β-ray spectrum is $2{\cdot}25 \times 10^6$ volts. The maximum energy liberated in the thorium C′ branch is therefore $2{\cdot}25 + 8{\cdot}95 = 11{\cdot}20 \times 10^6$ volts.

The fastest α-particles from thorium C have an energy of $6{\cdot}20 \times 10^6$ volts. Ellis and Mott (*loc. cit.*) have shown that in the disintegration of thorium C″ the two γ-rays of $2{\cdot}62 \times 10^6$ volts and $0{\cdot}582 \times 10^6$ volts energy are excited in every disintegration. The upper limit of the thorium C″ β-ray spectrum was found to be $1{\cdot}79 \times 10^6$ volts, so the total energy of disintegration for thorium C″ is $4{\cdot}99 \times 10^6$ volts. The maximum energy liberated in the thorium C″ branch is therefore $6{\cdot}20 + 4{\cdot}99 = 11{\cdot}19 \times 10^6$ volts and we conclude that the maximum energies liberated in the two branches balance.

It is reasonable to expect that the same relation will hold for the other branching bodies although data are not yet available to test this conclusion. Beck (*loc. cit.*) has attempted to show that there is a balance of the maximum energies released in the actinium C→actinium D and radium C→radium D branches, by estimating the unknown upper limits of the β-ray spectra of radium C″ and actinium C from Sargent's† curves. It is, however, not at all clear what interpretation is to be put on these empirical curves connecting the observed upper limits and the disintegration constants. The upper limits alone give no certain information about the total energy of disintegration since the whole question of the excitation of γ-rays is left out of account and there are many examples to show how widely different elements vary in the extent of excitation in which they are left by a disintegration. Using the evidence from the thorium C→ thorium D branch where all the quantities have been measured it seems better to assume a balance of the maximum energies in the other branches and reverse the calculations to find the difference in binding energy between the nuclei of actinium C → actinium C′ and radium C″→ radium D. It is found that the energy of disintegration of radium C″ to radium D is $5 \cdot 89 \times 10^6$ volts and of actinium C to actinium C′ is $0 \cdot 7 \times 10^6$ volts.

---

* 'Nature,' vol. 132, p. 967 (1933).

† 'Proc. Roy. Soc.,' vol. 139, p. 659 (1933).

The very high energy difference between the radium C″ and radium D nuclei is interesting, but at present there is no evidence to decide in what form it is mainly emitted. If there is any direct transition from the normal state of radium C″ to that of radium D then there will be a β-ray spectrum with an upper limit at $5 \cdot 89 \times 10^6$ volts, but it seems more probable that with this high energy of disintegration there will be frequent excitation of the product nucleus. We might reasonably expect therefore that radium C″ emits hard γ-rays, possibly harder than those of thorium C,″ but their detection will be very difficult owing to the small number of atoms following this branch.

In conclusion, the author wishes to express his thanks to Lord Rutherford for the interest he has taken in this work and also to Dr. C. D. Ellis for much helpful advice and encouragement.

§ 5—SUMMARY

The upper limits and the high energy parts of the continuous β-ray spectra of thorium C and thorium C″ have been investigated by the method of magnetic focussing. A special coincidence counter which was relatively insensitive to γ-rays was used to count the β-rays. The values found for the upper limits of the spectra are interpreted in connection with modern views concerning the difference in binding energy between the parent and product nuclei of a β-ray disintegration.

The Excitation Potential of the Nitrogen Second Positive Bands

By N. THOMPSON, Chattock Research Student, and S. E. WILLIAMS, 1851 Exhibitioner (Sydney), Wills Physics Laboratory, The University, Bristol

(*Communicated by A. M. Tyndall, F.R.S.—Received August* 10, 1934)

INTRODUCTION

The electronic levels of the nitrogen molecule fall into two groups, the triplet and singlet systems, the latter including the ground state, the two being unconnected by any known optical transition.* The most direct method of determining the relative position of the two groups is to measure the excitation potential of one of the Positive (triplet) systems of bands, usually, for convenience, the Second Positive system. The standard determination is that of Sponer† whose results have been generally accepted as giving the most reliable value. Two earlier experimenters‡ give only rough values, and, in addition, apply no correction for the contact potential of the electrodes. This Sponer and subsequent workers have done by determining also the excitation potential of some other atom, the value of which was calculable from spectroscopic data, deducing the additive correction to be applied in this case, and assuming that it remained the same when the nature of the gas in the apparatus was altered. The method used by Sponer was to take spectrograms of the Second Positive bands excited by electrons of known energies at intervals of 0·2 volt, and compare the photographs visually to detect the first appearance of the bands. The calibration for contact potentials, however, was done visually with a pocket spectroscope, so that Sponer's estimate of her accuracy may be a little optimistic. The value obtained was 13·0 ± 0·3 volts.

---

* A new band system recently reported by Kaplan (' Phys. Rev.,' vol. 45, pp. 675, 898 (1934)) has been identified by Herzberg and Sponer ('Z. phys. Chem.,' B, vol. 26, p. 1 (1934)) as such an intercombination. This interpretation, however, is by no means definitely established. See ' Nature,' vol. 134, p. 322 (1934).

† ' Z. Physik,' vol. 34, p. 622 (1925).

‡ Bloch, C. R. Acad. Sci. Paris,' vol. 173, p. 225 (1921) ; Duncan, ' Astrophys. J.,' vol. 62, p. 145 (1925).

An obvious improvement was effected by Ornstein and Langstroth[*] who used the well-known Utrecht technique to compare intensities at different voltages. The observations in the neighbourhood of the excitation potential are, however, rather sparse, and the resulting extrapolation to zero intensity too lengthy to be very accurate. Their limits of error are not stated, but some idea of the accuracy can be obtained from the fact that the excitation potentials of the (0, 2), (1, 3) and (2, 4) bands are given as being the same (13·4 volts) while spectroscopic data indicate that they should extend over a range of 0·48 volt. A further source of error which becomes appreciable when this more refined method of measuring the intensities is used, is the possibility of a change in the spatial distribution of the glow discharge with the voltage, which would produce spurious variations in the intensity voltage curve. The method of using a defined pencil of electrons as used by Hanle and his co-workers, takes cognizance of this, but although Thieme[†] has determined the excitation function for the Second Positive system over the range 16–30 volts, he quotes no value for the excitation potential. An estimate from the published curves would be 13·6 ± 0·5 volts (this for the (1, 4) band), but the result is not very reliable since the extrapolation is again very lengthy.

A recent paper by Weizel and Fischer[‡] gives a determination from the so-called excitation dispersion phenomenon. The method is approximate only, but the result (10·9 ± 0·5 volts) differs from the general run by more than the quoted limits of error. It is of interest since no correction for contact potentials is needed, and no explanation of the discordant result is apparent. A summary of the results hitherto obtained for the energy of the $v = 0$ level of the $C\,^3\Pi$ state is appended.

	volts
Bloch (*loc. cit.*)	12·0
Duncan (*loc. cit.*)	12·0 ± 0·5
Sponer (*loc. cit.*)	13·0 ± 0·3
Ornstein and Langstroth (*loc. cit.*)	13·4 ± 0·5
Thieme (*loc. cit.*)	13·3 ± 0·5
Kneser[§]	14·8 ± 0·4
Weizel and Fischer (*loc. cit.*)	10·9 ± 0·5

[*] 'Proc. Acad. Sci., Amst.,' vol. 36, p. 384 (1933).

[†] 'Z. Physik,' vol. 78, p. 412 (1932).

[‡] *Ibid.*, vol. 89, p. 283 (1934).

[§] 'Ann. Physik,' vol. 79, p. 597 (1926). This determination, at best approximate, appears subject to some undetected error, since the values given for the excitation potentials of the various systems are inconsistent to more than a volt.

It is conceivable that the position of the triplet levels might be fixed by other indirect methods, based on a knowledge of the energies and products of dissociation of the various molecular states, but at present a more hopeful line of approach is to fix the levels by a direct method, and then proceed to a consideration of the dissociation products and dissociation energies.

Thus in the light of the above table, and considering the importance of the quantity concerned for the nitrogen molecular energy diagram and the theory of active nitrogen, a careful re-determination of the excitation potential seemed desirable. The method of using a defined pencil of electrons had been further developed in this laboratory by Lees* in his work on helium, and it appeared to us that his arrangement promised to yield the most reliable results. In addition the spreading phenomenon observed by him in helium could be examined for nitrogen at the same time, in order to provide a further test of the explanation suggested by Lees and Skinner.†

EXPERIMENTAL

The apparatus used in the experimental work is similar to that described by Lees (*loc. cit.*) and is shown diagrammatically in fig. 1. An indirectly heated, oxide coated nickel surface A served as the source of electrons, which were accelerated to the slit B by a potential of about 110 volts. B was so shaped as to shield the optical system from stray light from the filament. The slit C had a focussing action on the electron pencil, and by varying its potential (about 40 volts) over a range of about 6 volts, it could also be used to keep constant the electron current to the collector E, so compensating for small changes in the emission from the cathode. The third slit D determined the electron energy with which the nitrogen molecules were excited. This was usually between 13 and 20 volts. The actual slits in B, C, and D were 5 mm by 1 mm and the collecting cylinder E, placed very close to D, had an aperture about 8 mm by 4 mm. D and E were at the same potential, but the current to E only was recorded by the milliammeter M. The observations were made immediately behind the opening in E through a window in the side of the collector. A suitable light trap eliminated errors due to reflected light.

The electron current to E was between 0·5 and 1·0 mA, and owing to ionization by collision in the space BCD, there was also a small positive ion current. With D and E at zero potential with respect to A, this could be measured, and was found to be less than 4 microamps, which was insufficient to cause appreciable errors, either in the measured electron current or in the observed light intensities. These figures refer to a gas pressure of 3×10^{-3} mm Hg, at which the observations were made; at higher pressures the beam became less well defined, and there was also a tendency for the discharge to pass over into an arc. The nitrogen was prepared by the decomposition of sodium azide, and a continuous slow stream, controlled by a variable leak, passed through the apparatus during observations. The pressure was measured at frequent intervals. Since the probability of collision is proportional to this quantity, it was necessary to correct the observed light intensities for any small variations revealed.

---

* ' Proc. Roy. Soc.,' A, vol. 137, p. 173 (1932).

† *Ibid.*, p. 180.

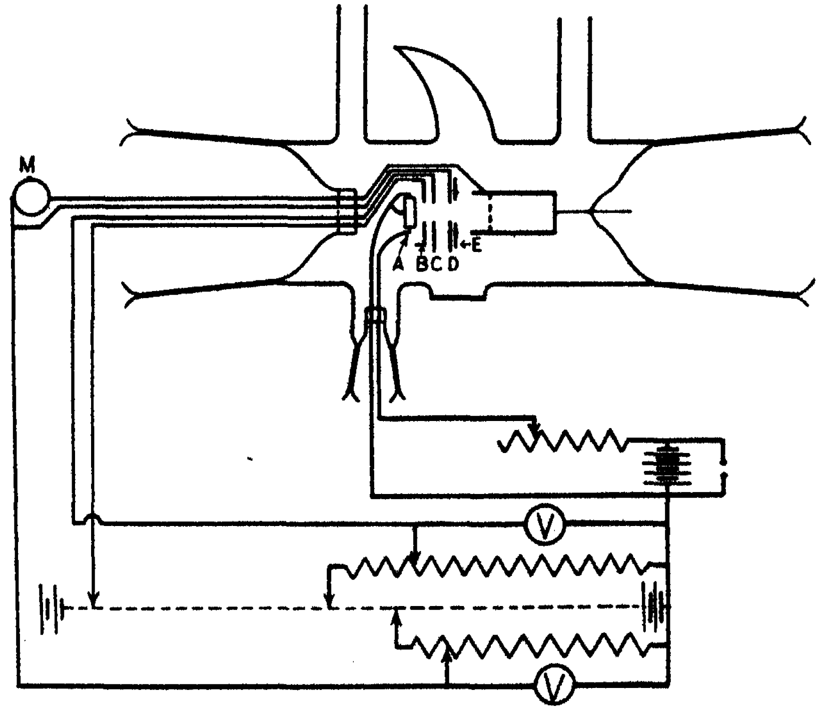

FIG. 1—Diagram of apparatus

Through a quartz window an image of the electron beam just behind the entrance to the collector was focussed on the slit of a Hilger E1 quartz spectrograph. The slit width, 0·5 mm, was magnified twice by the tilt of the plate, so that the rotation structure was completely merged. The exposures varied from 20 to 70 minutes and were so graded that all the spectra taken at different voltages were of a convenient density for photometering. Calibration of the plates was effected by means of a stepped slit used with a tungsten ribbon filament lamp. The plates were examined with the photoelectric microphotometer described by Lees,* modified for the direct recording of intensities by the method of Thompson.†

To guard against errors due to changes in the structure of the electron pencil, and also to include all the light emitted in the process of spreading, should this occur, precautions were taken that the full cross-section of the electron beam should be photographed. Consequently the contours of the bands on the plate were not sharply defined in the direction perpendicular to the dispersion, nor was the intensity distribution in this direction necessarily constant for different voltages. In addition the integrated intensity along the band was required, and not merely the peak intensity of the band head. Accordingly, the procedure adopted was to photometer both across and along the dispersion, passing in each case through the blackest part of the negative. The area of the first curve, indicating the shape of the beam, was divided by its maximum height, and the resulting " shape factors " averaged for the various bands excited at each voltage. The area of the curve taken along the dispersion was then multiplied by its appropriate shape factor to give a measure of the total intensity of the band. The resulting figures were corrected for pressure variations, and reduced to a common exposure time.

The primary object of the experiment being the determination of the excitation potential, a knowledge of the distribution of the velocities in the electron beam was considered to be of greater importance than the attainment of a very homogeneous pencil. Actually, the variation in voltage covered, about 5 volts, compares favourably with the range accepted by most workers as giving a sufficiently homogeneous pencil. It is obviously only necessary to know accurately the maximum electron velocity for a given applied potential difference between the electrodes; increased homogeneity merely lessens the necessary exposure times. The distribution curves were obtained by measuring the electron current for various stopping potentials on E, D being maintained at a constant known potential. A typical curve, obtained with D at a potential of 14 volts, is shown in fig. 2 *a*, whilst 2 *b* shows the lower part of the curve drawn on a larger scale. The differentiated curve, 2 *c*, shows the velocity distribution of the electrons, and is used later in calculating the form of the excitation function. The slight tail on the high velocity side of the maximum is probably due to the Boltzmann distribution of the electrons from the hot cathode, whose temperature, estimated from its colour, was about 800° C, indicating an extension of the size of that observed.*

---

* 'J. Sci. Instr.,' vol. 8, p. 273 (1931).

† 'Proc. Phys. Soc.,' vol. 45, p. 441 (1933).

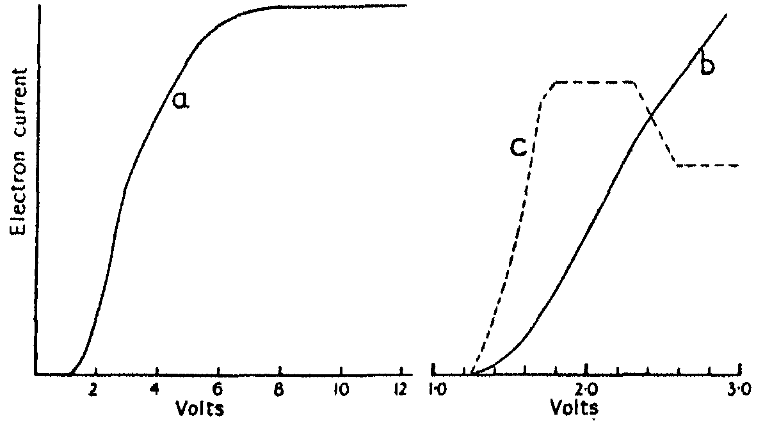

Fig. 2—Curves showing the velocity distribution of the electrons in the jet.

The potential difference between D and E at which the current to the latter drops to zero, gives the correction to be applied to the electron velocities indicated by the voltmeter between A and D, in order to take account of the contact potentials. That this is so, may most easily be seen from fig. 3, in which α, β, and γ represent the contact potentials of the electrodes, and V and V_s the accelerating and stopping potentials.

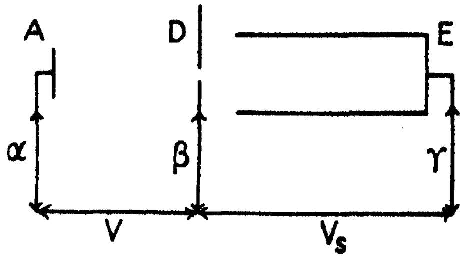

Fig. 3

When V_s is zero, electrons enter the collector with an energy equal to $V - \alpha + \gamma$, so that the correction to be subtracted from V is $(\alpha - \gamma)$. When a finite V_s is applied such that the electrons just fail to reach E, then $V - \alpha + \beta = V_s + \beta - \gamma$. This gives that $(\alpha - \gamma)$, the correction due to contact potentials, equals $(V - V_s)$, the indicated potential difference between D and E. The only assumption involved is that γ does not change with changing electron bombardment (as might the contact potential due to the charging of a grease film). Since no change in $(V - V_a)$ was observed with a ten-fold change in the electron current, this assumption appears to be justified. The method avoids the use of a second gas for the evaluation of contact potentials, with the consequent possibility of a change in their values when the gas is changed.

---

* *Cf.* Richardson and Brown, 'Phil. Mag.,' vol. 16, p. 353 (1908).

RESULTS

The curves of intensity *vs* electron voltage published by many workers in this field generally show an almost linear rise from zero at the excitation potential to a maximum which is reached a few volts above this value, but few have investigated in detail the shape of the curve immediately above the excitation potential. Over the limited range to which our results refer, which is generally insufficient to include the maximum of the intensity function, the curve was not linear, and it was found necessary to make observations at small intervals of voltage beginning well below the estimated value of the excitation potential.

The most reliable set of curves is reproduced in fig. 4, where the voltage scale is already corrected for contact potentials. Six bands were examined three whose upper vibrational level was zero, (0, 0) (0, 1), (0, 2), and three from the next higher level, (1, 0), (1, 2), (1, 3). The curves for the latter set have been shifted one volt to the right in the figure. The points at which the extrapolated curves cut the axis of zero intensity are as follows:—

(0, 0), 13·13 ; (0, 1), 13·11 ; (0, 2), 13·17 ; mean, 13·14 volts.
(1, 0), 13·40; (1, 2), 13·44 ; (1, 3), 13·40 ; mean, 13·41 volts.

The $v' = 1$ is known from spectroscopic data to lie 0·24 volts above the $v' = 0$ level, so that the mean value for the excitation potential of the lowest vibrational level is 13·16 volts. The possible error in this figure, including the error in the determination of the maximum electron velocity is estimated at 0·05 volts, which is a considerable advance on the accuracy of previous work.

We do not intend to add more to the volume of literature on the structure of the nitrogen molecular levels; the experimental result only is given, and discussion must be reserved for future papers. A word may be added, however, on the unexpected departure from linearity of the intensity-voltage curve. Undoubtedly this is partly due to the velocity distribution of the electrons, and Michels' method was used to apply a correction.* Various forms were tried for the excitation function, and combined in turn with the electron distribution curve, fig. 2 *c*, to give an intensity-voltage relation. The best agreement with the observations was obtained with an excitation function which fell to a minimum and rose again to a sharp maximum within 0·5 volt of the excitation potential. The theory offers no support for such a fine structure, previous workers would not have detected it, and the data here obtained are not sufficient to draw any definite conclusions, but the question might repay a more detailed investigation.

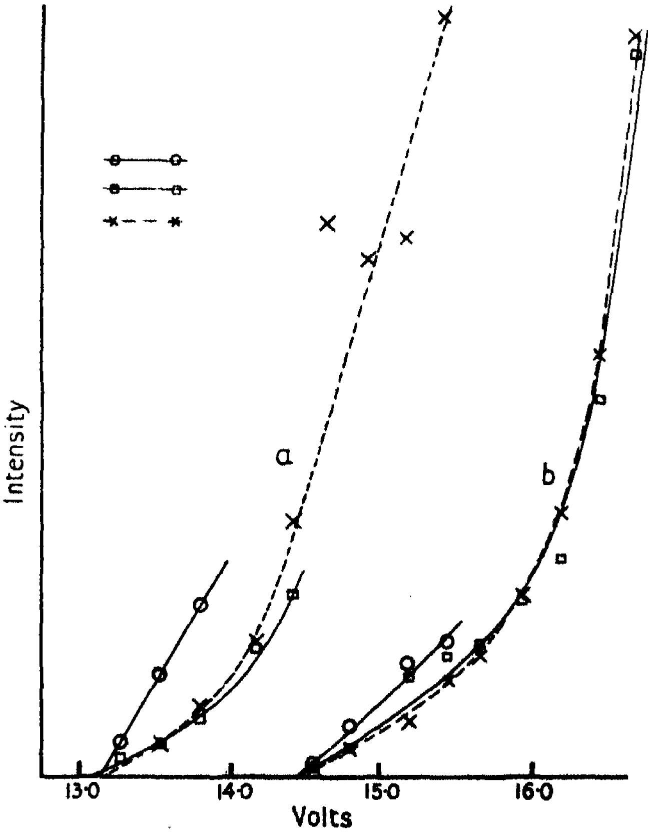

Fig. 4—The resulting curves of intensity *vs* electron voltage. The group marked *b* have been shifted one volt to the right, to avoid confusion

(*a*) (0, 0) } ○, (0, 1) } □, (0, 2) } ×.
(*b*) (1, 0) } ○, (1, 2) } □, (1, 3) } ×.

---

* 'Phys. Rev.,' vol. 38, p. 712 (1931).

Finally we may mention some observations which we made on the First Positive group of bands. When the energy of the exciting electron beam was more than about 10·5 volts, a red glow was seen to fill almost the whole of the collecting cylinder E. This was due to the First Positive bands. In addition to coming partly from the directly excited molecules in the path of the beam, they were emitted from regions so far from the electron pencil that the process of their excitation was necessarily a secondary one. This effect is the " spreading " phenomenon observed by Lees (*loc. cit.*) for some helium lines.

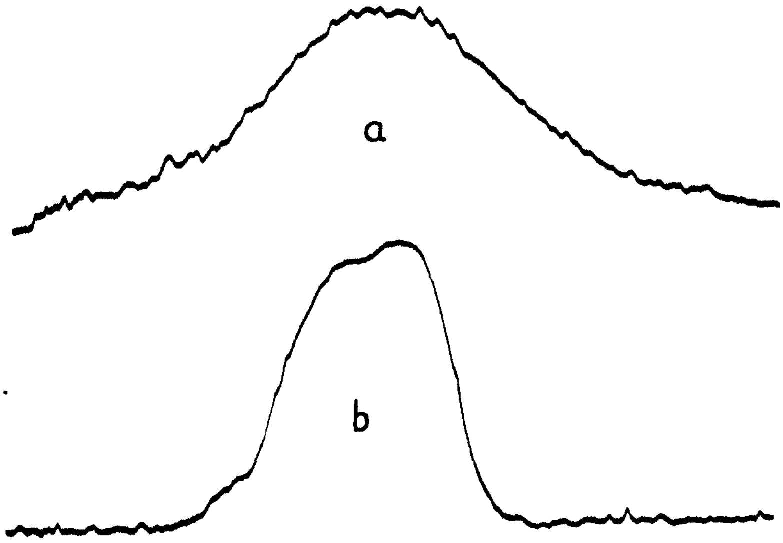

FIG. 5—Photometer traces perpendicular to the dispersion, to show the spreading effect. (*a*) a First Positive band, and (*b*) a Second Positive band.

With a Hilger constant deviation glass spectrograph, photographs were taken in the visible and near infra-red. Unfortunately the intensity of the source was small, and the only infra-red plates available very slow, so that the exposure times became inconveniently long. A photograph obtained on an Ilford hypersensitive panchromatic plate, with electrons of energy 15·75 volts, showed the limits of the Second Positive bands clearly defined, whilst the First Positive group extend to the edge of the field of view (limited by the size of the window in the collector). A simple calculation showed that a lack of achromatism in the optical system was quite inadequate to account for this effect. The two groups of First Positive bands which appeared on the plate were identified as that at 5900 A, (12, 8) to (5, 1), and that at 6500 A, (10, 7) to (4, 1). Another photograph on an Ilford infra-red plate showed only a small group at 8000 A, namely, the (7, 6), (6, 5), and (2, 0) ? bands, all of which spread in the same manner. Fig. 5 shows two photometer traces taken perpendicular to the dispersion, (*a*) for one of the First Positive bands, and (*b*) for one of the Second Positive group. The difference in shape shows the spreading effect quite clearly.

These observations are in accord with the explanation of the phenomenon suggested by Lees and Skinner (*loc. cit.*). The electrons will excite by direct impact, in addition to other systems, the Lyman bands, and these, being absorbed by molecules outside the beam, will raise them to the $a\,^1\Pi$ level. Collisions of the second kind then produce a population of excited molecules in the $B\,^3\Pi$ state which can emit the First Positive bands in falling to the $A\,^3\Sigma$ metastable level. The Birge-Hopfield bands are not excited strongly enough to produce such a marked spreading of the Second Positive bands by populating the $C\,^3\Pi$ level in a similar manner. The objection to this explanation is that the collision process concerned, involving as it does a change from a singlet to a triplet level, is theoretically very improbable, unless there is present also a considerable number of free electrons to take part in the reaction. It must be admitted therefore that the alternative explanation, following the lead of Maxwell,* cannot be rejected out of hand. This would postulate the absorption and subsequent re-emission of the First Positive bands by a population of molecules outside the beam in the metastable $A\,^3\Sigma$ level. The Second Positive group would not be expected to spread on this theory either. Some doubt as to the adequacy of this in its turn is caused by the fact that it does not account nearly so well as the other for the phenomena occurring in helium, as reported in Maxwell's original paper. In particular, the $S - P$ and $D - P$ transitions, both in ortho- and para-helium, which in emission are of comparable probability, would have to be assumed not to be so in absorption, in order to account for the spreading of the $D - P$ lines, and the non-spreading of the $S - P$ lines. To test the value of this theory for nitrogen, therefore, the voltages on our discharge tube were arranged to produce a large population in the $A\,^3\Sigma$ level without exciting the First Positive bands, other conditions remaining unaltered. The electron jet was then strongly illuminated from above by the light from a second nitrogen discharge, excited in a glass tube so as to filter out the Lyman bands. Although the intensity of the First Positive bands from the auxiliary source was at least one thousand times as great as that from the jet itself under normal conditions, there was visible no trace of spreading. Thus in this case at least, absorption by excited molecules seems to play no part in the causation of the spreading effect.

---

* 'J. Franklin Inst.,' vol. 214, p. 533 (1932.)

[*Note added in proof, November*, 1934—Since this paper was completed, evidence has accumulated that Kaplan's band system is the A — X intercombination.* Vegard's revised constants for ε-bands of solid nitrogen† also offer support to the lower value of 6·14 volts for this interval rather than the value 8·34 volts obtained by us. If Kaplan's value is correct, then our results must be interpreted to mean that the excitation function for the Second Positive bands has the peculiar property of remaining zero for all practical purposes for more than two volts above the excitation potential and then rising steeply to a maximum in the normal way.]

It is a pleasure to express our thanks to the staff of the Wills Physical Laboratory, and in particular to Dr. Appleyard, for many helpful suggestions and discussions during the course of this work.

SUMMARY

An accurate method of determining the excitation potential of optical levels by electron impact is described. A value of 13·16 ± 0·05 volts was found for the energy of the C $^3\Pi$ level of the nitrogen molecule, which is in agreement with previous less accurate determinations. Indications were obtained of a possible fine structure of the excitation function near the excitation potential. It was observed that the First Positive bands spread beyond the limits of the electron beam, while the Second Positive group do not, and possible explanations are suggested and discussed.

* Kaplan, 'Phys. Rev.,' vol. 45, p. 675 (1934); Kaplan, 'Phys. Rev.,' vol. 45, p. 898 (1934); Herzberg and Sponer, 'Z. phys. Chem.,' B, vol. 26, p. 1 (1934).

† Vegard, 'Nature,' vol. 134, p. 697 (1934).

A Note on the Spectrum of the Frequencies of a Polar Crystal Lattice

By M. Born and J. H. C. Thompson

(*Communicated by E. A. Milne, F.R.S.—Received August* 13, 1934)

1—Introduction

The following considerations deal with those vibrations of a polar crystal lattice in which the ions are moving as a whole. The frequencies of these vibrations extend from the slow macroscopic elastic waves to the infra-red region, and can be calculated by the methods of classical mechanics. (Higher frequencies occurring in optical phenomena are connected with excitations of electrons. They are not considered here.)

The oldest problem, which depends on a knowledge of the lattice frequency spectrum, is that of the calculation of specific heat; other such problems are those of the calculation of thermal expansion and other thermodynamical properties of crystals. Very rough approximations (Debye's method) are generally used, and give quite reasonable results. But a close comparison of theoretical results with experimental observations shows that the method is not completely satisfactory (*e.g.*, Debye's characteristic temperature, Θ, is not constant). The most important vibration in a binary polar lattice is that in which the vibrations of the two kinds of ions are in opposite phase—it gives rise to the infra-red absorption known as residual rays (reststrahlen). Recently the existence of secondary absorption maxima in the infra-red region has been discovered*: their explanation† depends on a knowledge of the *whole* frequency spectrum of the lattice.

Another group of problems, in which this frequency spectrum is *fundamental*, is that connected with the strength of crystals. For instance, it is known that a new crystal shows almost no resistance to gliding.

---

* Czerny, 'Z. Physik,' vol. 65, p. 600 (1930); Czerny and Barnes, 'Z. Physik,' vol. 72, p. 447 (1931); Barnes, 'Z. Physik,' vol. 75, p. 732 (1932).

† Born and Blackman, 'Z. Physik,' vol. 82, p. 551 (1933); Blackman, 'Z. Physik,' vol. 86, p. 421 (1933).

It follows that, either some of the vibrations of the lattice particles are unstable, or else that a new crystal has not a perfect lattice.* To investigate these alternatives it is indispensable to know the *whole* frequency spectrum, for instability of a vibration is signalled by an imaginary value of the corresponding frequency. Finally we mention the question of the " secondary structure " of crystals, raised by Zwicky,† as a problem connected intimately with the stability of the lattice, and therefore with the reality of the frequencies over the whole spectrum. Zwicky attempted to show‡ that there is a structure with periodic irregularities, at almost macroscopic distances apart, having lower energy (more exactly, free-energy) than the regular lattice. Assuming that such a structure really exists, the question is raised whether the regular lattice could change over to the less regular structure on account of mechanical instability, or whether the energies of these two structures are both minima separated by an energy maximum. In the latter case only at high temperatures could the thermal agitation transform the regular configuration into the less regular one, and at low temperatures the regular lattice would exist.

No attempt has ever been made to determine the whole frequency spectrum for a polar lattice, taking into account the real forces between the ions, *i.e.*, the electrical interactions of the charges and the " repulsive forces." In the few papers§ which deal with this problem, these real forces are replaced by quasi-elastic bindings between neighbouring ions. It is evident that such simple models must sometimes lead to bad results, and be completely unreliable for stability criteria. For the electrical forces are not in the least confined to actions between neighbouring ions, but, according to Coulomb's Law, they diminish very slowly with increasing distance. It is precisely this fact that makes the exact calculation of these forces very difficult, on account of the bad convergence of the series representing the forces of all ions on the one considered.

We thought it worth while to attempt an exact calculation of the frequency equation for polar lattices, in order to obtain a weapon to attack the problems mentioned. Here we explain briefly how we attacked the initial mathematical problem. A detailed exposition of the mathematics and numerical results, together with physical applications will be given by one of us in separate publications.

---

* G. I. Taylor, 'Proc. Roy. Soc.' A, vol. 145, p. 362 (1934) bases his theory of the gliding strength of crystals on an assumed imperfect lattice.

† 'Proc. Nat. Acad. Amer.,' vol. 15, pp. 253, 816 (1929) and vol. 17, p. 524 (1931) ; 'Helv. Phys. Acta,' vol. 3, pp. 269, 446 (1930).

‡ Zwicky's calculations appear to be wrong—*cf.* E. Orowan, 'Z. Physik,' vol. 79, p. 573 (1932)—but the problem raised is nevertheless worthy of consideration.

§ Born and v. Kármán, 'Phys. Z.,' vol. 13, p. 297 (1912).

2—FORMULATION OF THE PROBLEM

We treat the crystal simply as a conservative mechanical system; and, to determine its modes of vibration (given by the normal frequencies and the corresponding normal co-ordinates), we attempt to use the well-known method of classical mechanics. But, for a crystal lattice, this method has to be modified for two reasons.

The first difficulty is that it is not possible to obtain an expression for the potential energy of the Coulomb forces* by any direct mathematical method when the charged particles (ions) have *arbitrary* displacements. This problem is rather difficult for the regular arrangement of the particles in the equilibrium state; though, for this case, the problem has been solved by the methods of Madelung† and Ewald.‡ The problem of irregularly displaced particles cannot, however, be attacked immediately by these methods.

The second difficulty lies in the fact that the electrical interactions of vibrating charges are not described by electrostatic potentials, but since they have a finite speed of propagation, by electromagnetic potentials. It might be thought that this fact could not be very important for the relatively long waves that occur in the infra-red region, but such a conclusion is incorrect. For it is known from the theory of lattice models, mentioned above, that the displacements of the particles in any normal mode of vibration form a wave in the crystal, and that the frequencies split up into two groups. One group, called the elastic or acoustical frequencies, have a vanishing frequency as the wave-length becomes infinitely great; but there is another group, known as optical frequencies (experimentally exhibited as residual rays), which tend to finite frequencies with increasing wave-length. For these latter the finite speed of propagation plays an essential role, and the case of infinitely great wave-length requires special consideration.

---

* The so-called "repulsive forces" cause no difficulty, because they decrease so rapidly with the distance (as r^{-9} approximately). They are not considered in this paper.

† 'Phys. Z.,' vol. 19, p. 524 (1918).

‡ 'Ann. Physik,' vol. 64, p. 253 (1921).

3—THE CALCULATION OF THE ELECTRICAL INTERACTION FORCES

We indicate briefly the way to overcome these two difficulties. We consider the most general type of polar crystal lattice: there are s particles in each cell, which has sides $\boldsymbol{\alpha}_1$, $\boldsymbol{\alpha}_2$, $\boldsymbol{\alpha}_3$; the kth particle has a charge e_k.

The first difficulty met in the calculation of the Coulomb forces is avoided by reversing the processes of the summation of the elementary forces (to obtain the equations of motion) and the calculation of the normal co-ordinates and their frequencies. We know, not only that these normal modes exist, but also something about the displacements of the particles in these normal modes. This is simply a consequence of the lattice arrangement and is independent of the forces acting.

All vibrations which are short enough to determine the inner state of thermal agitation of the crystal are almost independent of its shape and special boundary conditions. The boundary conditions can thus be replaced by fictitious conditions which are more convenient for the mathematical calculations. The method introduced by Born* is that of the "*cyclic lattice.*" The infinite lattice is divided into blocks of the same shape as the cell, but containing just as many cells, N say, as the particular piece of crystal considered. Then the displacements in the infinite lattice are restricted by the condition of periodicity with this big block as period. The fictitious system has 3sN degrees of freedom, just like the real piece of crystal, but its behaviour is much simpler than that of a piece of crystal with irregular boundaries. For it can be shown that an arbitrary set of displacements of the particles in the block can be represented as a superposition of N independent sets of displacements. Each set consists of displacements which form a harmonic wave: the 3s amplitude-components in a cell are coupled together for a wave of given wave-length and direction, but are entirely independent of all the other waves. The problem of finding 3sN normal frequencies is reduced in this way to N similar problems of finding 3s normal frequencies.

The next step is to calculate the electrical part of the forces separately for each of the N wave-like motions, represented by

$$\mathbf{r}_k{}^l = \mathbf{r}_k{}^{0l} + \mathbf{u}_k\, e^{iq(\mathbf{s}\cdot\overline{\mathbf{r}_k{}^{0l} - \mathbf{r}_k{}^{0}})}, \; (k = 1, 2, \ldots .\, s). \;\ldots\ldots \quad (3.1)$$

Here $\mathbf{r}_k{}^{0l}$ is the vector co-ordinate of the kth particle in the lth cell for the equilibrium configuration, $\mathbf{r}_k{}^l$ that for the displaced configuration ; $\mathbf{r}_k{}^0$

---

* "Atomtheorie des festen Zustandes," 'Enc. Math. Wiss.,' vol. 5, iii, p. 587.

is the vector co-ordinate of the particle in the "origin-cell" for the equilibrium configuration; $\mathbf{u}_k$ (a function of the time) is the maximum amplitude of the displacement; $q/2\pi\ (= 1/\lambda)$ is the wave number of the displacement, and $\mathbf{s}$ is the unit vector denoting the direction of the wave normal. The quantities q and $\mathbf{s}$ must satisfy a certain relation expressing the boundary conditions.

The problem of the calculation of the electric forces can now be related to the problem for the undeformed lattice, solved by Madelung and Ewald. The first step is to split up the total potential into a sum of terms, each of which belongs to one kind of ion only. Just as in Ewald's theory of the undeformed lattice, this is made possible only by adding to the charge distribution of the point charges (of the ions of the kth type say) a fictitious uniform charge distribution of the opposite sign and the same total amount per cell. (The addition of these fictitious uniform charge distributions is permissible, as the total charge in a cell, Σe_k, is zero.) We have now to consider only the potential of the ions of the kth type, forming a lattice distorted in wave-like form according to (3.1). To get rid of this distortion we consider a transformation of the whole space,

$$\mathbf{r} = \mathbf{r}' + \mathbf{u}_k\, e^{iq(\mathbf{s}\cdot\overline{\mathbf{r}' - \mathbf{r}^0_k})}, \qquad \ldots\ldots\ldots\ldots\ldots\ldots \quad (3.2)$$

where $\mathbf{r}$ is the co-ordinate vector of the real space, and $\mathbf{r}'$ that of an "image space." The transformation has the property that for $\mathbf{r}' = \mathbf{r}_k^{0l}$ we have $\mathbf{r} = \mathbf{r}_k^{l}$; or, in other words, the positions of particles of the kth type in the displaced lattice have as "images" the positions of these particles in the undisplaced lattice.

Ewald's method for the undisplaced lattice was to express the charge density for each kind of ion (modified as above by the addition of a fictitious charge density) as a three-dimensional Fourier series, and then solve Poisson's equation to obtain the corresponding term in the expression for the electrostatic potential.

We are now in a position to obtain a similar type of expression for the charge density in the strained lattice. The charge density is connected with the charge density in the image space by the equation expressing the conservation of charge, so that an equation between the charge density in the strained lattice and that in the unstrained lattice is obtained. By this means we express the charge density of the strained lattice in terms of the *co-ordinates of real space.*

It is not now sufficient to find a solution of Poisson's equation, as we have to take account of the finite speed of propagation of the electric forces. However, the calculation is restricted to the infra-red region and magnetic forces are very small for these relatively small frequencies, so it is not necessary to work with the vector potential. It is sufficient to replace Poisson's equation by the wave equation

$$\nabla^2 \Psi + \frac{\omega^2}{c^2} \Psi = -4\pi\rho,$$

where ρ is the charge density, ω the frequency, and c the velocity of light.

Having found the total potential of the lattice in the manner described above, the potential of all particles except one can be obtained. The method employed and the method of making the series more rapidly convergent are similar to the methods adopted by Ewald.

4—THE FREQUENCY EQUATION AND THE DETERMINATION OF ITS ROOTS

The forces on one particle can now be obtained by partial differentiation*; and the $3s$ equations of motion (linear in the $3s$ displacement components) and the determinantal frequency equation are obtained in the usual manner. The frequency equation for ω^2 is of order $3s$—for a binary salt, of the sixth order. To obtain a knowledge of the whole spectrum of normal frequencies it is necessary to solve the frequency equation for each value of $q\mathbf{s}_x$, $q\mathbf{s}_y$, $q\mathbf{s}_z$. In certain simple cases (*e.g.*, $q\mathbf{s}_x = q\mathbf{s}_y = q\mathbf{s}_z$) the equation may split up into two or more equations of lower order, so that the roots may be directly calculable. But usually the calculation of the roots is almost outside the scope of direct numerical calculation. Fortunately it is possible to calculate them with the help of Mallock's calculating machine,† so that the complete description of the frequency spectrum is made possible.

SUMMARY

The importance of the knowledge of the frequency spectrum of a crystal lattice is discussed. A method for its determination is briefly outlined.

---

* The "repulsive forces" must be added, of course.

† 'Proc. Roy. Soc.,' A, vol. 140, p. 457 (1933).

CORRECTION

H. J. BHABHA and H. R. HULME. The Annihilation of fast Positrons by Electrons in the K-shell. 'Proc. Roy. Soc.,' A, vol. 146, p. 723 (1934)

On p. 726 the expression for the ratio of the number of spontaneous transitions to stimulated ones *should read* $8\pi\nu^3/c^2$ *instead of* $4\pi\nu^3/c^2$, so that all the values for the absorption coefficient should be doubled. We wish to thank Dr. Bethe for pointing out this slip.

INDEX TO VOLUME CXLVII (A)

Adam (N. K.), Danielli (J. F.) and Harding (J. B.) The structure of surface films. XXI—Surface potentials of dibasic esters, alcohols, aldoximes and ketones, 491.
Alloys, applications of Bloch theory (Jones), 396.
Alpha rays, energies (Wilson), 240.
Anthracene, powdered, reflection of X-rays (Robinson), 467.
Atoms, hydrogen, mean lives of excited (Griffiths), 547.

Bangham (D. H.) The swelling of charcoal. IV—Stoichiometric relations for the films of the alcohols, 175.
Bangham (D. H.), Fakhoury (N.) and Mohamed (A. F.) The swelling of charcoal. III—Experiments with the lower alcohols, 152.
Beta-rays, energies (Wilson), 240.
Beta-rays of low energy from radium E (Richardson), 442.
Bismuth, applications of Bloch theory (Jones), 396.
Bloch theory, applications to study of alloys and to properties of bismuth (Jones), 396.
Bone (W. A.) and Tei (L. J.) Researches on the chemistry of coal. VII—An investigation of German brown coals and Irish peat, 58.
Booker (H. G.) Some general properties of the formulæ of the magneto-ionic theory, 352.
Born (M.) and Infeld (L.) On the quantization of the new field equations, I, 522.
Born (M.) and Thompson (J. H. C.) A note on the spectrum of the frequencies of a polar crystal lattice, 594.
Butler (J. A. V.) *See* Connell and others.

Cæsium, magnetic moment of the nucleus (Jackson), 500.
Catalysis, contact, new phenomenon (Chapman and Gregory), 68.
Catalysis, decomposition of iron salts by hydrogen peroxide (Haber and Weiss), 332.
Chapman (D. L.) and Gregory (G.) The catalysis by palladium of the union of hydrogen and oxygen. A new phenomenon of contact catalysis, 68.
Charcoal, swelling, IV (Bangham), 175.
Charcoal, swelling, III (Bangham and others), 152.
Chlorine, active (Willey and Foord), 309.
Chlorine, induction period of the photochemical reaction with hydrogen (Griffiths and Norrish), 140.
Coal, researches on chemistry (Bone and Tei), 58.
Conductivity electrical of some salts in water-ethyl alcohol solutions (Connell and others), 418.
Connell (L. C.), Hamilton (R. T.) and Butler (J. A. V.) The behaviour of electrolytes in mixed solvents. VI—The electrical conductivities of some salts in water-ethyl alcohol solutions, 418.

Danielli (J. F.) *See* Adam and others.
Diamagnetic susceptibilities of salts forming ions, with inert gas configurations, I (Hoare), 88.

Electrolytes, behaviour in mixed solvents, VI (Connell and others), 418.
Equations, difference, explicit solution (Milne-Thomson), 76.
Ethylene, spectrum of the flame (Vaidya), 513.

Fakhoury (N.) *See* Bangham and others.
Field equations, new, quantization (Born and Infeld), 522.
Films, surface, structure, XXI (Adam and others), 491.
Fletcher (C. J. M.) The thermal decomposition of methyl alcohol, 119.
Foord (S. G.) *See* Willey and Foord.
Foster (A. G.) The sorption of vapours by ferric oxide gel. I—Aliphatic alcohols, 128.

Gamma-rays, energies (Wilson), 240.
Gases at high temperatures, determination of specific heat by sound velocity method, I (Sherratt and Griffiths), 292.
Gel, ferric oxide, sorption of vapours, I (Foster), 128.
Gels, isoelectric gelatin (Lloyd and Moran), 382.
Gliadin, cataphoresis, I and II (Kemp and Rideal), 1, 11.
Gregory (G.) *See* Chapman and Gregory.
Griffiths (E.) *See* Sherratt and Griffiths.
Griffiths (J. G. A.) and Norrish (R. G. W.) The induction period of the photochemical reaction between hydrogen and chlorine, 140.
Griffiths (J. H. E.) The mean lives of excited hydrogen atoms, 547.

Haber (F.) and Weiss (J.) The catalytic decomposition of hydrogen peroxide by iron salts, 332.
Halides of sodium and potassium, diamagnetic susceptibilities (Hoare), 88.
Hamilton (R. T.) *See* Connell and others.
Harding (J. B.) *See* Adams and others.
Heat, specific, of gases at high temperatures, determination by sound velocity method, I (Sherratt and Griffiths), 292.
Helium, liquefaction by an adiabatic method (Kapitza), 189.
Henderson (W. J.) The upper limits of the continuous β-ray spectra of thorium C and C″, 572.
Herzberg (G.) and Spinks (J. W. T.) Absorption bands of HCN in the photographic infra-red, 434.
Hinshelwood (C. N.), Williamson (A. T.) and Wolfenden (J. H.) The reaction between oxygen and the heavier isotope of hydrogen, 48.
Hoare (F. E.) The diamagnetic susceptibilities of salts forming ions with inert gas configurations. Part I—The Halides of sodium and potassium, 88.
Hydrogen atoms, excited, mean lives (Griffiths), 547.
Hydrogen, heavier isotope, reaction with oxygen (Hinshelwood and others), 48.
Hydrogen, induction period of photochemical reaction with chlorine (Griffiths and Norrish), 140.
Hydrogen, molecular, spectrum (Richardson and Rymer), 24, 251, 272.
Hydrogen peroxide, catalytic decomposition by iron salts (Haber and Weiss), 332.

Infeld (L.) *See* Born and Infeld.

Jackson (D. A.) The magnetic moment of the nucleus of cæsium, 500.

Jones (H.) Applications of the Bloch theory to the study of alloys and of the properties of bismuth, 396.

Kapitza (P.) The liquefaction of helium by an adiabatic method, 189.
Kemp (I.) and Rideal (E. K.) On the cataphoresis of gliadin. I—The adsorption of gliadin on quartz, 1.
Kemp (I.) and Rideal (E. K.) On the cataphoresis of gliadin. II—The effect of strong electrolytes upon the mobility, 11.
King (L. V.) On the acoustic radiation pressure on spheres, 212.

Lattice, polar crystal, spectrum of the frequencies (Born and Thompson), 594.
Lloyd (D. J.) and Moran (T.) Pressure and the water relations of proteins. I—Isoelectric gelatin gels, 382.

Magneto-ionic theory, general properties of the formulæ (Booker), 352.
Methyl alcohol, thermal decomposition (Fletcher), 119.
Milne-Thomson (L. M.) On the explicit solution of certain difference equations, 76.
Mohamed (A. F.) *See* Bangham and others.
Moran (T.) *See* Lloyd and Moran.
Moullin (E. B.) Measurement of shot voltage used to deduce the magnitude of secondary thermionic emission, 100.

Newitt (D. M.) and Szego (P.) Slow oxidations at high pressures. I—Methane and ethane. II—Methyl alcohol, ethyl, alcohol, acetaldehyde, and acetic acid, 555.
Nitrogen second positive bands, excitation potential (Thompson and Williams), 583.
Norrish (R. G. W.) *See* Griffiths and Norrish.

Oxidations, slow, at high pressures (Newitt and Szego), 555.
Oxygen afterglow (Stoddart), 454.
Oxygen, reaction with heavier isotope of hydrogen (Hinshelwood and others), 48.

Palladium, catalysis of the union of hydrogen and oxygen (Chapman and Gregory). 68.
Photochemical reaction between hydrogen and chlorine (Griffiths and Norrish), 140,
Proteins, pressure and the water relations, I (Lloyd and Moran), 382.
Prussic acid, absorption bands in the photographic infra-red (Herzberg and Spinks), 434.

Radiation pressure, acoustic, on spheres (King), 212.
Radium E, low energy β-rays (Richardson), 442.
Relativity, Milne's kinematical, principle of least action (Walker), 478.
Richardson (H. O. W.) The low energy β-rays of radium, E, 442.
Richardson (O. W.) and Rymer (T. B.) The spectrum of H_2 (the ordinary hydrogen molecule). Part I—The 3, $4d\,^3\Sigma, \Pi, \Delta \rightarrow 2p\,^3\Pi$ and $3s\,^3\Sigma \rightarrow 2p\,^3\Pi$ systems, 24.
Richardson (O. W.) and Rymer (T. B.) The spectrum of H_2. II—The band systems due to transitions from four new tiplet states to $2p\,^3\Pi$, 251.
Richardson (O. W.) and Rymer (T. B.) The Spectrum of H_2. III—New bands and band systems ending on $2s\,^3\Sigma$ and an extension of the singlet system $^1Q \rightarrow 2p\,^1\Sigma$, 272.

Rideal (E. K.) *See* Kemp and Rideal.
Robinson (B. W.) The reflection of X-rays from powdered anthracene, 467.
Rymer (T. B.) *See* Richardson and Rymer.

Sherratt (G. G.) and Griffiths (E.) The determination of the specific heat of gases at high temperatures by the sound velocity method. I—Carbon Monoxide, 292.
Spectra, continuous β-ray of thorium C and C″ (Henderson), 572.
Spectrum, band of nitrogen second positive, excitation potential (Thompson and Williams), 583.
Spectrum, molecular, of hydrogen (Richardson and Rymer), 24, 251, 272.
Spectrum of the flame of ethylene (Vaidya), 513.
Spectrum of the frequencies of a polar crystal lattice (Born and Thompson), 594.
Spectrum of HCN in the infra-red (Herzberg and Spinks), 434.
Spheres, acoustic radiation pressure (King), 212.
Spinks (J. W. T.) *See* Herzberg and Spinks.
Stoddart (E. M.) The oxygen afterglow, 454.
Szego (P.) *See* Newitt and Szego.

Tei (L. J.) *See* Bone and Tei.
Thermionic emission, secondary, magnitude measured by shot voltage (Moullin), 100.
Thompson (J. H. C.) *See* Born and Thompson.
Thompson (N.) and Williams (S. E.) The excitation potential of the nitrogen second positive bands, 583.
Thorium C and C″, upper limits of continuous β-ray spectra (Henderson), 572.

Vaidya (W. M.) Spectrum of the flame of ethylene, 513.
Voltage, shot, measurement to deduce magnitude of secondary thermionic emission (Moullin), 100.

Walker (A. G.) The principle of least action in Milne's kinematical relativity, 478.
Weiss (J.) *See* Haber and Weiss.
Willey (E. J. B.) and Foord (S. G.) On active chlorine, 309.
Williams (S. E.) *See* Thompson and Williams, 583.
Williamson (A. T.) *See* Hinshelwood and others.
Wilson (H. A.) The energies of alpha, beta and gamma rays, 240.
Wolfenden (J. H.) *See* Hinshelwood and others.

X-rays, reflection from powdered anthracene (Robinson), 467.

END OF THE ONE HUNDRED AND FORTY-SEVENTH VOLUME (SERIES A)

I. A. R. I. 75.

INDIAN AGRICULTURAL RESEARCH
INSTITUTE LIBRARY
NEW DELHI.

Date of issue.	Date of issue.	Date of issue

S. C. P.—1/8/47 P. J.-3-5-48-2000